UCLA School of Engineering and Applied Science

Final Report

Optimization Methods and Numerical Silicon Solar Cell Models

by

K.J. Girardini and S.E. Jacobsen

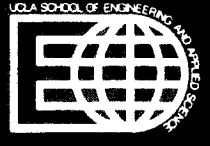

9950-1254

Final Report

"Optimization Methods and Silicon Solar Cell Numerical Models"

by
K. Girardini
S.E. Jacobsen, Professor

Department of Electrical Engineering
School of Engineering and Applied Science
University of California, Los Angeles, CA 90024

JPL Contract No. 957170

October, 1986

This work was performed for the Jet Propulsion Laboratory, California Institute of Technology, and was sponsored by the U.S. Department of Energy through an agreement with the National Aeronautics and Space Administration.

Table of Contents

List of Figures

List of Tables

Nomenclature List

symbol	description	units
α	absorption coefficient	m
ε	permittivity of material	Farad/*cm*
ΔE_g	reduction in bandgap	eV
Δ_g	effective reduction in bandgap	eV
$\Delta\chi$	electron affinity	
γ	effective asymmetry factor	
Γ	shadowing and reflection factor	
∇	gradient	
λ	wavelength	μm
μ_n	electron mobility	$cm^2/V\text{-}s$
μ_p	hole mobility	$cm^2/V\text{-}s$
$\mu_{n,p}^{L}$	Lattice scattering component of mobility	$cm^2/V\text{-}s$
$\mu_{n,p}^{I}$	Ionized impurity component of mobility	$cm^2/V\text{-}s$
ϕ	incident flux	photons/cm^3
τ_{n0}	electron saturation lifetime	ms
τ_{p0}	hole saturation lifetime	ms
τ_{Auger}	lifetime associated with Auger recombination	ms
τ_{bulk}	minority carrier lifetime in the bulk of the cell	ms
τ_{Rad}	lifetime associated with Radiative recombination	ms
τ_{SRH}	lifetime associated with SRH recombination	ms
Θ_n	reduction in bandgap (conduction band)	eV
Θ_p	reduction in bandgap (valence band)	eV
A	asymmetry factor	
A_n	electron Auger capture coefficient	cm^6/s
A_p	hole Auger capture coefficient	cm^6/s
BR	bulk resistivity	Ω–cm
BSF	back surface field cell (n-p-p^+ or p-n-n^+)	
BSR	back surface reflector	
C_{eff}	collection efficiency	%
CPU	central processor unit	
CV	conventional cell (n-p or p-n diode)	
DF	drift field cell (BSF cell with thick p^+ or n^+ region)	
D_0	net front surface doping concentration	atoms/cm^3
D_B	net bulk doping concentration	atoms/cm^3
D_L	back surface doping concentration	atoms/cm^3
Δn	diffusion coefficient for electrons	cm^2/s
Δp	diffusion coefficient for holes	cm^2/s

E_c	energy level of conduction band	eV
E_{fn}	Fermi energy for electrons	eV
E_{fp}	Fermi energy for holes	eV
E_v	energy level of valence band	eV
eff	efficiency	%
ff	fill factor	
G	generation rate	electron-hole pairs/cm^3
HLE	high-low emitter cell (p^+-p-n or n^+-n-p)	
I_{mp}	maximum power current	mA
I_{sc}	short circuit current	mA
J_n	electron current density	mA/cm^2
J_{mp}	maximum power current density	mA/cm^2
J_p	hole current density	mA/cm^2
J_{sc}	short circuit current density	mA/cm^2
k	Boltzmann constant	J/K
L_d	diffusion length	cm
N_A	concentration of ionized acceptor atoms	atoms/cm^3
N_D	concentration of ionized donor atoms	atoms/cm^3
n_{ie}	effective intrinsic carrier concentration	carriers/cm^3
n_{io}	equilibrium intrinsic carrier concentration	carriers/cm^3
n	electron concentration	electrons/cm^3
O_{pl}	optical path factor	
p	hole concentration	holes/cm^3
q	electronic charge constant (1.602×10^{-19})	coulomb
R	recombination rate	electron-hole pairs/cm^3
R_b	back surface reflectance	
R_f	front surface reflectance (internal)	
S_b	back surface recombination velocity	cm/s
S_f	front surface recombination velocity	cm/s
SCAP1D	Solar Cell Analysis Program in 1 Dimension	
T	temperature	K
V	voltage	volts
V_{bias}	bias voltage	volts
V_{mp}	maximum power voltage	volts
V_{oc}	open circuit voltage	volts
$\mathbf{X}$	a matrix	
$\mathbf{X}^k$	kth in a series of matrices	
$\mathbf{x}$	a vector quantity	
$\mathbf{x}^k$	kth in a series of vectors	

x_k	kth component of a vector	
X_b	back junction depth	μm
X_f	front junction depth	μm
X_L	cell thickness	μm

Acknowledgements

The authors wish to extend their appreciation to Dr. Anant Mokashi of JPL for his encouragement and guidance throughout the duration of the project. We wish to also thank Dr. Taher Daud of JPL who provided valuable insight and Professor Richard Schwartz of Purdue University for his assistance with the SCAP1D code's capabilities, as well as with interpretations of some of the results.

Abstract

The goal of this project is the development of an optimization algorithm for use with numerical silicon solar cell models. By coupling an optimization algorithm with a solar cell model, it is possible to simultaneously vary design variables such as impurity concentrations, front junction depth, back junction depth, and cell thickness to maximize the predicted cell efficiency. An optimization algorithm has been developed and interfaced with the Solar Cell Analysis Program in 1 Dimension (SCAP1D). SCAP1D uses finite difference methods to solve the differential equations which, along with several relations from the physics of semiconductors, describe mathematically the performance of a solar cell. A major obstacle is that the numerical methods used in SCAP1D require a significant amount of computer time, and during an optimization the model is called iteratively until the design variables converge to the values associated with the maximum efficiency. This problem has been alleviated by designing an optimization code specifically for use with numerically intensive simulations, to reduce the number of times the efficiency has to be calculated to achieve convergence to the optimal solution. Adapting SCAP1D so that it could be called iteratively by the optimization code provided another means of reducing the CPU time required to complete an optimization. Instead of calculating the entire I-V curve, as is usually done in SCAP1D, only the efficiency is calculated (maximum power voltage and current). The solution from a previous calculation is used to initiate the next efficiency calculation. Optimizations have been run for a variety of substrate qualities and levels of front and back surface passivation. This was done to determine how these variables affect the optimized efficiency and the values of the optimized design variables. The sensitivity of efficiency to each of the design variables was investigated. Several modifications were made to the SCAP1D model to allow other objective functions to be optimized, identify the effects of the physical mechanisms limiting cell efficiency, and use light trapping to define high efficiency designs.

1 Introduction

There has been considerable research in recent years to make solar cells a more economical source of energy. A large part of that research has been devoted to gaining a better understanding of the parameters that affect the performance of solar cells. One means of achieving a better understanding of solar cells is to develop a model, a mathematical representation or simulation of a system which incorporates the available physical knowledge of the system. A model can be used as an analytical tool to provide insight about the effects of and the relationships between the components that make up the model. For instance, a model is a valuable tool for investigating the performance of different solar cell designs without having to build the device that corresponds to each design.

Silicon is a leading candidate material for solar cells because there is a large body of knowledge about its properties and fabrication techniques due to its use in the semiconductor industry. It is possible to model a silicon solar cell using Poisson's equation, the continuity equations, and knowledge from the physics of semiconductors. The resulting set of differential equations does not permit an analytical solution unless several simplifying assumptions are made. One way of incorporating fewer assumptions than in analytic models (in an effort to increase the accuracy of the model), is to solve the differential equations numerically.

Accurate numerical models of silicon solar cells have been developed and used to determine the effects of cell design on performance. One method that has been used is to vary one design variable while holding the rest of the design variables constant [e.g., 1.1-1.7]. This leads to an understanding of the effect of the variable that is varied, but the knowledge obtained is valid only at the current values of the other inputs. The problem of finding the design which optimizes performance is very tedious and inexact using this approach, particularly if more than two design variables are considered. Such methods use the definition of optimum rather loosely.

Another means of arriving at an optimum design is to use analytical methods along with several simplifying assumptions to derive the optimum design [e.g., 1.8 and 1.9]. This approach, while instructive, defeats the primary purpose of developing a numerical model which is to avoid many of the assumptions required for an analytical analysis.

The need for a numerical model implies that the process modeled is sufficiently sophisticated and complex to make the above methods of analysis less than ideal. In this work, optimization theory, which can be used to define the optimum design in an exact and rigorous manner, will be used to solve the problem of arriving at an optimum design. An optimization algorithm provides an automated method for arriving at an optimum silicon solar cell design. The use of an optimization algorithm does not serve as a substitute for the knowledge of the system that is modeled, since knowledge of the physical system is necessary to insure the validity and correct interpretation of the results that are obtained from the optimization. The knowledge of the system can be extended and/or quantified by correctly interpreting the results obtained by optimization.

The first goal of this work is to develop an optimization method that can be used effectively with cpu intensive simulations. The second goal is to couple the optimization algorithm developed with the Solar Cell Analysis Program in 1 Dimension (SCAP1D). SCAP1D uses numerical methods to solve the differential equations that represent solar cell performance. The third goal is to demonstrate the effectiveness of using the optimization algorithm coupled with the SCAP1D model by doing an analysis of solar cell designs.

There are several difficulties in performing an optimization when the objective function is an output from a complex numerical process such as SCAP1D. Optimization methods require that the objective function be calculated iteratively until the optimization converges. Hence, a major obstacle in applying optimization techniques to SCAP1D is the amount of computational effort required to execute the model. The major design criterion for the optimization method to be described is that it converge reliably without requiring an excessive number of function calls. The computational burden required to complete an optimization can be reduced by properly adapting SCAP1D to an iterative environment to insure that only the calculations necessary to determine the objective function are performed. Another difficulty is that the execution of SCAP1D requires the use of several iterative algorithms that may affect the comparison of objective function evaluations associated with different values of the design variables.

The optimization method to be presented is not limited for use with SCAP1D, but was designed to be efficient (in terms of the number of objective evaluations required), reliable, and easy to interface with any numerical model. The changes

made to SCAP1D are specific to that model, but the same steps can be used to adapt any numerical silicon solar cell model with the optimization method presented. More generally, any numerical model can be successfully adapted for use with the optimization method presented by using techniques similar to the ones presented in this work.

In the next chapter, the optimization problem to be solved is stated mathematically, previous work to solve this problem is summarized, and an outline is given of the optimization method to be used to solve the problem. Understanding the model is critical to insure that valid results are obtained and the results are properly interpreted. Therefore, the third chapter describes the SCAP1D model. The equations to be solved are given and the parameters used are mathematically defined. The program inputs are described, and the effect of the inputs on the coefficients of the equations is noted. Then, the numerical method used to solve the equations during a single run of SCAP1D is described.

In the fourth chapter, the strategy used to adapt SCAP1D to an optimization environment is described. The emphasis is on changes required to insure the objective function is calculated to sufficient accuracy for an optimization and to reduce the computational burden of calculating the objective function iteratively. In the fifth chapter, the optimization code developed for use with SCAP1D is described in detail, stressing those aspects that make it appropriate for use with cpu intensive simulations.

In the sixth chapter, the results of numerous optimization runs are given for cells modeling various levels of technology. A sensitivity analysis is presented for the design variables and for the variables related to the level of technology modeled. In the seventh chapter, the effects of lateral resistance on cell efficiency are further investigated.

In the eighth chapter, a limit analysis is carried out by considering each of the loss mechanisms individually. The results along with the conclusions from the previous two sections are used to define high efficiency designs.

2 Overview of Problem

To illustrate more clearly the ideas presented in the introduction, the problem of optimizing the design of a silicon solar cell (simulated by SCAP1D) will be formulated and stated mathematically. Some knowledge of the operation of solar cells and the design variables involved is assumed. Previous work to solve this problem is summarized. The optimization code developed will then be outlined to more clearly illustrate the required interface with SCAP1D.

2.1 Mathematical Formulation

The use of optimization techniques requires two basic components, an objective function and decision variables (also referred to as design variables in this application). In addition, constraints may be specified to restrict the values that the decision variables may attain. SCAP1D has several outputs (results) that may be used as an objective function. With regard to cell design, the primary objective is to maximize the cell efficiency. The efficiency of a solar cell is defined as the power output (electrical output of the cell) divided by the power input (incident solar illumination).

The decision variables in the optimization are those aspects of solar cell design over which an engineer can exercise a reasonable degree of control. A single crystal silicon solar cell is a large area diode. A diode has the doping concentration as a function of x (since SCAP1D is a one dimensional model) and the cell thickness as design variables. Other design variables can be defined exterior to the single crystal silicon cell (e.g., anti-reflection coating, contact grids, etc.), but these are not modeled by SCAP1D.

Ideally, it is desirable to optimize the doping concentration for all x, but the required representation would lead to an exorbitant number of variables for an optimization application. Instead, a representation must be chosen that will specify the doping concentration throughout the device using a manageable number of

variables. In figure 2.1, the doping concentration between the front surface and the bulk of the device is defined by a complementary error function. The front junction occurs where the net doping density is equal to zero. The doping concentration of the bulk of the device is assumed constant. A complementary error function is also used between the bulk of the device and the back surface. The back junction depth is measured from the back of the device. Hence, the doping concentration is defined for all x by the the front surface doping concentration (D_0), the front junction depth (X_f), the bulk doping concentration (D_B), the back junction depth (X_b), and the back surface doping concentration (D_L). These variables, along with the cell thickness (X_L), are the decision variables for the optimization problem.

Figure 2.1 illustrates the doping concentration for a n-p-p^+ cell. The optimization and simulation program described in this work may be used for cells with a p-type type emitters and a n-type base (p-n). Also, any number of hi-lo junctions can be defined and included in the optimization (e.g., chapter 7 considers a n^+-n-p-p^+).

Upper and lower bounds may be defined for each of the decision variables to insure they take on values that are practically achievable and/or within the validity of the model. Linear constraints may also be used to insure that the same considerations are enforced for relationships that involve more than one variable.

The problem statement is (referred to as problem P1 in the text):

$$\text{maximize} \quad \text{eff}(D_0, X_f, D_B, X_b, D_L, X_L) \tag{P1}$$

Subject to the following constraints: [†]

$$14 \le \log D_0 \le 20.6$$

$$14 \le \log D_B \le 20.6$$

$$14 \le \log D_L \le 20.6$$

$$0.1 \le X_f \le 10.0$$

$$0.2 \le X_b \le 50.0$$

$$10.0 \le X_L \le 300.0$$

$$0.0 \le \log D_L - \log D_B$$

$$0.0 \le X_L - X_f - X_b \ ,$$

[†] The log denotes $\log_{10}$ and is used to transform the magnitude of the doping concentrations. Therefore, the constraints involving the log of the doping concentrations are linear constraints.

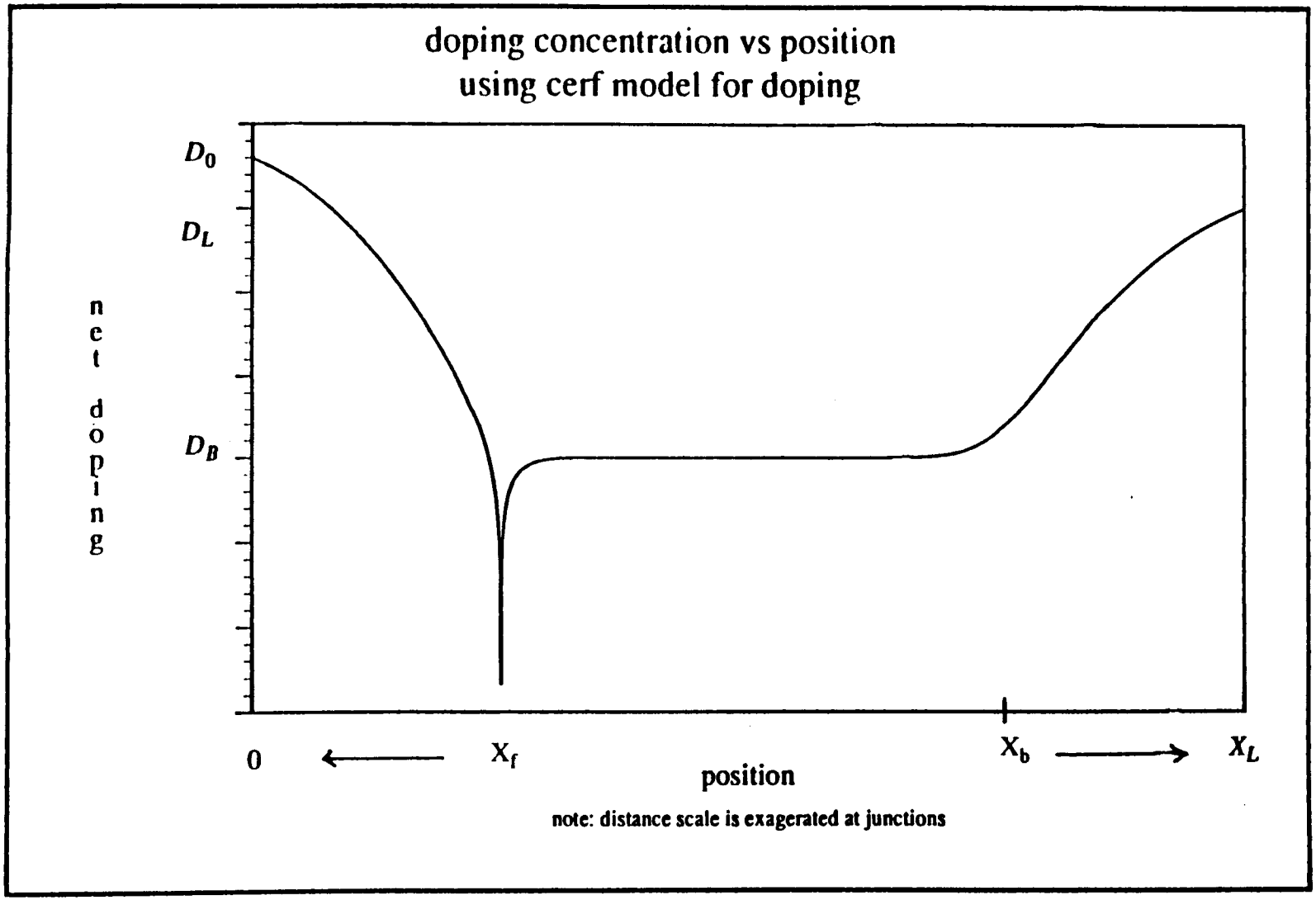
doping concentration vs position
using cerf model for doping
D_0
D_L
D_B
net doping
0
X_f
X_b
X_L
position
note: distance scale is exagerated at junctions

figure 2.1

eff = efficiency %

D_0 = net front surface doping concentration [P atoms - B atoms]/cm^3 ‡

D_B = net bulk doping concentration [B atoms - P atoms]/cm^3

D_L = net back surface doping concentration [B atoms - P atoms]/cm^3

X_f = Front junction depth μm

X_b = Back junction depth μm

X_L = Cell thickness μm.

There is an efficiency associated with each point in the design variable space. Hence, an efficiency surface in the six dimensional space of the decision variables is defined (e.g., analogous to the case with two decision variables which results in a 3-D plot). The constraints define the region in the decision space that may be searched for the maximum efficiency (referred to as the feasible region).

Some inputs to the solar cell model are determined by the fabrication techniques used and the current state of technology. Such inputs, which will be referred to as technology variables in this work, are not included in the optimization as decision variables (see section 3.6 for a more complete discussion). Technology and fabrication considerations may also affect the bounds on the decision variables (the feasible region to be searched). Changing technology variables can be thought of as altering the efficiency surface described above. This may change the maximum value of the efficiency and/or where it is located in the decision space. Hence, to do a complete analysis of silicon solar cell design it is necessary to solve the above problem more than once.

A complete analysis of a variety of devices can be used to compare the best efficiency predicted for different fabrication techniques and levels of technology. It is hoped that this will point out the possible benefits of certain fabrication techniques and/or the most promising directions for future research in terms of increasing efficiency. The study is limited to single crystal silicon solar cells of conventional geometry (i.e., front and back surface contacts) that can be modeled using SCAP1D. Since SCAP1D is a one dimensional code, it cannot be used to simulate the performance of designs that are two dimensional in nature (e.g., interdigitated back contact cells).

‡P, which stands for Phosphorus, is a donor or n-type impurity. B, which stands for Boron, is an acceptor or p-type impurity. Therefore, this optimization is for a n-p-p$^+$ silicon solar cell with conventional geometry (i.e., contacts on front and back surfaces).

In problem P1, a solar cell without a back surface field (referred to as a conventional or CV cell) is defined if the optimization converges to a point where $D_B = D_L$. However, the optimization, as formulated in problem P1, may not result in a CV cell. By removing decision variables X_b and D_L from problem P1, a new optimization problem is defined that is guaranteed to result in a CV cell and requires fewer decision variables.

$$\text{maximize} \quad \text{eff}(D_0, X_f, D_B, X_L) \tag{P2}$$

Subject to the following constraints:

$$14 \leq \log D_0 \leq 20.6$$

$$14 \leq \log D_B \leq 20.6$$

$$0.1 \leq X_f \leq 10.0$$

$$10.0 \leq X_L \leq 300.0$$

$$0.0 \leq X_L - X_f$$

The mathematical formulation P2 is similar to P1 in that it consists of an objective function, decision variables, and constraints.

2.2 Previous Work

In this section, previous work done to investigate the effects of cell design on efficiency will be reviewed. Some of the most recent studies are shown in table 2.1 . The studies are classified according to the type of model and the method of analysis used. Numerical models solve the governing differential equations using numerical methods (e.g., finite difference methods). Using this approach the cell parameters (doping concentration, mobility, lifetime, etc.) can be different at each finite difference mesh point. The middle entry in table 2.1 refers to models that divide the cell into a limited number of regions (or layers) associated with different values of the cell parameters. Analytical models use an explicit expression, which is based on an analytical solution of the governing differential equations, for the cell efficiency. The more sophisticated analytical models (e.g., those including bandgap narrowing, doping dependence of lifetime, etc.) involve complex expressions and are usually implemented on a computer for analysis (e.g., model used in [1.9]). In general, analytic models require more assumptions (less generality in the cell parameters, so that an analytic solution of the differential equations can be found) and are therefore regarded as less accurate.

Table 2.1 Previous Work

	Analytic	Numerical(layers)	Numerical
Parametric	Verlinden (1985), Chen & Wu (1981), Green (1982), Ruiz (1984)	Wolf (1985), Lin (1985)	JPL (1985), Weaver (1982), Lindholm & Sah (1984)
Optimization	Chen & Wu (1985)		

To investigate the effects of cell design on efficiency, the method of analysis may be parametric analysis or optimization. With one exception, the method of analysis used in the studies shown in table 2.1 has been limited to parametric analysis [1.1-1.7]. Using parametric analysis, one variable is varied while the other design variables are held fixed. This investigates the efficiency surface along a line in the decision space. Parametric methods are used primarily to investigate the effect of one or two of the design variables (e.g., base doping [1.3], back junction depth [1.7]). In the absence of other methods, parametric studies have provided knowledge as to the effects of some design variables on cell efficiency. However, the conclusions about the effect of the parametrically varied variable are valid only at the values assumed for the other design variables. If the value of any of the other design variables is changed, a move is made to a different place on the efficiency surface, where the effects of the variable being investigated may be different.

Some of the more extensive parametric studies are summarized below. This is done so that the conclusions can be easily referenced and compared to the results to be presented in this work (the comparisons are made in chapters six and seven). In particular, it is of interest to determine whether the conclusions of the parametric analyses agree with those of an optimization. As opposed to the fixed values of design variables used in a parametric analysis, in an optimization all the design variables are allowed to vary simultaneously.

It is stressed that the values assumed for the variables that are held fixed during a parametric analysis are critical and will affect the conclusions of a study.

When available, the values of the variables held constant are given for each of the studies discussed. The model used will also affect the results of a study. However, since all of the models are fairly sophisticated, the use of different models should not lead to different conclusions. The models used in the studies are classified in table 2.1 but are not discussed individually.

M. Wolf [1.1] studied the effects of the design of the emitter and a thick BSF. For the BSF study, the bulk of the device is 200 μm, the bulk doping concentration as 5×10^{16}, with a lifetime of 0.8 ms (at 5×10^{16}), the back contact is taken as ohmic, and the BSF is thick with a uniform profile. The doping concentration in the BSF region was varied from 5×10^{16} (no BSF) to 5×10^{20}. The conclusion was that no benefit in efficiency could be achieved with a thick BSF, but that the same efficiency could be achieved with a thinner cell when compared to a CV (conventional, n-p) cell.

The emitter study used a bulk doping of 2×10^{17}, front junction depth of 0.3 μm, and a exponential profile for the emitter. Different combinations of the front surface doping concentration and the front surface recombination velocity (S_f) were investigated. The main conclusion of this study was that higher doping concentrations are optimal at high values of S_f, while lower concentrations should be used when good surface passivation is possible. Furthermore, to take advantage of good surface passivation it is necessary to use a lightly doped emitter, or the beneficial effects of surface passivation are defeated by heavy doping effects in the emitter. For instance, cell performance was found to be practically independent of S_f (i.e., lowering S_f did not significantly improve the cell efficiency) at surface doping concentrations of 2×10^{21} (at $S_f > 10^6$ this doping level was optimal).

Lin [1.3] did a whole series of parametric studies on many variables (technology as well as design variables). For a cell thickness of 250 μm, front junction depth 0.3 μm, S_f of 10^4, S_b of 10^7, and constant front and back surface doping concentrations and profiles, several combinations of bulk resistivity (BR, higher doping in base leads to lower BR), diffusion length, and back junction depths were investigated. The conclusion was that best cell performance would be obtained from low BR cells for which there was little or no improvement with the addition of a BSF. A BSF was observed to improve performance for high BR cells. For high BR cells, a thicker back surface junction (investigated up to 10 μm) showed the greatest amount of improvement.

Parametric analysis of CV cells for S_f (X_L = 250 μm, X_f = 0.2 μm, and S_b = 10^7) and for S_b (X_L = 250 μm, X_f = 0.2 μm, and S_f = 10^4) resulted in the conclusion that low BR cells were less sensitive to the effects of surface recombination.

An investigation of numerous emitter profiles resulted in the conclusion that there was almost no sensitivity to profile.

Efficiency was insensitive to cell thickness over the range 100 to 350 μm for cells with a back surface reflector (BSR).

Weaver [1.5] used parametric analysis to compare a BSF and a CV solar cell. The variables held fixed included $D_0 = 1 \times 10^{20}$, $D_L = 2 \times 10^{20}$, $X_f = 0.35$ μm, $X_b = 1.0$ μm, $S_f = 10$ cm/s, back contact ohmic, profiles of emitter and BSF were Gaussian, and $X_L = 300$ μm. The bulk doping was then varied. The conclusion was that a CV cell can do as well as a BSF cell by using high bulk doping. Furthermore, back surface passivation fails to improve efficiency if a highly doped BSF is in use (similar to conclusions made by Wolf for the emitter). The author noted that at a cell thickness of 50 μm a BSF cell is superior to a CV cell.

An analysis of a HLE (high-low emitter) was completed with the conclusion that a CV cell did just as well. Where as Chen [1.4], using different cell parameters suggests that HLE is superior to CV due to lower lateral resistance.

Lindholm and Sah [1.7] investigated the effect of a drift-field (DF, a thick diffused BSF) as compared to the more standard thin diffused BSF. The fixed parameters were $X_L = 50$ μm, $D_B = 10^{17}$, $\tau = 20$ μs, and an ohmic back contact. The conclusion was that DF cell was superior to the standard BSF cell.

All of the above results are valid only for the values of the technology variables used in the studies and for the fixed values of the other design variables. The latter represents a major limitation of doing a design study using parametric analysis. For this reason, some of the conclusions of the above studies appear to contradict each other (e.g., on the effect of a BSF). In some of the studies summarized above, not all the values of the design and technology variables held fixed were specified in the published results.

A very desirable result of studies investigating the effects of design variables on solar cell performance would be the solution of problem P1 and/or P2. However, the solution of problem P1 is very difficult using parametric (heuristic) methods. For more than two design variables, the effort required to find the optimal design is prohibitive using heuristic methods (commonly referred to as the curse of dimensionality). An optimization algorithm can be coupled with a solar cell model to more effectively solve problems posed in the form of P1 and/or P2. Optimization is the other method of analysis referred to in table 2.1 .

In [1.9], Chen and Wu recognized the limitations of heuristic methods to solve problems such as P1 and P2. They developed an analytical model of a solar cell and used it in conjunction with a direct search (i.e., no use of gradients) optimization algorithm [2.1] to solve a problem related to problem P2. They also

suggested that the same methods had been used to solve a problem similar to P1 (i.e., included a back surface field).

The analysis in [1.9] is limited by the simplifying assumptions required to derive the analytical model (e.g., uniform doping). The reason stated for using an analytical model is to avoid the computational effort associated with a numerical solution of the semiconductor equations.

In [1.9], the front surface and back surface recombination velocities were included in the problem statement as decision variables. When optimized, the recombination velocities did not always go to their lower bounds; suggesting the model used in [1.9] predicts greater efficiencies at higher recombination velocities, or that there are convergence difficulties with the optimization algorithm used in [1.9]. In this work, recombination velocities are not included as decision variables in the optimization because they display a monotonic relationship with respect to efficiency and will only converge to their lower bound. Including them in the optimization simply increases the number of variables, hence increasing the numerical effort required to complete an optimization. The method used to investigate the effects of recombination velocities, which are classified as technology variables in this work, is discussed more thoroughly in section 3.6 .

The results published in [1.9] did not constitute a comprehensive analysis of solar cell designs. Rather, the results of a few optimizations were given. The optimizations showed large increases in efficiency from the initial to the final point of the optimization. However, the optimizations were initiated from very poor designs (efficiency $\leq$ 5 %). This tended to obscure the main point of the authors (i.e., the benefit of using an optimization in the design processes), since such designs would probably never be proposed in the first place. Also, the authors made no mention of the possibility of local maximums or any references to the concavity of the efficiency surface.

The authors suggested the development of better analytical models and strongly convergent optimization algorithms as goals for future research.

In this work, a strongly convergent optimization algorithm is developed specifically for use with CPU intensive simulations. However, deviating from the suggestions of Chen and Wu, the model used in this work is a one dimensional numerical model. This work is unique among the studies completed to date (i.e., this work would be classified in the lower right corner of table 2.1). The computational effort required to optimize a numerical model is not prohibitive if the model is properly adapted for use with an optimization algorithm. The use of finite difference and finite element models directly with optimization algorithms is well established in the fields of mechanical and civil engineering. Such work has been

particularly common in the area of structural design (see [2.2] for a historical survey). The problem of optimizing solar cell design is particularly well suited to such techniques due to the numerical solution methods used to solve the differential equations and the small number of decision variables in the optimization.

This work will stress the use of the optimization algorithm coupled with a one dimensional numerical model as a tool for doing a comprehensive analysis of silicon solar cell designs. A sensitivity analysis will be provided for the solutions found that will point out the possible pitfalls of using an optimization with a simulation program (e.g., nonconcavity of efficiency which could lead to the optimization converging to a local maximum that is not the global maximum).

2.3 Overview of Method of Solution

Figure 2.2 shows an overview of the optimization algorithm designed for use with SCAP1D and similar cpu intensive simulations. The basic components of the algorithm are the calculation of the numerical approximation of the gradient, definition of the search direction, implementation of the constraints, solution of the one dimensional subproblem, and test for convergence.

The efficiency associated with the initial guess for the optimal solution is calculated first. The optimization algorithm passes the decision vector (the vector $\mathbf{x} = [D_0, D_B, D_L, X_f, X_b, X_L]$)[†] to SCAP1D. SCAP1D then calculates the efficiency associated with the decision vector and passes it back to the optimization code. The SCAP1D model and how it is used to calculate the efficiency of a solar cell is described in the next chapter.

The optimization algorithm then calculates the numerical approximation of the n-dimensional gradient vector (∇eff), where n is the number of decision variables (6 in P1 and 4 in P2). This is done by offsetting each component of the decision vector one at a time and re-calculating the efficiency to determine the effect of each component. For example, the first component of the gradient is

$$\nabla \mathrm{eff}_1 = \frac{\mathrm{eff}(D_0 + \Delta D_0, X_f, D_B, X_b, D_L, X_L) - \mathrm{eff}(D_0, X_f, D_B, X_b, D_L, X_L)}{\Delta D_0} , \qquad (2.1)$$

[†] Scalar quantities are represented by normal type (e.g., D_0), vectors by lower case bold type (e.g., $\mathbf{x}$), a particular component of a vector by the vector symbol in normal type and a subscript denoting the component (e.g., x_1 = first component of vector $\mathbf{x}$), and matrices by upper case bold type (e.g., $\mathbf{H}$).

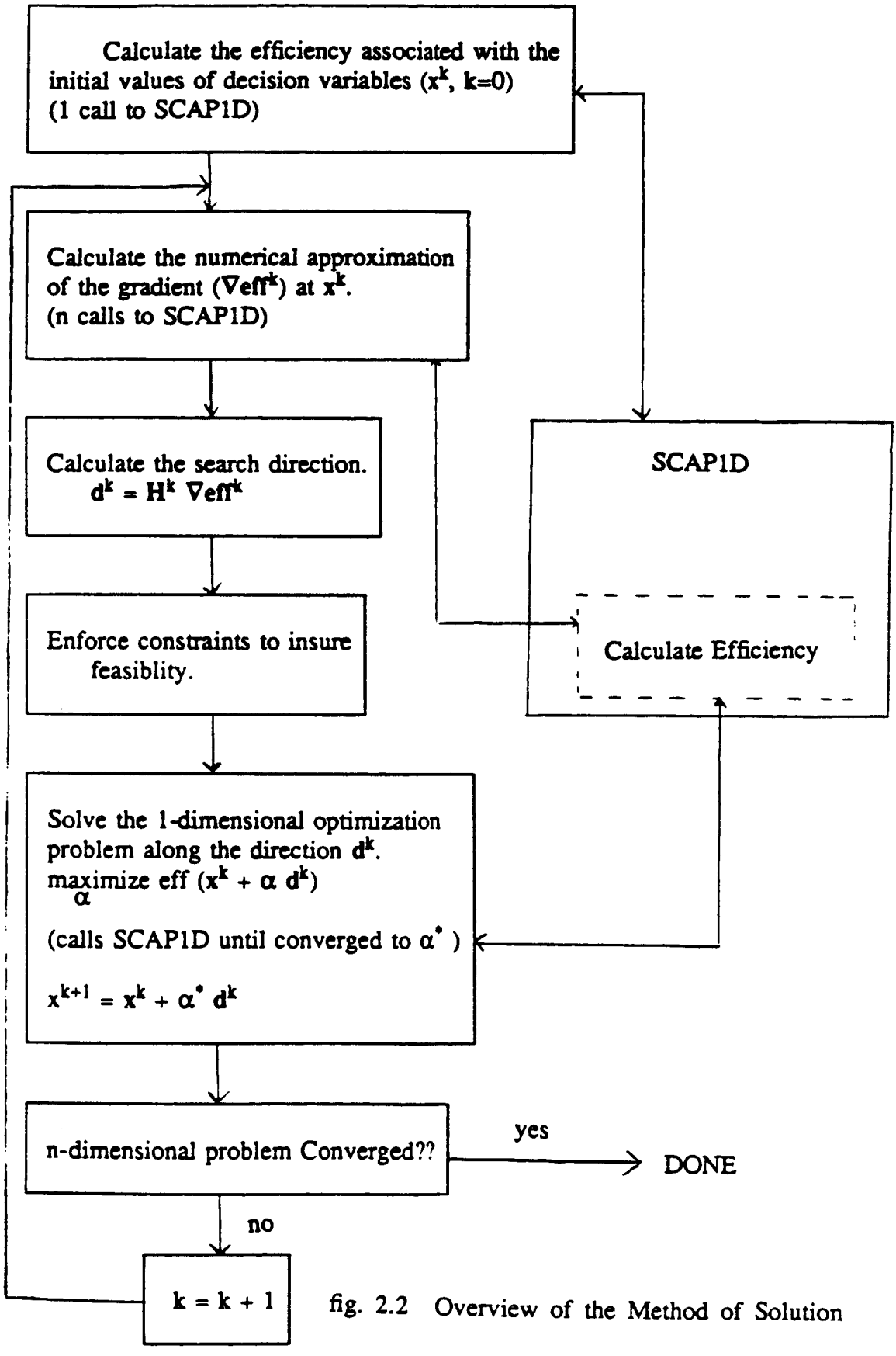

fig. 2.2 Overview of the Method of Solution

where ΔD_0 is the offset in the front surface doping concentration. The above procedure is repeated for each of the decision variables. The result is a numerical approximation of ∇eff.

The calculation of the numerical gradient is significantly complicated by the fact that the efficiency is a result of a complex numerical process which requires the use of iterative algorithms. This concern will be addressed in chapter 4. The calculation of the gradient has significant impact on the reliability of the optimization code and the number of function evaluations required for an optimization to converge (e.g., it is within the iterative loop of the optimization method outlined in figure 2.2). For these reasons, the actual method used is more involved than equation 2.1 and is completely described in chapter 5.

Unlike the initial call to SCAP1D, it is not necessary to execute the model in its entirety to calculate the efficiency for subsequent calls to SCAP1D (as illustrated in figure 2.2). It is possible to avoid calculations that are not necessary to determine the efficiency by using the results of previous objective function evaluations to initiate the iterative solution techniques employed in SCAP1D. This results in significant savings in computational effort, and the methods used are discussed in chapter 4.

Once ∇eff has been calculated, it is possible to define a search direction to be used in solving the one dimensional subproblem. The direction of search, $\mathbf{d}$, is

$$\mathbf{d} = -\mathbf{H}\ \nabla\mathrm{eff}\ . \tag{2.2}$$

$\mathbf{H}$ is the approximation to the inverse Hessian matrix (inverse of the matrix of second partial derivatives). $\mathbf{H}$ is initiated as the negative of the identity matrix, so that the first search direction is simply ∇eff (steepest ascent direction). For subsequent search directions (note iterative loop in figure 2.2), the matrix $\mathbf{H}$ is updated to approximate the inverse Hessian by using the quasi-Newton condition [2.3, 2.4],

$$\gamma^k = \mathbf{H}^{k+1}\,\delta^k\ , \tag{2.3}$$

where $\delta^k = \mathbf{x}^{k+1} - \mathbf{x}^k$ and $\gamma^k = \nabla\mathrm{eff}^{k+1} - \nabla\mathrm{eff}^k$. The quasi-Newton condition forces a condition that would be satisfied by a quadratic function on the inverse Hessian approximation. The solution of (2.3) for $\mathbf{H}$ is not unique, so an updating formula is used. By enforcing the condition (2.3) at each iteration (i.e., by updating the estimate $\mathbf{H}^k$ at each iteration), a local quadratic approximation is built up. Numerous update formulas exist, and any member of the Broyden family [2.5] of updates can be chosen in the code. The BFGS formula [2.5-2.8],

$$\mathbf{H}_{\mathrm{BFGS}}^{k+1} = \mathbf{H} + \left[1 + \frac{\gamma^t \mathbf{H}\,\gamma}{\delta^t\gamma}\right]\frac{\delta\,\delta^t}{\delta^t\gamma} - \left[\frac{\delta\,\gamma^t\mathbf{H} + \mathbf{H}\,\gamma\,\gamma^t}{\gamma^t\gamma}\right] \tag{2.4}$$

(the superscript k and the subscript BFGS are suppressed on the right side), has been the update formula most often used for the application to be studied in this work, because the line search algorithm to be described is not an exact line search [2.9]. The vector -**H** ∇**eff** represents the offset from the current point to the optimal point of the local quadratic approximation. This is seen by solving the necessary conditions for a maximum (gradient = 0) of the truncated Taylor series,

$$\mathbf{eff}(\mathbf{x}+\Delta\mathbf{x}) \approx q(\Delta\mathbf{x}) = \mathbf{eff}(\mathbf{x}) + \tfrac{1}{2}\,\Delta\mathbf{x}^{t}\,\mathbf{B}\,\Delta\mathbf{x} + \nabla\mathbf{eff}^{t}\,\Delta\mathbf{x} \quad . \tag{2.5}$$

$\mathbf{H} = \mathbf{B}^{-1}$. Since variable metric (quasi-Newton) methods take into account second order information, they are more successful than always moving in the direction ∇**eff** (steepest ascent direction) which makes use of only first order information.

It is necessary to insure that the search direction is feasible and that the one dimensional maximization along the search direction remains feasible (this defines a maximum step size α_{max}). The methods used to accomplish this are detailed in chapter 5.

Once the feasible search direction and a maximum feasible step size in that direction have been defined, it is possible to solve the one dimensional optimization problem,

$$\begin{aligned} &\text{maximize } \mathbf{eff}(\,\mathbf{x} + \alpha\,\mathbf{d}\,) \quad . \\ &0 \le \alpha \le \alpha_{max} \end{aligned} \tag{2.6}$$

The n-dimensional optimization is solved by iteratively solving the one dimensional subproblem. Hence, the one dimensional optimization routine is a very important component of the optimization code. The routine used in this work is based on restricted polynomial approximation and is described in detail in chapter 5.

The code iterates by solving for the numerical gradient at the best point found by the one dimensional optimization routine, defining a direction of search, and solving the one dimensional subproblem. A number of criteria are used to test for convergence, and these are defined in chapter 5. Once again, it is stressed that the problem is solved more than one time, so that the algorithm outlined above is used on a number of occasions.

3 The Silicon Solar Cell Model - SCAP1D

The efficiency associated with different solar cell designs can be calculated using the Solar Cell Analysis Program in 1 Dimension (SCAP1D). In figure 2.2, SCAP1D is shown as a black box; which, given the decision vector, calculates the associated efficiency. This chapter will describe the block box.

SCAP1D uses finite difference methods to solve the differential equations which, along with several relations from the physics of semiconductors, describe mathematically the performance of a solar cell. The differential equations to be solved, the coefficients of the equations, and the boundary conditions of the equations will be described in detail. The method used to solve the equations and how the solution is used to calculate the performance of a solar cell will be described. The variables (inputs to SCAP1D) will be discussed, and the manner in which the variables are treated in the analysis will be presented.

3.1 The Differential Equations

In general, models (numerical as well as analytic) involve assumptions that allow the physical process to be described mathematically. The equations given in this section are valid only if certain assumptions used in their definition hold for the solar cell to be simulated. The assumptions must be completely understood and properly implemented in the optimization for valid results to be obtained. This section will present the equations in a manner that emphasizes the considerations raised above.

The equations that form the basis of numerical methods for modeling semiconductor devices can be derived from Maxwell's equations, several relations from the physics of semiconductors, and several simplifying assumptions (e.g., see [3.1]). The resulting system of equations includes Poisson's equation and electron and hole continuity equations. Poisson's equation is:

$$\nabla^2 V = \frac{q}{\varepsilon} (n - p + N_D - N_A) \qquad (3.1)$$

where,

V = voltage
q = electronic charge constant (1.602×10^{-19})
ε = permittivity of the material
n = electron concentration
p = hole concentration
N_D = concentration of ionized donor atoms
N_A = concentration of ionized acceptor atoms.

Poisson's equation models the potential difference that is a result of the variation in charge distribution through the device. The writing of Poisson's equation has necessitated the use of several commonly accepted assumptions (e.g., homogeneity of permittivity).

The continuity equation is written as two equations by considering the holes and electrons separately. The resulting equations are:

$$\nabla J_n = q (R - G) \tag{3.2a}$$

$$\nabla J_p = -q (R - G) \tag{3.2b}$$

where,

J_n = electron current density
J_p = hole current density
R = Recombination rate
G = Generation rate.

Because we are interested in only steady state results (no transients), the equations above do not include terms that involve differentiation with respect to time. Hence, the interpretation of the continuity equations becomes equivalent to the principle of conservation of charge.

The terms J_n and J_p used in (3.2a) and (3.2b) describe the transport of carriers in a semiconductor. The derivation of equations to describe carrier transport in semiconductors is quite complex and involves many of the most important assumptions to be made. The derivation of the carrier transport equations used in SCAP1D is presented in detail in [3.2]. The objective here is to present the equations in a manner that illustrates the main assumptions that must be invoked for valid implementation. This will be done by writing the carrier transport equations in several intermediate forms. The basic carrier transport equations are given below:

$$J_n = -q\,\mu_n\, n\, \nabla V + q\, D_n\, \nabla n \qquad (3.3a)$$

$$J_p = -q\,\mu_p\, p\, \nabla V - q\, D_p\, \nabla p \qquad (3.3b)$$

where,

D_n = diffusion coefficient for electrons
D_p = diffusion coefficient for holes
μ_n = mobility of electrons
μ_p = mobility of holes.

These equations illustrate the drift and diffusion components of carrier transport. Many assumptions have been made to write the equations in the above form. Three of the most important assumptions are:

(1) Valid only for very lightly doped (or intrinsic) semiconductors (i.e., does not take into account positional variations in the band gap).

(2) Effects of degeneracy have been ignored.

(3) Parabolic energy bands are assumed.

The first assumption implies that the equations will not properly treat moderate heavy doping effects. This omission can be avoided by including a term involving the intrinsic carrier concentration which is a measurable parameter (e.g., [3.3-3.5]). The result is:

$$J_n = -q\,\mu_n\, n\, \nabla V + q\, D_n\, \nabla n - \mu_n\, n\, k\, T\, \nabla(\, \ln\,(n_{ie})\,) \qquad (3.4a)$$

$$J_p = -q\,\mu_p\, p\, \nabla V - q\, D_p\, \nabla p - \mu_p\, p\, k\, T\, \nabla(\, \ln\,(n_{ie})\,) \qquad (3.4b)$$

n_{ie} = effective intrinsic carrier concentration.

The last term in the equations can be thought of as a quasi-electric field that affects the transport of carriers. It accounts for positional variations in the bandgap due to doping. This equation still contains two important assumptions related to heavily doped semiconductors. First, the equation is not valid for degenerate semiconductors because Boltzmann statistics are used in the derivation. The use of Boltzmann statistics implies that the Fermi energy for electrons, E_{fn}, (holes, E_{fp},) has been assumed to be sufficiently below (above) the conduction (valence) band edge, E_c (E_v). This is mathematically stated as the relation

$$(\, E_{fn} - E_c\,) / kT \ll -1, \quad \text{or for holes} \quad (\, E_v - E_{fp}\,) / kT \ll -1\ . \qquad (3.5)$$

This condition is not true in heavily (degenerately) doped semiconductors. Second, the use of the intrinsic concentration implies knowledge of the band structure. The band structure, however, is not well characterized in heavily doped semiconductors.

The equations can be rewritten by defining the reduction in the bandgap ΔE_g. ΔE_g is related to the effective intrinsic carrier concentration by the equation

$$n_{ie}^2 = n_{io}^2 \, e^{(\Delta E_g / kT)} \quad . \tag{3.6}$$

The equations can be further generalized with the addition of an asymmetry factor. The asymmetry factor, A, is defined in terms of the electron affinity, $\Delta\chi$ ($A = \Delta\chi / \Delta E_g$), and allows for unequal shifts in the band edges of the valence and conduction bands. The resulting equations are :

$$J_n = -q \, \mu_n \, n \left[\nabla(V + A \frac{\Delta E_g}{q}) \right] + q \, D_n \, \nabla n \tag{3.7a}$$

$$J_p = -q \, \mu_p \, p \left[\nabla(V - (1-A) \frac{\Delta E_g}{q}) \right] - q \, D_p \, \nabla p \quad . \tag{3.7b}$$

Some authors have proceeded from these equations by making use of the rigid band approximation for heavily doped silicon and including Fermi-Dirac statistics directly into the equation. Adler [3.6-3.8] contends that using an experimently measured ΔE_g correctly accounts for Fermi-Dirac statistics and that the choice of the asymmetry factor does not affect some aspects of the model. This approach was used by Lundstrom [3.2] in deriving the transport equations that are implemented in SCAP1D. No specific shape is assumed for the bands, only the presence of sharp mobility edges is assumed. The terms $\Delta\chi$ and ΔE_g account for the position dependence of the band edges (i.e., the rigid band effect). In [3.2], Lundstrom introduces two new terms, Θ_n and Θ_p, that account for both the modified band shape (density-of-states effect) and the influence of Fermi-Dirac statistics (these effects are hard to separate in degenerately doped semiconductors). The resulting equations are:

$$J_n = -q \, \mu_n \, n \left[\nabla(V + \gamma \frac{\Delta_g}{q}) \right] + q \, D_n \, \nabla n \tag{3.8a}$$

$$J_p = -q \, \mu_p \, p \left[\nabla(V - (1-\gamma) \frac{\Delta_g}{q}) \right] - q \, D_p \, \nabla p \tag{3.8b}$$

where,

$$\Delta_g = \left[\Delta E_g + \Theta_n + \Theta_p \right] , \tag{3.9a}$$

and

$$\gamma = \frac{\Delta\chi + \Theta_n}{\Delta_g} . \tag{3.9b}$$

Δ_g is the effective gap shrinkage, and γ is the effective asymmetry factor. It is argued that the use of experimental values for Δ_g and γ correctly accounts for the effects of heavy doping [3.2, 3.6-3.8]. Therefore, no explicit correction for Fermi-Dirac statistics needs to be included in (3.8a) and (3.8b). The Boltzmann type structure, which is convenient for numerical models, is retained.

Procedures for obtaining electrical measurements of Δ_g and γ are provided in [3.2]. Δ_g does not necessarily equal the actual reduction in the bandgap. Equality would only exist if there were no change in the shape of the bands and the use of Boltzmann statistics were justified ($\Theta_n = \Theta_p = 0$). The effective bandgap is related to the effective intrinsic concentration (equilibrium np product) by the equation below (generalization of equation 3.6).

$$n_{ie}^2 = n_{io}^2 \, e^{(\Delta_g / kT)} \tag{3.10}$$

The interpretation of effective gap shrinkage is supported by the differences reported between electrical measurements and optical measurements (or theoretical predictions) of the bandgap in heavily doped semiconductors [3.6-3.10]. Electrical measurements are related to Δ_g, while optical measurements and theoretical predictions result in ΔE_g. No measurements have been made of the effective asymmetry factor. However, it has been argued in [3.2, 3.6-3.8] that the carrier concentrations, minority carrier current densities, and current-voltage characteristics of typical heavily doped solar cells are not affected by the choice of γ. Without γ it is not possible to correctly model all aspects of a solar cell (e.g., γ must be known to determine the built in voltage).

Equations (3.8a) and (3.8b) substituted into (3.2a) and (3.2b) along with (3.1) are the equations used in SCAP1D. Several assumptions are required for the validity of these equations. The most important assumptions are:

(1) Complete ionization of the dopants is assumed. This assumption defines the terms N_D and N_A to be equal to the doping concentrations.

(2) The heavily doped regions of the device are assumed to be quasi-neutral and in low injection, so that the majority carrier concentration is approximately equal to the doping density.

(3) The parameters Δ_g and γ are assumed to be functions of the carrier concentrations.

(4) The heavy doping parameters Δ_g and γ do not change when the device is not in equilibrium (related to the low injection assumption above).

These assumptions must be carefully taken into account to insure that valid results are obtained from the model.

3.2 The Coefficients of the Equations

In the previous section, to simplify the presentation of the equations, the dependence of the coefficients on other variables was suppressed (i.e., they were presented as constants). Each of the coefficients, however, is a function of one or more variables. In this section, each of the coefficients will be mathematically defined. Since SCAP1D is a one dimensional code, the ∇ used in presenting the equations simplifies to $\frac{d}{dx}$. The independent variable of the differential equations, x, is the distance into the solar cell perpendicular to and measured from the front surface.

It has already been indicated that γ can be chosen arbitrarily. SCAP1D allows γ to be defined as a function of x. However, since no reliable measurements of γ exist, γ will be defined as a constant in this work. In accordance with the assumptions given above, the ionized doping concentrations (N_D and N_A) are defined to be equal to the doping concentrations which are functions of x (e.g., see figure 2.1).

The terms G, R, μ_n, μ_p, and Δ_g are all defined by equations that include terms that fit experimental data. A review of the literature shows a profusion of equations and/or different constants to be used with the same equations [3.1]. To complicate matters, it has been argued [3.6] that the differences between models can often be traced back to the modeling of the above parameters, particularly Δ_g. For this reason, the equations that describe each of the above parameters will be given. References are given for the papers that derive the equations and/or define the constants that are used in this work.

For a solar cell, the generation rate for electron hole pairs (G in equations 3.2a and 3.2b) is modeled by the equation:

$$G(x) = \int_0^{\infty} (1 - \Gamma) \phi \alpha e^{-\alpha x} d\lambda \qquad (3.11)$$

where,

λ = wavelength

ϕ = incident flux.

The term Γ takes into account both reflection at the surface and shadowing losses (an approximation for a 1-D model). α, the absorption coefficient for silicon, is taken from a fit of experimental data [3.11]. Equation 3.11 is the integrated, or accumulated, generation rate at a given distance x into the cell.

Figure 3.1 is a graph of equation 3.11 with Γ equal to 0.07 (this is the value that will be used in chapter 6) at a temperature of 300 K. The variable x in equation 3.11 is expressed as the optical path length, since if the light is reflected or refracted the optical path will no longer be equal to the position in the device (referred to in this work as x). Figure 3.2 is a plot of the percentage of the photons of energy greater than the bandgap of silicon, $\approx$ 1.1 eV at 300 K, absorbed versus the optical path length. The majority of the incident photons of energy greater than 1.1 eV are absorbed very rapidly. Over 60% are absorbed by 5 μm, and over 70% are absorbed by 10 μm.

A graph of the percentage of the incident energy absorbed versus the optical path length would differ from figure 3.2 . Since high energy ($\gg$ 1.1 eV) electrons are more quickly absorbed in silicon, over 99% of the incident energy is absorbed by 300 μm. However, only 95% of the total number of photons of energy greater than 1.1 eV are absorbed by 300 μm. It takes an optical path of over 1000 μm to absorb 99% of the photons of energy greater than 1.1 eV. This is because the absorption coefficient of silicon for photons just greater than the bandgap energy is relatively small in magnitude. It is the percentage of photons greater than 1.1 eV that are absorbed, not the percentage of the incident energy, that is of primary importance in solar cells.

The recombination rate (R in equations 3.2a and 3.2b) is the sum of the Auger (AU) and singe-level Shockley-Read-Hall (SRH) processes. The Auger process dominates in heavily doped silicon due to a squared dependence on the doping concentration (all dopants are considered ionized, and the recombination rates are a function of the carrier densities). The equation for Auger recombination is:

$$R^{AU} = (A_n n + A_p p) (n p - n_{ie}^2) \quad . \tag{3.12}$$

The coefficients A_n and A_p (Auger capture coefficients) are taken from measurements by Dziewior and Schmid [3.12]. If Boltzmann statistics and a single trap level are assumed, the equation for SRH [3.13, 3.14] recombination is:

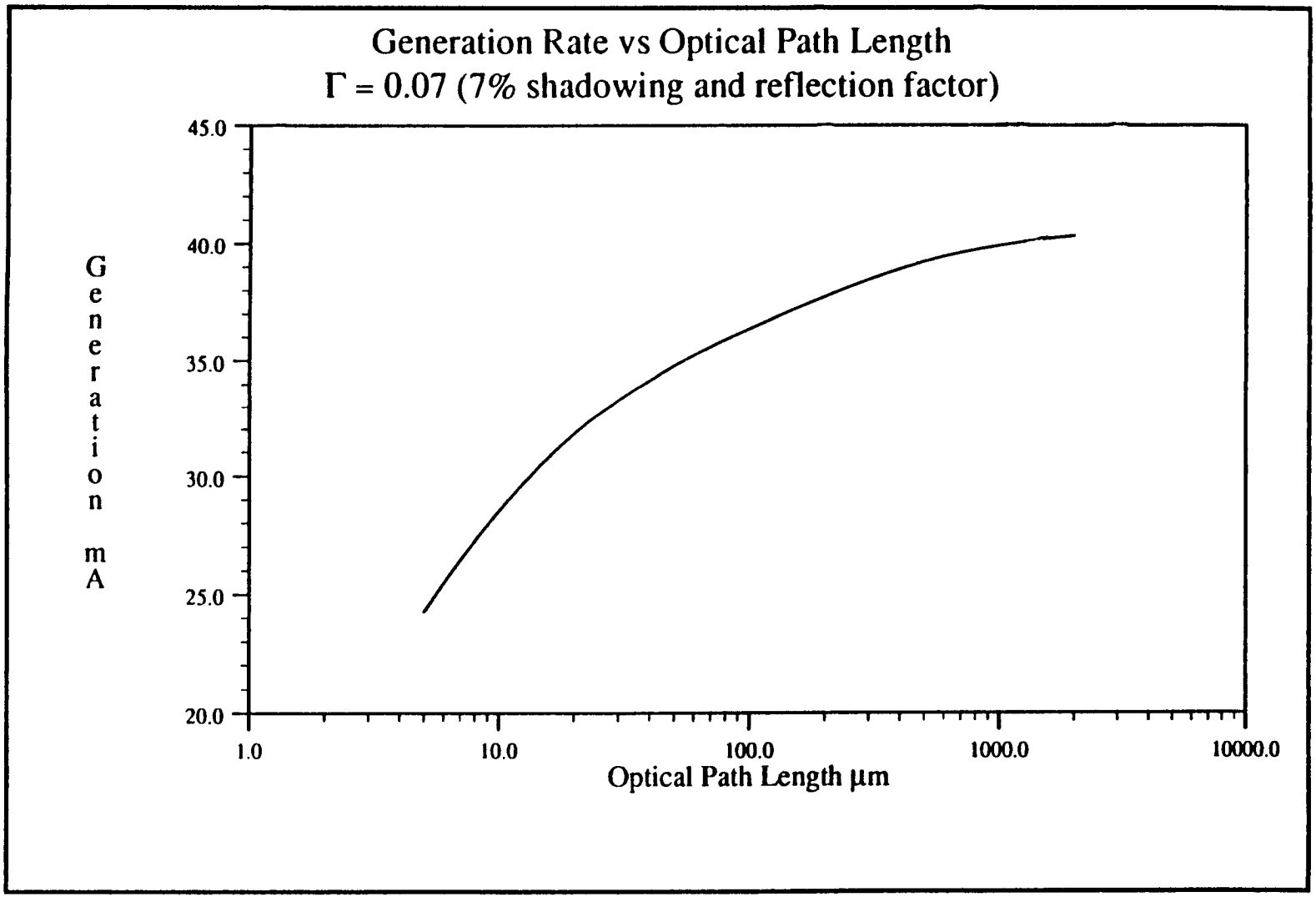
Generation Rate vs Optical Path Length
Γ = 0.07 (7% shadowing and reflection factor)
Generation mA
45.0
40.0
35.0
30.0
25.0
20.0
1.0
10.0
100.0
1000.0
10000.0
Optical Path Length µm

figure 3.1

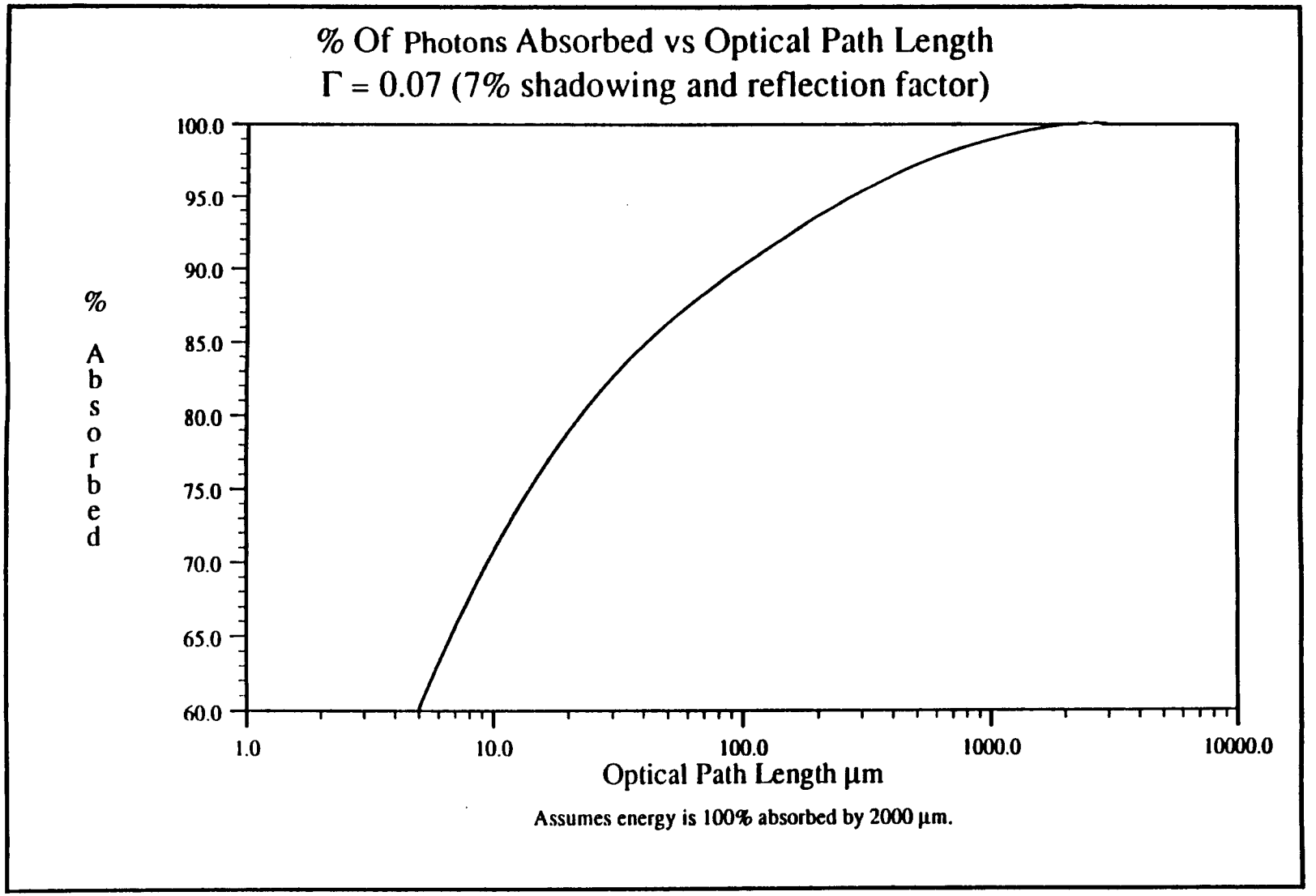
% Of Photons Absorbed vs Optical Path Length
Γ = 0.07 (7% shadowing and reflection factor)
100.0
95.0
90.0
85.0
80.0
75.0
70.0
65.0
60.0
% Absorbed
1.0
10.0
100.0
1000.0
10000.0
Optical Path Length µm
Assumes energy is 100% absorbed by 2000 µm.

figure 3.2

$$R^{SRH} = \frac{(n\,p - n_{ie}^{2})}{\tau_{pk} (n + n_1) + \tau_{nk} (p + p_1)} \quad . \tag{3.13}$$

The concentrations n_1 and p_1 relate the emission and capture rates at equilibrium and are a function of the trap level (middle of the bandgap in SCAP1D). The effective intrinsic concentration n_{ie} is defined in equation 3.10 . The terms τ_{pk} and τ_{nk} represent the reciprocals of the capture rates per single carrier. The capture rates are defined as the product of the capture cross section, the thermal velocity, and the concentration of the traps. Experimental evidence suggests that at high doping concentrations, the trap concentration increases. Therefore, it is necessary to make the lifetimes in equation 3.13 doping dependent. The doping dependence is modeled using the equations,

$$\tau_{nk} = \frac{\tau_{n0}}{1 + \dfrac{N_D + N_A}{Z_{kn}}} \tag{3.14a}$$

$$\tau_{pk} = \frac{\tau_{p0}}{1 + \dfrac{N_D + N_A}{Z_{kp}}} \quad , \tag{3.14b}$$

which were derived from experimental data. The parameters τ_{n0} and τ_{p0} are the reciprocal capture rates (lifetimes) for lightly doped silicon. They are input to SCAP1D and describe the quality of the silicon wafer used to build the solar cell. The parameters Z_{kp} and Z_{kn} are defined as 7.1×10^{15} [3.15]. The total recombination is the sum of R^{AU} and R^{SRH}, $R = R^{SRH} + R^{AU}$ (surface recombination is modeled using the boundary conditions).

To aid the engineer in the physical understanding of the device, recombination rates are often related to the minority carrier lifetime in the literature. At equilibrium, the generation and recombination rates associated with the physical phenomenon described by equations 3.12 and 3.13 must balance (i.e., $n\,p = n_{ie}^{2}$, so there is no net recombination). The lifetime is calculated by considering small deviations from equilibrium in the electron and hole concentrations (i.e., $n = n_e + dn$ and $p = p_e + \Delta p$). For example, in a p-type material the lifetime associated with the Auger process is calculated as follows:

$$\tau_{Auger} = \frac{\Delta n}{(\alpha_n n + \alpha_p p) (n\,p - n_{ie}^{2})} \tag{3.15a}$$

$$= \frac{\Delta n}{(\alpha_n n + \alpha_p p) [(n_e + \Delta n) (p_e + \Delta p) - n_{ie}^2]} \qquad (3.15b)$$

Using the fact that $n_{ie} = n_e\, p_e$.

$$= \frac{\Delta n}{(\alpha_n n + \alpha_p p) (\Delta n\, p_e - \Delta p\, n_e)} \qquad (3.15c)$$

Since the material is p-type, $p \gg n$, and the only term of importance involves p^2. If low injection is assumed, $p = N_A$ (i.e., low injection assumes that the majority carrier concentration is not raised significantly above the doping concentration).

$$\tau_{Auger} = \frac{1}{\alpha_p N_A^2} \qquad (3.16)$$

Identical arguments can be used to determine that the lifetime associted with SRH recombination is $\tau_{SRH} = \tau_{nk}$, where τ_{nk} is defined in equation 3.14a above. The combined lifetime is the reciprocal sum of the lifetimes associated with each process (since the recombination rates are additive).

$$\frac{1}{\tau_n} = \frac{1}{\tau_{Auger}} + \frac{1}{\tau_{SRH}} \qquad (3.17)$$

Figure 3.3 shows a graph of lifetime versus the net doping concentration, N ($N = N_A$ in the bulk of a n-p solar cell). The graphs are of equations 3.14a (SRH), 3.16 (Auger), and 3.17 (combined). The position of the graph for τ_{SRH} is moved vertically depending on the value assumed for τ_{n0} (1 ms is used in figure 3.3). As mentioned above, τ_{n0} is related to the quality of the substrate. The Auger lifetime is more fundamental and is not affected by the quality of the substrate. Figure 3.3 clearly shows the deterioration of lifetime (i.e., increase in recombination rates) that occurs when the doping concentration is increased. At light doping, the lifetime is dominated by τ_{SRH}. While at heavy doping, τ_{Auger} dominates.

Carrier mobility is modeled as the combination of scattering due to lattice vibrations and ionized impurities. Lattice scattering ($\mu_{n,p}^L$) is calculated using the power formula:

$$\mu_n^L = \mu_n^{max} \left[\frac{T}{300\ K} \right]^{-\alpha_n} \qquad (3.18a)$$

$$\mu_p^L = \mu_p^{max} \left[\frac{T}{300\ K} \right]^{-\alpha_p} . \qquad (3.18b)$$

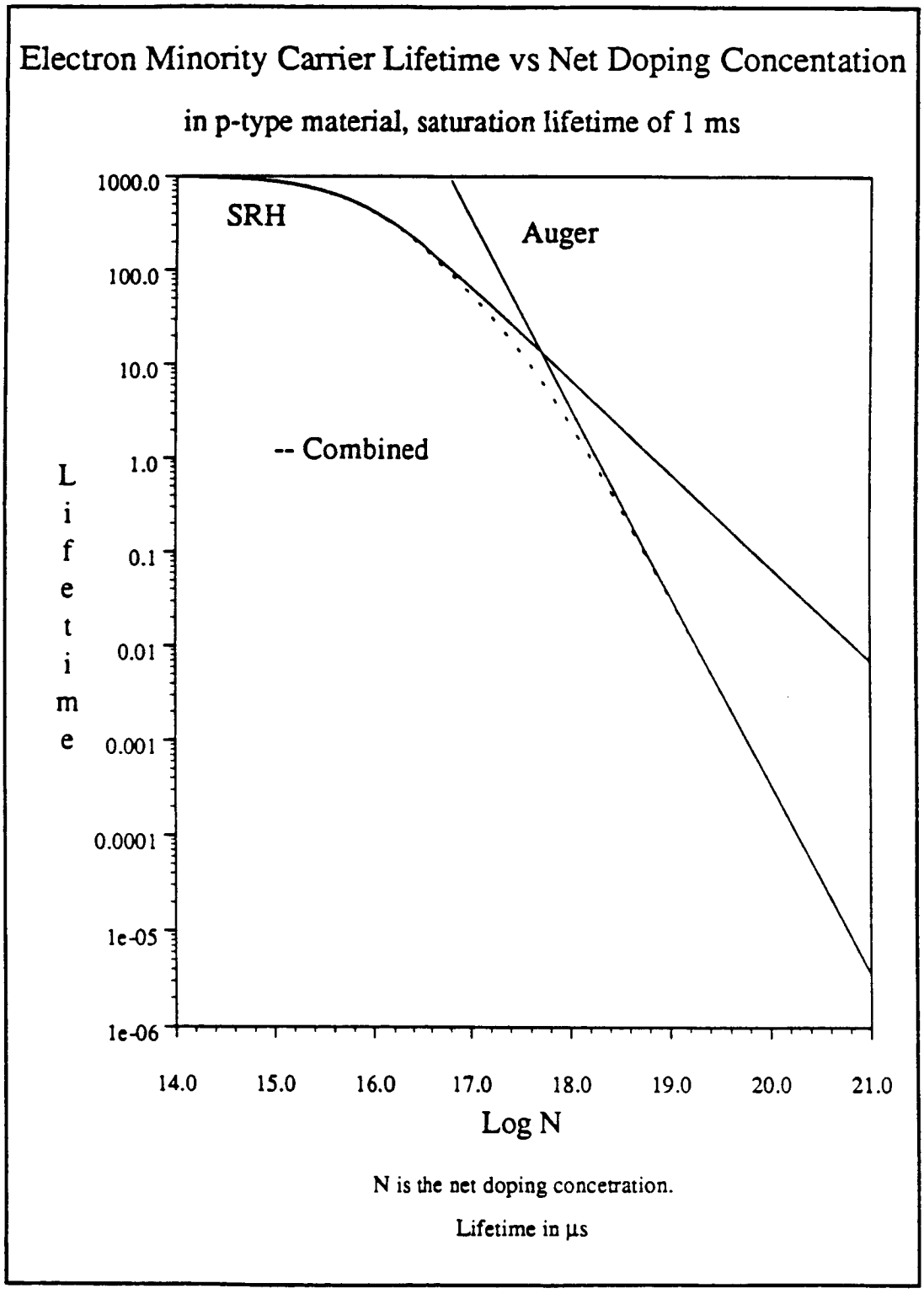
Electron Minority Carrier Lifetime vs Net Doping Concentation
in p-type material, saturation lifetime of 1 ms
SRH
Auger
-- Combined
Lifetime
1000.0
100.0
10.0
1.0
0.1
0.01
0.001
0.0001
1e-05
1e-06
14.0
15.0
16.0
17.0
18.0
19.0
20.0
21.0
Log N
N is the net doping concetration.
Lifetime in µs

figure 3.3

The constants μ_n^{max} and α_n are taken from [3.16], and μ_p^{max} and α_p are taken from [3.17]. The model for ionized impurity scattering ($\mu_{n,p}^{I}$) is based on the equation due to Caughey and Thomas [3.17]. The constants used in the equation have been updated by many authors, for holes [3.18] is used and for electrons [3.19]. In SCAP1D, the equation has been changed to include a temperature dependence taken from [3.20]. The combined mobility is determined by the Mathiessen rule,

$$\frac{1}{\mu_{p,n}^{U}} = \frac{1}{\mu_{p,n}^{L}} + \frac{1}{\mu_{p,n}^{I}} \quad . \tag{3.19}$$

All the results in this report were calculated at room temperature (300 K). Therefore, equation 3.19 is used to model the decrease in mobility that is experimently observed with increased doping concentration. The mobility as a function of the net doping concentration ($N = |N_D - N_A|$) is graphed for both electrons and holes in figure 3.4 . The reciprocal sum in equation 3.19 implies that the highest value achievable for electron mobility is μ_n^{max} (μ_p^{max} for holes).

The diffusion coefficients D_n and D_p, which appear in equations 3.8a and 3.8b, are related to the mobility by the Einstein relations.

$$D_n = \frac{k\,T}{q}\,\mu_n \quad \text{and} \quad D_p = \frac{k\,T}{q}\,\mu_p \tag{3.20}$$

In the [3.2], the generalized Einstein relations are used. However, the relations given above can be used to approximate an important physical parameter, the diffusion length. In a p-type material, the equation for the diffusion length,

$$L_d = \sqrt{\tau_n\, D_n} \quad . \tag{3.21}$$

is completely defined by substituting in equations 3.17, 3.19, and 3.20. Figure 3.5 is a graph of the diffusion length as a function of the net doping concentration for τ_{n0} = 1 ms (same value used in figure 3.3). The diffusion length decreases rapidly as the doping concentration increases, since both the mobility and the lifetime decrease with increasing doping concentration.

Bandgap narrowing is calculated using the empirical equation due to Slotboom and DeGraf [3.21-3.23],

$$\Delta_g = V_1\,[\,F + (\,F^2 + C\,)^{1/2}\,] \qquad F = \ln\frac{N}{N_0} \quad . \tag{3.22}$$

In the equation above, N is the net doping concentration ($|N_D - N_A|$), and the values of the constants V_1, N_0, and C, which are determined from experimental

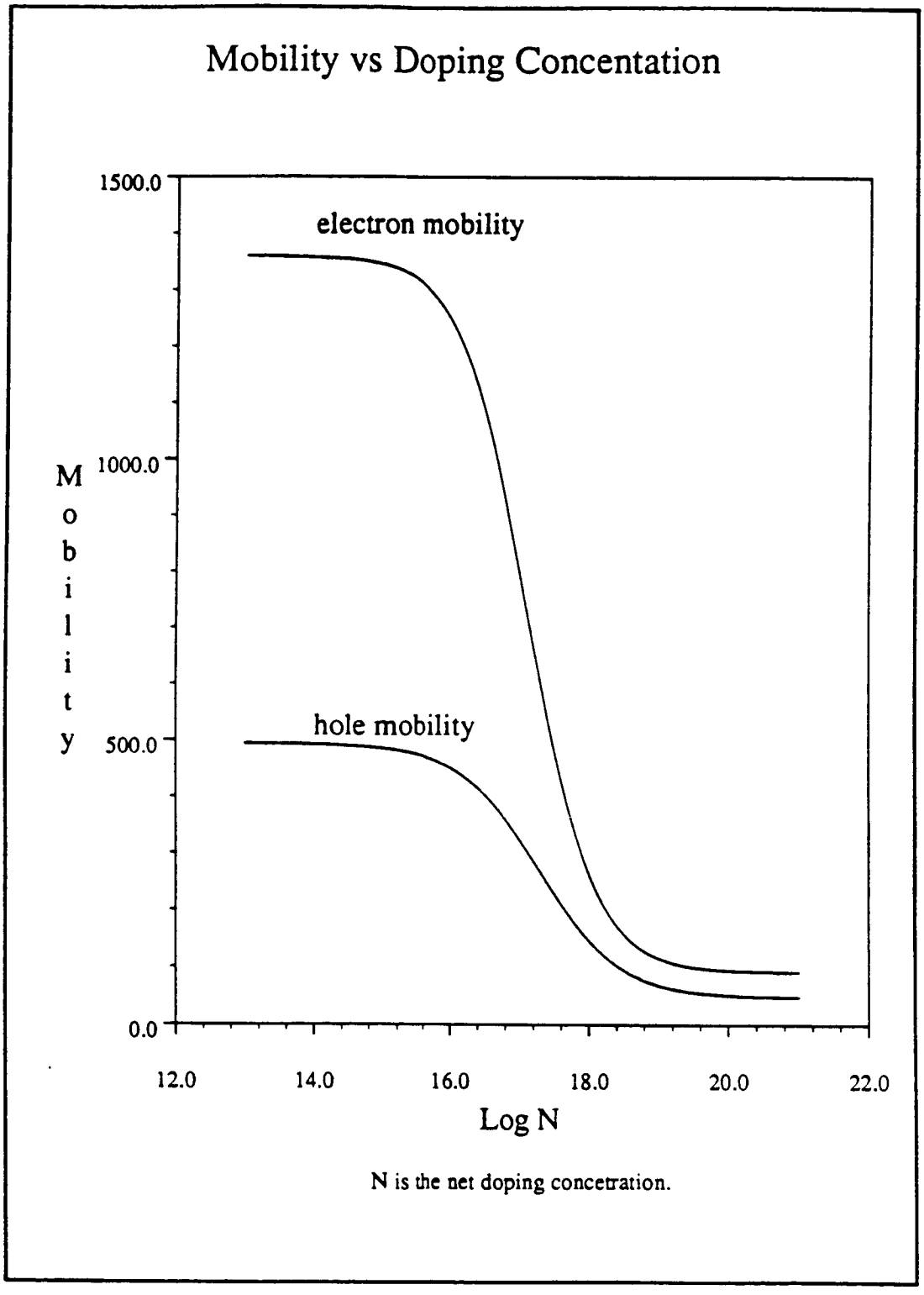
Mobility vs Doping Concentation
1500.0
electron mobility
1000.0
M
o
b
i
l
i
t
y
hole mobility
500.0
0.0
12.0
14.0
16.0
18.0
20.0
22.0
Log N
N is the net doping concetration.

figure 3.4

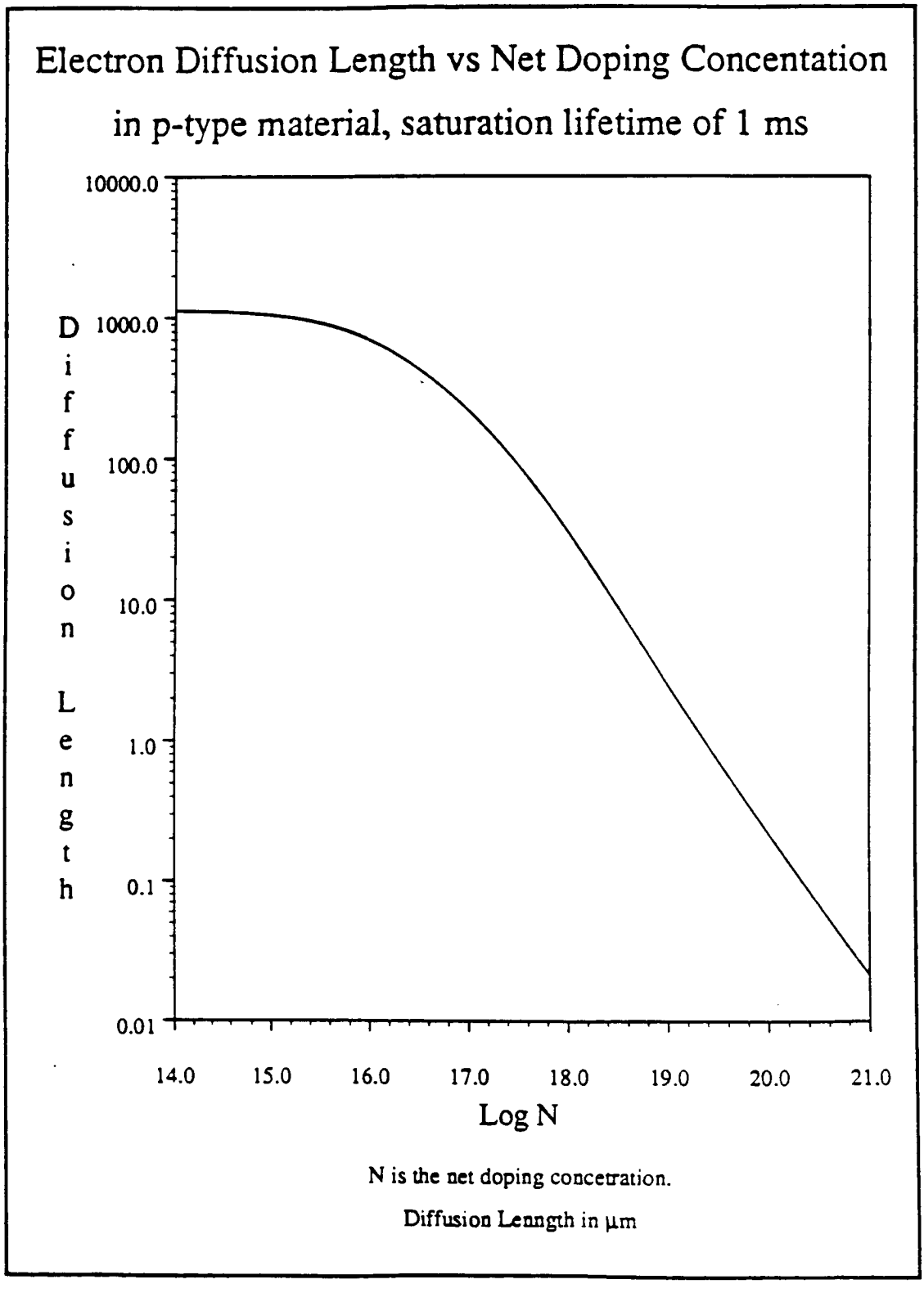
Electron Diffusion Length vs Net Doping Concentation
in p-type material, saturation lifetime of 1 ms
10000.0
1000.0
100.0
10.0
1.0
0.1
0.01
Diffusion Length
14.0
15.0
16.0
17.0
18.0
19.0
20.0
21.0
Log N
N is the net doping concetration.
Diffusion Lenngth in µm

figure 3.5

data, are taken from [3.23]. In figure 3.6, Δ_g is graphed versus the log of the net doping concentrations (Atoms/cm^3). Bandgap narrowing is not a factor for doping concentrations less than 10^{16}.

3.3 Boundary Conditions

To completely specify the differential equations, it is necessary to define the boundary conditions. Conditions are required at x=0 and x=L for V, n, and p or their derivatives. The boundary conditions on V were obtained by requiring that the semiconductor be space charge neutral at the contacts. This condition is valid if the contacts are ohmic, and is valid for nonohmic contacts if it is assumed the semiconductor is heavily doped at the contacts. Hence, $V_0 = V_{0eq}$ and $V_L = V_{Leq} - V_{bias}$. V_{bias} is the forward voltage bias across the device. The subscript eq (equilibrium) refers to the conditions in the device when there is no incident radiation.

The boundary conditions for the carrier concentrations are set equal to their equilibrium values if the contacts are specified as ohmic (equivalent to infinite surface recombination velocity). If the contacts are specified in terms of finite recombination velocities, the majority concentrations are still set equal to their equilibrium values (assumes heavy doping at the contacts and low injection), but for the minority carriers a current is defined:

$$J_n = \pm S (n - n_{eq}) \tag{3.23a}$$

if p-type at the contact, and

$$J_p = \pm S (p - p_{eq}) \tag{3.23b}$$

if n-type at the contact. The transport equations can then be substituted into the above equations to determine the minority carrier concentrations at the contacts. S_f and S_b (units of cm/s), which are inputs to the code, are used to differentiate between the front and back surfaces. The boundary conditions of an actual device are different for the cell surface that is located under the metallic grid and the surface that is not located under the metallic grid. Since the code is one dimensional, the recombination velocities are effective recombination velocities and represent the net effect of both areas.

3.4 Solving the Differential Equations

In the last three sections, the equations used in SCAP1D to describe the physics of a solar cell have been presented. The resulting system of equations is a set of three coupled, nonlinear, second order, ordinary differential equations. The

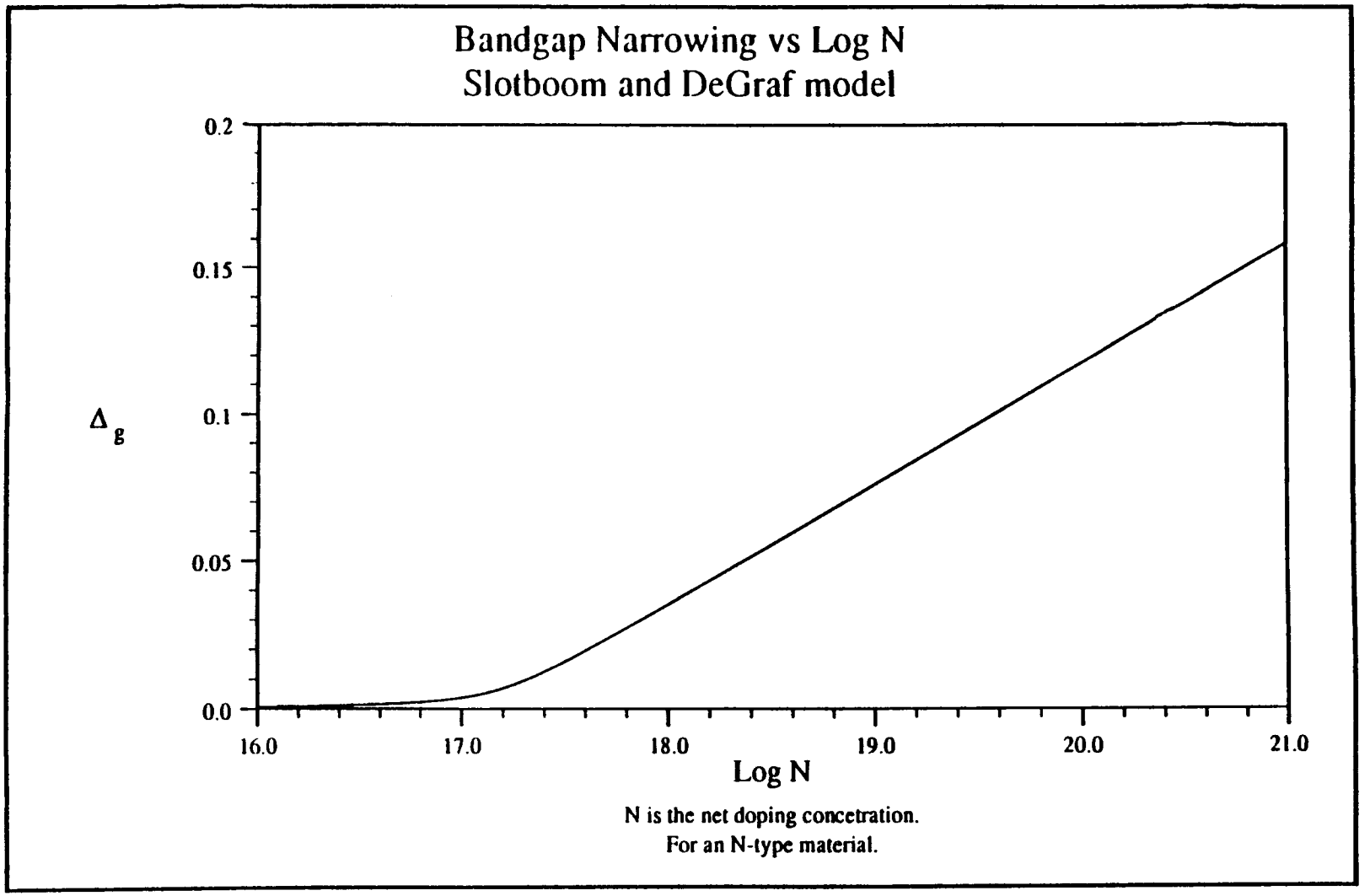
Bandgap Narrowing vs Log N
Slotboom and DeGraf model
0.2
0.15
0.1
0.05
0.0
Δ_g
16.0
17.0
18.0
19.0
20.0
21.0
Log N
N is the net doping concetration.
For an N-type material.

figure 3.6

solution to the equations is expressed as the values of voltage (V), electron carrier concentration (n), and hole carrier concentration (p) as a function of the independent variable x. It is not possible to solve these equations in their most general form using analytical methods. Hence, the differential equations are discretized using finite difference methods to transform them into a system of algebraic equations. Numerical procedures can then be used to solve the system of algebraic equations. The result is a discrete approximation to the analytic solution of the differential equations. In this section, the method used in SCAP1D to numerically solve the equations is described.

Because the model is one dimensional, the differential operators in equations 3.1, 3.2, and 3.8 simplify to differentiation with respect to x. The variable x denotes the position in the device measured from the front surface to the back surface. The equations are normalized to scale the variables and to simplify the calculations when solving the equations numerically. The resulting system of equations is:

$$\frac{d^2}{dx^2}V = n - p + N_D - N_A \tag{3.24a}$$

$$\frac{d}{dx}J_p = (G - R) \tag{3.24b}$$

$$\frac{d}{dx}J_n = -(G - R) \tag{3.24c}$$

$$J_p = -\mu_p \left[p \frac{d}{dx}(V - (\gamma - 1) V_G) - \frac{d}{dx}p \right] \tag{3.24d}$$

$$J_n = -\mu_p \left[p \frac{d}{dx}(V - (\gamma - 1) V_G) - \frac{d}{dx}p \right] \tag{3.24e}$$

where $V_G = \Delta_g/kT$.

The above differential equations are discretized by using finite difference techniques. The conventional difference approximation to the second derivative is used for Poisson's equation, while the technique of Scharfetter-Gummel [3.24] is used to discretize the current relations. A variably spaced mesh is used to place nodes throughout the device. A variable mesh is required because the solution of the semiconductor equations exhibit a smooth behavior in some regions (e.g., the bulk

of the device), whereas in others it varies rapidly (e.g., at the front junction). All results described in this report were calculated using 250 nodes. As a result of the finite difference transformation, at each node (j) a nonlinear algebraic equation is defined for Poison's equation (V) and the hole (p) and electron (n) current relations,

$$f_{V_j} = f(V_{j-1}, p_j, n_j, V_j, V_{j+1}) = 0 \tag{3.25}$$

$$f_{p_j} = f(p_{j-1}, V_{j-1}, p_j, n_j, V_j, p_{j+1}, V_{j+1}) = 0 \tag{3.26}$$

$$f_{n_j} = f(n_{j-1}, V_{j-1}, p_j, n_j, V_j, n_{j+1}, V_{j+1}) = 0 \ . \tag{3.27}$$

This is done for each of the 250 nodes used, resulting in a system of 750 nonlinear algebraic equations.

Let $\mathbf{u}$ be the vector $[p_1, n_1, V_1, \ldots, p_{250}, n_{250}, V_{250}]$, and $\mathbf{f(u)}$ be the associated vector whose components are the values of the left hand side of equations 3.25-3.27 at each node (disregarding the equality to zero). Just as one could use the Newton algorithm to determine the root of a single nonlinear algebraic equation, a system of nonlinear algebraic equations can be solved by using a Newton-like method. Analogous to the one dimensional case, the Newton-like method for a system of equations requires an initial estimate of the roots of the equations, $\mathbf{u}^0$ (the values of V, n, p at each of the 250 nodes). The vector $\mathbf{f}(\mathbf{u}^0)$ represents the error associated with the initial estimate in equations 3.25-3.27. The error can be used along with the Jacobian matrix (analogous to the derivative for the one dimensional case) of the system of equations to define a correction term that can be added to $\mathbf{u}^0$ to get an improved estimate of the solution $\mathbf{u}^1$.

The correction vector is defined as follows,

$$\mathbf{K}(\mathbf{u}^k)\ \Delta\ \mathbf{u}^{k+1} = -\mathbf{f}(\mathbf{u}^k) \ , \tag{3.28}$$

and is solved for by inverting the Jacobian matrix $\mathbf{K}$ (i.e., solving the system of linear equations). The correction vector $\Delta\ \mathbf{u}^{k+1}$ is added to the vector $\mathbf{u}^k$. The result is a better estimate, $\mathbf{u}^{k+1}$, to the solution vector $\mathbf{u}$ for which the equality to zero in equations 3.25-3.27 holds. The process iterates until the correction vector and the values of the components of $\mathbf{f}$ are deemed small enough to imply convergence.

The Jacobian matrix, $\mathbf{K}$ takes on the special form of a band matrix of bandwidth nine because the equations at each node are only a function of the values of n, p, and V at that node and the two adjacent nodes. Since $\mathbf{K}$ is a very

sparse matrix, solving the system of linear equations associated with (3.28) is simplified. Also, the solution strategy implemented in the code may use the same Jacobian for several iterations. Hence, the inversion required to solve 3.28 may not have to be done every iteration. However, due to the large dimension (750 for 250 nodes) and the fact that the linear equations 3.28 must be solved iteratively to obtain the solution of the nonlinear equations 3.25-3.27, the solution procedure requires considerable effort.

The basic Newton algorithm is modified in [3.2] to improve the convergence properties (correct the overshoot phenomenon) and expand the region of convergence for the initial guess. It is still the property of the algorithm, however, that the initial guess must be sufficiently close to the answer for convergence to be achieved (similar to the one dimensional Newton algorithm). This point is crucial to the method used to adapt SCAP1D to an optimization environment (described in chapter 4).

3.5 Simulating Solar Cell Performance

The method of obtaining a numerical solution of the differential equations has been given. How that solution is used to simulate the performance of a solar cell and to calculate the efficiency will now be presented. The first task is to arrive at an initial estimate of the values of V, n, and p for some mode of device operation. This is done by considering the solutions to the equations during equilibrium (the state of the device when there is no illumination or other external stimuli). Also, the equilibrium solution is required to define the boundary conditions to the nonequilibrium (illuminated) problem. In equilibrium, the current densities J_n and J_p are equal to zero. This simplifies the set of equations 3.24 to the following,

$$\frac{d^2}{dx^2}V_{eq} = \exp\left(V_{eq} + \gamma V_G \right) - \exp\left(-veq - \left(\gamma - 1 \right) V_G \right) - N_D + N_A \quad . \qquad (3.29)$$

Although this equation must also be solved by an iterative Newton-type numerical algorithm, a convergent initial solution can be defined by assuming space charge equilibrium throughout the device. The resulting equation,

$$\frac{d^2}{dx^2}V_{eq} = 0 \quad , \qquad (3.30)$$

has an analytic solution that can be used to calculate the voltage at each node.

Once the equilibrium voltage has been calculated, the equilibrium hole and electron carrier concentrations can be solved for at each mesh point from an analytic equation. The actual implementation of the equilibrium problem in SCAP1D

is more complex due to the need to define a variably spaced mesh that will result in an accurate solution of the equations. The considerations for the spacing of the mesh points are that the generation rate (for monochromatic illumination) between nodes does not significantly change, the distances between adjacent nodes does not change significantly, and the potential (V_{eq}) does not change significantly between any two nodes. An initial estimate for the mesh is automatically defined by the code using fewer nodes than requested in the input (in this work 250). The equilibrium problem is solved several times, each time increasing the number of nodes and/or redistributing the nodes, until all the conditions above are satisfied and the desired number of nodes is reached.

The solution to the equilibrium problem provides an initial estimate close enough to solve the nonequilibrium (illuminated) problem for a short circuit condition ($V_{bias} = 0$). The system of 750 nonlinear algebraic equations is then solved to determine the values of n, p, and V at each node by the Newton-like iterative algorithm described above. The bias can then be increased to 0.1 volt, with the solution vectors of n, p, and V from the short circuit problem being used as the initial estimate to the solution. Once again, the system of nonlinear equations is solved. This process continues, increasing the bias voltage by 0.1 volt and re-solving the system of nonlinear equations, until a negative or very small current results (the voltage offset is decreased if the code senses it is close to the crossover from positive to negative current). A current of zero would result if V_{bias} were set equal to the open circuit voltage (V_{oc}) of the cell. Negative currents represent a V_{bias} greater than V_{oc}. It may take as many as nine voltage offsets for V_{bias} to be increased to the vicinity of V_{oc}. Then, an iterative linear interpolation algorithm is used to solve for the open circuit voltage to within a specified tolerance (current sufficiently close to zero). The algorithm is iterative and in general several biases must be solved for (i.e., the system of nonlinear equations must be solved several times) before convergence to V_{oc} is reached.

Changing V_{bias} is interpreted as changing the resistance of the load attached to the solar cell. There is a load resistance that results in the maximum power being transferred to the load. The resulting V_{bias} is referred to as V_{mp}, the maximum power voltage. A good estimate of V_{mp} is calculated by using V_{oc} and I_{sc}, which have already been determined, in the ideal diode equation. Then a linear interpolation algorithm is used to converge to V_{mp}. This requires solving the system of nonlinear equations for several bias voltages until convergence to V_{mp} is achieved.

In following the above procedure, SCAP1D has completely defined the I-V curve associated with the solar cell. Figure 3.7 shows an example of an I-V curve. V_{mp} is the voltage associated with the largest area rectangle under the I-V curve

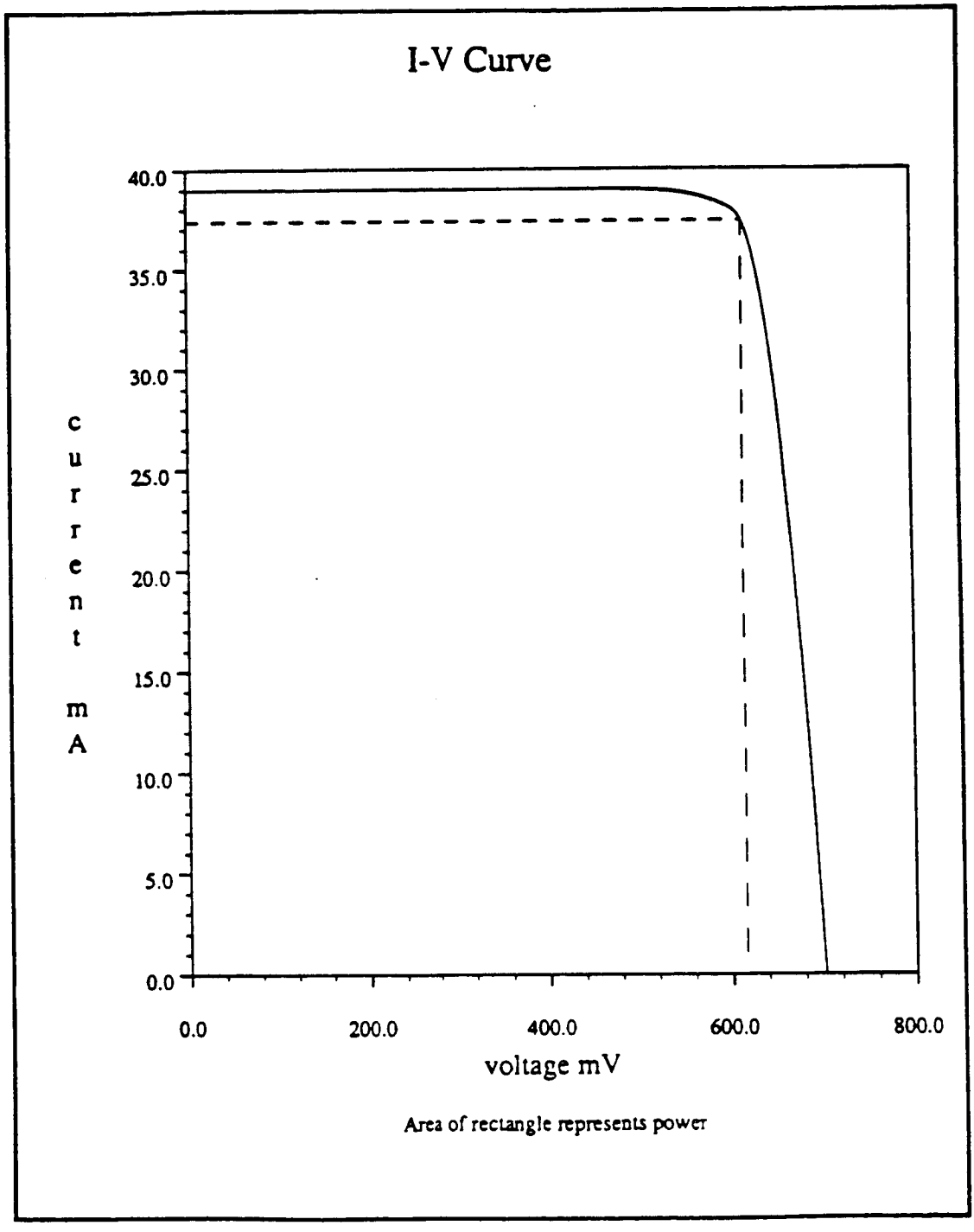
I-V Curve
40.0
35.0
30.0
25.0
20.0
15.0
10.0
5.0
0.0
current mA
0.0
200.0
400.0
600.0
800.0
voltage mV
Area of rectangle represents power

figure 3.7

(in the coordinates of current and voltage, area is equal to power). The efficiency of the device is calculated by dividing the power generated at V_{mp} by the power (in the form of illumination) incident on the cell.

3.6 The Variables

In the previous sections, it was seen that the efficiency of a solar cell can be calculated by solving the differential equations at a voltage bias equal to the maximum power voltage. Different solar cell designs are defined by changing the coefficients and the boundary conditions of the differential equations. Changing the coefficients and/or the boundary conditions of the equations affects the solution of the equations at all the biases (including V_{mp}) and the the value of V_{mp}, hence affecting the efficiency. The coefficients of the equations were seen to be a function of several variables.

The equations are completely defined by specifying the following inputs to the model; the operating temperature, the incident illumination, the shadowing and reflection factor, the SRH lifetimes for lightly doped silicon (τ_{n0} and τ_{p0}), the impurity concentration (as a function of x), the thickness of the device, and the effective surface recombination velocities (S_f and S_b). The operating temperature (300 K) and the incident illumination (AM1.5) are chosen in accordance with a standard established so that the results of different studies can be compared [3.25]. The shadowing and reflection factor is defined in this work as 7%. It represents the percent of the incoming illumination that is not available for power generation due to shadowing of the top contact grid and reflection at the front surface of the cell.

The doping concentration and the cell thickness are controllable to the extent that they can be considered decision or design variables in the optimization. In designing a silicon solar cell, the design engineer is able to specify these variables with a reasonable degree of accuracy within the bounds given in the problem statement P1.

The variables τ_{n0}, τ_{p0}, S_f, and S_b are not completely controllable. They are closely related to the fabrication process and level of technology used to build the cell. Hence, they will be referred to as technology variables. Since the level of technology and the fabrication process are fixed during the manufacture of a cell, the design engineer is not free to specify a desired value for the technology variables. The effect of the technology variables on efficiency is monotonic regardless of the values of the other design variables (i.e., increasing lifetimes increases efficiency and decreasing surface recombination velocities increases efficiency for any cell design). Since it is known that the technology variables will go to their

more favorable bound, including them in an optimization provides no useful information, while increasing the computational effort required to complete an optimization. The level of technology and fabrication processes may change in the future, so the effects of such variables should be investigated. Since technology variables should not be included in the optimization, they can only be investigated parametrically while re-optimizing the cell design. The re-optimization of the design variables is critical, since it is desirable to compare only the highest efficiency designs associated with different levels of technology and/or fabrication processes.

3.7 Summary

The equations used to simulate a solar cell in SCAP1D are a set of three coupled, nonlinear, second order, ordinary differential equations. The solution of the equations includes the values of the voltage, electron concentration, and hole concentration as a function of the independent variable x. The method of solution is to transform the equations using finite difference methods into a system of nonlinear algebraic equations. A Newton-like algorithm, which requires a good initial approximation of the solution to converge, can be used to solve the system of nonlinear algebraic equations.

The performance of a solar cell for a given voltage bias is simulated by solving the system of nonlinear algebraic equations and using the solution to determine the current and the terminal voltage of the cell. A number of voltage biases, which define the I-V curve, must be solved for to insure the convergence of the Newton-like algorithm and to determine the value of the maximum power voltage. The efficiency is defined by solving the system of nonlinear equations at a bias equal to the maximum power voltage.

Different solar cells are modeled by changing the values of variables which affect the coefficients and boundary conditions of the differential equations. The variables D_0, D_B, D_L, X_f, X_b, and X_L are decision (design) variables in the optimization. Variables such as the operating temperature and the incident illumination are chosen to standardize the results. The variables S_f, S_b, τ_{n0}, and τ_{p0} are referred to as technology variables and are not included in the optimization. By solving the optimization problem at different values of the technology variables, it is possible to compare the best predicted efficiency associated with different processes and levels of technology. Cell design must be optimized to make such comparisons valid.

4 Adapting SCAP1D to an Optimization Environment

To maximize efficiency, the objective function discussed in the problem statement section, it is necessary to couple SCAP1D with an optimization code (e.g., see figure 2.2). The optimization code requires that the objective function be calculated iteratively until convergence is reached. Hence, a major consideration when adapting a numerical model like SCAP1D for use in an optimization (i.e., iterative) environment is to insure that only the calculations necessary to compute the objective function are performed. The repetition of unnecessary calculations will increase the computational burden required to complete an optimization. It is also important to note that SCAP1D requires the use of iterative algorithms (Newton-like algorithm and secant algorithm). Hence, each calculation of efficiency is affected by the convergence tolerances of the iterative algorithms (referred to henceforth as convergence error) as well as numerical roundoff error, truncation error, etc. It is important that such sources of error do not significantly affect the comparison of the efficiencies associated with different values of the decision variables. This chapter will detail the changes made to adapt SCAP1D to an optimization environment stressing the above considerations.

4.1 A Strategy for Iteratively Calculating Efficiency

One way to interface SCAP1D to an optimization code would be to run SCAP1D in its entirety each time the objective function is requested by the optimization code. However, because the objective function requires that only the efficiency be calculated (not the entire I-V curve), it was possible to develop a strategy that allowed considerable savings in the computational effort required to complete an optimization. As part of this task, an analysis was made to determine the routines in SCAP1D that required significant cpu time. Table 4.1 shows the results of the analysis for a single execution of SCAP1D on a Gould PN9080 minicomputer. These times are only representative of an average run. Since SCAP1D involves several iterative processes, the times will be different for runs initiated with different data. The only activities that require significant amounts of time are

the solution of the nonequilibrium (illuminated) problem, the solution of the equilibrium (nonilluminated) problem, and the calculation of the generation rate (i.e., how the solar energy is absorbed through the device).

The time spent solving the nonequilibrium problem is accumulated by solving the system of nonlinear equations described in the previous chapter for a number of different values of V_{bias} (20 biases were solved for in the run that is the basis of table 4.1). Since

$$\text{efficiency} = V_{mp}\, I_{mp} / (\text{ incident power }), \tag{4.1}$$

the only bias required to determine the efficiency is the maximum power voltage, V_{mp}. In table 4.1, the time spent solving the nonequilibrium problem is further subdivided into the categories of I-V offsets, solving for V_{oc}, and solving for V_{mp}. This suggests that considerable effort can be saved in calculating the efficiency if an initial estimate can be provided that is within the region of convergence of the Newton-type algorithm for biases near V_{mp}. In an iterative environment, this estimate is provided by the previous call to SCAP1D. Because no estimate of the solution exists for the initial calculation of the efficiency, the first simulation must still be executed in its entirety.

Table 4.1 Time Analysis of a Single Execution of SCAP1D

Routine	cpu seconds	cpu seconds
Solve Non-Equilibrium Problem	63.12	
I-V Offsets		31.51
Solve For V_{oc}		9.46
Solve For V_{mp}		22.15
Solve Equilibrium Problem	9.34	
Calculate Generation Rate	6.86	
All Other Routines	0.71	

Figure 4.1 shows a flow chart of the strategy that was implemented. First, the efficiency associated with the initial estimate of the decision variables is calculated by running SCAP1D in its entirety. The values of n, p, and V at each node of the finite difference mesh (i.e., the solution to equations 3.25-3.27) associated with the maximum power voltage are saved along with the value of V_{mp}. The optimization

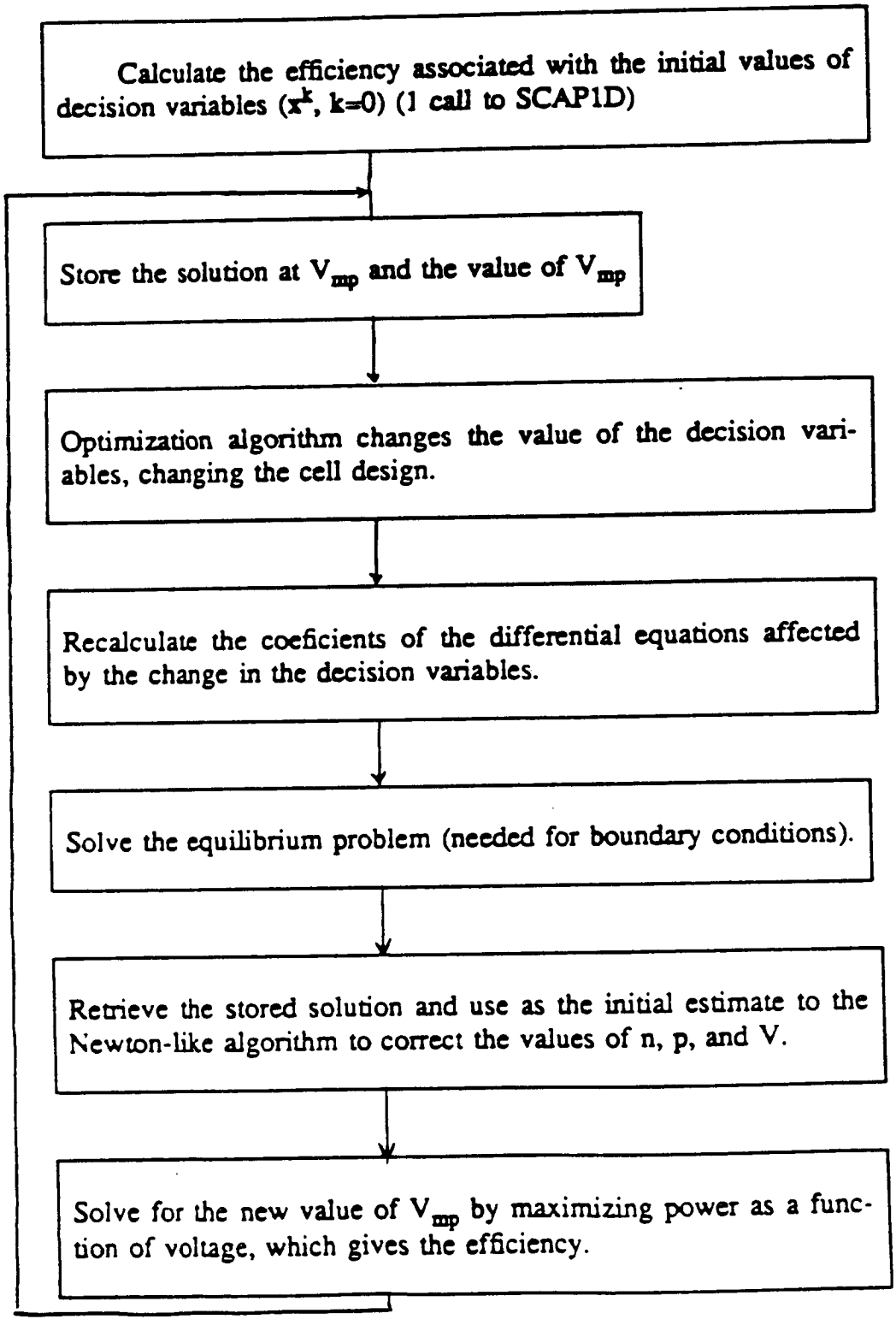

fig. 4.1 Iterative Solution Technique

code then changes the values of the decision variables to increase the efficiency. The next step actually depends on which decision variables change value. Figure 4.1 shows the simpler case of only the variables associated with the doping concentrations changing value (e.g., front surface doping concentration, bulk doping concentration, and back surface doping concentration). The routines required to modify the coefficients of the equations to reflect the changes in the decision variables are executed. The parameters R, Δ_g, μ_n, and μ_p are all recalculated because they are a functions of the doping concentrations (the defining equations are given in section 3.2). The variably spaced mesh from the previous solution can still be used (i.e., the value of x associated with the finite difference mesh points does not change). Therefore, it is not necessary to recalculate the generation rate (G in the equations 3.25-3.27), since it is only a function of x.

The retention of the variably spaced mesh also simplifies the solution of the equilibrium problem. The equilibrium problem must be solved, because it is required to define the boundary conditions for the nonequilibrium problem. An initial estimate of the new equilibrium solution can be calculated by assuming space charge equilibrium (equation 3.30). The resulting analytic expression is used to solve for the voltage at each of the 250 nodes. Then, the equilibrium voltage can be calculated by solving equation (3.29). The equilibrium carrier concentrations are solved using the same analytic expressions used in a standard run of SCAP1D. This defines all the terms needed to calculate the boundary conditions.

The solution vector from the previous nonequilibrium problem is retrieved from storage and used as the initial estimate to the solution of the nonequilibrium problem. The previous value of V_{mp} is used as the voltage bias. The equations 3.25-3.27 are re-solved using the Newton-like algorithm to iteratively solve equation 3.28 (repeated below),

$$\mathbf{K}(\mathbf{u}^k)\,\Delta\,\mathbf{u}^{k+1} = -\mathbf{f}(\mathbf{u}^k) \quad . \tag{4.2}$$

The initial estimate, $\mathbf{u}^0$ (k=0), is the retrieved solution vector from the previous calculation of efficiency. However, this estimate is no longer correct, because it was associated with different values of the doping concentrations. The solution of the nonequilibrium problem results in the solution vector associated with the new values of the doping concentrations at the V_{mp} associated with the old values of the doping concentrations. Since the doping concentrations have changed, the new value of V_{mp} will be different. The new value of V_{mp} is determined by solving the one dimensional maximization of power as a function of voltage,

$$\max_{V} \text{Power}(V) \quad . \tag{4.3}$$

A one dimensional optimization routine was written to solve the one dimensional optimization problem expressed in equation 4.3 . The optimization routine replaced the secant method (based on linear interpolation). The reasons for this and the one dimensional optimization algorithm developed are discussed in the next section.

Figure 4.2 illustrates the above process. The initial execution of SCAP1D defines the entire I-V curve (shown as a solid line in figure 4.2). Changing the doping concentrations defines a new I-V curve (the dotted curve shifted from the solid curve). By correcting the solution vectors at the old value of V_{mp}, a move is made vertically from the V_{mp} of the solid curve to the dotted curve. Maximizing power as a function of voltage implies a move along the dotted curve to the maximum power voltage associated with the dotted curve. The dotted I-V curve is never completely solved for. Rather, the system of 750 nonlinear equations described in section 3.4 is only solved for at a few biases in the vicinity of V_{mp} (as depicted in figure 4.2). Power as a function of voltage is plotted for the dotted curve in figure 4.3 . When the power has been maximized, the value of V_{mp} and the associated solution vectors are stored if they improve the efficiency. Since the optimization code is maximizing the efficiency, the solution associated with the current best point will provide the best initial estimate for the next set of decision variables defined by the optimization algorithm.

All subsequent calculations of efficiency required by the optimization are done by making use of the current stored solution. Hence, none of the subsequent I-V curves is ever completely defined. The above strategy will only work if the estimate that is retrieved from storage is within the region of convergence of the Newton-like algorithm (equation 4.2) used to solve the system of nonlinear equations. Originally, SCAP1D defined the I-V curve to obtain a voltage offset that was close to V_{mp} (within the convergence region of the Newton-like algorithm), while the cell design remained constant. The convergence region of the Newton-like algorithm includes I-V curves associated with similar cell designs. Hence, it is possible to use the iterative strategy described above. The process iterates until the optimization converges to the optimal efficiency.

The effects of the above changes were illustrated by timing an optimization initiated from the same inputs used as a basis for table 4.1 . The time taken for the initial execution of SCAP1D was subtracted from the time required for the optimization. The result was divided by the number of function evaluations (minus one) required for the optimization. The average time to determine the efficiency for subsequent runs was 9.7 seconds. Time spent in the optimization code is negligible. This represents a better than 800% reduction when compared to the time to call SCAP1D and solve it in its entirety. Since all the objective evaluations, except

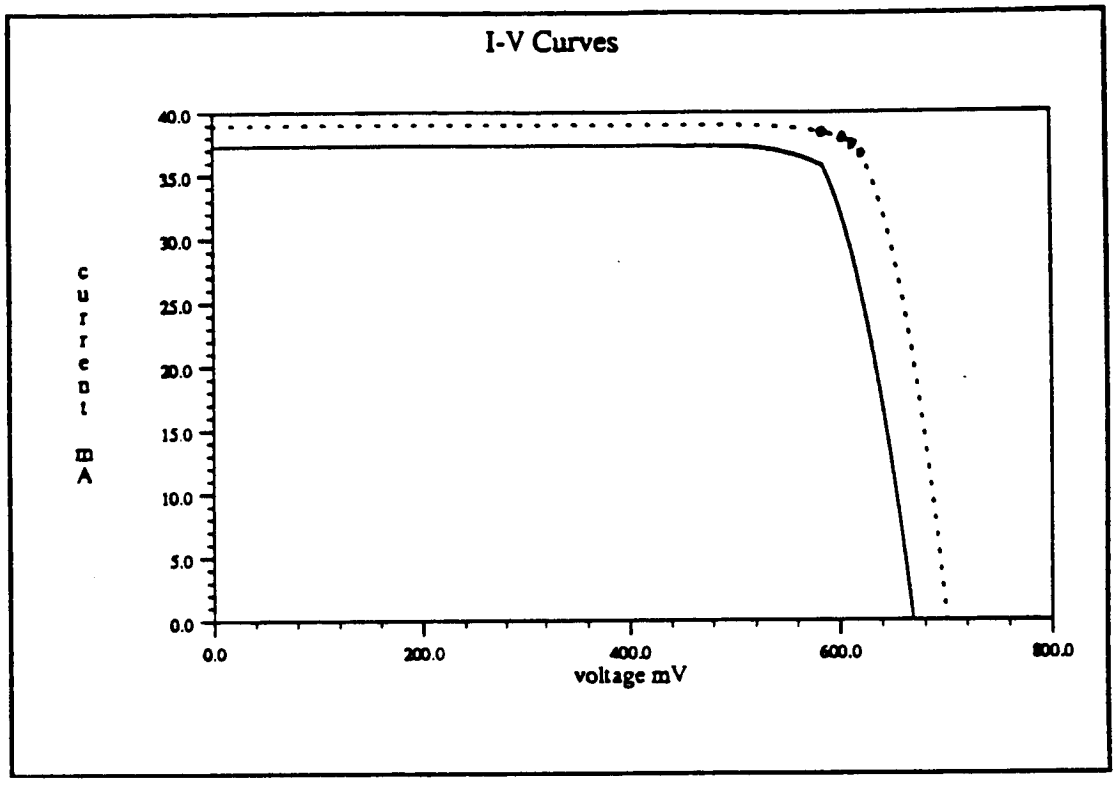

figure 4.2

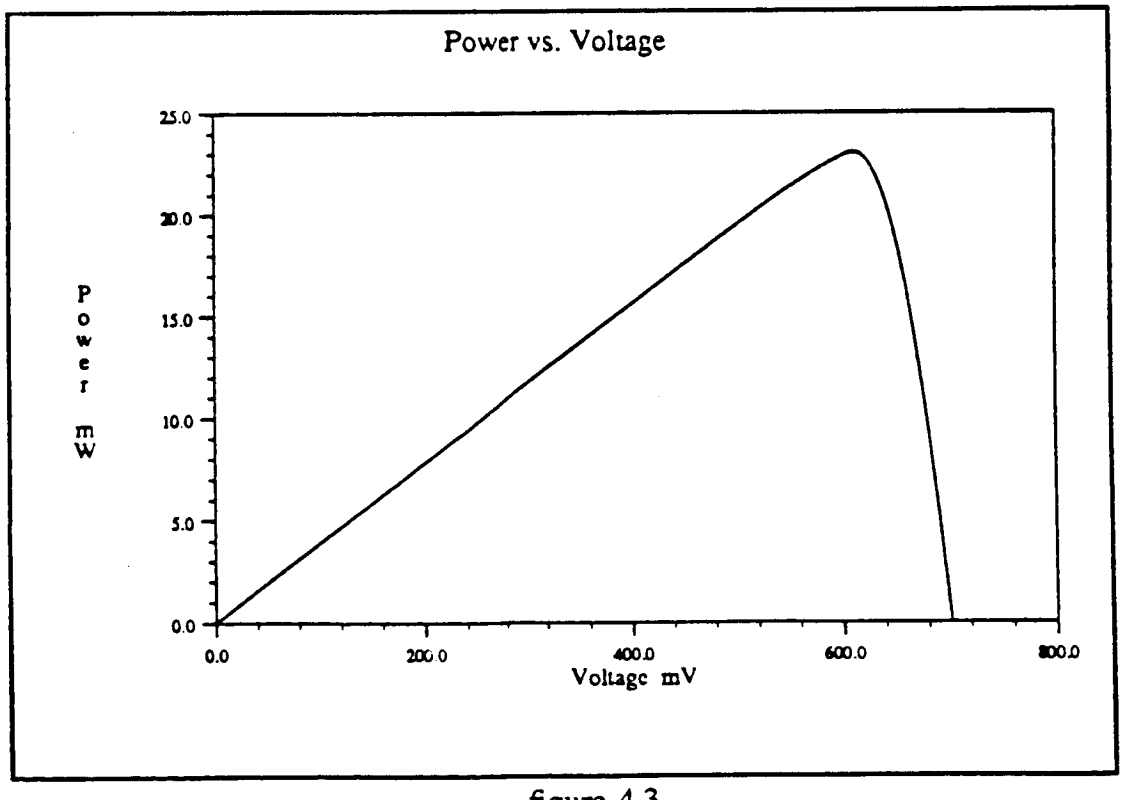

figure 4.3

the first one, are calculated using the iterative strategy outlined above, the time required for an optimization is reduced 800%. Since solving problem P1 can require that the efficiency be calculated many times (10-40, or more depending on the initial estimates of the decision variables), this represents a tremendous savings in computational effort. The 800% reduction reflects the fact that the generation rate did not have to be recalculated, the finite difference mesh did not have to be changed (simplifying the solution of the equilibrium problem), the I-V offsets and V_{oc} were not calculated, and the number of bias voltages needed to converge to V_{mp} was reduced. The latter was achieved by replacing the secant algorithm originally used in SCAP1D with the one dimensional optimization routine to be described in the next section.

The value of 9.7 seconds is the average time required to calculate the efficiency using the iterative strategy. Because the Newton-like algorithm and the maximization for V_{mp} depend on the quality of the initial estimate of the solution, the amount of time required for each efficiency calculation depends on the magnitude of the changes in the decision variables. For the Newton-like algorithm, the initial estimate is the value of n, p, and V at the 250 nodes. For the maximization of power, the initial estimate is the value of V_{mp}. If the changes in the decision variables are small, the time required will be less than 9.7 seconds. This was a dominant reason for using an optimization algorithm that uses finite difference approximations of the gradient. To numerically approximate the gradient requires that the efficiency be calculated after small changes have been made in the decision variables. Therefore, these efficiency calculations can be done with less effort because a high quality initial estimate is provided to the iterative algorithms.

If the changes in the decision variables are large, the time required to calculate the efficiency can be significantly more than 9.7 seconds because the iterative algorithms required to calculate the efficiency will require more time to converge. If the changes in the decision variables are too large, the Newton-like algorithm will not converge. This makes it impossible to make use of the stored solution associated with a previous calculation of efficiency. It would then be necessary to execute SCAP1D in its entirety to determine the efficiency, negating the savings outlined above. It will be shown in the next section that the one dimensional maximization of power as a function of voltage will always converge, so only the Newton-like algorithm may cause the iterative strategy defined above to fail.

The above description is valid if the doping concentrations are the only variables changed by the optimization code. A slightly different sequence of operations must be done if the front junction depth, back junction depth, and/or the cell thickness (referred to as geometric variables) change value. If any of the geometric variables changes value, it is necessary to solve the equilibrium problem

in its entirety and redefine the finite difference mesh. This must be done to insure that the mesh covers the entire device and the equations are solved accurately. The dominating factor determining where the nodes are placed within the device is the position of the junctions (the mesh is defined by a routine in SCAP1D). Due to the large variations in the solution vector in the vicinity of the junctions (particularly the front junction), an increased number of nodes is required in said regions to insure that the equations are accurately solved. Redefining the mesh changes the discretized values of the independent variable x. Hence, it is necessary to recalculate the generation rate as well as the other parameters in the equations (R, Δ_g, μ_n, and μ_p). Even when one of the geometric variables changes value, the considerations used to determine the positions of the nodes result in the nodes being distributed in a similar manner (similar number on each side of the junction, etc.). Therefore, the previous solution vector can still be used as an initial estimate even though the value of the independent variable associated with the solution has changed. The rest of the solution procedure is identical to that described above.

An optimization was initiated from the run that is a basis of table 4.1 allowing only the geometric variables to change. The average time for calculating the efficiency, after the initial call, was 21.8 seconds. This represents a 367% decrease in time compared to running SCAP1D in its entirety, but an increase by a factor of 2.2 when compared to the solution procedure for changes in the doping concentrations only.

The code determines which variables have changed value and follows the appropriate solution procedure. If the solution vector associated with the previous set of decision variables is not in the region of convergence of the Newton algorithm, SCAP1D is run in its entirety to determine the efficiency for the new values of the decision variables. The magnitude of the changes in the decision variables is considered by the optimization algorithm (see section 5.4). Therefore, rerunning SCAP1D in its entirety is a rare occurrence. The computational savings for completing an optimization will be between 400% and 800% when compared to executing SCAP1D in its entirety for each efficiency calculation.

4.2 Maximizing Power as a Function of Voltage

The region of convergence of the secant algorithm originally used in SCAP1D was very limited. This was not a problem because the I_{sc} and V_{oc} were solved for and could be used with the ideal diode equation to provide an excellent estimate of V_{mp}. By comparison, the strategy outlined above uses the V_{mp} of the solution that is stored in memory as the initial estimate of the new value of V_{mp}. Changes in the decision variables during the optimization could result in the failure of the secant algorithm to converge. The magnitude of the changes in the decision

variables that could be solved for using the recursive strategy outlined above is already limited to the region of convergence of the Newton-like algorithm for correcting the solution vectors V, n, and p. It is undesirable to further restrict the magnitude of the changes in the decision variables that can be tolerated before the iterative strategy described in the previous section fails, making it necessary to rerun SCAP1D in its entirety to calculate the efficiency associated with the new values of the decision variables.

Although it was possible to enlarge the region of convergence for the secant algorithm, doing so caused the algorithm to require an excessive number of iterations. Therefore, a one dimensional optimization routine was written and appended to SCAP1D to solve the problem of maximizing power as a function of voltage,

$$\underset{\Delta V}{\text{maximize}} \; (V_{mp}^{old} + \Delta V) \, I_V \; . \tag{4.4}$$

In the above equation, V_{mp}^{old} is the maximum power voltage for the solution that is stored; I_V, which is a function of the voltage, is the current; and ΔV is the change in the voltage. Since determining the current associated with a bias voltage requires the solution of the system of 750 nonlinear equations, it is important that this problem be solved efficiently for the ΔV that results in the new V_{mp}. Only function values are available, and a direction of ascent cannot be assumed. There are no constraints on the value of V_{bias}. As in figure 4.3, the problem will always have a well defined maximum (i.e., power is a concave function of voltage, assured by the physics of a solar cell).

A one dimensional routine was designed to solve the above problem and appended to SCAP1D. The power associated with V_{mp}^{old} is calculated (the vertical move from the solid to the dotted curve in figure 4.2). Then, since the main optimization algorithm (the optimization that is changing the solar cell design variables) is trying to increase efficiency, the one dimensional routine increases V_{bias} by an initial step size. The initial step size used depends on the magnitude of the changes in the design variables (as compared to the values associated with the stored solution), since larger changes suggest a larger change in V_{mp}. If the power associated with the initial offset increases, offsets are continued in the direction of increasing ΔV until the power decreases. Because power is a concave function of voltage, consecutive offsets in voltage changing from increasing to decreasing power implies that the maximum power voltage is contained in that interval (i.e., a bracket is obtained around V_{mp}, see figure 4.3). If the power decreases after the initial offset, the offsets are made in the negative direction (decreasing V_{bias}) until a bracket is obtained around V_{mp}. The magnitude of the initial and any additional

offsets prior to obtaining a bracket around V_{mp} is determined by a heuristic formula that was observed to work well for this application.

Once a bracket is found around the maximum power voltage, restricted quadratic or cubic interpolation is used to determine the optimal offset, ΔV^*. Quadratic interpolation is used if the output powers associated with three voltages are known. Cubic interpolation is used if the output powers associated with four or more voltages are known. As more interpolations are done, the bracket around V_{mp} is tightened, and the voltages associated with the four highest values of power are used to form the next cubic approximation. The interpolation process continues until a sufficiently tight bracket is found around the voltage associated with the maximum power.

There is no convergence region associated with the above algorithm (it will always converge regardless of the initial estimate). However, the quality of the initial estimate of the maximum power voltage, which is determined by the magnitude of the changes in the decision variables, will affect the number of bias voltages required to achieve convergence.

4.3 Convergence Error

SCAP1D was originally designed to report the efficiency to an accuracy of ± 0.005. However, for an optimization algorithm, the calculation of efficiency has to be more accurate by orders of magnitude (± 0.00005). Where accuracy is not defined with respect to a physical device, but rather refers to the ability of the model to predict changes in efficiency due to changes in design. For example, SCAP1D must be able to predict the change in efficiency that would occur if the front surface doping concentration were raised by 1% in a design. The efficiencies predicted do not need to be within 0.00005 of the efficiencies associated with the actual physical devices, but the trend in the efficiencies must be predicted accurately.

The calculation of efficiency using SCAP1D requires two iterative algorithms, the Newton-like algorithm and the maximization of power as a function of voltage. So; as well as the errors due to roundoff, cancellation, and finite precision on a computer (e.g., see [4.1]); each objective function (efficiency) evaluation will be affected by the error associated with solving the iterative algorithms to a finite convergence tolerance. The latter will be referred to as convergence error. Convergence error will generaly far exceed the other forms of numerical error.

The accuracy required in solving the maximization of power as a function of voltage described in the previous section is of critical importance due to the fact that it is embedded in the optimization of the solar cell design variables for

maximum efficiency. To insure that differences in efficiency resulting from relatively small changes in the decision variables (particularly for gradient calculations) will not be obscured or significantly affected, tight convergence criteria are used in the maximization of power as a function of voltage. An example of varying a single variable using the original secant algorithm and convergence criteria used in SCAP1D, which were not designed for such an application, is given in Figure 4.4 . The result of running a nonlinear optimization code to maximize such a function would be disastrous due to the highly nonconcave surface. The algorithm would be prone to stop at any of the numerous local maximums or fail to converge due to bad gradient information, and this was in fact observed in the initial attempts to optimize efficiency. Figure 4.5 is identical to figure 4.4, but the former was generated using tighter (by a factor of 100) convergence criteria and the one dimensional maximization routine described in the previous section. It is seen that the efficiency is in fact concave along the line searched.

Even with much tighter convergence criteria, the one dimensional maximization algorithm requires fewer bias voltages to converge to the V_{mp} than the original algorithm and replaced the former even for single runs of SCAP1D. The reason is made clear by observing that the region around the maximum in figure 4.3 is much better fit by higher order approximations (cubic versus linear in the original algorithm in SCAP1D). Since obtaining the solution vector for a bias involves the solution of 750 nonlinear equations, the reduction in the number of biases required is significant. This is particularly true in an optimization, since V_{mp} must be solved for each time the decision variables are changed.

By changing the numerical methods used in the model, it was possible to tighten the convergence criteria to an acceptable level while decreasing the computational effort. This made it possible to achieve the level of accuracy desired in the decision variables. If figure 4.5 were redone by choosing much smaller increments in the back junction depth, eventually it would start to once again resemble figure 4.4 . For some models, the increase in computational effort that results from tightening the convergence tolerance may be excessive. The optimization code to be described in the next chapter can still operate on a function like that shown in figure 4.4 . The objective evaluations are only taken at points that are sufficiently distant from each other to reflect differences in the objective function that are not obscured by the numerical accuracy of the model. Therefore, the level of accuracy desired in the optimization of the decision variables must be traded off against the computational effort required to reflect that accuracy in the model.

Since the Newton-like algorithm used to solve the system of nonlinear equations is also required for each objective evaluation, the convergence tolerance used could have caused a problem with respect to the concavity of the objective

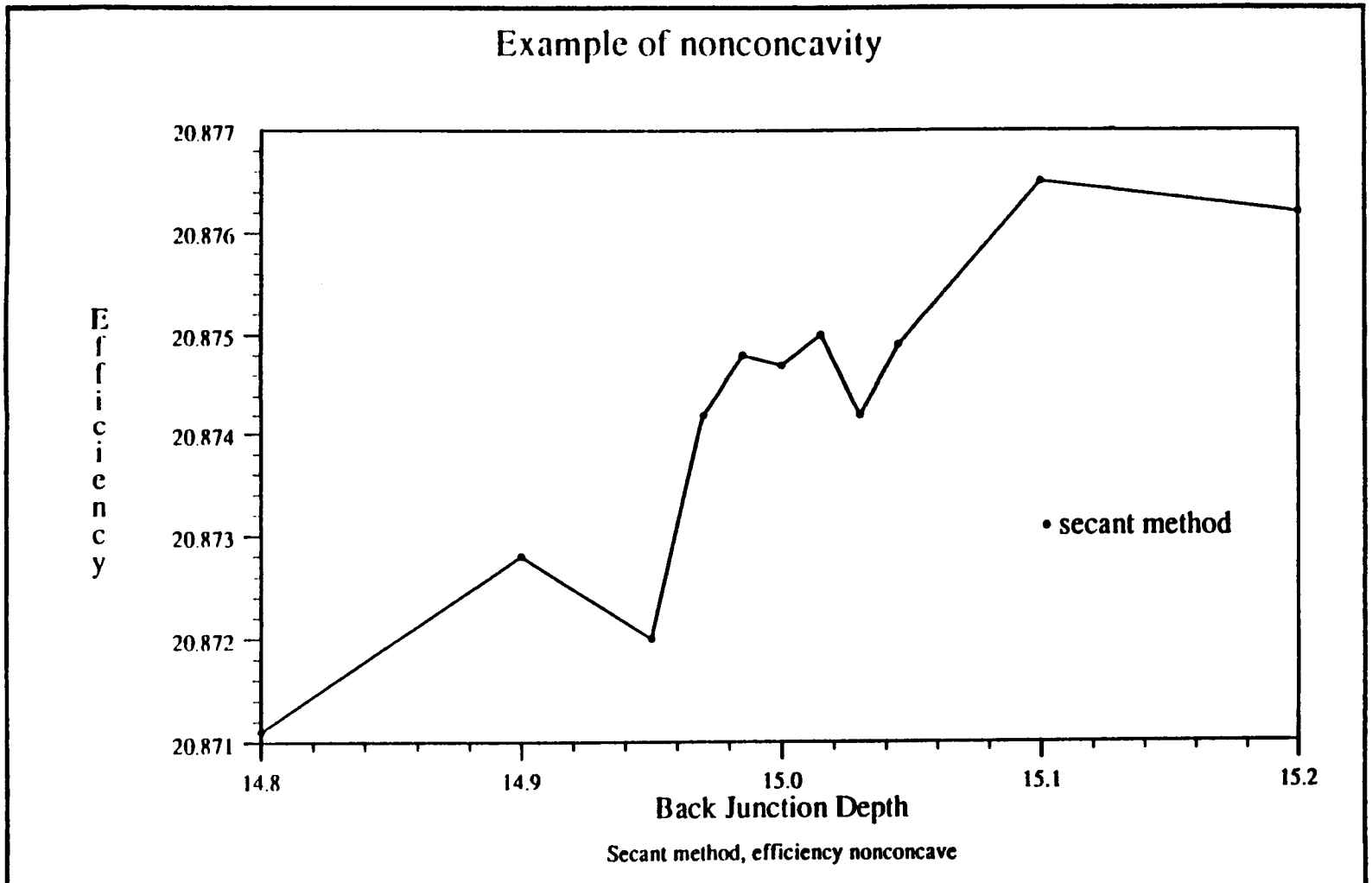
Example of nonconcavity
20.877
20.876
20.875
20.874
20.873
20.872
20.871
Efficiency
14.8
14.9
15.0
15.1
15.2
Back Junction Depth
• secant method
Secant method, efficiency nonconcave

figure 4.4

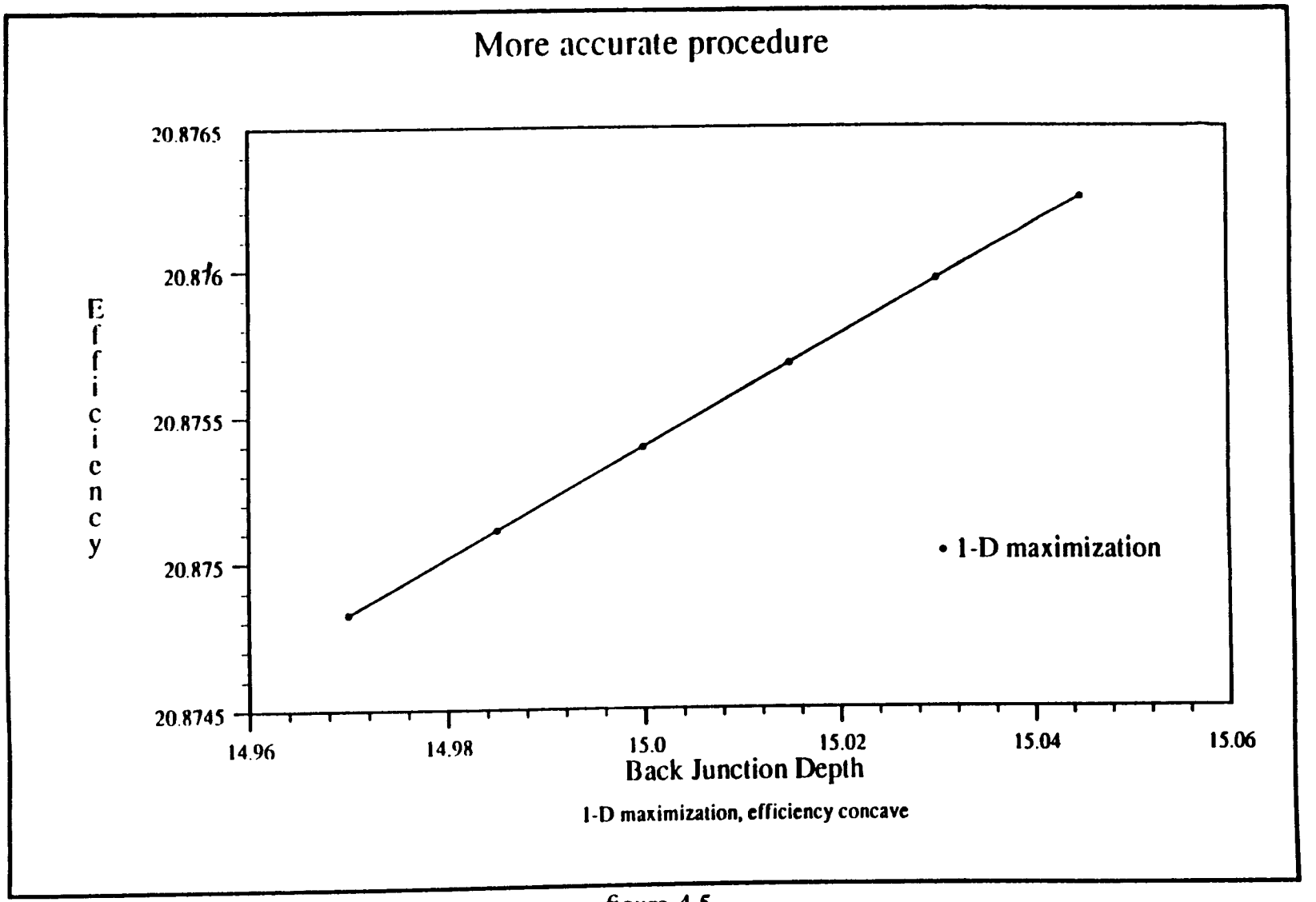
More accurate procedure
20.8765
20.876
20.8755
20.875
20.8745
Efficiency
14.96
14.98
15.0
15.02
15.04
15.06
Back Junction Depth
• 1-D maximization
1-D maximization, efficiency concave

figure 4.5

function. However, the convergence criteria used in SCAP1D were tight enough, and no problems were observed for the accuracy desired in the decision variables.

4.4 Summary

It has been established that significant savings (400% to 800%) in the computational effort required to complete an optimization can be realized by properly adapting SCAP1D to an optimization environment. The savings are realized by avoiding the calculation of the I-V curve each time (except the first) that the optimization requires the efficiency to be calculated to solve problem P1. Instead, the solution of a previous calculation of efficiency is used to initiate the iterative algorithms used in SCAP1D to calculate the efficiency for the new value of the decision variables. This was achieved by developing a new routine for use with SCAP1D that solved the problem of maximizing the power output of the cell as a function of the voltage bias to determine the maximum power voltage.

The system of nonlinear algebraic equations, which is associated with the finite difference transformation of the differential equations, is solved using a Newton-like algorithm. The only limitation of the above method is that the change in the decision variables cannot be so large that the Newton-like algorithm fails to converge.

Depending on which variables change value, different schemes for making use of prior solutions for the calculation of efficiency are implemented. The geometric variables (X_f, X_b, and X_L) affect the finite difference mesh, hence they require more computational effort than the doping variables (D_0, D_B, and D_L).

The one dimensional optimization for the maximum power voltage affects the efficiency associated with a decision vector in the maximization of cell efficiency. Therefore, tight convergence criteria are used. When optimizing a model that requires the use of iterative algorithms to calculate the objective function (some output of the model), the accuracy desired for the decision variables must be traded off against the computational effort required to reflect that accuracy in the objective function.

5 The Optimization Code

The optimization code used to optimize SCAP1D has been outlined in section 2.3 . Several of the components were not discussed in detail. In this chapter, the calculation of the numerical gradient, the implementation of the constraints, the one dimensional optimization routine, and the test for convergence will be discussed in detail. Also, a summary of the intended application will be presented.

The routines will be discussed from the point of view of a minimization. A maximization is simply the minimization of the negative of the objective function. The objective function is represented by f, the gradient by g, and the decision vector by **x**.

5.1 Summary of Application

For best performance, an optimization code should be designed specifically for the intended application. At the same time, it is desirable to write a code that is useful for solving a wide variety of problems. Both objectives are achieved by using inputs to trigger the more specialized options used for optimizing cpu intensive simulations. The discussion in this section will proceed as though the appropriate options are in effect and the code is tailored to the application.

In the previous section, it was shown that the amount of work required to calculate the efficiency depends on which variables are changed with respect to the last solution that was saved (the current best point of the optimization). The amount of computation required is also dependent on the magnitude of the change in the decision vector, since this affects the quality of the initial estimates for both the Newton algorithm and the maximization of power as a function of voltage (both are iterative procedures). If the changes in the decision variables are too large, the Newton algorithm may not converge because the previous solution will not provide a good enough estimate. This will make it necessary to rerun SCAP1D in its entirety, negating the reductions in computational effort explained in the previous section. These considerations suggest that special capabilities will

have to be designed into the code.

The dominating factor in this application is that any calculation of efficiency can be considered expensive enough that a premium should be placed on the number of times the optimization code requires the efficiency to be calculated before achieving convergence.

Assuming it is possible to model the doping concentration throughout the device using a reasonable number of variables, the number of decision variables in the optimization should not be large. Since the objective function is extremely difficult to calculate, an optimization with a large number of variables would be prohibitively expensive in terms of computer time. Therefore, the optimization code could be designed for an application with a limited number of decision variables (e.g., < 20). The formulation in the problem statement (problem P1) has just six decision variables, and a similar formulation without a back surface field (problem P2) requires only four decision variables. Also, the formulation given in the problem statement requires that the optimization code have the capacity to handle simple bounds on the decision variables and linear constraints.

5.2 Calculation of the Numerical Gradient

SCAP1D can be viewed as a black box. The black box supplies an output (the efficiency), which is the objective function for the optimization, when provided with an input (the decision vector, x) There is no closed form representation for what is in the black box, hence analytic gradients are not available. Therefore, the gradient must be calculated numerically. Due to this consideration, algorithms were considered that use only function evaluations (referred to as direct search algorithms).

A major disadvantage of most direct search algorithms is that they require that the objective evaluations be spread out over the feasible region to be searched. This raised difficulties with the recursive scheme described in the previous chapter for using the solution of a previous efficiency calculation to initiate the next calculation, because the changes in the decision variables were too large. A comparison between two algorithms (nonlinear algorithm based on searching the decision space with simplexes [5.1-5.3] and the code described in this report) suggested that it was more efficient, accurate, and reliable to use a variable metric algorithm with numerically calculated gradients.

The calculation of numerical gradients is particularly desirable for optimizing a model such as SCAP1D for two reasons. First, the number of decision variables is small (n is small). Second, the computational effort required to calculate the efficiency is reduced if a good estimate of the solution is provided. This is

because the initial correction of the solution vector (vertical move from the solid to the dotted I-V curve in figure 4.2) and the maximization of power as a function of voltage converge faster. Numerical gradients are taken at the optimum of the last line search (the solution at such a point is stored using the strategy developed in the previous chapter) by slightly offsetting one component of the decision vector (see equation 5.1 below). Hence, an excellent estimate for the next solution is available.

The use of the optimization code described in this report with models that cannot make use of previous objective evaluations to reduce the computational effort may not be as advantageous when compared to direct search algorithms. For example, a model that involves the solution of a large system of linear equations using direct methods or a time simulation that must be run in its entirety for every objective evaluation would require the same effort if a large change or a slight offset was made in the values of the decision variables. However, the first order gradient information provided by numerical gradients allows second order information to be approximated using the quasi-Newton condition. Several authors [e.g., 5.4] favor the calculation of numerical gradients so that the more sophisticated gradient based algorithms can be used, as compared to the generally less sophisticated direct search algorithms. However, care must be taken in applying optimization algorithms such as quasi-Newton algorithms, which were theoretically developed assuming the use of analytic gradients, with numerical approximations of the gradient [5.5-5.7].

The gradient at a given point can be calculated (approximated) numerically by using the the forward difference formula,

$$g_i = \frac{f(x_1,x_2, \ldots, x_i + \Delta x_i, \ldots, x_n) - f(x_1,x_2, \ldots, x_i, \ldots, x_n)}{\Delta x_i} \quad . \qquad (5.1)$$

Δx_i represents a small offset in the ith component of the vector of decision variables. Equation 5.1 provides the ith component of the gradient. The above calculation is repeated for each component of the vector of decision variables. Hence, n objective evaluations are required to determine the gradient using the forward difference formula.

In optimization problems, roundoff error is usually the primary concern when deciding on Δx_i [5.5]. Assuming absolute accuracy, as Δx_i goes to zero, the forward difference approximation approaches the true gradient. For this reason, it is desirable to make Δx_i as small as possible. However, extra care must be taken in the selection of Δx_i when the objective function is a complicated numerical process. For instance, the calculation of efficiency in SCAP1D requires the use of two

iterative algorithms (Newton-iteration and the maximization of power as a function of voltage) whose convergence may obscure the true results of equation 5.1 for small offsets (e.g., see figure 4.4). It is necessary to make Δx_i large enough to insure that the forward difference formula is not affected by such considerations. In general, Δx_i is determined by the numerical processes used in the simulation. It represents the accuracy in the decision variables that can be reflected in the objective function. This can be determined by an analysis similar to the one used to generate figures 4.4 and 4.5 . Δx_i is calculated as a percentage (input to the code) of the current value of x_i. If the absolute magnitude of x_i becomes too small; an absolute, rather than a percentage, offset is used.

A major difficulty with the forward difference approximation of the derivative is that it may suggest a direction that is not a direction of descent. Figure 5.1 illustrates this case. The figure only represents one component of a n dimensional problem. By incorrectly calculating one component of the gradient, it is possible that the direction defined and/or the steepest descent direction may not truly be directions of descent. For example, this is particularly likely to occur when the surface of the objective function has a steep sided valley. The algorithm will halt if the line search subproblem fails to make progress in the direction of search. This may occur far from the true optimum of the n dimensional problem, and the objective may be significantly greater at the point where the algorithm halted. This situation is more likely to occur if one is forced to use fairly large offsets to avoid the numerical problems associated with objectives that are the result of complex computational processes (e.g., computer simulations). The only way to detect such an error is to use the central difference approximation of the gradient.

$$g_i = \frac{f(x_1,x_2, \ldots, x_i + \Delta x_i, \ldots, x_n) - f(x_1,x_2, \ldots, x_i - \Delta x_i, \ldots, x_n)}{2\,\Delta x_i} \qquad (5.2)$$

The central difference formula is modified so that g_i is set to zero if both offsets fail to improve the objective. Figure 5.2 shows a function that would give an erroneous direction of descent using the central difference formula without the above modification. When using this formula, the offset should be chosen to reflect the desired accuracy in the decision variables.

The disadvantage of the modified central difference formula is that it requires two objective evaluations, as opposed to one for the forward difference formula. Therefore, it is desirable to take central differences only when absolutely necessary. Several options are given in the code ranging from always using forward differences to always using central differences to approximate the components of the gradient. The most useful option for numerically intensive simulations uses

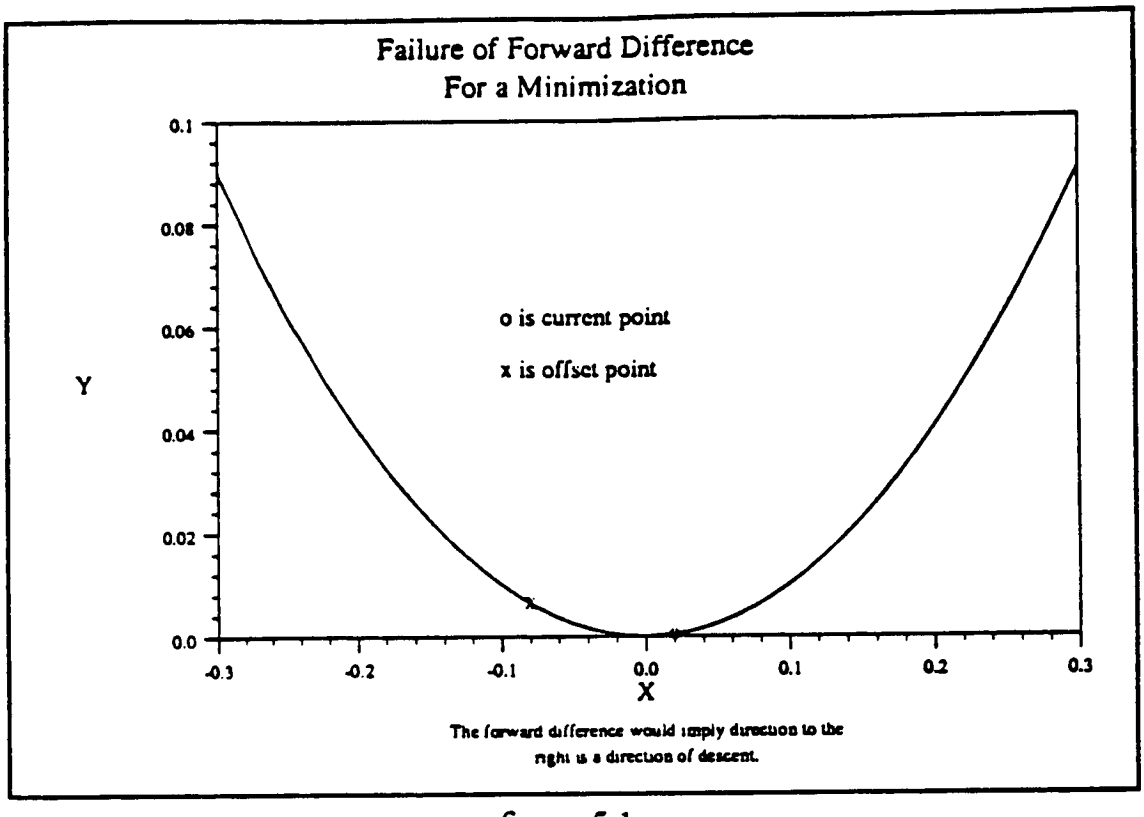

figure 5.1

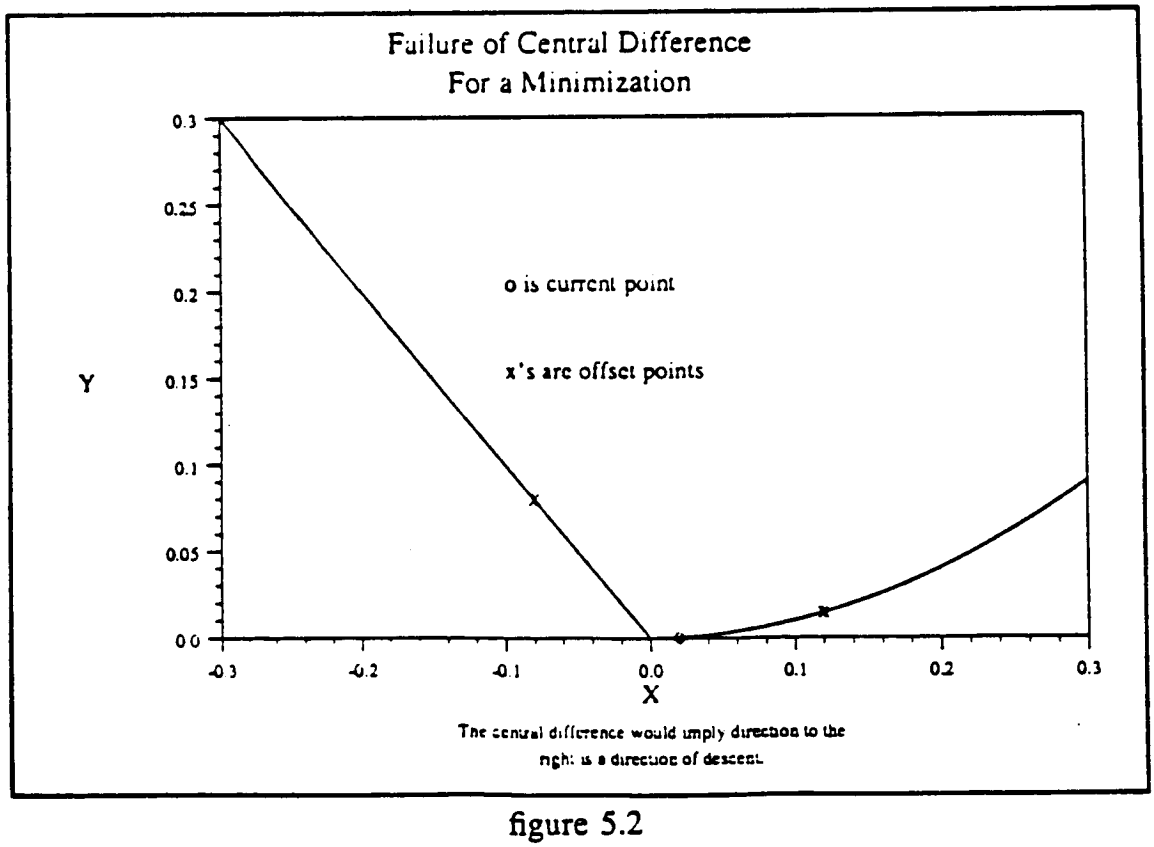

figure 5.2

forward differences until the program is halted due to failure of the one dimensional subproblem to improve the objective function (if this occurs). Any of the decision variables which did not improve the objective function when offset in the forward direction are then offset in the backward direction. The existing gradient and the backward difference are used to calculate the modified central difference. This either results in the numerical gradient being set equal to zero, or a true direction of descent being defined.

Offsets in n linear independent directions are required to solve for the n components of the gradient using equation 5.1. The n directions chosen are usually the component directions, but this is not necessary. This fact can be used to save one of the objective function evaluations needed to calculate the gradient. In finding the minimum along a direction of search, polynomial approximations are used to approximate the objective function along the search direction and locate the minimum. After a point has been accepted (i.e., one dimensional search is completed) another polynomial approximation is made that includes the accepted minimum point. The gradient of the polynomial approximation is calculated at the accepted minimum to the line search and used as the directional derivative at that point. Certain conditions can be used to assure the accuracy of the approximation of the directional derivative (e.g., distance of nearest point along search direction and magnitude of the approximation). If the conditions are met, the component of the search direction of greatest absolute value is not offset. The components of the gradient in the other directions are solved for as usual and used with the approximation of the directional derivative to calculate the remaining gradient component. If forward differences are in use, this saves one objective evaluation each iteration. If n is small, a significant savings in the number of objective function evaluations needed to complete the optimization can result.

5.3 Constraints

Once the gradient has been solved for, the direction of search must be calculated. The method used to solve for the search direction, which has already been presented in section 2.3, uses the BFGS update of the inverse Hessian approximation. Once the direction has been defined, it is necessary to insure that the direction is feasible (satisfies the constraints) and that the minimization along that line remains feasible. The only constraints in problems P1 and P2 are simple bounds on the decision variables and linear constraints. The upper and lower bounds are handled by limiting the step size to insure the one dimensional search along the search direction remains feasible. If any upper or lower bounds are active and the search direction would cause the bound(s) to be violated, those component(s) of the search direction are set to zero.

Linear constraints are handled by reducing the search direction (-Hg) (see [5.8]) and/or limiting the step size to maintain feasibility. The direction of search is reduced only if one of the linear inequalities is tight, so as not to disrupt the convergence properties of the quasi-Newton directions [5.9]. Linear equality constraints should be handled by solving for one of the variables in the constraint in terms of the other variables in the constraint, hence eliminating one of the variables and the constraint from the optimization. In general, models do not require the use of equality constraints to simulate a feasible design, unless such constraints can be easily handled.

5.4 The One Dimensional Optimization Routine

Once a feasible direction has been defined and a maximum feasible step size set (may be infinite), it is possible to solve the one dimensional subproblem. As can be seen from figure 2.1, the one dimensional optimization routine (henceforth referred to as the line search routine) is a very important component of the optimization code. During the course of an n-dimensional optimization, it is generally necessary to execute the line search routine many times. Therefore, considerable effort was made to develop the most efficient code possible.

The problem statement to be solved by the line search is,

$$\text{minimize } f(\mathbf{x} + \alpha \mathbf{d}) \quad . \qquad (5.3)$$
$$0 \le \alpha \le \alpha_{max}$$

The line search routine is provided with the search direction (**d**) and the directional derivative. This makes the application considerably different than the one dimensional routine described in section 4.2 for which a direction of improvement could not be assumed (α can be positive or negative).

The line search routine searches in the given direction until it satisfies the convergence criteria. The convergence criteria used in line search routines vary widely depending on the application. For the application being discussed, it is not of interest to solve the one dimensional subproblem exactly. To do so may require an excessive number of function evaluations, and the n-dimensional optimization may still be far from the region of the true minimum. For the routine described in section 4.2, it was necessary to solve the one dimensional problem with a high degree of accuracy, since there was only one dimension.

The routine used to solve the one dimensional subproblem given in equation 5.3 is based on restricted polynomial approximation. All the step sizes are calculated based on a polynomial approximation of the objective function along the line of search. The step size that minimizes the polynomial approximation is either

accepted or restricted by upper and lower bounds. No effort is made exclusively to reduce the interval of uncertainty for the minimum, and the convergence criterion is not based on a desired bracket of the best step size. Rather, at any step the best possible estimate of the minimum along the search direction is used and incorporated into the approximation, or the line search is terminated.

Figure 5.3 shows the logic of the line search routine. The initial estimate of the step size, α_1, is the smaller of the natural quasi-Newton step size ($|\mathbf{Hg}|$), the optimal step size from the previous line search, the maximum feasible step size, or a limit that is input by the user. The value of the objective function, f_0, and the directional derivative, f_0', are known at the starting point of the search. The initial point of the search is associated with a step size $\alpha_0 = 0$. Once the objective is evaluated at the initial step size, f_1; it is possible to form a quadratic approximation (three conditions for the three coefficients of a scalar quadratic).

$$
\begin{aligned}
c_2\,\alpha^2 + c_1\,\alpha + c_0 &= f(\alpha) \qquad (5.4)\\
c_2\,\alpha_1^2 + c_1\,\alpha_1 + c_0 &= f_1\\
c_0 &= f_0\\
c_1 &= f_0'
\end{aligned}
$$

The coefficient c_2 is solved for, and the minimum of the quadratic is calculated by solving the necessary conditions (gradient = 0), $\alpha_2 = -c_1/2c_2$. The value of α_2 is either accepted as the next step size, a restricted value is used, or convergence is detected. The restriction on the value of α_2 takes the form,

$$\beta_1\,\alpha_1 \le \alpha_2 \le \beta_2\,\alpha_1 \quad , \qquad (5.5)$$

where the values of β_1 and β_2 are different if the polynomial approximation is used for an interpolation or an extrapolation.

The objective value f_2, which is associated with α_2, is included in a cubic polynomial approximation.

$$
\begin{aligned}
c_3\,\alpha^3 + c_2\,\alpha^2 + c_1\,\alpha + c_0 &= f(\alpha) \qquad (5.6)\\
c_3\,\alpha_2^3 + c_2\,\alpha_2^2 + c_1\,\alpha_2 + c_0 &= f_2\\
c_3\,\alpha_1^3 + c_2\,\alpha_1^2 + c_1\,\alpha_1 + c_0 &= f_1\\
c_0 &= f_0\\
c_1 &= f_0'
\end{aligned}
$$

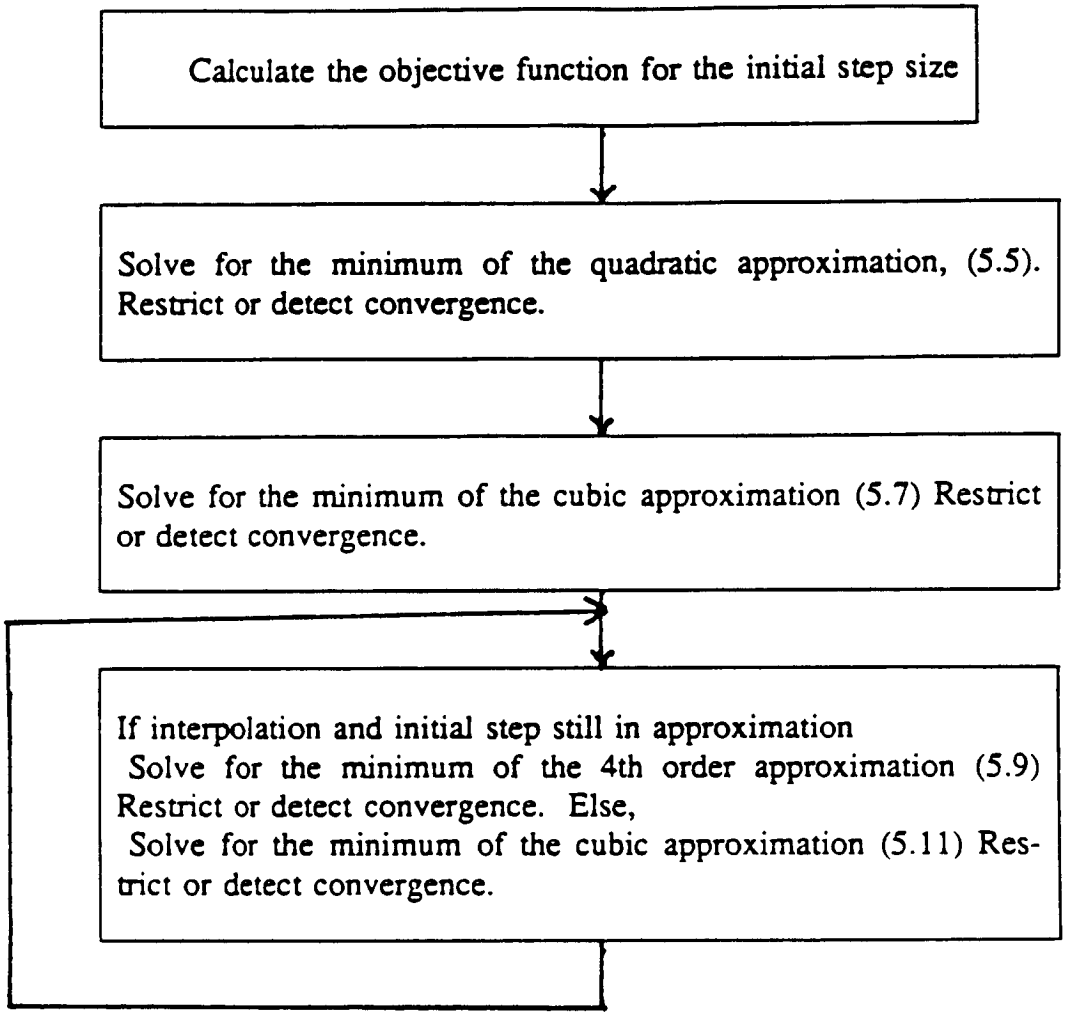

fig. 5.3 Overview of Line Search Algorithm

From the above system of equations, it is possible to solve for the coefficients of the cubic approximation. The necessary conditions for a minimum of the cubic approximation result in a quadratic equation,

$$3\, c_3\, \alpha^2 + 2\, c_2\, \alpha + c_1 = 0 \quad . \tag{5.7}$$

The ambiguity of which root of the quadratic to use is cleared up by using the general form of the solution in the derivative of equation 5.7 and requiring it to be positive (e.g., the minimum is always associated with a positive second derivative). This condition implies that the root associated with adding the radical in the quadratic equation always represents the minimum of the cubic approximation. The value of α_3 (determined from equation 5.7, but rather messy to write down) is either accepted as the next step size, a restricted value is used, or the problem is considered completed.

The logic of the routine now depends on whether a bracket has been found around the optimal step size. If a bracket has (not) been found, the polynomial approximation will be used for an interpolation (extrapolation).

The case of an interpolation is considered first. For an interpolation, the order of the polynomial approximation increases to degree four.

$$c_4\, \alpha^4 + c_3\, \alpha^3 + c_2\, \alpha^2 + c_1\, \alpha + c_0 = f(\alpha) \tag{5.8}$$

$$c_4\, \alpha_3^4 + c_3\, \alpha_3^3 + c_2\, \alpha_3^2 + c_1\, \alpha_3 + c_0 = f_3$$

$$c_4\, \alpha_2^4 + c_3\, \alpha_2^3 + c_2\, \alpha_2^2 + c_1\, \alpha_2 + c_0 = f_2$$

$$c_4\, \alpha_1^4 + c_3\, \alpha_1^3 + c_2\, \alpha_1^2 + c_1\, \alpha_1 + c_0 = f_1$$

$$c_0 = f_0$$

$$c_1 = f_0'$$

The above equations can be used to solve for the coefficients of the fourth order polynomial that approximates the objective function along the line. The necessary condition is now the cubic,

$$4\, c_4\, \alpha^3 + 3\, c_3\, \alpha^2 + 2\, c_2\, \alpha + c_1 = 0 \quad . \tag{5.9}$$

The root is found for this equation by starting a Newton-Raphson iteration from the current best point. This requires very little computational effort, and convergence usually occurs after a few iterations. The value of the minimizing step size calculated from equation 5.9 (α_4) is either accepted, restricted, or convergence is detected.

In the case of an extrapolation, a cubic polynomial approximation, which is based on the objective at four points, is used.

$$c_3 \alpha^3 + c_2 \alpha^2 + c_1 \alpha + c_0 = f(\alpha) \tag{5.10}$$

$$c_3 \alpha_3^3 + c_2 \alpha_3^2 + c_1 \alpha_3 + c_0 = f_3$$

$$c_3 \alpha_2^3 + c_2 \alpha_2^2 + c_1 \alpha_2 + c_0 = f_2$$

$$c_3 \alpha_1^3 + c_2 \alpha_1^2 + c_1 \alpha_1 + c_0 = f_1$$

$$c_0 = f_0$$

The coefficients of the cubic polynomial that approximates the objective along the line can be solved for using the above equations. The solution for the minimum is based on equation 5.7 . The root associated with adding the radical in the quadratic formula is associated with the minimum of the cubic approximation.

The best four points are always retained and any further polynomial approximations are based on these points. If the initial point is no longer one of the best four, one condition (the directional derivative) is lost so that for any further approximations the conditions in the set of equations 5.10 are used. All the step sizes are translated so that the least value of the four retained step sizes is zero.

The formula used to solve for the optimum step size for each of the above polynomial approximations is explicitly coded into the program. This was done by solving each of the linear systems of equations (5.4, 5.6, 5.8, and 5.10) for the coefficients as a function of the step sizes (α's) and the function values (f's). The optimal step size is expressed as a function of the coefficients of the approximating polynomial. The increase in the computational effort required by the higher order approximations is insignificant, particularly for the application being considered in this work, and results in higher accuracy.

The convergence of the line search routine occurs in one of three ways. 1) The accepted step size may be within a tolerance, input by the user, of the current accepted minimum along the line. This implies that the new polynomial approximation did not change significantly. Hence, it is assumed that no significant progress can be made and the line search is terminated. 2) A limit is input on the number of successful interpolations after the minimum is bracketed. If this limit is reached, the line search is terminated. 3) A limit is input on the number of unsuccessful interpolations after the minimum has been bracketed. If this limit is reached, the line search is terminated. The above convergence criteria result in an inexact line search.

The standard practice of doubling the step size until the minimum is bracketed and reducing the step size by one half until the objective is improved is not used. This method can lead to line searches that require excessive objective evaluations for the application being considered and is too dependent on the quality of the initial step size used. The method described above is more tolerant of poor initial step sizes and rarely takes more than four objective evaluations to converge (usually less).

The restricted extrapolation makes it easy to allow the user to control the magnitude of the change in the decision variables allowed at any single step. By making the restrictions functions of the magnitude of the step size, the next step size can be defined to be 100 times the current step size without causing convergence problems (in SCAP1D). Or, if the step size is large, the increase can proceed at a slower pace (e.g., 1.5 times the step size).

5.5 Convergence Criteria

The convergence of the optimization can occur in several ways. A direction of search may be defined, but the line search may fail to improve the objective function. Failure of the search direction is detected when a user input lower limit (ε_x) on the step size is reached while interpolating along the line of search for a point of improvement. If this occurs, attempts are made to define a direction of descent. The search direction is checked to see if it is the direction of steepest descent (reduced and feasible). If not, the objective is calculated along the steepest descent direction at the step size ε_x. If this fails to improve the objective and the forward difference formula was used to calculate the gradient, the modified central difference formula is calculated using the existing forward difference and a backward difference calculation. If the directional derivative along the last line search was used, the component of the gradient approximated is calculated using the modified central difference formula. There are then three possibilities. 1) The numerical approximation of the gradient has a magnitude of zero (all components zero because all offsets failed to improve the objective function), and execution is halted. Else, a function evaluation is made at the step size ε_x in the direction of descent specified by the modified central difference approximation to the gradient. 2) If the objective improves, the line search is completed and execution continues. 3) If the objective fails to improve, execution is halted. This last situation should not occur. If it does, the user should check the offsets being used to calculate the gradient and/or the numerical properties of the objective function (e.g., convergence tolerance of iterative algorithms used in the calculation of the objective, convexity, etc.).

The optimization code has been designed so that it can optimize a function like that shown in figure 4.4. By choosing the gradient offset and the input ε_x correctly, the optimization will only consider decision variables that are far enough apart to disguise the local nonconvexity (sawtooth nature) of the objective. This is important for the intended application because for some simulations it may not be possible to get a smooth (locally convex) objective function, due to the complexity of the numerical process and/or convergence tolerances of iterative algorithms used to calculate the objective function.

There are also convergence criteria for the change in the objective and the change in the decision variables. If the objective function changes by less then ε_f for i_{max} consecutive iterations, execution is halted. If all the decision variables change by less than ε_x for i_{max} consecutive iterations, execution is halted. The values ε_f, ε_x, and i_{max} are all user inputs.

There is also a convergence criterion for the magnitude of the gradient (ε_g). Experience has shown that when calculating the gradient numerically the use of ε_g can result in prematurely halting the optimization. Also, the use of the modified central difference formula insures that once no improvement can be made from a given point the magnitude of the gradient will be set to zero. Therefore, when numerical gradients are used it is advisable to set ε_g very tight.

5.6 Prescaling the Decision Variables

There are numerous examples of how the scaling of the decision variables affects the convergence of nonlinear optimization algorithms. If it is known a priori that the objective function is more sensitive to certain variables, those variables should be appropriately scaled to improve the convergence properties of the optimization. This information is not always known prior to execution of the optimization code. However, for many simulations favorable scaling factors can be defined by examination of the physics of the system modeled and the units (or magnitudes) of the decision variables. In general, a model will be optimized for several different cases defined by variables that are not included in the optimization. Hence, the results of previous runs can be used to arrive at scaling factors for the decision variables. The code has an optional input vector that can be used to scale the variables. Assuming lower and upper bounds on a variable, the range of the variable is reduced by the scaling vector. In equation 5.1, the values of f do not change while the value of Δx_i is reduced by the scaling factor, hence multiplying that component of the gradient by the scaling factor.

5.7 Summary

The iterative processes required to calculate the cell efficiency are dependent on the quality of the initial estimate provided. This makes it desirable to use a code which makes use of numerical approximations to the gradient. The routine used to calculate the numerical approximation of the gradient has been designed to reduce the number of function calls required and improve the reliability of the code.

The quasi-Newton condition is used to approximate the inverse Hessian so that second order information can be used in defining the direction of search. Simple bounds and linear constraints are implemented in a manner that maintains the convergence properties of the quasi-Newton directions.

The one dimensional optimization routine for the line search problem uses restricted polynomial interpolation and extrapolation. The code is very efficient, is less sensitive than standard methods to the quality of the initial step size, and allows the user some control over the magnitude of the change in the decision variables during the one dimensional search (so that prior objective evaluations remain good estimates to the next objective evaluation). Prior scaling of the decision variables is included.

6 Results

In this chapter, some optimization results will be given for the problem statement given in section 2.1 and repeated below for convenience.

$$\text{maximize } \text{eff}(\, D_0, X_f, D_B, X_b, D_L, X_L \,) \qquad \text{(P1)}$$

Subject to the following constraints:

$$14 \le \log D_0 \le 20.6$$

$$14 \le \log D_B \le 20.6$$

$$14 \le \log D_L \le 20.6$$

$$0.1 \le X_f \le 10.0$$

$$0.2 \le X_b \le 50.0$$

$$10.0 \le X_L \le 300.0$$

$$0.0 \le \log D_L - \log D_B$$

$$0.0 \le X_L - X_f - X_b$$

eff = efficiency %
D_0 = net front surface doping concentration [P atoms - B atoms]/cm^3
D_B = net bulk doping concentration [B atoms - P atoms]/cm^3
D_L = net back surface doping concentration [B atoms - P atoms]/cm^3
X_f = Front junction depth μm
X_b = Back junction depth μm
X_L = Cell thickness μm

This formulation uses the complementary error function model for the doping profile (see figure 2.1).

Nonlinear optimization algorithms converge in an iterative fashion to a solution. Models (e.g., SCAP1D) will inevitably will have inaccuracies when compared to the actual physical device. This suggest that nothing is to be gained by enforcing exceedingly strict convergence criteria on a model that is at best an approximation. The manner in which the results are used, however, can also affect the choice of the convergence criteria. It should be possible to compare the results of several related optimizations without the comparison being affected by the convergence criteria. Due to this factor, tight convergence criteria are used, and the results are reported to high accuracy. Despite this fact, the convergence tolerance may affect the comparison of some closely related runs.

Nonlinear optimization algorithms will find only a local extremum (in this problem a maximum) of the objective function. The local maximum may or may not be the global maximum. If certain conditions, pseudo-concavity, hold over the feasible region, then the local maximum will be the global maximum. For general functions, however, such conditions are impossible to establish. No methods exist which can guarantee finding the global maximum for a general function. The concavity of the efficiency surface for a given solar cell design problem, as defined by the technology variables, cannot be established. A sensitivity analysis is used to insure that the solutions found are globally optimal. Solving the optimization for different values of the technology variables also helps to insure the maximums converged to are global.

Due to the volume of results to be presented, the point where the optimization was initiated from will not be presented. A large difference from the initial efficiency to the final efficiency will only result if there is very little knowledge of the effects of the decision variables. The optimizations can be purposefully started from points with very low efficiency to show large improvements in the efficiency. This was done in the early stages of analysis to insure that the problem was concave over reasonably large regions and the code was robust.

It is desirable to start an optimization from the best estimate available as this will tend to decrease the number of function evaluations and the cpu time required to complete the optimization. When doing a series of related optimizations, the optimal solution from a completed optimization usually provides the best estimate for the next optimization to be performed.

Efficiency is shown in problem P1 to be a function of the decision variables only. Efficiency is, however, a function of other inputs to SCAP1D that are not included in the optimization. The illumination (100 mW/cm^3 AM1.5) and the temperature (28 degrees C) are held constant in accordance with the standard conditions presented in [3.25]. The contact and grid resistance are taken as zero (negligible). Shadowing and reflection are assumed to reduce the generation rate by 7%.

It is important to note the shadowing and reflection factor, since its value is not standard in the reporting of results in the general literature. The results presented may be linearly converted to different shadowing factors; 23% efficiency at 7% shadowing and reflection is = 24.73% efficiency with no shadowing and reflection. The relationship is not exactly linear due to variations in efficiency with concentration.

The physics of solar cells assures that efficiency is a monotonic function of some variables (e.g., the technology variables τ_{p0}, τ_{n0}, S_f, and S_b). Such variables would only go to their more favorable bound if included in an optimization as decision variables. The technology variables are of interest because they can be used to represent different levels of technology and/or fabrication processes. By solving optimizations at different values of the technology variables, it is possible to determine their effect on the optimal efficiency and the associated optimal values of the decision variables. This information is valuable for evaluating the benefit of extra processing steps (e.g., surface passivation) and evaluating the likely benefits of technological advances (e.g., higher quality substrate).

To fully investigate the design of silicon solar cells a number of optimizations had to be solved. The main inputs to SCAP1D and the methods used to include them in the analysis are summarized in table 6.1 (all tables and figures for this chapter are in appendix B). Results are presented in this chapter for six different cases, which are defined by specifying the inputs S_f, S_b, and τ_{n0} (τ_{p0} = 1/2 τ_{n0}). In addition, each case considers the effects of other design variables not easily incorporated into the optimization (e.g., back surface reflector). The interpretations of the results are valid only for the case being discussed, and the reader must be cognizant of all the inputs to SCAP1D.

For each case, problem P1 is solved by simultaneously optimizing all the decision variables. A sensitivity analysis is then performed on the optimal solution to determine the effect of using nonoptimal values of the design variables. One method used is to vary one variable while re-optimizing the others. This is equivalent to solving P1 with one of the decision variables held fixed (at a nonoptimal value for P1). A second method of sensitivity analysis is to vary one variable while holding the others fixed at the optimal values associated with problem P1.

The effects of the technology variables are further investigated by parametrically varying them and re-solving the optimization problem. The results are presented as graphs of efficiency versus minority carrier lifetime and contour plots of efficiency as a function of front and back effective surface recombination velocities.

The analysis presented in this section exemplifies the usefulness of using optimization techniques in conjunction with a model. It would be impossible to do such an analysis using heuristic methods to determine the best design. Using such methods one optimization can be very time consuming. Also, the inexact nature of heuristic methods would cloud the comparisons of related runs.

6.1 Case 1

For the first case to be investigated the technology variables were taken as τ_{n0} = 2 ms, S_f = 100 cm/s, and S_b = 100 cm/s. The minority carrier lifetime for holes, τ_{p0}, is taken as half the value for electrons. This represents a cell manufactured from an excellent substrate (may not be currently achievable) with very good surface passivation. A perfect back surface reflector was assumed (R_b = 1.0). Hence, the optical length of the cell is two times the cell thickness. The back surface reflectance represents another variable that should not be included in the optimization as a decision variable (obviously complete reflectance will always be optimal).

Table 6.2 (all tables and figures for this chapter are in appendix B) displays the design that results from solving problem P1. In all the tables to follow, the entry corresponding to table 6.2 will be printed in bold type, as it will form the base line for the sensitivity analysis.

The high sheet resistance of the emitter results because lateral resistance is not included in SCAP1D. This clearly illustrates how an optimization will bring out the weaknesses of a model. For instance, a model which did not include heavy doping effects would result in high doping concentrations being optimal. This is why it is necessary to incorporate the most accurate model possible in an optimization study. The objectionably high sheet resistance will be addressed later in this section.

Tables 6.3-6.10 display the results of all the optimizations done to complete the sensitivity analysis for case 1. The table headings are as follows:

eff = efficiency (%)
V_{oc} = open circuit voltage (mV)
V_{mp} = maximum power voltage (mV)
J_{sc} = short circuit current density (mA/cm^2)
ff = fill factor ([eff x 1000]/[V_{oc} x J_{sc}])
C_{eff} = collection efficiency (% of the generated carriers that are collected)
τ_{bulk} = minority carrier lifetime in the bulk (μs)
L_d = diffusion length in the bulk (μm)
X_L = cell thickness (μm)
X_f = front junction depth (μm)

X_b = back junction depth (μm)
log D_0 = log of the net front surface doping concentration ([P atoms - B atoms]/cm^3)
log D_B = log of the net bulk doping concentration ([B atoms - P atoms]/cm^3)
log D_L = log of the net back surface doping concentration ([B atoms - P atoms]/cm^3)
O_{pl} = multiplicative factor that relates X_L to the optical path length (e.g., a perfect back surface reflector implies $O_{pl} = 2$).

The bulk minority carrier lifetime and diffusion length are calculated using equations 3.17 ($\tau_{bulk} = \tau_n$) and 3.21 respectively. In the code, these parameters are actually a function of the electron and hole concentrations. Therefore, the values that appear in the tables will be accurate as long as the bulk of the device is in low injection (i.e., the majority carrier concentration is approximately equal to the doping concentration). The low injection assumption is explained in detail in section 3.2 . Low injection in the bulk of the device is usually a valid assumption for the incident illumination used in this work (AM1.5 at a concentration of 1.2022, 100 mW/cm^2), and the actual values of τ_{bulk} and L_d will only be slightly less than those that appear in the tables. However, certain designs may result in high injection in the bulk of the device even at an incident power level of 100 mW/cm^2, and these cases will be pointed out.

In solving problem P1, the lower bound on the back junction depth could not be set to zero or a solution may have resulted that had a back surface field ($D_B < D_L$) with a junction depth that was impractically thin. Therefore, the constraint $D_L - D_B \geq 0$ was used to allow the possibility of no back surface field. If the optimization converges to a design that includes a BSF, the question still remains as to the quantitative improvement that the back surface field provides. This is answered by solving the following optimization problem,

$$\text{Maximize } \text{Eff}(D_0, X_f, D_B, X_L) \qquad \text{(P2)}$$

Subject to the following constraints:

$$14 \leq D_0 \leq 20.6$$

$$14 \leq D_B \leq 20.6$$

$$0.1 \leq X_f \leq 10.0$$

$$10.0 \leq X_L \leq 300.0$$

$$0.0 \leq X_L - X_f$$

Table 6.3 shows the results of optimizations for a cell with a back surface field (BSF), with and without a back surface reflector (no BSR, $O_{pl} = 1$); and a cell without a BSF (referred to as a conventional or CV cell), with and without a BSR. Both the BSF and the BSR can only be treated as on/off design decisions (either included or not).

For this case, the cumulative effect of the BSF and BSR resulted in an absolute improvement in efficiency of 1.1% (4.6% improvement). Because efficiency is expressed as a percentage, differences in efficiency will be reported first in absolute terms and then parenthetically in percent difference to avoid confusion. Without re-optimizing for each case, it is dubious if the true difference in performance could be found. Not surprisingly, removal of the BSR results in the cell thickness going to the upper bound of 300 μm to increase the absorption of the lower energy photons. Elimination of the BSF results in higher doping in the bulk of the device (a lower base resistivity). With the increase in bulk doping, the bulk lifetime and diffusion length both deteriorate. In this case, because of the lower bulk doping used in the optimized BSF design, the integrated base doping is lower in the BSF cell. Hence, the BSF results in higher V_{oc} due to decreased bulk and back surface recombination. Also, the BSF results in slightly higher J_{sc} due to better collection efficiency, which is a result of lower bulk doping. Together, these two effects result in an improved cell efficiency.

The conclusion is that a BSF provides a reasonable increase in performance, despite the excellent back surface passivation that is being modeled in this case. The BSF is beneficial because the high lifetime results in a very long diffusion length. The sensitivity to surface recombination is very closely related to the quality of the substrate (see section 6.7), and the high quality substrate in this case results in an improvement with a BSF even for a well passivated back surface.

A sensitivity analysis was completed for each decision variable in problem P1 (the two methods used are described at the beginning of this section). The first decision variable to be investigated was cell thickness. Table 6.4 and figure 6.1 display the results of solving problem P1, but holding the cell thickness fixed. Also, problem P2 was re-optimized at different values of the cell thickness. This allowed a comparison between cells with and without a BSF at a variety of values of the cell thickness. The results are displayed in figures 6.1 and 6.2 and table 6.5 .

The beneficial effect of the BSF is relatively constant from 10 μm to 500 μm with a slight peak at 50 μm. An absolute difference in efficiency of 0.44% (2.0% difference) remains all the way out to 500 μm. Thicker cells with a BSF are superior to CV cells of the same thickness primarily due to the lower bulk doping,

which results in a higher collection efficiency, that can be used in a BSF cell. By contrast, the thinner cells with a BSF are superior to CV cells of the same thickness primarily due to higher V_{oc}. This is very quickly observed by comparing the C_{eff} and V_{oc} columns in tables 6.4 and 6.5 .

The cell thickness is a relatively insensitive variable for both BSF and CV cells at thicknesses $\geq$ 100 μm, which agrees with the conclusions of Lin [1.3]. In fact, the lack of change in the re-optimized values (with BSF) suggests that a parametric analysis should be accurate in observing this trend.

As mentioned above, no definite trend exists in the re-optimized values of the doping concentrations in table 6.4 (with a BSF). Since nonlinear optimization is an iterative process, an optimization cannot be guaranteed to result in the exact optimal values for even a local optimum point. The optimization often halts due to a lack of improvement in the objective function. This only suggests a region has been found where very little progress is being made toward further increasing the efficiency, not necessarily that the decision variables are at their exact optimal values. For a series of related runs, the best interpretations can be made if the differences between the solutions are significant and consistent enough that they can not be explained by convergence tolerances. Therefore, no comment or graphs will be made on changes in the optimal values of the decision variables unless the above criteria are met.

The exponential absorption of the suns energy is the predominate reason that the very thin cells (10 to 25 microns) do so well. In fact, the very thin cells have excellent performance except for the short circuit current. The thinner cells have better V_{oc}, fill factor, and C_{eff} in both BSF and CV cells.

Figure 6.2 displays the optimal value of bulk doping as the cell thickness is varied for a CV cell. As the cell thickness is increased, the bulk doping decreases.

Table 6.6 and the solid line in figure 6.3 display the solution to problem P1 with the front junction depth held fixed while the other variables are re-optimized. The dotted line in figure 6.3 represents the efficiency that results if the other decision variables are fixed at the optimal values associated with a front junction depth of 0.1 μm (bold entry in table 6.6) while varying the front junction depth. Figure 6.4 displays the optimal value of the front surface doping concentration for the re-optimized solution. It is important to re-optimize the front surface doping concentration when varying the front junction depth. Simply changing the junction depth without changing the front surface doping concentration is not a valid comparison. The effect of lowering the bound on the junction depth below 0.1 μm is shown to be minimal.

The re-optimized values of the other design variables suggests that in this case the design of the BSF appears independent of the changes in the front junction depth (i.e., X_b and D_L do not change). The cell thickness does show small changes. Increasing the junction depth results in a larger value of cell thickness being optimal, and this probably leads to the very slight changes that occur in the bulk doping.

Because SCAP1D is a one dimensional code, it does not include the effects of lateral resistance. The optimality in a real cell with a front junction depth of 0.1 μm is suspect if coupled with front surface doping concentrations below 10^{20}. The sensitivity analysis of X_f implies that the lateral resistance can be decreased by increasing X_f without significantly affecting efficiency. Although increasing X_f leads to a lower optimal value for the front surface doping concentration, the lateral resistance still decreases.

Table 6.7 and figures 6.5 and 6.6 illustrate the solution to problem P1 with the back junction depth held fixed. The obvious trend is in the value of the optimized back surface concentration. The optimal value of D_L decreases as the optimization is re-solved at an increased value of the junction depth (figure 6.6). The trends are similar to those observed for front junction depth, but the relative effect on the efficiency is less. Decreasing the lower bound on the back junction depth results in stronger fields near the back surface and a smaller region (though more heavily doped) of the device subject to heavy doping effects, both of which combine to result in a slightly higher V_{oc} (and efficiency).

The cell thickness, which increases slightly as X_b is increased, is the only other design variable to show any change in the re-optimization. The sensitivity analysis of X_f and X_b suggests that the sensitivity analysis could have been achieved by re-optimizing D_0 and D_L respectively.

Table 6.8 and figures 6.7 and 6.8 display the results of the sensitivity analysis for front surface doping concentration. Each point on the graph represents a doubling of the optimal value of the front surface doping concentration The far left point is 1/8 the optimal doping concentration, and the far right point is eight times the optimal doping concentration. The fixed and re-optimized cell designs are represented by the same point in the middle of the graph (i.e., front surface doping concentration is equal to the optimal value). Therefore, variation between the solid and dashed line in figure 6.7 can only occur on either end.

There is very little difference between the efficiencies if the other decision variables are fixed or re-optimized. The re-optimized value of the cell thickness is shown in figure 6.8 . If the front surface doping concentration is increased above the optimal value, the cell thickness is increased. If the front surface doping is too

low, the front surface becomes a more effective recombination center due to the weaker fields and higher minority carrier diffusivity associated with a lower front surface doping. Therefore, the cell thickness is again increased. More will be said about how the optimization uses cell thickness to isolate recombination centers near the surfaces when the recombination velocities are investigated (section 6.8). The bulk doping concentration decreases as the cell thickness increases reflecting the increased importance of bulk recombination in thicker cells.

The results here are in good agreement with the conclusions of Wolfe [1.1], who argued that the beneficial effects of good front surface passivation may be negated by heavy doping effects in the emitter. With good surface passivation, the detrimental effects of heavy doping in the emitter are seen in the steep drop off in efficiency in figure 6.7 . The heavy doping effects in the emitter result in a rapid decrease in V_{oc}. Also, it should be noted that this is at a very thin junction depth (0.1 μm). For a constant profile, a deeper junction would result in a larger region under the influence of heavy doping (hence a more rapid decrease in efficiency as the front surface doping is raised beyond its optimal value). The sensitivity analysis suggests that it is better to dope too low than too high, and there is little that can be done in the re-optimization to avoid the effects of using nonoptimal front surface doping.

There are two other points of interest: 1) While increasing the front junction depth and holding it fixed resulted in a lower value for the optimal front surface doping concentration, the reverse situation is not true. The front junction depth remains at the lower bound as the front surface doping concentration is decreased and held fixed. 2) The optimal value of D_0 results in the highest value of V_{oc} in the sensitivity analysis. The same situations exist with respect to the back junction depth and the back surface doping concentration.

Table 6.9 and figures 6.9 and 6.10 show the results of the sensitivity analysis for bulk doping. The scale for efficiency in figure 6.9 is much coarser than in figure 6.7, reflecting the fact that in this case bulk doping is a more sensitive variable than front surface doping. The maximum cell thickness in figure 6.10 is associated with the optimal bulk doping.

The re-optimization results in much thinner cells when the bulk doping is greater than the optimal value. This is primarily to offset the increased bulk recombination that would result at the higher doping concentrations. As a result, V_{oc} does not deteriorate dramatically, but the decrease in cell thickness results in a decrease in the short circuit current.

When the bulk doping is decreased from the optimal value, the cell thickness decreases again in response to the increasing series resistance. The increase in

series resistance is due to a loss of base conductivity modulation [6.1]. Although thinner cells with lower bulk doping result in a cell with higher V_{oc}, the rapid fall off in the fill factor due to high series resistance results in a cell of lower efficiency.

Table 6.10 and figures 6.11 and 6.12 show the results of the sensitivity analysis for back surface doping concentration. The trends are very similar to those for front surface doping concentration. In the re-optimization, the cell thickness is increased to isolate the generated carriers from the recombination that occurs near the back surface. When a back surface doping concentration greater than the optimal value is used, the increased Auger recombination results in a decrease in V_{oc}. At the same time, the re-optimization results in a thicker cell with lower bulk doping, which results in a slight increase in J_{sc}.

When a back surface doping concentration less than the optimal value is used, the cell thickness again increases to isolate the carriers generated from the more effective recombination center, which is due to weaker electric fields and higher minority carrier diffusivity, at the back surface. The cell efficiency is considerably less sensitive to using a nonoptimal value of D_L than D_0. However, the same arguments made by Wolf about the front surface hold for the back surface (i.e., the effects of better surface passivation are negated if the surface doping concentration is too high), as suggested by Weaver [1.5]. The increasing negative slope in figure 6.11 suggest that doping more than eight times the optimal value would seriously affect cell performance. Once again, it is better to dope too low than too high.

6.2 Case 2

For the second case to be investigated, the technology variables were taken as τ_{n0} = 1 ms, S_f = 1,000 cm/s, and S_b = 1,000 cm/s. The minority carrier lifetime for holes, τ_{p0}, is taken as half the value for electrons. This represents a cell manufactured from an excellent substrate and with good surface passivation. The lifetime of 1 ms has been reported for substrates manufactured using the float-zone (FZ) process.

The results for the solution to problem P1 are given in table 6.11 . Tables 6.12-6.19 and figures 6.13-6.23 present the sensitivity analysis in the same fashion as for case 1. Most off the trends are the same qualitatively, but not quantitatively. For instance, the increase in surface recombination velocities results in several quantitative changes. The discussion will be limited to avoid repetition.

One result of the increase in back surface recombination velocity is that BSF cells do considerably better than CV cells. The best BSF cell has absolute increase in efficiency of 1.15% (5.57% improvement) over the best CV cell if the upper

bound of 300 μm on X_L is observed. The increase is primarily due to better collection efficiency in the cell with a BSF, as the increase in V_{oc} is only about 6 mV. The use of a BSF allows a lower value of bulk doping to be used. The lower value of D_B results in higher C_{eff} and J_{sc} due to better minority carrier lifetime and diffusion length. The maximum difference in efficiency for BSF and CV cells of the same cell thickness occurs at 100 μm. Unlike the first case, there is a significant variation in the benefit of a BSF with cell thickness.

In figure 6.14, decreasing cell thickness with a BSF and re-optimizing leads to a reduction in bulk doping concentration (i.e., a higher resistivity base). This is opposite the trend observed without a BSF. The combined effects of the BSF and the BSR result in an absolute increase in efficiency of 1.49% (7.3% improvement).

This case provides an excellent example of how optimizing with and without a BSF effects the cell design. A standard rule of thumb in cell design is to compare the diffusion length with the cell thickness. If the diffusion length is greater than the cell thickness, then the BSF should provide a reasonable increase in cell efficiency. However, both the diffusion length and the cell thickness are dramatically affected depending on whether or not the optimization is done for a CV or BSF cell. Lower bulk doping and thinner cells invariably result when a BSF is included. The optimal value of cell thickness for the CV cell was 500 μm with a bulk doping of 6.7×10^{16}, while the BSF cell had an optimal thickness of 280.1 μm with a bulk doping of 2.0×10^{16}. For the CV cell, the diffusion length is 461 μm, which is less than the cell thickness of 500 μm. Hence, one could reach the erroneous conclusion that the best cell design is a CV cell if problem P2 were solved first and problem P1 was not solved.

The sheet resistance given in table 6.11 that is associated with the optimal junction depth is once again too high (988 Ω/□). The sensitivity analysis with respect to front junction depth suggests that the junction can be made deeper if the front surface doping concentration is re-optimized. For example, the efficiency at a fixed junction depth of 0.5 μm is only slightly lower if the problem is re-optimized, but the sheet resistance of the emitter decreases to 360 Ω/□. Once again, it is necessary to re-optimize or the efficiency drops off radically. This suggests that a parametric analysis in which only the front junction depth is changed would lead to an entirely different conclusion about the sensitivity of the front junction depth. As the junction depth is increased, the front surface doping concentration must be decreased or a large region of the cell is subject to heavy doping effects, and the cell quickly becomes emitter dominated.

The sensitivity to the front junction depth is greater in this case than it was in the previous case. This is because the front surface recombination velocity is

greater. The decrease in minority carrier lifetime results in the opposite trend (i.e., less sensitivity to the surfaces), but the former dominates the differences between cases one and two. As the front surface passivation is degraded (S_f is increased), the cells will become increasingly sensitive to the front junction depth, and the blue response of the cell will deteriorate if the junction depth is increased to reduce the lateral resistance.

For the sensitivity analysis of the back junction depth, the same trends are observed as in the previous case. However, the increase in the back surface recombination velocity makes the back junction depth a more sensitive variable.

Since the optimal cell thickness is near the upper bound, the re-optimization when the front or back surface doping concentration is varied has less effect (in the last case the cell thickness was the primary means of compensating for nonoptimal doping concentrations at the surfaces). Also, the higher recombination velocities result in higher doping concentrations at the surfaces, for stronger electric fields and lower minority carrier diffusivities. Hence, increasing the doping concentrations to eight times their optimal values results in significant Auger recombination and bandgap narrowing, and larger reductions in efficiency (as compared to the first case). There is less effect if the doping concentrations are reduced from their optimal values. Once again, if unsure of the optimal value of surface (front or back) doping concentration, it is better to dope too low than too high.

As in the previous case, in the sensitivity analysis for the bulk doping concentration, the thickest cell is associated with the optimal value of the bulk doping concentration. In the sensitivity analyses for D_0 and D_L, the optimal value results in the highest value of V_{oc}.

6.3 Case 3

For the third case to be investigated, the technology variables were taken as τ_{n0} = 1 ms, S_f = 1,000 cm/s, and $S_b = \infty$ cm/s. The infinite back surface recombination velocity represents an ohmic contact. The minority carrier lifetime for holes, τ_{p0}, is taken as half the value for electrons. This is identical to the previous case, but without back surface passivation.

The results for problem P1 are given in table 6.20 . Both the upper bound for cell thickness and back junction depth are active (the front junction depth remains at the lower bound). The optimal values for these variables without an upper bound were found in their respective sensitivity analysis (X_L = 390.7 μm and X_b = 112 μm). The results of the sensitivity analysis for case 3 is given in tables 6.21-6.28 and figures 6.24-6.32 .

The advantage of the cell with a BSF (absolute difference of 1.3%) is not much greater than the previous case (absolute difference of 1.15%). However, the sensitivity analysis with respect to cell thickness with and without a BSF results in much greater differences for thin cells. a comparison between tables 6.13 and 6.22 shows that poor back surface passivation severely effects the efficiency of thin cells even with a BSF. The drop in efficiency is a result of poor V_{oc}. V_{oc} deteriorates due to increased back surface recombination and recombination in the BSF (more heavily doped in thin cells).

In table 6.21, the optimal CV cell has a higher V_{oc} than the optimal BSF cell because the higher bulk doping used in the CV cell results in significantly greater integrated base doping. The reason that the cell with a BSF is superior in efficiency is that it attains a better collection efficiency and hence improved J_{sc}. The cells are of the same thickness, so this increase is due to lower bulk doping. The lower D_B for the BSF cell results in significantly higher τ_{bulk} and L_d.

The effectiveness of the BSF is clearly illustrated by the effect of the BSR on the CV and BSF cells. The cell with a BSF still shows about one half percentage point improvement with the addition of a BSR. Even though both cells are the same thickness (300 μm), the use of a BSR for a CV cell provides only half as much improvement in efficiency. This is because with the addition of a BSR most of the increased generation occurs near the back of the cell where the collection probability is low for the CV cell.

The optimality of a thicker back junction for this case agrees well with the conclusions of Lindholm and Sah [1.7]. Figure 6.28 suggests that whether the sensitivity of X_b is studied parametrically or re-optimized the same conclusion would be reached, although the actual numbers would differ slightly. The sensitivity of the back junction depth reflects the need to keep the generated minority carriers from diffusing to the recombination center at the back surface. The very thick back junction depth can almost be considered a form of nonconstant bulk doping (referred to as a drift field or DF cell in [1.7]).

The optimal value of the back surface doping concentration decreases as the junction depth is increased (figure 6.29) to avoid excessive recombination. The doping concentration, however, remains at a level high enough to significantly degrade the minority carrier diffusivity as this is the mechanism for shielding the minority carriers from the back surface in the DF cell. In figure 3.4, the electron mobility decreases rapidly for doping concentrations between 10^{16} and 2.5×10^{18} (the log of which is 18.4).

All the previous results have suggested that it is better to dope the surfaces too low than too high. In figure 6.32, however, the efficiency decreases more

rapidly if the back surface doping concentration is below the optimal value. This is because if the doping concentration is reduced below 2 x 10^{18} the electron mobility increases rapidly. Hence, the effectiveness of the BSF, which relied primarily on decreasing the electron (minority carrier) mobility, is reduced.

If D_L is greater than the optimal value, the re-optimization reacts by decreasing the back junction depth. This is done to reduce the region of the device subject to heavy doping. In [6.2], the minority carrier reflecting capacity of high-low junctions was found to be significantly impacted by Auger recombination.

The fact that the bound on cell thickness is active results in little change between the fixed and re-optimized values calculated during the sensitivities of the front and back surface doping concentrations. In the first two cases, the cell thickness was the variable that changed most significantly.

6.4 Case 4

For the fourth case to be investigated, the technology variables were taken as τ_{n0} = 0.4 ms, S_f = 10,000 cm/s, and S_b = 10,000 cm/s. This was the lifetime first suggested when equation (3.14) was derived. The surface recombination velocities are high enough to have substantial impact on the efficiency. The minority carrier lifetime for holes, τ_{p0}, is taken as half the value for electrons. This represents a cell manufactured from a medium quality substrate with ineffective front and back surface passivation.

The results for problem P1 are given in table 6.29 . Due to the higher front surface recombination velocity, the optimal value of the front surface doping concentration is higher than in the previous cases. Higher surface doping concentrations are required to provide stronger electric fields to shield the generated minority carriers from the surfaces and reduce minority carrier diffusivity. The higher front surface doping concentration lowers the sheet resistance of the emitter, hence it will not be necessary to make the junction as deep to lower the lateral resistance. This is fortunate because with poor front surface passivation the sensitivity to junction depth is greater (see figure 6.35), and the blue response of the cell falls off rapidly.

Both the upper bound for cell thickness and back junction depth are active (the front junction depth remains at the lower bound). The true optimal value for these variables is determined in their respective sensitivity analysis. The results of the sensitivity analysis for case 4 is given in tables 6.30-6.37 and figures 6.33-6.42 .

The sensitivity due to back junction depth is of particular interest, because it reveals that the efficiency is not always a concave function of the decision

variables. If the optimization were started at a back junction depth less than 1.0 μm, a local minimum that is not the true global minimum would result. This suggests the necessity of a complete sensitivity analysis. The optimal value for the back junction depth changes discontinuously from the lower bound to the upper bound as the back surface recombination velocity is increased from 1,000 cm/s to 10,000 cm/s (this was observed by performing a series of optimizations as S_b was varied). The change occurs when the efficiency associated with deep junction depths (a local maximum) is greater than the efficiency associated with thin junction depths (also a local maximum). Throughout the region tested ($1{,}000 \leq S_b \leq 10{,}000$), both local maximum existed. This very clearly illustrates how the technology variables perturb the efficiency surface (the surface of the objective function).

Due to the high value of S_f, the optimal value of the front surface doping concentration is quite high (7.2×10^{19}). Therefore, when the value of D_0 is increased beyond the optimal value in the sensitivity analysis, there is a significant reduction in the efficiency due to extreme heavy doping effects.

6.5 Case 5

For the fifth case to be investigated, the technology variables were taken as τ_{n0} = 0.1 ms, S_f = 1,000 cm/s, and S_b = 1,000 cm/s. This lifetime is meant to represent those available in the sheet technologies. Hence, the upper bound for cell thickness was decreased to 100 μm for problems P1 and P2. It may be that even lower lifetimes have to be considered, and this is done in the investigation of the technology variables. Both surfaces are passivated in this case. The minority carrier lifetime for holes, τ_{p0}, is taken as half the value for electrons.

The results for problem P1 are given in table 6.38 . The upper bound for cell thickness is active (the front junction depth remains at the lower bound). The true optimal value for cell thickness is given in the sensitivity analysis. The results of the sensitivity analysis for case 5 is given in tables 6.39-6.46 and figures 6.43-6.52 .

Table 6.40 shows that at this lifetime it is still possible to get high values of V_{oc}, fill factor, and C_{eff} from very thin cells. In figure 6.44, the bulk doping concentration (with a BSF) increases with decreasing cell thickness, until very thin cells (<25 μm). This is different than in the first four cases and reflects the importance of bulk recombination for a low-lifetime substrate. The optimal value of the cell thickness is much less than in case 2. Also, there is significantly less reduction in efficiency for the very thin cells, when compared to the efficiency at the optimal cell thickness. These are both expected results for a lower lifetime

substrate.

6.6 Case 6

For the sixth case to be investigated, the technology variables were taken as τ_{n0} = 0.1 ms, S_f = 1,000 cm/s, and S_b = ∞ cm/s. This case is the same as case 5, except there is no back surface passivation.

The results for problem P1 are given in table 6.47 . The upper bound for cell thickness is active (the front junction depth remains at the lower bound). The true optimal value is determined in the sensitivity analysis for cell thickness. The results of the sensitivity analysis for case 6 are given in tables 6.48-6.55 and figures 6.53-6.61.

Due to the thin cell and the poor lifetime the optimal value of the back junction depth does not reach the upper bound. The BSF field provides considerable improvement at very thin cell thicknesses when compared to the same thickness cells with no BSF. As in the previous cases with poor back surface passivation (three and four), the thin cells no longer provide improved V_{oc}, fill factor, or C_{eff}.

In figure 6.61, significant differences result between the re-optimized and the fixed cases because the back junction depth is used to compensate for the use of nonoptimal back surface doping concentrations (see table 6.55).

6.7 Analysis of Lifetime

The effects of varying τ_{n0}, the minority carrier lifetime in lightly doped silicon (saturation lifetime), are given in table 6.56 and figure 6.62. Each point on figure 6.62 is the result of an optimization and represents a different cell design. The optimal values of the decision variables for each point are given in table 6.56 . The results are given at seven different levels of surface passivation. The front and back surface recombination velocities are taken as the same value. In the next section, all combinations of the surface recombination velocities will be considered. Lifetimes greater than those currently achievable are included in the analysis. The efficiency of 25.258 % would convert to ≥ 27.16 % if shadowing and reflection were disregarded, which is approaching the theoretical maximum.

The most obvious trend is the increasingly detrimental effect that recombination velocities have at higher lifetimes. As the substrate quality increases, cell performance is easily dominated by the surfaces. The contribution to the saturation current by surface recombination, even at relatively low values of surface recombination velocity, becomes increasingly important. At very high lifetimes, recombination velocities as low as 100 cm/s will result in large losses in efficiency. Improvements in the saturation lifetime beyond 1 ms will not yield significant

increases in efficiency unless the effective front and back surface recombination velocities are ≈ 100 cm/s or lower.

Table 6.56 illustrates that higher lifetimes generally result in higher values of the front and back surface doping concentrations being optimal. However, the trend in the bulk doping concentration is less clear, as this value is strongly influenced by the cell thickness, which varies drastically for the different lifetimes.

The curves in figure 6.62 are affected by the upper bound on the cell thickness (300 μm) in problem P1 for recombination velocities greater than 1 cm/s. The results in table 6.56 show that the upper bound is almost always active at the higher lifetimes. The lower lifetimes tend to have lower values of optimal cell thickness and are not as severely affected by the upper bound. The increases in efficiency for cell thicknesses greater than 300 μm would be the result of isolating the generated carriers from the recombination centers at the surfaces. Previous results suggest that the increase in efficiency that would result from increasing the cell thickness beyond 300 μm would be marginal, and increasing cell thickness beyond 300 μm for cells fabricated from a high quality silicon substrate may not be a cost effective design strategy.

The curve for 1 cm/s (log sf = log sb = 0) shows a sudden increase in slope at higher lifetimes. This is due to the emergence of a new local maximum which becomes the global maximum at high lifetimes and low surface recombination velocities. This illustrates the nonconcavity of efficiency as a function of the decision variables and how the technology variables affect the efficiency surface. Table 6.57 shows a comparison of the local maximums for different values of the technology variables. At a lifetime of 10 ms and surface recombination velocities of 1 cm/s, the usual maximum ($D_B \approx 10^{16}$) disappears. For several other cases, both local maximums exist. Finally, for the last case in table 6.57, the local maximum around $D_B = 10^{14}$ disappears. Where both maximums exist, the solution that the optimization will converge to depends on where the optimization is started from. The true optimum value of the decision variables will change discontinuously as the recombination velocities are lowered and the lifetime is increased.

The bulk minority carrier lifetimes and diffusion lengths given in table 6.57 for the thin cells with low bulk doping may be significantly lower due to the fact that some of the cells may be approaching high injection in the bulk.

In table 6.57, the thinner cells have higher V_{oc} and C_{eff}. However, thinner cells result in a shorter optical path and a decrease in J_{sc}. The very thin cells are extremely sensitive to surface recombination, and the associated local maximum exists only for cells with excellent front and back surface passivation. The optimal thickness drops substantially with lifetime (145.1 μm at 10 ms, 94.8 μm at 5 ms,

and 49.7 μm at 2 ms). As the lifetime drops and the optimal cell thickness decreases, the local maximum is no longer globally optimal due to the rapid decrease in J_{sc}.

The fill factor, which is a strong function of V_{oc}, in some cases is considerably higher for the local maximum associated with a lower value of V_{oc}. This is due to a loss of base conductivity modulation (i.e., increased series resistance) that occurs at low bulk doping. This, as well as lower bulk recombination, is the reason that the optimal value cell thickness is so thin.

If the back surface is well passivated, it would be expected that the CV cell would do almost as well as the BSF cell. For example, the case of log $S_f = 0$ and log $S_b = 0$ represents excellent surface passivation, and the above statement is true for the cases where the more common local maximum ($D_B \approx 10^{16}$) is the global maximum. However, at the lifetimes of 10, 5, and 2 ms the CV efficiency approaches the local maximum which is not global (see table 6.58). The true optimal design in these cases requires a BSF even with a well passivated surface to attain the global maximum. This may be due to better conductivity modulation with the BSF cell, but the boundary conditions of the model require that the majority carrier concentration equal the net doping concentration at the contacts. Because the back contact is not heavily doped, which was assumed in the formulation of the boundary conditions, the effect of doping concentrations as low as 10^{14} at the back contact may be equivalent to surface recombination. From a practical standpoint, the BSF design is more desirable due to better contact properties (lower contact resistance at the back contact due to higher doping). The above consideration is important in analyzing the usefulness of a design because contact resistance is assumed negligible and is not included in the calculation of efficiency in this work.

When the lower bound on bulk doping was lowered to 10^{10}, the optimal bulk doping went to the lower bound resulting in a very slight increase in efficiency (for the maximums associated with very light bulk doping).

6.8 Analysis of Surface Recombination Velocities

The next runs were made to examine the sensitivity of the efficiency to the recombination velocities. The surface recombination velocities quoted are "effective" surface recombination velocities. In reality, the device will have different recombination velocities at the silicon - silicon dioxide interface and the silicon - metal interface. Even a cell with passivation under the contacts (a thin SiO_2 layer) can still be expected to have different recombination velocities due to the differences in the levels of surface passivation. In a one dimensional code, the

effective surface recombination velocity is assumed to equal the overall recombination velocity that would result on a two dimensional surface. It is not meant to be the recombination velocity measured away from the contacts.

To optimize all combinations of SF and SB of interest required considerable effort. It was decided that the problems would be solved in the form of problem P1 and P2 with R_b = 1.0 (O_{p1} = 2). This was required because it was not known a priori what the optimal cell thickness would be. The upper bound for cell thickness varied depending on the lifetime being considered. It was shown in the previous results that a back surface reflector used with a BSF cell results in an absolute increase in efficiency of 0.46 percentage points at a cell thickness of 300 μm.

The results for solving problem P1 at τ_{n0} = 2.0 ms with an upper bound on cell thickness of 500 μm for a variety of combinations of recombination velocities are given in table 6.59 . In the cases with poor surface passivation, the upper bound of 500 μm was reached. As discussed above, since all runs were made with R_b = 1.0, this does not appear to be done primarily to increase the optical absorption. Rather, the optimization was reacting to the recombination centers at the front and back surfaces and the large value of the diffusion length that is associated with this lifetime. Thin cells resulted only when both the front and back recombination velocities were 100 cm/s or less. As expected, when the back surface recombination velocity was high, the optimization increased the cell thickness to isolate the carriers generated by the light from the back surface by increasing the cell thickness. When the front surface recombination velocity is increased, the optimization reacts by increasing the cell thickness to isolate the carriers generated by the light reflected off the BSR from the front surface. This is observed by the increase in cell thickness even when the back surface recombination velocity is very low, which implies the increase was not due to the large value of the bulk diffusion length (e.g., compare the design for log S_f = 0 and log S_b =0 to the design for log S_f = 3 and log S_b = 0). The optimization is trading off all the effects of increased cell thickness, which include increased absorption, increased bulk recombination, and isolating the generated carriers from the surfaces. The results suggest that for a lifetime of 2 ms isolating the generated carriers from the surfaces is the most important. Hence, recombination velocities are strong factors in determining the optimal cell thickness.

The results of table 6.59 are easily understood by analyzing how the surface recombination velocities are used in the code. In SCAP1D, the front and back surface recombination velocities are used to determine the boundary conditions of n and p (electron and hole concentrations). If ohmic contacts are specified, the boundary conditions of n and p are set to their equilibrium values (essentially infinite recombination velocity). If there were significant generation occurring near a

surface, the hole electron pairs are lost (recombined) due to the fact that the boundary conditions are at equilibrium, and the solution vectors of n and p are forced to satisfy the boundary conditions. By increasing the cell thickness, the generated carriers are moved farther from the boundaries. Hence, the electron and hole concentrations, the solution vectors n and p, are not as strongly affected by the boundary conditions. The interpretation is that the minority carriers have an increased probability of being collected before diffusing to a surface (i.e., avoid recombining at a surface). For finite recombination velocities, the principles are the same but the actual calculations in SCAP1D are more complex (see equation 3.23).

The observations made above must be viewed in the light of the previous results that suggested large changes in the cell thickness can have a small effect on efficiency. Table 6.60 shows the results when the case with ohmic boundary conditions is optimized with no upper bounds on cell thickness or back junction depth. The thickness increases to beyond 700 microns. The difference in efficiency is only 0.03 when compared to the optimal result with the bounds used to generate table 6.59 ($X_L \leq 500$ and $X_b \leq 50$). The optimization code will vary the variables significantly even if the resulting increase in efficiency could not be measured experimentally. This is not meant to be a practical design, but only to determine how large the optimal values are and illustrate the importance of a complete sensitivity analysis.

The results of table 6.59 were used to initiate a second set of runs that set the upper bound on the cell thickness at the more practical limit of 300 microns. The results of these runs are given in table 6.61 . Any entries in table 6.59 that resulted in a cell thickness of less than 300 microns were not rerun, but are included in table 6.61 for completeness. Figure 6.63 is a contour plot of optimal efficiency versus front and back effective surface recombination velocities based on the results of table 6.61 . The contour plot is for "optimal efficiency", so that all of the points in the two dimensional surface of S_f and S_b correspond to a different cell design. Table 6.61 shows that significant differences exist in the cell design as the recombination velocities are varied. Therefore, the contour plot of efficiency for a set design would be significantly different.

As the front surface recombination velocity is raised, the front surface doping concentration is increased. This occurs until the front surface doping concentration reaches its upper bound, at which point the front junction depth increases from its lower bound. Numerically, this increases the integrated charge in the emitter, which is important in determining the effects of the boundary conditions (i.e., the surface recombination). Although it would appear that increasing the junction depth would be harmful, the probability of collecting the carriers generated near the surface is so low that the optimal design forsakes some of these carriers to

raise the probability of collection of the carriers generated slightly farther from the surface.

The sensitivity analysis of the six cases treated earlier in the section made it clear that the optimal value of the front surface doping concentration must be low to gain the full benefit of good front surface passivation. If the front surface doping concentration is raised above its optimal value, the gains of surface passivation will be negated by heavy doping effects in the emitter. However, when the front surface recombination velocity is high, the strong fields and reduction in minority carrier diffusivity associated with heavy doping deter surface recombination and this is more beneficial than the heavy doping effects are harmful. In determining the optimal value of the front surface doping concentration and junction depth, the optimization finds the optimal tradeoff between heavy doping effects and surface recombination.

Some of the designs given in table 6.61 (particularly those associated with low values of S_f) would result in extremely high lateral resistance in the emitter. If the front surface is well passivated, it is no longer critical to make the front junction depth as thin as possible. This was shown in the sensitivity analysis performed for front junction depth for the six cases described earlier. When the front surface recombination velocity is high (and junction depth becomes critical), the optimal value of the doping concentration is higher resulting in lower lateral resistance. The conclusion is that including lateral resistance in the analysis would not significantly affect the optimal efficiency contours (figures 6.63-72). However, the optimal values of the front junction depth and front surface doping concentration listed in the tables would change, particularly for low S_f.

The back surface doping concentration increases with the back surface recombination velocity until log $S_b = 4$. At that point, the design changes from a BSF to a DF cell (i.e., the back junction depth changes from the lower to the upper bound). The back surface doping concentration decreases to reflect the change in junction depth, then rises slightly as S_b continues to increase. The deeper junction results in a significant decrease in the probability of collection for the carriers generated near the back surface. However, it is apparent from the optimization results that the deeper junction provides better shielding from the back surface for a majority of the generated carriers (the number of carriers generated decreases exponentially from the front surface, disregarding the photons reflected from the BSR).

Once the back surface recombination velocity reaches 10^5 cm/s, there is little further change in the efficiency or the optimal values of the design variables.

The effect of back surface recombination velocity is not nearly so strong as front surface recombination velocity, as can be expected since so many more carriers are generated near the front surface. Since the substrate modeled is of excellent quality, 2 ms electron minority carrier lifetime in lightly doped silicon, the device is very easily dominated by the surfaces.

All the runs were initiated with a back surface field (six variable optimization). It was not expected that the BSF would make a difference for the cases with very low back surface recombination velocities (disregarding the results from the previous section). It was anticipated that the BSF could be eliminated by converging to a point where the back surface and bulk doping concentrations were equal. This never occurred, however, and there are a couple of possible explanations. It has already been observed that the optimization code is sensitive to very small numerical differences in the efficiency. It may be that a cell with a BSF is incrementally better than a cell without a BSF (even at low back surface recombination velocities). This may not be due to any shielding effects, but just a result of a slight boost in V_{oc} combined with a decrease in the optimal value of the bulk doping and cell thickness. Or, it may be that the results are at a local minimum and it is not possible to converge to a cell with no BSF, depending on where one initiates the optimization from.

The same set of runs was made for τ_{n0} = 2 ms while solving problem P2 (i.e., an optimized CV cell). The results are shown in table 6.62 and figure 6.64 . The effect of the back surface field is quite obvious when comparing figures 6.63 and 6.64 . The intersection of the contour lines along the axis log S_b = 0 does not change significantly, but the BSF cell is far superior as the back surface recombination velocity is increased.

Looking at the case log S_f = 0 and log S_b = 5 in tables 6.61 and 6.62 it is again seen that the optimal CV design results in a higher V_{oc} than the optimal BSF design. Both cells are 300 μm thick (the upper bound for X_L). The BSF cell is superior because the use of the back surface field allows lower bulk doping to be used. This results in better minority carrier lifetime and diffusion length in the bulk, which increases J_{sc} and C_{eff}.

When good front surface passivation is coupled with very poor back surface passivation, the optimization reacts by increasing the front junction depth. This is done to help increase the collection probability of the carriers generated deeper in the cell. Since there is not a significant recombination center at the front surface, the front junction depth does not have to be at its lower bound to collect the carriers generated at the front surface.

With low S_f, the optimal CV design in table 6.62 uses low front surface doping to avoid heavy doping effects in the emitter. However, it is then necessary to heavily dope the base to get high V_{oc}. As S_b increases for a given value of S_f, the bulk doping is further increased to reduce the back surface recombination. The highest bulk doping occurs with low S_f and high S_b. The highest optimal value of the bulk doping is $\approx 2.0 \times 10^{17}$ (bulk resistivity of 0.12 Ω-cm).

Several other lifetimes were solved for and the results are given in tables 6.63-6.70 and the corresponding contour plots in figures 6.65-6.72 . Many of the same trends discussed above are observed. As the lifetime decreases the sensitivity to the surfaces decreases.

For the lowest lifetimes (0.1 and 0.05 ms) the upper bound on cell thickness was decreased to 100 μm. Comparison of figures 6.70 and 6.71 illustrates the substantial benefits of using a BSF with a thin cell when the back surface is poorly passivated.

Figure 6.69 was generated by raising the upper bound on cell thickness from 100 to 300 μm at τ_{n0} = 0.1 ms. Comparison of figures 6.69 and 6.70 clearly illustrates the effects of using the cell thickness to isolate the surfaces for cells with poor surface passivation. The tradeoff for increased cell thickness also includes the increased generation that occurs when the cell thickness is increased beyond 100 μm.

6.9 Summary

In this chapter, the cell designs for six cases (see below), defined by the technology variables, were optimized.

Table 6.71 Summary of Cases

case	τ_{n0}	S_f	S_b	$X_L \leq$
1	2 ms	100 cm/s	100 cm/s	300 μm
2	1 ms	1,000 cm/s	1,000 cm/s	300 μm
3	1 ms	1,000 cm/s	∞	300 μm
4	0.4 ms	10,000 cm/s	10,000 cm/s	300 μm
5	0.1 ms	1,000 cm/s	1,000 cm/s	100 μm
6	0.1 ms	1,000 cm/s	∞	100 μm

A sensitivity analysis was performed on each of the optimal solutions. Also, the technology variables were varied parametrically and the cell design reoptimized. Some of the results are summarized below.

- The high sheet resistivities for the emitters of the optimal designs reflected the fact that lateral resistance is not in the SCAP1D model. This will be further investigated in the next chapter.
- Several examples were cited that showed that for some values of the technology variables the efficiency is not a concave function of the design variables.
- The optimal cell design, the sensitivities of the optimal solution, and the optimal value of the efficiency vary drastically as the technology variables are changed. Therefore, all the optimization results must be stated in reference to the values of the technology variables used.
- The strongest interactions in the cell design are between X_f and D_0 (greater if S_f is high), X_b and D_L (greater if S_b is high), and X_L and D_B (greater if τ_{n0} is low).
- As well as the surface doping concentrations and the junction depths, the optimal value of the cell thickness is very dependent on the surface recombination velocities.
- Heavily doping well passivated surfaces will result in a cell that is dominated by heavy doping effects, and the benefits of surface passivation will be lost.
- For unpassivated or poorly passivated surfaces a thick BSF results in higher efficiency than a thin heavily doped BSF.
- For all the cases considered, a cell with a BSF resulted in a higher efficiency than a CV (conventional n-p, no BSF) cell. The optimal design with a BSF invariably resulted in a thinner cell with lower bulk doping. This suggests that parametric analysis will not accurately predict the effects of a BSF since it is necessary to vary many variables simultaneously. The optimal cell with a BSF often had lower V_{oc} then the optimal CV cell, but better efficiency due to higher J_{sc}.
- The cells optimized while cell thickness was held at a low value had the highest values of V_{oc}, fill factor, and collection efficiency, but both surfaces had to be well passivated. Thin cells will be further investigated in chapter 8.
- At very high lifetimes, recombination velocities as low as 100 cm/s will result in large losses in efficiency. Improvements in the saturation lifetime beyond 1 ms will not yield significant increases in efficiency unless the effective front and back surface recombination velocities are $\simeq$ 100 cm/s or lower.

- The efficiency associated with the optimal cell design is insensitive to S_b for values greater than 10^5 and S_f for values greater than 10^7. Sensitivity to S_f and S_b is highly dependent on the value of τ_{n0}.

7 Lateral Resistance

In this section, the effect of lateral resistance on the results in the previous section will be discussed. An approximate correction term for lateral resistance will be derived and appended to the objective function. Results will then be given for the new objective function.

7.1 Correction for Lateral Resistance

Lateral resistance occurs in the emitter of a solar cell with conventional geometry (i.e., front and back surface contacts) and can significantly affect the performance of a cell. Current generally flows perpendicular to the surfaces in the bulk of a solar cell. Because the top metal contact grid only partially covers the top surface, the current must flow laterally in the emitter to be collected by the grid. If the emitter is very thin, significant current crowding can occur leading to a resistive voltage drop in the emitter. The doping concentration in the emitter determines the resistivity of the material (resistivity is a function of the hole and electron concentrations). Higher doping concentrations result in lower resistivities. Hence, to minimize lateral resistance, the cell should be designed with a thick heavily doped emitter.

The above criterion is in direct conflict with other considerations that affect cell performance. Due to the exponential absorption of the incident radiation, the majority of the electron-hole pairs are generated near the front surface. The probability of collecting an electron-hole pair generated near the front surface may be significantly reduced if the front surface is an effective recombination center. If this occurs, it is desirable to make the junction as close as possible to the front surface. Also, heavy doping in the emitter results in the detrimental effects of band gap narrowing and Auger recombination.

In the previous section, the results of the optimization runs reflected the fact that SCAP1D does not include lateral resistance. In each of the six cases studied, the optimal value of the front junction depth was at the lower bound of 0.1 μm.

This junction depth led to high values of sheet resistivity in the emitter which would result in a lower efficiency if the effects of lateral resistance were included in the calculations.

The sensitivity analyses performed on the front junction depth implied that the front junction depth could be increased as long as the other variables were re-optimized (e.g., figure 6.3). The re-optimization generally resulted in a lower value of front surface doping concentration being optimal. Combined with the increase in junction depth, however, the sheet resistivity of the emitter decreased. The sensitivity of the efficiency to such changes was dependent on the value of the effective front surface recombination velocity.

The higher the effective front surface recombination velocity, the more sensitive the efficiency is to the front junction depth. A higher front surface recombination velocity, however, resulted in a greater value of the front surface doping concentration being optimal and lower sheet resistivities for the emitter. The higher front surface doping concentration results because stronger electric fields and lower minority carrier diffusivities are required near the surface to collect the minority carriers before they recombine.

In conclusion, in situations where the front junction depth is a particularly sensitive variable (high S_f), the lateral resistance is less of a problem. When the front surface recombination velocity is low, the lateral resistance of the designs given in the previous section is too high, but the junction depth is less sensitive and can be increased to lower the lateral resistance.

The above conclusions can be validated by including a correction for the lateral resistance in the optimization. Since SCAP1D is a one dimensional code, the correction term is an approximation. The derivation of a lateral resistance correction term for use with SCAP1D is based on figure 7.1 which shows the top and side views of a solar cell with a contact grid on the front surface. Although different geometries are used in designing contact grids, the majority of the cell surface is covered by fingers (narrow grid lines which are used for collecting the current generated in the cell). The fingers are usually connected to a thicker grid line referred to as a busbar. In the simple approximation to be given, however, only the fingers will be included.

Assuming an n-type emitter, the electrons which enter the emitter must flow laterally to the closest grid line. In figure 7.1, all those electrons a distance d/2 or less from a finger will flow to that finger [7.1]. The resistive losses can be calculated by the following integral,

$$P_{loss} = \int_{x=0}^{x=d/2} I_{mp}^2 \, dR \quad . \tag{7.1}$$

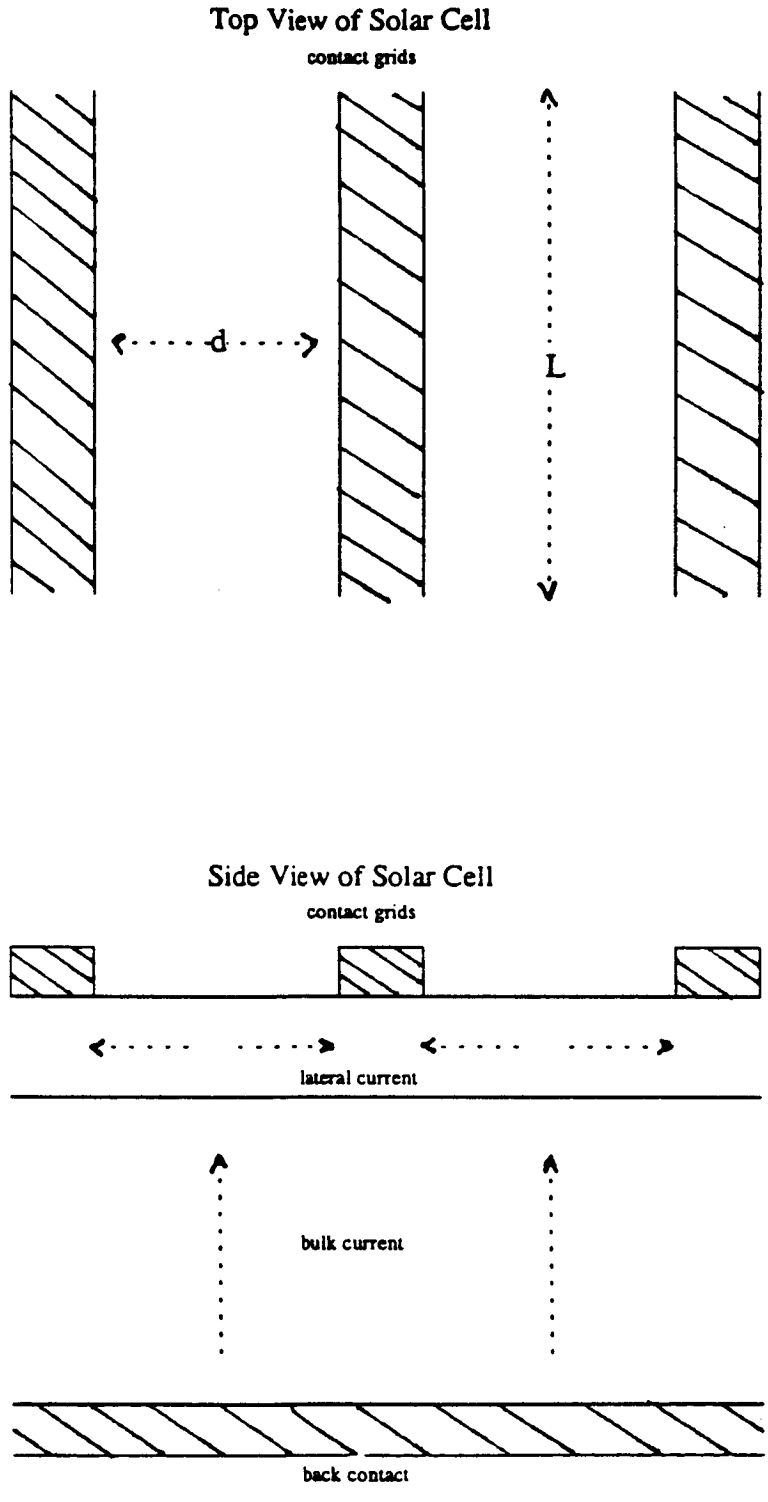

fig. 7.1 Grid Pattern Used for Lateral Resistance Correction Factor

The incremental resistance, dR, is $\frac{\rho_e\, dx}{L}$. The maximum power current, I_{mp}, is equal to $J_{mp}Lx$. Hence, the integral in equation 7.1 is

$$P_{loss} = \frac{J_{mp}^2\, L\, \rho_e\, d^3}{24} \tag{7.2}$$

Since SCAP1D is a one dimensional code, the correction term must be of the form P_{loss}/cm^2. The area the losses are integrated over is Ld/2, so

$$P_{loss}/cm^2 = \frac{J_{mp}^2\, \rho_e\, d^2}{12} \quad . \tag{7.3}$$

The term in equation 7.3 can be incorporated into the expression for the power generated by the cell as follows:

$$P_{cell} = \left[V_{mp} - \frac{J_{mp}\, \rho_e\, d^2}{12} \right] I_{mp} \quad . \tag{7.4}$$

The cell efficiency is simply the power generated by the cell divided by the power incident in the form of illumination. The optimization is identical to the statement of problem P1, except that the above definition of the cell power is used.

Equation 7.3 is an approximate correction factor for the effects of lateral resistance. As already mentioned, a very simple geometry is used in describing the top contact design. The voltage drop that is approximated is not included in the solution of Poisson's equation. In reality, the voltage drop would be distributed in the emitter, but a two dimensional model would be required to simulate such an effect. Also, the assumption of current flow perpendicular to the junction in the bulk of the device is used in the derivation of the correction term.

7.2 Results

In this section, the optimizations for the six cases used in the previous chapter are repeated using an objective function based on equation 7.4 . In equation 7.4, the value of d represents the distance between the fingers of the top contact. Runs were made at the values of 1 mm, 2 mm, and 3 mm. Also, the sensitivity analysis for the front junction depth was repeated for each case and value of finger separation. The sensitivity analysis was done by holding the front junction depth fixed and re-optimizing the other design variables. The results are presented in tables 7.1-7.18 and figures 7.2-7.7 (located at the back of the chapter). The design associated with the optimal value of the front junction depth is printed in bold in the tables.

The column headings of tables 7.1-7.18 are:

lr eff = efficiency with lateral resistance correction included (%)

V_{oc} = open circuit voltage (mV)

J_{sc} = short circuit current density (mA/cm^2)

note: The lateral resistance correction is not included in the calculation J_{sc}.

lr ff = fill factor using lateral resistance correction.

C_{eff} = collection efficiency (%)

ρ_e = sheet resistance of the emitter ($\Omega/\square$)

eff = efficiency without correction for lateral resistance (%)

ff = fill factor without correction for lateral resistance

X_L = cell thickness (μm)

X_f = front junction depth (μm)

X_b = back junction depth (μm)

log D_0 = log of the net front surface doping concentration ([P atoms - B atoms]/cm^3)

log D_B = log of the net bulk doping concentration ([B atoms - P atoms]/cm^3)

log D_L = log of the net back surface doping concentration ([B atoms - P atoms]/cm^3)

The results for case 1 are given in tables 7.1-7.3 and figure 7.2. In figure 7.2, the dashed line is the sensitivity analysis for X_f given in chapter 6 which did not include a correction for lateral resistance. The other three curves represent the sensitivity analysis with d equal to 1 mm, 2 mm, and 3 mm. The trend is significantly different for the analyses that were done with a correction for lateral resistance included. The very thin junction depth of 0.1 μm is no longer optimal. In fact, the sensitivity analyses suggest that with a correction for lateral resistance included the efficiency would drop off sharply if a junction depth of 0.1 μm were used.

The results agree with the statements made in the previous section that the lateral resistance could be reduced by increasing the front junction depth while lowering the front surface doping concentration. The doping concentrations, however, are not equal to those found in the sensitivity analysis illustrated in table 6.6. Comparison of the front surface doping concentrations for the same front junction depth show that those in table 7.1 are always higher than those in table 6.6. Comparison of table 7.1 with 7.2 and 7.3 shows a further increase in the front surface doping concentration as the distance between the grid fingers is increased. This is due to the fact that higher doping concentrations reduce ρ_e.

Figure 7.2 illustrates that for this case it is better to increase the junction depth to decrease the lateral resistance. The least favorable alternative to reduce

the detrimental effects of lateral resistance is to retain a thin emitter and resort to very heavy doping to reduce the sheet resistance. The conclusions given above become more pronounced as the grid finger spacing, d, is increased. Also, as in chapter six, tables 7.1-7.3 show that the optimal value of the front surface doping concentration varies significantly as the front junction depth is changed.

Heavily doping a thin emitter results in a substantial drop in V_{oc} due to increased Auger recombination and bandgap narrowing in the emitter. When X_f is held fixed at a small value, the sheet resistivity remains fairly high because the only way to decrease the lateral resistance is to raise the front surface doping concentration. Comparison of the results at 0.1 μm shown in tables 7.1-7.3 show that further increasing the front surface doping concentration is a bad tradeoff, so it is better to allow for a more substantial loss due to lateral resistance. Even the efficiencies without the lateral resistance correction factor (eff column) are less for the thin emitters as a result of the effects of heavy doping.

The optimality of a front junction depth of 10 μm (for d = 3 mm) occurs because the cell being modeled in this case has excellent front surface passivation. The main reason for designing a cell with a very thin junction is to avoid recombination at the front surface. If the front surface is well passivated, it is no longer critical to have very thin junctions. For example, the above observation is critical to the successful design of IBC cells. In IBC cells, all the current is collected at the back of the cell ($X_f = X_L$).

The results for cases 2 and 3 are similar to those for case 1. The optimal value of the front junction depth decreases due to the higher front surface recombination velocity in cases 2 and 3. Because the doping concentrations are higher (for a given value of X_f), the value of ρ_e is lower.

The solutions for case 4 are significantly different than the first three cases. The poorly passivated front surface ($S_f = 10^4$) results in significant recombination at the front surface if the front junction depth is increased. In figure 7.5, this is illustrated by the sharp decline in efficiency to the right of the optimal junction depth.

For d = 1 mm, a front junction depth of 0.11 μm is optimal. As compared to the optimization without a lateral resistance term, the reduction in ρ_e is accomplished primarily by increasing the front surface doping concentration from 7.24 x 10^{19} to 1.35 x 10^{20}. The tradeoff for increasing the front surface doping concentration is better in this case because as well as lowering ρ_e it also helps shield the carriers generated near the front surface from the poorly passivated surface. If the front surface is well passivated, the benefit derived from the latter consideration is substantially less, so that the heavy doping effects dominate the tradeoff.

As d is increased, however, the value of the optimal junction depth increases as in the previous cases. The doping concentration has become so high that the tradeoff again favors increasing the front junction depth to reduce ρ_e.

Cases 5 and 6 are similar to the first three cases.

Table 7.19 is a summary of the effect of including the lateral resistance correction for each of the cases. The numbers refer to the absolute and percentage difference from the optimal efficiency without the lateral resistance correction factor. The percentage difference is given in parenthesis.

Table 7.19 Effect of Lateral Resistance on Optimal Efficiency

	case 1	case 2	case 3	case 4	case 5	case 6
d=1mm	-0.34 (-1.5%)	-0.39 (-1.8%)	-0.35 (-1.6%)	-0.31 (-1.5%)	-0.36 (-1.8%)	-0.32 (-1.8%)
d=2mm	-0.66 (-2.9%)	-0.85 (-3.9%)	-0.78 (-3.6%)	-0.77 (-3.8%)	-0.82 (-4.1%)	-0.74 (-3.8%)
d=3mm	-1.02 (-4.4%)	-1.35 (-6.2%)	-1.26 (-5.9%)	-1.26 (-6.2%)	-1.34 (-6.7%)	-1.23 (-6.2%)

Case 1, which models a cell with excellent front surface passivation, is affected the least by the inclusion of the correction for lateral resistance.

In the above analysis, the shadowing and correction factor was taken as 7% regardless of the value of d. In general, as the spacing between the grid fingers is reduced the shadowing will increase (it may be possible to reduce the thickness of the grid lines, but there is a lower limit on the thickness imposed by the metalization technology). The analysis was not intended to compare the efficiencies at different spacings but rather to illustrate the change in the optimal design that occurs as the front contact grid is changed. The results imply that the front contact design must be specified (e.g., from an optimization that trades off shadowing, grid resistance, and lateral resistance) to determine which design is optimal or that the front grid and the cell must be optimized simultaneously. The latter would require a two (or three) dimensional model.

7.3 The High-Low Emitter (HLE) Design

In the previous section, including the lateral resistance correction resulted in an absolute decrease in efficiency of about 0.3 to 0.4 percentage points in efficiency for each case. Furthermore, not taking into account the effects of shadowing, for each increase of 1 mm in the grid spacing the efficiency dropped another 0.4 to 0.6 percentage points for each case.

One method that has been suggested to reduce the effects of lateral resistance is the High Low Emitter (HLE) [1.4]. In this section, the effectiveness of the HLE will be investigated by solving the optimization with the lateral resistance correction factor included.

Figure 7.8 shows the doping profile used to model the HLE cell. The profile follows a complementary error function from x=0 to $x=X_f$. The doping concentration is then constant from $x=X_f$ to $x=X_e$ (different doping profiles were tried here, but the profiles tried did not make a significant difference). At $x=X_e$ the doping concentration changes from D_e to D_B in step fashion. The high-low junction at the back of the device is defined in the same manner as in the previous sections. The HLE profile introduces two new variables into the optimization, X_e and D_e.

Tables 7.20-7.22 show the optimal solution for each case for d equal to 1mm, 2mm, and 3mm. The benefit of the HLE design is minimal for all the cases for each value of d. In fact, the HLE design leads to a reduction in efficiency for case 4 ($S_f = 10^4$) at d = 2 mm and d = 3 mm. There are two entries in tables 7.21 and 7.22 for case 4. The first is the point that the optimization converged to, which effectively eliminated the high-low junction ($X_f \approx X_e$). In the second entry, the value of X_f was fixed at 0.1 μm to force the HLE design. The latter case results in a reduction in efficiency, illustrating the importance of keeping a strong gradient in the doping concentration near the front surface when the front surface is poorly passivated. The optimization of the HLE design attempts to achieve a strong gradient by reducing D_e to the lower bound.

The lower bound for X_f was then decreased from 0.1 to 0.04 μm. This still represents a practical design with an HLE because the high-low junction can be used to reduce the lateral resistance. The efficiencies that resulted were only slightly better than those given in tables 7.20 - 7.22 .

7.4 Summary

An approximate lateral resistance correction factor was derived and appended to the objective function. The conclusions of the optimizations are as follows:

- The sensitivity analysis for the front junction depth changes drastically as compared to the results of chapter six. Without the lateral resistance correction, the efficiency monotonically decreased with increasing front junction depth. Where as, with the lateral resistance correction, the efficiency generally fell off sharply at very thin junction depths, reached an optimal value, and then fell off very slowly (except case 4 $S_f = 10^4$, in which the decrease beyond the optimal junction depth was rather sharp).
- The optimal values of the front junction depth and the front surface doping concentration vary significantly with the spacing of the grid fingers.
- For cells with good front surface passivation ($< 10^4$), the most effective means of reducing the sheet resistivity of the emitter is to increase the front junction depth, as opposed to heavily doping a thin emitter.
- For cells with poor front surface passivation ($> 10^4$), the tradeoff favors increasing the front surface doping concentration more than in cells with good front surface passivation. However, particularly for wider grid spacings, it is still beneficial to increase the front junction depth to decrease the lateral resistance.
- The high-low emitter (HLE) design does not show significant improvement in efficiency (< 0.2 percentage point) over the conventional emitter design.

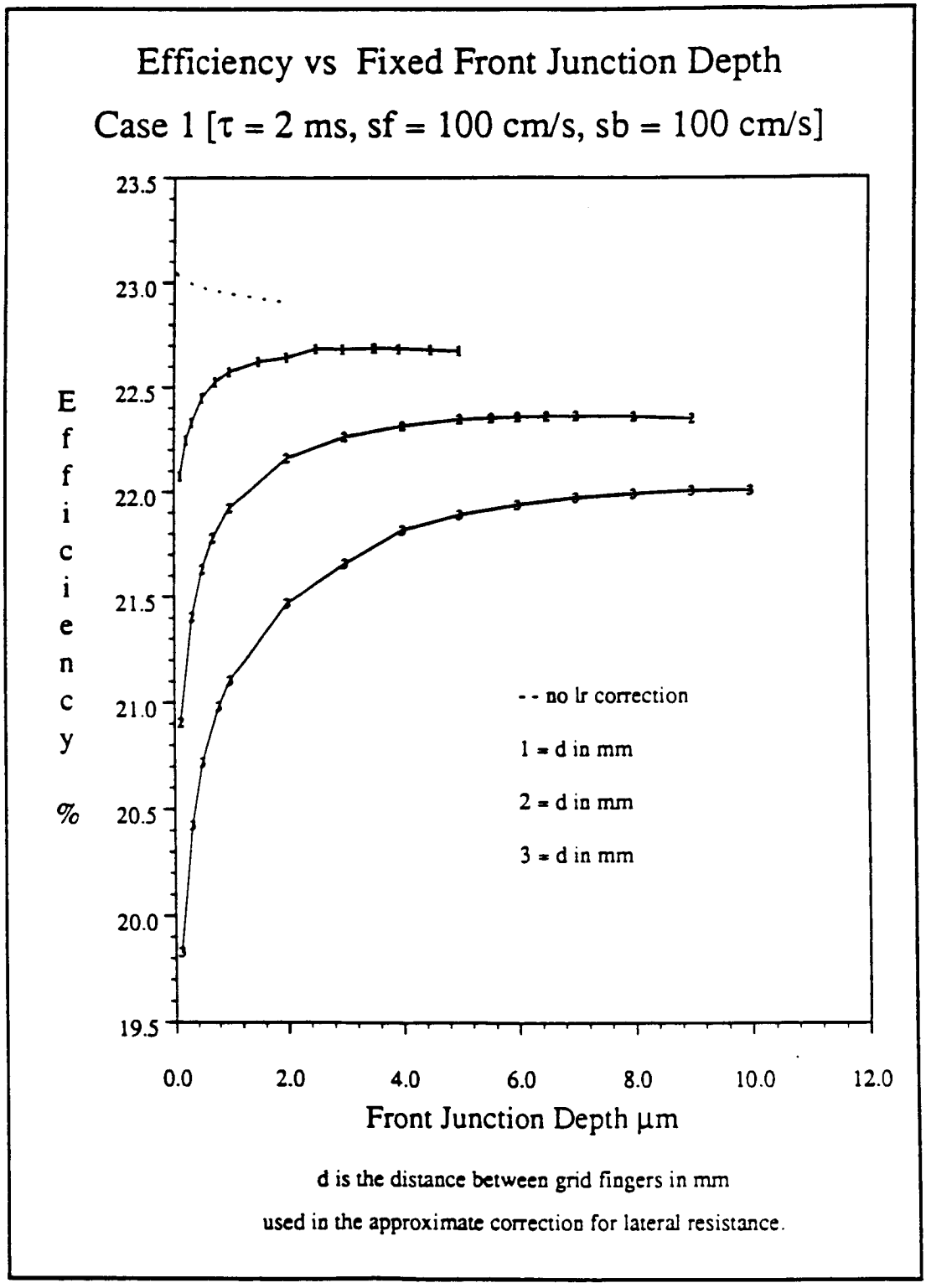
Efficiency vs Fixed Front Junction Depth
Case 1 [τ = 2 ms, sf = 100 cm/s, sb = 100 cm/s]
Efficiency %
23.5
23.0
22.5
22.0
21.5
21.0
20.5
20.0
19.5
0.0
2.0
4.0
6.0
8.0
10.0
12.0
Front Junction Depth μm
- - no lr correction
1 = d in mm
2 = d in mm
3 = d in mm
d is the distance between grid fingers in mm
used in the approximate correction for lateral resistance.

figure 7.2

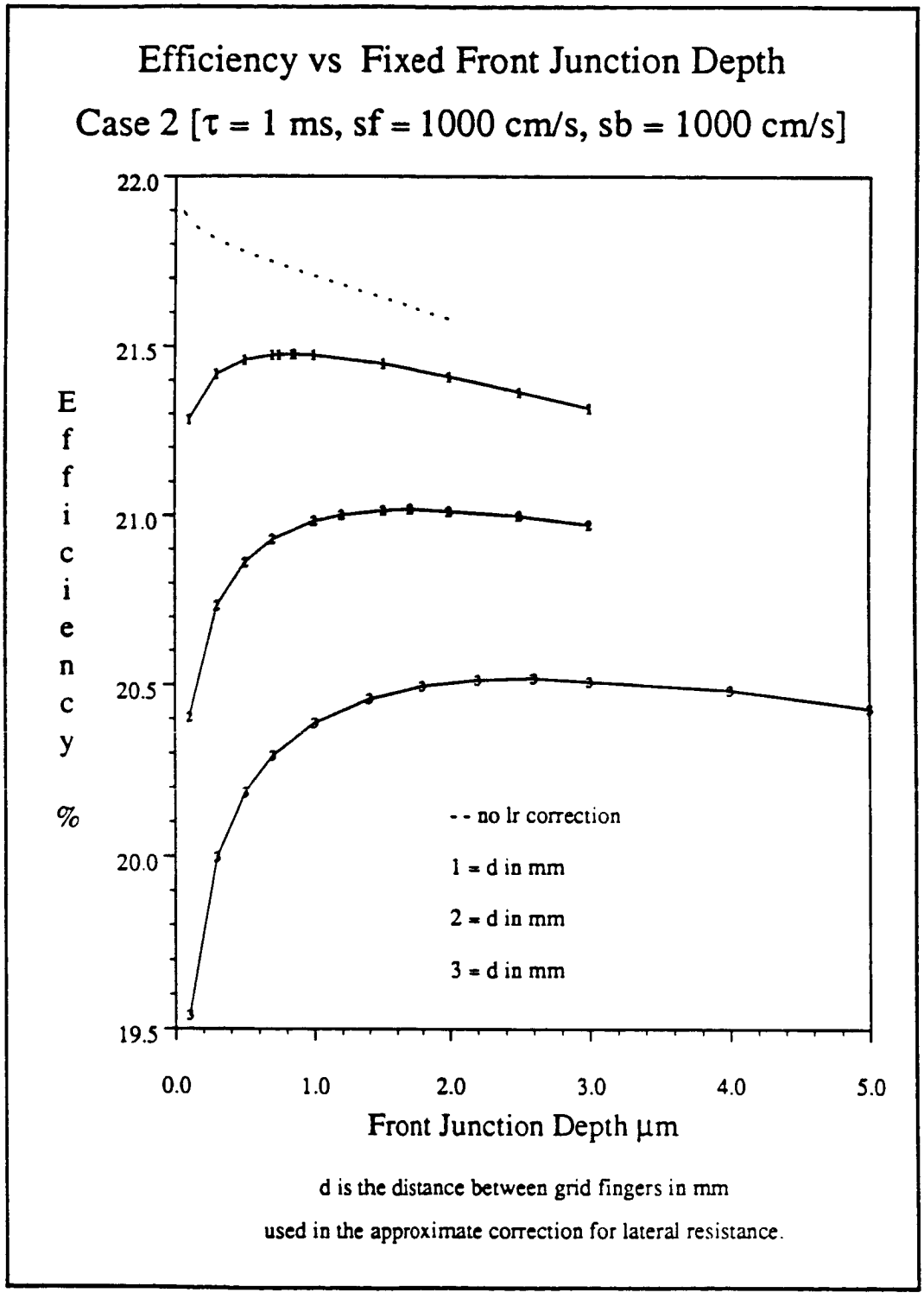
Efficiency vs Fixed Front Junction Depth
Case 2 [τ = 1 ms, sf = 1000 cm/s, sb = 1000 cm/s]
22.0
21.5
21.0
20.5
20.0
19.5
Efficiency %
- - no lr correction
1 = d in mm
2 = d in mm
3 = d in mm
0.0
1.0
2.0
3.0
4.0
5.0
Front Junction Depth µm
d is the distance between grid fingers in mm
used in the approximate correction for lateral resistance.

figure 7.3

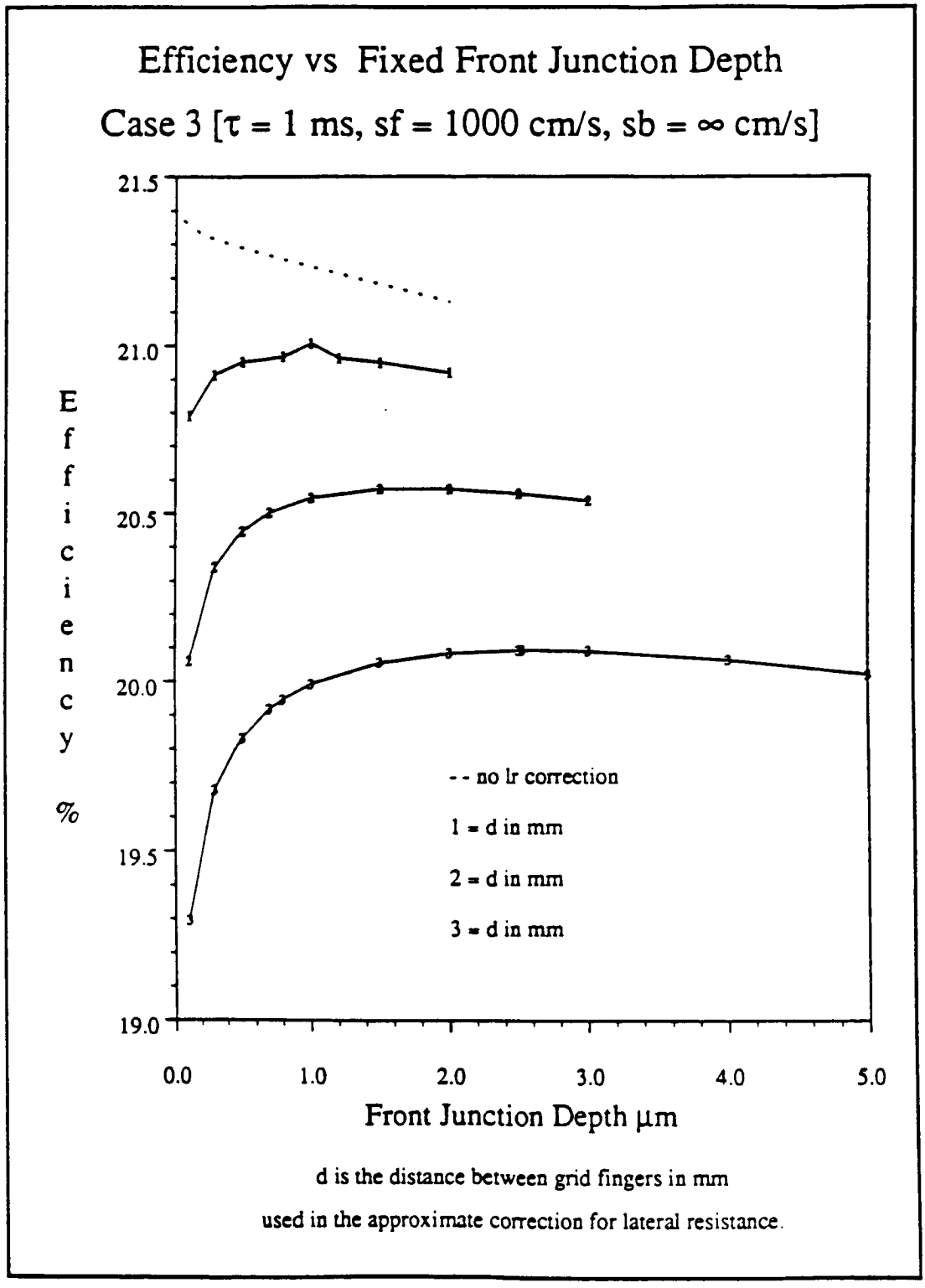
Efficiency vs Fixed Front Junction Depth
Case 3 [τ = 1 ms, sf = 1000 cm/s, sb = ∞ cm/s]
21.5
21.0
20.5
20.0
19.5
19.0
Efficiency %
- - no lr correction
1 = d in mm
2 = d in mm
3 = d in mm
0.0
1.0
2.0
3.0
4.0
5.0
Front Junction Depth µm
d is the distance between grid fingers in mm
used in the approximate correction for lateral resistance.

figure 7.4

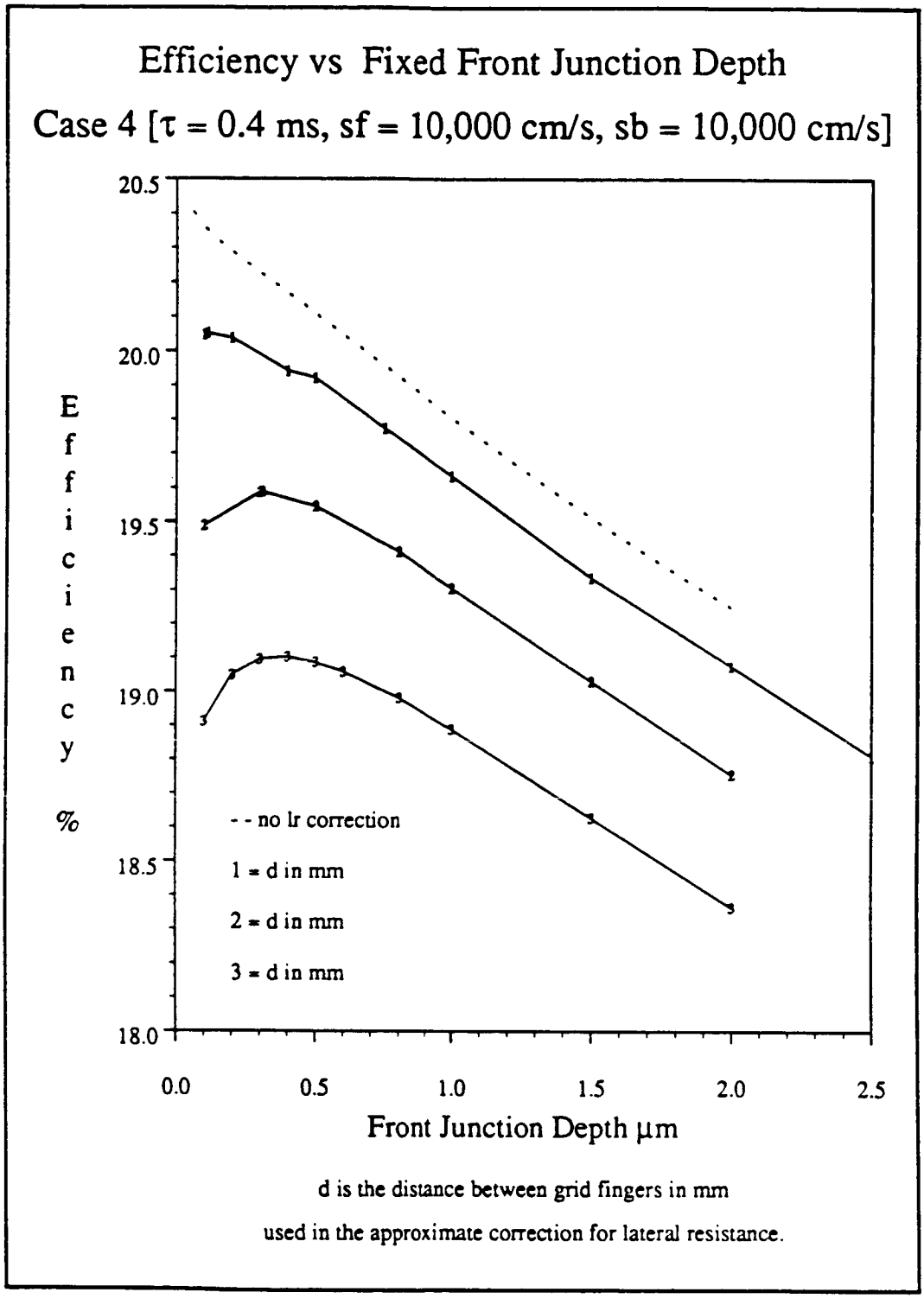
Efficiency vs Fixed Front Junction Depth
Case 4 [τ = 0.4 ms, sf = 10,000 cm/s, sb = 10,000 cm/s]
20.5
20.0
19.5
19.0
18.5
18.0
Efficiency %
- - no lr correction
1 = d in mm
2 = d in mm
3 = d in mm
0.0
0.5
1.0
1.5
2.0
2.5
Front Junction Depth µm
d is the distance between grid fingers in mm
used in the approximate correction for lateral resistance.

figure 7.5

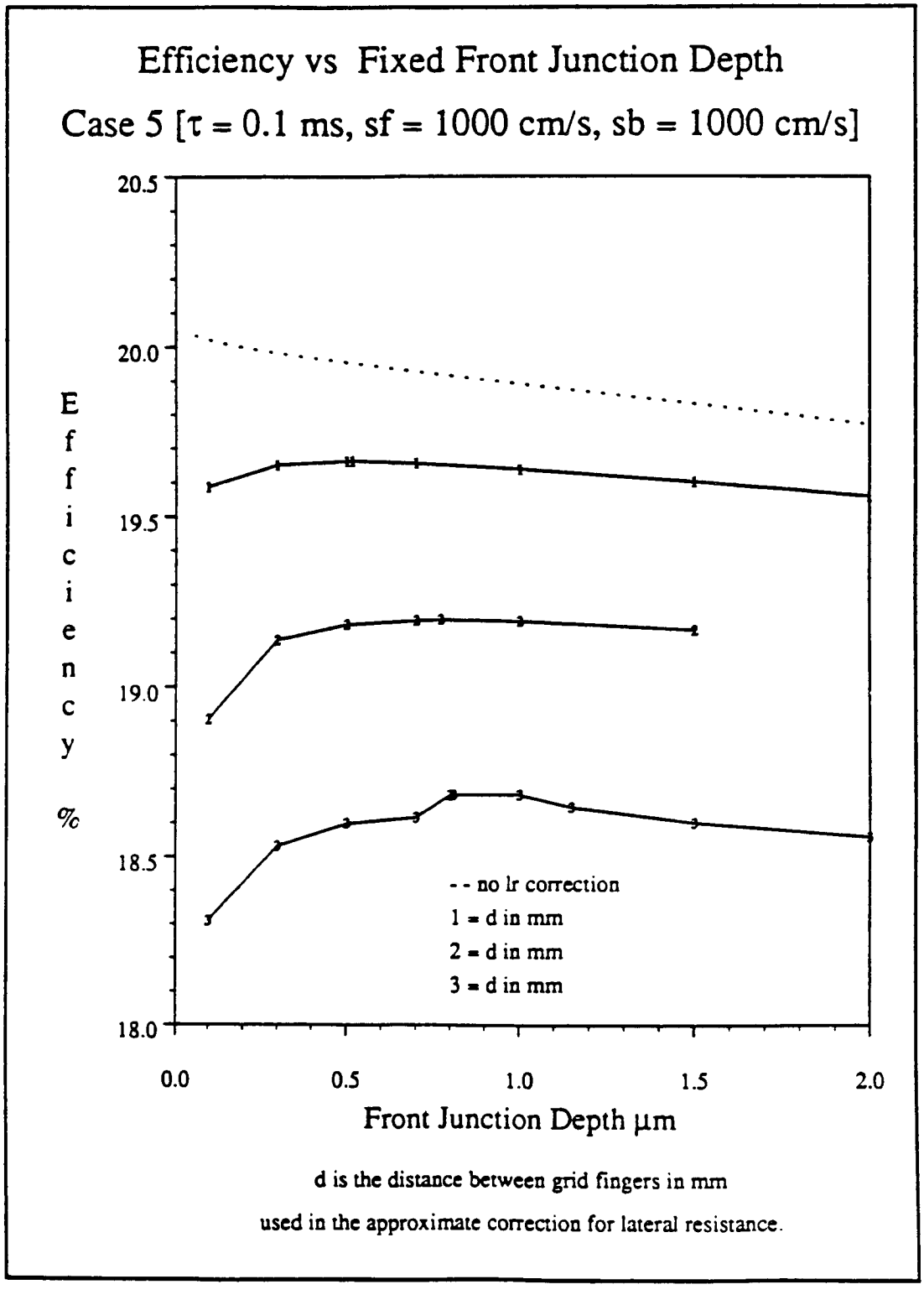
Efficiency vs Fixed Front Junction Depth
Case 5 [τ = 0.1 ms, sf = 1000 cm/s, sb = 1000 cm/s]
20.5
20.0
19.5
19.0
18.5
18.0
Efficiency %
- - no lr correction
1 = d in mm
2 = d in mm
3 = d in mm
0.0
0.5
1.0
1.5
2.0
Front Junction Depth µm
d is the distance between grid fingers in mm
used in the approximate correction for lateral resistance.

figure 7.6

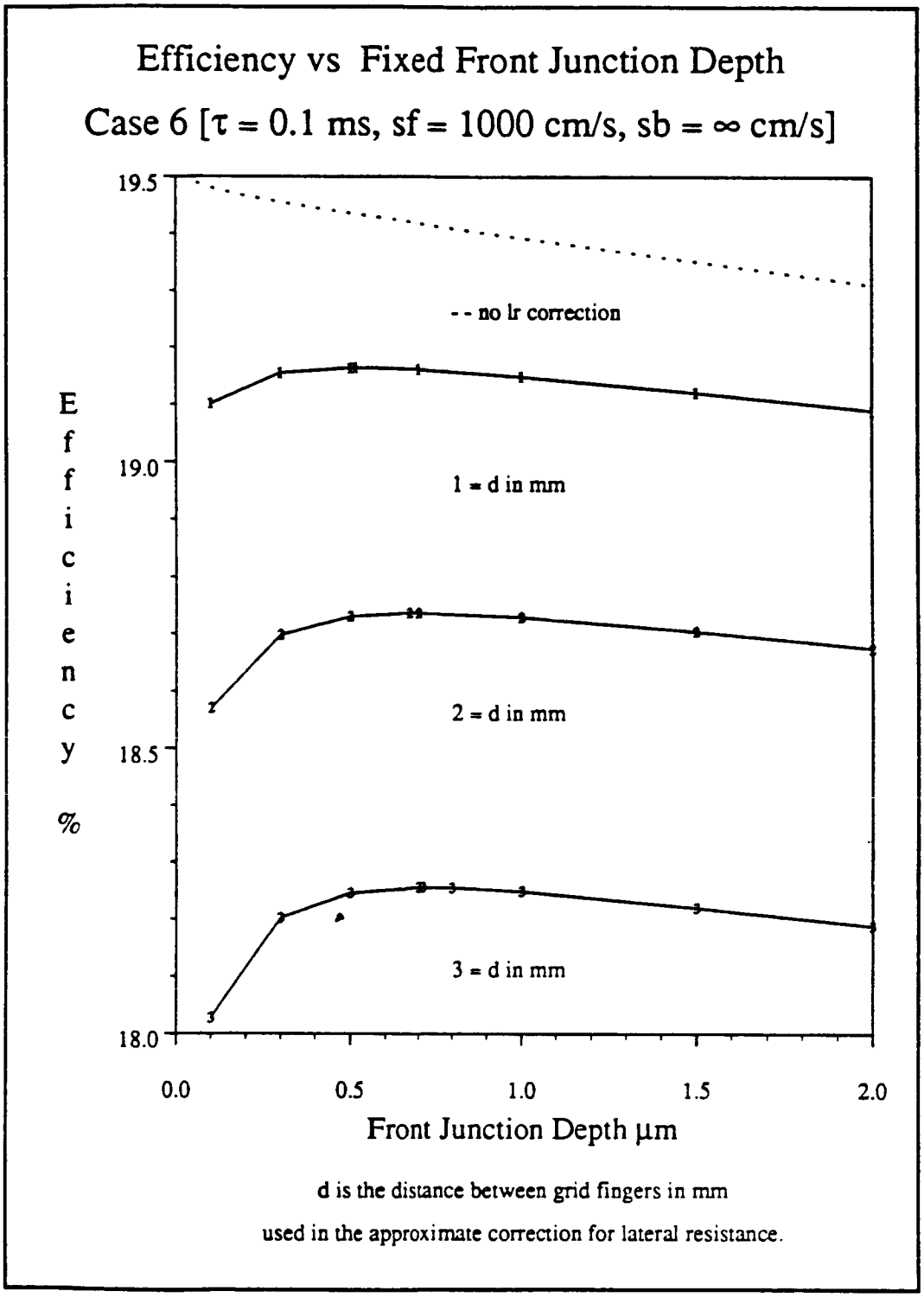
Efficiency vs Fixed Front Junction Depth
Case 6 [τ = 0.1 ms, sf = 1000 cm/s, sb = ∞ cm/s]
19.5
19.0
18.5
18.0
Efficiency %
-- no lr correction
1 = d in mm
2 = d in mm
3 = d in mm
0.0
0.5
1.0
1.5
2.0
Front Junction Depth µm
d is the distance between grid fingers in mm
used in the approximate correction for lateral resistance.

figure 7.7

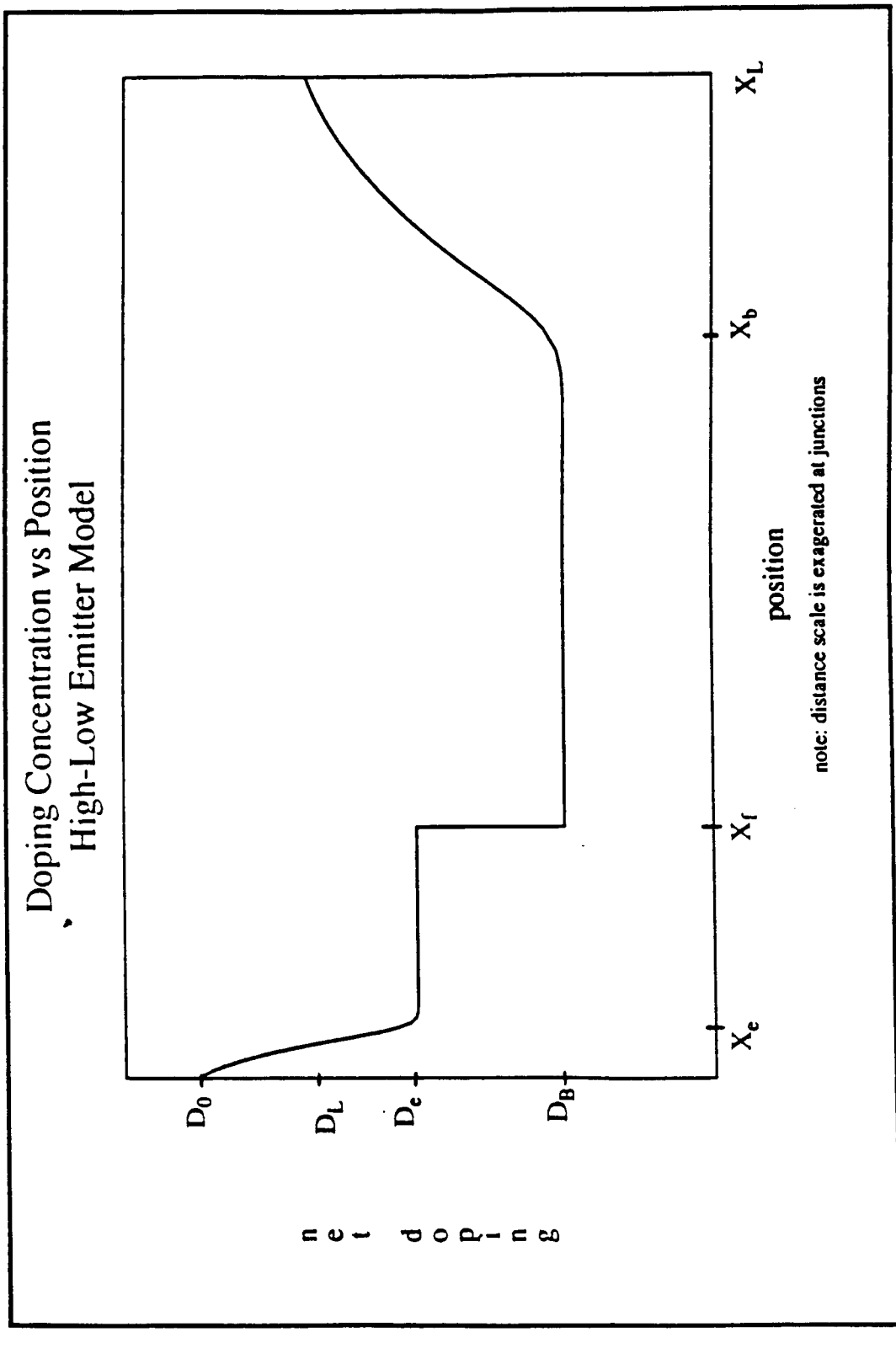
Doping Concentration vs Position
High-Low Emitter Model
net doping
D_0
D_L
D_e
D_B
X_e
X_f
X_b
X_L
position
note: distance scale is exagerated at junctions

figure 7.8

Table 7.1 Sensitivity of Front Junction Depth, Case 1, d = 1 mm, O_{pl} = 2

η eff	V_{oc}	J_{sc}	FF	C_{eff}	ρ_e	eff	ff	X_L	X_f	X_b	log D_0	log D_B	log D_L
22.075	687.9	39.18	.819	99.6	515.2	22.67	.841	276.6	0.10	0.4	19.69	16.45	18.47
22.250	692.1	39.09	.822	99.6	444.6	22.76	.841	251.1	0.20	0.4	19.38	16.42	18.62
22.331	694.0	38.98	.826	99.5	403.7	22.80	.843	236.2	0.30	0.6	19.18	16.54	18.78
22.450	693.8	39.06	.828	99.6	317.6	22.82	.842	249.3	0.50	0.6	19.00	16.47	18.71
22.524	695.4	39.03	.830	99.6	285.0	22.85	.842	243.0	0.75	0.6	18.77	16.48	18.77
22.573	696.0	39.03	.831	99.6	259.3	22.87	.842	242.7	1.00	0.6	18.62	16.46	18.66
22.623	695.9	39.03	.833	99.6	208.4	22.86	.842	243.4	1.50	0.6	18.45	16.44	18.60
22.642	694.8	39.06	.834	99.5	167.6	22.84	.842	251.8	2.00	0.6	18.39	16.44	18.73
22.684	**695.4**	**39.07**	**.835**	**99.5**	**152.4**	**22.86**	**.841**	**254.3**	**2.50**	**0.2**	**18.27**	**16.44**	**18.89**
22.681	696.4	38.98	.835	99.6	141.8	22.85	.841	236.3	2.97	0.2	18.18	16.44	18.73
22.680	695.6	39.01	.836	99.5	127.2	22.83	.841	244.6	3.50	0.2	18.12	16.44	18.87
22.679	695.2	39.06	.835	99.5	130.3	22.84	.841	253.9	3.54	0.2	18.09	16.42	18.89
22.678	694.8	39.08	.835	99.5	123.6	22.83	.841	257.5	3.94	0.2	18.04	16.41	18.96
22.678	694.0	39.10	.836	99.5	113.1	22.81	.840	266.3	4.49	0.2	18.00	16.40	18.89
22.671	694.2	39.07	.836	99.5	106.7	22.80	.840	260.8	4.99	0.2	17.96	16.40	18.90

Table 7.2 Sensitivity of Front Junction Depth, Case 1, d = 2 mm, O_{pl} = 2

η eff	V_{oc}	J_{sc}	FF	C_{eff}	ρ_e	eff	ff	X_L	X_f	X_b	log D_0	log D_B	log D_L
20.906	669.6	39.27	.795	99.6	245.6	22.06	.839	300.0	0.10	0.2	20.07	16.38	18.86
21.405	678.6	39.24	.804	99.5	206.7	22.37	.840	300.0	0.30	0.2	19.58	16.43	18.87
21.629	683.9	39.22	.806	99.5	195.8	22.55	.840	291.8	0.50	0.2	19.32	16.40	18.89
21.777	685.8	39.17	.811	99.4	175.1	22.60	.841	287.1	0.70	0.2	19.17	16.48	18.90
21.921	688.7	39.12	.814	99.4	161.1	22.67	.842	275.5	1.00	0.2	18.98	16.50	18.89
22.161	690.8	39.13	.820	99.4	125.4	22.75	.841	281.5	2.00	0.2	18.64	16.47	18.91
22.261	691.3	39.15	.823	99.3	108.0	22.77	.841	290.8	3.00	0.2	18.42	16.46	18.90
22.315	691.5	39.13	.825	99.3	94.2	22.76	.841	288.6	4.00	0.2	18.28	16.44	18.90
22.346	692.3	39.07	.826	99.3	83.4	22.73	.841	273.0	5.00	0.2	18.19	16.41	18.95
22.352	691.9	39.06	.827	99.3	77.0	22.71	.840	276.1	5.55	0.2	18.16	16.40	18.94
22.357	691.7	39.09	.827	99.3	76.4	22.71	.840	283.3	6.00	0.2	18.10	16.38	18.93
22.359	691.3	39.10	.827	99.2	73.3	22.70	.840	288.7	6.50	0.2	18.06	16.37	18.93
22.361	**692.4**	**39.02**	**.828**	**99.3**	**72.1**	**22.70**	**.840**	**269.0**	**7.00**	**0.2**	**18.01**	**16.38**	**18.97**
22.359	691.7	39.04	.828	99.2	66.7	22.67	.839	278.1	8.00	0.2	17.96	16.35	18.95
22.351	691.0	39.06	.828	99.1	63.6	22.65	.839	287.3	9.00	0.2	17.89	16.35	18.93

Table 7.3 Sensitivity of Front Junction Depth, Case 1, d = 3 mm, O_{pl} = 2

η eff	V_{oc}	J_{sc}	FF	C_{eff}	ρ_e	eff	FF	X_L	X_f	X_b	log D_0	log D_B	log D_L
19.829	648.7	39.23	.779	99.4	136.0	21.26	.835	300.0	0.10	2.8	20.36	16.37	18.33
20.424	663.7	39.15	.786	99.3	129.4	21.78	.838	300.0	0.30	3.0	19.83	16.45	18.32
20.717	670.4	39.15	.789	99.3	124.3	22.02	.839	300.0	0.50	2.8	19.58	16.42	18.20
20.981	675.8	39.13	.793	99.2	117.0	22.21	.840	300.0	0.80	2.8	19.34	16.42	18.29
21.103	678.3	39.09	.796	99.1	112.9	22.29	.840	297.7	1.00	2.9	19.22	16.47	18.34
21.469	684.4	39.08	.803	99.1	97.6	22.49	.841	295.9	2.00	2.7	18.84	16.46	18.35
21.656	686.2	39.07	.808	99.1	84.6	22.54	.841	296.5	3.00	2.7	18.63	16.44	18.36
21.816	689.0	39.08	.810	99.1	78.3	22.64	.841	292.8	4.00	0.2	18.45	16.42	18.62
21.891	690.9	39.01	.812	99.2	73.2	22.66	.841	271.6	5.00	0.2	18.31	16.41	18.65
21.939	691.2	38.99	.814	99.2	67.8	22.65	.840	271.0	6.00	0.2	18.21	16.39	18.65
21.973	690.8	38.96	.816	99.0	60.9	22.61	.840	272.4	7.00	0.2	18.17	16.38	18.65
21.991	691.2	38.96	.817	99.1	58.9	22.61	.839	270.8	8.00	0.2	18.08	16.34	18.63
22.008	690.5	38.93	.819	98.9	53.3	22.56	.839	275.5	9.00	0.2	18.06	16.35	18.75
22.010	690.8	38.92	.819	99.0	52.6	22.56	.839	272.6	10.00	0.2	17.97	16.32	18.63

Table 7.4 Sensitivity of Front Junction Depth, Case 2, d = 1 mm, O_{pl} = 2

η eff	V_{oc}	J_{sc}	η ff	C_{eff}	ρ_e	eff	ff	X_L	X_f	X_b	log D_0	log D_B	log D_L
21.284	662.8	39.11	.821	99.2	364.6	21.71	.837	300.0	0.10	0.2	19.88	16.29	19.52
21.419	663.7	39.10	.825	99.1	264.3	21.73	.837	297.5	0.30	0.2	19.46	16.28	19.52
21.461	663.9	39.07	.827	99.1	224.1	21.72	.837	297.3	0.50	0.2	19.25	16.29	19.52
21.476	663.9	39.05	.828	99.0	198.6	21.71	.837	297.4	0.70	0.2	19.11	16.28	19.52
21.477	663.9	39.04	.829	99.0	194.2	21.70	.837	297.3	0.75	0.2	19.08	16.29	19.52
21.478	**663.9**	**39.03**	**.829**	**99.0**	**188.8**	**21.70**	**.837**	**297.6**	**0.84**	**0.2**	**19.01**	**16.29**	**19.52**
21.476	663.7	39.01	.829	98.9	173.3	21.68	.837	298.2	1.00	0.2	18.95	16.28	19.52
21.451	663.1	38.96	.830	98.8	148.6	21.62	.837	300.0	1.50	0.2	18.76	16.26	19.52
21.412	662.6	38.89	.831	98.6	134.0	21.57	.837	300.0	2.00	0.2	18.61	16.25	19.52
21.367	662.1	38.83	.831	98.4	123.2	21.51	.837	300.0	2.50	0.2	18.49	16.24	19.52
21.319	661.5	38.77	.831	98.3	115.5	21.45	.836	300.0	3.00	0.2	18.39	16.22	19.52

Table 7.5 Sensitivity of Front Junction Depth, Case 2, d = 2 mm, O_{pl} = 2

η eff	V_{oc}	J_{sc}	η ff	C_{eff}	ρ_e	eff	ff	X_L	X_f	X_b	log D_0	log D_B	log D_L
20.406	652.0	39.10	.800	99.1	194.1	21.31	.836	299.3	0.10	0.2	20.20	16.28	19.57
20.733	657.0	39.06	.808	99.0	157.7	21.46	.836	299.3	0.30	0.2	19.74	16.28	19.58
20.862	659.1	39.02	.811	98.9	141.6	21.52	.837	299.3	0.50	0.2	19.52	16.28	19.52
20.930	660.3	38.98	.813	98.8	131.5	21.54	.837	299.3	0.70	0.2	19.37	16.29	19.52
20.985	661.1	38.92	.816	98.7	119.8	21.54	.837	300.0	1.00	0.2	19.20	16.29	19.53
21.004	661.6	38.89	.816	98.6	116.0	21.54	.837	300.0	1.20	0.2	19.10	16.30	19.56
21.017	662.1	38.85	.817	98.5	111.9	21.53	.837	300.0	1.50	0.2	18.97	16.30	19.57
21.021	661.9	38.82	.818	98.4	105.2	21.50	.837	300.0	1.70	0.2	18.93	16.26	19.54
21.022	**661.9**	**38.82**	**.818**	**98.4**	**105.8**	**21.51**	**.837**	**300.0**	**1.71**	**0.2**	**18.92**	**16.27**	**19.53**
21.015	662.2	38.74	.819	98.2	101.7	21.48	.837	300.0	2.00	0.2	18.83	16.32	19.58
21.001	662.0	38.69	.820	98.1	95.5	21.44	.837	300.0	2.50	0.2	18.70	16.28	19.56
20.975	661.7	38.64	.820	98.0	91.8	21.39	.837	300.0	3.00	0.2	18.59	16.25	19.56

Table 7.6 Sensitivity of Front Junction Depth, Case 2, d = 3 mm, O_{pl} = 2

η eff	V_{oc}	J_{sc}	η ff	C_{eff}	ρ_e	eff	ff	X_L	X_f	X_b	log D_0	log D_B	log D_L
19.538	641.5	39.10	.779	99.1	131.9	20.92	.834	300.0	0.10	0.2	20.39	16.24	19.51
19.999	648.1	38.99	.791	98.8	105.9	21.10	.835	300.0	0.30	0.2	19.95	16.26	19.52
20.185	652.4	38.92	.795	98.7	99.8	21.22	.836	300.0	0.50	0.2	19.71	16.26	19.52
20.292	654.9	38.86	.797	98.5	95.6	21.28	.836	300.0	0.70	0.2	19.55	16.28	19.52
20.389	657.3	38.79	.800	98.3	91.2	21.33	.836	299.9	1.00	0.2	19.37	16.29	19.52
20.460	659.1	38.71	.802	98.1	86.5	21.35	.837	299.7	1.40	0.2	19.19	16.29	19.52
20.497	659.9	38.65	.804	98.0	82.6	21.34	.837	300.0	1.80	0.2	19.06	16.27	19.51
20.515	660.5	38.59	.805	97.8	79.4	21.33	.837	300.0	2.20	0.2	18.95	16.27	19.50
20.520	**660.8**	**38.52**	**.806**	**97.6**	**76.6**	**21.30**	**.837**	**300.0**	**2.60**	**0.2**	**18.85**	**16.27**	**19.49**
20.510	662.0	38.39	.807	97.6	75.6	21.27	.837	271.0	3.00	0.2	18.75	16.27	19.48
20.486	660.8	38.33	.809	97.2	69.8	21.19	.837	300.0	4.00	0.2	18.58	16.25	19.49
20.432	660.9	38.18	.810	96.9	66.7	21.10	.836	285.2	5.00	0.2	18.42	16.21	19.51

Table 7.7 Sensitivity of Front Junction Depth, Case 3, d = 1 mm, O_{pl} = 2

η eff	V_{oc}	J_{sc}	FF	C_{eff}	ρ_e	eff	ff	X_L	X_f	X_b	log D_0	log D_B	log D_L
20.790	651.4	38.88	.821	98.6	327.1	21.16	.836	300.0	0.10	36.6	19.94	16.17	19.14
20.912	652.1	38.88	.825	98.6	240.4	21.19	.836	300.0	0.30	36.6	19.52	16.14	19.08
20.950	652.4	38.86	.826	98.5	206.7	21.19	.836	300.0	0.50	36.6	19.31	16.14	19.08
20.967	652.5	38.83	.827	98.4	180.5	21.17	.836	300.0	0.80	36.6	19.10	16.13	19.08
21.007	**653.8**	**38.80**	**.828**	**98.4**	**171.1**	**21.20**	**.836**	**300.0**	**1.00**	**50.0**	**18.98**	**16.12**	**18.93**
20.963	652.4	38.79	.828	98.3	159.2	21.14	.836	300.0	1.20	36.6	18.90	16.13	19.08
20.950	652.2	38.76	.829	98.3	149.3	21.12	.835	300.0	1.50	36.6	18.78	16.12	19.07
20.920	651.7	38.73	.829	98.2	138.6	21.08	.835	300.0	2.00	36.6	18.61	16.08	19.07

Table 7.8 Sensitivity of Front Junction Depth, Case 3, d = 2 mm, O_{pl} = 2

η eff	V_{oc}	J_{sc}	FF	C_{eff}	ρ_e	eff	ff	X_L	X_f	X_b	log D_0	log D_B	log D_L
20.060	643.2	38.88	.802	98.6	174.9	20.86	.834	300.0	0.10	50.0	20.26	16.13	18.92
20.339	647.4	38.83	.809	98.4	142.1	20.99	.835	300.0	0.30	50.0	19.81	16.12	18.92
20.446	649.3	38.79	.812	98.3	129.5	21.04	.835	300.0	0.50	50.0	19.59	16.12	18.92
20.502	650.5	38.75	.813	98.2	121.8	21.06	.835	300.0	0.70	50.0	19.43	16.12	18.93
20.546	651.3	38.71	.815	98.1	113.7	21.06	.835	300.0	1.00	50.0	19.25	16.10	18.92
20.574	**652.1**	**38.64**	**.816**	**98.0**	**105.3**	**21.05**	**.835**	**300.0**	**1.50**	**50.0**	**19.04**	**16.09**	**18.93**
20.574	652.4	38.57	.818	97.8	98.8	21.02	.835	300.0	2.00	50.0	18.88	16.10	18.93
20.560	652.3	38.51	.818	97.6	93.7	20.98	.835	300.0	2.50	50.0	18.75	16.08	18.92
20.538	652.2	38.45	.819	97.5	89.8	20.94	.835	300.0	3.00	50.0	18.63	16.06	18.92

Table 7.9 Sensitivity of Front Junction Depth, Case 3, d = 3 mm, O_{pl} = 2

η eff	V_{oc}	J_{sc}	FF	C_{eff}	ρ_e	eff	ff	X_L	X_f	X_b	log D_0	log D_B	log D_L
19.296	631.2	38.87	.786	98.5	108.4	20.41	.832	300.0	0.10	50.0	20.49	16.08	18.90
19.679	640.0	38.78	.793	98.3	98.1	20.69	.833	300.0	0.30	50.0	20.00	16.07	18.92
19.831	643.9	38.69	.796	98.1	93.1	20.78	.834	300.0	0.50	50.0	19.77	16.09	18.92
19.917	646.2	38.61	.798	97.9	89.4	20.83	.835	300.0	0.70	50.0	19.60	16.12	18.92
19.946	647.2	38.57	.799	97.8	88.3	20.84	.835	300.0	0.80	50.0	19.53	16.14	18.92
19.992	648.4	38.54	.800	97.7	86.3	20.87	.835	300.0	1.00	50.0	19.42	16.13	18.92
20.056	650.3	38.44	.802	97.4	81.7	20.88	.835	300.0	1.50	50.0	19.20	16.14	18.92
20.084	651.2	38.37	.804	97.3	78.6	20.88	.835	300.0	2.00	50.0	19.04	16.14	18.93
20.093	651.6	38.31	.805	97.1	75.8	20.86	.835	300.0	2.50	50.0	18.90	16.12	18.93
20.094	**651.5**	**38.31**	**.805**	**97.1**	**75.3**	**20.85**	**.835**	**300.0**	**2.52**	**50.0**	**18.90**	**16.12**	**18.93**
20.090	651.9	38.23	.806	96.9	73.0	20.82	.835	300.0	3.00	50.0	18.79	16.13	18.93
20.064	651.8	38.12	.808	96.6	69.5	20.76	.835	300.0	4.00	50.0	18.60	16.11	18.93
20.022	651.3	38.03	.808	96.4	66.5	20.68	.835	300.0	5.00	50.0	18.45	16.07	18.93

Table 7.10 Sensitivity of Front Junction Depth, Case 4, d = 1 mm, O_{pl} = 2

lr eff	V_{oc}	J_{sc}	lr ff	C_{eff}	ρ_e	eff	ff	X_L	X_f	X_b	log D_0	log D_B	log D_L
20.048	630.0	38.76	.821	98.3	221.2	20.30	.831	292.3	0.10	50.0	20.15	16.02	18.68
20.051	**629.5**	**38.78**	**.821**	**98.3**	**206.3**	**20.29**	**.831**	**300.0**	**0.11**	**50.0**	**20.13**	**16.01**	**18.69**
20.037	629.9	38.65	.823	98.1	182.7	20.24	.831	285.1	0.20	50.0	19.90	16.04	18.68
19.942	629.0	38.52	.823	98.2	145.5	20.11	.830	251.9	0.40	50.0	19.67	15.82	18.69
19.922	628.7	38.45	.824	97.5	150.8	20.09	.831	300.0	0.50	50.0	19.51	16.02	18.68
19.773	628.4	38.19	.824	97.0	149.1	19.94	.831	277.4	0.75	50.0	19.28	15.99	18.68
19.634	627.9	37.91	.825	96.4	126.5	19.77	.831	272.5	1.00	50.0	19.20	15.95	18.69
19.337	626.3	37.45	.824	95.3	125.9	19.47	.830	265.2	1.50	50.0	18.93	15.91	18.69
19.077	622.8	37.23	.823	94.4	141.3	19.22	.829	300.0	2.00	50.0	18.62	15.91	18.68
18.811	620.9	36.89	.821	93.9	142.9	18.96	.828	262.1	2.50	50.0	18.43	15.73	18.69

Table 7.11 Sensitivity of Front Junction Depth, Case 4, d = 2 mm, O_{pl} = 2

lr eff	V_{oc}	J_{sc}	lr ff	C_{eff}	ρ_e	eff	ff	X_L	X_f	X_b	log D_0	log D_B	log D_L
19.489	624.8	38.75	.805	98.4	134.0	20.10	.830	283.6	0.10	50.0	20.40	15.97	18.59
19.587	626.5	38.58	.810	97.8	107.2	20.07	.830	297.4	0.30	50.0	19.97	15.97	18.63
19.588	**626.5**	**38.55**	**.811**	**97.7**	**104.6**	**20.06**	**.830**	**300.0**	**0.31**	**50.0**	**19.96**	**16.00**	**18.66**
19.545	627.3	38.35	.813	97.2	96.9	19.98	.830	300.0	0.50	50.0	19.75	15.99	18.66
19.413	627.4	38.02	.814	96.4	89.8	19.81	.830	300.0	0.80	50.0	19.54	15.97	18.66
19.305	627.4	37.81	.814	95.9	90.7	19.70	.830	292.5	1.00	50.0	19.41	15.95	18.61
19.032	626.4	37.34	.814	94.6	87.5	19.40	.830	300.0	1.50	50.0	19.19	15.88	18.72
18.756	625.3	36.87	.813	93.5	88.4	19.12	.829	300.0	2.00	50.0	18.99	15.86	18.69

Table 7.12 Sensitivity of Front Junction Depth, Case 4, d = 3 mm, O_{pl} = 2

lr eff	V_{oc}	J_{sc}	lr ff	C_{eff}	ρ_e	eff	ff	X_L	X_f	X_b	log D_0	log D_B	log D_L
18.912	617.0	38.75	.791	98.2	87.3	19.81	.828	300.0	0.10	50.0	20.60	15.95	18.72
19.050	620.5	38.59	.796	97.8	79.4	19.86	.829	300.0	0.20	50.0	20.31	15.96	18.69
19.096	622.7	38.46	.798	97.5	76.3	19.87	.830	300.0	0.30	50.0	20.14	15.97	18.71
19.103	**623.8**	**38.31**	**.799**	**97.1**	**72.9**	**19.83**	**.830**	**300.0**	**0.40**	**50.0**	**20.02**	**15.97**	**18.71**
19.088	624.9	38.19	.800	96.8	72.4	19.81	.830	300.0	0.50	50.0	19.91	15.98	18.73
19.060	625.4	38.07	.801	96.5	71.2	19.76	.830	300.0	0.60	50.0	19.82	15.97	18.73
18.982	626.5	37.81	.801	95.9	70.8	19.67	.830	300.0	0.80	49.5	19.67	15.99	18.74
18.889	626.9	37.57	.802	95.3	69.8	19.56	.830	300.0	1.00	49.5	19.55	15.99	18.75
18.628	627.1	37.02	.803	93.8	69.2	19.27	.830	300.0	1.50	49.5	19.32	15.97	18.74
18.364	626.0	36.55	.803	92.7	67.7	18.98	.829	300.0	2.00	49.5	19.17	15.88	18.73

Table 7.13 Sensitivity of Front Junction Depth, Case 5, d = 1 mm, O_{pl} = 2

η_{eff}	V_{oc}	J_{sc}	η_{ff}	C_{eff}	ρ_e	eff	ff	X_L	X_f	X_b	log D_0	log D_B	log D_L
19.588	638.6	37.34	.821	98.9	270.1	19.87	.833	100.0	0.10	0.2	20.03	16.29	19.21
19.652	639.5	37.31	.824	98.8	221.4	19.89	.833	100.0	0.30	0.2	19.56	16.29	19.25
19.663	639.8	37.27	.824	98.7	204.0	19.88	.833	100.0	0.50	0.2	19.30	16.30	19.25
19.663	**639.8**	**37.28**	**.824**	**98.8**	**203.8**	**19.88**	**.833**	**100.0**	**0.52**	**0.2**	**19.29**	**16.29**	**19.27**
19.659	639.8	37.27	.825	98.7	199.4	19.87	.833	100.0	0.70	0.2	19.10	16.29	19.27
19.642	639.7	37.22	.825	98.6	187.9	19.84	.833	100.0	1.00	0.2	18.89	16.29	19.22
19.606	639.1	37.19	.825	98.5	180.4	19.79	.833	100.0	1.50	0.2	18.60	16.28	19.23
19.563	638.5	37.14	.825	98.4	172.9	19.74	.833	100.0	2.00	0.2	18.38	16.27	19.14

Table 7.14 Sensitivity of Front Junction Depth, Case 5, d = 2 mm, O_{pl} = 2

η_{eff}	V_{oc}	J_{sc}	η_{ff}	C_{eff}	ρ_e	eff	ff	X_L	X_f	X_b	log D_0	log D_B	log D_L
18.906	628.3	37.33	.806	98.9	142.3	19.51	.832	100.0	0.10	3.5	20.35	16.19	18.43
19.138	634.8	37.23	.810	98.6	129.2	19.68	.833	100.0	0.30	0.2	19.85	16.30	19.21
19.183	636.5	37.19	.810	98.5	127.9	19.72	.833	100.0	0.50	0.2	19.58	16.29	19.22
19.196	637.2	37.15	.811	98.4	124.9	19.72	.833	100.0	0.70	0.2	19.40	16.29	19.20
19.200	**636.9**	**37.12**	**.812**	**98.3**	**117.1**	**19.69**	**.833**	**100.0**	**0.77**	**0.2**	**19.38**	**16.28**	**19.23**
19.195	637.6	37.09	.812	98.3	121.4	19.70	.833	100.0	1.00	0.2	19.20	16.28	19.21
19.169	637.9	37.02	.812	98.0	119.4	19.67	.833	100.0	1.50	0.2	18.93	16.28	19.20

Table 7.15 Sensitivity of Front Junction Depth, Case 5, d = 3 mm, O_{pl} = 2

η_{eff}	V_{oc}	J_{sc}	η_{ff}	C_{eff}	ρ_e	eff	ff	X_L	X_f	X_b	log D_0	log D_B	log D_L
18.311	620.3	37.28	.792	98.8	93.8	19.20	.830	100.0	0.10	0.2	20.55	16.20	18.11
18.533	626.9	37.13	.796	98.3	86.9	19.35	.831	100.0	0.30	0.2	20.05	16.21	18.15
18.598	630.5	37.04	.796	98.1	89.0	19.43	.832	100.0	0.50	0.4	19.78	16.23	18.21
18.618	631.8	36.97	.797	97.9	87.9	19.44	.832	100.0	0.70	0.2	19.60	16.22	18.18
18.684	634.0	36.93	.798	97.8	86.7	19.49	.832	100.0	0.80	0.2	19.53	16.27	19.27
18.684	**633.9**	**36.92**	**.798**	**97.8**	**85.9**	**19.48**	**.832**	**100.0**	**0.81**	**0.2**	**19.53**	**16.27**	**19.27**
18.684	634.8	36.87	.798	97.7	86.5	19.49	.832	100.0	1.00	0.2	19.40	16.28	19.34
18.647	635.7	36.71	.799	97.2	85.9	19.44	.833	100.0	1.15	0.2	19.31	16.40	18.86
18.601	634.6	36.78	.797	97.4	89.6	19.43	.832	100.0	1.50	0.9	19.13	16.26	18.33
18.561	634.4	36.74	.796	97.3	90.3	19.39	.832	100.0	2.00	1.0	18.93	16.22	18.21

Table 7.16 Sensitivity of Front Junction Depth, Case 6, d = 1 mm, O_{pl} = 2

lr eff	V_{oc}	J_{sc}	lr ff	C_{eff}	ρ_e	eff	ff	X_L	X_f	X_b	log D_0	log D_B	log D_L
19.102	628.0	37.06	.821	98.2	239.0	19.35	.831	100.0	0.10	24.3	20.11	16.06	19.00
19.156	629.0	37.02	.823	98.1	202.2	19.37	.831	100.0	0.30	24.3	19.63	16.07	19.02
19.164	629.5	36.99	.823	98.0	193.0	19.36	.832	100.0	0.50	24.3	19.36	16.07	19.05
19.165	**629.6**	**36.98**	**.823**	**97.9**	**190.8**	**19.36**	**.832**	**100.0**	**0.52**	**24.3**	**19.35**	**16.08**	**19.03**
19.162	629.5	36.96	.823	97.9	182.7	19.35	.831	100.0	0.70	24.3	19.18	16.08	19.01
19.148	629.6	36.94	.823	97.8	180.5	19.33	.831	100.0	1.00	24.3	18.95	16.07	19.04
19.121	629.3	36.90	.824	97.7	174.4	19.30	.831	100.0	1.50	24.3	18.66	16.06	19.00
19.090	628.9	36.87	.823	97.6	172.5	19.27	.831	100.0	2.00	24.3	18.42	16.05	19.00

Table 7.17 Sensitivity of Front Junction Depth, Case 6, d = 2 mm, O_{pl} = 2

lr eff	V_{oc}	J_{sc}	lr ff	C_{eff}	ρ_e	eff	ff	X_L	X_f	X_b	log D_0	log D_B	log D_L
18.571	621.5	37.05	.807	98.1	131.1	19.12	.830	100.0	0.10	24.2	20.40	16.04	19.01
18.699	625.0	36.95	.810	97.9	118.2	19.19	.831	100.0	0.30	24.2	19.91	16.06	18.99
18.731	626.3	36.90	.811	97.7	114.8	19.20	.831	100.0	0.50	24.2	19.66	16.05	18.99
18.737	627.1	36.83	.811	97.6	112.4	19.20	.831	100.0	0.67	24.1	19.50	16.07	19.04
18.737	**627.1**	**36.83**	**.811**	**97.6**	**112.1**	**19.20**	**.831**	**100.0**	**0.70**	**24.2**	**19.48**	**16.07**	**19.00**
18.730	627.9	36.77	.811	97.4	113.1	19.19	.831	100.0	1.00	24.2	19.26	16.07	19.03
18.705	628.2	36.70	.811	97.2	112.2	19.16	.831	100.0	1.50	24.2	19.00	16.06	19.03
18.676	628.4	36.65	.811	97.1	114.4	19.14	.831	100.0	2.00	24.2	18.77	16.07	19.03

Table 7.18 Sensitivity of Front Junction Depth, Case 6, d = 3 mm, O_{pl} = 2

lr eff	V_{oc}	J_{sc}	lr ff	C_{eff}	ρ_e	eff	ff	X_L	X_f	X_b	log D_0	log D_B	log D_L
18.027	613.8	37.04	.793	98.1	87.0	18.84	.829	100.0	0.10	24.3	20.60	15.97	18.95
18.203	620.1	36.83	.797	97.5	81.5	18.96	.830	100.0	0.30	24.2	20.10	16.02	19.04
18.246	622.7	36.73	.798	97.3	80.8	18.99	.830	100.0	0.50	24.3	19.85	16.02	19.05
18.256	624.1	36.68	.798	97.1	82.1	19.01	.830	100.0	0.70	24.3	19.66	16.01	19.00
18.256	**624.2**	**36.66**	**.798**	**97.1**	**81.9**	**19.01**	**.831**	**100.0**	**0.72**	**24.3**	**19.65**	**16.02**	**19.00**
18.255	624.5	36.63	.798	97.0	81.3	19.00	.831	100.0	0.80	24.3	19.59	16.02	19.00
18.249	625.6	36.55	.798	96.8	82.7	19.00	.831	100.0	1.00	24.3	19.45	16.06	19.03
18.220	626.6	36.45	.798	96.6	84.0	18.98	.831	100.0	1.50	24.3	19.19	16.06	19.04
18.188	626.8	36.41	.797	96.4	85.0	18.96	.831	100.0	2.00	24.3	18.99	16.03	19.00

Table 7.20 High-Low Emmitter, Cases 1-6, d = 1 mm, O_{pl} = 2

lr eff	V_{oc}	J_{sc}	lr ff	C_{eff}	ρ_e	eff	ff	X_L	X_f	X_e	X_b	log D_0	log D_e	log D_B	log D_L
22.796	695.6	39.16	.837	99.5	109.9	22.92	.841	253.4	0.1	5.7	0.2	18.76	17.22	16.43	18.95
21.580	667.2	38.91	.831	98.9	150.1	21.75	.838	293.1	0.1	5.6	0.2	19.37	16.92	16.29	19.53
21.086	656.4	38.68	.830	98.3	151.0	21.24	.836	300.0	0.1	5.6	50.0	19.37	16.89	16.16	18.93
20.057	630.4	38.71	.822	98.3	207.8	20.28	.831	300.0	0.1	2.1	50.0	20.11	16.18	16.01	18.70
19.717	624.8	37.70	.837	95.8	194.4	19.57	.831	100.0	0.1	2.2	0.2	19.42	17.29	16.30	19.34
19.208	618.2	37.87	.821	96.2	187.3	19.41	.829	100.0	0.1	2.6	24.0	19.47	17.16	16.11	19.02

Table 7.21 High-Low Emmitter, Cases 1-6, d = 2 mm, O_{pl} = 2

lr eff	V_{oc}	J_{sc}	lr ff	C_{eff}	ρ_e	eff	ff	X_L	X_f	X_e	X_b	log D_0	log D_e	log D_B	log D_L
22.528	694.4	39.07	.830	99.3	61.3	22.81	.841	251.5	0.1	10.2	0.2	18.76	17.22	16.38	18.96
21.201	666.7	38.69	.822	98.3	89.3	21.61	.838	290.6	0.1	5.7	0.2	19.33	17.30	16.28	19.51
20.718	656.0	38.44	.821	97.6	87.7	21.09	.836	300.0	0.1	5.7	50.0	19.34	17.29	16.15	18.93
19.587	626.8	38.52	.811	97.9	104.9	20.05	.830	300.0	0.4	0.7	50.0	20.00	14.17	15.99	18.71
19.515	626.9	38.61	.806	98.1	132.5	20.10	.831	300.0	0.1	2.3	50.0	20.31	16.41	15.99	18.71
19.259	623.6	37.56	.822	95.4	120.4	19.45	.830	100.0	0.1	3.6	0.2	19.43	17.36	16.28	19.33
18.776	617.2	37.68	.807	95.7	115.3	19.28	.829	100.0	0.1	4.2	23.9	19.45	17.26	16.09	19.03

Table 7.22 High-Low Emmitter, Cases 1-6, d = 3 mm, O_{pl} = 2

lr eff	V_{oc}	J_{sc}	lr ff	C_{eff}	ρ_e	eff	ff	X_L	X_f	X_e	X_b	log D_0	log D_e	log D_B	log D_L
22.181	693.4	39.01	.820	99.1	53.6	22.74	.841	264.0	0.1	7.9	0.2	18.77	17.51	16.38	18.96
20.773	666.1	38.46	.811	97.7	67.4	21.46	.838	295.5	0.1	6.2	0.2	19.32	17.46	16.27	19.53
20.314	655.5	38.19	.812	97.0	63.9	20.93	.836	300.0	0.1	7.2	50.0	19.34	17.38	16.14	18.92
19.103	624.4	38.26	.800	97.2	74.2	19.83	.830	300.0	0.5	0.4	50.0	20.02	14.00	15.98	18.70
18.902	618.5	38.63	.791	98.1	90.0	19.80	.829	300.0	0.1	3.0	50.0	20.56	15.96	15.94	18.68
18.734	622.0	37.35	.806	94.9	87.6	19.28	.830	100.0	0.1	5.4	0.2	19.42	17.33	16.23	19.25
18.280	616.1	37.43	.793	95.1	86.1	19.11	.829	100.0	0.1	5.6	24.0	19.43	17.30	16.06	19.02

8 High Efficiency Concepts

In this chapter, the results from the previous two sections will be used along with several modifications to the SCAP1D code to define cell designs which achieve high efficiencies. Two new objectives, the maximization of V_{oc} and J_{sc}, will be used to determine the limitations on efficiency and explore possible improvements in cell design. Light trapping will be used to define higher efficiency designs, and results will be given for the six cases defined in chapter six. A limit analysis will be carried out to determine how cell efficiency is affected by the different physical mechanisms that limit cell efficiency and to define upper bounds for efficiency. The results given in this work will be compared to the theoretical upper bounds.

8.1 Maximizing V_{oc} and J_{sc}

In this section, two new objective functions, the maximization of V_{oc} and J_{sc}, will be considered. The designs that optimize V_{oc} and J_{sc} will have efficiencies that are less than the designs found in chapter six that optimize efficiency. The results of this section, however, will determine to what extent V_{oc} or J_{sc} limit the efficiency of the cells discussed in chapter 6.

In chapter six, the sensitivity analysis with respect to cell thickness suggested that, for cells with both surfaces passivated, the best values of open circuit voltage, fill factor, and collection efficiency were attained by thin cells. This can be validated by maximizing V_{oc}. Also, comparing the designs for maximum V_{oc} and the designs for maximum J_{sc} will illustrate the tradeoffs that must be made in designing a cell for maximum efficiency.

The numerical methods used to implement the maximization of V_{oc} and J_{sc} are similar to those described in chapter four for the maximization of efficiency. The solution associated with a previous function call in the optimization is used to initiate SCAP1D so that the numerical effort required to complete an optimization is significantly reduced. The methods used are described in appendix A.

Table 8.1 shows the results of maximizing the open circuit voltage for each of the six cases defined in chapter six. If both surfaces are passivated, the optimal thickness for maximum V_{oc} is very thin. Case six, which models a cell with an ohmic back contact, also results in a thin cell because of the low value of SRH lifetime used (τ_{n0} = 0.1 ms).

The bulk doping concentration also varies significantly between the cases that do and do not have both surfaces passivated. If both surfaces are passivated, the optimal D_B for maximum V_{oc} is at or near the lower bound of 10^{14}. The low bulk doping, coupled with a thin cell thickness, results in excellent collection efficiency as well as maximum V_{oc}. For cells with poor surface passivation, the optimal value of D_B for maximum V_{oc} is around 2 x 10^{17}.

The differences in the optimal value of D_B illustrate two diametrically opposite cell designs for increasing V_{oc}. For cells with both surfaces well passivated, the emphasis is on decreasing the bulk recombination to increase V_{oc}. This is achieved with the low bulk doping and the thin cell thickness. If the back surface is not well passivated, however, decreasing the cell thickness results in significant back surface recombination. Hence, the tradeoff is no longer favorable. Instead, the cell thickness is increased to isolate the generated minority carriers, and the bulk doping concentration is raised to increase the integrated base doping.

Table 8.2 shows the results of maximizing the short circuit current density for the six cases defined in chapter six. The optimal value of J_{sc} shows significantly less variation than V_{oc}. There is a slight decrease in the optimal value of J_{sc} in cases five and six reflecting the lower value of SRH saturation lifetime modeled in these cases.

The optimal cell design for maximum J_{sc} also shows little variation. The bulk doping is at the lower bound to preserve the SRH lifetime and diffusion length. The cell thickness is at the upper bound to increase the absorption of the incident energy. The thick BSF, which was optimal when maximizing efficiency for a cell with a poorly passivated back surface, is eliminated to reduce the bulk recombination. The back surface recombination is decreased instead by a thin heavily doped BSF.

The emitter is doped significantly lower to maximize J_{sc} than to maximize V_{oc}. The situation is reversed for the BSF. This reflects the need to avoid Auger recombination near the front surface, where most of the carriers are generated, when maximizing J_{sc}.

Table 8.3 shows the percent improvement of the maximized values of V_{oc} and J_{sc} compared to the V_{oc} and J_{sc} that results when the efficiency is optimized (from

Table 8.1 Maximization of V_{oc}, Cases 1-6

case	eff	V_{oc}	J_{sc}	V_{mp}	ff	C_{eff}	X_L	X_f	X_b	log D_0	log D_B	log D_L	O_{pt}
1	21.360	732.2	34.64	645.3	.842	100.0	23.5	0.10	0.2	18.84	14.00	18.92	2
2	20.290	683.1	35.72	597.2	.832	99.9	36.7	0.10	0.2	19.38	14.44	19.45	2
3	19.930	666.6	35.63	584.5	.839	90.3	300.0	0.10	10.4	19.29	17.46	19.34	2
4	18.700	638.4	35.13	557.5	.834	90.2	204.5	0.10	1.4	19.82	17.35	19.22	2
5	17.500	673.8	31.83	583.6	.816	99.9	10.0	0.10	0.2	19.32	14.00	19.37	2
6	17.930	641.9	33.50	560.6	.834	91.9	51.2	0.10	16.8	19.20	17.23	19.18	2

Table 8.2 Maximization of J_{sc}, Cases 1-6

case	eff	V_{oc}	J_{sc}	V_{mp}	ff	C_{eff}	X_L	X_f	X_b	log D_0	log D_B	log D_L	O_{pt}
1	21.930	702.7	39.44	600.5	.791	100.0	300.0	0.10	1.6	18.13	14.00	19.05	2
2	19.870	647.1	39.43	548.8	.779	100.0	300.0	0.10	0.2	16.99	14.00	19.60	2
3	18.790	596.6	39.43	510.6	.799	100.0	300.0	0.10	0.5	18.87	14.00	20.60	2
4	18.240	617.3	39.40	514.7	.750	99.9	300.0	0.10	0.2	19.02	14.00	19.87	2
5	15.720	591.9	39.32	463.9	.676	99.7	300.0	0.10	0.2	19.03	14.00	19.55	2
6	15.650	574.7	39.32	459.5	.692	99.7	300.0	0.10	0.7	18.40	14.00	20.51	2

Table 8.3 Percent Improvement in V_{oc} and J_{sc}

	V_{oc}	J_{sc}
case 1	4.4%	1.2%
case 2	2.2%	0.9%
case 3	1.5%	1.4%
case 4	1.1%	1.6%
case 5	4.8%	5.3%
case 6	1.6%	6.1%

chapter six). Disregarding the large improvements in J_{sc} in cases 5 and 6, which are the result of raising the upper bound on cell thickness from 100 μm to 300 μm, in all the cases but one there is more to be gained in V_{oc} than in J_{sc}. Furthermore, the values for J_{sc} are at or near the upper bound for an optical path of 600 μm (see figure 3.1), and there is very little improvement to be gained by further increasing the optical path (figure 3.2 suggests that by 600 μm 98% of the photons of energy greater than 1.1eV have been absorbed). An upper bound for V_{oc} is not as easily established, but, as expected, the V_{oc}'s in table 8.1 do not approach the theoretical maximum of 1.1 V.

Both surfaces must be passivated for a design to exist that significantly increases V_{oc}. The better the surface passivation (e.g., case 1), the greater the increase in V_{oc}. Assuming both surfaces are passivated, a lower SRH lifetime (e.g., case 5) results in a greater percentage increase in V_{oc} by changing to a thin cell design.

8.2 Light Trapping

The results of chapter six and the previous section suggest that significant improvements in cell efficiency can be made for cells with both surfaces passivated if the absorption of thin cells can be increased. This has also been reported in the literature by several authors [e.g., 8.1-8.3]. The absorption of thin cells can be increased by increasing the optical path that the incident illumination must pass through before leaving the cell (without increasing the cell thickness). By assuming the use of a perfect back surface reflector, the optical path is twice the cell thickness ($O_{pl} = 2$). By taking advantage of the high index of refraction of silicon and using surface texturing (or other light scattering schemes), it is possible to use refraction and/or total internal reflection to trap the light in the cell so that the optical path is many times the cell thickness [8.2, 8.4-8.7]. This section will investigate the use of light trapping in designing high efficiency silicon solar cells. It was necessary to modify SCAP1D to include light trapping in the code (see appendix A).

For all the results in this section, the effects of lateral resistance will be calculated using a grid spacing, defined in chapter 7, of d = 1 mm. The reflection and shadowing factor is 7%. The doping profile makes use of the complementary error function, as illustrated in figure 2.1 .

Tables 8.4-8.6 show the results of optimizing cases 1-6 with $O_{pl} = 2$ (summarized from results given in chapter 7), $O_{pl} = 10$, and $O_{pl} = 20$. For all the cases, the optimal value of the cell thickness decreases as absorption is enhanced. For almost all the cases, the optimal values of the doping concentrations decrease slightly as

Table 8.4 From chapter 7, O_{pl} = 2, cases 1-6

case	lr eff	V_{oc}	J_{sc}	lr ff	C_{eff}	ρ_e	eff	ff	X_L	X_f	X_b	log D_0	log D_B	log D_L
1	22.684	695.4	39.07	.835	99.5	152.4	22.86	.841	254.3	2.50	0.2	18.27	16.44	18.89
2	21.478	663.9	39.03	.829	99.0	188.8	21.70	.837	297.6	0.84	0.2	19.01	16.29	19.52
3	21.007	653.8	38.80	.828	98.4	171.1	21.20	.836	300.0	1.00	50.0	18.98	16.12	18.93
4	20.051	629.5	38.78	.821	98.3	206.3	20.29	.831	300.0	0.11	50.0	20.13	16.01	18.69
5	19.663	639.8	37.28	.824	98.8	203.8	19.88	.833	100.0	0.52	0.2	19.29	16.29	19.27
6	19.165	629.6	36.98	.823	97.9	190.8	19.36	.832	100.0	0.52	24.3	19.35	16.08	19.03

Table 8.5 Light trapping included, O_{pl} = 10, cases 1-6

case	lr eff	V_{oc}	J_{sc}	lr ff	C_{eff}	ρ_e	eff	ff	X_L	X_f	X_b	log D_0	log D_B	log D_L
1	23.750	713.0	39.84	.836	99.8	179.0	23.97	.844	82.2	2.27	0.2	18.21	16.40	18.88
2	22.309	673.3	39.89	.831	99.5	198.6	22.55	.839	112.6	0.83	0.2	18.99	16.28	19.43
3	21.617	655.0	39.88	.828	98.3	177.0	21.83	.836	262.0	0.84	50.0	19.09	16.06	18.93
4	20.680	632.4	39.74	.823	98.3	184.8	20.90	.832	205.1	0.18	50.0	19.96	15.92	18.62
5	21.109	653.5	39.12	.826	99.3	226.3	21.37	.836	47.3	0.50	0.2	19.24	16.35	19.29
6	20.260	631.5	38.98	.823	97.5	184.1	20.47	.832	91.1	0.69	24.1	19.19	16.03	18.96

Table 8.6 Light trapping included, O_{pl} = 20, cases 1-6

case	lr eff	V_{oc}	J_{sc}	lr ff	C_{eff}	ρ_e	eff	ff	X_L	X_f	X_b	log D_0	log D_B	log D_L
1	23.996	716.5	40.03	.837	99.9	177.4	24.21	.844	59.4	2.38	0.2	18.18	16.34	18.88
2	22.501	673.9	40.19	.831	99.5	195.8	22.74	.840	103.9	0.85	0.2	18.99	16.26	19.42
3	21.787	655.1	40.18	.828	98.2	168.0	21.99	.836	264.4	1.01	50.0	19.00	16.04	18.91
4	20.851	632.9	40.06	.822	98.3	195.8	21.09	.832	204.5	0.15	50.0	20.02	15.93	18.63
5	21.464	658.4	39.46	.826	99.5	233.0	21.74	.837	33.4	0.54	0.2	19.17	16.36	19.30
6	20.434	631.8	39.29	.823	97.5	182.9	20.65	.832	87.3	0.58	23.6	19.31	16.00	18.96

Table 8.7 Percent Improvement in Efficiency, V_{oc}, and J_{sc} (O_{pl} = 2 as baseline)

	eff		V_{oc}		J_{sc}	
	O_{pl} = 10	O_{pl} = 20	O_{pl} = 10	O_{pl} = 20	O_{pl} = 10	O_{pl} = 20
case 1	4.7%	5.8%	2.5%	3.0%	2.0%	2.5%
case 2	3.9%	4.8%	1.4%	1.5%	2.2%	3.0%
case 3	2.9%	3.7%	0.2%	0.2%	2.8%	3.6%
case 4	3.1%	4.0%	0.5%	0.5%	2.5%	3.3%
case 5	7.4%	9.2%	2.1%	2.9%	4.9%	5.8%
case 6	5.7%	6.6%	0.3%	0.3%	5.4%	6.2%

absorption is enhanced.

In table 8.7, the effect of light trapping on cell efficiency, V_{oc}, and J_{sc} is compared to the results of chapter 7 (given in table 8.4). Cases 5 and 6 show the largest percent improvements in efficiency. The large increases in J_{sc} in cases 5 and 6 reflect the fact that the upper bound for cell thickness was 100 μm in chapter 7.

Only the cells that have good front and back surface passivation show improvement in V_{oc}, and they fail to achieve the maximum V_{oc} solved for in the previous section at $O_{pl} = 2$ (including light trapping in the maximization of V_{oc} results in only small increases in the maximum value of V_{oc} associated with increasing the excess carrier concentration). The main reason these cells fail to achieve the maximum V_{oc} is the maximum efficiency cell design has significantly higher bulk recombination. The cell designs for maximum V_{oc} are thinner and the bulk doping is at the lower bound. It was shown in section 6.7 that there is a local maximum for efficiency associated with very thin cells and very light base doping at high lifetimes and low values of surface recombination velocities. Although this local maximum exist for cases 1 and 2, it is not the global maximum with respect to efficiency.

8.3 Limit Analysis

In this section, an upper bound will be set for the best efficiency that can be achieved by a silicon solar cell by making use of the SCAP1D and optimization codes. This will be achieved by disabling many of the physical mechanisms which lower the efficiency (e.g., recombination, shadowing and reflection, and bandgap narrowing). The upper bound will then be tightened by including unavoidable losses in the optimization runs. The results will then be compared to the efficiencies calculated in the previous section.

The first upper bound on cell efficiency requires only the spectrum of the incident illumination and the bandgap of silicon. Figure 8.1 illustrates the generation rate versus the optical path for the AM1.5 spectrum of concentration 1.2022 ($100mW/cm^2$) with a reflection and shadowing factor of 0%. Assuming each photon of energy greater than the bandgap generates one electron hole pair and the incident energy is almost entirely absorbed by 2000 μm (checked by integrating the AM1.5 spectrum for the number of photons greater than the bandgap of silicon), the maximum possible current density for a silicon cell is 43.36 mA/cm^2. Assuming each photon contributes the maximum energy to the load (1.1 eV per photon), an upper bound for the efficiency of a silicon solar cell is 47.7%.

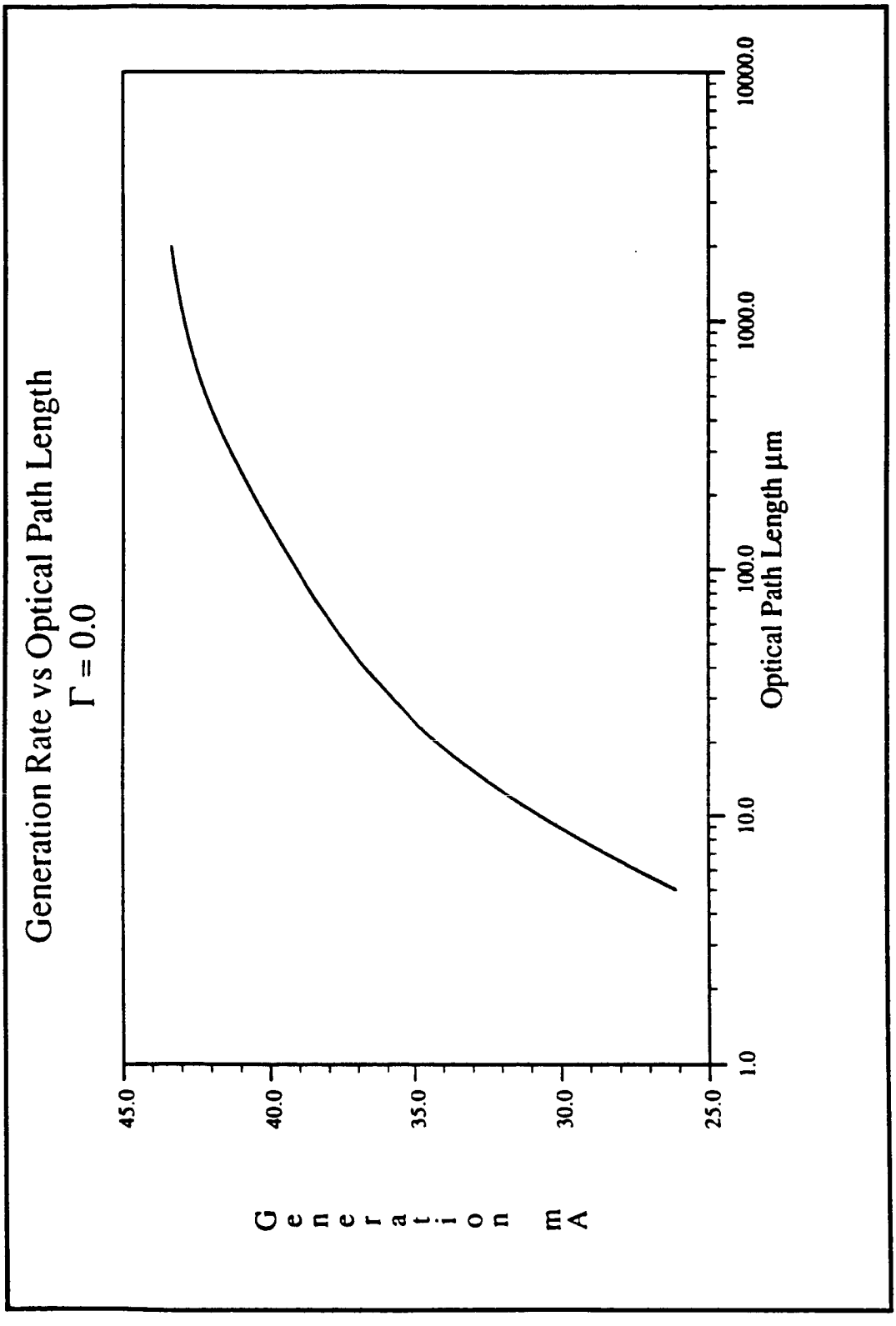
Generation Rate vs Optical Path Length
Γ = 0.0
Generation mA
45.0
40.0
35.0
30.0
25.0
1.0
10.0
100.0
1000.0
10000.0
Optical Path Length µm

figure 8.1

The next bound is calculated by considering only the effects of radiative recombination. To do this it was necessary to modify SCAP1D to include radiative recombination (see appendix A). Auger recombination, SRH recombination and bandgap narrowing are all disabled. SRH recombination is disabled by setting τ_n = 10 seconds and τ_p = 5 seconds (τ_{n0} = 10 seconds, τ_{p0} = 5 seconds, and Z_{kn} = Z_{kp} = 1 x 10^{50} in equation 3.14a and 3.15b). Therefore, radiative recombination is the dominant recombination process over the range of doping concentrations considered (1 x 10^{14} to 4 x 10^{20}). The surface recombination velocities are set to zero, and the reflection and shadowing factor is set to zero.

Table 8.8 shows the results of optimizing the cell efficiency under the above conditions. Three optical path length factors were considered; O_{pl} = 2, O_{pl} = 10, and O_{pl} = 20. The optical path length factor, O_{pl}, is a multiplicative factor that relates the cell thickness and the actual optical path of the incident energy. By assuming a perfect back surface reflector, the optical path traversed by the incident illumination is twice the cell thickness (O_{pl} = 2). Optical paths greater than twice the cell thickness are achieved by light trapping (see appendix A).

The results, ≈ 30%, agree well with the limit calculated by Shockley and Queisser [8.8]. In [8.8], an upper bound of 30% was calculated for the efficiency of a silicon solar cell by considering the energy distributions of the radiation emitted by 300 K (solar cell) and 6000 K (the sun) black bodies and assuming radiative recombination as the only loss mechanism. The differences in the limits are a result of the differences between a 6000 K black body spectrum and the AM1.5 spectrum.

The lifetime associated with radiative recombination is a linear function of the doping concentration. The lifetime is high enough that it is still possible to heavily dope the emitter, bulk, and BSF to increase V_{oc}. At a doping concentration of 1 x 10^{17} (≈ D_B), the lifetime associated with radiative recombination is 4 ms.

The effect of light trapping is to decrease the value of cell thickness that is optimal. This decreases the amount of recombination in the cell and increases the excess carrier concentrations, both of which increase V_{oc}. For all three cases, the optical path is long enough that over 98% of the photons of energy greater than 1.1 eV are absorbed.

The bound can be further tightened by including Auger recombination in the model. The results are shown in table 8.9 . For the case with O_{pl} = 2, the effect on efficiency is a drop of 1.0 percentage point compared to table 8.8 . The inclusion of Auger recombination does not cause a larger drop in efficiency because the optimization results in lower doping concentrations. The reductions in the doping

Table 8.8 Radiative Recombination Only

eff	V_{oc}	J_{sc}	V_{mp}	ff	C_{eff}	X_L	X_f	X_b	log D_0	log D_B	log D_L	O_{pl}
29.250	808.5	42.02	721.2	.861	100.0	224.7	0.18	0.4	19.90	16.77	19.60	2
31.150	852.4	42.17	763.8	.867	100.0	41.4	0.19	0.4	19.90	16.96	19.61	10
31.793	867.5	42.21	778.4	.868	100.0	23.2	0.19	0.5	19.90	17.05	19.61	20

Table 8.9 Radiative and Auger Recombination

eff	V_{oc}	J_{sc}	V_{mp}	ff	C_{eff}	X_L	X_f	X_b	log D_0	log D_B	log D_L	O_{pl}
28.315	756.4	42.34	688.8	.884	100.0	282.1	0.65	0.2	15.75	15.98	17.42	2
29.803	785.9	42.54	719.4	.892	100.0	55.5	0.24	0.2	15.84	16.17	16.57	10
30.285	796.2	42.57	730.0	.894	100.0	31.1	0.10	0.2	15.77	16.27	16.67	20

Table 8.10 Radiative and Auger Recombination and BGN

eff	V_{oc}	J_{sc}	V_{mp}	ff	C_{eff}	X_L	X_f	X_b	log D_0	log D_B	log D_L	O_{pl}
28.279	755.3	42.35	687.7	.884	100.0	283.9	0.10	0.2	14.83	15.92	16.32	2
29.758	784.4	42.55	718.0	.891	100.0	56.2	0.11	0.2	15.65	16.09	16.60	10
30.232	794.4	42.59	728.1	.893	100.0	31.9	0.10	0.2	14.86	16.13	16.54	20

Table 8.11 Radiative and Auger Recombination, BGN, S_f = 1 cm/s, and S_b = 1 cm/s

eff	V_{oc}	J_{sc}	V_{mp}	ff	C_{eff}	X_L	X_f	X_b	log D_0	log D_B	log D_L	O_{pl}
28.197	753.6	42.41	685.1	.882	100.0	300.0	0.10	0.2	17.81	15.88	17.95	2
29.506	778.8	42.77	710.0	.886	100.0	69.8	0.10	0.2	17.80	15.98	17.86	10
29.880	786.6	42.87	717.2	.886	100.0	43.1	0.10	0.2	17.82	15.99	17.85	20

Table 8.12 Radiative and Auger Recombination, BGN, S_f = 10 cm/s, and S_b = 10 cm/s

eff	V_{oc}	J_{sc}	V_{mp}	ff	C_{eff}	X_L	X_f	X_b	log D_0	log D_B	log D_L	O_{pl}
27.800	749.9	42.42	677.5	.874	100.0	300.0	0.10	0.2	18.36	14.00	18.61	2
28.753	760.9	43.27	687.1	.873	100.0	142.5	0.10	0.2	18.32	15.73	18.44	10
29.005	761.2	43.63	687.2	.873	100.0	143.1	0.10	0.2	18.39	14.48	18.52	20

Table 8.13 Radiative and Auger Recombination, BGN, S_f = 100 cm/s, and S_b = 100 cm/s

eff	V_{oc}	J_{sc}	V_{mp}	ff	C_{eff}	X_L	X_f	X_b	log D_0	log D_B	log D_L	O_{pl}
26.554	732.2	42.42	651.3	.855	100.0	300.0	0.10	0.2	18.91	14.00	19.13	2
27.397	732.9	43.71	652.0	.855	100.0	300.0	0.10	0.2	18.91	14.00	19.13	10
27.625	733.1	44.06	652.2	.855	100.0	300.0	0.10	0.2	18.91	14.00	19.13	20

Table 8.14 Radiative Recombination, S_f = 100 cm/s, and S_b = 100 cm/s

eff	V_{oc}	J_{sc}	V_{mp}	ff	C_{eff}	X_L	X_f	X_b	log D_0	log D_B	log D_L	O_{pl}
29.239	807.8	42.04	720.5	.861	100.0	228.5	0.10	0.2	20.60	16.76	20.60	2
31.089	849.3	42.26	760.7	.866	100.0	44.4	0.10	0.2	20.60	14.00	20.60	10
31.689	862.3	42.36	773.3	.868	100.0	26.0	0.10	0.2	20.60	14.00	20.60	20

Table 8.15 Radiative and Auger Recombination, BGN, S_f = 100 cm/s, S_b = 100 cm/s, and Γ = .07

eff	V_{oc}	J_{sc}	V_{mp}	ff	C_{eff}	X_L	X_f	X_b	log D_0	log D_B	log D_L	O_{pl}
24.629	730.6	39.45	649.6	.855	100.0	300.0	0.10	0.2	18.91	14.00	19.13	2
25.411	731.3	40.65	650.3	.855	100.0	300.0	0.10	0.2	18.90	14.00	19.13	10
25.622	731.5	40.98	650.5	.855	100.0	300.0	0.10	0.2	18.91	14.00	19.13	20

concentrations, however, result in a decrease in the integrated doping in the base and emitter. This results in a reduction in V_{oc}.

The optimal value of the front surface doping concentration is very low ($\simeq 6 \times 10^{15}$). This implies that the emitter may be in high injection at the contacts. The boundary conditions for the majority carrier concentration used in SCAP1D assumed heavy doping at the contacts so that ohmic boundary conditions could be used. If this boundary condition is violated, it would be equivalent to surface recombination. Hence, the efficiency predicted by SCAP1D would be low.

Table 8.10 shows the results of also including bandgap narrowing in the model. The emitter and the BSF are doped at concentrations that avoid the detrimental effects of heavy doping. Therefore, the change in efficiency from the previous case is minimal.

At this point one could argue that all the fundamental losses are included in the analysis. Other losses such as SRH recombination, surface recombination, and shadowing and reflection, although not unavoidable, are more closely related to the technology used to produce the cell. Hence, we find that the upper limit on efficiency is $\simeq$ 30% if light trapping can be successfully employed to achieve O_{pl} = 20. The limit would be slightly higher if O_{pl} were increased. The upper limit on efficiency is 28.3% for O_{pl} = 2. The results in the previous section fall well below this limit.

Of course, it is not possible to achieve the above limits because other loss mechanisms exist in the cell including surface recombination, SRH recombination, and reflection. Also, for the conventional geometry considered in this work, there are losses associated with shadowing and lateral resistance.

The effects of surface recombination are shown in tables 8.11-8.13 . The front and back surface recombination velocities are equal, and runs were made at 1, 10, and 100 cm/s. The upper bound on efficiency is substantially decreased as the surface recombination velocities are increased to 100 cm/s.

As the surface recombination velocities are increased, it is necessary to more heavily dope the emitter and BSF. Also, the cell thickness is increased to isolate the generated carriers from the surfaces. Both of the above result in higher recombination. Although the collection efficiency remains approximately at 100%, the increase in recombination and bandgap narrowing result in a substantial decrease in the V_{oc} of the cell as the surface recombination velocities are increased.

Table 8.14, which shows the optimization results including surface and radiative recombination only, illustrates that it is the combination of heavy doping effects and surface recombination which results in the sudden decrease in the upper bound for efficiency. If either surface recombination or heavy doping effects are

not included in the model, a cell design can be found which achieves an efficiency very close to the upper bound established by considering radiative recombination only.

The effect of a 7% shadowing and reflection factor is illustrated in table 8.15 . By comparing tables 8.13 and 8.15 it is seen that not only is the short circuit current density decreased by 7%, but the V_{oc} also decreases slightly due to a decrease in the excess carrier concentrations. This is the same effect which results in higher efficiencies at higher sun concentrations. The effect of the 7% shadowing factor is approximately a 7.25% reduction in efficiency.

Figure 8.2 summarizes how the upper bound of efficiency is affected by each of the loss mechanisms considered so far in this section. The largest reductions in the upper bound are a result of heavy doping effects in conjunction with surface recombination velocities ≈ 10 cm/s or greater and the inclusion of the reflection and shadowing factor.

The effect of varying the SRH saturation lifetime (τ_{n0}) has been discussed in section 6.7 . Now those results will be extended to include the effects of light trapping and compared to the limits derived above.

In figure 8.2, cases E (table 8.11), F (table 8.12), and G (table 8.13) are each extended by considering SRH recombination with a saturation lifetime (τ_{n0}) of 100 ms, 10 ms, 1 ms, and 0.1 ms. The results of the optimizations are given in tables 8.16-8.27 .

The addition of light trapping favors the local maximum associated with thin cells and light bulk doping. In several cases, the design associated with the global maximum changes as O_{pl} is increased (e.g., table 8.21, 8.22, and 8.23). In generating the results given in tables 8.16-8.27, it was necessary to solve the maximization of efficiency twice. One run was initiated from a cell with a bulk doping concentration of 10^{16}, while the other was initiated from a cell with a bulk doping concentration of 10^{14}. If the two optimizations converged to different cell designs (for some runs one or the other of the local maximums did not exist, as described in section 6.7), the one with the greatest efficiency was reported.

For τ_{n0} = 0.1 ms, the optimal value of the bulk doping is never at the lower bound. This could be due to the lower bound of 10 μm on the cell thickness. For the local maximums associated with $D_B = 10^{14}$, the lower bound on cell thickness was active. If the lower bound for cell thickness was lowered and/or O_{pl} was increased, the local maximum associated with light bulk doping would be the global maximum.

Figure 8.3 illustrates the effect on efficiency of including SRH recombination at different levels on cases E, F, and G from figure 8.2 . The bulk lifetime

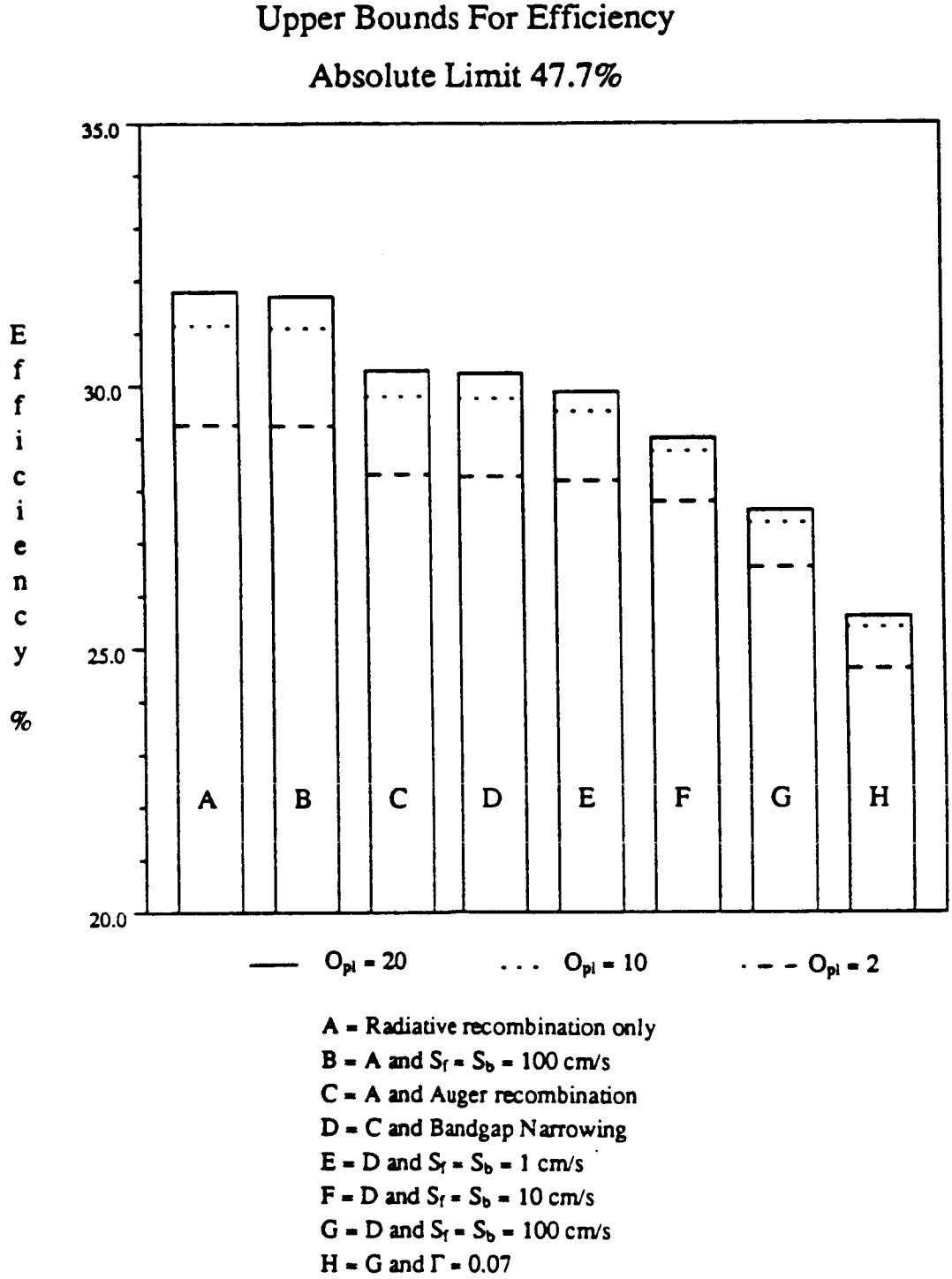
Upper Bounds For Efficiency
Absolute Limit 47.7%
Efficiency %
35.0
30.0
25.0
20.0
A
B
C
D
E
F
G
H
O_{pl} = 20
O_{pl} = 10
O_{pl} = 2
A = Radiative recombination only
B = A and $S_f = S_b$ = 100 cm/s
C = A and Auger recombination
D = C and Bandgap Narrowing
E = D and $S_f = S_b$ = 1 cm/s
F = D and $S_f = S_b$ = 10 cm/s
G = D and $S_f = S_b$ = 100 cm/s
H = G and Γ = 0.07

Figure 8.2

Table 8.16 BGN, Auger, Rad, SRH (τ_{n0} = 100 ms), S_f = 1 cm/s, S_b = 1 cm/s, Γ = 0

eff	V_{oc}	J_{sc}	V_{mp}	ff	C_{eff}	X_L	X_f	X_b	log D_0	log D_B	log D_L	O_{pt}
28.006	755.0	42.26	684.9	.878	100.0	266.4	0.10	0.2	17.88	14.00	18.06	2
29.432	779.9	42.70	710.2	.884	100.0	64.6	0.10	0.2	17.88	14.00	17.95	10
29.833	787.9	42.81	717.7	.884	100.0	40.0	0.10	0.2	17.88	14.00	17.93	20

Table 8.17 BGN, Auger, Rad, SRH (τ_{n0} = 100 ms), S_f = 10 cm/s, S_b = 10 cm/s, Γ = 0

eff	V_{oc}	J_{sc}	V_{mp}	ff	C_{eff}	X_L	X_f	X_b	log D_0	log D_B	log D_L	O_{pt}
27.665	749.5	42.42	676.1	.870	100.0	300.0	0.10	0.2	18.40	14.00	18.61	2
28.695	764.2	43.12	689.0	.871	100.0	111.3	0.10	0.2	18.37	14.00	18.49	10
28.950	765.4	43.43	690.1	.871	100.0	102.5	0.10	0.2	18.42	14.00	18.49	20

Table 8.18 BGN, Auger, Rad, SRH (τ_{n0} = 100 ms), S_f = 100 cm/s, S_b = 100 cm/s, Γ = 0

eff	V_{oc}	J_{sc}	V_{mp}	ff	C_{eff}	X_L	X_f	X_b	log D_0	log D_B	log D_L	O_{pt}
26.474	731.9	42.42	650.3	.853	100.0	300.0	0.10	0.2	18.91	14.00	19.13	2
27.315	732.6	43.71	651.1	.853	100.0	300.0	0.10	0.2	18.91	14.00	19.13	10
27.543	732.8	44.06	651.3	.853	100.0	300.0	0.10	0.2	18.91	14.00	19.13	20

Table 8.19 BGN, Auger, Rad, SRH (τ_{n0} = 10 ms), S_f = 1 cm/s, S_b = 1 cm/s, Γ = 0

eff	V_{oc}	J_{sc}	V_{mp}	ff	C_{eff}	X_L	X_f	X_b	log D_0	log D_B	log D_L	O_{pt}
27.060	763.3	41.30	686.9	.858	100.0	144.4	0.10	0.2	17.86	14.00	17.96	2
28.984	783.9	42.35	710.7	.873	100.0	47.3	0.10	0.2	17.88	14.00	17.92	10
29.493	791.0	42.57	717.9	.876	100.0	31.1	0.10	0.2	17.85	14.00	17.91	20

Table 8.20 BGN, Auger, Rad, SRH (τ_{n0} = 10 ms), S_f = 10 cm/s, S_b = 10 cm/s, Γ = 0

eff	V_{oc}	J_{sc}	V_{mp}	ff	C_{eff}	X_L	X_f	X_b	log D_0	log D_B	log D_L	O_{pt}
26.724	753.5	41.77	672.5	.849	100.0	191.0	0.10	0.2	18.40	14.00	18.53	2
28.248	768.3	42.78	688.5	.859	100.0	70.5	0.10	0.2	18.38	14.00	18.46	10
28.590	772.5	42.99	692.2	.861	100.0	50.4	0.10	0.2	18.40	14.00	18.44	20

Table 8.21 BGN, Auger, Rad, SRH (τ_{n0} = 10 ms), S_f = 100 cm/s, S_b = 100 cm/s, Γ = 0

eff	V_{oc}	J_{sc}	V_{mp}	ff	C_{eff}	X_L	X_f	X_b	log D_0	log D_B	log D_L	O_{pl}
25.884	722.4	42.36	636.1	.846	99.9	300.0	0.10	0.2	18.81	16.33	18.99	2
26.827	735.2	43.18	649.9	.845	100.0	123.9	0.10	0.2	18.89	14.00	19.00	10
27.061	735.3	43.55	650.0	.845	100.0	126.6	0.10	0.2	18.90	14.00	19.00	20

Table 8.22 BGN, Auger, Rad, SRH (τ_{n0} = 1 ms), S_f = 1 cm/s, S_b = 1 cm/s, Γ = 0

eff	V_{oc}	J_{sc}	V_{mp}	ff	C_{eff}	X_L	X_f	X_b	log D_0	log D_B	log D_L	O_{pl}
24.420	704.6	41.14	618.7	.842	99.7	142.4	0.10	0.2	17.79	16.55	17.79	2
26.939	792.8	40.66	702.0	.836	100.0	17.2	0.10	0.2	17.67	14.00	17.70	10
27.751	797.7	41.32	709.1	.842	100.0	13.3	0.10	0.2	17.69	14.00	17.71	20

Table 8.23 BGN, Auger, Rad, SRH (τ_{n0} = 1 ms), S_f = 10 cm/s, S_b = 10 cm/s, Γ = 0

eff	V_{oc}	J_{sc}	V_{mp}	ff	C_{eff}	X_L	X_f	X_b	log D_0	log D_B	log D_L	O_{pl}
24.386	702.4	41.22	616.7	.842	99.7	149.7	0.10	0.2	18.25	16.55	18.26	2
26.435	770.2	41.45	675.7	.828	100.0	26.2	0.10	0.2	18.32	14.00	18.36	10
27.104	773.6	41.99	681.2	.834	100.0	20.0	0.10	0.2	18.31	14.00	18.37	20

Table 8.24 BGN, Auger, Rad, SRH (τ_{n0} = 1 ms), S_f = 100 cm/s, S_b = 100 cm/s, Γ = 0

eff	V_{oc}	J_{sc}	V_{mp}	ff	C_{eff}	X_L	X_f	X_b	log D_0	log D_B	log D_L	O_{pl}
24.208	693.0	41.52	608.1	.841	99.5	183.3	0.10	0.2	18.79	16.49	18.90	2
25.704	715.5	42.53	629.4	.845	99.9	57.8	0.10	0.2	18.77	16.55	18.85	10
26.080	721.1	42.76	634.9	.846	99.9	39.3	0.10	0.2	18.78	16.54	18.84	20

Table 8.25 BGN, Auger, Rad, SRH (τ_{n0} = 0.1 ms), S_f = 1 cm/s, S_b = 1 cm/s, Γ = 0

eff	V_{oc}	J_{sc}	V_{mp}	ff	C_{eff}	X_L	X_f	X_b	log D_0	log D_B	log D_L	O_{pl}
21.880	659.1	39.68	576.4	.837	99.2	75.0	0.10	0.2	17.86	16.44	16.96	2
23.906	688.7	41.30	603.9	.840	99.8	25.4	0.10	0.2	17.99	16.56	17.21	10
24.539	700.9	41.62	615.1	.841	99.9	16.2	0.10	0.2	17.94	16.58	16.98	20

Table 8.26 BGN, Auger, Rad, SRH (τ_{n0} = 0.1 ms), S_f = 10 cm/s, S_b = 10 cm/s, Γ = 0

eff	V_{oc}	J_{sc}	V_{mp}	ff	C_{eff}	X_L	X_f	X_b	log D_0	log D_B	log D_L	O_{pt}
21.871	658.6	39.70	575.9	.836	99.2	75.8	0.10	0.2	18.16	16.43	17.70	2
23.880	687.2	41.35	602.8	.840	99.8	26.2	0.10	0.2	18.11	16.57	17.70	10
24.499	698.3	41.70	612.7	.841	99.9	17.1	0.10	0.2	18.12	16.58	17.66	20

Table 8.27 BGN, Auger, Rad, SRH (τ_{n0} = 0.1 ms), S_f = 100 cm/s, S_b = 100 cm/s, Γ = 0

eff	V_{oc}	J_{sc}	V_{mp}	ff	C_{eff}	X_L	X_f	X_b	log D_0	log D_B	log D_L	O_{pt}
21.821	655.3	39.83	572.9	.836	99.1	82.0	0.10	0.2	18.63	16.41	18.59	2
23.747	679.9	41.59	596.2	.840	99.7	30.6	0.10	0.2	18.61	16.53	18.58	10
24.309	688.6	41.98	604.3	.841	99.8	20.8	0.10	0.2	18.60	16.56	18.58	20

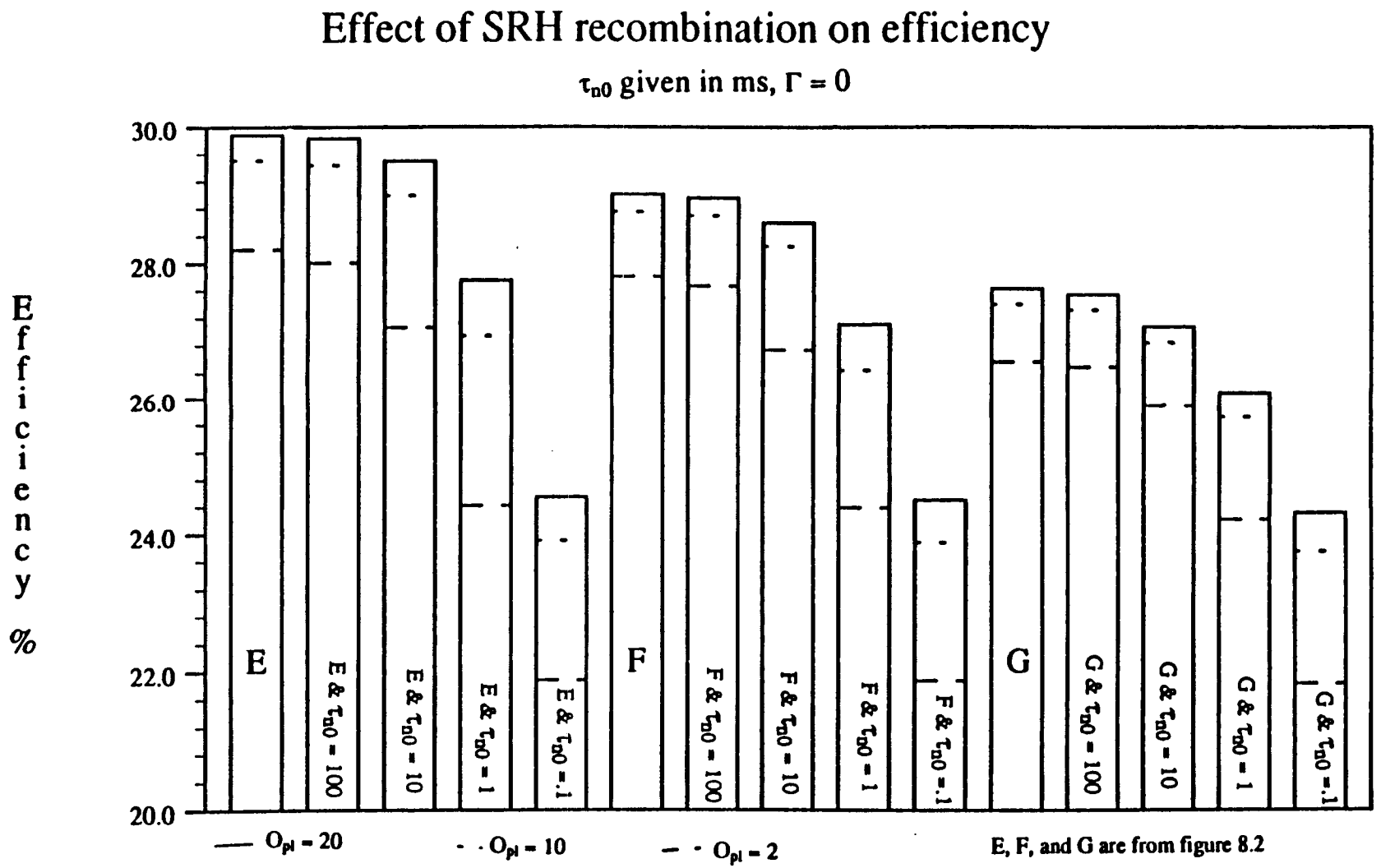
Effect of SRH recombination on efficiency
τ_{n0} given in ms, $\Gamma = 0$
Efficiency %
30.0
28.0
26.0
24.0
22.0
20.0
E
E & τ_{n0} = 100
E & τ_{n0} = 10
E & τ_{n0} = 1
E & τ_{n0} = .1
F
F & τ_{n0} = 100
F & τ_{n0} = 10
F & τ_{n0} = 1
F & τ_{n0} = .1
G
G & τ_{n0} = 100
G & τ_{n0} = 10
G & τ_{n0} = 1
G & τ_{n0} = .1
— O_{pl} = 20
- - O_{pl} = 10
— - O_{pl} = 2
E, F, and G are from figure 8.2

Figure 8.3

associated with cases E, F, and G is determined by radiative recombination and ranges, since lifetime is dependent on the bulk doping, from 5000 to 500 ms. As already observed in previous results, the higher lifetime cases are more significantly affected by surface passivation.

A value of τ_{n0} of 100 ms results in almost no change from the efficiencies calculated without including SRH recombination. A small difference exists at τ_{n0} = 10 ms. The effect becomes quite apparent, particularly at $S_f = S_b = 1$ cm/s, as τ_{n0} is further decreased to 1 ms and 0.1 ms.

All the cells benefit from increasing O_{pl}, but the lowest lifetimes benefit the most, since the lower lifetimes show greater decreases in bulk recombination.

The efficiencies calculated for cases 5 and 6 are substantially less than for the same lifetime with lower surface recombination velocities even after the shadowing and reflection factor is accounted for. Although figure 8.3 suggests that at τ_{n0} = 0.1 ms, the efficiency is insensitive to the recombination velocities up to 100 cm/s, the efficiency does decrease when the recombination velocities are increased to 1,000 cm/s.

8.4 Summary

The main conclusions of this chapter are summarized below.

- For cells with good front and back surface passivation, the maximum V_{oc} is attained by thin cells with very low bulk doping ($\approx 10^{14}$). Where as, for cells with poor back surface passivation, the maximum V_{oc} is attained by thicker cells with high bulk doping ($\approx 2 \times 10^{17}$).
- The cell design for maximum J_{sc} is a thick cell with low bulk doping and a thin BSF.
- Light trapping results in a much thinner value of cell thickness being optimal, particularly if both surfaces are well passivated and/or the cell is made from a substrate with a low value of SRH saturation lifetime.
- Heavy doping effects combined with surface recombination, shadowing and reflection, and SRH saturation lifetimes below 10 ms are the primary mechanisms that lower cell efficiency.

References

[1.1] M. Wolf,"The Influence of Heavy Doping Effects on Si Solar Cell Performance", Proc. 18th IEEE Photovoltaic Specialists Conference, Las Vegas, Nevada, Oct. 21-25, pp. 33-38, 1985

[1.2] P. Verlinden, F. Van de Wiele, G. Stehelin, J.P. David, "Optimized Interdigitated Back Contact (IBC) Solar Cell for High Concentration Sunlight", Proc. 18th IEEE Photovoltaic Specialists Conference, Las Vegas, Nevada, Oct. 21-25, pp. 33-38, 1985

[1.3] E.I.H. Lin, "Sensitivity Analysis of Low Bulk Resistivity Solar Cells", Proc. 18th IEEE Photovoltaic Specialists Conference, Las Vegas, Nevada, Oct. 21-25, pp. 715-719, 1985

[1.4] W.Z. Chen, C.Y. Wu, "An Analytical Model for High-Low-Emitter (HLE) Solar Cells in Concentrated Sunlight", Solid State Electronics, vol. 24, num. 11, pp. 1025-1037, 1981

[1.5] H.T. Weaver, "Ineffectiveness of Low-High Junctions in Optimizing Solar Cell Designs", Solar Cells, vol. 5, pp. 275-292, 1982

[1.6] J.M. Ruiz, A. Cuevos, M. Cid, "Influence of the Bulk Region on the Performance of Silicon Solar Cells", Proc. 17th IEEE Photovoltaic Specialists Conference, Kissimmee, Florida, May 1-4, pp. 615-620, 1984

[1.7] F.A. Lindholm, C.T. Sah, "Theoretical Performance Limits and Measured Performance of Thin Extended BSF P/N Junction Silicon Solar Cells", Proc. 17th IEEE Photovoltaic Specialists Conference, Kissimmee, Florida, May 1-4, pp. 1202-1206, 1984

[1.8] M.A. Green, Solar Cells, Prentice-Hall, Englewood Cliffs, N.J., pp. 138-152, 1982

[1.9] W.Z. Chen, C.Y. Wu, "A New Method for Computer Aided Optimization of Solar Cell Structures", Cells in Concentrated Sunlight", Solid State Electronics, vol. 28, num. 8, pp. 751-761, 1985

[2.1] H. Rosenbrock, "An automatic Method for Finding the Greatest or Least Value of a Function", Computer Journal, vol. 3, pp. 175-184, 1960

[2.2] L.A. Schmit, "Structural Synthesis - Its Genesis and Development", AIAA Journal, vol. 19, num. 10, pp. 1249-1263, 1981

[2.3] W.C. Davidon, "Variable Metric Method for Minimization", AEC Res. and Dev. Report ANL-5990 (revised)

[2.4] R. Fletcher, M.J.D. Powell, "A Rapidly Convergent Descent Method for Minimization", Computer Journal, vol. 6, pp. 163-168, 1963

[2.5] C.G. Broyden, "The convergence of a Class of Double Rank Minimization Algorithms", Journal of the Institute of Mathematics and its Applications, vol. 6, pp. 76-90, 1970

[2.6] R. Fletcher, "A New Approach to Variable Metric Algorithms", Computer Journal, vol. 13, pp. 317-321, 1970

[2.7] D. Goldfarb, "A Family of Variable Metric Methods Derived by Variational Means", Maths. Comput., vol. 24, pp. 23-26, 1970

[2.8] D.F. Shanno, "Conditioning of Quasi-Newton Methods for Function Minimization", Maths. Comput., vol. 24, pp. 647-656, 1970

[2.9] R. Fletcher, Practical Methods of Optimization: Volume 1, John Wiley and Sons, pp. 54-60, 1980

[3.1] S. Selberherr, Analysis and Simulation of Semiconductor Devices, Wien Springer-Verlag, 1984

[3.2] M.S. Lundstrum, "Numerical Analysis of Silicon Solar Cells", Report no. TR-EE 80-27, School of Electrical Engineering, Purdue University, Lafayette, Indiana, December 1980

[3.3] A. Marshack, and K. M. Van Vliet, "Electrical Currents in Solids with Position-Dependent Band Structure", Solid State Electronics, vol. 21, pp. 417-427, 1978

[3.4] A. Marshack, and K. M. Van Vliet "Carrier Densities and Emitter Efficiency in Degenerate Materials with Position Dependent Band Structure", Solid State Electronics, vol. 21, pp. 429-434, 1978

[3.5] A. Marshack, and K. M. Van Vliet, "The Shockley-like equations for the Carrier Densities and Current Flows in Materials with a Nonuniform Composition", Solid State Electronics, vol. 23, pp. 49-53, 1980

[3.6] M.S. Adler,"A Method for Achieving and Choosing Variable Density Grids in Finite Difference Formulations and the Importance of Degeneracy and Bandgap Narrowing in Device Modeling", Proc. of the NASACODE I Conference, Trinity College, Dublin, Ireland, pp. 3-30, 1979

[3.7] M.S. Adler, "Achieving Accuracy in Transistor and Thyristor Modeling", Tech. Digest, 1978, Washington D.C., pp. 550-555

[3.8] M.S. Adler, "An Operational Method to Model Carrier Degeneracy and Bandgap Narrowing", Solid State Electronics, vol. 26, num. 5, pp. 387-396, 1983

[3.9] H.S. Bennett, "Heavy Doping Effects on Bandgaps, Effective Intrinsic Carrier Concentration, and Carrier Mobilities and Lifetimes", Solid State Electronics, vol. 28, num. 1, pp. 193-200, 1985

[3.10]J.A. del Alamo, R.M. Swanson, A. Lietoila, "Photovoltaic Measurement of Bandgap Narrowing in Moderately Doped Silicon", Solid State Electronics, vol. 26, num. 6, pp. 483-489, 1983

[3.11]K. Rajkanan, R. Singh, and J. Shewchun Solid State Electronics, vol. 22, pp. 793-795, 1979

[3.12]J. Dziewior, and W. Schmid, "Auger Coefficients for Highly Doped and Highly Excited Silicon", Applied Physics Letters, vol. 31, pp. 346-348, 1977

[3.13]W. Shockley, and W. Read, "Statistics of the Recombinations of Holes and Electrons", Physical Review, vol. 87, No. 5, pp. 835-842, 1952

[3.14]R. Hall, "Electron-Hole Recombination in Germanium", Physical Review, vol. 87, pp. 387, 1952

[3.15]J. G. Fossum, "Computer-Aided Numerical Analysis of Silicon Solar Cells", Solid State Electron, vol. 19, pp. 269-277, 1976

[3.16]W. L. Engl, H. Dirks, "Introduction to the Numerical Analysis of Semiconductor Devices and Integrated Circuits", pp. 42-46, Dublin, Boole Press, 1981

[3.17]D. M. Caughey, R. E. Thomas, "Carrier Mobilities in Silicon Empirically Related to Doping and Field", Proc. IEEE, vol. 55, pp. 2192-2193, 1967

[3.18]G. Baccarani, P. Ostoja, "Electron Mobility Empirically Related to the Phosphorus Concentration in Silicon", Solid-State Electron, vol. 18, pp. 579-580, 1975

[3.19]J. C. Plunkett, J. L. Stone, A. Leu, "A Computer Algorithm for Accurate and Repeatable Profile Analysis Using Anodization and Stripping of Silicon", Solid-State Electron, vol. 20, pp. 447-453, 1977

[3.20]S. M. Sze, Physics of Semiconductor Devices, New York, Wiley, 1969

[3.21]J. W. Slotboom, H. C. DeGraf, "Measurements of Bandgap Narrowing in Si Bipolar Transistors", Solid-State Electron, vol. 19, pp. 857-862, 1976

[3.22]J. W. Slotboom, H. C. DeGraf, "Bandgap Narrowing in Silicon Bipolar Transistors", IEEE Tans. Electron Devices ED-24, No. 8, pp. 123-1125, 1977

[3.23]J. W. Slotboom, "The pn-Product in Silicon", Solid-State Electron, vol. 20, pp. 279-283, 1977

[3.24]D.L. Scharfetter and H.K. Gummel, "Large-Signal Analysis of a Silicon Read Diode Oscillator", IEEE Trans. Electron Devices, vol. ED-16, pp. 64-67, 1969

[3.25]Terrestrial Photovoltaic Measurement Procedures, Report ERDA/NASA /1022-77/16, June 1977

[4.1] P.E. Gill, W. Murray, and M.H. Wright, Practical Optimization, Academic Press, pp. 7-14, 1981

[5.1] G.E.P. Box, "Evolutionary Operation: A Method for Increasing Industrial Productivity", Applied Statistics, vol. 6, pp. 81-101, 1957

[5.2] W. Spendly, G.R. Hext, F.R. Himsworth, "Sequential Application of Simplex Designs in Optimization and Evolutionary Operation", Technometrics, vol. 4, pp. 441-461, 1962

[5.3] J.A. Nelder and R. Mead, "A Simplex Method for Function Minimization", Computer Journal, vol. 7, 1965

[5.4] R. Fletcher, Practical Methods of Optimization: Volume 1, John Wiley and Sons, pp. 19-20, 1980

[5.5] G.W. Stewart, "A Modification of Davidon's Minimization Method to Accept Difference Approximations of Derivatives", Journal Ass. Comput. Mach., vol. 14, pp. 72-83, 1967

[5.6] W. Murray, "Failures, the Causes and Cures", in Numerical Methods for Unconstrained Optimization (ed. W. Murray), Academic Press, London, 1972

[5.7] P.E. Gill, W. Murray, "Quasi-Newton Methods for Unconstrained Optimization", J. Inst. Maths. Applns., vol. 12, pp. 91-108, 1972

[5.8] P. Wolfe, "Methods of Nonlinear Programming", in Recent Advances in Mathematical Programming (eds. R.L. Graves and P. Wolfe), MaGraw-Hill, New York, 1963

[5.9] M.L. Lenard, "A Computational Study of Active Set Strategies in Nonlinear Programming with Linear Constraints", Mathematical Programming, vol. 16, pp.81-97, 1979

[6.1] R.J. Schwartz, and M.S. Lundstrum, "Degradation of BSF Solar Cell Performance At High Intensities Due to Loss of Base Conductivity Modulation", Proc. 14th IEEE Photovoltaic Specialists Conference, San Diego, California, January 7-10, pp. 1392-1393, 1980

[6.2] R. Girisch, R.P. Mertens, and R. Van Overstraeten, "Experimental and Theoretical Evaluations of Boron Diffused High-Low Junctions For BSF Cells", Solid State Electronics, vol. 29, num. 6, pp. 677-676, 1986

[7.1] M.A. Green, Solar Cells, Prentice-Hall, Englewood Cliffs, N.J., pp. 145-147, 1982

[8.1] S.A. Jain, R. Mertens, and R. Van Overstraeten, "High Efficiency Approaches", Proc. 16th IEEE Photovoltaic Specialists Conference, San Diego, California, Sept. 27-30, pp. 333-339, 1982

[8.2] M. Spitzer, J. Shewchun, E.S. Vera, and J.J. Loferski, "Ultra High Efficiency Thin Silicon p-n Junction Solar Cells Using Reflecting Surfaces", Proc. 14th IEEE Photovoltaic Specialists Conference, San Diego, California, January 7-10, pp. 375-380, 1980

[8.3] M. Wolfe, "High Efficiency Silicon Solar Cells", Proc. 14th IEEE Photovoltaic Specialists Conference, San Diego, California, January 7-10, pp. 674-679, 1980

[8.4] M.G. Mauk and A.M. Barnett, "Thin Silicon Solar Cells With Internal Reflection and Their Fabrication By Solution Growth", Proc. 18th IEEE Photovoltaic Specialists Conference, Las Vegas, Nevada, Oct. 21-25, pp. 192-???, 1985

[8.5] T. Chappel, "The V-Groove Multijunction Solar Cell", IEEE Trans. Electron Devices, vol. ED-26, no. 7, pp. 1091-1097, 1979

[8.6] E. Yablonovich and G.D. Cody, "Intensity Enhancement in Texturized Optical Sheets for Solar Cells", IEEE Trans. Electron Devices, vol. ED-29, no. 2, pp. 300-305, 1982

[8.7] A. Goetzberger, "Optical Confinement in Thin Si-Solar Cells by Diffuse Back Reflector", Proc. 15th IEEE Photovoltaic Specialists Conference, Kissimmee, Florida, May 12-15, pp. 867-870, 1981

[8.8] W. Shockley and H.J. Queisser, "Detailed Balance Limit of Efficiency of p-n Junction Solar Cells", Journal of Applied Physics, vol. 32, num. 3, pp. 510-519, 1961

Appendix A Modifications to SCAP1D

This appendix describes in detail some of the modifications made to the SCAP1D code. These modifications include numerical (i.e., how the code arrives at a solution) as well as modeling changes. Chapter four described modifications that were made to adapt SCAP1D for use with the optimization code to maximize cell efficiency. Chapter seven described a correction for lateral resistance that was appended to the efficiency calculation. In this appendix, the numerical changes required to optimize V_{oc} and J_{sc} will be described. Also, the methods used to include light trapping, radiative recombination, and reflection calculations for thin film coatings in the model will be described.

A.1 Maximization of V_{oc}

The maximization of V_{oc} is implemented in a fashion similar to that described in chapter four for maximizing efficiency. The first execution of SCAP1D is halted after the open circuit voltage is calculated. The solution vectors V, n, and p are then stored.

After the optimization has changed the design variables, the next calculation is initiated at the solution vectors and value of V_{oc} retrieved from storage. The solution vectors must first be corrected at the old value of V_{oc} to correspond to the new design. The Newton-type algorithm is used to solve the system of nonlinear algebraic equations associated with the finite difference transformation of the differential equations. The same convergence considerations, which were related to the change in the magnitude of the design variables and the Newton-like algorithm's need for a good initial estimate of the solution to converge, that were discussed in chapter four hold for this step.

Once the solution vectors have been corrected for the new design, it is necessary to determine the new value of V_{oc}. A linear interpolation scheme is used since the relationship between current and voltage is almost linear near V_{oc} (see figure 4.2). A routine was written and appended to the code. The convergence

error of this step will profoundly effect the progress of the optimization (see section 4.3) so tight convergence criteria were used. This step also significantly affects the computational effort required to complete an optimization. The code written was specialized for this application so that it would converge as rapidly as possible to the new value of V_{oc} and was safeguarded against divergence.

The optimization proceeds iteratively, retrieving a solution stored from a previous objective evaluation to initiate the next objective evaluation, until the design variables converge to the optimal solution.

The time required to optimize V_{oc} is comparable to the time required to optimize efficiency. The solution strategy closely parallels the strategy described in chapter four for maximizing the efficiency. The amount of effort required is different if the design variables that changed value are geometric variables, since geometric variable require that the equilibrium problem be re-solved in its entirety and the generation rate be recalculated (see chapter 4).

A.2 Maximization of J_{sc}

The maximization of J_{sc} differs significantly from the maximization of V_{oc} and efficiency. This is because the voltage bias for short circuit is known, $V_{bias} = 0$.

The initial execution of SCAP1D is halted after J_{sc} has been determined. This occurs on the first solution of the nonequilibrium problem at $V_{bias} = 0$. The solution vectors V, n, and p are then stored.

After the cell design has been changed by the optimization, which is maximizing J_{sc}, the stored solution is retrieved. The solution vectors must be corrected to correspond to the new cell design at $V_{bias} = 0$. The Newton-type algorithm is used to solve the system of nonlinear algebraic equations associated with the finite difference transformation of the differential equations. The same convergence considerations for the Newton-like algorithm that were discussed in chapter four hold for this step.

Since the voltage bias associated with J_{sc} is known and does not change as the cell design changes, there is no need to solve the nonequilibrium problem for more than one voltage bias. For this reason, it takes considerably less effort to maximize J_{sc} than V_{oc} or efficiency (on the average 1/4 the CPU time). The difficulties posed by convergence error are also alleviated, since one of the iterative algorithms required to calculate the objective function is eliminated.

A.3 Implementation of Light Trapping

Most of the results in this work have had an optical path equal to two times the cell thickness ($O_{pl} = 2$) due to the use of a perfect back surface reflector. The SCAP1D model has been modified to include the possibility of light trapping. Light trapping is defined as a design which allows a solar cell to achieve an optical path greater than twice the cell thickness.

A variety of methods have been proposed for achieving light trapping in silicon solar cells. Most involve the use of textured front and/or back surfaces. These designs take advantage of refraction and total internal reflection to increase the optical path the incident illumination has to pass through before escaping the solar cell. This results in increased number of photons being absorbed (electron-hole pairs generated) for a given cell thickness.

The actual location where the increased generation takes place is dependent on the design used to achieve light trapping. For example, on a textured front surface light striking the side of a pyramid is refracted due to the high index of refraction of silicon. Because the textured surface is at an angle with the bulk of the cell, the light travels a greater distance through the cell before reaching the back surface. The increased generation will predominately occur near the front surface due to the exponential absorption of the incident illumination. Where as, if the back surface is textured or a light scattering back surface is provided, most of the increased absorption will occur near the back surface.

Light trapping is implemented in SCAP1D by specifying a front surface reflection coefficient for light reflected off the back surface. This coefficient can be thought of as the percentage of the light that is internally reflected at the front surface. Another input specifies the number of internal reflections off the front surface. In the results described in this work, the front and back surface reflectors are assumed to be perfect ($R_b = 1.0$ and $R_f = 1.0$). Hence, the optical path is equal to two times the number of internal reflections specified times the cell thickness. The incident illumination is assumed to remain perpendicular to the cell surfaces (this determines where the additional generation occurs).

It is not possible to have a perfect front (or back) surface reflector. In reality, a certain percentage of the remaining light will escape at each optical interface (surface). This will actually occur an infinite number of times. Or, from a practical point of view, until the internally reflected energy becomes negligible in magnitude. However, to simulate such an occurrence would require an enormous amount of computational effort. Hence, the more simplified approach of perfect front and back surface reflectors were used in the results of this work.

The inclusion of light trapping following the strategy stated above is implemented using the equation that determines the generation rate at a given position, x, in the cell. For a solar cell, the generation rate for electron hole pairs is modeled by the equation:

$$G(x_i) = \int_0^{\infty} (1 - \Gamma) \phi \alpha e^{-\alpha x_i} d\lambda \qquad (A.1)$$

λ = wavelength
ϕ = incident flux.

The integral is integrated numerically over the wavelength. The value $G(x_i)$ is the accumulated generation rate by the time the incident energy has traveled a distance equal to x_i. Hence, the generation rate between x_i and x_{i-1} is equal to $G(x_i)$ - $G(x_{i-1})$ (assuming $x_i > x_{i-1}$). The total generation rate at a given node (TG_i) in the finite difference mesh is the sum over the number of times the incident energy passes that node (the irradiance at each wavelength is reduced by $1\text{-}R_b$ at the back surface and $1\text{-}R_f$ at the front surface).

$$TG_i = \sum_{k=1}^{O_{pl}} G(x_i^k) - G(x_{i-1}^k) \qquad (A.2)$$

For k=1 the values of x_i^k and x_{i-1}^k are the position of the midpoints between the two adjacent nodes measured from the front surface. For k=2,...,O_{pl}; the values of x_i^k and x_{i-1}^k are the distance that the incident energy has traveled through the cell when it reaches the midpoints around node i.

A.4 Inclusion of Radiative Recombination

The original version of SCAP1D did not include radiative recombination. This omission is not important for most of the results reported in this work because the lifetime associated with radiative recombination is far greater than that associated with SRH recombination at low values of doping (and possibly at high levels of doping depending on the value of τ_{n_0}) and Auger recombination at high levels of doping. However, for the limit analysis done in section 8.3 it was important to have radiative recombination in the model.

The equation for radiative recombination is

$$R_{RAD} = B (n p - n_{ie}^2) \ . \qquad (A.3)$$

The constant B is equal to 2.0×10^{-15} and was obtained from [A.1].

The lifetime associated with radiative recombination can be derived using the assumptions described in section 3.3 . Assuming a P-type substrate, the lifetime is

$$\tau_{RAD} = \frac{1}{B\ N_A} \quad . \tag{A.4}$$

The lifetime associated with radiative recombination is a linear function of the doping concentration. Figure A.1 shows the lifetime of radiative and Auger recombination as a function of the net doping concentration. Both of these lifetimes may be considered fundamental, since they are not related to the quality of the substrate (as the SRH lifetime is).

A.4 Thin Film Coatings

In the original version of SCAP1D, reflection and shadowing were accounted for with the single input Γ. The generation rate at each node was reduced by Γ (i.e., multiplied by 1-Γ). This was equivalent to reducing the irradiance at each wavelength equally.

In changing the code to include thin film coatings, it was first necessary to separate the effects of shadowing and reflection. Shadowing was used to reduce the active area of the cell. Hence, the calculation of the efficiency is as follows:

$$eff = \frac{V_{mp}\ J_{mp}\ A_{act}}{P_{inc}\ A_{tot}} \quad . \tag{A.5}$$

A_{tot} is the total area of the cell and A_{act} is the area of the cell which is not shadowed (i.e., A_{act} = [1-shadow] A_{tot}, where shadow is the fraction of the front surface covered by the collection grid). P_{inc} is the incident energy in the illumination per cm^2 (100 mW/cm^2 in this work). The equation above can be generalized to include the effects of lateral resistance.

$$eff = \frac{\left[\left[V_{mp} - \frac{J_{mp}\ \rho_e\ d^2}{12}\right] J_{mp}\right] A_{act}}{P_{inc}\ A_{tot}} \quad . \tag{A.6}$$

To maintain continuity with previous results a reflection factor was defined which uniformly, as a function of wavelength, reduced the irradiance of the incident spectrum. This factor has the same effect as the previous shadowing and reflection factor. It can be set to zero if a thin film coating is being used to calculate the reflectance.

Because of the high index of refraction of silicon, it is necessary to apply thin film coatings to a solar cell to reduce the reflection. For solar cell work, the

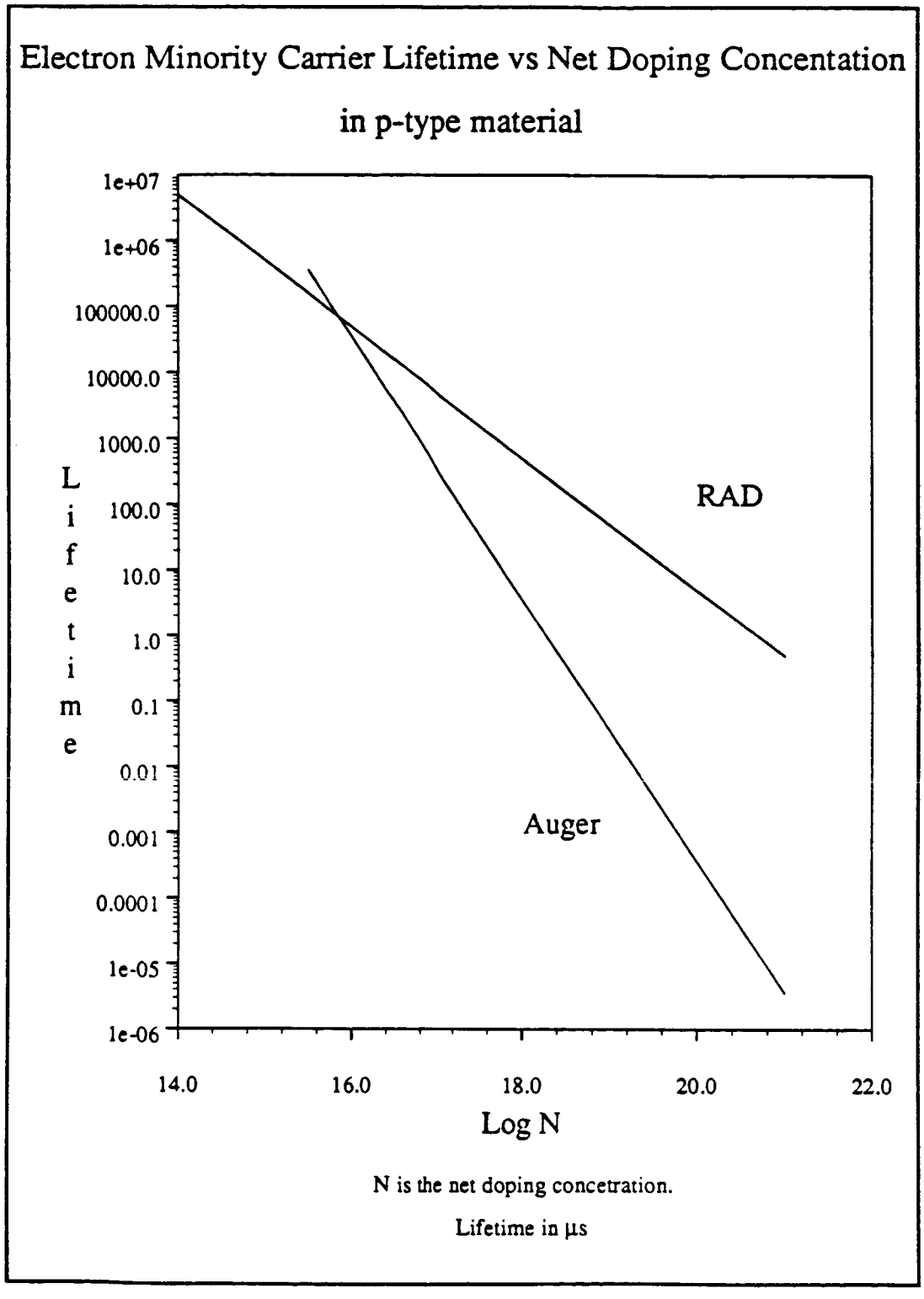
Electron Minority Carrier Lifetime vs Net Doping Concentation
in p-type material
1e+07
1e+06
100000.0
10000.0
1000.0
100.0
10.0
1.0
0.1
0.01
0.001
0.0001
1e-05
1e-06
Lifetime
RAD
Auger
14.0
16.0
18.0
20.0
22.0
Log N
N is the net doping concetration.
Lifetime in µs

figure A.1

reflectance of a thin film coating is a function of wavelength for two reasons. The complex index of refraction of silicon, $n_{Si} + i\ k_{Si}$, changes with wavelength (see figure A.2, data from [A.2]), and interference effects in thin films (constructive or destructive) are a function of the wavelength. The wavelength dependence of interference in thin films is a function of the film thickness.

The equation for reflection with a single layer antireflection coating will now be presented. n_0 is the index of refraction of the medium (glass or air), n_1 is the index of refraction of the thin film, and d_1 is the thickness of the thin film. Let:

$$r_1 = \frac{n_0 - n_1}{n_0 + n_1} \tag{A.7}$$

$$r_2 = \frac{n_1 - n_{Si} + i\ k_{Si}}{n_1 + n_{Si} - i\ k_{Si}} \tag{A.8}$$

$$\Delta_1 = \frac{4\ \pi\ n_1\ d_1}{\lambda} \tag{A.9}$$

Since n_{Si} and k_{Si} are a function of lamda, r_2 is also a function of lamda. The complex fraction represented by r_2 is expressed as a complex number by multiplying by complex conjugate of the denominator.

$$r_{2r} = \frac{(\ n_1 - n_{Si}\ )\ (\ n_1 + n_{Si}\ ) - k_{Si}^2}{(\ n_1 + n_{Si}\ )^2 + k_{Si}^2} \tag{A.10}$$

$$r_{2i} = \frac{2\ n_1\ k_{Si}}{(\ n_1 + n_{Si}\ )^2 + k_{Si}^2} \tag{A.11}$$

The amplitude and phase of the reflected wave taking into account interference in the thin film is [A.3]:

$$r\ e^{i\varepsilon} = \frac{r_1 + r_2\ e^{-i\Delta_1}}{1 + r_1\ r_2\ e^{-i\Delta_1}} \tag{A.12}$$

Let:

$$P_{1r} = r_{2r}\ \cos(\Delta_1) + r_{2i}\ \sin(\Delta_1) \tag{A.13}$$

$$P_{1i} = r_{2i}\ \cos(\Delta_1) - r_{2r}\ \sin(\Delta_1) \tag{A.14}$$

Substituting in the appropriate expressions gives:

$$r\ e^{i\varepsilon} = \frac{r_1 + P_{1r} + i\ P_{1i}}{1 + r_1\ P_{1r} + i\ r_1\ P_{1i}} \tag{A.15}$$

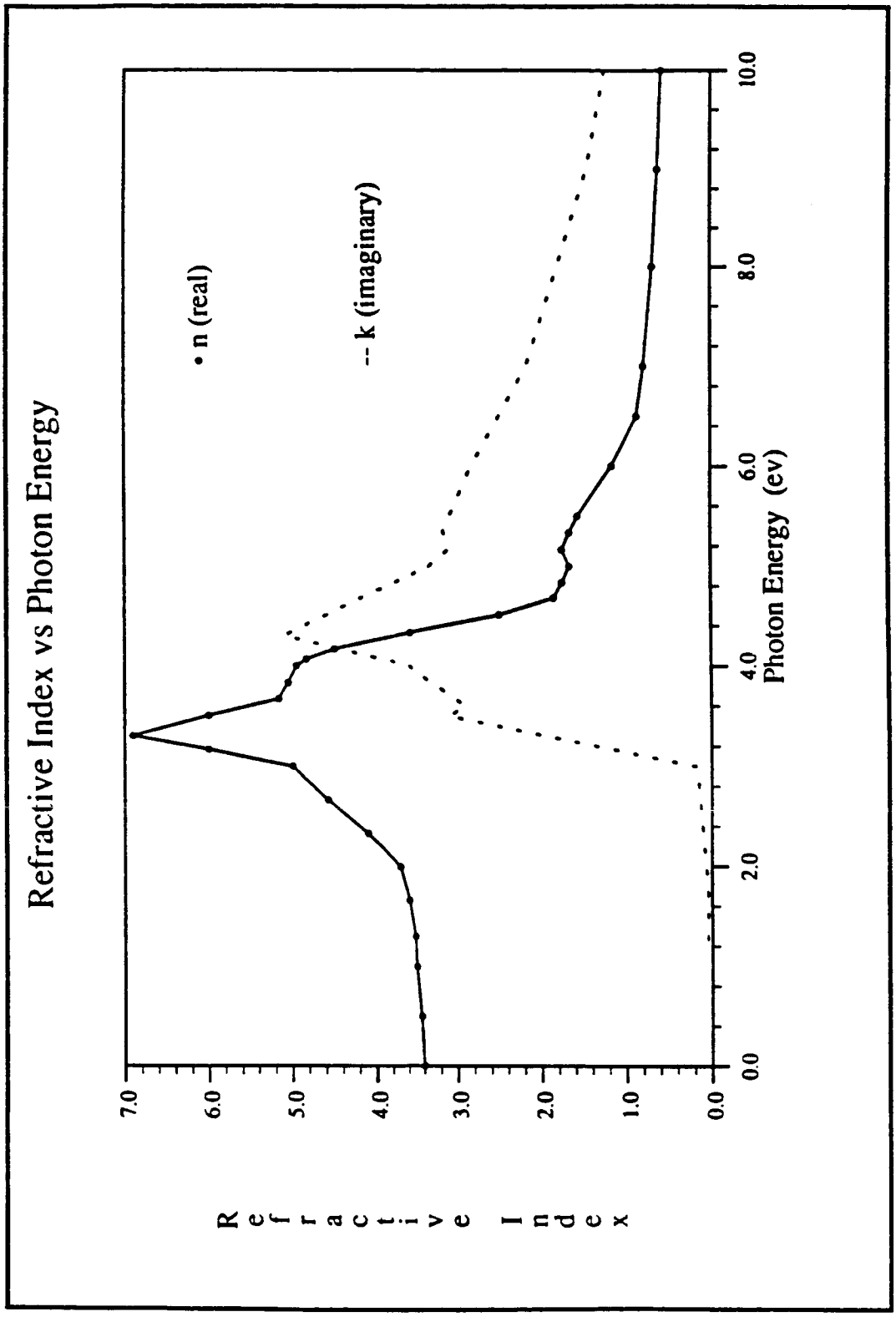
Refractive Index vs Photon Energy
• n (real)
-- k (imaginary)
Refractive Index
7.0
6.0
5.0
4.0
3.0
2.0
1.0
0.0
0.0
2.0
4.0
6.0
8.0
10.0
Photon Energy (ev)

Figure A.2

The reflection, R, is obtained by multiplying equation A.15 by the complex conjugate.

$$R = \frac{(r_1 + P_{1r})^2 + P_{1i}^2}{(1 + r_1 P_{1r})^2 + (r_1 P_{1i})^2} \tag{A.16}$$

The reflection is different for light of different wavelengths. The design of the single layer antireflection coating is specified by the inputs n_0 (1.0 for air or 1.5 for glass), n_1, and d_1.

The equation for reflection with a double layer antireflection coating will now be presented. n_0 is the index of refraction of the medium (glass or air), n_1 is the index of refraction of the thin film closest to the medium, d_1 is the thickness of the thin film closest to the medium, n_2 is the index of refraction of the thin film closest to the substrate, and d_2 is the thickness of the thin film closest to the substrate. Let:

$$r_1 = \frac{n_0 - n_1}{n_0 + n_1} \tag{A.17}$$

$$r_2 = \frac{n_1 - n_2}{n_1 + n_2} \tag{A.18}$$

$$r_3 = \frac{n_2 - n_{Si} + i\, k_{Si}}{n_2 + n_{Si} - i\, k_{Si}} \tag{A.19}$$

$$\Delta_1 = \frac{4 \pi n_1 d_1}{\lambda} \tag{A.20}$$

$$\Delta_2 = \frac{4 \pi n_2 d_2}{\lambda} \tag{A.20}$$

Since n_{Si} and k_{Si} are a function of lamda, r_2 is also a function of lamda. The complex fraction represented by r_3 is expressed as a complex number by multiplying by complex conjugate of the denominator.

$$r_{3r} = \frac{(n_2 - n_{Si}) (n_2 + n_{Si}) - k_{Si}^2}{(n_2 + n_{Si})^2 + k_{Si}^2} \tag{A.21}$$

$$r_{3i} = \frac{2 n_2 k_{Si}}{(n_2 + n_{Si})^2 + k_{Si}^2} \tag{A.22}$$

The amplitude and phase of the reflected wave taking into account interference in the thin film is [A.4]:

$$r\,e^{i\varepsilon} = \frac{r_1 + r_2\,e^{-i\Delta_1} + r_3\,e^{-i(\Delta_1+\Delta_2)} + r_1\,r_2\,r_3\,e^{-i\Delta_2}}{1 + r_1\,r_2\,e^{-i\Delta_1} + r_1\,r_3\,e^{-i(\Delta_1+\Delta_2)} + r_2\,r_3\,e^{-i\Delta_2}} \tag{A.23}$$

Let:

$$P_{1r} = r_2\cos(\Delta_1) \tag{A.24}$$

$$P_{1i} = -r2\sin(\Delta_1) \tag{A.25}$$

$$P_{2r} = r_{3r}\cos(\Delta_1+\Delta_2) + r_{3i}\sin(\Delta_1+\Delta_2) \tag{A.26}$$

$$P_{2i} = r_{3i}\cos(\Delta_1+\Delta_2) - r_{3r}\sin(\Delta_1+\Delta_2) \tag{A.27}$$

$$P_{3r} = r_{3r}\cos(\Delta_2) + r_{3i}\sin(\Delta_2) \tag{A.28}$$

$$P_{3i} = r_{3i}\cos(\Delta_2) - r_{3r}\sin(\Delta_2) \tag{A.29}$$

Substituting in the appropriate expressions gives:

$$r\,e^{i\varepsilon} = \frac{r_1 + P_{1r} + r_3\,P_{2r} + r_1\,r_2\,P_{3r} + i\,(\,P_{1i} + r_3\,P_{2i} + r_1\,r_2\,P_{3i}\,)}{1 + r_1\,P_{1r} + r_1\,P_{2r} + r_2\,P_{3r} + i\,(\,r_1\,P_{1i} + r_1\,P_{2i} + r_2\,P_{3i}\,)} \tag{A.30}$$

The reflection, R, is obtained by multiplying equation A.30 by the complex conjugate.

$$R = \frac{(\,r_1 + P_{1r} + r_3\,P_{2r} + r_1\,r_2\,P_{3r}\,)^2 + (\,P_{1i} + r_3\,P_{2i} + r_1\,r_2\,P_{3i}\,)^2}{(\,1 + r_1\,P_{1r} + r_1\,P_{2r} + r_2\,P_{3r}\,)^2 + (\,r_1\,P_{1i} + r_1\,P_{2i} + r_2\,P_{3i}\,)^2} \tag{A.31}$$

The reflection is different for light of different wavelengths. The design of a double layer antireflection coating is specified by the inputs n_0 (1.0 for air or ≈ 1.5 for glass), n_1, d_1, n_2, and d_2.

SCAP1D and the optimization code can be used to design a single or double layer antireflection coating which maximizes the generation rate in the cell. This does not involve the solution of the differential equations for modeling solar cell performance and is accomplished with considerably less computational effort than the maximization of V_{oc}, J_{sc}, or efficiency discussed earlier in this work. The variables associated with the antireflection coating can also be included in the maximization of V_{oc}, J_{sc}, or efficiency along with the other cell design variables discussed earlier in this work.

A.5 References

[A.1]J.I. Pankove, Optical Processes in Semiconductors, Englewood Cliffs, N.J., Prentice Hall, 1971

[A.2]H.R. Phillip and E.A. Taft, Physical Review, vol. 120, pp. 37-38, 1960

[A.3]H. Anders, Thin Films in Optics, The Focal Press, p. 26, 1967

[A.4]H. Anders, Thin Films in Optics, The Focal Press, p. 46, 1967

Appendix B Tables and Figures for Chapter 6

This appendix contains the figures and tables for chapter six. They are arranged and numbered as they are referenced in chapter six.

Parameters Held Constant

Illumination	100mW/cm^3 (AM 1.5)
Temperature	28 degrees C
Doping Profile	erfc
Shadowing (including reflection)	7%
Auger Recombination	considered
Band Gap Narrowing	Slootboom Degraff model

Parameters Varied Parametrically

Front surface recombination velocity (S_f)

Back surface recombination velocity (S_b)

Minority carrier lifetime (used same formulas as in last progress report)

τ_{n0} is electron minority carrier lifetime.

τ_{p0} is hole minority carrier lifetime (always taken as one half τ_{n0})

For .2 ohm-cm substrate the input τ_{n0} = 2 ms, 1 ms, .4 ms gives bulk minority carrier lifetimes of 54, 30, and 13 micro seconds respectively.

R_b (back surface reflection, 1.0 or 0.0)

Parameters Varied Parametrically or Optimized

Front junction depth (X_f)

Back junction depth (X_b)

Cell thickness (X_L)

Front surface doping concentration (D_0)

Bulk doping concentration (D_B)

Back surface doping concentration (D_L)

Table 6.1 Base Input Parameters for Problem P1

Parameters Held Constant During Optimization (see also table 6.1).

Front surface recombination velocity (S_f)	100.0	cm/s
Back surface recombination velocity (S_b)	100.0	cm/s
Electron minority carrier lifetime[1] (τ_{n0})	2.00	ms
Hole minority carrier lifetime[1] (τ_{p0})	1.00	ms

Optimal Values of Decision Variables

Front junction depth (X_f)	0.10	μm (lower bound)
Back junction depth (X_b)	0.20	μm (lower bound)
Cell thickness (X_L)	230.9	μm
Front surface doping concentration (D_0)	6.211×10^{18}	P atoms/cm^3
Bulk doping concentration (D_B)	3.038×10^{16}	B atoms/cm^3
Back surface doping concentration (D_L)	7.985×10^{18}	B atoms/cm^3

Cell Performance Parameters

Efficiency	23.025	%
Open circuit voltage (V_{oc})	701.16	mV
Short circuit current density (J_{sc})	38.983	mA/cm^2
Maximum power voltage (V_{mp})	615.63	mV
Fill factor	0.8424	
Collection efficiency	99.65	%
Bulk resitivity	0.509	ohm-cm
Sheet resistance layer 1	2204.5	ohm/□
layer 2	21.76	ohm/□
Bulk lifetime	366.2	μs
Bulk diffusion length	1017	μm

[1] Values in lightly doped silicon.

Table 6.2 Optimal Solution For Case 1

Table 6.3 Effect of BSF and BSR, case 1 (S_f = 100 cm/s, S_b = 100 cm/s, τ_{n0} = 2 ms)

eff	V_{oc}	J_{sc}	V_{mp}	ff	C_{eff}	τ_{bulk}	L_d	X_L	X_f	X_b	log D_0	log D_B	log D_L	O_{pl}
23.025	**701.2**	**38.98**	**615.6**	**.842**	**99.7**	**366.2**	**1017**	**230.9**	**0.10**	**0.20**	**18.79**	**16.48**	**18.90**	**2**
22.418	695.4	38.30	610.3	.842	99.6	370.8	1025	300.0	0.10	0.20	18.79	16.48	18.91	1
22.481	689.7	38.66	606.5	.843	98.5	174.6	640	253.4	0.10	0.	18.79	16.83	0.	2
21.956	687.2	37.91	604.1	.843	98.5	181.6	656	300.0	0.10	0.	18.79	16.81	0.	1

Table 6.4 Optimizations at Fixed Cell Thickness (X_L), with bsf, case 1

eff	V_{oc}	J_{sc}	V_{mp}	ff	C_{eff}	τ_{bulk}	L_d	X_L	X_f	X_b	log D_0	log D_B	log D_L	O_{pl}
19.660	728.4	31.83	642.8	.848	99.9	597.7	1358	10.0	0.10	0.20	18.80	16.21	18.85	2
21.422	726.7	34.79	640.8	.847	99.9	409.3	1087	25.0	0.10	0.20	18.80	16.42	18.85	2
22.231	722.4	36.37	636.4	.846	99.9	358.0	1003	50.0	0.10	0.20	18.81	16.49	18.86	2
22.700	716.1	37.51	630.1	.845	99.9	340.6	973	90.0	0.10	0.20	18.81	16.52	18.87	2
22.757	716.0	37.72	628.4	.843	99.9	456.8	1161	100.0	0.10	0.20	18.82	16.37	18.85	2
22.818	713.3	37.88	627.5	.844	99.9	340.4	973	110.0	0.10	0.20	18.80	16.52	18.87	2
22.952	709.2	38.40	622.7	.843	99.8	399.6	1072	150.0	0.10	0.20	18.77	16.44	18.89	2
23.021	703.1	38.85	617.5	.843	99.7	360.2	1007	207.8	0.10	0.20	18.79	16.49	18.91	2
23.025	701.5	38.96	616.0	.842	99.7	363.5	1012	226.5	0.10	0.20	18.80	16.49	18.88	2
23.025	**701.2**	**38.98**	**615.6**	**.842**	**99.7**	**366.2**	**1017**	**230.9**	**0.10**	**0.20**	**18.79**	**16.48**	**18.90**	**2**
23.016	698.5	39.14	613.1	.842	99.6	376.6	1034	266.1	0.10	0.20	18.81	16.47	18.94	2
23.003	697.3	39.17	612.3	.842	99.5	344.6	980	280.0	0.10	0.20	18.82	16.51	19.09	2
22.946	693.0	39.37	607.9	.841	99.4	385.3	1049	350.0	0.10	0.20	18.81	16.46	18.85	2
22.893	690.3	39.47	605.1	.840	99.3	414.0	1095	400.0	0.10	0.20	18.81	16.42	19.03	2
22.832	687.8	39.53	602.6	.840	99.3	434.9	1127	450.0	0.10	0.20	18.81	16.39	19.01	2
22.778	685.8	39.59	600.3	.839	99.2	463.4	1170	500.0	0.10	0.20	18.88	16.36	19.27	2
22.598	680.4	39.60	595.6	.839	98.8	442.2	1138	650.0	0.10	0.20	19.11	16.38	19.19	2

Table 6.5 Optimizations at Fixed Cell Thickness (X_L), no bsf, case 1

eff	V_{oc}	J_{sc}	V_{mp}	ff	C_{eff}	τ_{bulk}	L_d	X_L	X_f	X_b	log D_0	log D_B	log D_L	O_{pl}
19.140	711.6	31.76	627.7	.847	99.8	38.5	229	10.0	0.10	0.	18.77	17.42	0.	2
20.824	709.3	34.68	625.5	.847	99.7	63.9	326	25.0	0.10	0.	18.78	17.24	0.	2
21.612	705.6	36.20	622.0	.846	99.5	87.1	403	50.0	0.10	0.	18.79	17.12	0.	2
22.164	700.1	37.46	616.7	.845	99.2	116.2	489	100.0	0.10	0.	18.79	17.00	0.	2
22.374	696.0	38.07	612.7	.844	99.0	138.1	549	150.0	0.10	0.	18.79	16.93	0.	2
22.459	692.7	38.42	609.4	.844	98.7	156.6	596	200.0	0.10	0.	18.80	16.88	0.	2
22.481	689.8	38.64	606.7	.843	98.5	174.1	639	250.0	0.10	0.	18.79	16.83	0.	2
22.481	689.7	38.66	606.5	.843	98.5	174.6	640	253.4	0.10	0.	18.79	16.83	0.	2
22.472	687.4	38.79	604.3	.843	98.3	190.0	676	300.0	0.10	0.	18.79	16.79	0.	2
22.446	685.3	38.88	602.1	.842	98.2	205.0	710	350.0	0.10	0.	18.80	16.76	0.	2
22.411	683.4	38.94	600.4	.842	98.0	217.9	738	400.0	0.10	0.	18.80	16.73	0.	2
22.371	681.8	38.98	598.8	.842	97.9	230.0	763	450.0	0.10	0.	18.80	16.71	0.	2
22.330	680.3	39.01	597.3	.841	97.7	241.3	787	500.0	0.10	0.	18.80	16.69	0.	2

Table 6.6 Optimizations at Fixed Front Junction Depth (X_f), case 1

eff	V_{oc}	J_{sc}	V_{mp}	ff	C_{eff}	τ_{bulk}	L_d	X_L	X_f	X_b	$\log D_0$	$\log D_B$	$\log D_L$	O_{pl}
23.047	701.8	38.98	616.2	.842	99.7	368.3	1021	231.1	0.04	0.20	19.04	16.48	18.92	2
23.038	701.5	38.99	615.9	.842	99.7	369.1	1022	231.2	0.06	0.20	18.93	16.48	18.93	2
23.031	701.3	38.99	615.8	.842	99.7	370.3	1024	231.1	0.08	0.20	18.85	16.48	18.93	2
23.025	**701.2**	**38.98**	**615.6**	**.842**	**99.7**	**366.2**	**1017**	**230.9**	**0.10**	**0.20**	**18.79**	**16.48**	**18.90**	**2**
23.007	700.5	38.99	615.0	.842	99.7	374.0	1030	232.4	0.20	0.20	18.63	16.47	18.93	2
22.995	700.2	38.99	614.7	.842	99.7	375.4	1032	232.2	0.30	0.20	18.54	16.47	18.93	2
22.986	699.6	39.02	614.1	.842	99.7	383.4	1045	236.8	0.40	0.20	18.46	16.46	18.93	2
22.978	699.4	39.02	613.9	.842	99.7	382.6	1044	236.6	0.50	0.20	18.41	16.46	18.93	2
22.971	699.3	39.01	613.9	.842	99.7	381.8	1043	235.5	0.60	0.20	18.36	16.46	18.93	2
22.958	699.1	39.02	613.5	.842	99.7	396.8	1067	235.1	0.80	0.20	18.28	16.44	18.93	2
22.948	698.2	39.04	612.9	.842	99.6	385.8	1050	241.5	1.00	0.20	18.25	16.46	18.93	2
22.926	697.5	39.06	612.0	.841	99.6	402.5	1076	245.5	1.50	0.20	18.12	16.43	18.93	2
22.906	696.8	39.07	611.3	.841	99.6	410.1	1088	248.7	2.00	0.20	18.05	16.42	18.92	2

Table 6.7 Optimizations at Fixed Back Junction Depth (X_b), case 1

eff	V_{oc}	J_{sc}	V_{mp}	ff	C_{eff}	τ_{bulk}	L_d	X_L	X_f	X_b	$\log D_0$	$\log D_B$	$\log D_L$	O_{pl}
23.090	703.1	38.99	617.3	.842	99.7	368.2	1020	229.8	0.10	0.05	18.86	16.48	19.90	2
23.048	701.8	38.99	616.2	.842	99.7	367.7	1020	231.1	0.10	0.10	18.79	16.48	19.23	2
23.025	**701.2**	**38.98**	**615.6**	**.842**	**99.7**	**366.2**	**1017**	**230.9**	**0.10**	**0.20**	**18.79**	**16.48**	**18.90**	**2**
23.014	700.9	38.98	615.3	.842	99.6	369.8	1023	231.1	0.10	0.30	18.80	16.48	18.80	2
23.006	700.7	38.98	615.1	.842	99.7	375.8	1033	231.1	0.10	0.40	18.78	16.47	18.70	2
23.000	700.5	38.98	615.0	.842	99.7	380.0	1040	230.9	0.10	0.50	18.80	16.46	18.66	2
22.979	699.6	39.00	614.2	.842	99.6	380.8	1041	235.8	0.10	1.00	18.79	16.46	18.47	2
22.967	699.1	39.01	613.7	.842	99.6	384.5	1047	238.0	0.10	1.50	18.79	16.46	18.36	2
22.957	698.8	39.02	613.4	.842	99.6	390.2	1057	238.3	0.10	2.00	18.79	16.45	18.28	2

Table 6.8 Optimizations at Fixed Front Surface Doping Concentration (D_0), case 1

eff	V_{oc}	J_{sc}	V_{mp}	ff	C_{eff}	τ_{bulk}	L_d	X_L	X_f	X_b	$\log D_0$	$\log D_B$	$\log D_L$	O_{pl}
22.947	698.4	39.03	612.9	.842	99.7	399.4	1071	238.0	0.10	0.20	17.89	16.44	18.92	2
22.987	699.6	39.01	614.2	.842	99.7	379.1	1038	236.1	0.10	0.20	18.19	16.46	18.94	2
23.014	700.8	38.98	615.3	.842	99.7	369.2	1022	230.7	0.10	0.20	18.49	16.48	18.93	2
23.025	**701.2**	**38.98**	**615.6**	**.842**	**99.7**	**366.2**	**1017**	**230.9**	**0.10**	**0.20**	**18.79**	**16.48**	**18.90**	**2**
23.006	700.4	39.00	614.9	.842	99.7	379.7	1039	233.8	0.10	0.20	19.09	16.46	18.93	2
22.917	696.3	39.10	611.1	.842	99.6	401.0	1074	254.1	0.10	0.20	19.40	16.44	18.92	2
22.690	687.2	39.29	602.6	.840	99.6	452.0	1153	300.0	0.10	0.20	19.70	16.37	18.97	2

Table 6.9 Optimizations at Fixed Bulk Doping Concentration (D_B), case 1

eff	V_{oc}	J_{sc}	V_{mp}	ff	C_{eff}	τ_{bulk}	L_d	X_L	X_f	X_b	$\log D_0$	$\log D_B$	$\log D_L$	O_{pl}
22.623	717.6	38.68	614.4	.815	99.9	1300.7	2099	172.8	0.10	0.20	18.85	15.58	18.95	2
22.814	710.7	38.92	612.5	.825	99.9	961.0	1777	204.9	0.10	0.20	18.81	15.88	18.94	2
22.968	703.8	39.04	613.6	.836	99.8	627.9	1397	229.0	0.10	0.20	18.81	16.18	18.95	2
23.025	**701.2**	**38.98**	**615.6**	**.842**	**99.7**	**366.2**	**1017**	**230.9**	**0.10**	**0.20**	**18.79**	**16.48**	**18.90**	**2**
22.947	701.5	38.72	617.6	.845	99.3	194.4	686	208.4	0.10	0.20	18.78	16.78	18.89	2
22.640	701.2	38.20	617.7	.845	98.9	95.1	428	166.5	0.10	0.20	18.79	17.08	18.85	2
22.026	698.8	37.31	615.4	.845	98.3	42.6	246	112.3	0.10	0.20	18.79	17.39	18.81	2

Table 6.10 Optimizations at Fixed Back Surface Doping Concentration (D_L), case 1

eff	V_{oc}	J_{sc}	V_{mp}	ff	C_{eff}	τ_{bulk}	L_d	X_L	X_f	X_b	$\log D_0$	$\log D_B$	$\log D_L$	O_{pl}
22.957	698.7	39.02	613.4	.842	99.6	380.8	1041	239.4	0.10	0.20	18.79	16.46	18.00	2
22.990	700.0	39.00	614.6	.842	99.6	378.4	1037	233.7	0.10	0.20	18.79	16.47	18.30	2
23.014	701.0	38.97	615.5	.842	99.6	366.2	1017	229.3	0.10	0.20	18.79	16.48	18.60	2
23.025	**701.2**	**38.98**	**615.6**	**.842**	**99.7**	**366.2**	**1017**	**230.9**	**0.10**	**0.20**	**18.79**	**16.48**	**18.90**	**2**
23.011	700.4	39.01	614.9	.842	99.6	377.1	1035	235.9	0.10	0.20	18.79	16.47	19.21	2
22.943	696.9	39.12	611.5	.841	99.6	405.9	1082	261.4	0.10	0.20	18.79	16.43	19.51	2
22.780	690.6	39.25	605.5	.840	99.5	460.8	1167	300.0	0.10	0.20	18.80	16.36	19.81	2

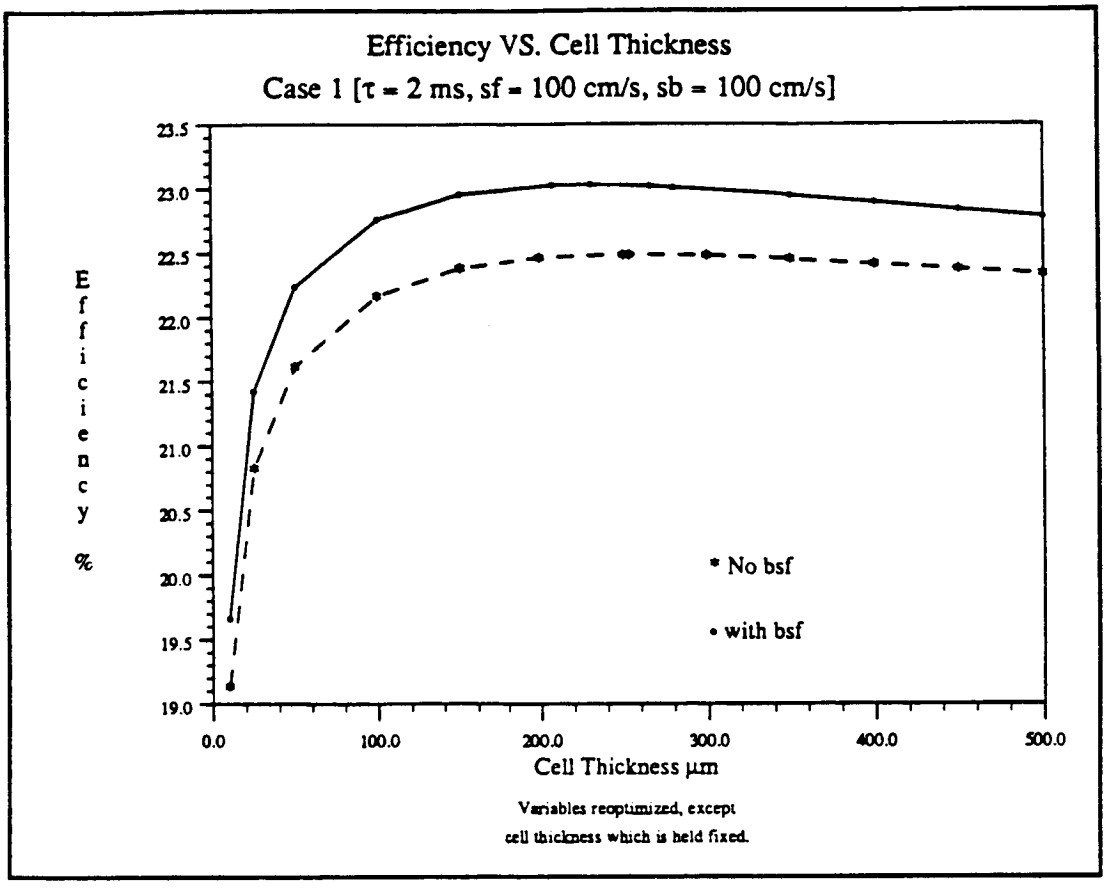

figure 6.1

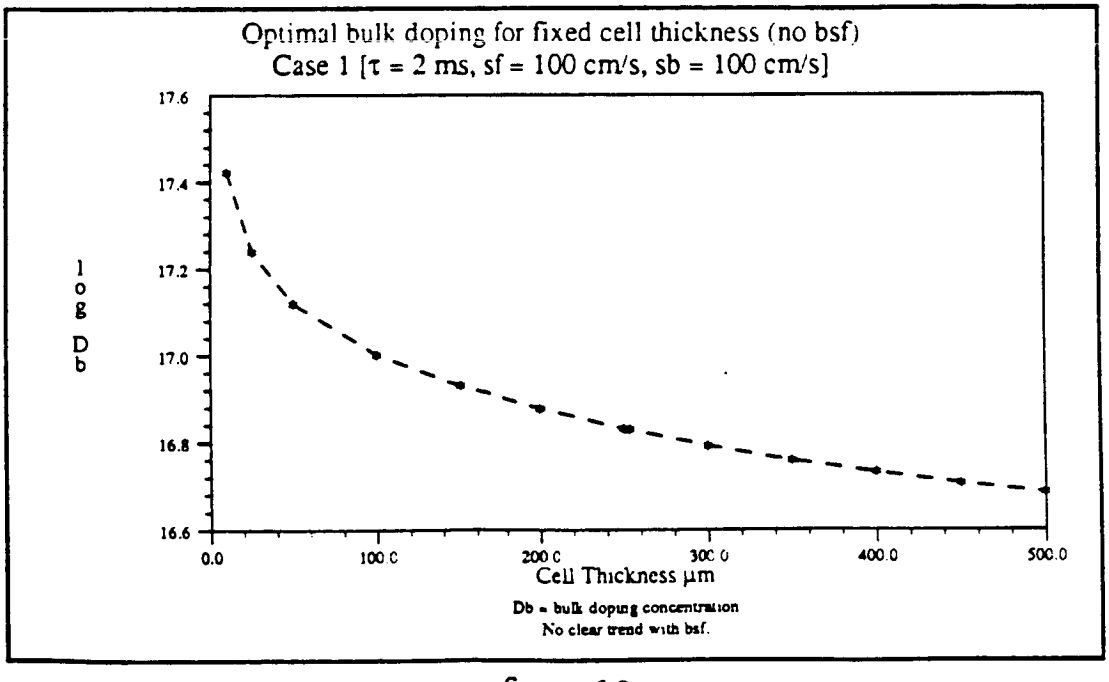

figure 6.2

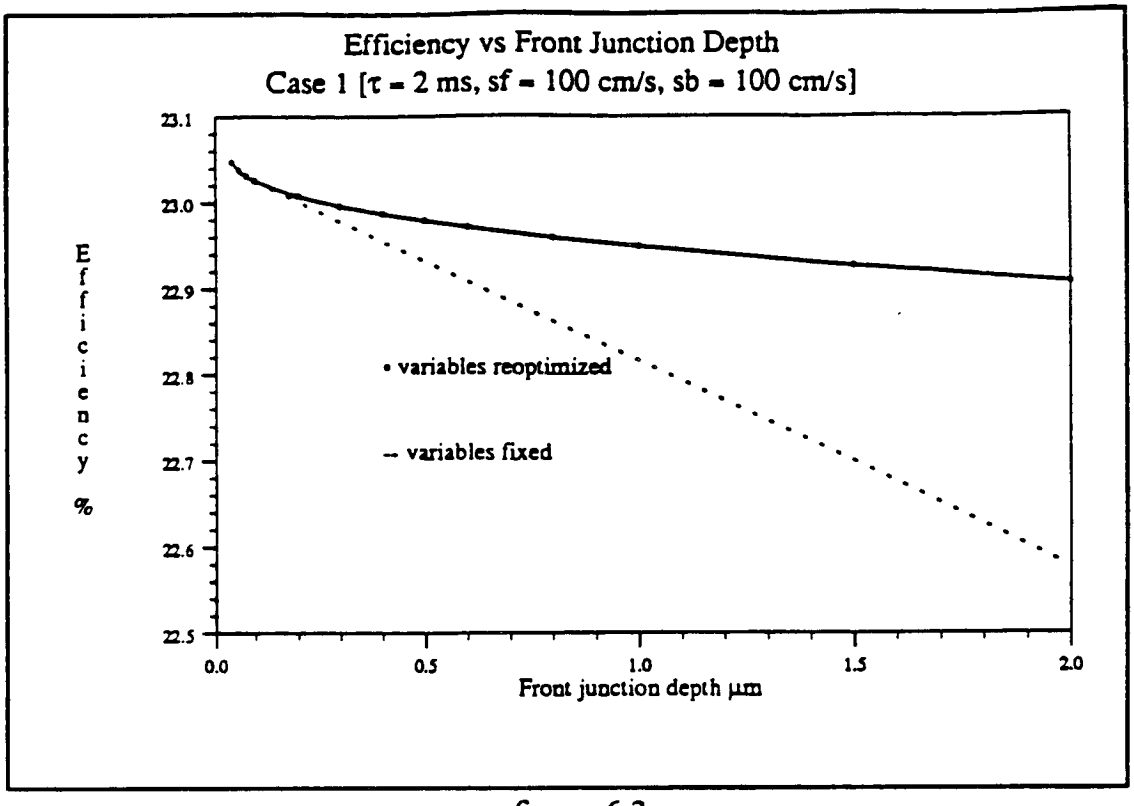

figure 6.3

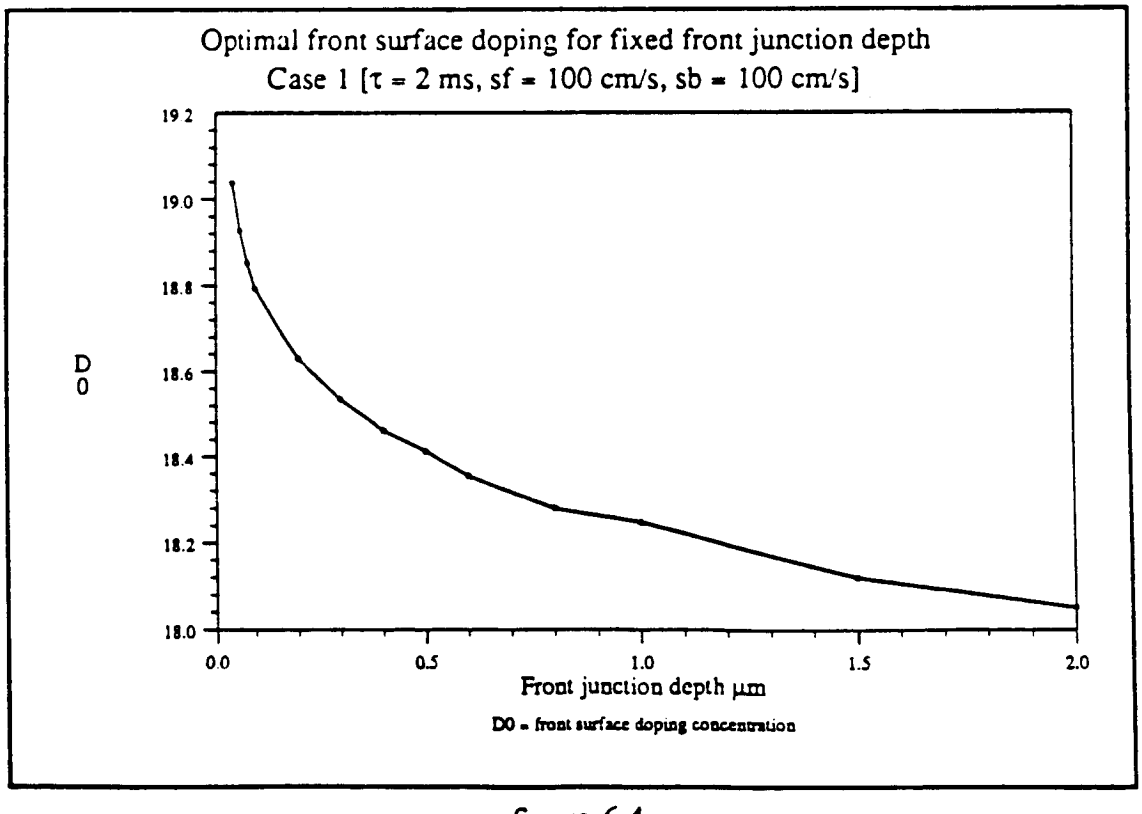

figure 6.4

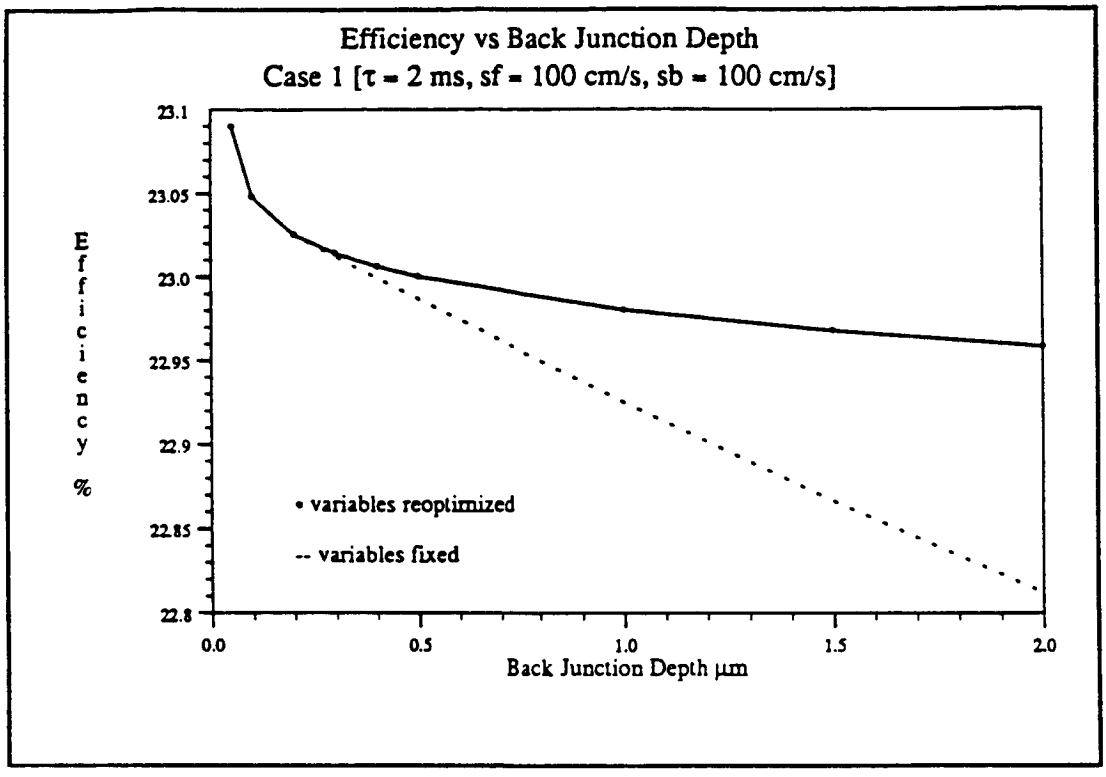

figure 6.5

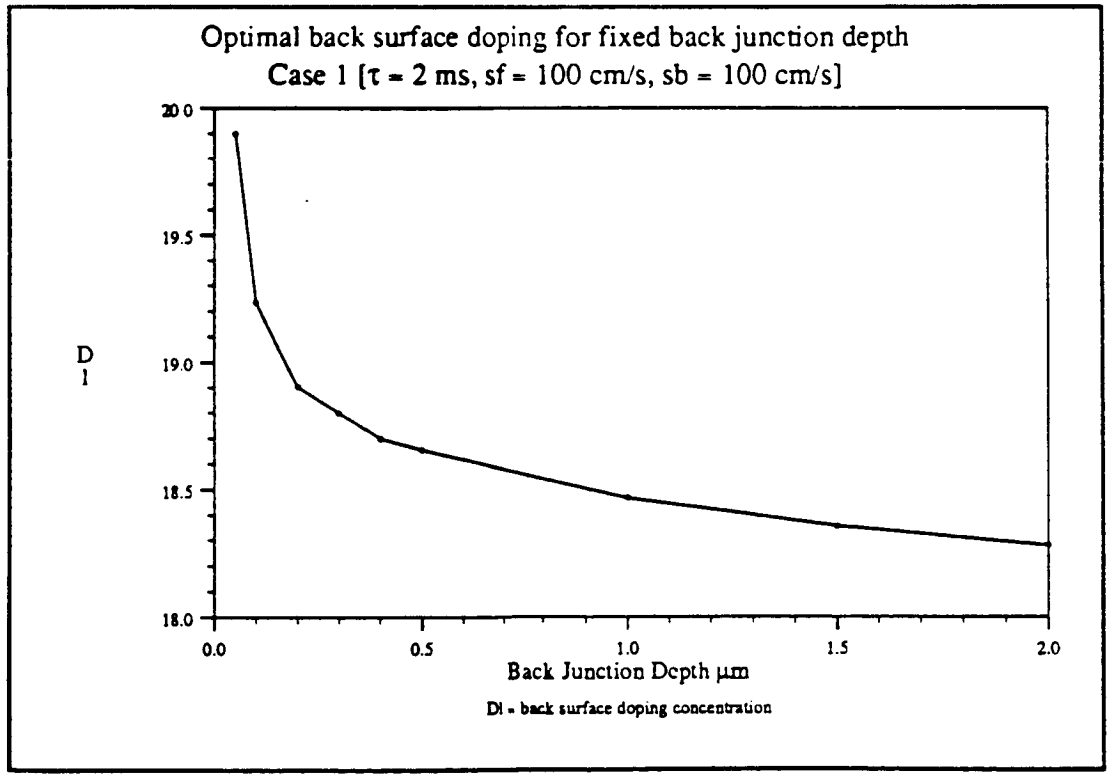

figure 6.6

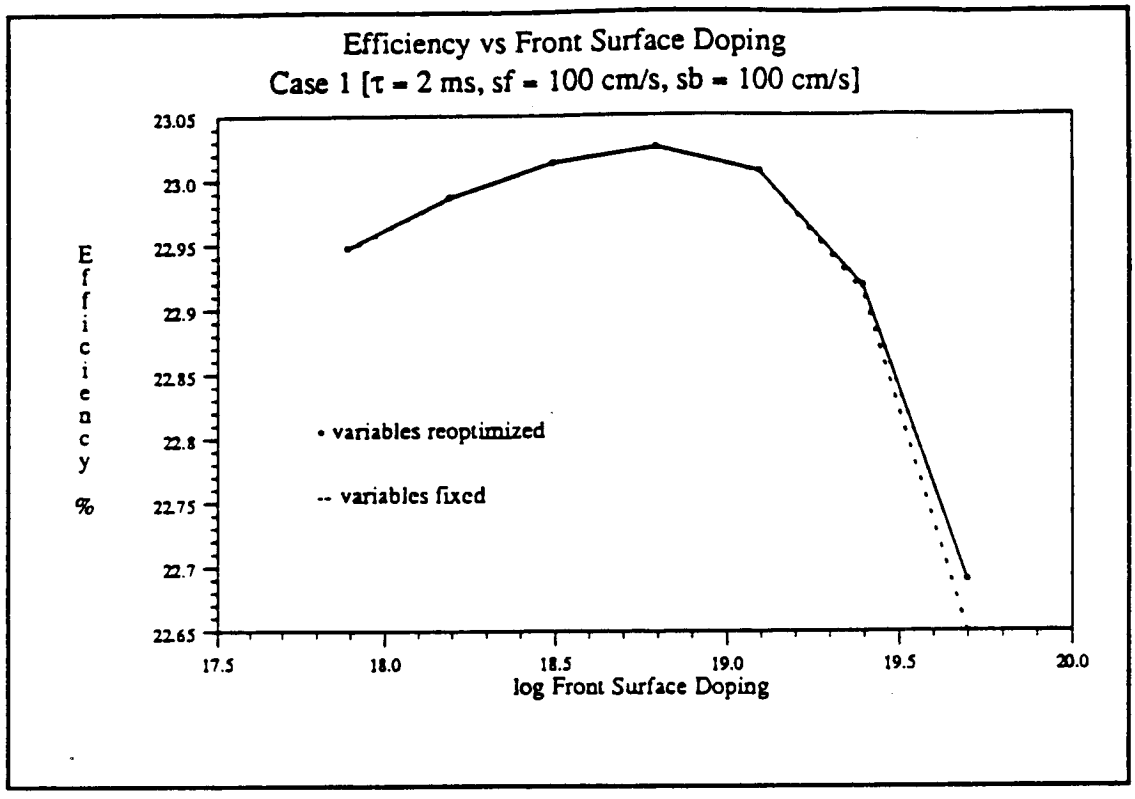

figure 6.7

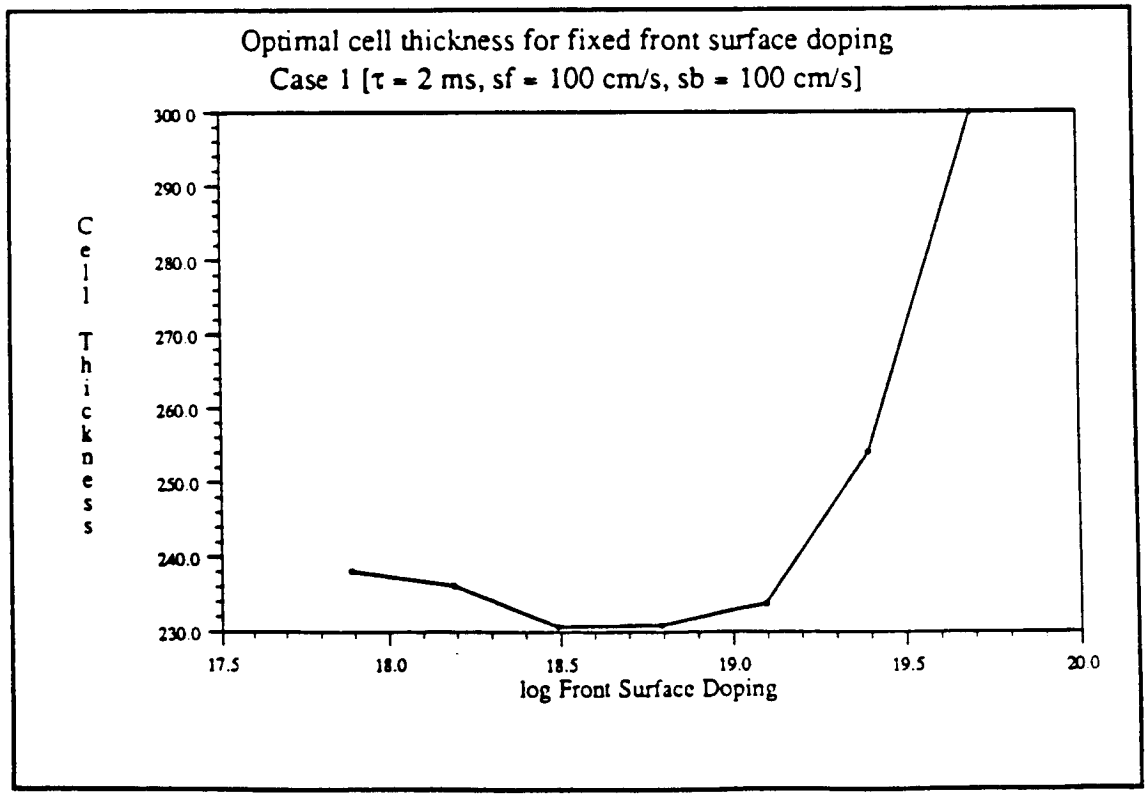

figure 6.8

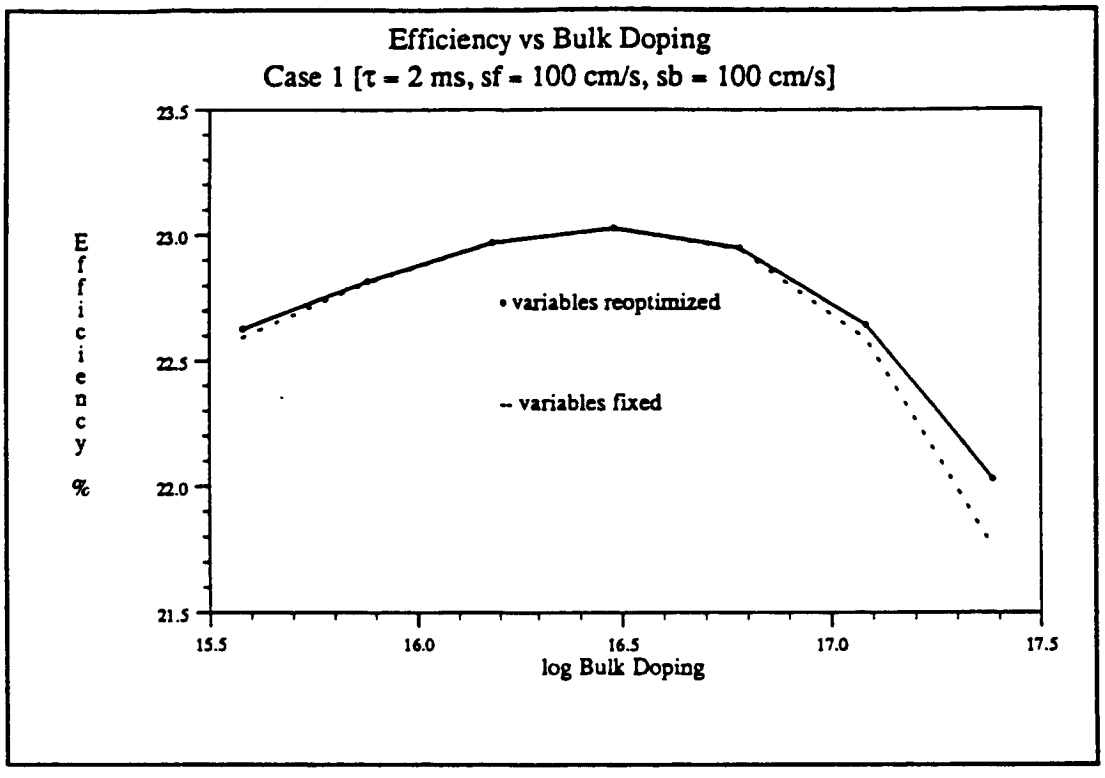

figure 6.9

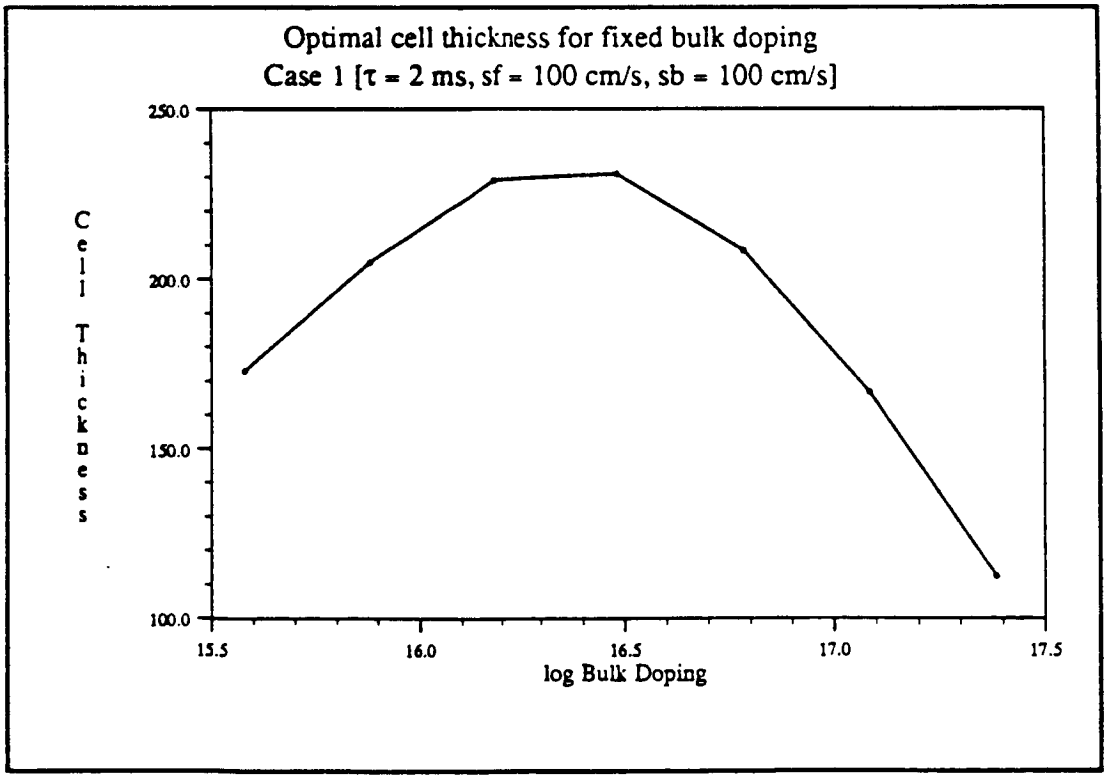

figure 6.10

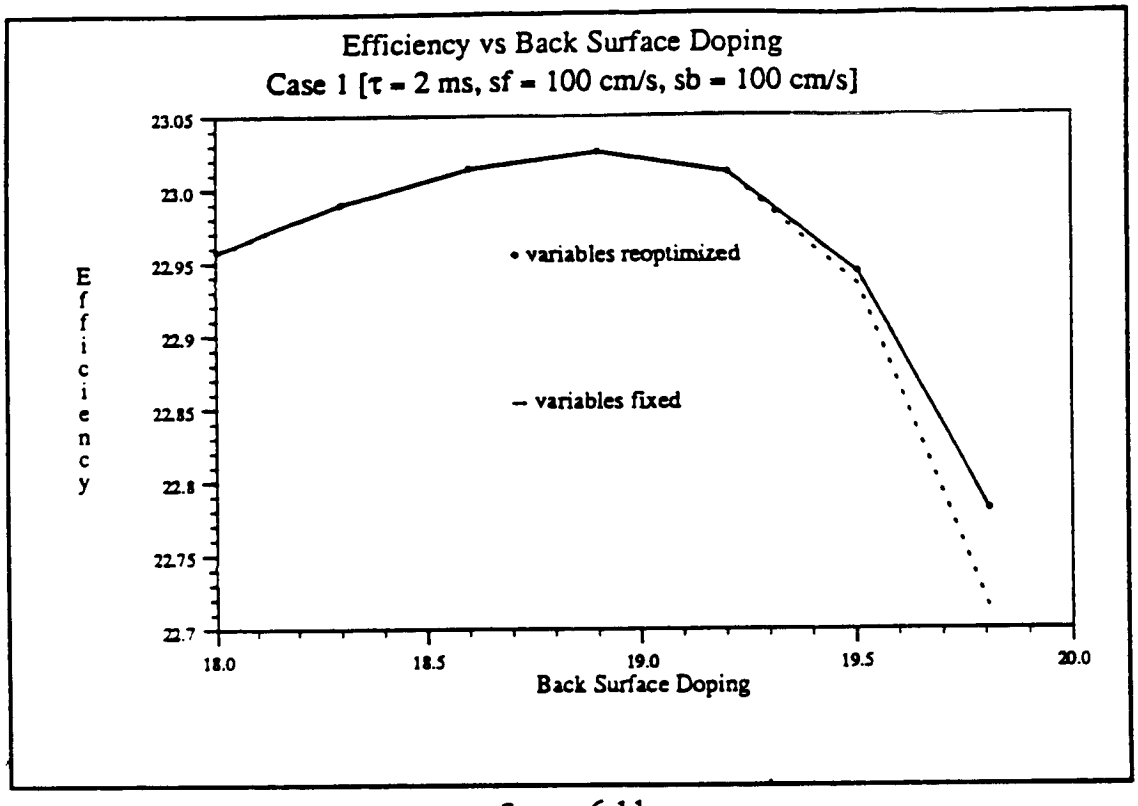

figure 6.11

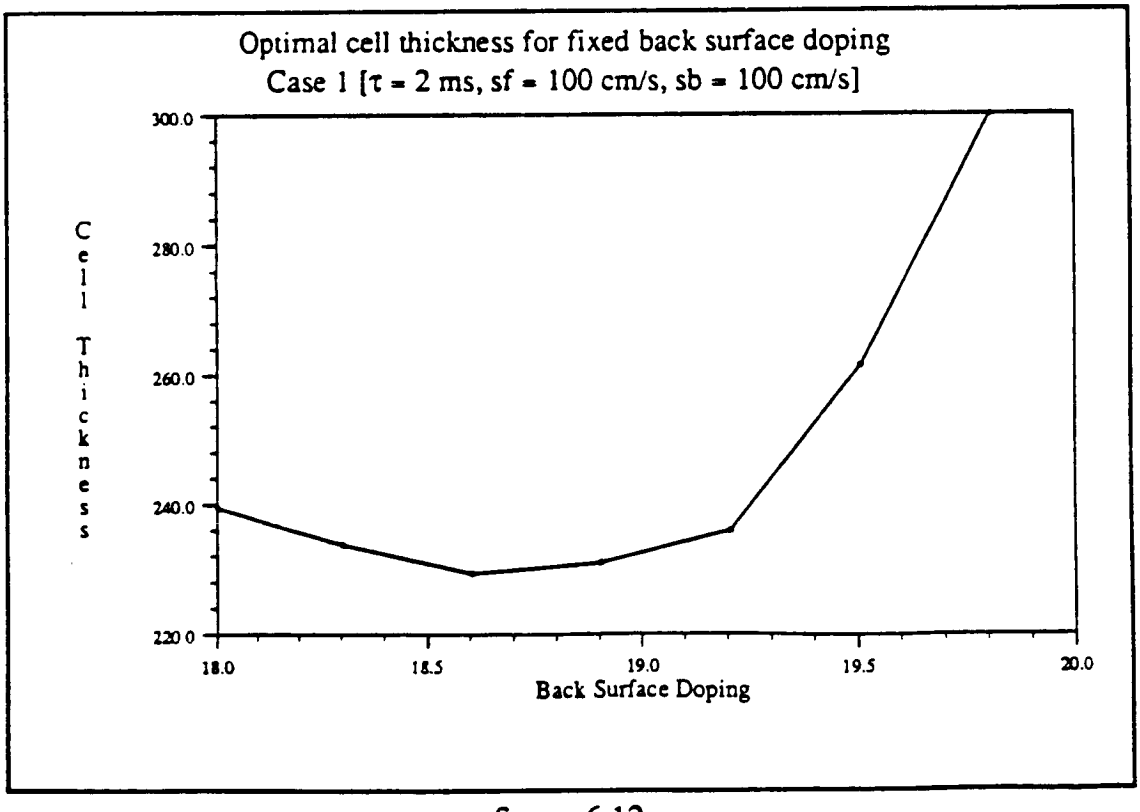

figure 6.12

Parameters Held Constant During Optimization (see also table 6.1).

Front surface recombination velocity (S_f)	1,000.0	cm/s
Back surface recombination velocity (S_b)	1,000.0	cm/s
Electron minority carrier lifetime[1] (τ_{n0})	1.00	ms
Hole minority carrier lifetime[1] (τ_{p0})	0.50	ms

Optimal Values of Decision Variables

Front junction depth (X_f)	0.10	μm (lower bound)
Back junction depth (X_b)	0.20	μm (lower bound)
Cell thickness (X_L)	280.1	μm
Front surface doping concentration (D_0)	2.153×10^{19}	P atoms/cm^3
Bulk doping concentration (D_B)	1.989×10^{16}	B atoms/cm^3
Back surface doping concentration (D_L)	3.214×10^{19}	B atoms/cm^3

Cell Performance Parameters

Efficiency	21.871	%
Open circuit voltage (V_{oc})	668.2	mV
Short circuit current density (J_{sc})	39.063	mA/cm^2
Maximum power voltage (V_{mp})	584.86	mV
Fill factor	0.8379	
Collection efficiency	99.23	%
Bulk resitivity	0.74	ohm-cm
Sheet resistance layer 1	988.0	ohm/□
layer 2	25.37	ohm/□
Bulk lifetime	260.4	μs
Bulk diffusion length	885	μm

[1] Values in lightly doped silicon.

Table 6.11 Optimal Solution For Case 2

Table 6.12 Effect of BSF and BSR, case 2 (S_f = 1,000 cm/s, S_b = 1,000 cm/s, τ_{n0} = 1 ms)

eff	V_{oc}	J_{sc}	V_{mp}	ff	C_{eff}	τ_{bulk}	L_d	X_L	X_f	X_b	log D_0	log D_B	log D_L	O_{pl}
21.871	**668.2**	**39.06**	**584.9**	**.838**	**99.2**	**260.4**	**885**	**280.1**	**0.10**	**0.20**	**19.33**	**16.30**	**19.51**	**2**
21.335	666.9	38.18	583.8	.838	99.2	245.4	855	300.0	0.10	0.20	19.33	16.33	19.51	1
20.717	661.8	37.33	579.9	.839	94.6	72.7	398	300.0	0.10	0.	19.31	16.93	0.	2
20.383	662.2	36.70	580.3	.839	95.4	68.0	381	300.0	0.10	0.	19.31	16.96	0.	1

Table 6.13 Optimizations at Fixed Cell Thickness (X_L), with bsf, case 2

eff	V_{oc}	J_{sc}	V_{mp}	ff	C_{eff}	τ_{bulk}	L_d	X_L	X_f	X_b	log D_0	log D_B	log D_L	O_{pl}
18.212	680.1	31.82	597.2	.841	99.9	413.1	1154	10.0	0.10	0.20	19.33	16.00	19.40	2
19.928	681.0	34.78	598.0	.841	99.9	307.9	976	25.0	0.10	0.20	19.33	16.20	19.38	2
20.789	680.1	36.34	597.0	.841	99.9	264.0	893	50.0	0.10	0.20	19.34	16.29	19.39	2
21.432	677.3	37.66	594.1	.840	99.7	250.0	865	100.0	0.10	0.20	19.34	16.32	19.42	2
21.698	674.5	38.32	591.2	.840	99.6	249.8	864	150.0	0.10	0.20	19.33	16.32	19.44	2
21.821	671.9	38.71	588.6	.839	99.5	253.7	872	200.0	0.10	0.20	19.34	16.31	19.46	2
21.858	670.0	38.92	586.6	.838	99.3	256.5	878	240.0	0.10	0.20	19.34	16.31	19.46	2
21.867	669.1	38.99	585.8	.838	99.3	256.4	877	260.0	0.10	0.20	19.34	16.31	19.46	2
21.871	**668.2**	**39.06**	**584.9**	**.838**	**99.2**	**260.4**	**885**	**280.1**	**0.10**	**0.20**	**19.33**	**16.30**	**19.51**	**2**
21.870	667.4	39.12	584.0	.838	99.2	260.6	886	300.0	0.10	0.20	19.33	16.30	19.49	2
21.864	666.6	39.16	583.3	.838	99.1	260.6	886	320.0	0.10	0.20	19.33	16.30	19.48	2
21.855	665.8	39.20	582.4	.837	99.0	263.5	892	341.4	0.10	0.20	19.33	16.29	19.50	2
21.803	663.1	39.30	579.7	.837	98.8	272.3	909	413.9	0.10	0.20	19.32	16.27	19.60	2
21.746	661.4	39.31	578.2	.836	98.5	256.4	877	500.0	0.10	0.20	19.41	16.31	19.62	2

Table 6.14 Optimizations at Fixed Cell Thickness (X_L), no bsf, case 2

eff	V_{oc}	J_{sc}	V_{mp}	ff	C_{eff}	τ_{bulk}	L_d	X_L	X_f	X_b	log D_0	log D_B	log D_L	O_{pl}
17.286	660.2	31.24	578.4	.838	98.1	19.3	157	10.0	0.10	0.	19.28	17.47	0.	2
18.759	660.3	33.89	578.5	.838	97.4	30.6	219	25.0	0.10	0.	19.28	17.30	0.	2
19.490	660.4	35.20	578.7	.838	96.7	40.0	264	50.0	0.10	0.	19.31	17.19	0.	2
20.080	661.0	36.22	579.3	.839	95.9	49.9	308	100.0	0.10	0.	19.31	17.09	0.	2
20.364	661.5	36.71	579.6	.839	95.4	56.9	337	150.0	0.10	0.	19.30	17.04	0.	2
20.533	661.8	37.00	579.9	.839	95.1	62.7	360	200.0	0.10	0.	19.31	17.00	0.	2
20.640	661.8	37.19	579.9	.839	94.8	67.9	380	250.0	0.10	0.	19.28	16.96	0.	2
20.717	661.8	37.33	579.9	.839	94.6	72.7	398	300.0	0.10	0.	19.31	16.93	0.	2
20.773	661.7	37.44	579.8	.838	94.5	77.7	416	350.0	0.10	0.	19.31	16.90	0.	2
20.816	661.7	37.52	579.7	.838	94.4	81.4	429	400.0	0.10	0.	19.31	16.88	0.	2
20.847	661.4	37.60	579.4	.838	94.4	85.9	445	450.0	0.10	0.	19.29	16.86	0.	2
20.873	661.1	37.67	579.1	.838	94.4	90.7	461	500.0	0.10	0.	19.30	16.83	0.	2

Table 6.15 Optimizations at Fixed Front Junction Depth (X_f), case 2

eff	V_{oc}	J_{sc}	V_{mp}	ff	C_{eff}	τ_{bulk}	L_d	X_L	X_f	X_b	$\log D_0$	$\log D_B$	$\log D_L$	O_{pl}
21.895	668.8	39.07	585.6	.838	99.2	261.2	887	280.7	0.06	0.20	19.47	16.30	19.51	2
21.871	**668.2**	**39.06**	**584.9**	**.838**	**99.2**	**260.4**	**885**	**280.1**	**0.10**	**0.20**	**19.33**	**16.30**	**19.51**	**2**
21.837	666.9	39.09	583.6	.838	99.2	268.3	901	286.8	0.20	0.20	19.16	16.28	19.52	2
21.814	666.1	39.10	582.9	.837	99.2	269.0	902	292.4	0.30	0.20	19.05	16.28	19.53	2
21.795	665.9	39.08	582.7	.838	99.2	265.2	895	289.1	0.40	0.20	18.98	16.29	19.51	2
21.778	665.3	39.10	582.0	.837	99.2	274.6	913	294.7	0.50	0.20	18.91	16.27	19.52	2
21.763	665.1	39.07	581.9	.837	99.1	266.9	898	293.3	0.60	0.20	18.86	16.28	19.51	2
21.707	664.0	39.05	580.8	.837	99.0	277.8	920	296.3	1.00	0.20	18.71	16.26	19.54	2
21.643	662.9	39.02	579.7	.837	98.9	288.3	940	300.0	1.50	0.20	18.53	16.24	19.51	2
21.581	662.2	38.96	579.0	.837	98.8	295.5	953	300.0	2.00	0.20	18.43	16.22	19.52	2

Table 6.16 Optimizations at Fixed Back Junction Depth (X_b), case 2

eff	V_{oc}	J_{sc}	V_{mp}	ff	C_{eff}	τ_{bulk}	L_d	X_L	X_f	X_b	$\log D_0$	$\log D_B$	$\log D_L$	O_{pl}
22.036	672.3	39.09	588.6	.838	99.3	240.7	845	280.1	0.10	0.05	19.43	16.34	20.60	2
21.927	669.4	39.09	585.9	.838	99.3	259.1	883	282.4	0.10	0.10	19.32	16.30	19.89	2
21.871	**668.2**	**39.06**	**584.9**	**.838**	**99.2**	**260.4**	**885**	**280.1**	**0.10**	**0.20**	**19.33**	**16.30**	**19.51**	**2**
21.847	667.5	39.07	584.1	.838	99.2	267.4	899	281.9	0.10	0.30	19.34	16.28	19.37	2
21.831	667.1	39.07	583.8	.838	99.2	270.6	905	282.5	0.10	0.40	19.34	16.28	19.28	2
21.819	666.7	39.07	583.4	.838	99.2	270.1	905	285.7	0.10	0.50	19.33	16.28	19.20	2
21.783	665.6	39.08	582.3	.837	99.2	278.7	921	290.0	0.10	1.00	19.33	16.26	19.02	2
21.761	665.4	39.06	582.1	.837	99.2	284.4	932	281.3	0.10	1.50	19.33	16.25	18.92	2
21.746	664.7	39.07	581.6	.837	99.1	280.9	925	289.6	0.10	2.00	19.34	16.25	18.85	2

Table 6.17 Optimizations at Fixed Front Surface Doping Concentration (D_0), case 2

eff	V_{oc}	J_{sc}	V_{mp}	ff	C_{eff}	τ_{bulk}	L_d	X_L	X_f	X_b	$\log D_0$	$\log D_B$	$\log D_L$	O_{pl}
21.738	663.8	39.11	580.7	.837	99.2	268.7	902	292.9	0.10	0.20	18.43	16.28	19.53	2
21.802	666.0	39.08	582.8	.838	99.2	266.6	898	284.2	0.10	0.20	18.73	16.28	19.50	2
21.850	667.4	39.08	584.1	.838	99.2	261.9	888	284.9	0.10	0.20	19.03	16.30	19.51	2
21.871	**668.2**	**39.06**	**584.9**	**.838**	**99.2**	**260.4**	**885**	**280.1**	**0.10**	**0.20**	**19.33**	**16.30**	**19.51**	**2**
21.833	666.7	39.10	583.4	.838	99.2	270.0	904	288.9	0.10	0.20	19.63	16.28	19.51	2
21.663	661.3	39.15	578.2	.837	99.3	293.5	949	300.0	0.10	0.20	19.94	16.23	19.51	2
21.251	649.8	39.19	567.1	.834	99.4	351.7	1054	300.0	0.10	0.20	20.24	16.11	19.51	2

Table 6.18 Optimizations at Fixed Bulk Doping Concentration (D_B), case 2

eff	V_{oc}	J_{sc}	V_{mp}	ff	C_{eff}	τ_{bulk}	L_d	X_L	X_f	X_b	log D_0	log D_B	log D_L	O_{pl}
21.376	673.5	38.96	576.2	.815	99.9	740.4	1593	213.2	0.10	0.20	19.37	15.40	19.54	2
21.629	669.7	39.15	578.2	.825	99.8	587.3	1404	252.4	0.10	0.20	19.35	15.70	19.52	2
21.809	667.5	39.19	581.5	.833	99.6	414.9	1157	279.0	0.10	0.20	19.34	16.00	19.52	2
21.871	**668.2**	**39.06**	**584.9**	**.838**	**99.2**	**260.4**	**885**	**280.1**	**0.10**	**0.20**	**19.33**	**16.30**	**19.51**	**2**
21.797	670.1	38.74	587.5	.840	98.6	148.0	630	261.7	0.10	0.20	19.32	16.60	19.47	2
21.547	672.1	38.15	589.8	.840	97.7	77.9	417	219.0	0.10	0.20	19.31	16.90	19.44	2
21.068	672.5	37.27	590.3	.841	96.6	38.6	258	161.1	0.10	0.20	19.29	17.20	19.39	2

Table 6.19 Optimizations at Fixed Back Surface Doping Concentration (D_L), case 2

eff	V_{oc}	J_{sc}	V_{mp}	ff	C_{eff}	τ_{bulk}	L_d	X_L	X_f	X_b	log D_0	log D_B	log D_L	O_{pl}
21.747	664.6	39.07	581.5	.837	99.1	276.6	917	293.8	0.10	0.20	19.33	16.26	18.60	2
21.806	666.5	39.06	583.3	.838	99.2	266.7	898	283.5	0.10	0.20	19.33	16.28	18.90	2
21.851	667.7	39.06	584.4	.838	99.2	260.5	886	280.6	0.10	0.20	19.33	16.30	19.21	2
21.871	**668.2**	**39.06**	**584.9**	**.838**	**99.2**	**260.4**	**885**	**280.1**	**0.10**	**0.20**	**19.33**	**16.30**	**19.51**	**2**
21.840	666.6	39.12	583.3	.837	99.2	270.6	906	300.0	0.10	0.20	19.33	16.28	19.81	2
21.699	663.0	39.11	579.7	.837	99.2	307.5	975	300.0	0.10	0.20	19.33	16.20	20.11	2
21.356	654.3	39.09	571.3	.835	99.1	387.1	1113	300.0	0.10	0.20	19.34	16.05	20.41	2

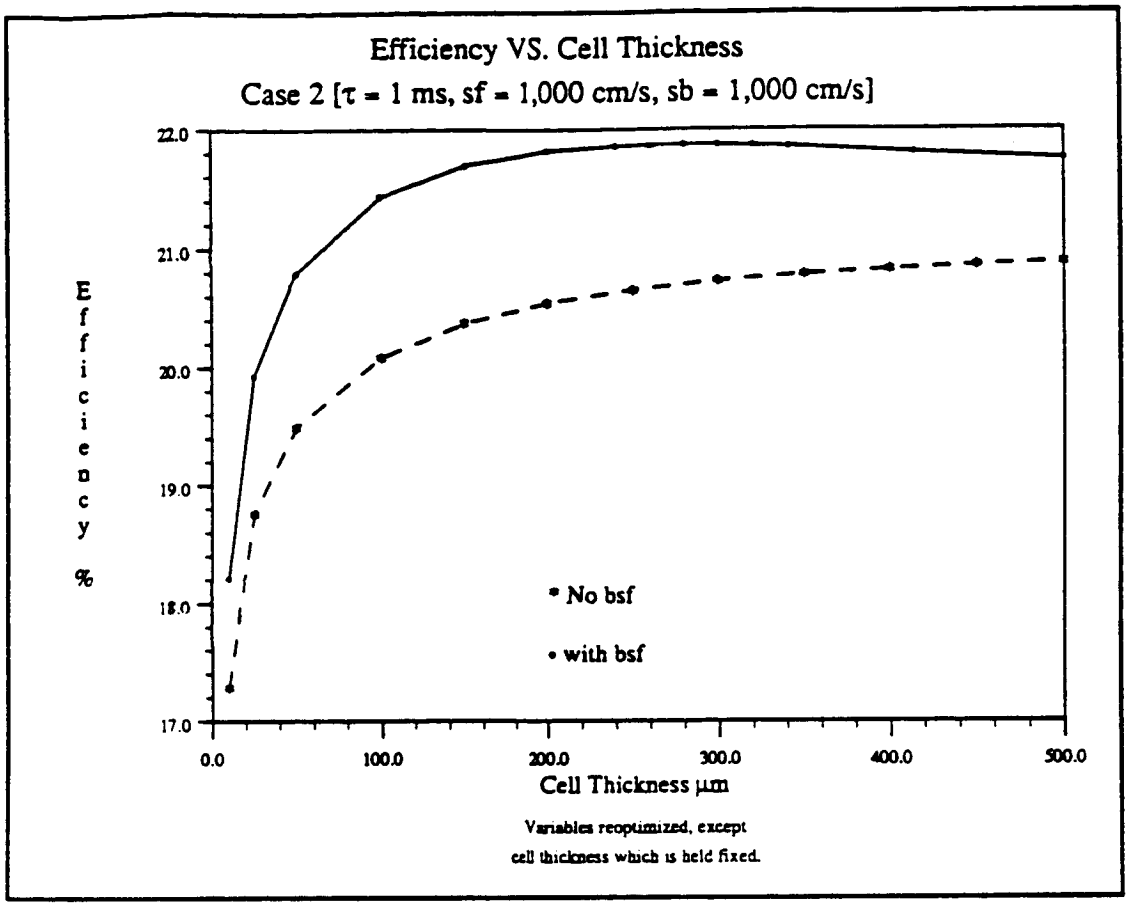

figure 6.13

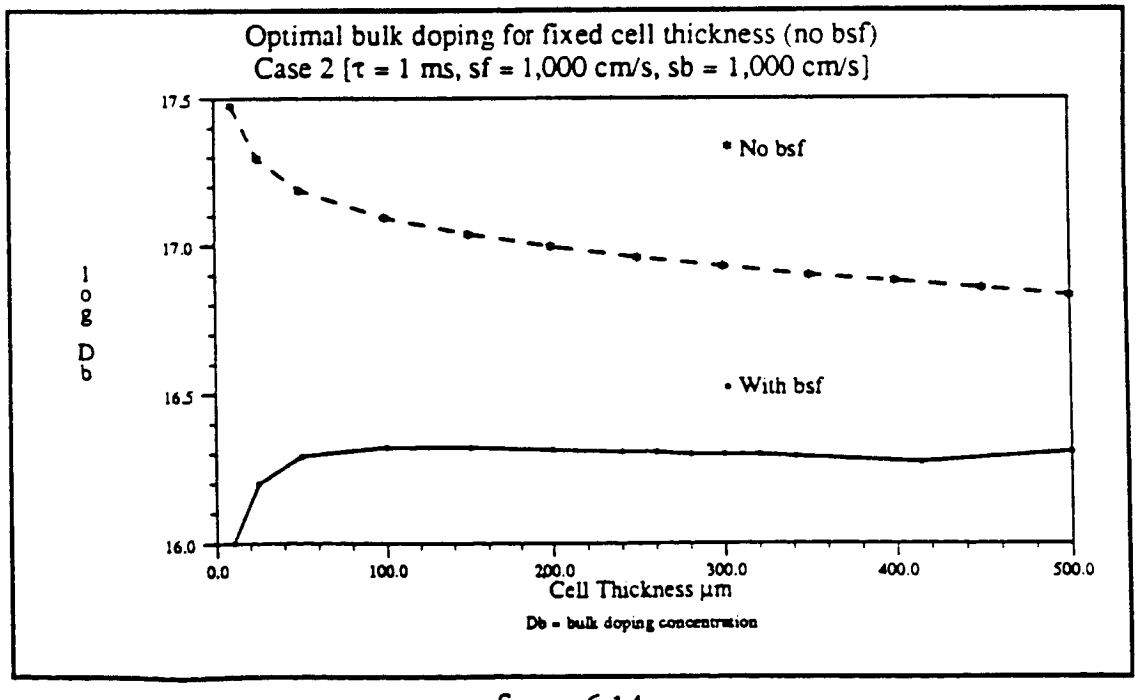

figure 6.14

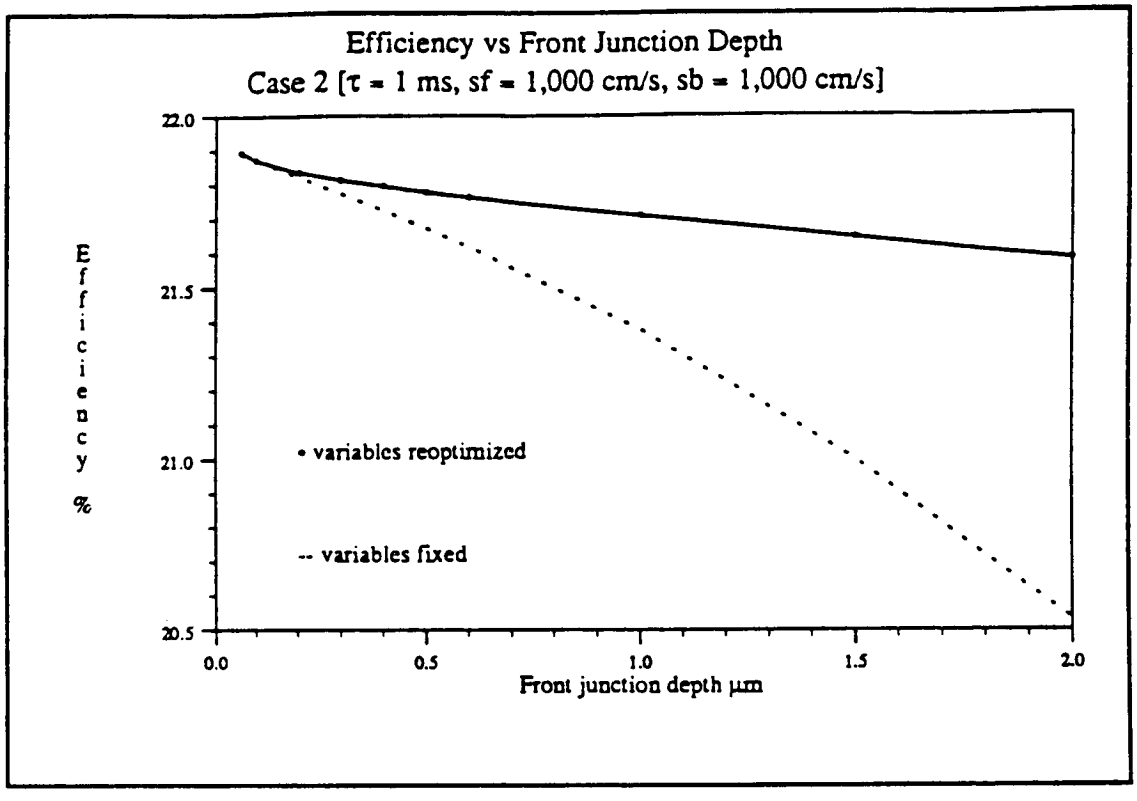

figure 6.15

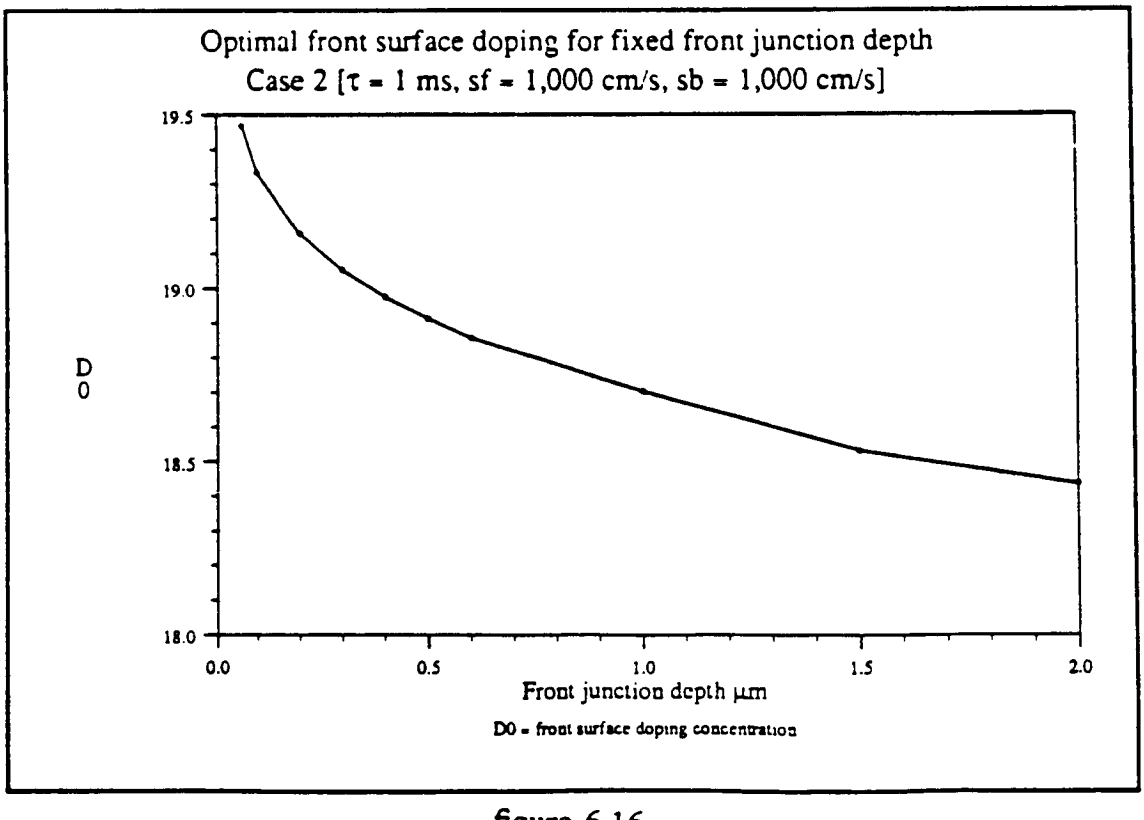

figure 6.16

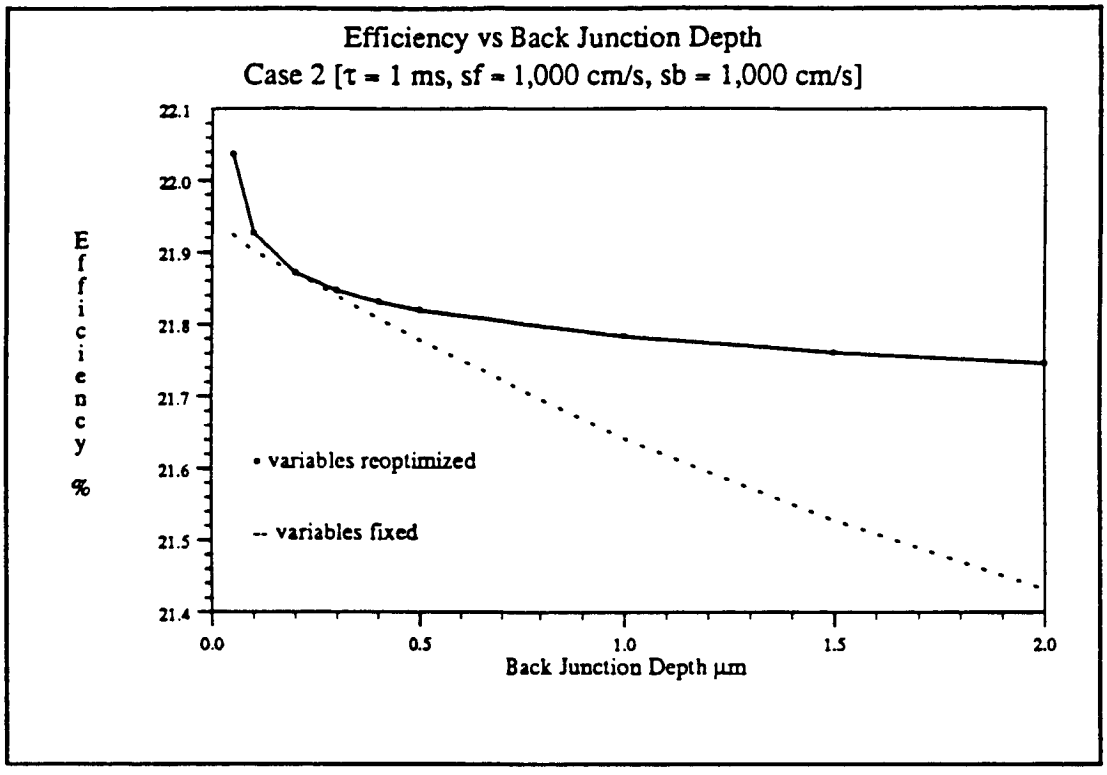

figure 6.17

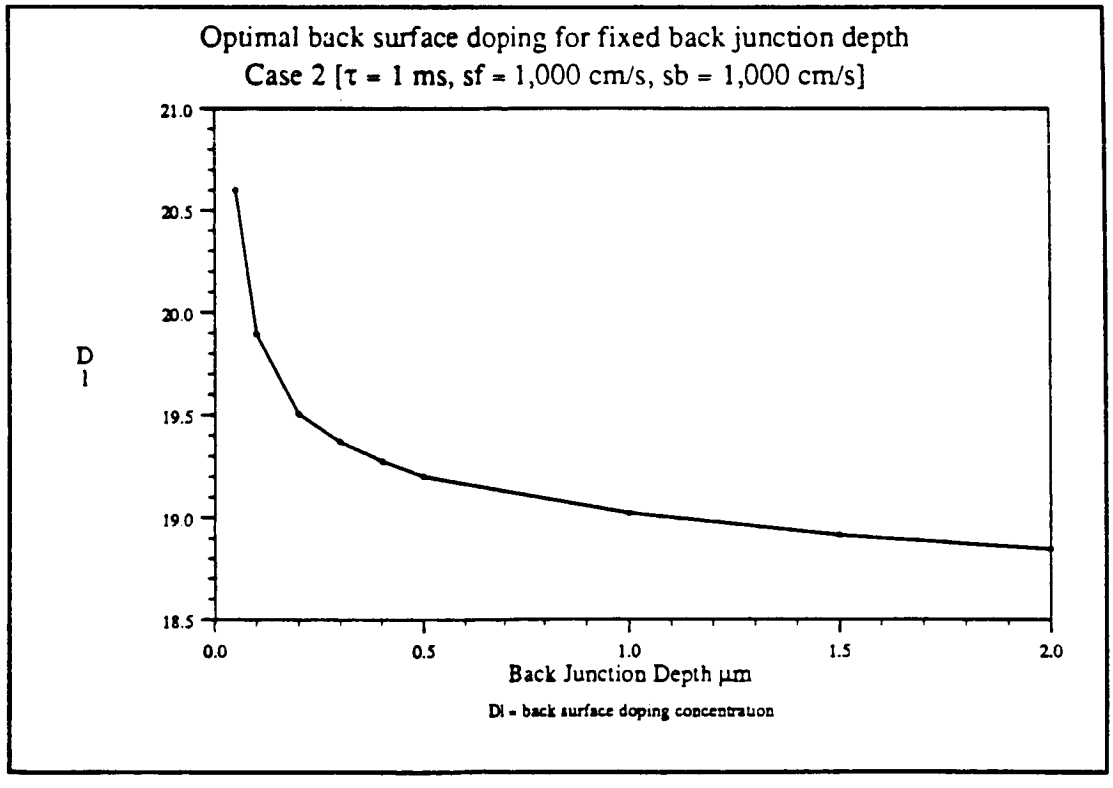

figure 6.18

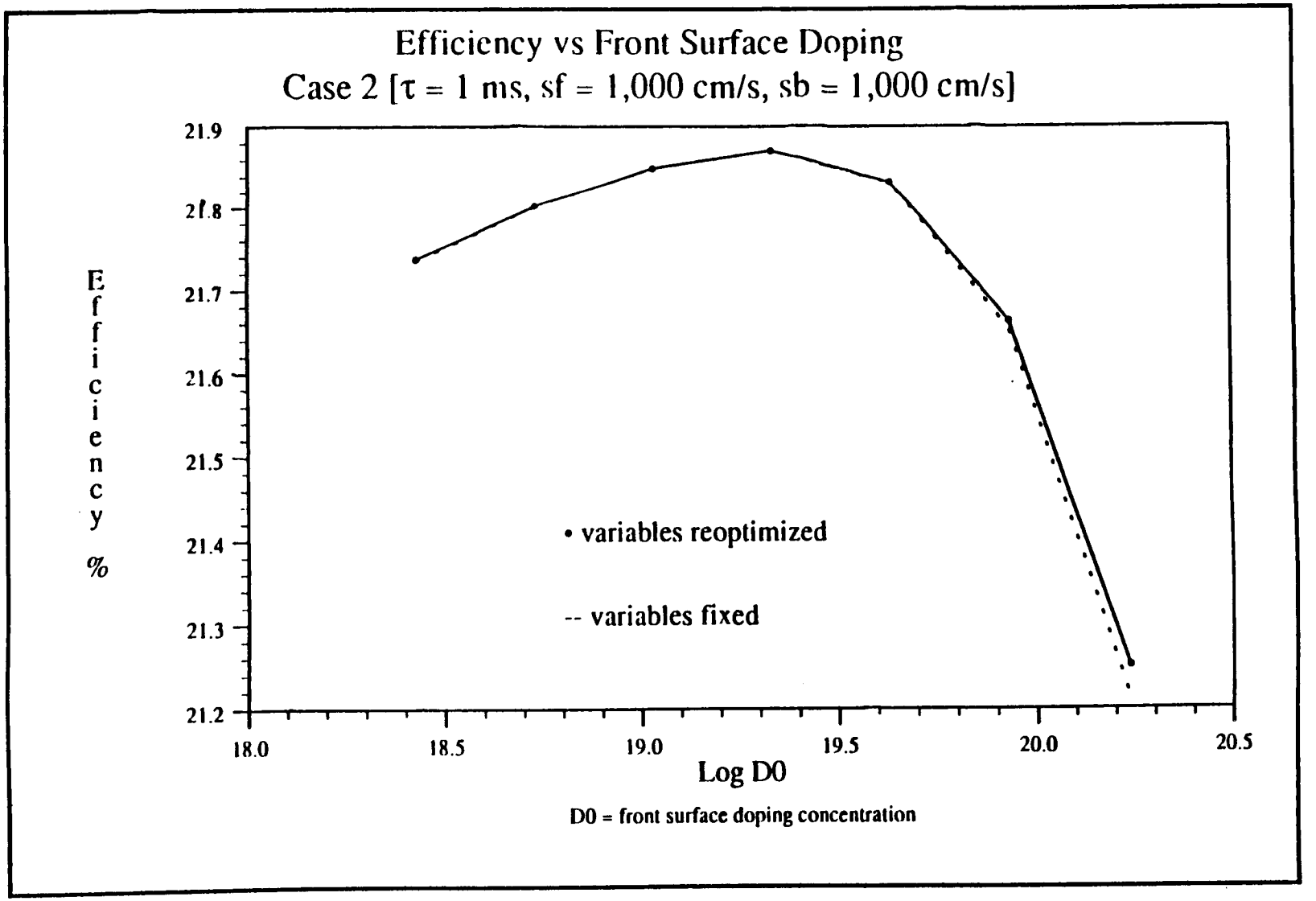
Efficiency vs Front Surface Doping
Case 2 [τ = 1 ms, sf = 1,000 cm/s, sb = 1,000 cm/s]
Efficiency %
21.9
21.8
21.7
21.6
21.5
21.4
21.3
21.2
18.0
18.5
19.0
19.5
20.0
20.5
Log D0
• variables reoptimized
-- variables fixed
D0 = front surface doping concentration

figure 6.19

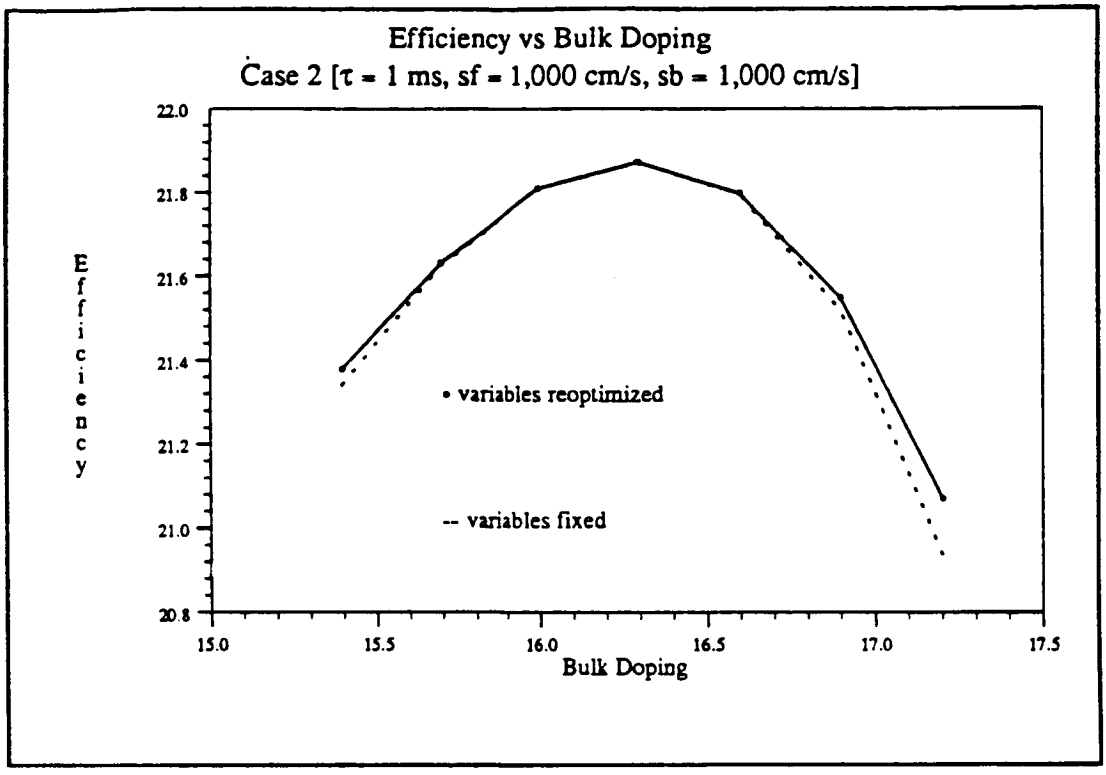

figure 6.20

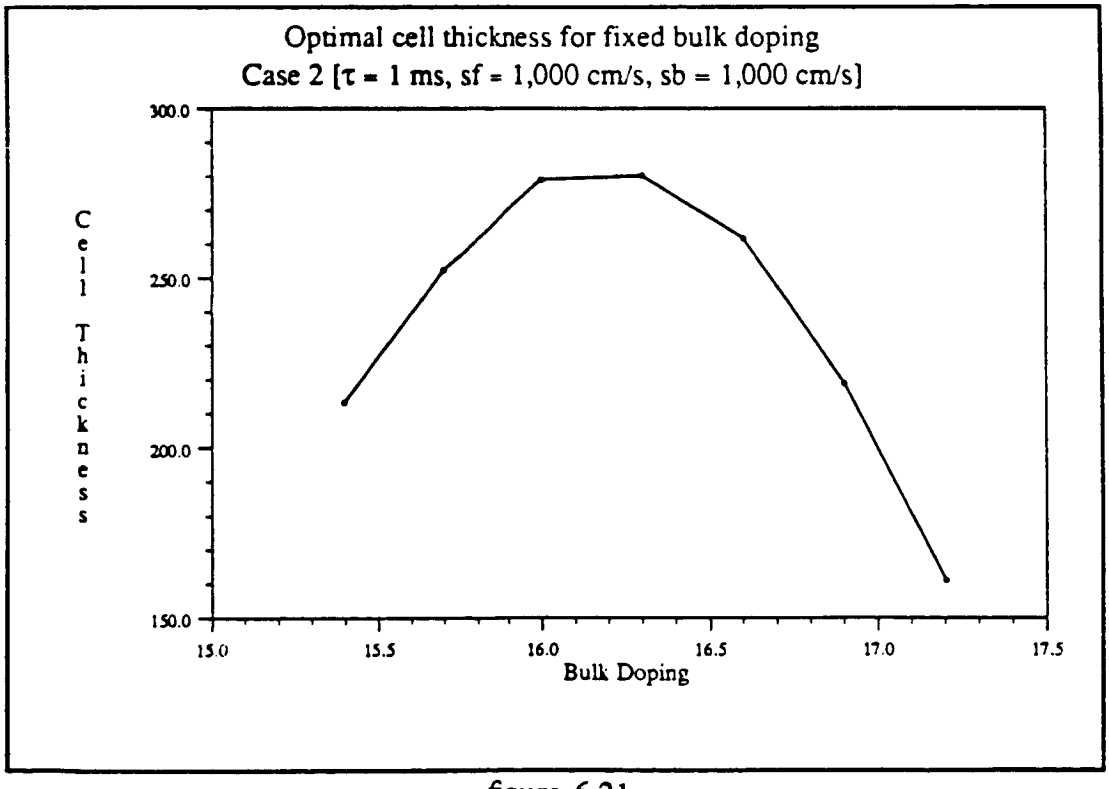

figure 6.21

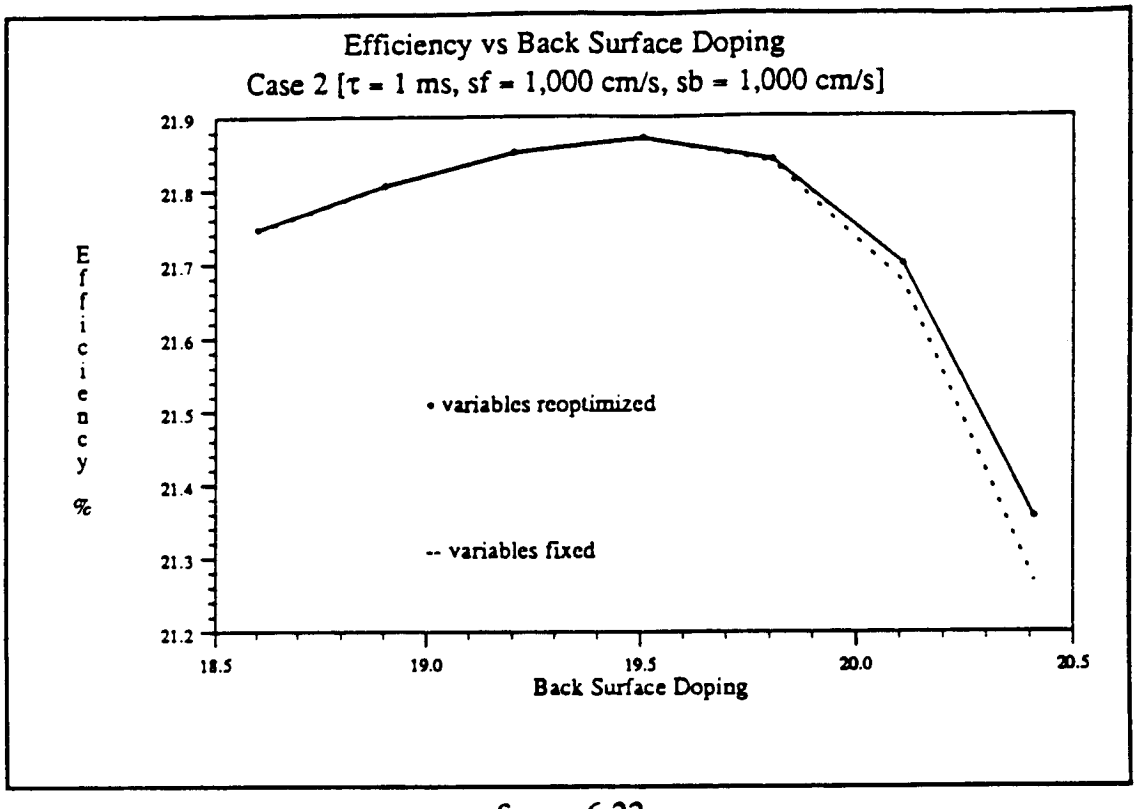

figure 6.22

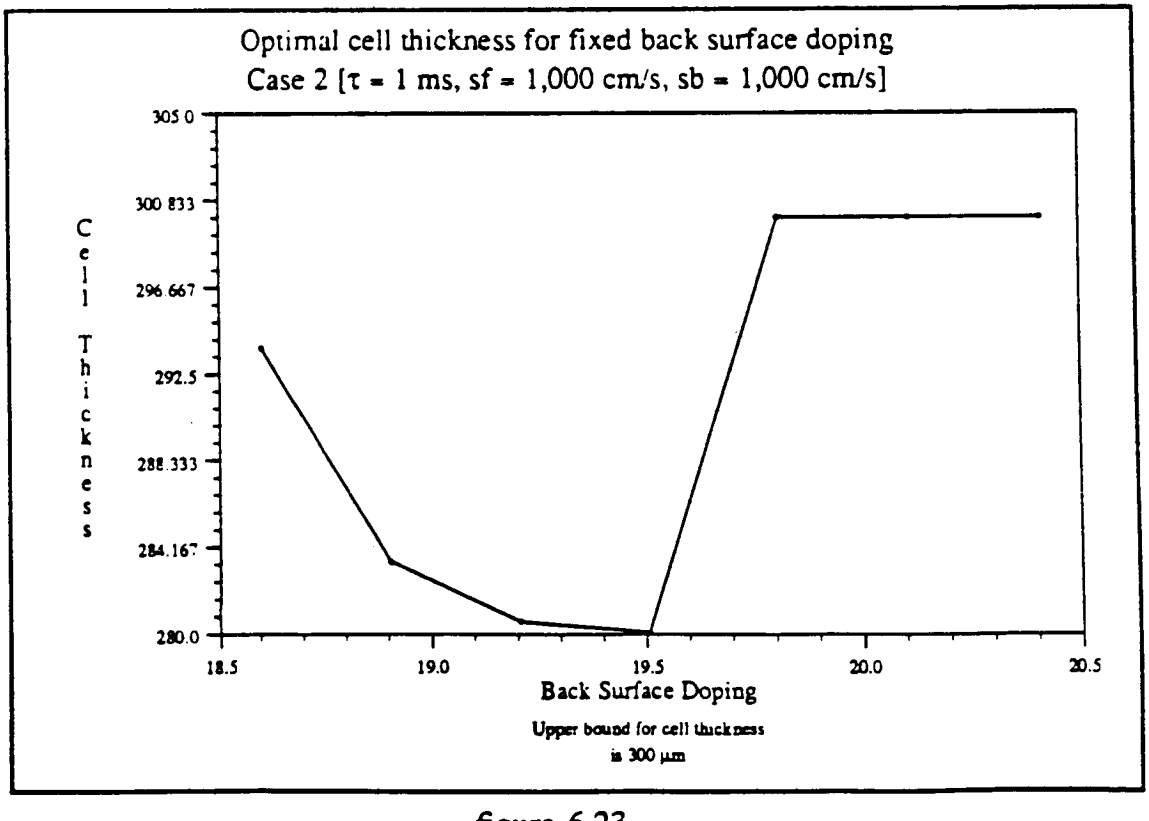

figure 6.23

Parameters Held Constant During Optimization (see also table 6.1).

Front surface recombination velocity (S_f)	1,000	cm/s
Back surface recombination velocity (S_b)	∞	cm/s
Electron minority carrier lifetime[1] (τ_{n0})	1.00	ms
Hole minority carrier lifetime[1] (τ_{p0})	0.50	ms

Optimal Values of Decision Variables

Front junction depth (X_f)	0.10	μm (lower bound)
Back junction depth (X_b)	50.0	μm (upper bound)
Cell thickness (X_L)	300.0	μm (upper bound)
Front surface doping concentration (D_0)	2.157×10^{19}	P atoms/cm^3
Bulk doping concentration (D_B)	1.368×10^{16}	B atoms/cm^3
Back surface doping concentration (D_L)	8.572×10^{18}	B atoms/cm^3

Cell Performance Parameters

Efficiency	21.355	%
Open circuit voltage (V_{oc})	656.5	mV
Short circuit current density (J_{sc})	38.903	mA/cm^2
Maximum power voltage (V_{mp})	573.9	mV
Fill factor	0.8362	
Collection efficiency	98.62	%
Bulk resitivity	1.04	ohm-cm
Sheet resistance layer 1	1010.1	ohm/□
layer 2	5.28	ohm/□
Bulk lifetime	339.5	μs
Bulk diffusion length	1032	μm

[1] Values in lightly doped silicon.

Table 6.20 Optimal Solution For Case 3

Table 6.21 Effect of BSF and BSR, case 3 (S_f = 1,000 cm/s, S_b = ∞ cm/s, τ_{n0} = 1 ms)

eff	V_{oc}	J_{sc}	V_{mp}	ff	C_{eff}	τ_{bulk}	L_d	X_L	X_f	X_b	log D_0	log D_B	log D_L	O_{pl}
21.355	656.5	38.90	573.9	.836	98.6	339.5	1032	300.0	0.10	50.0	19.33	16.14	18.93	2
20.882	656.5	38.02	574.2	.837	98.8	299.4	960	300.0	0.10	50.0	19.33	16.22	18.95	1
20.059	662.0	36.13	580.1	.839	91.6	42.1	274	300.0	0.10	0.	19.29	17.17	0.	2
19.849	662.0	35.76	580.1	.839	92.9	41.0	269	300.0	0.10	0.	19.30	17.18	0.	1

Table 6.22 Optimizations at Fixed Cell Thickness (X_L), with bsf, case 3

eff	V_{oc}	J_{sc}	V_{mp}	ff	C_{eff}	τ_{bulk}	L_d	X_L	X_f	X_b	log D_0	log D_B	log D_L	O_{pl}
16.158	625.9	31.03	545.5	.832	97.5	776.9	1635	10.0	0.10	2.9	19.33	15.31	20.06	2
18.341	644.3	34.08	563.0	.835	97.9	642.7	1475	25.0	0.10	9.3	19.35	15.60	19.56	2
19.569	653.9	35.77	572.0	.837	98.3	528.3	1324	50.0	0.10	20.5	19.36	15.80	19.23	2
20.525	659.1	37.19	576.8	.837	98.5	438.7	1194	100.0	0.10	39.8	19.36	15.96	18.96	2
20.951	659.7	37.93	577.2	.837	98.6	384.1	1108	150.0	0.10	50.0	19.33	16.05	18.87	2
21.173	658.7	38.41	576.1	.837	98.7	359.8	1067	200.0	0.10	50.0	19.35	16.10	18.90	2
21.290	657.4	38.72	574.7	.836	98.7	356.5	1062	250.0	0.10	50.0	19.33	16.10	18.92	2
21.355	**656.5**	**38.90**	**573.9**	**.836**	**98.6**	**339.5**	**1032**	**300.0**	**0.10**	**50.0**	**19.33**	**16.14**	**18.93**	**2**
21.382	655.3	39.04	572.6	.836	98.6	341.6	1036	349.3	0.10	50.0	19.36	16.13	18.95	2
21.387	654.6	39.10	572.0	.836	98.4	330.1	1016	390.7	0.10	50.0	19.35	16.15	18.95	2
21.376	653.5	39.16	570.9	.835	98.3	324.6	1006	450.0	0.10	50.0	19.32	16.17	18.94	2
21.358	652.8	39.17	570.2	.835	98.1	316.4	991	500.0	0.10	50.0	19.33	16.18	18.97	2
21.340	652.3	39.18	569.6	.835	98.0	311.6	983	542.6	0.10	50.0	19.34	16.19	18.96	2

Table 6.23 Optimizations at Fixed Cell Thickness (X_L), no bsf, case 3

eff	V_{oc}	J_{sc}	V_{mp}	ff	C_{eff}	τ_{bulk}	L_d	X_L	X_f	X_b	log D_0	log D_B	log D_L	O_{pl}
13.721	602.3	27.71	521.6	.822	87.1	2.7	40	10.0	2.71	0.	18.14	18.13	0.	2
15.630	619.5	30.52	538.2	.827	87.7	7.1	77	25.0	3.19	0.	17.85	17.83	0.	2
17.038	644.8	31.71	563.0	.833	87.2	8.0	84	50.0	1.31	0.	18.54	17.79	0.	2
18.437	657.5	33.48	575.8	.838	88.7	13.8	123	100.0	0.10	0.	19.29	17.60	0.	2
19.127	659.6	34.60	577.8	.838	89.9	21.2	168	150.0	0.10	0.	19.30	17.44	0.	2
19.552	660.6	35.30	578.9	.838	90.7	28.9	210	200.0	0.10	0.	19.29	17.32	0.	2
19.843	661.6	35.77	579.8	.838	91.2	35.1	241	250.0	0.10	0.	19.29	17.24	0.	2
20.059	662.0	36.13	580.1	.839	91.6	42.1	274	300.0	0.10	0.	19.29	17.17	0.	2
20.223	662.2	36.42	580.3	.839	91.9	48.8	304	350.0	0.10	0.	19.30	17.10	0.	2
20.353	662.5	36.63	580.6	.839	92.2	53.4	323	400.0	0.10	0.	19.31	17.07	0.	2
20.454	662.6	36.81	580.6	.839	92.4	58.5	344	450.0	0.10	0.	19.29	17.03	0.	2
20.538	662.8	36.95	580.8	.839	92.6	62.2	358	500.0	0.10	0.	19.29	17.00	0.	2

Table 6.24 Optimizations at Fixed Front Junction Depth (X_f), case 3

eff	V_{oc}	J_{sc}	V_{mp}	ff	C_{eff}	τ_{bulk}	L_d	X_L	X_f	X_b	$\log D_0$	$\log D_B$	$\log D_L$	O_{pl}
21.371	656.9	38.90	574.3	.836	98.6	337.9	1030	300.0	0.06	50.0	19.48	16.14	18.93	2
21.355	**656.5**	**38.90**	**573.9**	**.836**	**98.6**	**339.5**	**1032**	**300.0**	**0.10**	**50.0**	**19.33**	**16.14**	**18.93**	**2**
21.332	655.8	38.91	573.2	.836	98.6	345.1	1042	300.0	0.20	50.0	19.16	16.13	18.93	2
21.316	655.4	38.91	572.8	.836	98.6	350.3	1051	300.0	0.30	50.0	19.04	16.12	18.93	2
21.303	655.1	38.90	572.5	.836	98.6	350.5	1051	300.0	0.40	50.0	18.98	16.12	18.93	2
21.290	654.9	38.90	572.3	.836	98.6	352.2	1054	300.0	0.50	50.0	18.90	16.11	18.92	2
21.262	654.3	38.88	571.8	.836	98.6	356.5	1062	300.0	0.75	50.0	18.78	16.10	18.92	2
21.235	654.0	38.86	571.4	.836	98.5	356.0	1061	300.0	1.00	50.0	18.67	16.10	18.93	2
21.183	653.2	38.82	570.6	.835	98.4	368.3	1082	300.0	1.50	50.0	18.52	16.08	18.92	2
21.131	652.6	38.77	570.0	.835	98.3	372.4	1088	300.0	2.00	50.0	18.38	16.07	18.93	2

Table 6.25 Optimizations at Fixed Back Junction Depth (X_b), case 3

eff	V_{oc}	J_{sc}	V_{mp}	ff	C_{eff}	τ_{bulk}	L_d	X_L	X_f	X_b	$\log D_0$	$\log D_B$	$\log D_L$	O_{pl}
20.158	661.0	36.37	579.2	.838	92.2	49.8	308	300.0	0.10	0.5	19.29	17.10	20.60	2
20.228	660.3	36.54	578.5	.838	92.6	55.9	333	300.0	0.10	1.0	19.30	17.05	20.56	2
20.298	630.4	38.72	549.1	.832	98.2	461.9	1229	300.0	0.10	2.0	19.34	15.92	20.33	2
20.727	640.2	38.85	558.4	.833	98.5	415.3	1158	300.0	0.10	5.0	19.33	16.00	19.94	2
20.989	646.5	38.90	564.4	.834	98.6	380.6	1102	300.0	0.10	10.0	19.33	16.06	19.64	2
21.189	651.6	38.93	569.3	.835	98.7	353.7	1057	300.0	0.10	20.0	19.33	16.11	19.33	2
21.275	653.9	38.93	571.4	.836	98.7	345.1	1042	300.0	0.10	30.0	19.33	16.13	19.15	2
21.325	655.4	38.92	572.9	.836	98.7	341.3	1036	300.0	0.10	40.0	19.33	16.13	19.03	2
21.355	**656.5**	**38.90**	**573.9**	**.836**	**98.6**	**339.5**	**1032**	**300.0**	**0.10**	**50.0**	**19.33**	**16.14**	**18.93**	**2**
21.372	657.1	38.90	574.4	.836	98.6	345.7	1043	300.0	0.10	60.0	19.33	16.12	18.83	2
21.385	657.7	38.88	575.0	.836	98.6	347.4	1046	300.0	0.10	70.0	19.33	16.12	18.75	2
21.394	658.3	38.86	575.5	.836	98.5	349.6	1050	300.0	0.10	80.0	19.33	16.12	18.69	2
21.400	658.8	38.84	575.9	.836	98.5	354.9	1059	300.0	0.10	90.0	19.33	16.11	18.64	2
21.403	659.2	38.81	576.4	.837	98.4	356.9	1062	300.0	0.10	100.	19.33	16.10	18.58	2
21.404	659.6	38.79	576.8	.837	98.3	358.1	1064	300.0	0.10	110.	19.33	16.10	18.53	2
21.404	659.7	38.79	576.8	.837	98.3	363.8	1074	300.0	0.10	112.	19.33	16.09	18.53	2
21.404	659.9	38.76	577.1	.837	98.3	367.4	1080	300.0	0.10	120.	19.33	16.08	18.49	2

Table 6.26 Optimizations at Fixed Front Surface Doping Concentration (D_0), case 3

eff	V_{oc}	J_{sc}	V_{mp}	ff	C_{eff}	τ_{bulk}	L_d	X_L	X_f	X_b	$\log D_0$	$\log D_B$	$\log D_L$	O_{pl}
21.266	653.7	38.93	571.2	.836	98.7	354.5	1058	300.0	0.10	50.0	18.43	16.11	18.93	2
21.309	655.0	38.92	572.4	.836	98.7	349.9	1050	300.0	0.10	50.0	18.73	16.12	18.93	2
21.341	656.0	38.91	573.4	.836	98.6	341.5	1036	300.0	0.10	50.0	19.03	16.13	18.93	2
21.355	**656.5**	**38.90**	**573.9**	**.836**	**98.6**	**339.5**	**1032**	**300.0**	**0.10**	**50.0**	**19.33**	**16.14**	**18.93**	**2**
21.331	655.7	38.91	573.1	.836	98.7	348.6	1048	300.0	0.10	50.0	19.63	16.12	18.93	2
21.216	652.2	38.95	569.6	.835	98.7	376.2	1095	300.0	0.10	50.0	19.94	16.07	18.93	2
20.910	643.4	38.99	561.1	.833	98.9	432.6	1184	300.0	0.10	50.0	20.24	15.97	18.92	2

Table 6.27 Optimizations at Fixed Bulk Doping Concentration (D_B), case 3

eff	V_{oc}	J_{sc}	V_{mp}	ff	C_{eff}	τ_{bulk}	L_d	X_L	X_f	X_b	$\log D_0$	$\log D_B$	$\log D_L$	O_{pl}
20.924	654.2	39.23	560.9	.815	99.4	805.7	1668	300.0	0.10	50.0	19.33	15.23	18.93	2
21.156	654.3	39.17	565.7	.825	99.3	674.3	1514	300.0	0.10	50.0	19.35	15.53	18.97	2
21.305	654.8	39.08	570.3	.833	99.1	508.1	1296	300.0	0.10	50.0	19.35	15.84	18.95	2
21.355	**656.5**	**38.90**	**573.9**	**.836**	**98.6**	**339.5**	**1032**	**300.0**	**0.10**	**50.0**	**19.33**	**16.14**	**18.93**	**2**
21.301	659.0	38.58	577.0	.838	97.8	202.9	764	300.0	0.10	50.0	19.33	16.44	18.90	2
21.127	662.4	38.03	580.5	.839	96.4	111.0	525	300.0	0.10	50.0	19.31	16.74	18.87	2
20.808	665.8	37.24	583.7	.839	94.4	56.8	337	300.0	0.10	50.0	19.29	17.04	18.81	2

Table 6.28 Optimizations at Fixed Back Surface Doping Concentration (D_L), case 3

eff	V_{oc}	J_{sc}	V_{mp}	ff	C_{eff}	τ_{bulk}	L_d	X_L	X_f	X_b	$\log D_0$	$\log D_B$	$\log D_L$	O_{pl}
20.818	646.2	38.57	564.7	.835	97.8	299.7	961	300.0	0.10	50.0	19.33	16.21	18.03	2
21.118	651.4	38.78	569.4	.836	98.3	322.0	1001	300.0	0.10	50.0	19.33	16.17	18.33	2
21.302	655.2	38.88	572.8	.836	98.6	330.5	1017	300.0	0.10	50.0	19.33	16.15	18.63	2
21.355	**656.5**	**38.90**	**573.9**	**.836**	**98.6**	**339.5**	**1032**	**300.0**	**0.10**	**50.0**	**19.33**	**16.14**	**18.93**	**2**
21.329	656.2	38.88	573.5	.836	98.6	347.4	1046	300.0	0.10	50.0	19.33	16.12	19.23	2
21.290	655.7	38.84	573.0	.836	98.5	351.4	1053	300.0	0.10	50.0	19.34	16.11	19.54	2
21.255	655.2	38.81	572.6	.836	98.4	352.7	1055	300.0	0.10	50.0	19.33	16.11	19.84	2

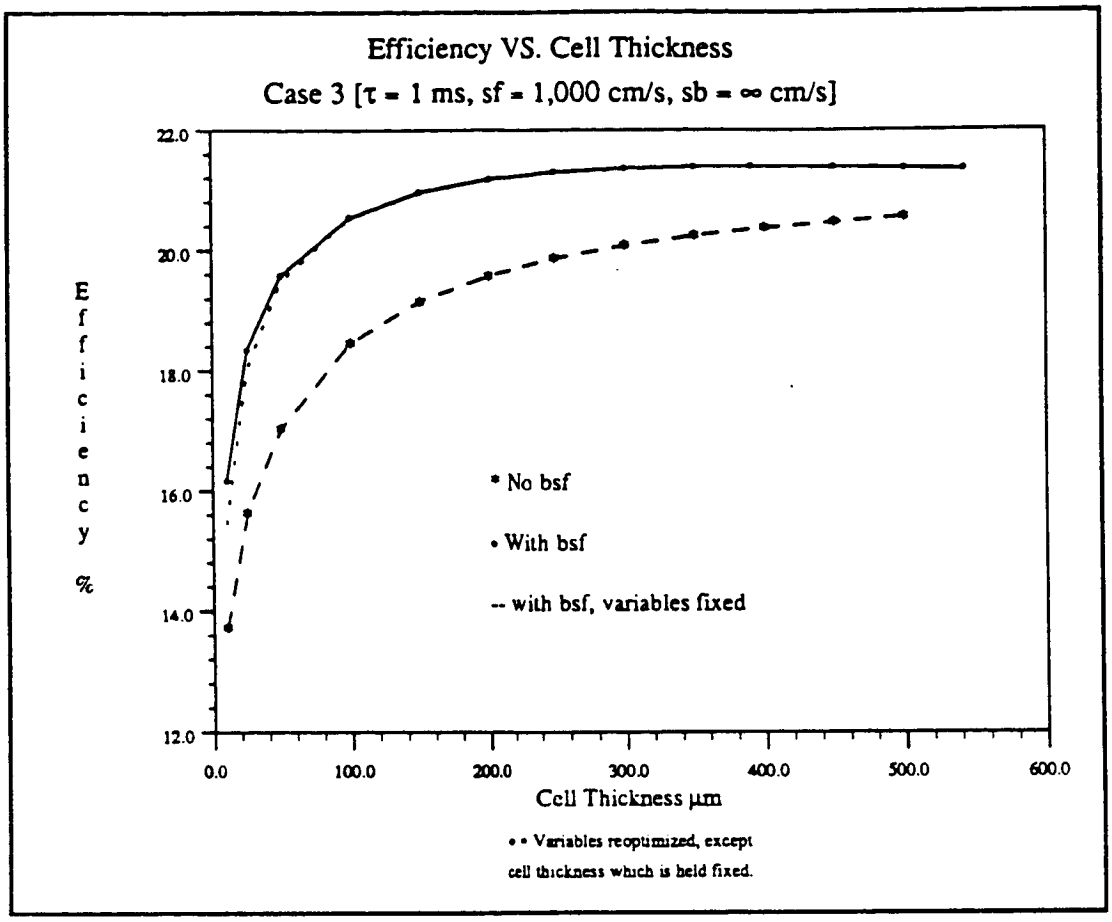

figure 6.24

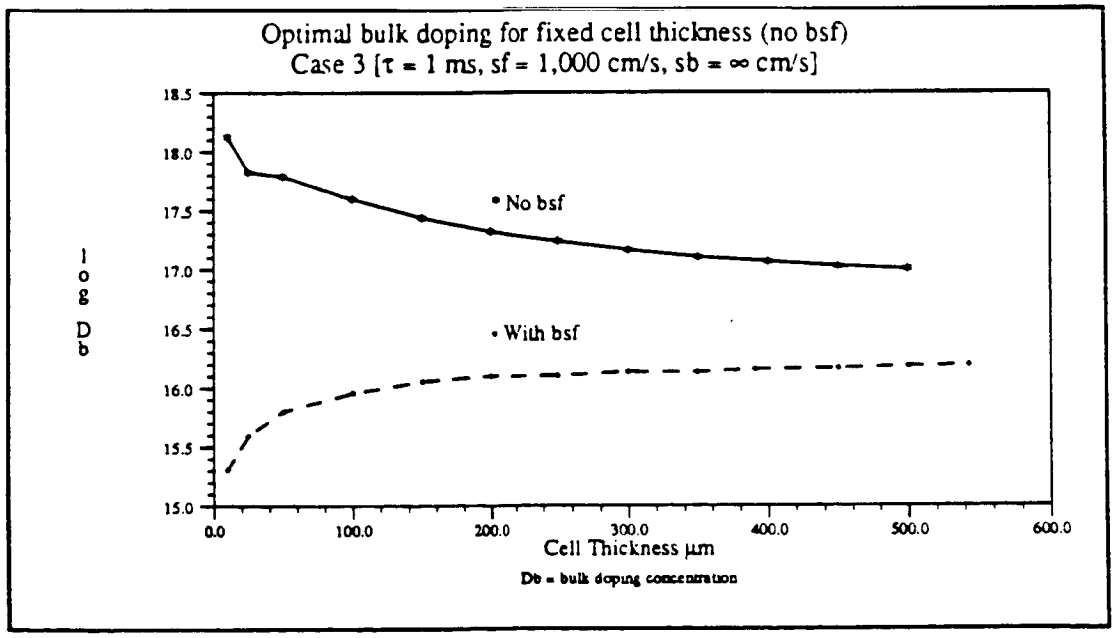

figure 6.25

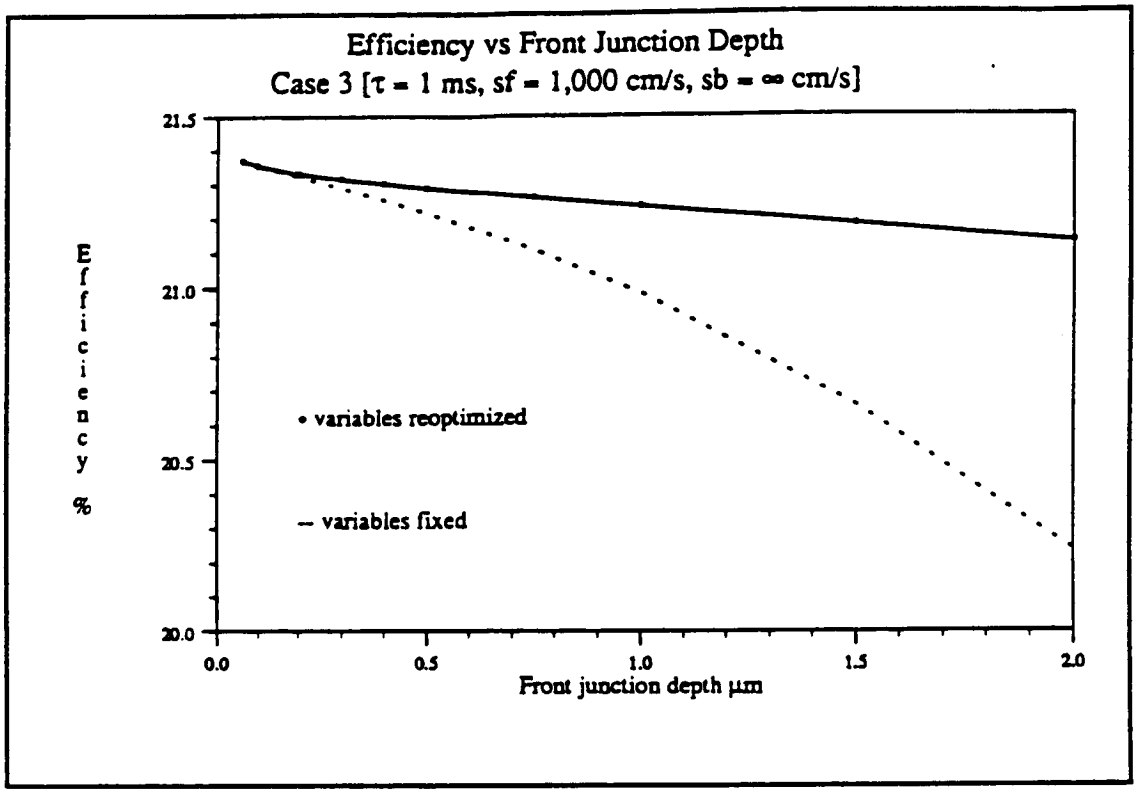

figure 6.26

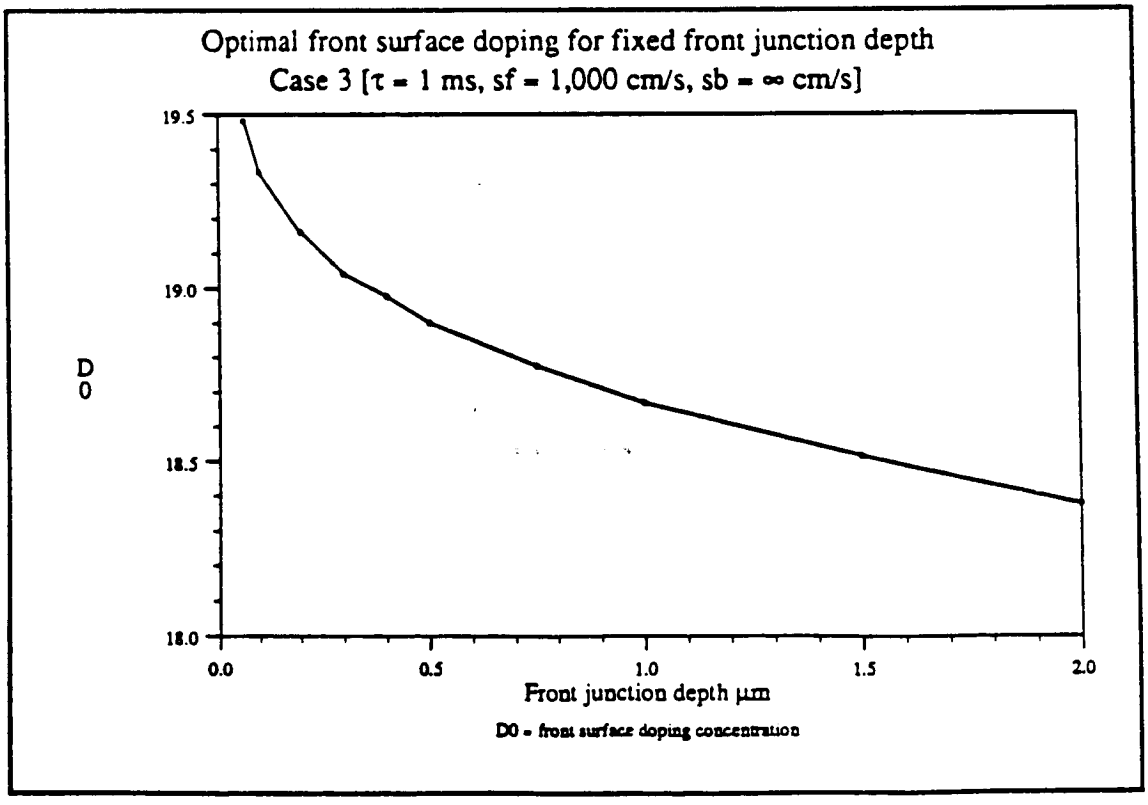

figure 6.27

C-3

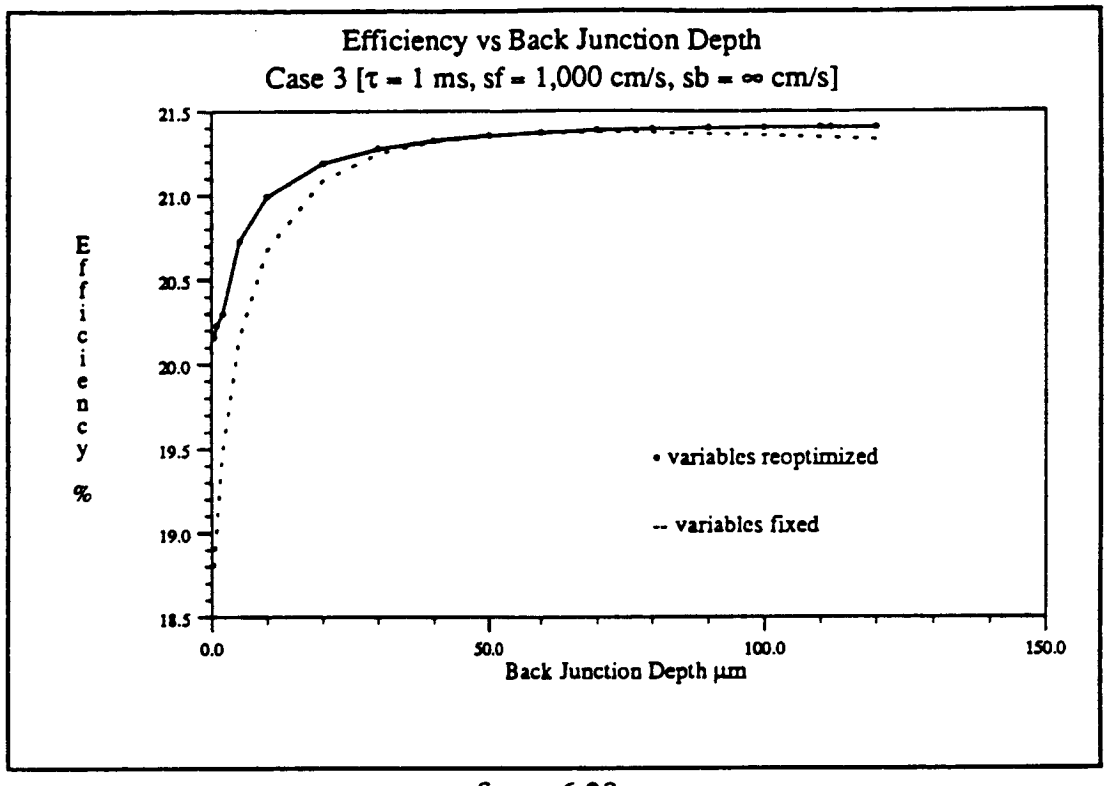

figure 6.28

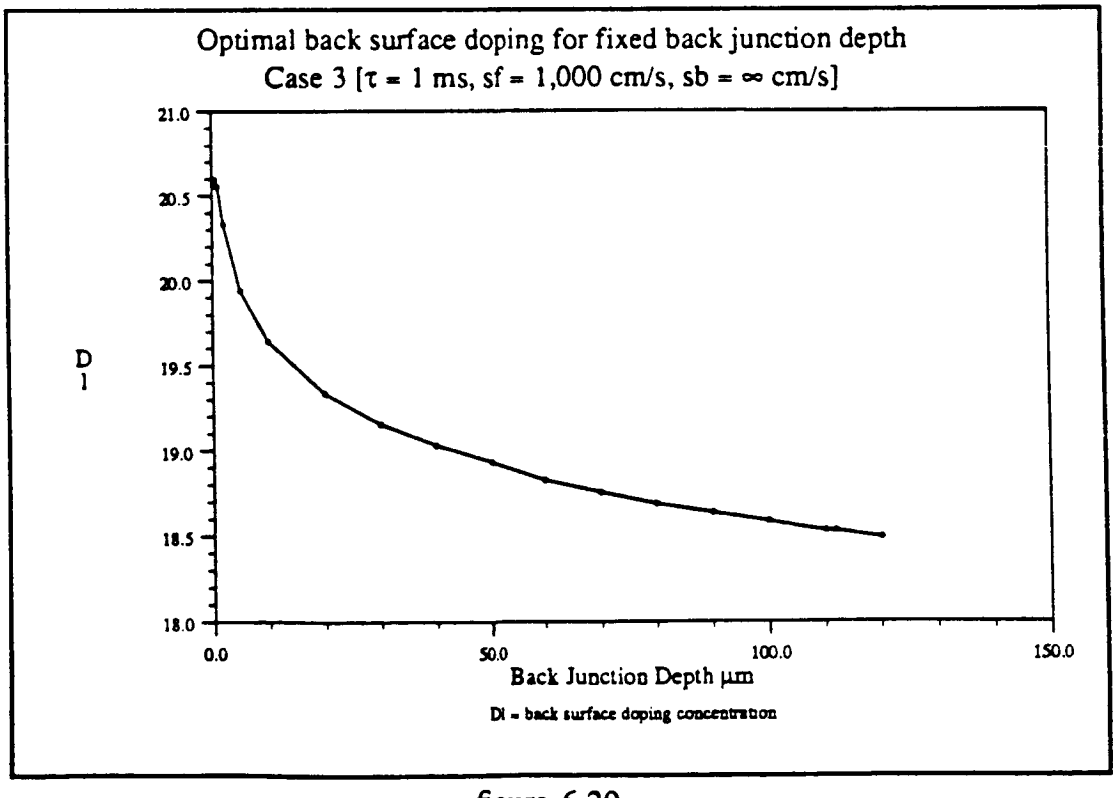

figure 6.29

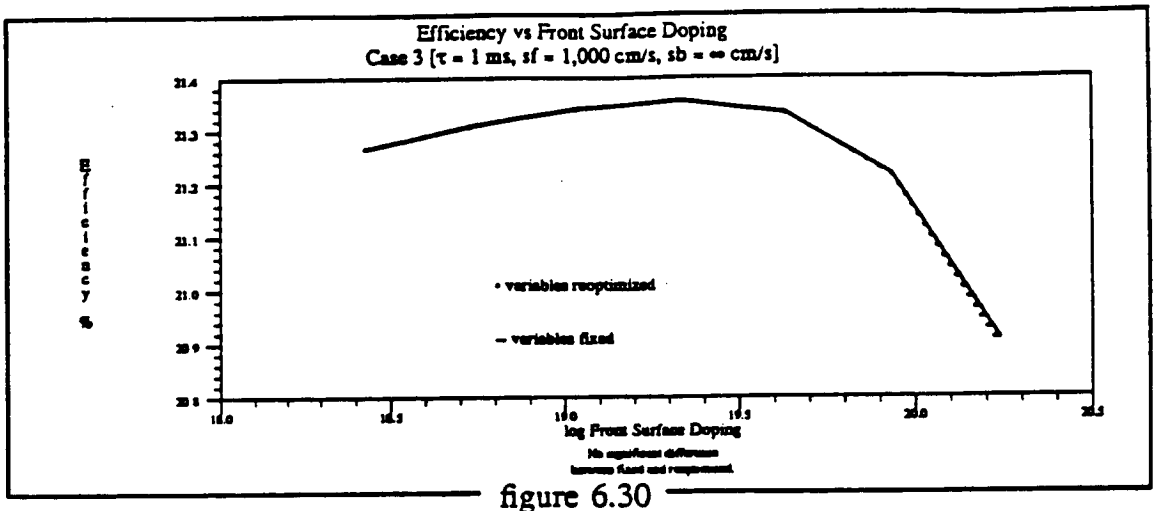

figure 6.30

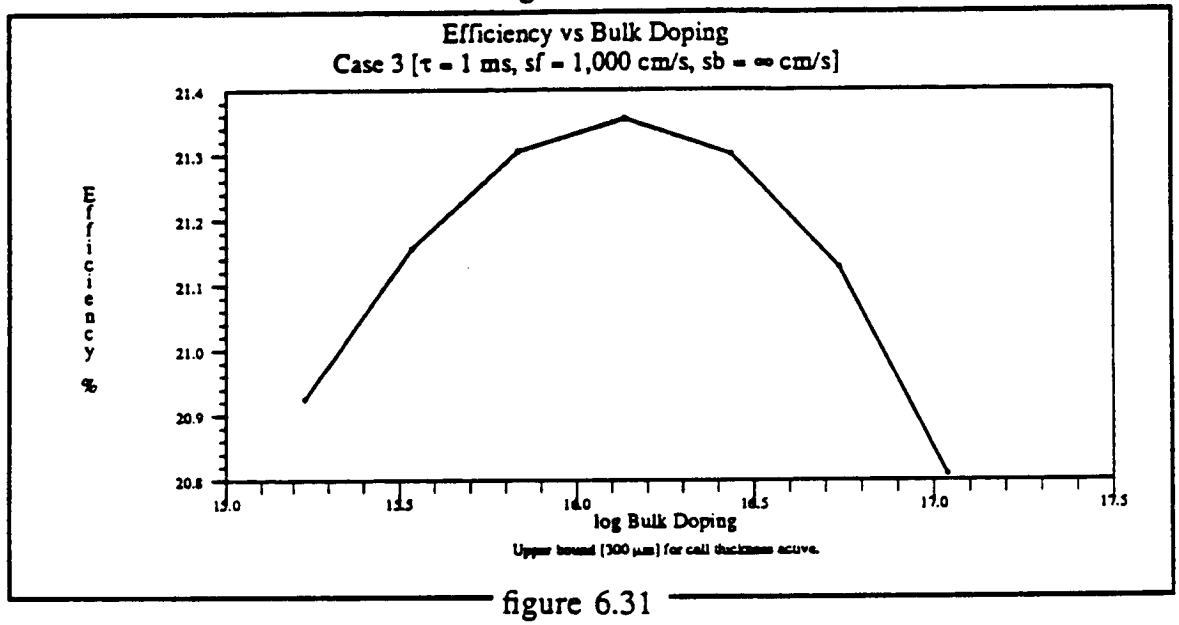

figure 6.31

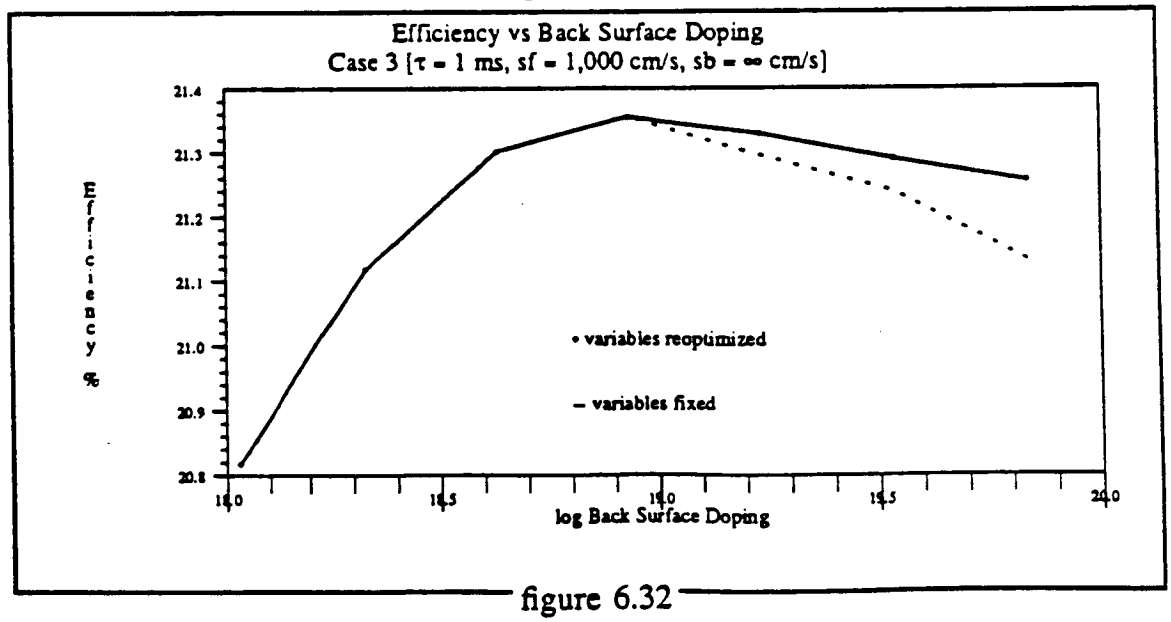

figure 6.32

Parameters Held Constant During Optimization (see also table 6.1).

Front surface recombination velocity (S_f)	10,000	cm/s
Back surface recombination velocity (S_b)	10,000	cm/s
Electron minority carrier lifetime[1] (τ_{n0})	0.40	ms
Hole minority carrier lifetime[1] (τ_{p0})	0.20	ms

Optimal Values of Decision Variables

Front junction depth (X_f)	0.10	μm (lower bound)
Back junction depth (X_b)	50.0	μm (upper bound)
Cell thickness (X_L)	300.0	μm (upper bound)
Front surface doping concentration (D_0)	7.228×10^{19}	P atoms/cm^3
Bulk doping concentration (D_B)	1.0×10^{16}	B atoms/cm^3
Back surface doping concentration (D_L)	5.724×10^{19}	B atoms/cm^3

Cell Performance Parameters

Efficiency	20.361	%
Open circuit voltage (V_{oc})	631.16	mV
Short circuit current density (J_{sc})	38.809	mA/cm^2
Maximum power voltage (V_{mp})	549.55	mV
Fill factor	0.8312	
Collection efficiency	98.38	%
Bulk resitivity	1.391	ohm-cm
Sheet resistance layer 1	395.4	ohm/□
layer 2	7.19	ohm/□
Bulk lifetime	165.8	μs
Bulk diffusion length	731	μm

[1] Values in lightly doped silicon.

Table 6.29 Optimal Solution For Case 4

Table 6.30 Effect of BSF and BSR, case 4 (S_f = 10,000 cm/s, S_b = 10,000 cm/s, τ_{n0} = 0.4 ms)

eff	V_{oc}	J_{sc}	V_{mp}	ff	C_{eff}	τ_{bulk}	L_d	X_L	X_f	X_b	log D_0	log D_B	log D_L	O_{pl}
20.361	**631.2**	**38.81**	**549.5**	**.831**	**98.4**	**165.8**	**731**	**300.0**	**0.10**	**50.0**	**19.86**	**16.00**	**18.72**	**2**
19.908	631.1	37.93	549.8	.832	98.6	151.5	695	300.0	0.10	50.0	19.85	16.06	18.74	1
19.170	634.1	36.28	553.3	.833	92.0	34.8	282	300.0	0.10	0.	19.82	16.86	0.	2
18.952	634.2	35.86	553.4	.833	93.2	33.3	274	300.0	0.10	0.	19.84	16.88	0.	1

Table 6.31 Optimizations at Fixed Cell Thickness (X_L), with bsf, case 4

eff	V_{oc}	J_{sc}	V_{mp}	ff	C_{eff}	τ_{bulk}	L_d	X_L	X_f	X_b	log D_0	log D_B	log D_L	O_{pl}
16.711	631.2	31.79	550.5	.833	99.9	246.8	912	10.0	0.10	0.2	19.82	15.64	19.91	2
18.308	632.9	34.73	552.0	.833	99.8	221.9	860	25.0	0.10	0.2	19.85	15.76	19.91	2
19.071	633.8	36.13	552.8	.833	99.3	200.4	813	50.0	0.10	10.0	19.87	15.85	19.11	2
19.782	635.1	37.40	553.8	.833	99.1	185.5	779	100.0	0.10	22.3	19.87	15.91	18.92	2
20.108	634.8	38.05	553.4	.832	98.9	173.9	751	150.0	0.10	29.9	19.90	15.96	18.86	2
20.258	634.1	38.39	552.6	.832	98.6	169.5	740	200.0	0.10	49.2	19.87	15.98	18.66	2
20.332	632.5	38.65	550.9	.832	98.5	168.8	738	250.0	0.10	49.8	19.86	15.99	18.68	2
20.361	**631.2**	**38.81**	**549.5**	**.831**	**98.4**	**165.8**	**731**	**300.0**	**0.10**	**50.0**	**19.86**	**16.00**	**18.72**	**2**
20.362	630.7	38.85	549.1	.831	98.3	164.1	727	319.1	0.10	50.0	19.85	16.01	18.72	2
20.358	630.0	38.89	548.3	.831	98.2	162.9	724	350.0	0.10	50.0	19.86	16.01	18.74	2
20.336	628.9	38.94	547.2	.830	98.0	160.8	719	400.0	0.10	50.0	19.87	16.02	18.75	2
20.296	627.7	38.95	546.0	.830	97.8	159.5	715	450.0	0.10	50.0	19.84	16.03	18.76	2
20.257	626.9	38.94	545.1	.830	97.6	157.4	710	500.0	0.10	50.0	19.86	16.04	18.78	2

Table 6.32 Optimizations at Fixed Cell Thickness (X_L), no bsf, case 4

eff	V_{oc}	J_{sc}	V_{mp}	ff	C_{eff}	τ_{bulk}	L_d	X_L	X_f	X_b	log D_0	log D_B	log D_L	O_{pl}
14.455	601.7	29.07	522.5	.826	91.3	20.4	196	10.0	0.10	0.	19.76	17.11	0.	2
15.823	614.3	31.06	534.5	.829	89.3	17.0	173	25.0	0.10	0.	19.79	17.18	0.	2
16.908	625.2	32.52	544.9	.831	89.4	14.2	152	50.0	0.10	0.	19.81	17.26	0.	2
17.958	631.1	34.17	550.5	.833	90.5	17.6	177	100.0	0.10	0.	19.81	17.17	0.	2
18.480	632.9	35.05	552.2	.833	91.1	22.3	208	150.0	0.10	0.	19.82	17.07	0.	2
18.802	633.9	35.60	553.2	.833	91.5	26.4	234	200.0	0.10	0.	19.82	16.99	0.	2
19.013	634.0	35.99	553.3	.833	91.7	30.7	260	250.0	0.10	0.	19.81	16.92	0.	2
19.170	634.1	36.28	553.3	.833	92.0	34.8	282	300.0	0.10	0.	19.82	16.86	0.	2
19.287	634.0	36.51	553.2	.833	92.2	38.7	303	350.0	0.10	0.	19.82	16.81	0.	2
19.379	633.8	36.70	553.0	.833	92.4	42.4	322	400.0	0.10	0.	19.83	16.77	0.	2
19.444	633.3	36.86	552.5	.833	92.5	46.3	340	450.0	0.10	0.	19.81	16.73	0.	2
19.503	633.0	36.99	552.1	.833	92.7	49.9	357	500.0	0.10	0.	19.82	16.69	0.	2

Table 6.33 Optimizations at Fixed Front Junction Depth (X_f), case 4

eff	V_{oc}	J_{sc}	V_{mp}	ff	C_{eff}	τ_{bulk}	L_d	X_L	X_f	X_b	$\log D_0$	$\log D_B$	$\log D_L$	O_{pl}
20.404	632.2	38.82	550.5	.831	98.4	164.1	727	300.0	0.06	50.0	20.00	16.01	18.70	2
20.361	**631.2**	**38.81**	**549.5**	**.831**	**98.4**	**165.8**	**731**	**300.0**	**0.10**	**50.0**	**19.86**	**16.00**	**18.72**	**2**
20.288	629.8	38.77	548.1	.831	98.3	170.7	743	300.0	0.20	50.0	19.67	15.98	18.69	2
20.226	629.1	38.71	547.5	.831	98.1	171.6	745	300.0	0.30	50.0	19.55	15.97	18.68	2
20.167	628.5	38.63	547.0	.831	97.9	173.2	749	300.0	0.40	50.0	19.45	15.97	18.70	2
20.107	628.0	38.56	546.4	.830	97.8	176.4	757	300.0	0.50	50.0	19.36	15.95	18.71	2
19.956	626.9	38.35	545.3	.830	97.2	181.9	770	300.0	0.75	50.0	19.19	15.93	18.70	2
19.804	625.7	38.15	544.1	.830	96.7	188.6	786	300.0	1.00	50.0	19.02	15.90	18.71	2
19.513	622.9	37.80	541.2	.829	95.8	199.8	812	300.0	1.50	49.5	18.69	15.85	18.69	2
19.249	619.0	37.58	537.2	.827	95.3	216.0	847	300.0	2.00	50.0	18.35	15.78	18.68	2

Table 6.34 Optimizations at Fixed Back Junction Depth (X_b), case 4

eff	V_{oc}	J_{sc}	V_{mp}	ff	C_{eff}	τ_{bulk}	L_d	X_L	X_f	X_b	$\log D_0$	$\log D_B$	$\log D_L$	O_{pl}
20.264	628.0	38.86	546.4	.830	98.5	171.8	746	300.0	0.10	0.2	19.86	15.97	20.07	2
20.200	626.7	38.83	545.1	.830	98.4	175.3	754	300.0	0.10	0.5	19.86	15.96	19.76	2
20.174	626.1	38.82	544.6	.830	98.4	177.3	759	300.0	0.10	1.0	19.86	15.95	19.60	2
20.167	626.0	38.81	544.6	.830	98.4	175.8	755	300.0	0.10	2.0	19.86	15.96	19.44	2
20.198	626.7	38.82	545.3	.830	98.4	173.7	750	300.0	0.10	5.0	19.86	15.97	19.29	2
20.250	628.0	38.83	546.4	.830	98.4	169.6	740	300.0	0.10	10.0	19.86	15.98	19.18	2
20.309	629.4	38.83	547.9	.831	98.4	165.8	731	300.0	0.10	20.0	19.86	16.00	19.04	2
20.336	630.2	38.83	548.6	.831	98.4	165.8	731	300.0	0.10	30.0	19.86	16.00	18.92	2
20.352	630.7	38.82	549.1	.831	98.4	165.8	731	300.0	0.10	40.0	19.86	16.00	18.82	2
20.361	**631.2**	**38.81**	**549.5**	**.831**	**98.4**	**165.8**	**731**	**300.0**	**0.10**	**50.0**	**19.86**	**16.00**	**18.72**	**2**
20.365	631.5	38.79	549.9	.831	98.3	165.9	731	300.0	0.10	60.0	19.86	16.00	18.62	2
20.368	631.8	38.77	550.2	.831	98.3	166.3	732	300.0	0.10	70.0	19.86	16.00	18.56	2
20.369	632.0	38.76	550.4	.831	98.3	168.7	738	300.0	0.10	80.0	19.86	15.99	18.49	2
20.369	632.1	38.76	550.4	.831	98.3	170.1	742	300.0	0.10	84.3	19.86	15.98	18.45	2
20.369	632.2	38.75	550.6	.831	98.2	170.6	743	300.0	0.10	90.0	19.85	15.98	18.40	2

Table 6.35 Optimizations at Fixed Front Surface Doping Concentration (D_0), case 4

eff	V_{oc}	J_{sc}	V_{mp}	ff	C_{eff}	τ_{bulk}	L_d	X_L	X_f	X_b	$\log D_0$	$\log D_B$	$\log D_L$	O_{pl}
20.151	624.8	38.86	543.4	.830	98.5	176.5	757	300.0	0.10	49.6	18.96	15.95	18.70	2
20.249	627.7	38.84	546.3	.830	98.5	171.7	746	300.0	0.10	50.0	19.26	15.97	18.71	2
20.325	630.1	38.81	548.5	.831	98.4	165.8	731	300.0	0.10	50.0	19.56	16.00	18.71	2
20.361	**631.2**	**38.81**	**549.5**	**.831**	**98.4**	**165.8**	**731**	**300.0**	**0.10**	**50.0**	**19.86**	**16.00**	**18.72**	**2**
20.298	629.4	38.82	547.8	.831	98.4	172.5	747	300.0	0.10	50.0	20.16	15.97	18.72	2
20.031	622.3	38.82	540.9	.829	98.4	183.7	774	300.0	0.10	49.4	20.46	15.92	18.67	2
19.813	616.5	38.82	535.3	.828	98.4	199.2	810	300.0	0.10	50.0	20.60	15.85	18.67	2

Table 6.36 Optimizations at Fixed Bulk Doping Concentration (D_B), case 4

eff	V_{oc}	J_{sc}	V_{mp}	ff	C_{eff}	τ_{bulk}	L_d	X_L	X_f	X_b	$\log D_0$	$\log D_B$	$\log D_L$	O_{pl}
19.849	631.6	38.66	540.4	.813	99.3	340.1	1086	201.7	0.10	50.0	19.90	15.10	18.65	2
20.100	629.3	38.93	541.8	.820	99.2	295.8	1007	254.6	0.10	50.0	19.86	15.40	18.69	2
20.291	628.9	39.00	545.3	.827	98.9	234.5	887	297.6	0.10	50.0	19.88	15.70	18.69	2
20.361	**631.2**	**38.81**	**549.5**	**.831**	**98.4**	**165.8**	**731**	**300.0**	**0.10**	**50.0**	**19.86**	**16.00**	**18.72**	**2**
20.290	633.6	38.45	552.5	.833	97.5	104.3	560	300.0	0.10	50.0	19.86	16.30	18.71	2
20.065	636.0	37.84	555.1	.834	96.0	59.7	400	292.1	0.10	50.0	19.84	16.60	18.70	2
19.670	638.1	36.95	557.2	.834	94.0	31.9	267	269.7	0.10	50.0	19.82	16.90	18.66	2

Table 6.37 Optimizations at Fixed Back Surface Doping Concentration (D_L), case 4

eff	V_{oc}	J_{sc}	V_{mp}	ff	C_{eff}	τ_{bulk}	L_d	X_L	X_f	X_b	$\log D_0$	$\log D_B$	$\log D_L$	O_{pl}
20.122	625.7	38.73	544.5	.830	98.2	177.7	760	300.0	0.10	50.0	19.86	15.95	17.82	2
20.256	628.6	38.78	547.2	.831	98.3	171.3	745	300.0	0.10	50.0	19.86	15.98	18.12	2
20.337	630.5	38.81	548.9	.831	98.4	165.8	731	300.0	0.10	50.0	19.86	16.00	18.42	2
20.361	**631.2**	**38.81**	**549.5**	**.831**	**98.4**	**165.8**	**731**	**300.0**	**0.10**	**50.0**	**19.86**	**16.00**	**18.72**	**2**
20.346	631.1	38.78	549.5	.831	98.3	165.8	731	300.0	0.10	48.0	19.86	16.00	19.02	2
20.323	630.9	38.76	549.3	.831	98.3	165.8	731	300.0	0.10	44.8	19.86	16.00	19.32	2
20.302	630.7	38.73	549.1	.831	98.2	165.8	731	300.0	0.10	43.9	19.86	16.00	19.63	2

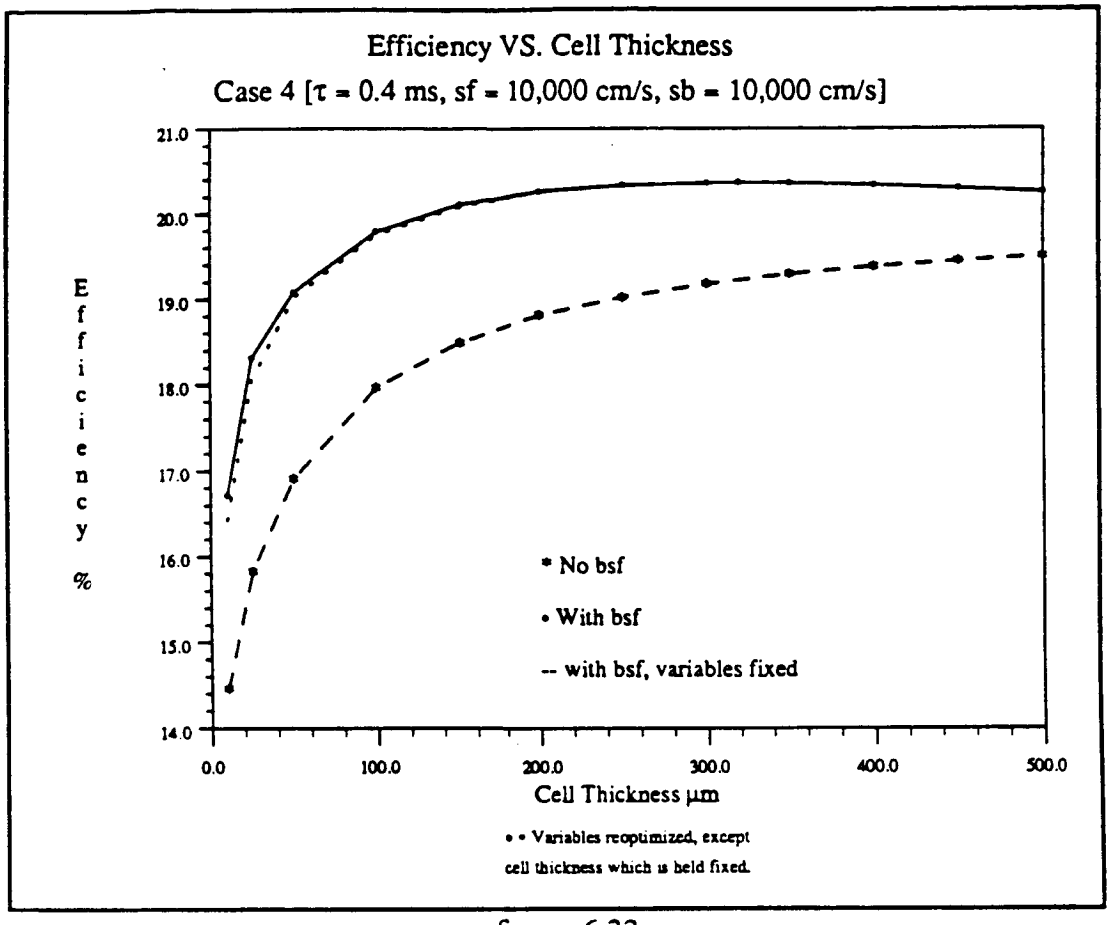

figure 6.33

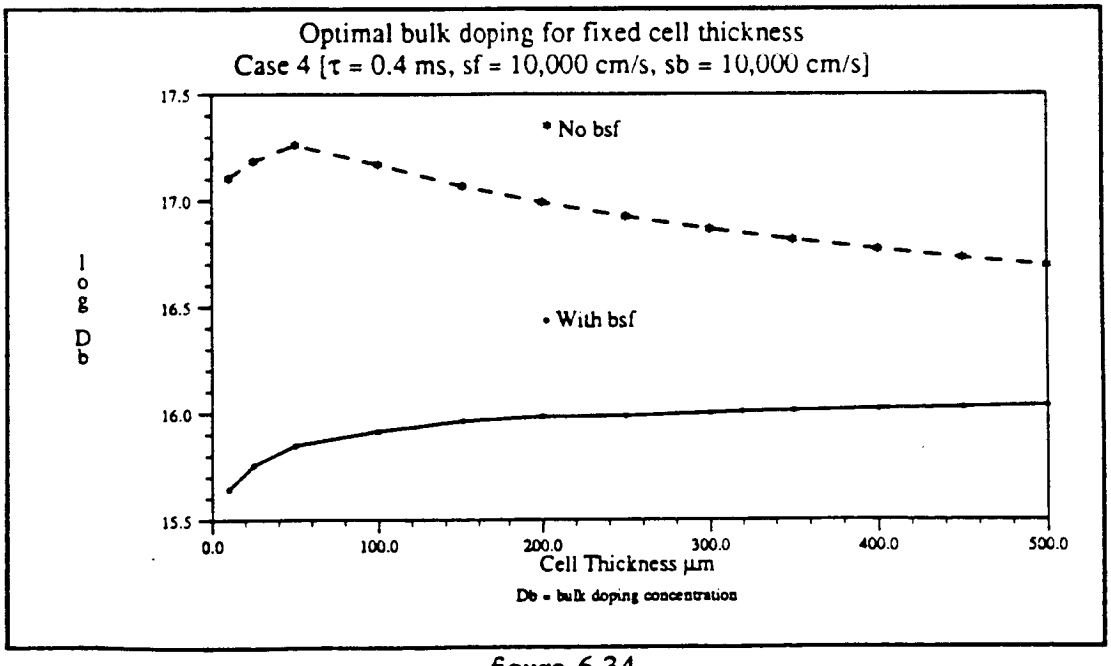

figure 6.34

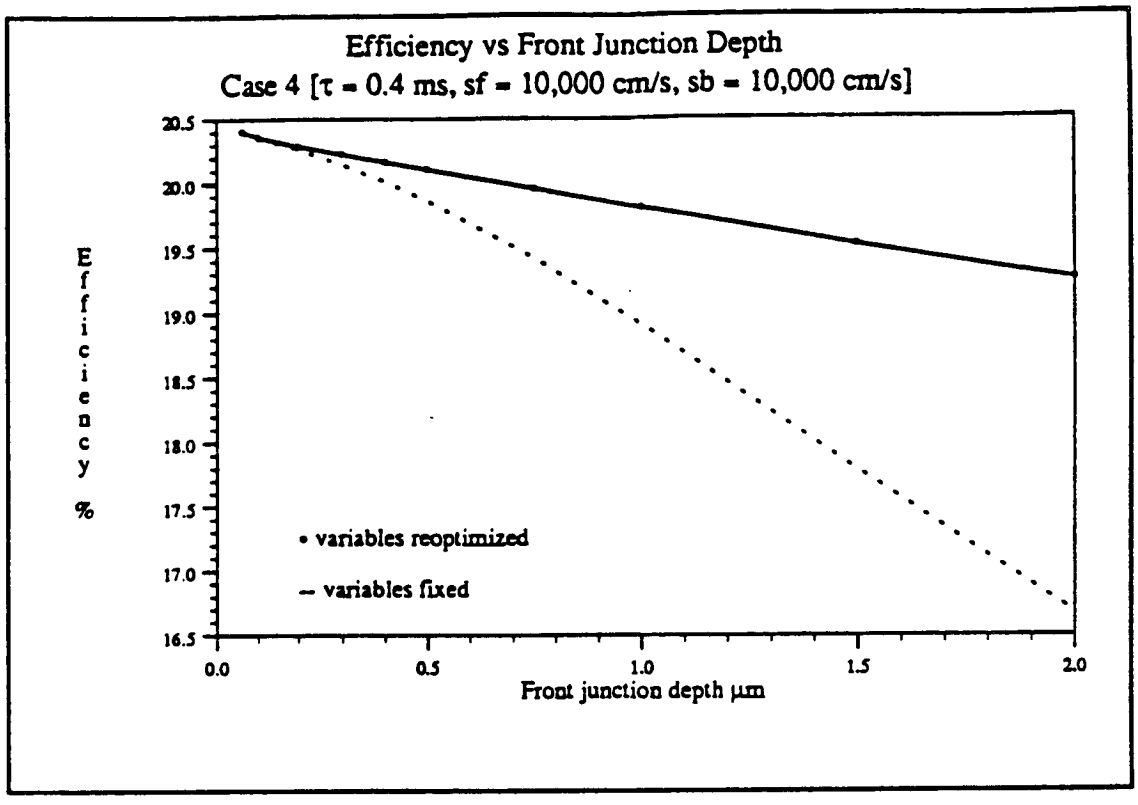

figure 6.35

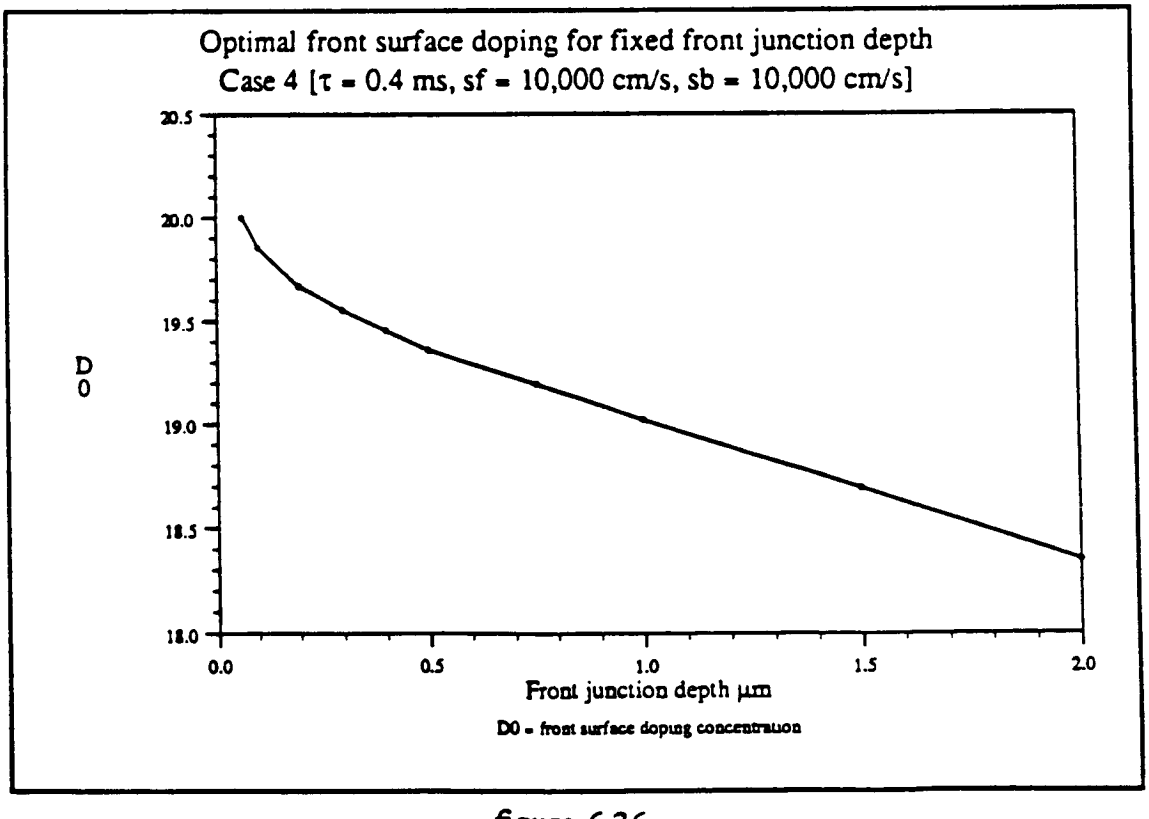

figure 6.36

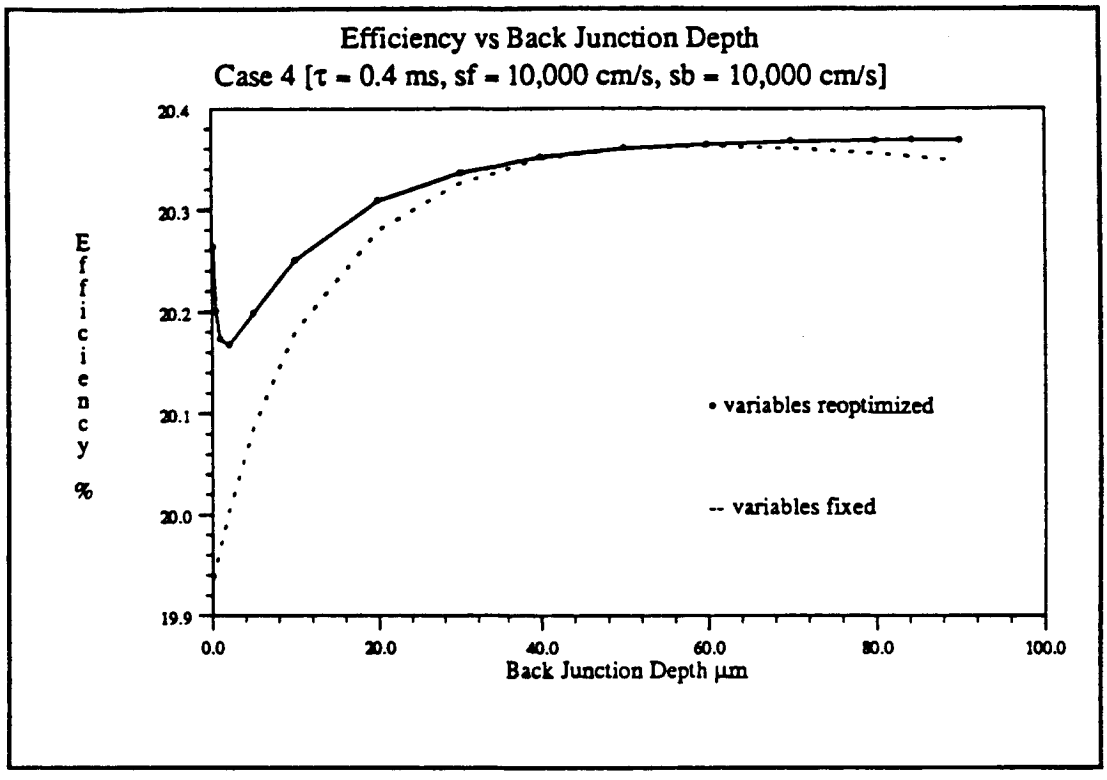

figure 6.37

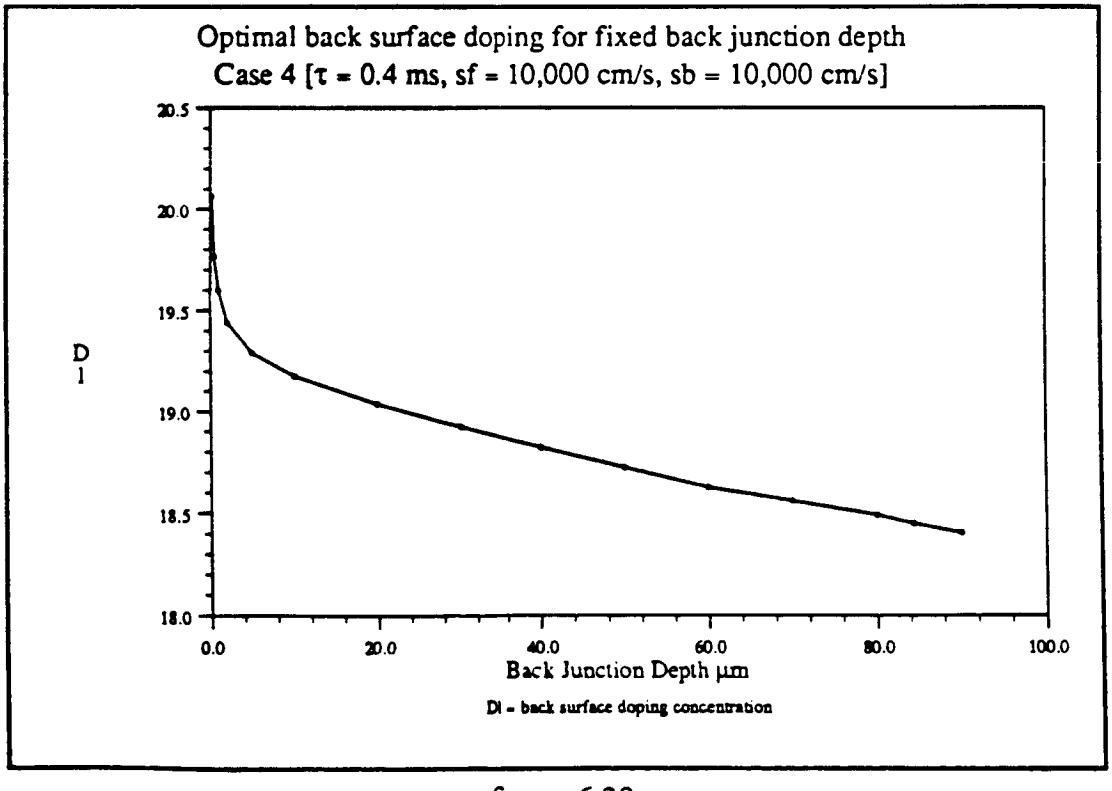

figure 6.38

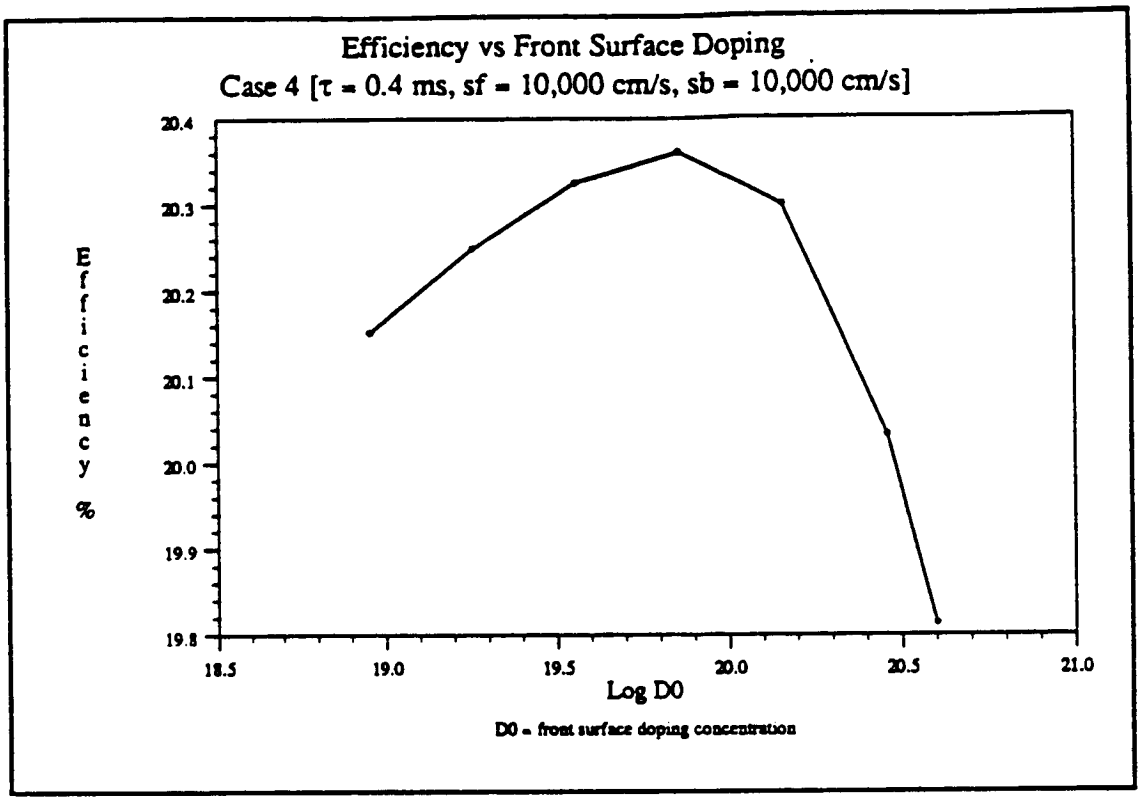

figure 6.39

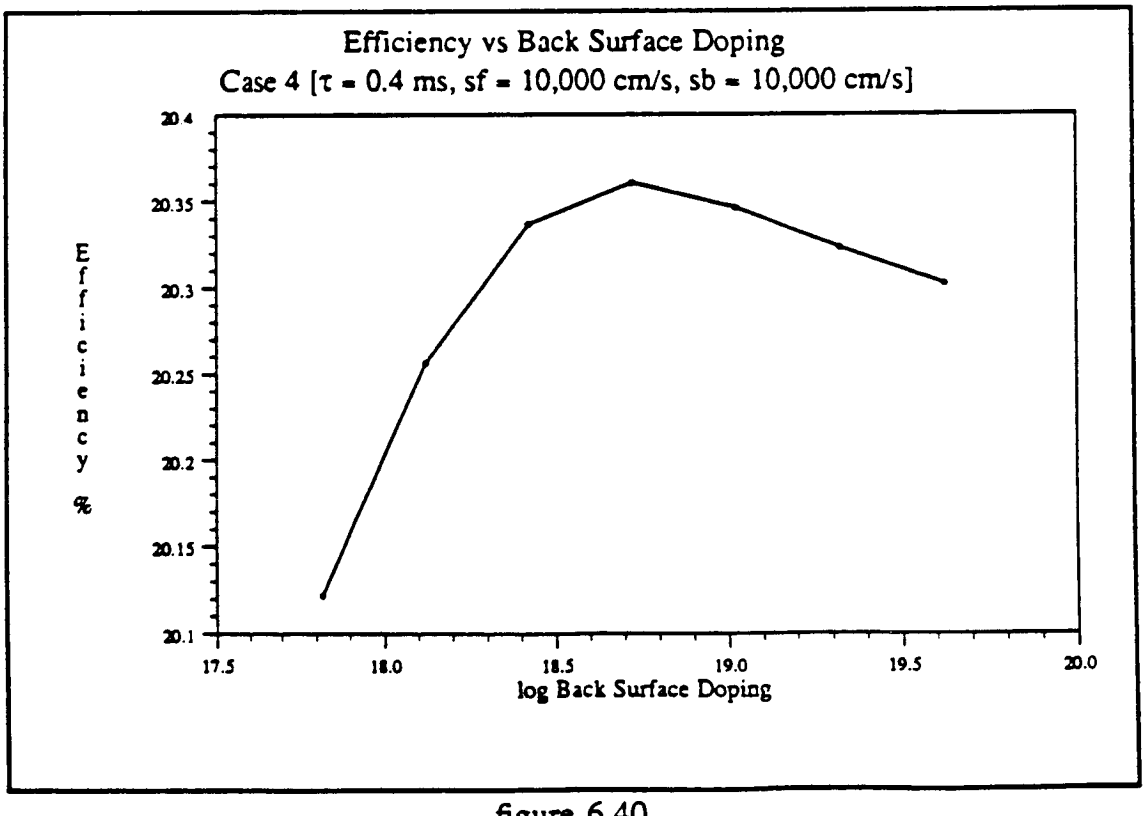

figure 6.40

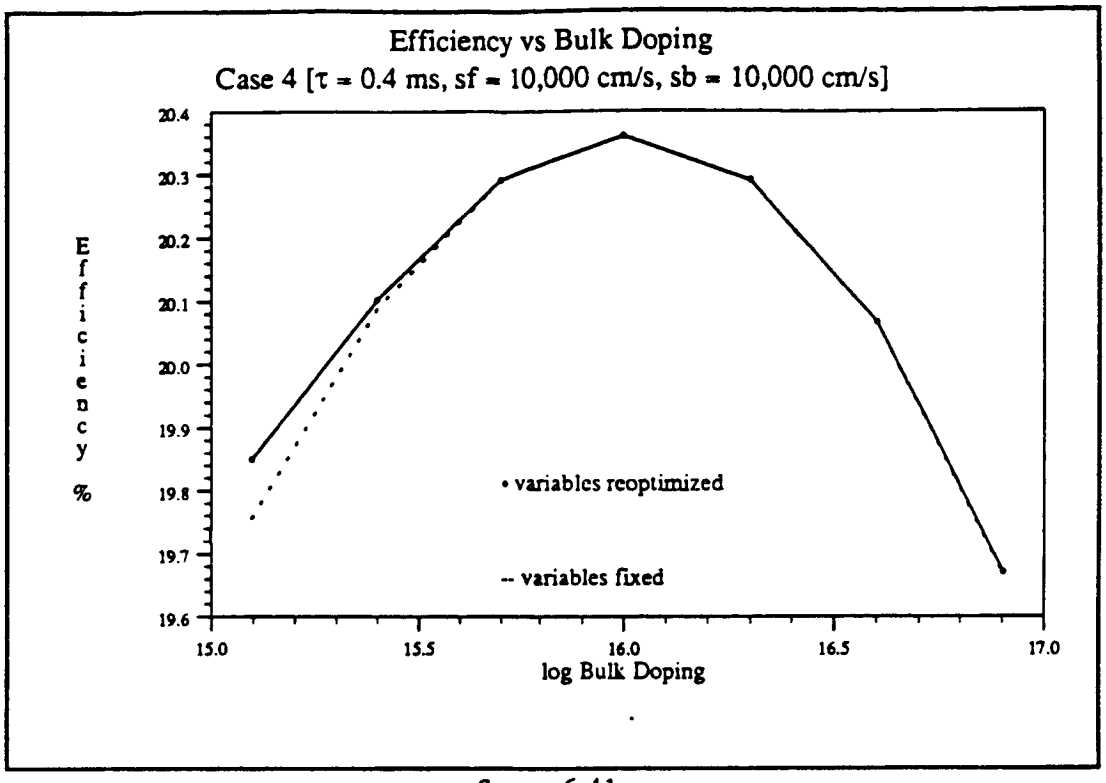

figure 6.41

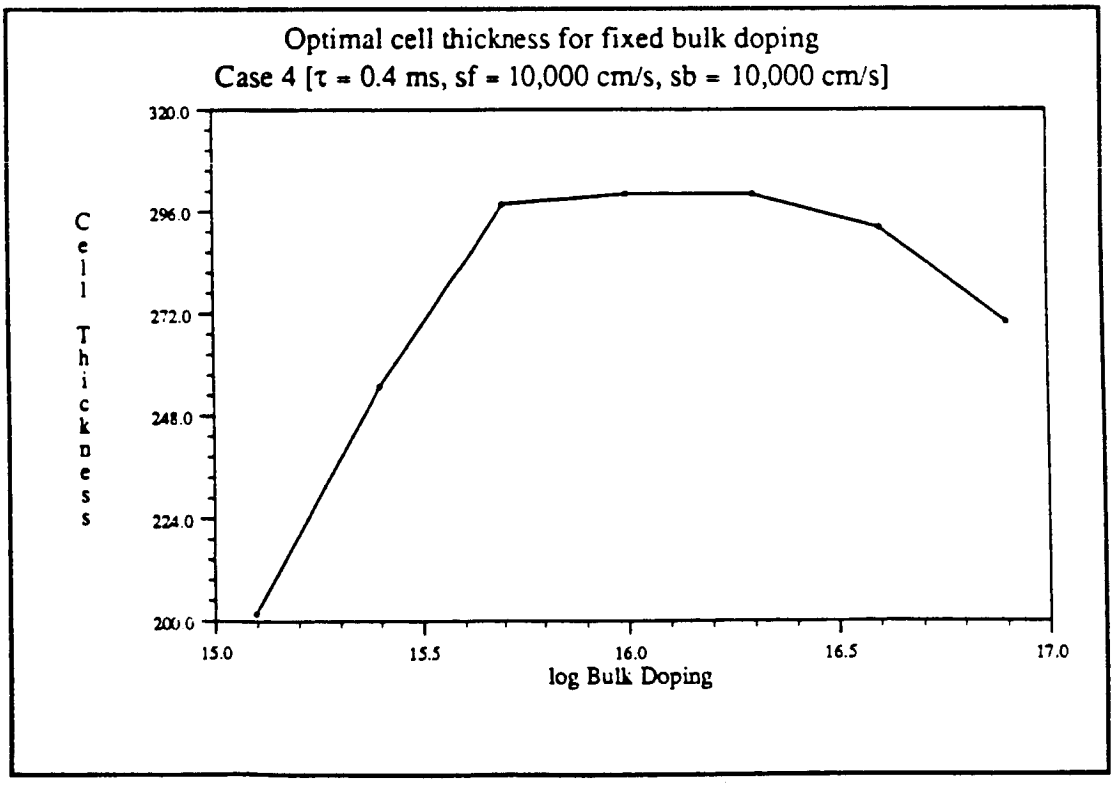

figure 6.42

Parameters Held Constant During Optimization (see also table 6.1).

Front surface recombination velocity (S_f)	1,000	cm/s
Back surface recombination velocity (S_b)	1,000	cm/s
Electron minority carrier lifetime[1] (τ_{n0})	0.1	ms
Hole minority carrier lifetime[1] (τ_{p0})	0.05	ms

Optimal Values of Decision Variables

Front junction depth (X_f)	0.10	μm (lower bound)
Back junction depth (X_b)	0.2	μm (lower bound)
Cell thickness (X_L)	100.0	μm (upper bound)
Front surface doping concentration (D_0)	1.863×10^{19}	P atoms/cm^3
Bulk doping concentration (D_B)	2.005×10^{16}	B atoms/cm^3
Back surface doping concentration (D_L)	2.139×10^{19}	B atoms/cm^3

Cell Performance Parameters

Efficiency	20.022	%
Open circuit voltage (V_{oc})	642.9	mV
Short circuit current density (J_{sc})	37.339	mA/cm^2
Maximum power voltage (V_{mp})	561.2	mV
Fill factor	0.8340	
Collection efficiency	98.91	%
Bulk resitivity	0.735	ohm-cm
Sheet resistance layer 1	1097.4	ohm/□
layer 2	67.67	ohm/□
Bulk lifetime	26.1	μs
Bulk diffusion length	280	μm

[1] Values in lightly doped silicon.

Table 6.38 Optimal Solution For Case 5

Table 6.39 Effect of BSF and BSR, case 5 (S_f = 1,000 cm/s, S_b = 1,000 cm/s, τ_{n0} = 0.1 ms)

eff	V_{oc}	J_{sc}	V_{mp}	ff	C_{eff}	τ_{bulk}	L_d	X_L	X_f	X_b	log D_0	log D_B	log D_L	O_{pl}
20.022	**642.9**	**37.34**	**561.2**	**.834**	**98.9**	**26.1**	**280**	**100.0**	**0.10**	**0.20**	**19.27**	**16.30**	**19.33**	**2**
19.296	642.3	36.02	560.7	.834	99.0	24.7	271	100.0	0.10	0.20	19.27	16.34	19.33	1
19.081	635.5	36.02	554.7	.833	95.4	11.8	172	100.0	0.10	0.	19.26	16.72	0.	2
18.502	635.9	34.91	555.1	.833	95.9	10.9	163	100.0	0.10	0.	19.27	16.76	0.	1

Table 6.40 Optimizations at Fixed Cell Thickness (X_L), with bsf, case 5

eff	V_{oc}	J_{sc}	V_{mp}	ff	C_{eff}	τ_{bulk}	L_d	X_L	X_f	X_b	log D_0	log D_B	log D_L	O_{pl}
17.878	669.8	31.80	587.2	.839	99.9	21.5	250	10.0	0.10	0.20	19.24	16.41	19.29	2
19.312	663.8	34.71	581.4	.838	99.8	20.5	242	25.0	0.10	0.20	19.25	16.44	19.30	2
19.832	655.1	36.19	572.9	.836	99.5	22.0	253	50.0	0.10	0.20	19.27	16.40	19.31	2
19.979	648.3	36.90	566.4	.835	99.2	24.1	267	75.0	0.10	0.20	19.27	16.35	19.31	2
20.022	**642.9**	**37.34**	**561.2**	**.834**	**98.9**	**26.1**	**280**	**100.0**	**0.10**	**0.20**	**19.27**	**16.30**	**19.33**	**2**
20.022	641.5	37.44	559.8	.834	98.8	26.9	285	107.1	0.10	0.20	19.25	16.29	19.33	2
20.013	638.4	37.63	556.7	.833	98.6	28.2	293	125.0	0.10	0.20	19.25	16.26	19.34	2
19.977	634.6	37.82	553.1	.832	98.3	29.6	301	150.0	0.10	0.20	19.26	16.23	19.36	2
19.865	628.6	38.03	547.3	.831	97.7	32.1	316	200.0	0.10	0.20	19.27	16.18	19.39	2
19.594	620.7	38.08	539.6	.829	96.5	34.9	331	300.0	0.10	0.20	19.26	16.12	19.45	2

Table 6.41 Optimizations at Fixed Cell Thickness (X_L), no bsf, case 5

eff	V_{oc}	J_{sc}	V_{mp}	ff	C_{eff}	τ_{bulk}	L_d	X_L	X_f	X_b	log D_0	log D_B	log D_L	O_{pl}
17.026	650.2	31.35	568.5	.835	98.5	4.5	89	10.0	0.10	0.	19.24	17.17	0.	2
18.331	646.8	33.93	565.4	.835	97.5	6.4	114	25.0	0.10	0.	19.24	17.01	0.	2
18.827	642.0	35.14	560.9	.835	96.6	8.5	138	50.0	0.10	0.	19.25	16.88	0.	2
18.999	638.3	35.69	557.4	.834	95.9	10.3	157	75.0	0.10	0.	19.24	16.79	0.	2
19.081	635.5	36.02	554.7	.833	95.4	11.8	172	100.0	0.10	0.	19.26	16.72	0.	2
19.119	633.6	36.22	552.8	.833	94.9	12.9	182	125.0	0.10	0.	19.24	16.68	0.	2
19.136	631.8	36.38	551.1	.833	94.6	14.1	192	150.0	0.10	0.	19.24	16.63	0.	2
19.139	630.0	36.50	549.4	.832	94.3	15.4	203	172.7	0.10	0.	19.25	16.59	0.	2
19.135	628.5	36.59	547.9	.832	94.0	16.6	213	200.0	0.10	0.	19.26	16.55	0.	2
19.086	624.9	36.75	544.3	.831	93.2	19.6	236	300.0	0.10	0.	19.24	16.46	0.	2

Table 6.42 Optimizations at Fixed Front Junction Depth (X_f), case 5

eff	V_{oc}	J_{sc}	V_{mp}	ff	C_{eff}	τ_{bulk}	L_d	X_L	X_f	X_b	log D_0	log D_B	log D_L	O_{pl}
20.035	643.3	37.34	561.5	.834	98.9	26.1	280	100.0	0.06	0.20	19.44	16.30	19.33	2
20.022	**642.9**	**37.34**	**561.2**	**.834**	**98.9**	**26.1**	**280**	**100.0**	**0.10**	**0.20**	**19.27**	**16.30**	**19.33**	**2**
19.999	642.4	37.34	560.6	.834	98.9	26.1	280	100.0	0.20	0.20	19.04	16.30	19.33	2
19.982	641.8	37.35	560.0	.834	98.9	27.0	285	100.0	0.30	0.20	18.91	16.28	19.33	2
19.968	641.4	37.34	559.7	.834	98.9	27.0	285	100.0	0.40	0.20	18.82	16.28	19.33	2
19.954	641.1	37.35	559.3	.833	98.9	27.4	288	100.0	0.50	0.20	18.73	16.27	19.32	2
19.922	640.6	37.32	558.8	.833	98.9	27.0	286	100.0	0.75	0.20	18.57	16.28	19.32	2
19.892	639.9	37.32	558.1	.833	98.9	27.9	291	100.0	1.00	0.20	18.41	16.26	19.26	2
19.835	638.9	37.29	557.1	.833	98.8	28.5	295	100.0	1.50	0.20	18.20	16.25	19.33	2
19.774	637.6	37.27	555.8	.832	98.7	30.0	304	100.0	2.00	0.20	18.01	16.22	19.07	2

Table 6.43 Optimizations at Fixed Back Junction Depth (X_b), case 5

eff	V_{oc}	J_{sc}	V_{mp}	ff	C_{eff}	τ_{bulk}	L_d	X_L	X_f	X_b	log D_0	log D_B	log D_L	O_{pl}
20.060	644.0	37.34	562.2	.834	98.9	25.1	274	100.0	0.10	0.05	19.26	16.32	19.87	2
20.040	643.4	37.35	561.6	.834	98.9	26.1	280	100.0	0.10	0.10	19.27	16.30	19.56	2
20.022	**642.9**	**37.34**	**561.2**	**.834**	**98.9**	**26.1**	**280**	**100.0**	**0.10**	**0.20**	**19.27**	**16.30**	**19.33**	**2**
20.010	642.7	37.33	560.9	.834	98.9	26.1	280	100.0	0.10	0.30	19.27	16.30	19.20	2
19.994	642.3	37.33	560.5	.834	98.9	26.4	281	100.0	0.10	0.50	19.28	16.30	19.03	2
19.980	641.8	37.34	560.1	.834	98.9	27.0	285	100.0	0.10	0.75	19.27	16.28	18.91	2
19.969	641.5	37.34	559.8	.834	98.9	27.4	288	100.0	0.10	1.00	19.27	16.27	18.83	2
19.952	641.0	37.34	559.3	.834	98.9	28.0	291	100.0	0.10	1.50	19.27	16.26	18.69	2
19.940	640.7	37.34	559.0	.834	98.9	28.1	292	100.0	0.10	2.00	19.27	16.26	18.59	2

Table 6.44 Optimizations at Fixed Front Surface Doping Concentration (D_0), case 5

eff	V_{oc}	J_{sc}	V_{mp}	ff	C_{eff}	τ_{bulk}	L_d	X_L	X_f	X_b	log D_0	log D_B	log D_L	O_{pl}
19.968	641.2	37.36	559.5	.834	98.9	27.0	286	100.0	0.10	0.20	18.37	16.28	19.33	2
19.995	642.1	37.34	560.5	.834	98.9	26.1	280	100.0	0.10	0.20	18.67	16.30	19.33	2
20.014	642.7	37.34	561.0	.834	98.9	26.1	280	100.0	0.10	0.20	18.97	16.30	19.33	2
20.022	**642.9**	**37.34**	**561.2**	**.834**	**98.9**	**26.1**	**280**	**100.0**	**0.10**	**0.20**	**19.27**	**16.30**	**19.33**	**2**
20.009	642.6	37.34	560.9	.834	98.9	26.1	280	100.0	0.10	0.20	19.57	16.30	19.33	2
19.947	640.5	37.36	558.9	.834	99.0	27.6	289	100.0	0.10	0.20	19.87	16.27	19.33	2
19.775	635.4	37.37	554.0	.833	99.0	29.5	301	100.0	0.10	0.20	20.17	16.23	19.32	2

Table 6.45 Optimizations at Fixed Bulk Doping Concentration (D_B), case 5

eff	V_{oc}	J_{sc}	V_{mp}	ff	C_{eff}	τ_{bulk}	L_d	X_L	X_f	X_b	$\log D_0$	$\log D_B$	$\log D_L$	O_{pl}
19.365	635.5	37.64	540.4	.810	99.7	73.9	503	100.0	0.10	0.20	19.31	15.40	19.37	2
19.715	636.8	37.60	549.6	.823	99.6	58.6	443	100.0	0.10	0.20	19.29	15.70	19.36	2
19.941	639.8	37.51	556.6	.831	99.4	41.4	365	100.0	0.10	0.20	19.28	16.00	19.35	2
20.022	**642.9**	**37.34**	**561.2**	**.834**	**98.9**	**26.1**	**280**	**100.0**	**0.10**	**0.20**	**19.27**	**16.30**	**19.33**	**2**
19.891	648.2	36.72	566.7	.836	98.1	13.4	186	84.3	0.10	0.20	19.25	16.66	19.31	2
19.633	651.9	36.02	570.3	.836	97.5	8.1	134	65.6	0.10	0.20	19.25	16.90	19.28	2
19.071	653.8	34.90	571.9	.836	96.7	4.2	84	43.7	0.10	0.20	19.26	17.21	19.25	2

Table 6.46 Optimizations at Fixed Back Surface Doping Concentration (D_L), case 5

eff	V_{oc}	J_{sc}	V_{mp}	ff	C_{eff}	τ_{bulk}	L_d	X_L	X_f	X_b	$\log D_0$	$\log D_B$	$\log D_L$	O_{pl}
19.965	641.4	37.33	559.7	.834	98.9	27.3	287	100.0	0.10	0.20	19.27	16.28	18.43	2
19.993	642.1	37.34	560.4	.834	98.9	26.9	285	100.0	0.10	0.20	19.27	16.29	18.73	2
20.013	642.8	37.34	561.0	.834	98.9	26.1	280	100.0	0.10	0.20	19.27	16.30	19.03	2
20.022	**642.9**	**37.34**	**561.2**	**.834**	**98.9**	**26.1**	**280**	**100.0**	**0.10**	**0.20**	**19.27**	**16.30**	**19.33**	**2**
20.008	642.6	37.33	560.9	.834	98.9	26.1	280	100.0	0.10	0.20	19.27	16.30	19.63	2
19.944	640.8	37.34	559.1	.833	98.9	28.2	293	100.0	0.10	0.20	19.27	16.26	19.93	2
19.768	636.1	37.32	554.6	.833	98.9	31.6	313	100.0	0.10	0.20	19.27	16.19	20.23	2

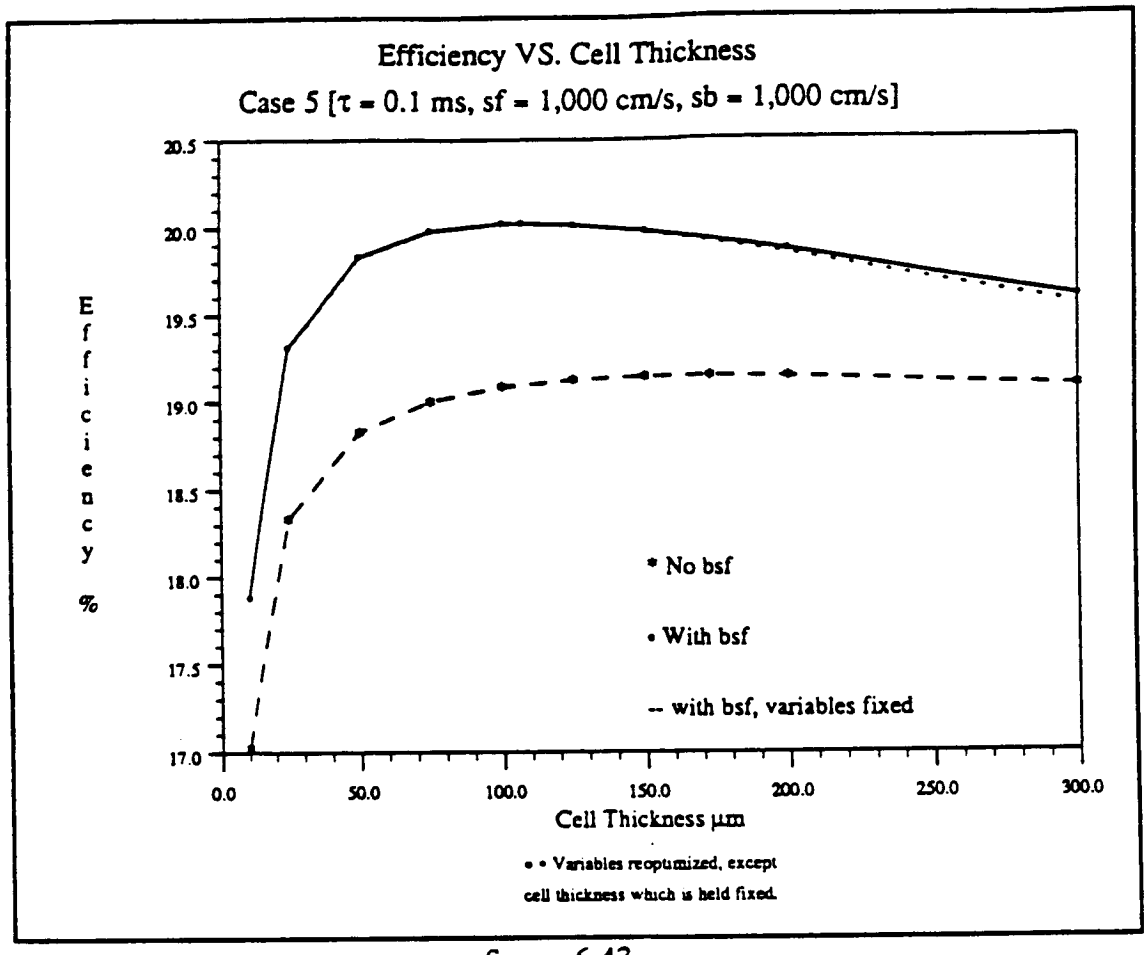

figure 6.43

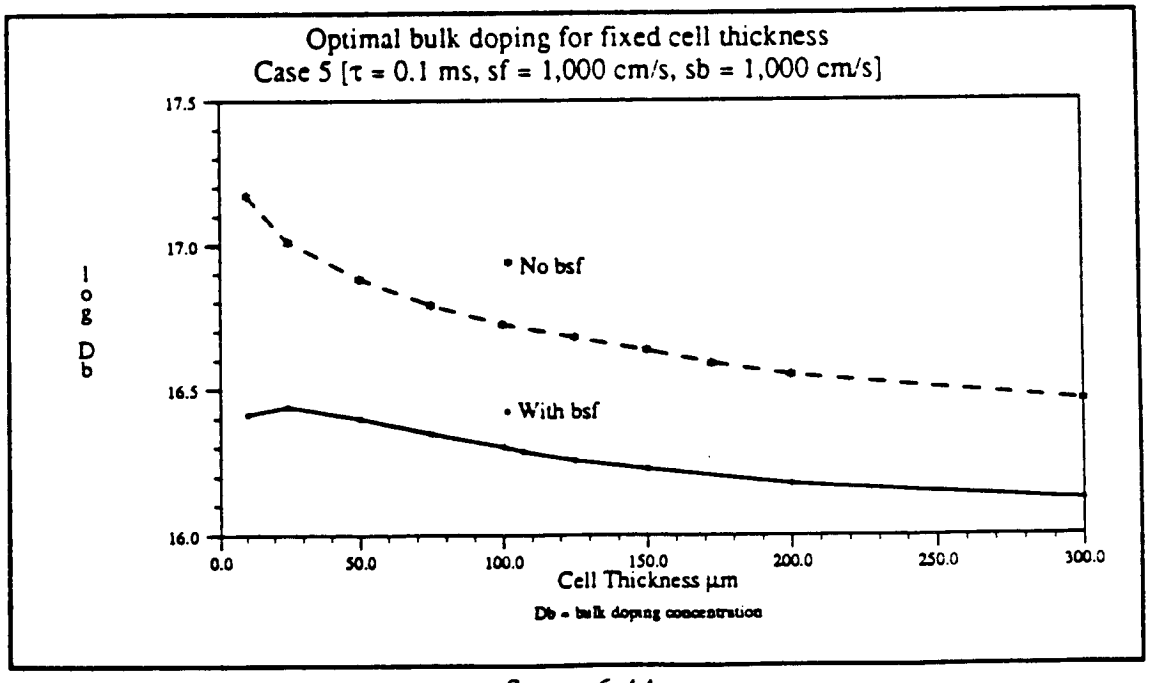

figure 6.44

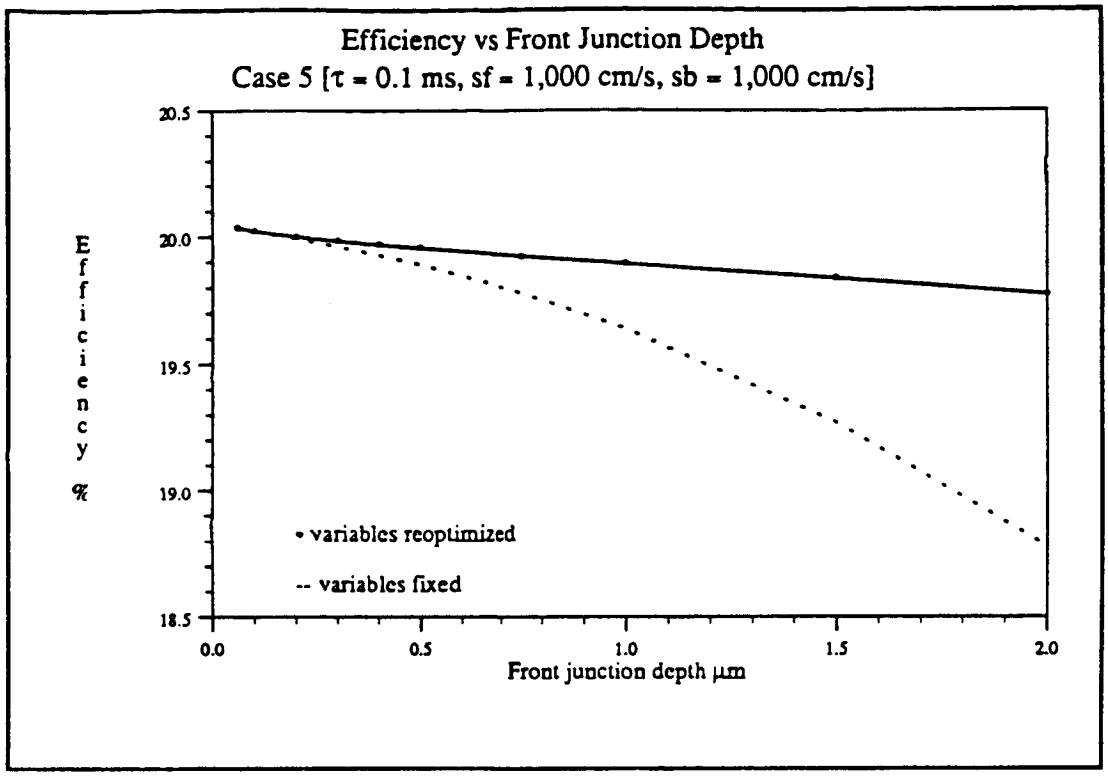

figure 6.45

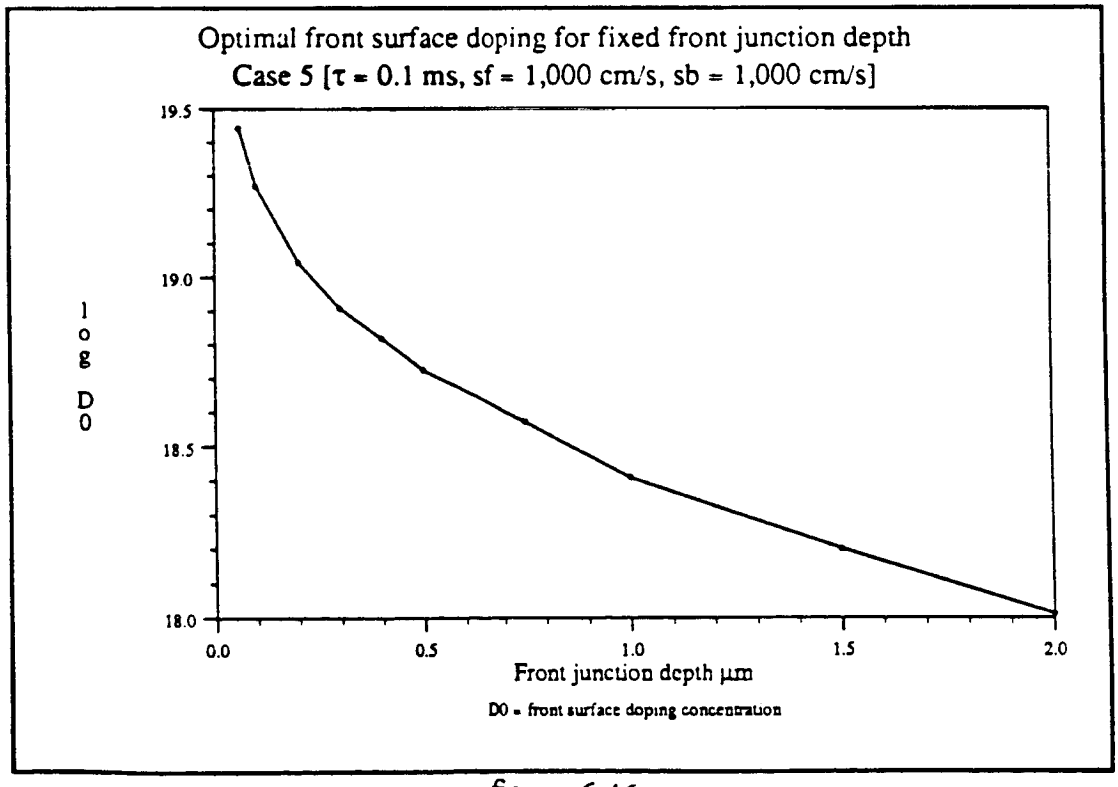

figure 6.46

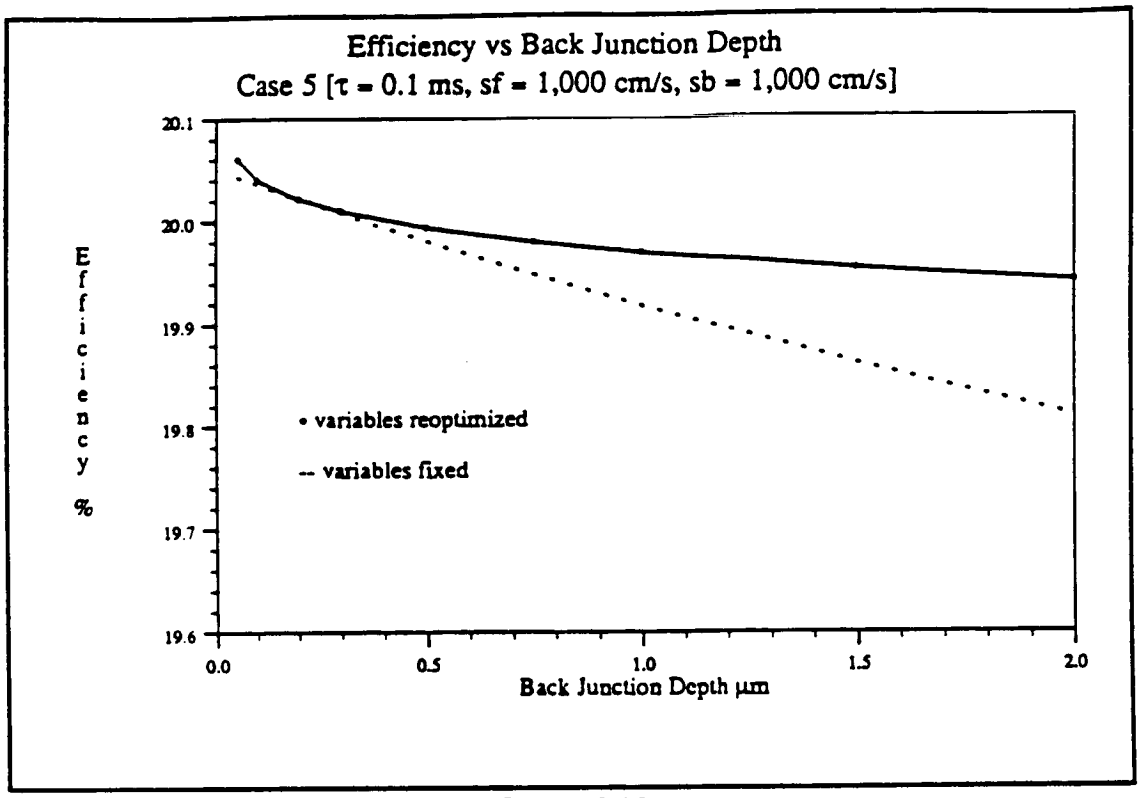

figure 6.47

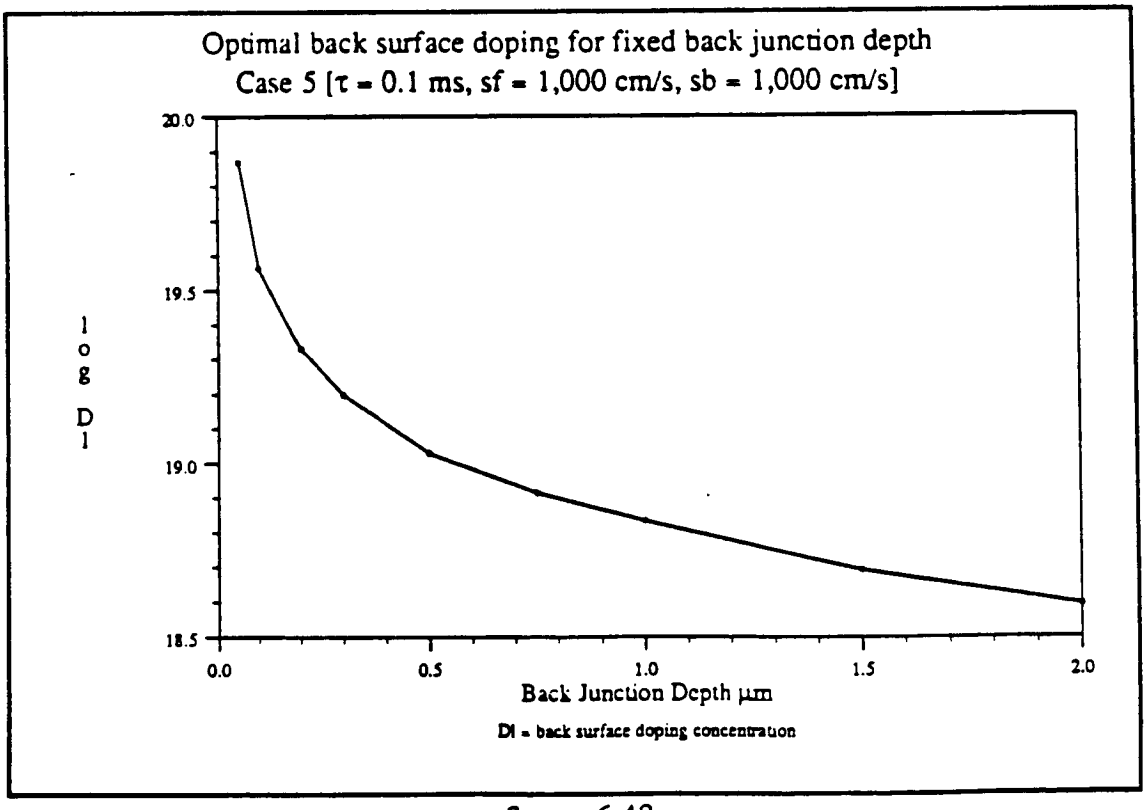

figure 6.48

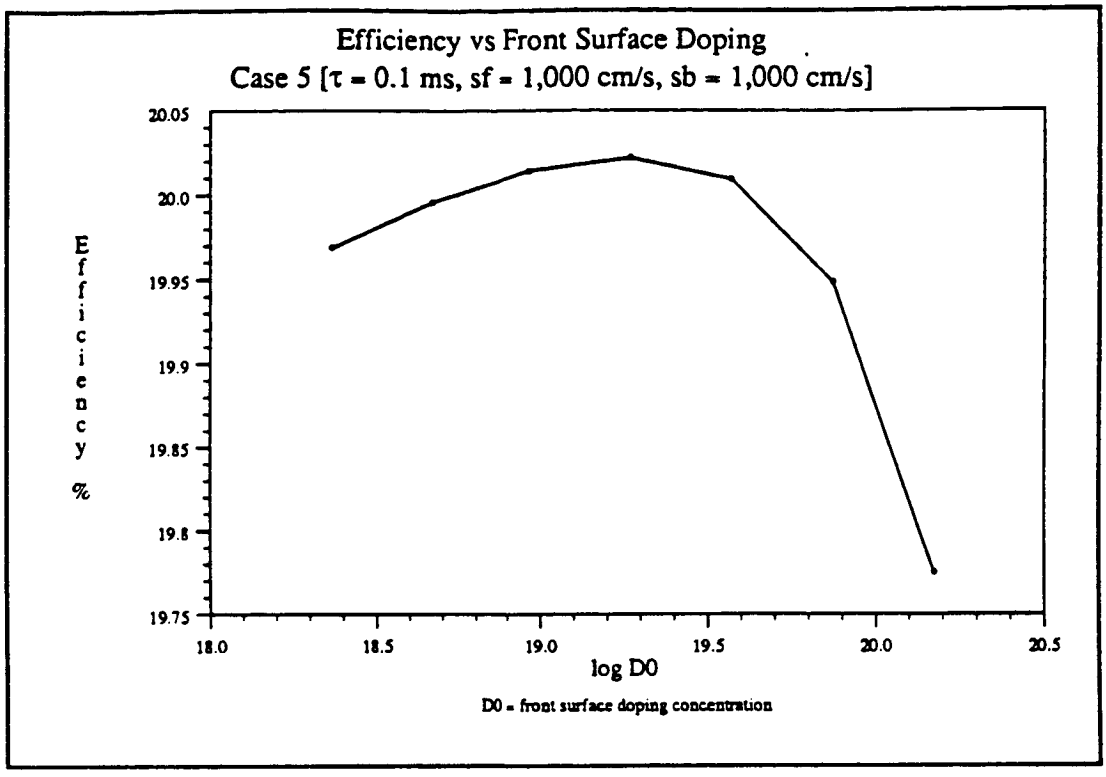

figure 6.49

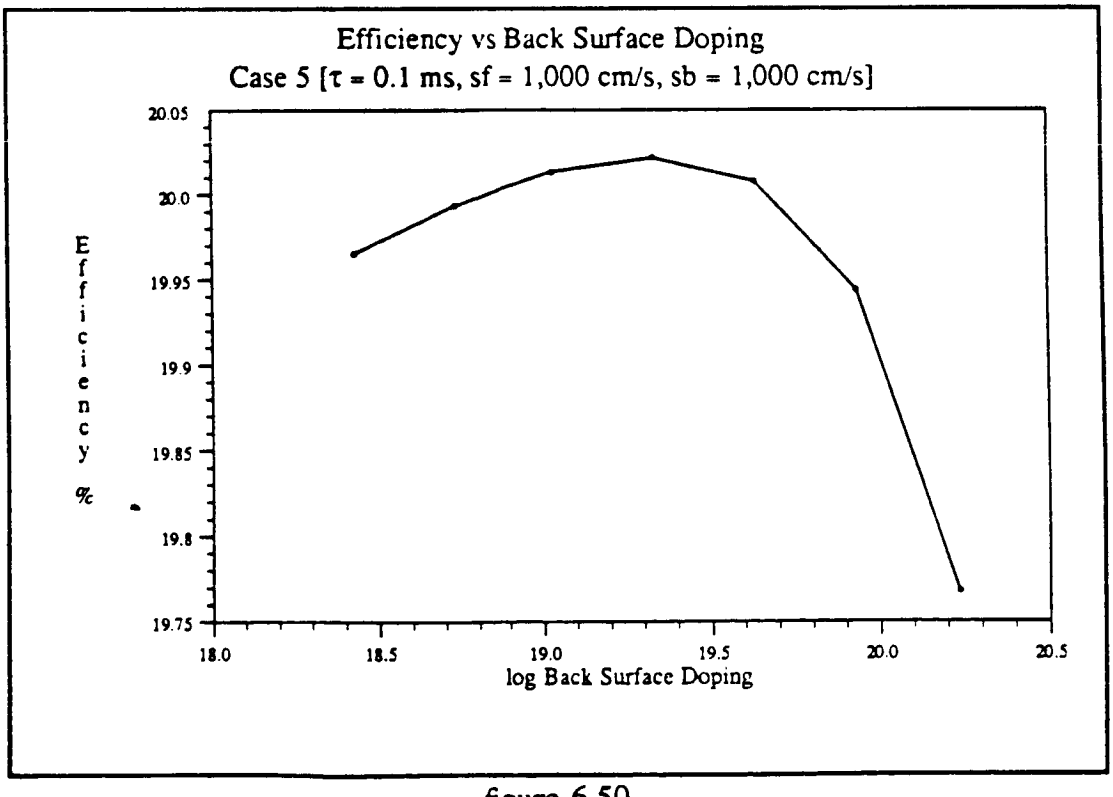

figure 6.50

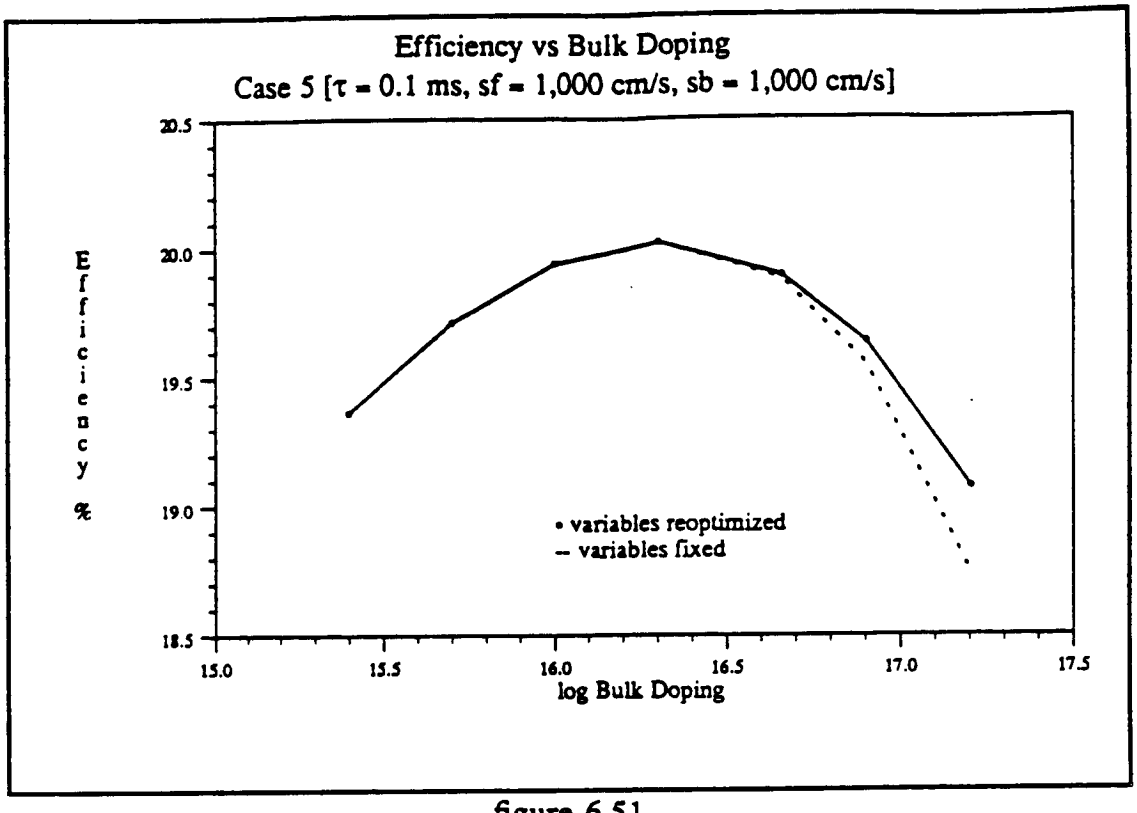

figure 6.51

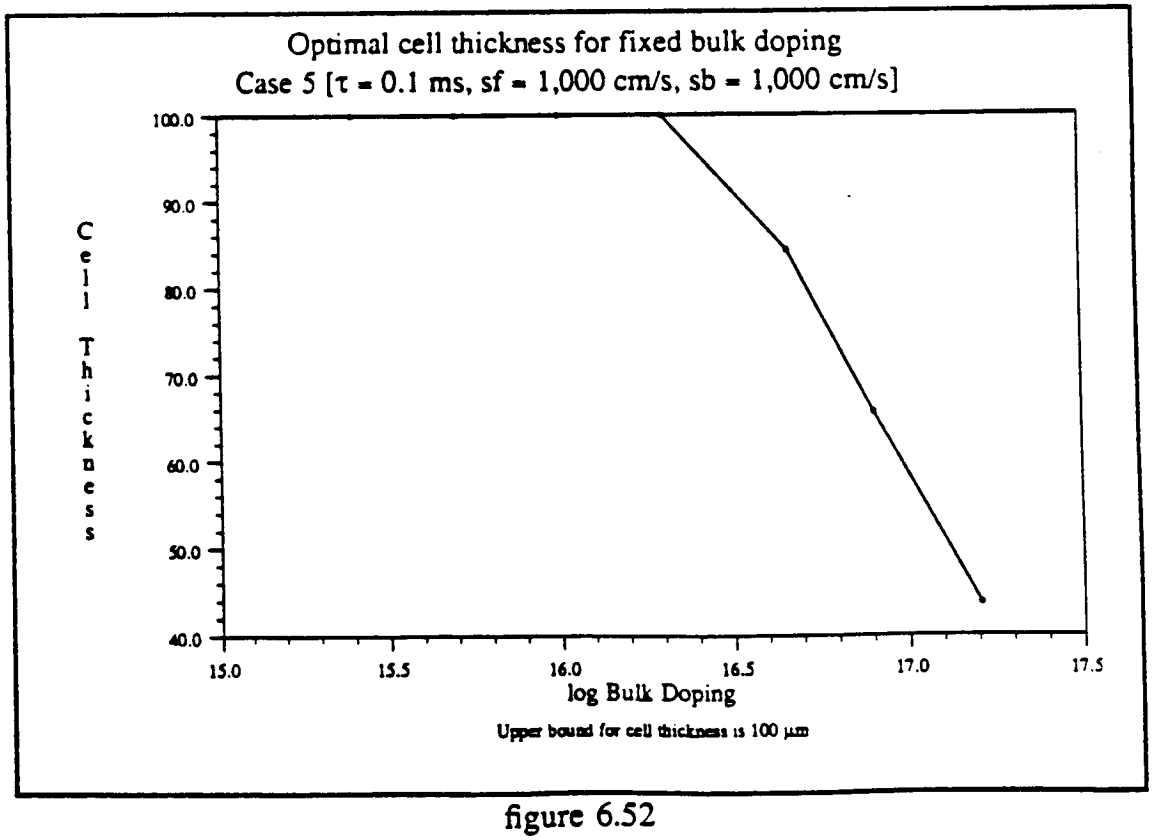

figure 6.52

Parameters Held Constant During Optimization (see also table 6.1).

Front surface recombination velocity (S_f)	1,000	cm/s
Back surface recombination velocity (S_b)	∞	cm/s
Electron minority carrier lifetime[1] (τ_{n0})	0.1	ms
Hole minority carrier lifetime[1] (τ_{p0})	0.05	ms

Optimal Values of Decision Variables

Front junction depth (X_f)	0.10	μm (lower bound)
Back junction depth (X_b)	24.17	μm
Cell thickness (X_L)	100.0	μm (upper bound)
Front surface doping concentration (D_0)	1.932×10^{19}	P atoms/cm^3
Bulk doping concentration (D_B)	1.236×10^{16}	B atoms/cm^3
Back surface doping concentration (D_L)	1.031×10^{19}	B atoms/cm^3

Cell Performance Parameters

Efficiency	19.481	%
Open circuit voltage (V_{oc})	631.2	mV
Short circuit current density (J_{sc})	37.05	mA/cm^2
Maximum power voltage (V_{mp})	550.74	mV
Fill factor	0.832	
Collection efficiency	98.14	%
Bulk resitivity	1.143	ohm-cm
Sheet resistance layer 1	1100.9	ohm/□
layer 2	10.61	ohm/□
Bulk lifetime	36.5	μs
Bulk diffusion length	340	μm

[1] Values in lightly doped silicon.

Table 6.47 Optimal Solution For Case 6

Table 6.48 Effect of BSF and BSR, case 6 (S_f = 1,000 cm/s, S_b = ∞ cm/s, τ_{n0} = 0.1 ms)

eff	V_{oc}	J_{sc}	V_{mp}	ff	C_{eff}	τ_{bulk}	L_d	X_L	X_f	X_b	log D_0	log D_B	log D_L	O_{pl}
19.481	**632.0**	**37.05**	**550.7**	**.832**	**98.1**	**36.5**	**340**	**100.0**	**0.10**	**24.2**	**19.29**	**16.09**	**19.01**	**2**
18.847	631.7	35.85	550.6	.832	98.5	33.7	324	100.0	0.10	24.2	19.28	16.15	19.05	1
17.553	633.5	33.28	552.7	.833	88.1	5.1	97	100.0	0.10	0.	19.27	17.12	0.	2
17.254	633.6	32.71	552.8	.833	89.9	4.9	94	100.0	0.10	0.	19.26	17.14	0.	1

Table 6.49 Optimizations at Fixed Cell Thickness (X_L), with bsf, case 6

eff	V_{oc}	J_{sc}	V_{mp}	ff	C_{eff}	τ_{bulk}	L_d	X_L	X_f	X_b	log D_0	log D_B	log D_L	O_{pl}
16.039	621.4	31.07	541.1	.831	97.6	56.7	435	10.0	0.10	2.5	19.22	15.73	20.07	2
18.008	633.2	34.15	552.2	.833	98.1	43.4	375	25.0	0.10	6.7	19.24	15.97	19.62	2
18.942	635.3	35.80	554.1	.833	98.4	38.4	350	50.0	0.10	12.8	19.27	16.06	19.32	2
19.304	633.9	36.58	552.7	.832	98.3	36.8	342	75.0	0.10	18.4	19.26	16.09	19.15	2
19.481	**632.0**	**37.05**	**550.7**	**.832**	**98.1**	**36.5**	**340**	**100.0**	**0.10**	**24.2**	**19.29**	**16.09**	**19.01**	**2**
19.568	629.8	37.37	548.6	.831	97.9	37.1	343	125.0	0.10	31.0	19.25	16.08	18.89	2
19.607	627.3	37.62	546.2	.831	97.8	37.2	344	150.0	0.10	29.8	19.26	16.08	18.93	2
19.613	625.7	37.74	544.6	.830	97.7	37.6	346	166.9	0.10	30.8	19.25	16.07	18.93	2
19.602	623.7	37.86	542.7	.830	97.3	37.4	345	200.0	0.10	39.4	19.27	16.07	18.79	2

Table 6.50 Optimizations at Fixed Cell Thickness (X_L), no bsf, case 6

eff	V_{oc}	J_{sc}	V_{mp}	ff	C_{eff}	τ_{bulk}	L_d	X_L	X_f	X_b	log D_0	log D_B	log D_L	O_{pl}
13.019	572.6	27.92	493.0	.814	87.7	2.2	52	10.0	3.05	0.	17.64	17.49	0.	2
14.895	591.5	30.75	510.9	.819	88.4	4.0	82	25.0	3.50	0.	17.31	17.22	0.	2
16.256	630.8	31.00	549.9	.831	85.2	2.7	60	50.0	0.10	0.	19.29	17.41	0.	2
17.064	632.7	32.41	551.8	.832	87.1	3.9	80	75.0	0.10	0.	19.27	17.24	0.	2
17.553	633.5	33.28	552.7	.833	88.1	5.1	97	100.0	0.10	0.	19.27	17.12	0.	2
17.878	634.2	33.85	553.4	.833	88.7	5.9	108	125.0	0.10	0.	19.26	17.05	0.	2
18.107	634.4	34.27	553.5	.833	89.1	6.8	119	150.0	0.10	0.	19.26	16.98	0.	2
18.402	633.9	34.85	553.1	.833	89.5	8.4	137	200.0	0.10	0.	19.26	16.89	0.	2
18.574	632.7	35.26	551.9	.833	89.9	10.0	154	250.0	0.10	0.	19.25	16.80	0.	2
18.684	631.4	35.55	550.7	.832	90.1	11.4	168	300.0	0.10	0.	19.25	16.74	0.	2

Table 6.51 Optimizations at Fixed Front Junction Depth (X_f), case 6

eff	V_{oc}	J_{sc}	V_{mp}	ff	C_{eff}	τ_{bulk}	L_d	X_L	X_f	X_b	$\log D_0$	$\log D_B$	$\log D_L$	O_{pl}
19.489	632.2	37.05	551.0	.832	98.1	36.5	340	100.0	0.06	24.3	19.44	16.09	19.01	2
19.481	**632.0**	**37.05**	**550.7**	**.832**	**98.1**	**36.5**	**340**	**100.0**	**0.10**	**24.2**	**19.29**	**16.09**	**19.01**	**2**
19.467	631.5	37.06	550.3	.832	98.2	37.1	343	100.0	0.20	24.3	19.05	16.08	19.00	2
19.455	631.1	37.06	549.9	.832	98.2	37.3	344	100.0	0.30	24.1	18.91	16.08	19.00	2
19.445	630.9	37.06	549.7	.832	98.2	37.4	345	100.0	0.40	24.1	18.80	16.07	19.01	2
19.436	630.7	37.05	549.5	.832	98.2	37.5	345	100.0	0.50	24.2	18.69	16.07	19.00	2
19.413	630.3	37.04	549.1	.832	98.1	37.2	344	100.0	0.75	24.0	18.51	16.08	19.00	2
19.392	629.7	37.04	548.5	.831	98.1	38.3	349	100.0	1.00	23.6	18.36	16.06	19.01	2
19.350	628.9	37.02	547.7	.831	98.1	38.4	350	100.0	1.50	22.3	18.12	16.06	19.05	2
19.309	628.3	36.99	547.0	.831	98.0	38.8	352	100.0	2.00	22.6	17.94	16.05	19.04	2

Table 6.52 Optimizations at Fixed Back Junction Depth (X_b), case 6

eff	V_{oc}	J_{sc}	V_{mp}	ff	C_{eff}	τ_{bulk}	L_d	X_L	X_f	X_b	$\log D_0$	$\log D_B$	$\log D_L$	O_{pl}
17.597	633.2	33.39	552.4	.833	88.4	5.3	100	100.0	0.10	0.0	19.27	17.10	20.60	2
17.645	632.9	33.49	552.1	.832	88.7	5.6	104	100.0	0.10	0.1	19.27	17.08	20.60	2
18.318	601.5	36.85	522.0	.826	97.6	48.4	398	100.0	0.10	0.5	19.27	15.88	20.60	2
18.732	608.4	37.23	528.0	.827	98.6	55.3	429	100.0	0.10	1.0	19.27	15.76	20.60	2
19.023	617.5	37.15	537.0	.829	98.4	43.4	375	100.0	0.10	2.0	19.25	15.97	20.31	2
19.302	625.0	37.17	544.2	.831	98.5	38.3	349	100.0	0.10	5.0	19.28	16.06	19.88	2
19.427	628.8	37.16	547.8	.831	98.4	36.5	340	100.0	0.10	10.0	19.27	16.09	19.54	2
19.478	631.3	37.09	550.1	.832	98.2	36.5	340	100.0	0.10	20.0	19.29	16.09	19.13	2
19.481	**632.0**	**37.05**	**550.7**	**.832**	**98.1**	**36.5**	**340**	**100.0**	**0.10**	**24.2**	**19.29**	**16.09**	**19.01**	**2**
19.477	632.6	37.00	551.3	.832	98.0	37.2	344	100.0	0.10	30.0	19.29	16.08	18.87	2
19.460	633.5	36.91	552.1	.832	97.8	39.0	353	100.0	0.10	40.0	19.29	16.05	18.69	2
19.435	634.2	36.82	552.8	.832	97.5	41.6	366	100.0	0.10	50.0	19.29	16.00	18.53	2

Table 6.53 Optimizations at Fixed Front Surface Doping Concentration (D_0), case 6

eff	V_{oc}	J_{sc}	V_{mp}	ff	C_{eff}	τ_{bulk}	L_d	X_L	X_f	X_b	$\log D_0$	$\log D_B$	$\log D_L$	O_{pl}
19.447	630.7	37.07	549.6	.832	98.2	37.5	345	100.0	0.10	24.2	18.38	16.07	19.01	2
19.464	631.4	37.05	550.2	.832	98.2	36.5	340	100.0	0.10	24.0	18.68	16.09	19.01	2
19.476	631.8	37.05	550.6	.832	98.1	36.5	340	100.0	0.10	24.1	18.98	16.09	19.01	2
19.481	**632.0**	**37.05**	**550.7**	**.832**	**98.1**	**36.5**	**340**	**100.0**	**0.10**	**24.2**	**19.29**	**16.09**	**19.01**	**2**
19.472	631.7	37.05	550.5	.832	98.1	36.5	340	100.0	0.10	24.1	19.59	16.09	19.01	2
19.429	630.2	37.07	549.0	.832	98.2	38.1	348	100.0	0.10	24.1	19.89	16.06	19.00	2
19.306	626.3	37.09	545.4	.831	98.3	39.7	357	100.0	0.10	22.7	20.19	16.03	19.04	2

Table 6.54 Optimizations at Fixed Bulk Doping Concentration (D_B), case 6

eff	V_{oc}	J_{sc}	V_{mp}	ff	C_{eff}	τ_{bulk}	L_d	X_L	X_f	X_b	$\log D_0$	$\log D_B$	$\log D_L$	O_{pl}
19.073	629.8	37.15	539.6	.815	98.4	82.1	533	100.0	0.10	50.0	19.31	15.19	18.54	2
19.287	630.8	37.07	545.5	.825	98.2	69.7	487	100.0	0.10	50.0	19.30	15.49	18.54	2
19.423	630.2	37.17	547.6	.829	98.4	53.5	421	100.0	0.10	31.2	19.29	15.79	18.86	2
19.481	**632.0**	**37.05**	**550.7**	**.832**	**98.1**	**36.5**	**340**	**100.0**	**0.10**	**24.2**	**19.29**	**16.09**	**19.01**	**2**
19.412	634.6	36.71	553.7	.833	97.3	22.3	255	100.0	0.10	22.3	19.26	16.39	19.04	2
19.176	637.6	36.07	556.7	.834	95.5	12.5	178	100.0	0.10	22.3	19.26	16.69	19.03	2
18.728	640.5	35.05	559.4	.834	92.9	6.7	117	100.0	0.10	19.4	19.26	16.99	19.08	2

Table 6.55 Optimizations at Fixed Back Surface Doping Concentration (D_L), case 6

eff	V_{oc}	J_{sc}	V_{mp}	ff	C_{eff}	τ_{bulk}	L_d	X_L	X_f	X_b	$\log D_0$	$\log D_B$	$\log D_L$	O_{pl}
19.327	630.7	36.83	549.7	.832	97.6	41.0	363	100.0	0.10	50.0	19.27	16.01	18.11	2
19.430	633.1	36.88	551.8	.832	97.7	40.1	359	100.0	0.10	46.2	19.27	16.02	18.41	2
19.469	632.5	36.99	551.3	.832	98.0	38.0	348	100.0	0.10	33.2	19.29	16.06	18.71	2
19.481	**632.0**	**37.05**	**550.7**	**.832**	**98.1**	**36.5**	**340**	**100.0**	**0.10**	**24.2**	**19.29**	**16.09**	**19.01**	**2**
19.476	631.4	37.07	550.3	.832	98.2	35.9	337	100.0	0.10	18.8	19.27	16.10	19.31	2
19.451	630.7	37.08	549.6	.832	98.2	36.2	338	100.0	0.10	16.1	19.27	16.10	19.62	2
19.421	630.3	37.04	549.2	.832	98.1	36.4	339	100.0	0.10	15.8	19.27	16.09	19.92	2

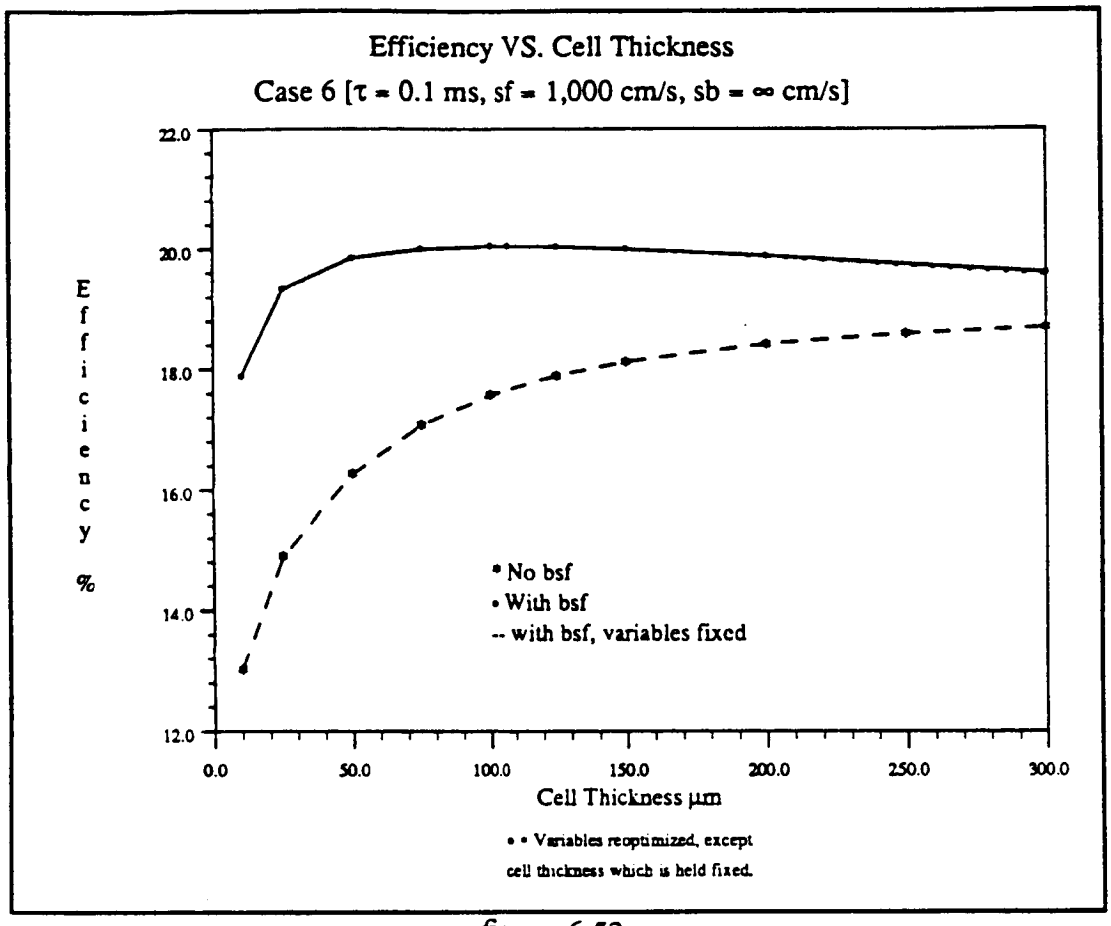

figure 6.53

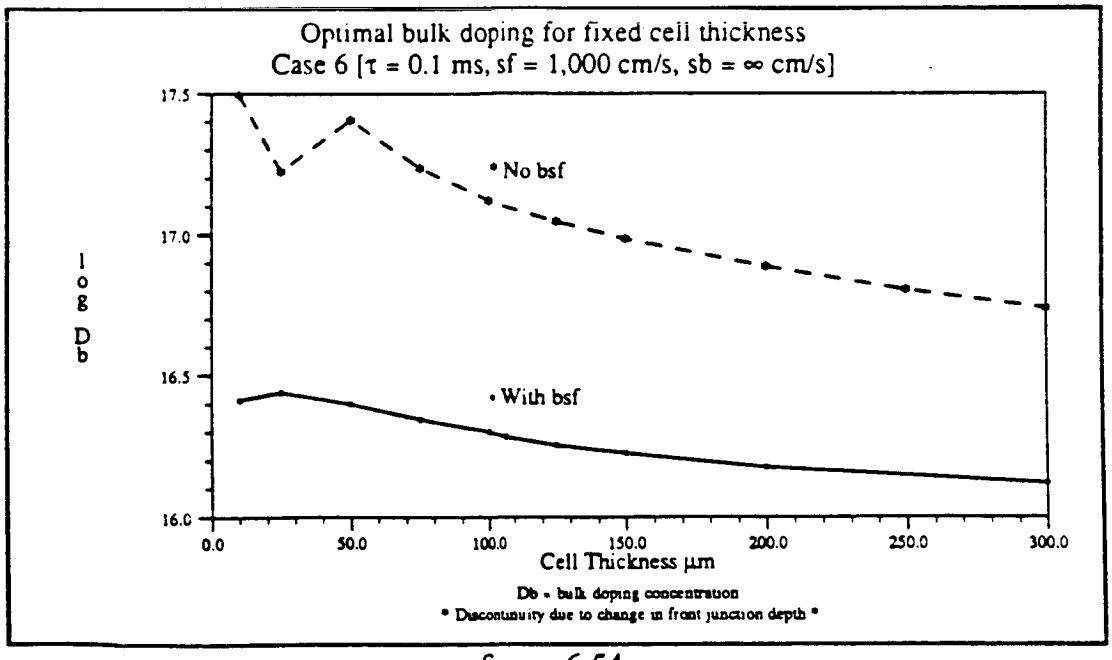

figure 6.54

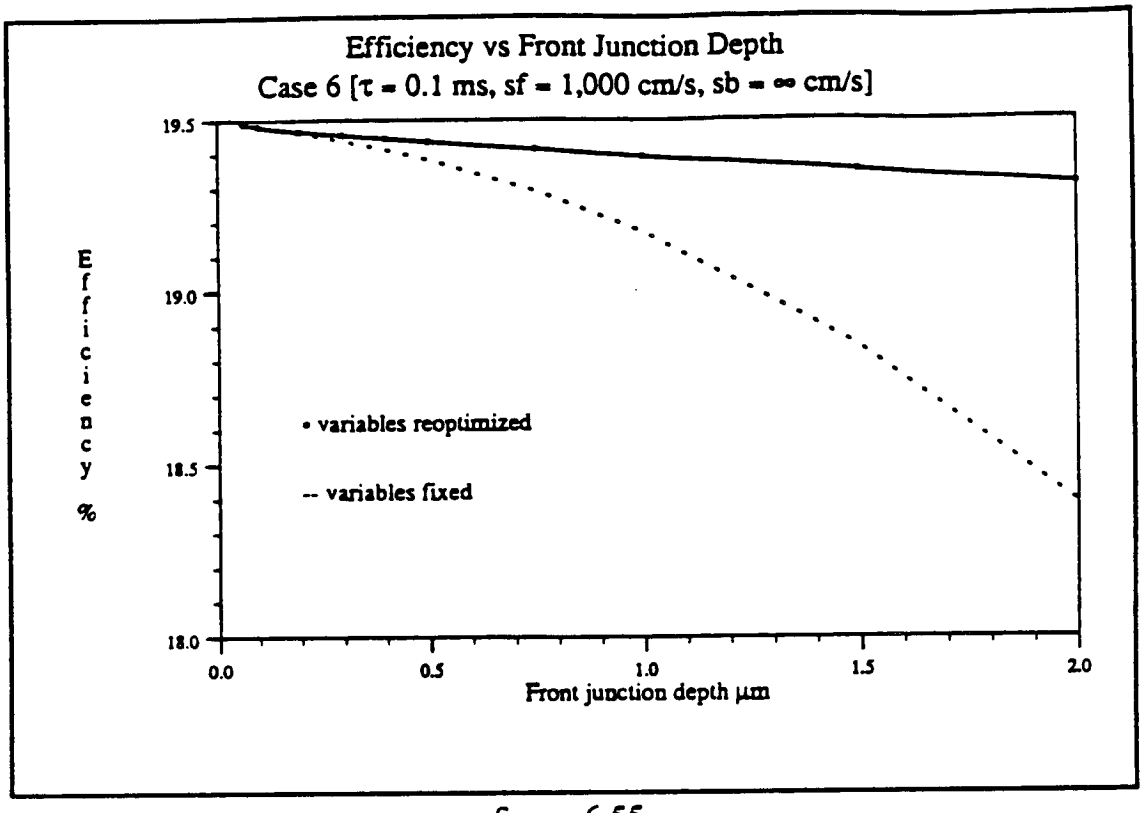

figure 6.55

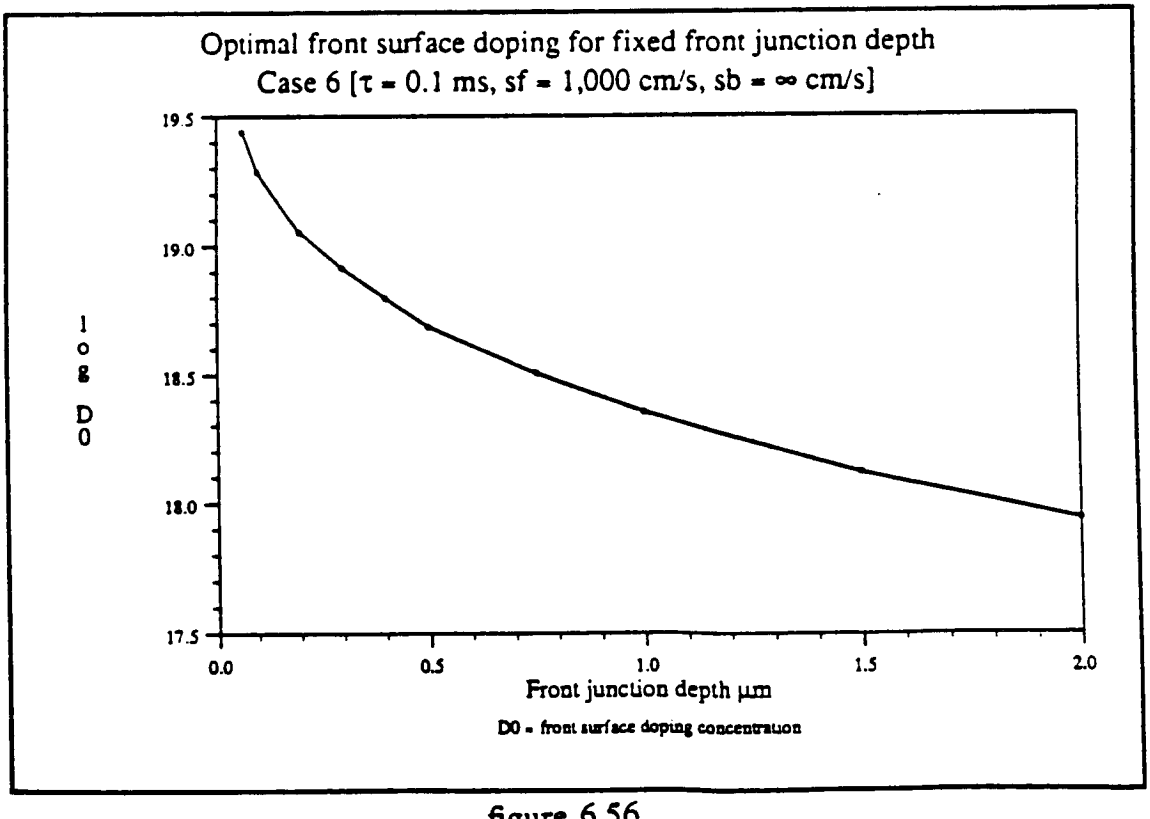

figure 6.56

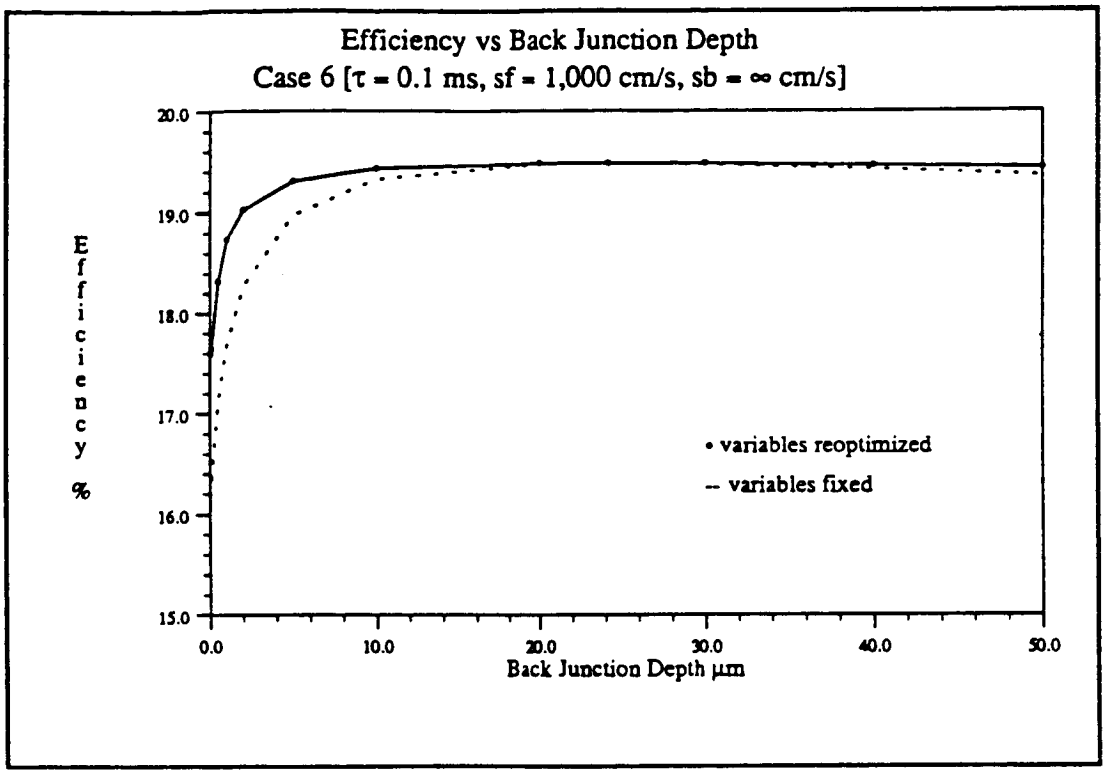

figure 6.57

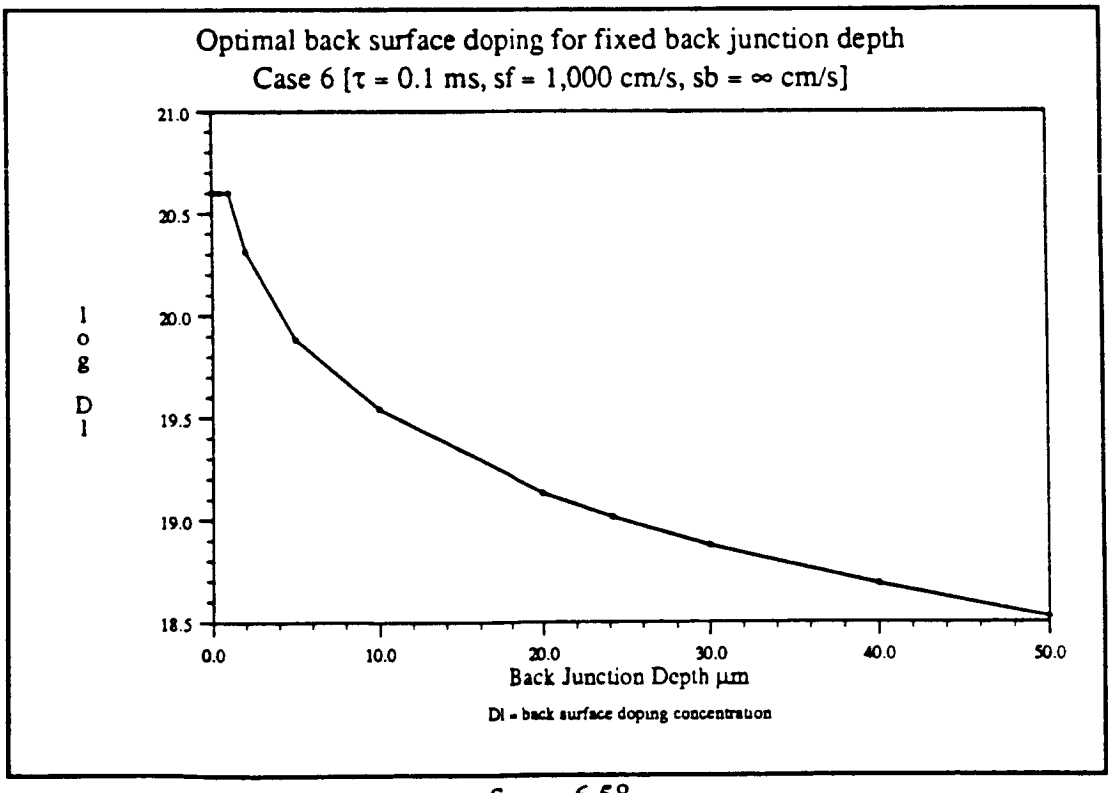

figure 6.58

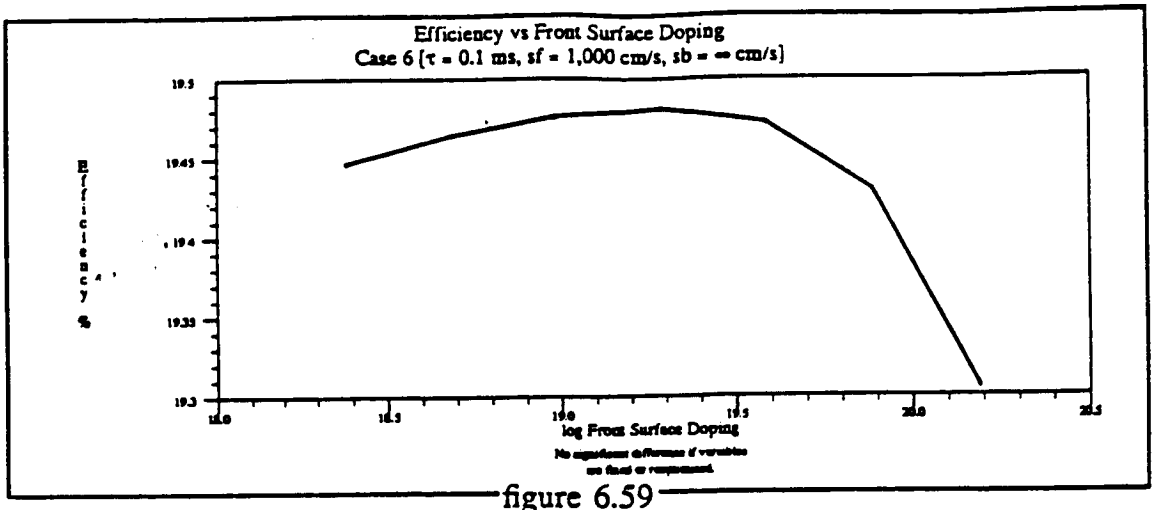

figure 6.59

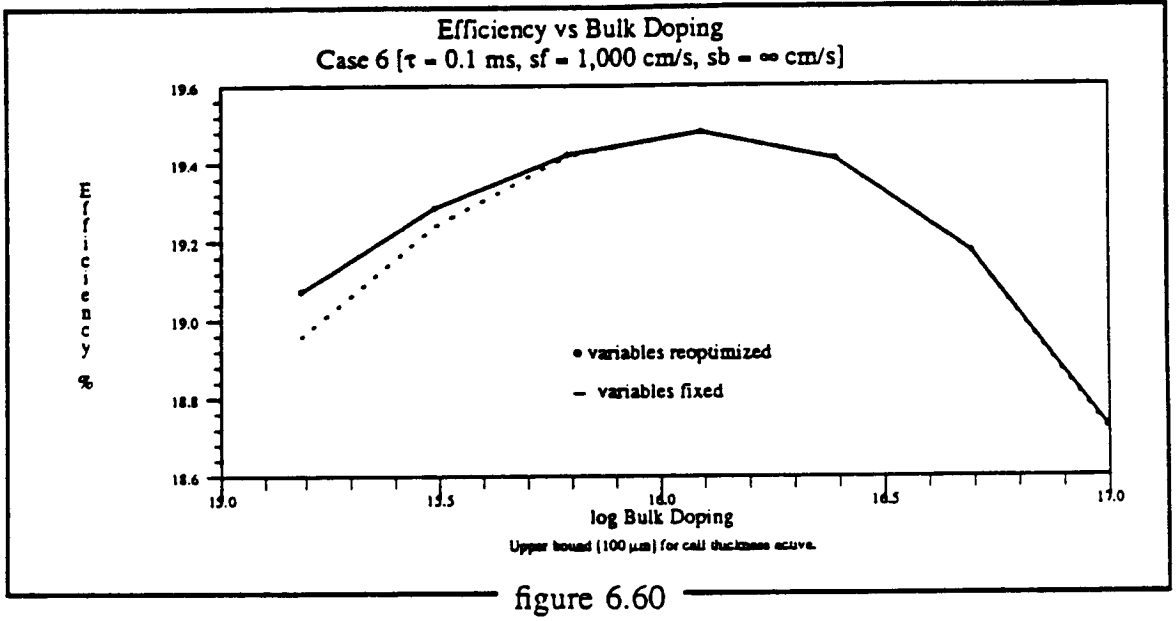

figure 6.60

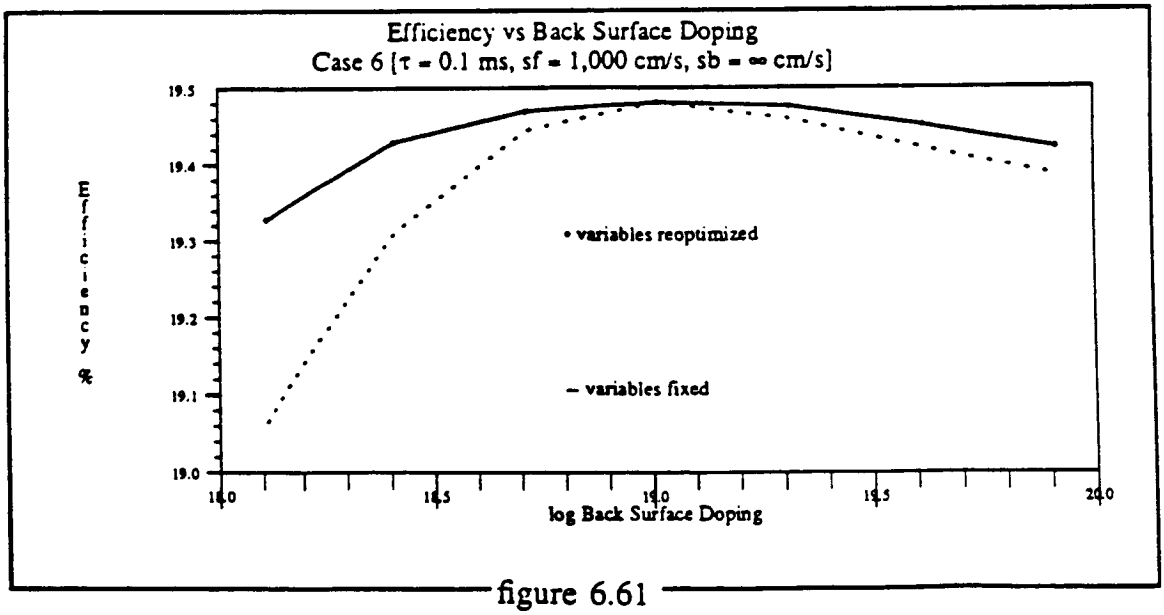

figure 6.61

Table 6.56 Effect of Lifetime, $X_L \leq 300$ μm, $O_{pl} = 2$

eff	V_{oc}	J_{sc}	V_{mp}	ff	C_{eff}	τ_{bulk}	L_d	X_L	X_f	X_b	log D_0	log D_B	log D_L	τ_{s0}	log S_f	log S_b
17.792	613.7	35.04	533.2	.827	98.5	2.9	93	34.1	.10	0.2	18.08	16.25	17.06	0.01	0	0
18.557	627.4	35.61	546.3	.831	98.8	5.2	125	42.4	.10	0.2	18.08	16.30	17.06	0.02	0	0
19.546	644.8	36.35	562.9	.834	99.1	11.2	181	58.0	.10	0.2	18.07	16.39	17.10	0.05	0	0
20.283	657.3	36.90	574.8	.836	99.2	20.6	243	74.6	.10	0.2	18.13	16.44	17.24	0.10	0	0
21.011	670.1	37.40	586.8	.838	99.4	38.1	328	94.4	.10	0.2	18.05	16.48	17.25	0.20	0	0
21.729	683.7	37.82	599.5	.840	99.5	69.7	440	115.2	.10	0.2	17.99	16.52	17.31	0.40	0	0
22.297	695.4	38.09	610.4	.842	99.6	114.6	560	131.2	.10	0.2	17.86	16.55	17.34	0.70	0	0
22.653	703.0	38.27	617.0	.842	99.7	167.4	679	142.6	.10	0.2	17.79	16.54	17.79	1.00	0	0
23.440	776.1	36.37	686.2	.830	100.0	1972.2	2631	49.7	.10	0.2	17.81	14.00	17.82	2.00	0	0
24.576	769.4	37.65	689.5	.848	100.0	4930.5	4161	94.8	.10	0.2	17.83	14.00	17.93	5.00	0	0
25.258	764.2	38.41	689.6	.860	100.0	9861.0	5885	145.1	.10	0.2	17.83	14.00	17.95	10.00	0	0
17.773	612.4	35.08	532.0	.827	98.5	2.9	94	35.1	.10	0.2	18.25	16.24	18.02	0.01	2	2
18.531	625.9	35.66	544.9	.830	98.8	5.4	127	43.4	.10	0.2	18.35	16.28	18.14	0.02	2	2
19.497	637.7	36.71	556.2	.833	98.8	12.4	191	73.8	.10	0.2	18.54	16.33	18.42	0.05	2	2
20.228	653.4	37.04	571.1	.836	99.1	21.7	250	81.8	.10	0.2	18.62	16.41	18.59	0.10	2	2
20.934	664.8	37.59	581.9	.838	99.3	41.0	343	107.0	.10	0.2	18.70	16.44	18.73	0.20	2	2
21.614	676.5	38.07	592.8	.839	99.4	77.4	469	135.8	.10	0.2	18.75	16.47	18.82	0.40	2	2
22.130	682.9	38.58	598.7	.840	99.4	134.8	619	185.8	.10	0.2	18.79	16.47	18.88	0.70	2	2
22.447	687.7	38.85	602.6	.840	99.5	213.8	788	217.4	.10	0.2	18.74	16.41	18.84	1.00	2	2
23.025	701.2	38.98	615.6	.842	99.7	366.2	1017	230.9	.10	0.2	18.79	16.48	18.93	2.00	2	2
23.675	713.0	39.36	626.6	.844	99.8	989.1	1692	300.0	.10	0.2	18.81	16.42	18.97	5.00	2	2
24.050	721.9	39.40	635.5	.846	99.9	2261.2	2600	300.0	.10	0.2	18.81	16.33	18.98	10.00	2	2
17.691	607.9	35.21	527.8	.827	98.4	3.2	99	37.9	.10	0.2	18.77	16.18	18.71	0.01	3	3
18.422	619.2	35.88	538.6	.829	98.6	5.9	134	50.4	.10	0.2	19.00	16.23	18.99	0.02	3	3
19.330	627.0	37.10	546.0	.831	98.3	14.9	213	99.1	.10	0.2	19.20	16.22	19.24	0.05	3	3
20.022	641.6	37.43	559.9	.834	98.8	26.7	284	106.9	.10	0.2	19.25	16.29	19.32	0.10	3	3
20.650	649.8	38.06	567.6	.835	98.9	52.2	396	151.4	.10	0.2	19.30	16.30	19.39	0.20	3	3
21.224	658.7	38.52	575.9	.836	99.1	103.3	557	195.0	.10	0.2	19.33	16.31	19.44	0.40	3	3
21.633	665.2	38.83	582.1	.837	99.2	180.1	735	235.0	.10	0.2	19.33	16.31	19.48	0.70	3	3
21.870	667.4	39.12	584.0	.838	99.2	264.1	893	300.0	.10	0.2	19.34	16.29	19.52	1.00	3	3
22.252	675.8	39.24	592.1	.839	99.5	542.8	1284	300.0	.10	0.2	19.34	16.27	19.52	2.00	3	3
22.561	682.5	39.32	598.7	.841	99.7	1493.9	2151	300.0	.10	0.2	19.33	16.20	19.52	5.00	3	3
22.690	685.2	39.36	601.4	.841	99.8	3359.9	3258	300.0	.10	0.2	19.34	16.11	19.53	10.00	3	3
17.346	586.5	35.97	507.3	.822	96.5	5.8	140	78.5	.10	50.0	19.59	15.70	17.47	0.01	4	4
17.993	596.9	36.55	517.3	.825	96.8	10.2	183	99.9	.10	50.0	19.72	15.84	17.76	0.02	4	4
18.812	608.9	37.35	528.7	.827	97.3	22.6	271	143.0	.10	50.0	19.79	15.93	18.14	0.05	4	4
19.395	617.0	37.93	536.3	.829	97.6	43.4	375	189.8	.10	50.0	19.83	15.97	18.40	0.10	4	4
19.915	624.4	38.43	543.2	.830	98.0	84.2	521	246.2	.10	50.0	19.85	15.99	18.59	0.20	4	4
20.361	631.2	38.81	549.5	.831	98.4	165.4	730	300.0	.10	50.0	19.85	16.00	18.71	0.40	4	4
20.626	636.3	38.95	554.4	.832	98.7	296.1	978	300.0	.10	50.0	19.87	15.98	18.77	0.70	4	4
20.751	638.7	39.01	556.8	.833	98.9	429.3	1179	300.0	.10	50.0	19.87	15.97	18.77	1.00	4	4
20.915	641.9	39.10	559.8	.833	99.1	910.4	1724	300.0	.10	50.0	19.87	15.92	18.79	2.00	4	4
21.028	644.0	39.16	561.9	.834	99.3	2446.4	2839	300.0	.10	50.0	19.86	15.86	18.82	5.00	4	4
21.069	644.8	39.18	562.7	.834	99.3	5006.9	4070	300.0	.10	50.0	19.87	15.83	18.82	10.00	4	4
16.913	574.5	35.93	495.9	.819	95.5	6.0	142	92.2	.10	50.0	20.23	15.67	17.81	0.01	5	5
17.489	581.7	36.61	502.6	.821	96.1	11.1	192	121.7	.10	49.9	20.30	15.75	18.04	0.02	5	5
18.184	589.7	37.48	510.1	.823	96.7	27.0	299	177.5	.10	49.9	20.35	15.78	18.35	0.05	5	5

eff	V_{oc}	J_{sc}	V_{mp}	ff	C_{eff}	τ_{walk}	L_d	X_L	X_f	X_b	log D_0	log D_B	log D_L	τ_{n0}	log S_f	log S_b
18.628	594.6	38.04	514.6	.823	97.2	53.6	422	232.7	.10	49.8	20.36	15.79	18.54	0.10	5	5
19.006	599.1	38.50	518.5	.824	97.6	104.2	587	300.0	.10	46.6	20.38	15.81	18.78	0.20	5	5
19.268	603.4	38.71	522.6	.825	98.1	205.0	823	300.0	.10	46.7	20.40	15.83	18.82	0.40	5	5
19.397	605.4	38.82	524.5	.825	98.4	369.5	1107	300.0	.10	50.0	20.40	15.80	18.82	0.70	5	5
19.453	606.3	38.86	525.4	.825	98.5	528.3	1324	300.0	.10	49.2	20.39	15.80	18.83	1.00	5	5
19.521	607.4	38.92	526.4	.826	98.7	1054.4	1871	300.0	.10	43.6	20.39	15.80	18.92	2.00	5	5
19.564	608.1	38.95	527.1	.826	98.8	2619.7	2949	300.0	.10	43.6	20.39	15.80	18.93	5.00	5	5
19.578	608.4	38.97	527.3	.826	98.8	5282.3	4191	300.0	.10	43.6	20.39	15.78	18.93	10.00	5	5
16.363	562.1	35.65	484.1	.817	94.3	6.5	148	101.6	.10	49.6	20.60	15.59	17.84	0.01	6	6
16.857	567.3	36.34	488.9	.818	94.9	12.4	204	136.3	.10	50.0	20.60	15.64	18.04	0.02	6	6
17.417	572.4	37.16	493.4	.818	95.5	30.2	318	200.7	.10	49.6	20.50	15.67	18.33	0.05	6	6
17.801	579.1	37.51	499.4	.819	95.4	58.5	442	268.3	.12	49.5	20.60	15.70	18.55	0.10	6	6
18.102	584.8	37.73	504.7	.820	95.6	112.7	613	300.0	.14	46.1	20.60	15.74	18.73	0.20	6	6
18.298	589.1	37.81	508.8	.821	95.9	222.5	861	300.0	.16	46.1	20.60	15.75	18.78	0.40	6	6
18.394	591.7	37.81	511.3	.822	95.9	382.3	1128	300.0	.17	49.5	20.60	15.77	18.81	0.70	6	6
18.436	593.0	37.81	512.5	.822	95.9	544.9	1347	300.0	.18	45.1	20.60	15.77	18.87	1.00	6	6
18.486	593.9	37.84	513.4	.823	95.9	1069.6	1885	300.0	.18	45.8	20.60	15.79	18.88	2.00	6	6
18.518	594.5	37.86	514.0	.823	96.0	2640.6	2962	300.0	.18	45.0	20.60	15.79	18.89	5.00	6	6
18.528	594.9	37.85	514.4	.823	95.9	5160.7	4138	300.0	.18	45.8	20.60	15.80	18.89	10.00	6	6
16.160	559.4	35.41	481.4	.816	93.7	6.6	149	102.5	.11	50.0	20.60	15.57	17.80	0.01	7	7
16.642	565.6	36.00	487.2	.817	93.9	12.6	206	139.2	.12	50.0	20.60	15.62	18.03	0.02	7	7
17.226	575.1	36.57	496.0	.819	94.0	29.8	316	199.4	.15	50.0	20.60	15.68	18.33	0.05	7	7
17.599	581.0	36.94	501.3	.820	94.1	57.8	440	257.3	.17	50.0	20.60	15.71	18.54	0.10	7	7
17.907	586.5	37.19	506.4	.821	94.3	112.5	613	300.0	.19	50.0	20.60	15.74	18.69	0.20	7	7
18.109	591.0	37.28	510.7	.822	94.5	221.3	859	300.0	.21	49.6	20.60	15.76	18.77	0.40	7	7
18.208	593.4	37.30	513.0	.823	94.6	381.1	1126	300.0	.22	49.6	20.60	15.77	18.81	0.70	7	7
18.252	594.4	37.32	513.9	.823	94.6	539.4	1339	300.0	.22	45.1	20.60	15.78	18.88	1.00	7	7
18.302	595.5	37.34	515.0	.823	94.6	1070.7	1887	300.0	.23	49.9	20.60	15.79	18.84	2.00	7	7
18.334	596.4	37.33	515.9	.823	94.6	2640.9	2962	300.0	.23	49.9	20.60	15.79	18.86	5.00	7	7
18.345	596.7	37.34	516.2	.823	94.6	5208.1	4159	300.0	.23	49.9	20.60	15.80	18.85	10.00	7	7

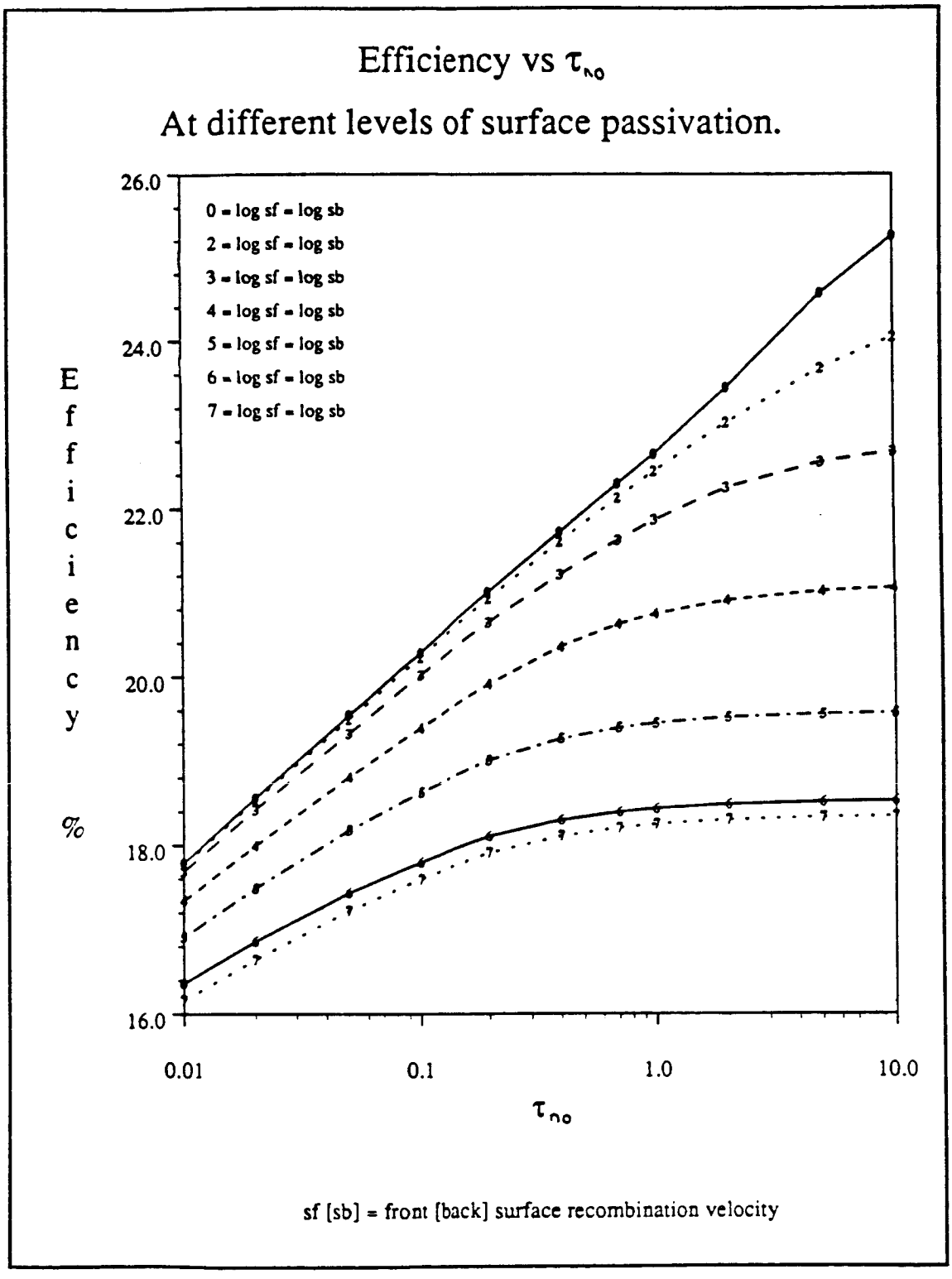
Efficiency vs τ_{no}
At different levels of surface passivation.
0 = log sf = log sb
2 = log sf = log sb
3 = log sf = log sb
4 = log sf = log sb
5 = log sf = log sb
6 = log sf = log sb
7 = log sf = log sb
Efficiency %
26.0
24.0
22.0
20.0
18.0
16.0
0.01
0.1
1.0
10.0
τ_{no}
sf [sb] = front [back] surface recombination velocity

figure 6.62

Table 6.57 Examples of Local Maximums, $X_L \leq 300$ μm, $O_{pl} = 2$

eff	V_{oc}	J_{sc}	V_{mp}	ff	C_{eff}	τ_{bulk}	L_d	X_L	X_f	X_b	log D_0	log D_B	log D_L	τ_{s0}	log S_f	log S_b
25.258	764.2	38.41	689.6	.860	100.0	9861.0	5885	145.1	.10	0.2	17.83	14.00	17.95	10.00	0	0
24.576	769.4	37.65	689.5	.848	100.0	4930.5	4161	94.8	.10	0.2	17.83	14.00	17.93	5.00	0	0
24.178	739.6	38.75	649.3	.844	99.9	899.5	1599	182.3	.10	0.2	17.79	16.47	17.73	5.00	0	0
23.440	776.1	36.37	686.2	.830	100.0	1972.2	2631	49.7	.10	0.2	17.81	14.00	17.82	2.00	0	0
23.328	718.4	38.51	630.9	.843	99.8	317.5	932	161.1	.10	0.2	17.82	16.55	17.69	2.00	0	0
22.440	776.9	35.54	675.9	.813	100.0	986.1	1861	34.0	.10	0.2	17.75	14.00	17.78	1.00	0	0
22.653	703.0	38.27	617.0	.842	99.7	167.4	679	142.6	.10	0.2	17.79	16.54	17.79	1.00	0	0
20.996	765.0	35.00	646.6	.784	100.0	394.4	1177	27.1	.10	0.2	17.76	14.00	17.76	0.40	0	0
21.729	683.7	37.82	599.5	.840	99.5	69.7	440	115.2	.10	0.2	17.99	16.52	17.31	0.40	0	0
23.978	728.9	39.44	641.6	.834	100.0	9861.0	5885	299.3	.10	0.2	18.89	14.00	19.13	10.00	2	2
24.050	721.9	39.40	635.5	.846	99.9	2261.2	2600	300.0	.10	0.2	18.81	16.33	18.98	10.00	2	2
23.459	728.6	38.94	638.0	.827	100.0	4930.5	4161	203.6	.10	0.2	18.92	14.00	19.05	5.00	2	2
23.675	713.0	39.36	626.6	.844	99.8	989.1	1692	300.0	.10	0.2	18.81	16.42	18.97	5.00	2	2
22.567	726.1	38.15	630.2	.815	100.0	1972.2	2631	124.7	.10	0.2	18.89	14.00	18.97	2.00	2	2
23.025	701.2	38.98	615.6	.842	99.7	366.2	1017	230.9	.10	0.2	18.79	16.48	18.93	2.00	2	2
22.474	687.5	39.44	600.7	.829	100.0	9861.0	5885	300.0	.10	0.2	19.41	14.00	19.65	10.00	3	3
22.690	685.2	39.36	601.4	.841	99.8	3359.9	3258	300.0	.10	0.2	19.34	16.11	19.53	10.00	3	3
22.190	685.9	39.42	596.7	.821	100.0	4930.5	4161	295.0	.10	0.2	19.42	14.00	19.64	5.00	3	3
22.561	682.5	39.32	598.7	.841	99.7	1493.9	2151	300.0	.10	0.2	19.33	16.20	19.52	5.00	3	3
21.600	683.0	38.87	591.6	.814	100.0	1972.2	2631	193.8	.10	0.2	19.42	14.00	19.56	2.00	3	3
22.252	675.8	39.24	592.1	.839	99.5	542.8	1284	300.0	.10	0.2	19.34	16.27	19.52	2.00	3	3
21.006	680.1	38.26	586.6	.807	100.0	985.1	1859	132.8	.10	0.2	19.40	14.03	19.52	1.00	3	3
21.870	667.4	39.12	584.0	.838	99.2	264.1	893	300.0	.10	0.2	19.34	16.29	19.52	1.00	3	3
21.224	658.7	38.52	576.0	.836	99.1	102.7	555	195.2	.10	0.2	19.33	16.31	19.44	0.40	3	3

Table 6.58 No BSF for cases with local maximums, $X_L \leq 300$ μm, $O_{pl} = 2$

eff	V_{oc}	J_{sc}	V_{mp}	ff	C_{eff}	τ_{bulk}	L_d	X_L	X_f	X_b	log D_0	log D_B	log D_L	τ_{s0}	log S_f	log S_b
23.315	717.1	38.54	630.1	.844	99.8	303.3	907	164.6	.10	0.	17.81	16.58	0.	2.00	0	0
24.144	735.7	38.82	647.1	.845	99.9	784.8	1474	192.8	.10	0.	17.82	16.53	0.	5.00	0	0
24.712	745.9	39.01	658.9	.849	99.9	1698.0	2200	216.1	.10	0.	17.81	16.46	0.	10.00	0	0

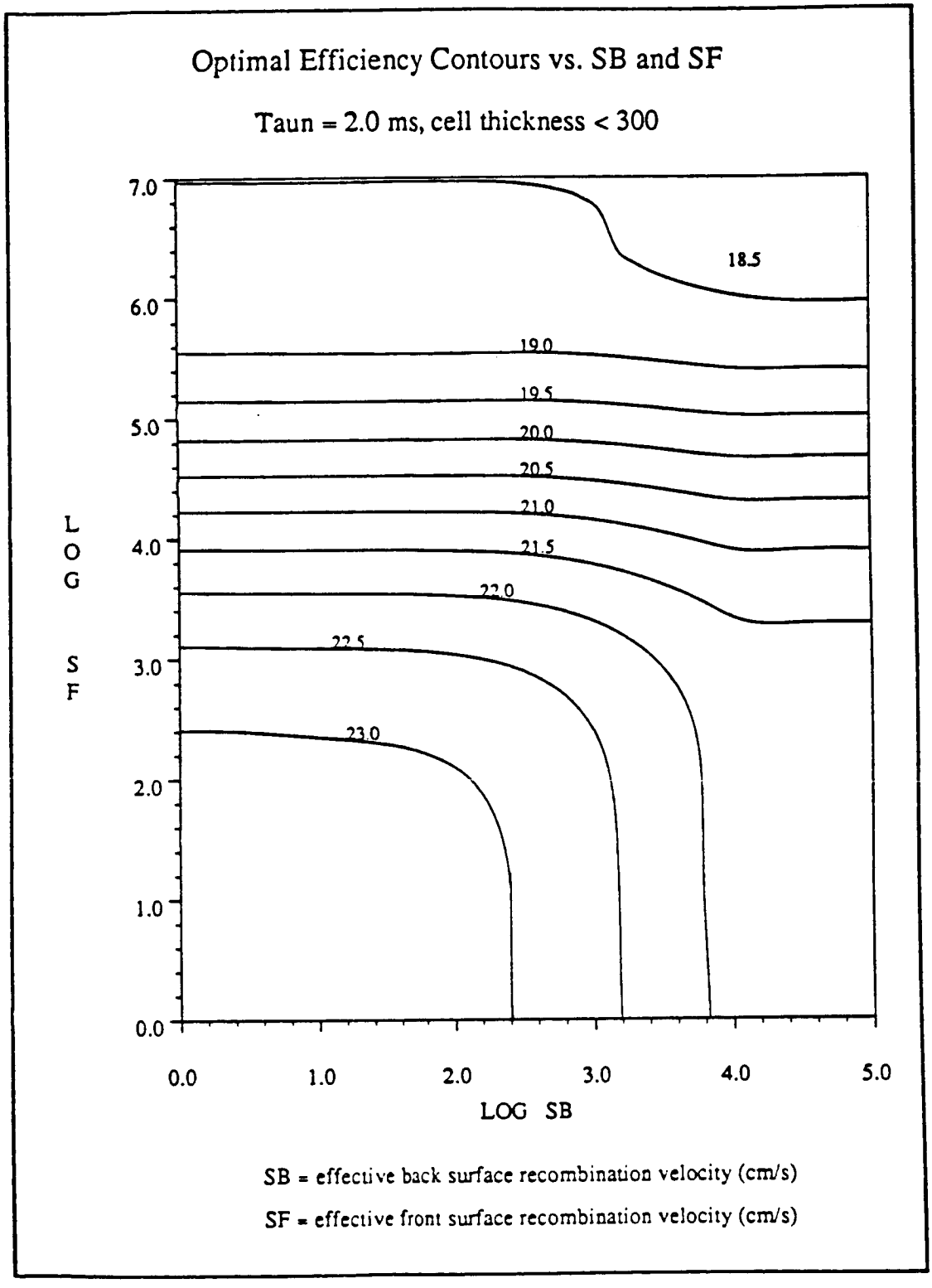
Optimal Efficiency Contours vs. SB and SF
Taun = 2.0 ms, cell thickness < 300
7.0
6.0
5.0
4.0
3.0
2.0
1.0
0.0
LOG SF
18.5
19.0
19.5
20.0
20.5
21.0
21.5
22.0
22.5
23.0
0.0
1.0
2.0
3.0
4.0
5.0
LOG SB
SB = effective back surface recombination velocity (cm/s)
SF = effective front surface recombination velocity (cm/s)

figure 6.63

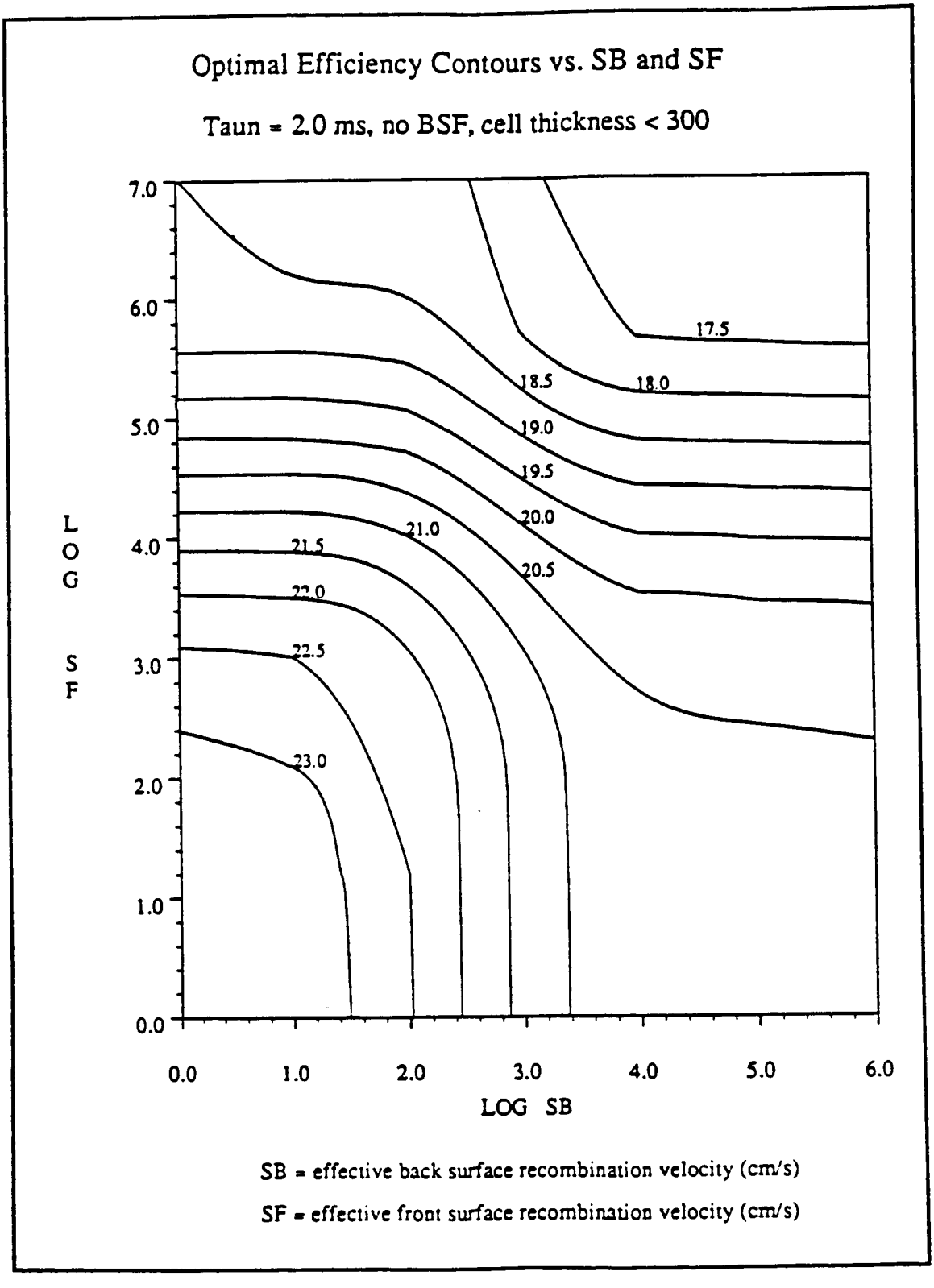
Optimal Efficiency Contours vs. SB and SF
Taun = 2.0 ms, no BSF, cell thickness < 300
7.0
6.0
5.0
4.0
3.0
2.0
1.0
0.0
LOG SF
17.5
18.0
18.5
19.0
19.5
20.0
20.5
21.0
21.5
22.0
22.5
23.0
0.0
1.0
2.0
3.0
4.0
5.0
6.0
LOG SB
SB = effective back surface recombination velocity (cm/s)
SF = effective front surface recombination velocity (cm/s)

figure 6.64

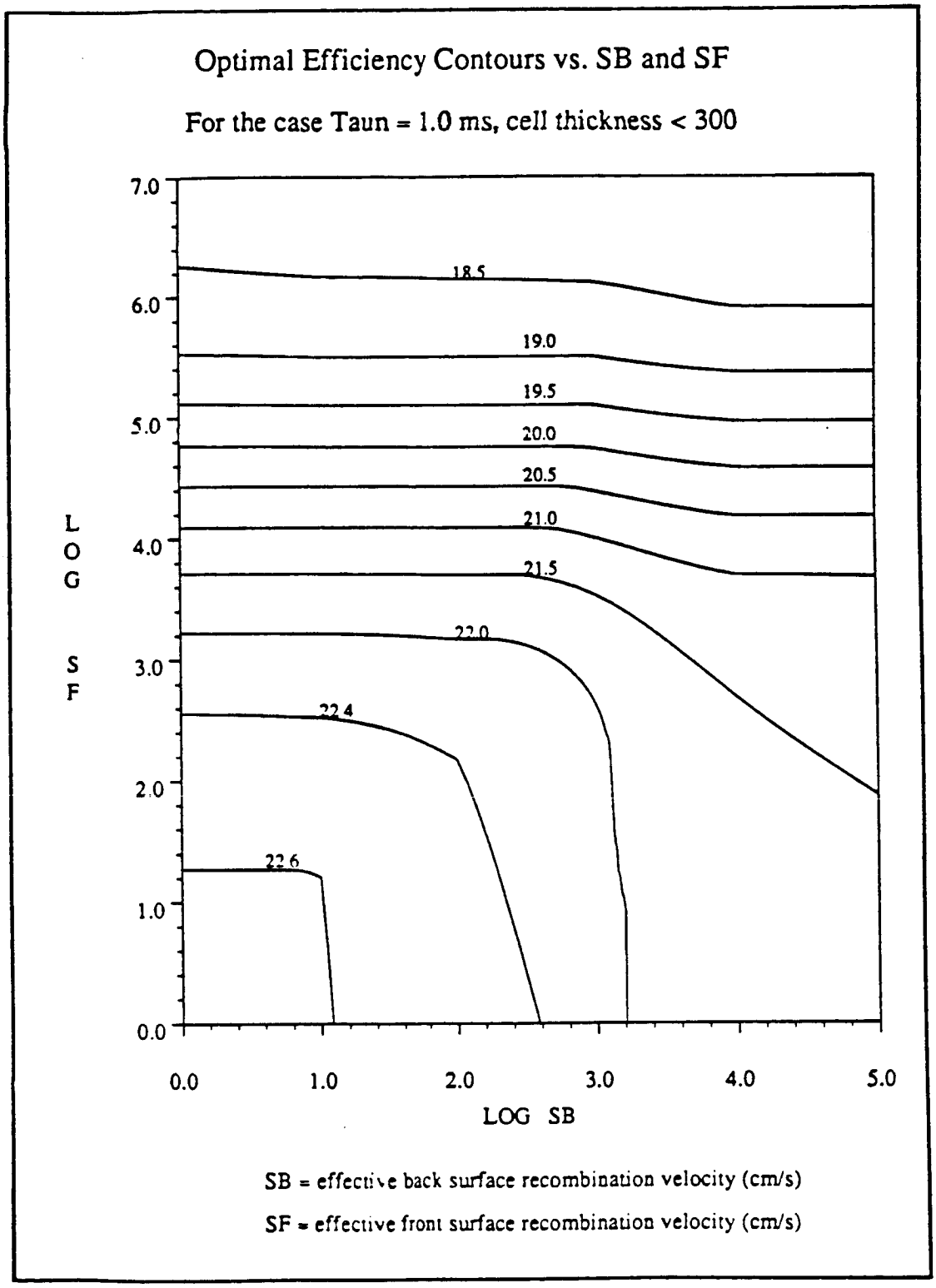
Optimal Efficiency Contours vs. SB and SF
For the case Taun = 1.0 ms, cell thickness < 300
7.0
6.0
5.0
4.0
3.0
2.0
1.0
0.0
LOG SF
18.5
19.0
19.5
20.0
20.5
21.0
21.5
22.0
22.4
22.6
0.0
1.0
2.0
3.0
4.0
5.0
LOG SB
SB = effective back surface recombination velocity (cm/s)
SF = effective front surface recombination velocity (cm/s)

figure 6.65

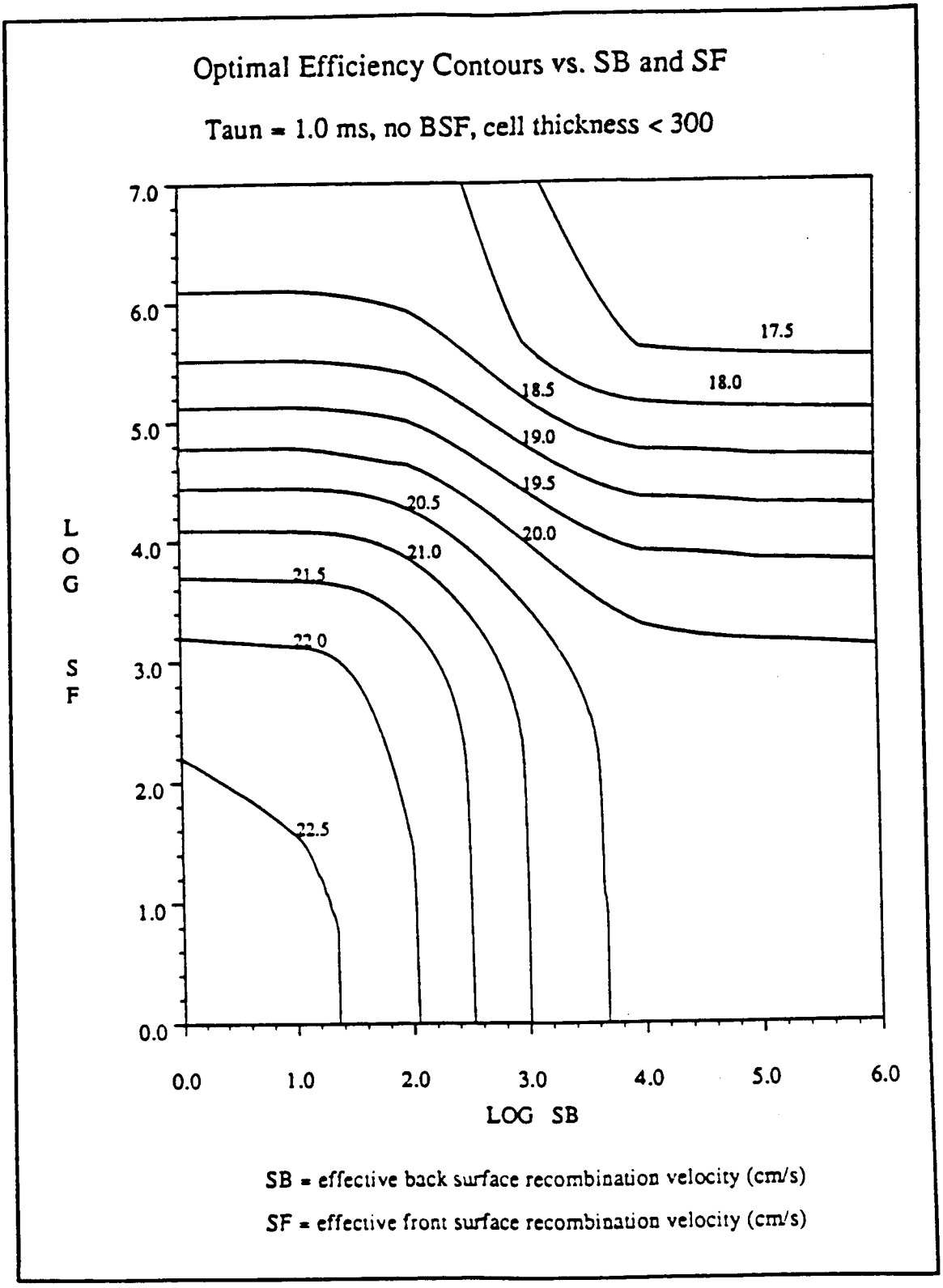
Optimal Efficiency Contours vs. SB and SF
Taun = 1.0 ms, no BSF, cell thickness < 300
7.0
6.0
5.0
4.0
3.0
2.0
1.0
0.0
LOG SF
17.5
18.0
18.5
19.0
19.5
20.0
20.5
21.0
21.5
22.0
22.5
0.0
1.0
2.0
3.0
4.0
5.0
6.0
LOG SB
SB = effective back surface recombination velocity (cm/s)
SF = effective front surface recombination velocity (cm/s)

figure 6.66

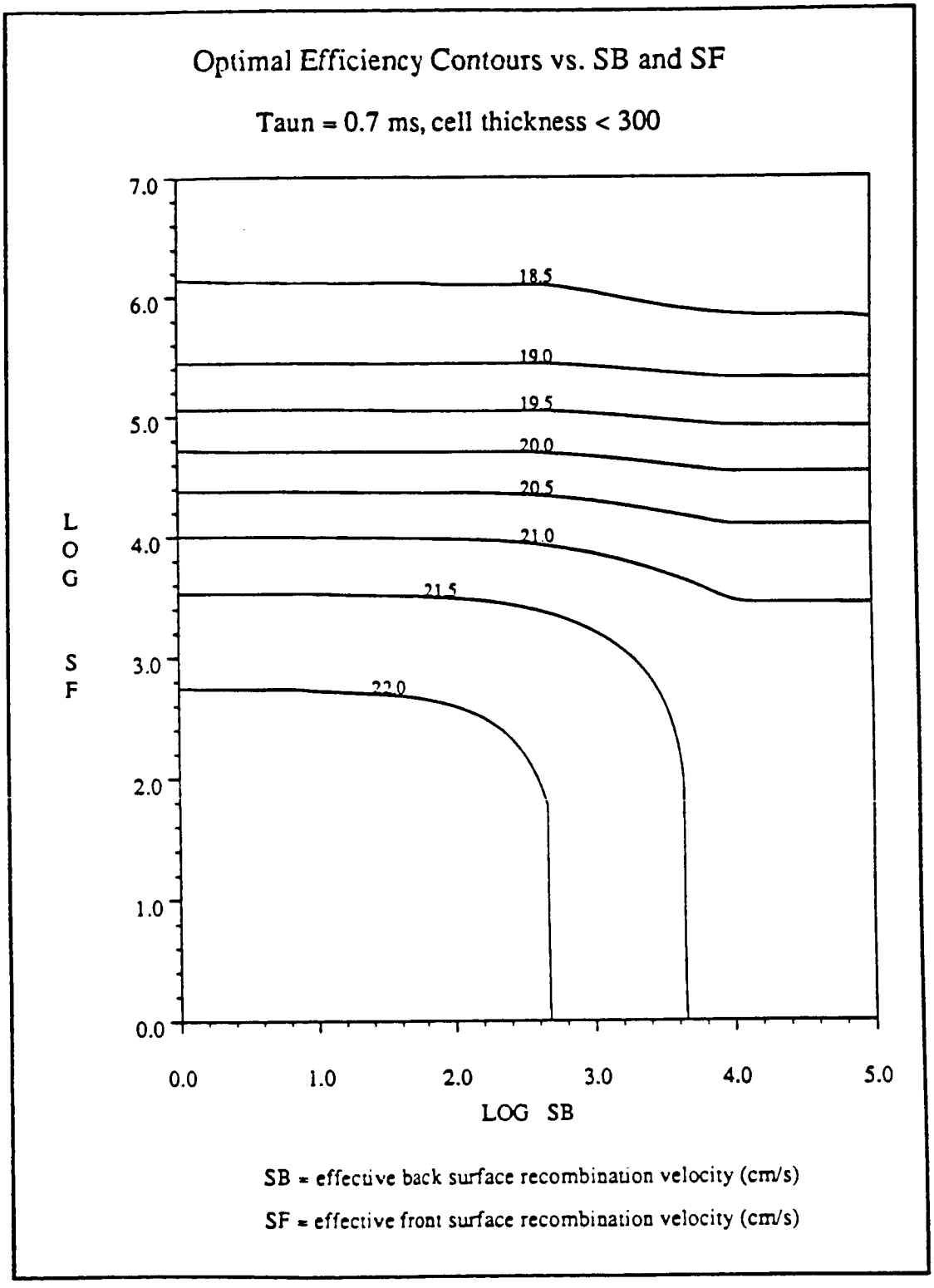
Optimal Efficiency Contours vs. SB and SF
Taun = 0.7 ms, cell thickness < 300
7.0
6.0
5.0
4.0
3.0
2.0
1.0
0.0
LOG SF
18.5
19.0
19.5
20.0
20.5
21.0
21.5
22.0
0.0
1.0
2.0
3.0
4.0
5.0
LOG SB
SB = effective back surface recombination velocity (cm/s)
SF = effective front surface recombination velocity (cm/s)

figure 6.67

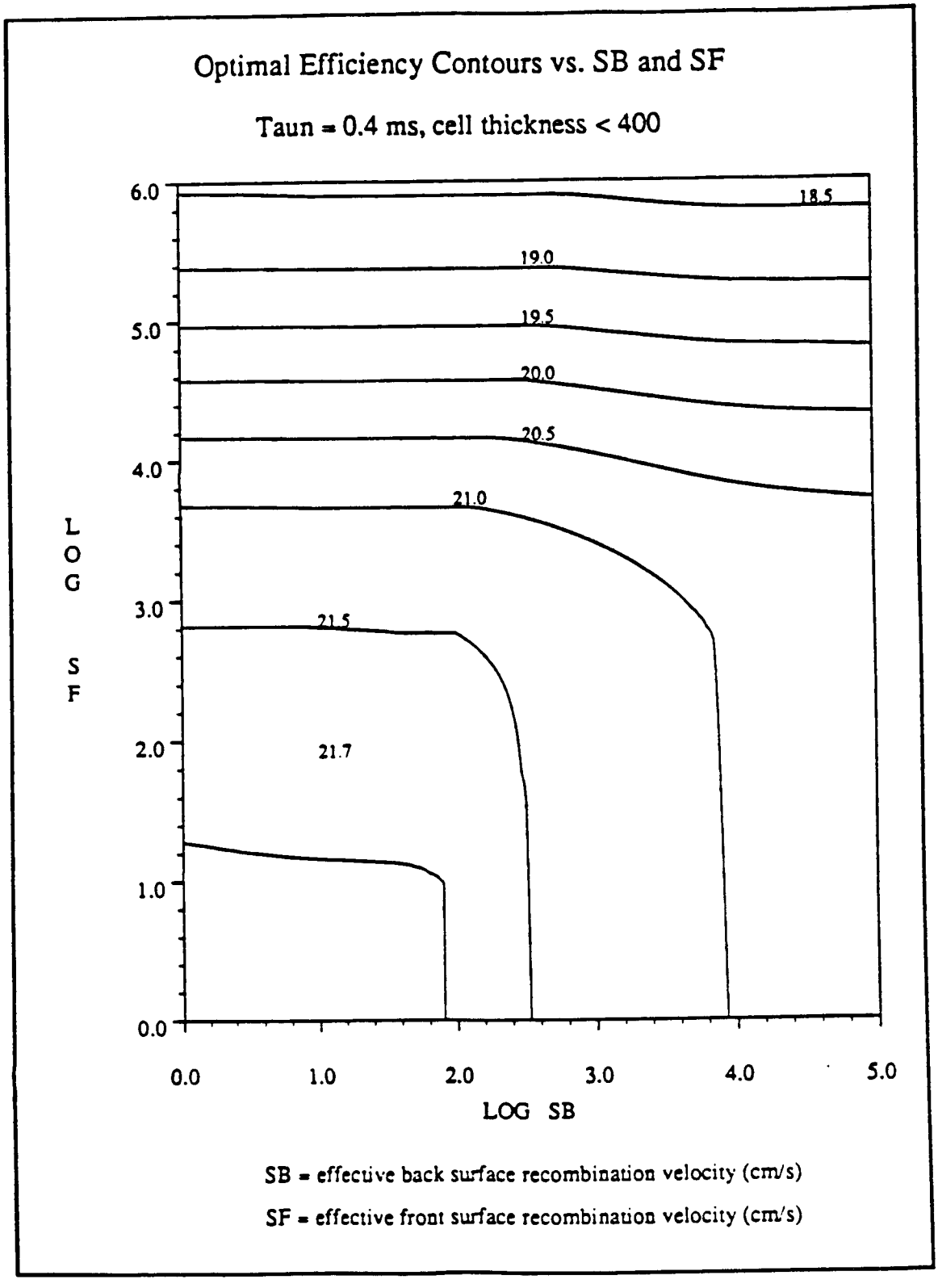
Optimal Efficiency Contours vs. SB and SF
Taun = 0.4 ms, cell thickness < 400
6.0
5.0
4.0
3.0
2.0
1.0
0.0
LOG SF
18.5
19.0
19.5
20.0
20.5
21.0
21.5
21.7
0.0
1.0
2.0
3.0
4.0
5.0
LOG SB
SB = effective back surface recombination velocity (cm/s)
SF = effective front surface recombination velocity (cm/s)

figure 6.68

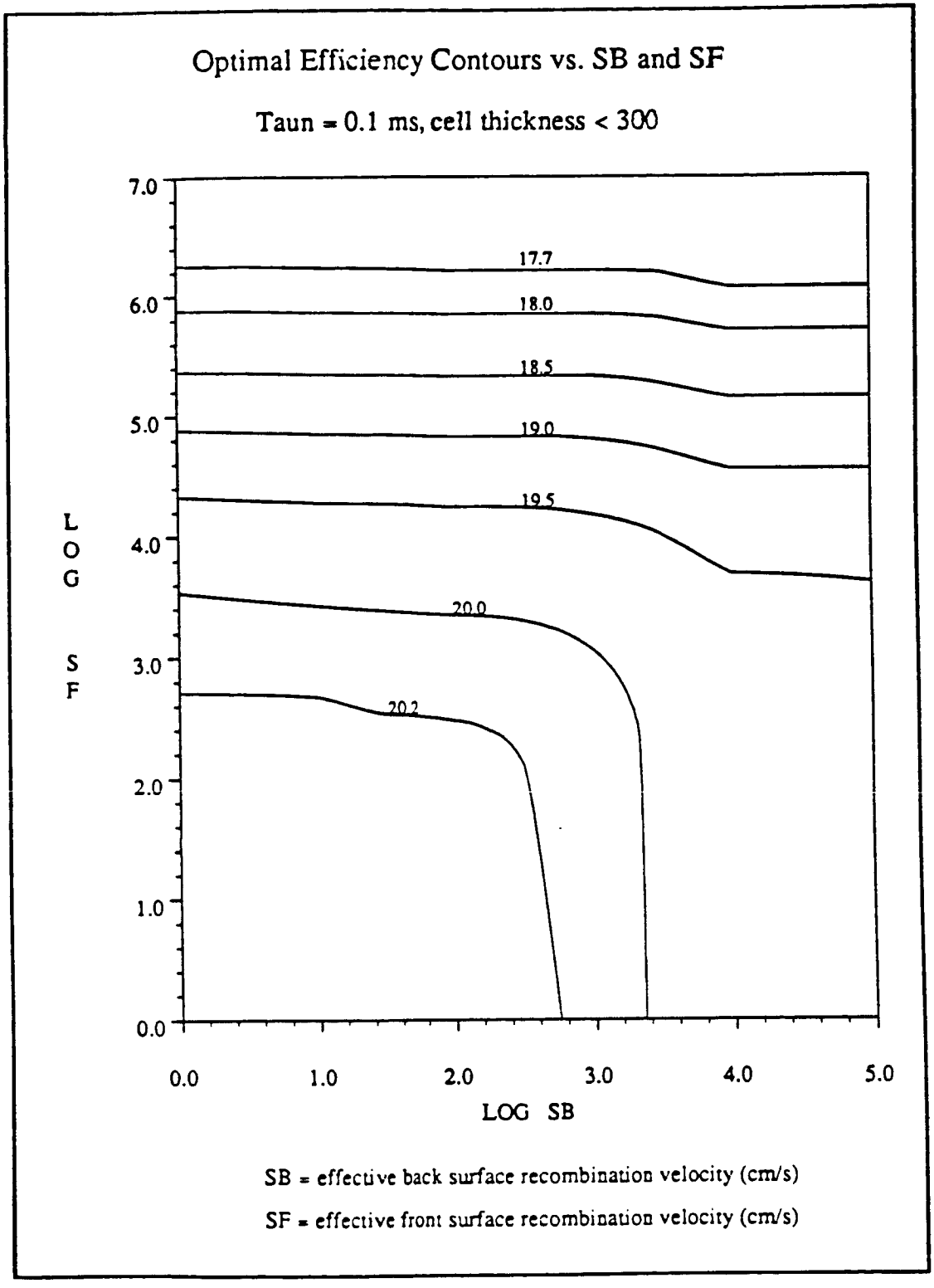
Optimal Efficiency Contours vs. SB and SF
Taun = 0.1 ms, cell thickness < 300
7.0
6.0
5.0
4.0
3.0
2.0
1.0
0.0
LOG SF
17.7
18.0
18.5
19.0
19.5
20.0
20.2
0.0
1.0
2.0
3.0
4.0
5.0
LOG SB
SB = effective back surface recombination velocity (cm/s)
SF = effective front surface recombination velocity (cm/s)

figure 6.69

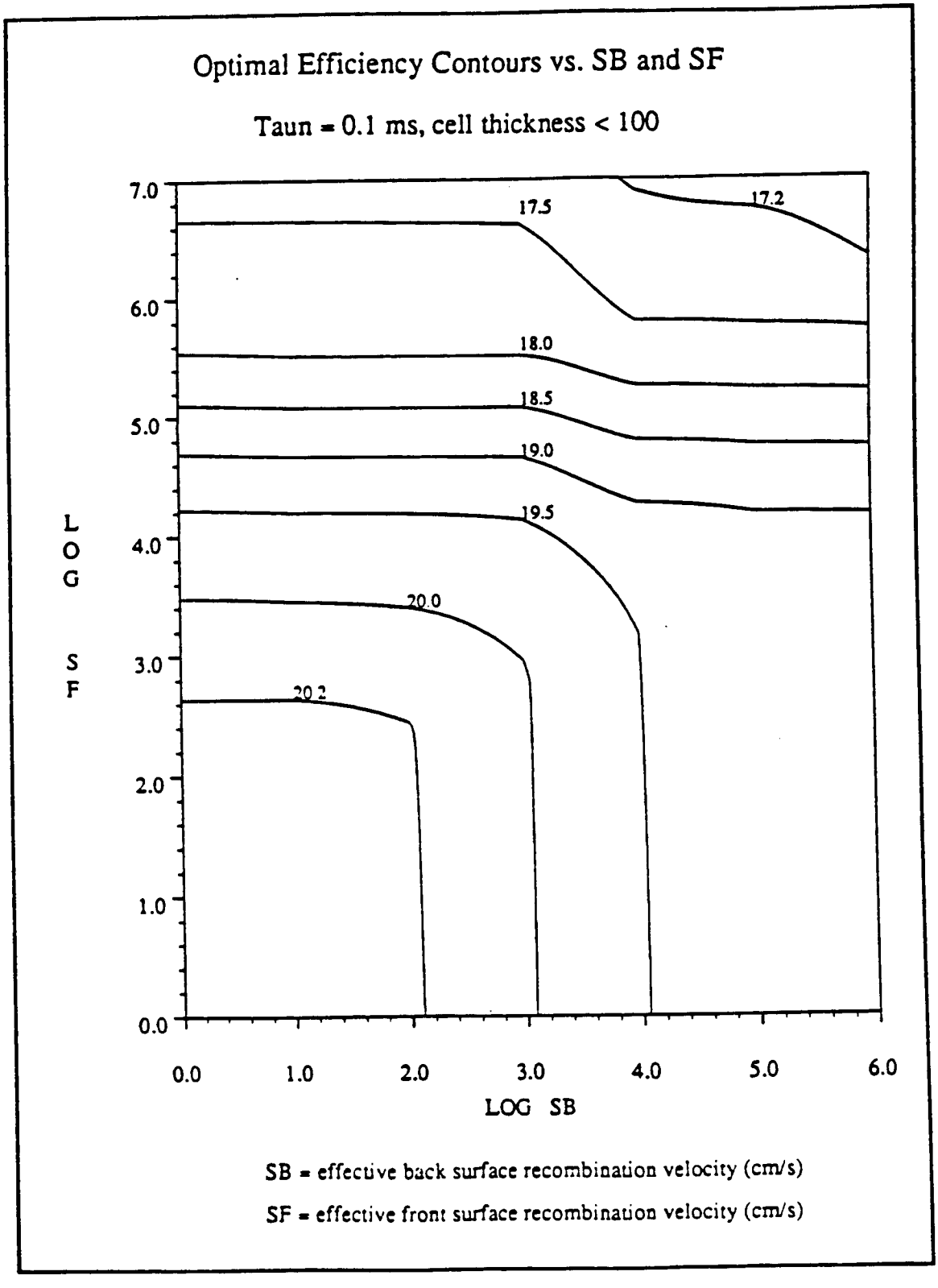
Optimal Efficiency Contours vs. SB and SF
Taun = 0.1 ms, cell thickness < 100
17.5
17.2
18.0
18.5
19.0
19.5
20.0
20.2
7.0
6.0
5.0
4.0
3.0
2.0
1.0
0.0
LOG SF
0.0
1.0
2.0
3.0
4.0
5.0
6.0
LOG SB
SB = effective back surface recombination velocity (cm/s)
SF = effective front surface recombination velocity (cm/s)

figure 6.70

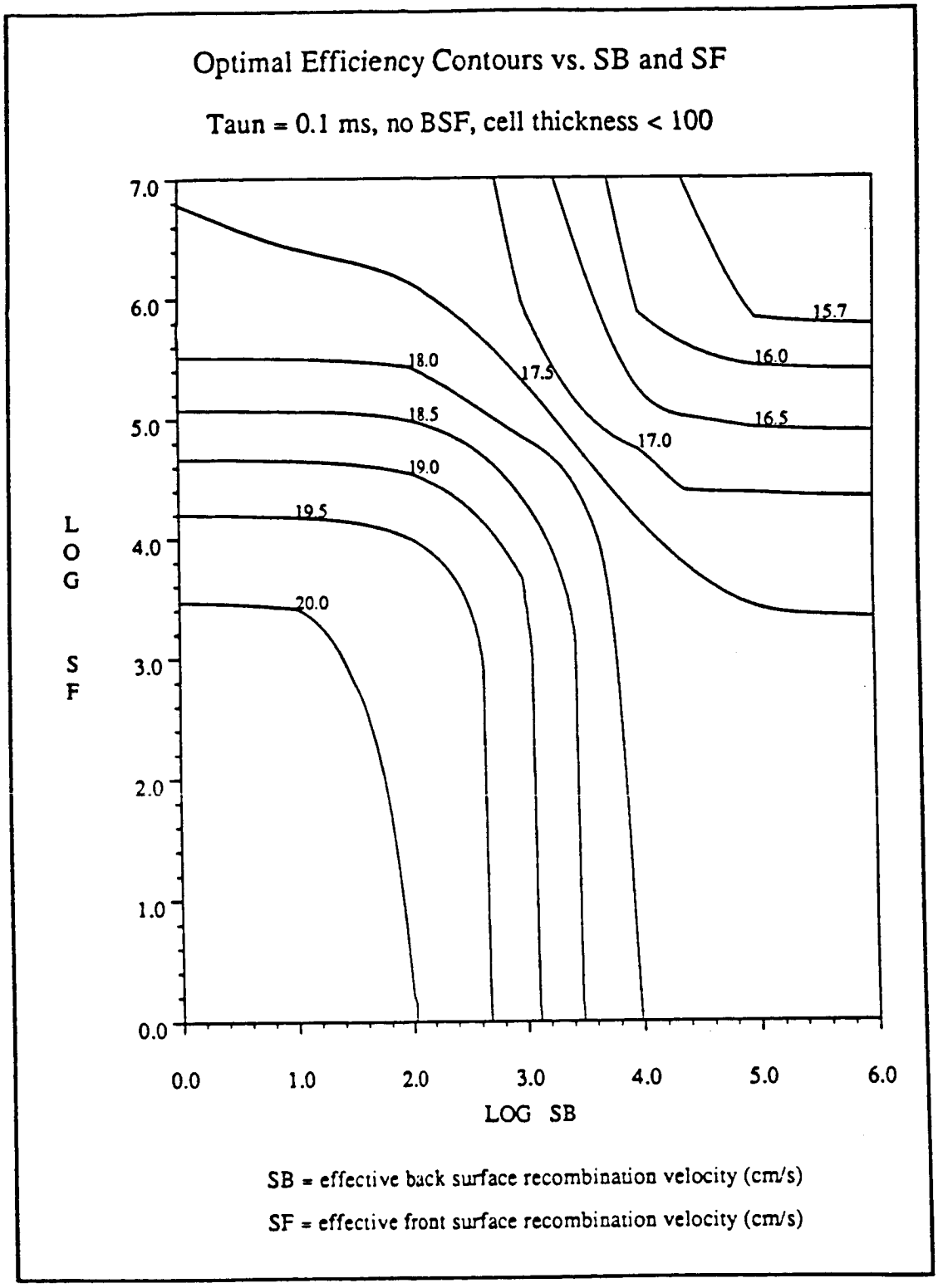
Optimal Efficiency Contours vs. SB and SF
Taun = 0.1 ms, no BSF, cell thickness < 100
7.0
6.0
5.0
4.0
3.0
2.0
1.0
0.0
LOG SF
0.0
1.0
2.0
3.0
4.0
5.0
6.0
LOG SB
15.7
16.0
16.5
17.0
17.5
18.0
18.5
19.0
19.5
20.0
SB = effective back surface recombination velocity (cm/s)
SF = effective front surface recombination velocity (cm/s)

figure 6.71

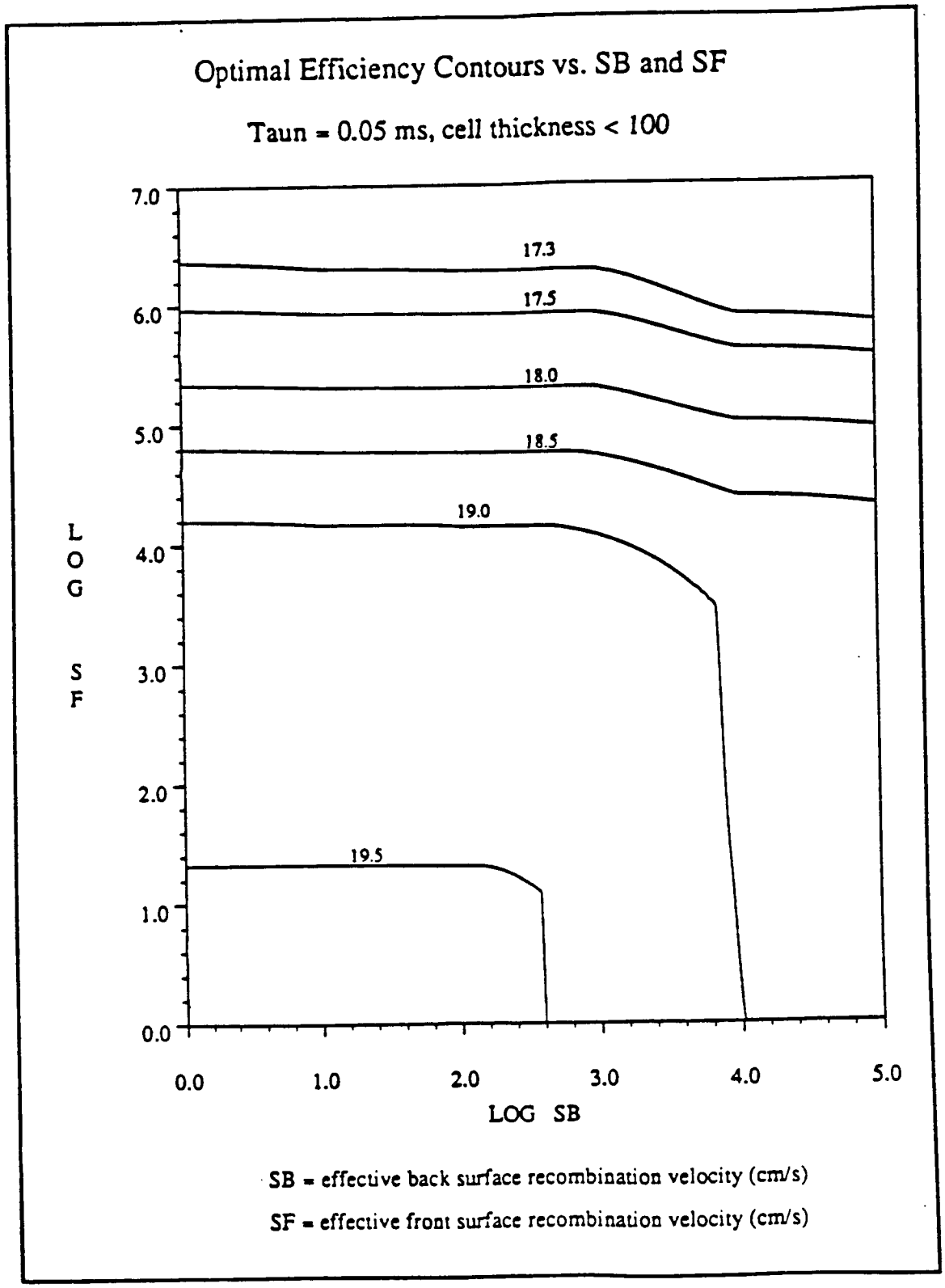
Optimal Efficiency Contours vs. SB and SF
Taun = 0.05 ms, cell thickness < 100
7.0
6.0
5.0
4.0
3.0
2.0
1.0
0.0
LOG SF
17.3
17.5
18.0
18.5
19.0
19.5
0.0
1.0
2.0
3.0
4.0
5.0
LOG SB
SB = effective back surface recombination velocity (cm/s)
SF = effective front surface recombination velocity (cm/s)

figure 6.72

Table 6.59 Effect of S_f and S_b at τ_{n0} = 2.0 ms, $X_L \leq 500$ μm, $O_{pl} = 2$

eff	V_{oc}	J_{sc}	V_{mp}	ff	C_{eff}	τ_{bulk}	L_d	X_L	X_f	X_b	log D_0	log D_B	log D_L	log S_f	log S_b
23.328	719.6	38.44	632.0	.843	99.8	317.5	932	154.1	0.10	0.2	17.82	16.55	17.84	0	0.
23.301	716.8	38.55	629.5	.843	99.8	323.8	944	166.1	0.10	0.2	17.98	16.54	18.37	0	1.0
23.159	707.9	38.81	621.7	.843	99.7	346.6	984	202.2	0.10	0.2	18.03	16.51	18.91	0	2.0
22.644	686.9	39.22	602.4	.840	99.4	464.0	1171	308.1	0.10	0.2	17.96	16.36	19.51	0	3.0
21.962	667.3	39.27	584.2	.838	98.4	559.7	1307	484.8	0.10	50.0	17.93	16.25	18.85	0	4.0
21.945	666.9	39.27	583.8	.838	98.4	556.0	1302	500.0	0.10	50.0	18.26	16.25	18.95	0	5.0
21.944	666.9	39.27	583.8	.838	98.4	554.5	1300	500.0	0.10	50.0	18.18	16.26	18.96	0	6.0
23.301	716.3	38.59	629.0	.843	99.8	327.2	950	169.5	0.10	0.2	18.31	16.54	17.93	1	0.
23.207	712.2	38.80	623.3	.840	99.8	449.1	1149	194.2	0.10	0.2	18.28	16.38	19.15	1	1.0
23.140	707.2	38.83	621.0	.843	99.7	357.8	1003	204.4	0.10	0.2	18.32	16.49	18.91	1	2.0
22.635	686.3	39.25	601.7	.840	99.3	467.2	1176	318.0	0.10	0.2	18.30	16.35	19.56	1	3.0
21.954	667.1	39.27	584.0	.838	98.4	546.3	1289	497.7	0.10	50.0	18.80	16.27	18.85	1	4.0
21.941	666.8	39.27	583.7	.838	98.4	556.4	1303	500.0	0.10	50.0	18.26	16.25	18.95	1	5.0
21.940	666.8	39.26	583.7	.838	98.4	552.3	1297	499.4	0.10	50.0	18.43	16.26	18.98	1	6.0
23.153	707.3	38.84	621.1	.843	99.7	348.0	986	203.5	0.10	0.2	18.81	16.51	17.92	2	0.
23.134	706.5	38.85	620.5	.843	99.7	345.1	981	205.0	0.10	0.2	18.79	16.51	18.38	2	1.0
23.025	701.2	38.98	615.6	.842	99.6	366.2	1017	230.9	0.10	0.2	18.79	16.48	18.90	2	2.0
22.578	684.5	39.25	600.2	.840	99.3	469.2	1179	319.3	0.10	0.2	18.81	16.35	19.54	2	3.0
21.929	666.0	39.30	582.9	.838	98.5	575.1	1328	495.9	0.10	50.0	18.81	16.23	18.84	2	4.0
21.913	665.9	39.27	582.9	.838	98.4	561.4	1309	500.0	0.10	50.0	18.80	16.25	18.95	2	5.0
21.911	665.7	39.29	582.7	.838	98.4	572.6	1325	500.0	0.10	50.0	18.81	16.24	18.96	2	6.0
22.605	684.0	39.33	599.8	.840	99.6	437.7	1132	311.1	0.10	0.2	19.32	16.39	18.24	3	0.
22.561	686.0	39.09	602.1	.841	99.7	398.4	1070	249.6	0.10	0.2	19.33	16.44	19.13	3	1.0
22.545	682.6	39.31	598.5	.840	99.6	444.4	1142	309.6	0.10	0.2	19.32	16.38	18.97	3	2.0
22.272	673.9	39.42	590.0	.838	99.4	557.8	1305	371.9	0.10	0.2	19.38	16.25	19.50	3	3.0
21.755	660.4	39.37	577.5	.837	98.6	643.2	1416	500.0	0.10	50.0	19.34	16.17	18.84	3	4.0
21.740	660.1	39.37	577.2	.837	98.6	655.0	1431	500.0	0.10	50.0	19.34	16.16	18.95	3	5.0
21.739	660.2	39.36	577.2	.837	98.6	649.4	1424	500.0	0.10	50.0	19.33	16.16	18.96	3	6.0
21.475	649.2	39.66	566.4	.834	99.4	596.4	1356	500.0	0.10	0.2	19.94	16.21	18.05	4	0.
21.473	649.2	39.66	566.4	.834	99.4	599.8	1360	500.0	0.10	0.2	19.95	16.21	18.85	4	1.0
21.457	648.9	39.65	566.1	.834	99.4	610.8	1375	498.0	0.10	0.2	19.94	16.20	18.95	4	2.0
21.377	647.2	39.63	564.4	.833	99.3	679.1	1461	500.0	0.10	0.2	19.95	16.13	19.98	4	3.0
21.042	640.1	39.52	557.4	.832	99.0	889.8	1702	500.0	0.10	50.0	19.78	15.94	18.78	4	4.0
21.040	640.3	39.48	557.8	.832	98.9	851.5	1661	499.9	0.10	50.0	19.86	15.98	18.97	4	5.0
21.039	640.4	39.47	557.9	.832	98.9	839.1	1647	499.9	0.10	50.0	19.86	15.99	18.96	4	6.0
19.930	611.0	39.49	529.6	.826	98.9	701.5	1488	500.0	0.10	0.2	20.47	16.11	18.09	5	0.
19.929	611.0	39.48	529.6	.826	98.9	687.7	1472	500.0	0.10	0.2	20.47	16.12	18.97	5	1.0
19.923	610.9	39.49	529.4	.826	98.9	722.2	1513	500.0	0.10	0.2	20.47	16.09	19.35	5	2.0
19.883	610.4	39.46	528.8	.825	98.9	788.9	1591	500.0	0.10	0.2	20.48	16.03	19.56	5	3.0
19.688	607.3	39.33	525.5	.824	98.5	962.7	1779	500.0	0.10	50.0	20.40	15.88	18.80	5	4.0
19.679	607.0	39.33	525.3	.824	98.5	965.8	1782	500.0	0.10	50.0	20.34	15.88	18.92	5	5.0
19.680	607.1	39.33	525.2	.824	98.5	992.6	1809	500.0	0.10	50.0	20.39	15.85	18.91	5	6.0
18.807	596.3	38.33	515.6	.823	96.0	709.4	1498	500.0	0.18	0.2	20.60	16.10	18.95	6	0.
18.806	596.1	38.34	515.4	.823	96.0	711.4	1500	500.0	0.18	0.2	20.60	16.10	18.96	6	1.0
18.801	596.2	38.32	515.5	.823	96.0	718.3	1509	500.0	0.18	0.2	20.60	16.10	19.22	6	2.0
18.766	595.7	38.31	514.7	.822	96.0	804.9	1609	500.0	0.18	0.2	20.60	16.02	19.68	6	3.0
18.659	594.0	38.25	512.7	.821	95.8	980.9	1797	500.0	0.18	50.0	20.60	15.86	18.80	6	4.0
18.653	594.0	38.24	512.7	.821	95.8	974.3	1790	500.0	0.18	50.0	20.60	15.87	18.91	6	5.0
18.652	594.0	38.24	512.7	.821	95.8	979.9	1796	500.0	0.18	50.0	20.60	15.86	18.93	6	6.0
18.629	598.0	37.83	517.3	.823	94.8	700.2	1487	500.0	0.23	0.2	20.60	16.11	18.15	7	0.
18.628	598.0	37.83	517.2	.823	94.8	704.1	1492	500.0	0.23	0.2	20.60	16.11	18.77	7	1.0

eff	V_{oc}	J_{sc}	V_{mp}	ff	C_{eff}	τ_{bulk}	L_d	X_L	X_f	X_b	log D_0	log D_B	log D_L	log S_f	log S_b
18.622	597.9	37.83	517.1	.823	94.8	718.7	1509	500.0	0.23	0.2	20.60	16.09	19.05	7	2.0
18.545	598.1	37.61	518.1	.824	94.2	512.5	1242	500.0	0.23	0.2	20.60	16.30	19.50	7	3.0
18.478	595.8	37.75	514.8	.822	94.6	988.2	1805	500.0	0.23	50.0	20.60	15.86	18.79	7	4.0
18.472	595.7	37.74	514.4	.822	94.5	986.9	1803	500.0	0.23	50.0	20.60	15.86	18.91	7	5.0
18.471	595.7	37.74	514.3	.822	94.6	988.2	1805	500.0	0.23	50.0	20.60	15.86	18.92	7	6.0
18.610	598.2	37.78	517.5	.823	94.7	701.7	1489	500.0	0.24	0.2	20.60	16.11	17.90	8	0.
18.609	598.2	37.78	517.5	.823	94.6	703.9	1491	500.0	0.24	0.2	20.60	16.11	18.77	8	1.0
18.603	598.1	37.78	517.3	.823	94.6	718.7	1509	500.0	0.24	0.2	20.60	16.09	19.13	8	2.0
18.568	597.7	37.76	516.6	.823	94.6	802.8	1607	500.0	0.24	0.2	20.60	16.02	19.68	8	3.0
18.459	595.9	37.70	514.5	.822	94.5	989.5	1806	500.0	0.23	50.0	20.60	15.86	18.79	8	4.0
18.453	595.9	37.69	514.5	.822	94.4	988.1	1805	500.0	0.23	50.0	20.60	15.86	18.91	8	5.0
18.452	595.9	37.69	514.5	.822	94.4	987.8	1804	500.0	0.23	50.0	20.60	15.86	18.92	8	6.0

Table 6.60 Effect of S_f and S_b at τ_{n0} = 2.0 ms, $X_L \leq 300$ μm, $O_{pl} = 2$

eff	V_{oc}	J_{sc}	V_{mp}	ff	C_{eff}	τ_{bulk}	L_d	X_L	X_f	X_b	log D_0	log D_B	log D_L	log S_f	log S_b
18.488	595.9	37.83	513.7	.820	94.2	921.4	1736	740.6	0.23	73.1	20.60	15.91	18.76	∞	∞

Table 6.61 Effect of S_f and S_b at τ_{n0} = 2.0 ms, $X_L \leq 300$ μm, O_{pl} = 2

eff	V_{oc}	J_{sc}	V_{mp}	ff	C_{eff}	τ_{bulk}	L_d	X_L	X_f	X_b	log D_0	log D_B	log D_L	log S_f	log S_b
23.328	718.4	38.51	630.9	.843	99.8	317.5	932	161.1	0.10	0.2	17.82	16.55	17.69	0	0.
23.302	716.7	38.56	629.4	.843	99.8	323.8	944	167.1	0.10	0.2	17.81	16.54	18.32	0	1.0
23.159	708.0	38.81	621.8	.843	99.7	346.6	984	201.5	0.10	0.2	17.82	16.51	18.92	0	2.0
22.643	687.3	39.20	602.7	.841	99.4	464.0	1171	300.0	0.10	0.2	17.81	16.36	19.51	0	3.0
21.872	669.2	38.98	586.1	.839	98.8	627.3	1396	300.0	0.10	50.0	17.81	16.18	18.83	0	4.0
21.847	668.8	38.96	585.8	.838	98.8	627.1	1396	300.0	0.10	50.0	17.80	16.18	18.94	0	5.0
23.301	716.3	38.59	629.0	.843	99.8	327.2	950	169.5	0.10	0.2	18.28	16.54	17.70	1	0.
23.272	712.1	38.77	625.3	.843	99.7	334.4	963	194.2	0.10	0.2	18.28	16.53	18.34	1	1.0
23.140	707.1	38.83	621.0	.843	99.7	352.1	993	204.4	0.10	0.2	18.28	16.50	18.91	1	2.0
22.634	687.0	39.20	602.4	.840	99.4	468.0	1177	300.0	0.10	0.2	18.27	16.35	19.52	1	3.0
21.868	669.0	38.98	586.0	.839	98.8	623.3	1391	300.0	0.10	50.0	18.28	16.19	18.82	1	4.0
21.843	668.7	38.96	585.6	.838	98.8	628.4	1398	300.0	0.10	50.0	18.29	16.18	18.94	1	5.0
23.153	707.1	38.84	621.2	.843	99.7	336.2	966	203.5	0.10	0.2	18.81	16.53	17.72	2	0.
23.135	706.5	38.85	620.6	.843	99.7	345.1	981	205.0	0.10	0.2	18.81	16.51	18.34	2	1.0
23.025	701.2	38.98	615.6	.842	99.7	366.2	1017	230.9	0.10	0.2	18.79	16.48	18.93	2	2.0
22.575	685.2	39.21	600.8	.840	99.4	478.7	1193	300.0	0.10	0.2	18.81	16.34	19.53	2	3.0
21.837	668.1	38.99	585.0	.838	98.8	640.5	1413	300.0	0.10	50.0	18.81	16.17	18.82	2	4.0
21.812	667.7	38.97	584.7	.838	98.8	643.4	1417	300.0	0.10	50.0	18.82	16.17	18.94	2	5.0
22.606	684.5	39.29	600.4	.841	99.6	419.2	1103	300.0	0.10	0.2	19.34	16.41	17.81	3	0.
22.579	686.5	39.10	602.5	.841	99.7	401.7	1075	249.6	0.10	0.2	19.33	16.43	18.37	3	1.0
22.545	683.0	39.28	598.9	.840	99.6	444.4	1142	300.0	0.10	0.2	19.34	16.38	18.97	3	2.0
22.252	675.8	39.24	592.1	.839	99.5	542.8	1284	300.0	0.10	0.2	19.34	16.27	19.52	3	3.0
21.653	662.5	39.03	579.7	.837	98.9	715.6	1505	300.0	0.10	50.0	19.35	16.10	18.82	3	4.0
21.630	662.2	39.01	579.4	.837	98.9	712.9	1502	300.0	0.10	50.0	19.34	16.10	18.94	3	5.0
21.357	650.4	39.31	568.2	.835	99.6	557.9	1305	300.0	0.10	0.2	19.86	16.25	17.77	4	0.
21.354	650.4	39.30	568.2	.835	99.6	562.3	1311	300.0	0.10	0.2	19.87	16.25	18.40	4	1.0
21.336	650.0	39.30	567.8	.835	99.6	582.4	1338	300.0	0.10	0.2	19.86	16.23	18.98	4	2.0
21.225	647.6	39.27	565.4	.834	99.5	696.6	1482	300.0	0.10	0.2	19.86	16.12	19.53	4	3.0
20.915	641.9	39.10	559.8	.833	99.1	910.4	1724	300.0	0.10	50.0	19.87	15.92	18.79	4	4.0
20.898	641.8	39.07	559.7	.833	99.0	905.1	1718	300.0	0.10	50.0	19.87	15.93	18.92	4	5.0
19.728	610.0	39.10	529.4	.827	99.1	663.2	1441	300.0	0.10	0.4	20.39	16.15	17.80	5	0.
19.727	610.0	39.10	529.4	.827	99.1	669.5	1449	300.0	0.10	0.2	20.39	16.14	18.42	5	1.0
19.720	609.9	39.10	529.3	.827	99.1	700.6	1487	300.0	0.10	0.2	20.39	16.11	19.00	5	2.0
19.679	609.3	39.07	528.5	.827	99.1	807.3	1612	300.0	0.10	0.2	20.38	16.01	19.54	5	3.0
19.534	607.5	38.95	526.4	.826	98.7	1049.7	1866	300.0	0.10	42.3	20.40	15.80	18.78	5	4.0
19.521	607.4	38.92	526.4	.826	98.7	1054.4	1871	300.0	0.10	43.6	20.39	15.80	18.92	5	5.0
18.664	596.5	37.96	516.5	.824	96.2	655.5	1432	300.0	0.18	0.2	20.60	16.15	18.42	6	0.
18.663	596.4	37.96	516.5	.824	96.2	647.6	1422	300.0	0.18	0.2	20.60	16.16	18.42	6	1.0
18.657	596.4	37.96	516.4	.824	96.2	682.8	1466	300.0	0.18	0.2	20.60	16.13	18.98	6	2.0
18.623	596.0	37.93	515.8	.824	96.2	804.9	1609	300.0	0.18	0.2	20.60	16.02	19.54	6	3.0
18.501	593.8	37.88	513.3	.823	96.0	1053.9	1870	300.0	0.18	35.5	20.60	15.80	18.84	6	4.0
18.489	593.9	37.84	513.4	.823	95.9	1064.8	1881	300.0	0.18	36.9	20.60	15.79	18.98	6	5.0
18.485	598.1	37.47	518.2	.825	95.0	645.5	1419	300.0	0.23	0.3	20.60	16.16	18.01	7	0.
18.484	598.2	37.46	518.2	.825	95.0	638.1	1410	300.0	0.23	0.2	20.60	16.17	18.57	7	1.0
18.478	598.1	37.46	518.1	.825	95.0	676.2	1457	300.0	0.23	0.2	20.60	16.13	18.99	7	2.0
18.442	597.5	37.45	517.3	.824	94.9	809.7	1614	300.0	0.23	0.2	20.60	16.01	19.54	7	3.0
18.318	595.6	37.37	515.1	.823	94.7	1067.4	1883	300.0	0.23	37.8	20.60	15.79	18.83	7	4.0
18.306	595.2	37.37	514.7	.823	94.7	1072.8	1889	300.0	0.23	38.5	20.60	15.78	18.97	7	5.0

Table 6.62 Effect of S_f and S_b at τ_{n0} = 2.0 ms, no BSF, $X_L \leq 300$ μm, O_{pl} = 2

eff	V_{oc}	J_{sc}	V_{mp}	ff	C_{eff}	τ_{bulk}	L_d	X_L	X_f	X_b	log D_0	log D_B	log D_L	log S_f	log S_b
23.315	717.4	38.53	630.2	.843	99.8	309.4	918	163.8	0.10	0.	17.82	16.57	0.	0	0.
23.183	710.1	38.64	624.9	.845	99.6	248.3	801	183.8	0.10	0.	17.85	16.67	0.	0	1.0
22.569	693.0	38.60	609.7	.844	98.5	166.1	620	240.5	0.10	0.	17.92	16.85	0.	0	2.0
21.303	675.0	37.56	592.3	.840	95.2	102.6	450	300.0	2.60	0.	17.71	17.05	0.	0	3.0
20.716	673.2	36.65	590.5	.840	92.9	62.2	320	300.0	2.60	0.	17.82	17.25	0.	0	4.0
20.639	673.3	36.51	590.5	.839	92.6	57.1	301	300.0	2.52	0.	17.84	17.28	0.	0	5.0
20.631	673.3	36.50	590.5	.839	92.5	56.6	300	300.0	2.50	0.	17.84	17.28	0.	0	6.0
23.285	713.0	38.72	626.4	.843	99.7	314.9	928	187.5	0.10	0.	18.27	16.56	0.	1	0.
23.156	706.3	38.83	621.4	.844	99.5	263.1	830	212.2	0.10	0.	18.28	16.64	0.	1	1.0
22.554	693.7	38.53	610.4	.844	98.6	161.2	608	222.4	0.10	0.	18.28	16.87	0.	1	2.0
21.293	675.1	37.53	592.4	.840	95.1	100.5	444	300.0	2.42	0.	17.78	17.06	0.	1	3.0
20.705	673.0	36.64	590.3	.840	92.9	62.8	322	300.0	2.57	0.	17.86	17.24	0.	1	4.0
20.628	673.0	36.51	590.3	.839	92.5	57.9	304	300.0	2.46	0.	17.87	17.27	0.	1	5.0
20.620	673.0	36.49	590.3	.839	92.5	57.3	302	300.0	2.45	0.	17.87	17.28	0.	1	6.0
23.138	704.9	38.94	619.2	.843	99.7	335.4	964	221.5	0.10	0.	18.79	16.53	0.	2	0.
23.034	701.8	38.89	617.2	.844	99.5	275.6	855	223.0	0.10	0.	18.79	16.62	0.	2	1.0
22.481	689.9	38.64	606.7	.843	98.5	174.3	639	248.9	0.10	0.	18.79	16.83	0.	2	2.0
21.223	675.5	37.36	593.1	.841	94.7	100.5	444	300.0	0.10	0.	18.79	17.06	0.	2	3.0
20.621	674.9	36.33	592.5	.841	92.1	58.4	306	300.0	0.10	0.	18.77	17.27	0.	2	4.0
20.543	675.1	36.18	592.8	.841	91.7	53.2	287	300.0	0.10	0.	18.79	17.31	0.	2	5.0
20.535	675.1	36.17	592.8	.841	91.7	52.7	285	300.0	0.10	0.	18.79	17.31	0.	2	6.0
22.599	684.3	39.28	600.3	.841	99.6	409.6	1088	300.0	0.10	0.	19.32	16.42	0.	3	0.
22.522	684.2	39.12	600.7	.841	99.5	339.8	972	267.6	0.10	0.	19.33	16.52	0.	3	1.0
22.111	676.8	38.85	594.1	.841	98.5	217.5	737	300.0	0.10	0.	19.31	16.73	0.	3	2.0
20.977	667.5	37.42	585.4	.840	94.9	112.3	478	300.0	0.10	0.	19.30	17.02	0.	3	3.0
20.378	667.0	36.39	584.9	.840	92.3	65.4	331	300.0	0.10	0.	19.30	17.23	0.	3	4.0
20.299	667.2	36.24	585.1	.840	91.9	59.5	310	300.0	0.10	0.	19.30	17.26	0.	3	5.0
20.290	667.2	36.22	585.1	.840	91.8	58.9	308	300.0	0.10	0.	19.30	17.27	0.	3	6.0
21.353	650.4	39.30	568.2	.835	99.6	557.9	1305	300.0	0.10	0.	19.86	16.25	0.	4	0.
21.317	649.8	39.26	567.8	.835	99.5	495.9	1218	300.0	0.10	0.	19.87	16.32	0.	4	1.0
21.058	646.9	38.95	565.4	.836	98.8	326.1	948	300.0	0.10	0.	19.86	16.54	0.	4	2.0
20.151	641.9	37.60	560.8	.835	95.3	167.5	623	300.0	0.10	0.	19.83	16.85	0.	4	3.0
19.560	641.6	36.51	560.6	.835	92.6	95.8	430	300.0	0.10	0.	19.82	17.08	0.	4	4.0
19.475	641.8	36.35	560.7	.835	92.1	85.4	398	300.0	0.10	0.	19.82	17.13	0.	4	5.0
19.467	641.8	36.33	560.8	.835	92.1	84.4	394	300.0	0.10	0.	19.82	17.13	0.	4	6.0
19.727	610.0	39.10	529.4	.827	99.1	663.2	1441	300.0	0.10	0.	20.39	16.15	0.	5	0.
19.708	609.8	39.07	529.3	.827	99.0	639.6	1412	300.0	0.10	0.	20.39	16.17	0.	5	1.0
19.548	608.5	38.82	528.4	.827	98.4	514.0	1244	300.0	0.10	0.	20.39	16.30	0.	5	2.0
18.828	605.5	37.59	525.8	.827	95.3	309.3	918	300.0	0.10	0.	20.36	16.57	0.	5	3.0
18.239	605.4	36.40	525.9	.827	92.3	165.1	617	300.0	0.10	0.	20.35	16.86	0.	5	4.0
18.146	605.6	36.20	526.1	.828	91.8	140.6	556	300.0	0.10	0.	20.35	16.92	0.	5	5.0
18.136	605.6	36.18	526.1	.828	91.7	138.1	549	300.0	0.10	0.	20.35	16.93	0.	5	6.0
18.663	596.3	37.96	516.4	.824	96.2	641.6	1414	300.0	0.18	0.	20.60	16.17	0.	6	0.
18.648	596.1	37.95	516.3	.824	96.2	628.9	1398	300.0	0.18	0.	20.60	16.18	0.	6	1.0
18.510	594.6	37.76	515.0	.824	95.7	551.9	1297	300.0	0.17	0.	20.60	16.26	0.	6	2.0
17.850	590.3	36.70	511.3	.824	93.0	374.9	1031	300.0	0.15	0.	20.60	16.47	0.	6	3.0
17.274	590.0	35.52	511.1	.824	90.1	196.4	690	300.0	0.14	0.	20.60	16.78	0.	6	4.0
17.180	590.3	35.31	511.4	.824	89.5	161.3	608	300.0	0.14	0.	20.60	16.87	0.	6	5.0
17.170	590.3	35.29	511.4	.824	89.5	159.6	604	300.0	0.14	0.	20.60	16.87	0.	6	6.0
18.484	598.2	37.46	518.2	.825	95.0	642.0	1415	300.0	0.23	0.	20.60	16.17	0.	7	0.
18.468	598.0	37.44	518.0	.825	94.9	638.1	1410	300.0	0.23	0.	20.60	16.17	0.	7	1.0

eff	V_{oc}	J_{sc}	V_{mp}	ff	C_{eff}	τ_{bulk}	L_d	X_L	X_f	X_b	log D_0	log D_B	log D_L	log S_f	log S_b
18.328	596.5	37.25	516.8	.825	94.4	544.2	1286	300.0	0.22	0.	20.60	16.27	0.	7	2.0
17.663	592.3	36.17	513.1	.824	91.7	366.6	1018	300.0	0.20	0.	20.60	16.48	0.	7	3.0
17.086	591.9	35.01	512.9	.825	88.8	191.8	680	300.0	0.19	0.	20.60	16.79	0.	7	4.0
16.993	592.3	34.79	513.3	.825	88.2	155.7	594	300.0	0.19	0.	20.60	16.88	0.	7	5.0
16.984	592.2	34.77	513.3	.825	88.2	156.9	597	300.0	0.19	0.	20.60	16.88	0.	7	6.0
18.465	598.4	37.41	518.5	.825	94.8	640.8	1413	300.0	0.23	0.	20.60	16.17	0.	8	0.
18.449	598.2	37.39	518.3	.825	94.8	631.6	1402	300.0	0.23	0.	20.60	16.18	0.	8	1.0
18.309	596.7	37.20	517.0	.825	94.3	547.7	1291	300.0	0.23	0.	20.60	16.26	0.	8	2.0
17.643	592.6	36.11	513.4	.824	91.5	366.8	1018	300.0	0.20	0.	20.60	16.48	0.	8	3.0
17.067	592.2	34.95	513.2	.825	88.6	190.2	676	300.0	0.19	0.	20.60	16.79	0.	8	4.0
16.974	592.5	34.74	513.5	.825	88.1	157.3	598	300.0	0.19	0.	20.60	16.88	0.	8	5.0
16.964	592.4	34.72	513.4	.825	88.0	156.2	595	300.0	0.19	0.	20.60	16.88	0.	8	6.0

Table 6.63 Effect of S_f and S_b at τ_{n0} = 1.0 ms, $X_L \leq 300$ μm, $O_{pl} = 2$

eff	V_{oc}	J_{sc}	V_{mp}	ff	C_{eff}	τ_{bulk}	L_d	X_L	X_f	X_b	log D_0	log D_B	log D_L	log S_f	log S_b
22.653	703.0	38.27	617.0	.842	99.7	167.4	679	142.6	0.10	0.2	17.79	16.54	17.79	0	0.
22.636	701.1	38.37	615.0	.841	99.7	179.2	708	151.7	0.10	0.2	17.93	16.50	18.30	0	1.0
22.531	693.3	38.67	607.8	.840	99.6	202.7	763	188.9	0.10	0.2	17.97	16.44	18.84	0	2.0
22.408	689.4	38.66	604.7	.841	99.5	193.9	743	192.5	0.10	0.2	17.85	16.46	19.18	0	2.5
22.161	678.9	38.89	594.8	.839	99.3	234.8	833	240.5	0.10	0.2	17.84	16.36	19.45	0	3.0
21.778	666.3	39.03	582.9	.837	98.9	286.5	936	300.0	0.10	0.2	17.84	16.24	19.79	0	3.5
21.547	662.1	38.88	579.2	.837	98.6	309.3	979	300.0	0.10	50.0	18.01	16.20	18.81	0	4.0
21.527	661.9	38.85	579.0	.837	98.5	305.3	971	300.0	0.10	50.0	18.26	16.20	18.92	0	5.0
21.526	661.9	38.85	579.0	.837	98.5	307.8	976	300.0	0.10	50.0	17.90	16.20	18.93	0	6.0
22.637	701.7	38.32	615.7	.842	99.7	174.6	697	147.5	0.10	0.2	18.25	16.52	17.88	1	0.
22.596	694.4	38.64	609.5	.842	99.5	167.9	681	188.8	0.10	0.2	18.23	16.54	19.02	1	1.0
22.531	693.9	38.61	608.4	.841	99.6	197.9	752	181.4	0.10	0.2	18.25	16.45	18.87	1	2.0
22.396	690.2	38.58	605.5	.841	99.5	191.6	738	181.4	0.10	0.2	18.26	16.47	19.17	1	2.5
22.154	678.4	38.91	594.4	.839	99.2	231.2	826	245.7	0.10	0.2	18.19	16.37	19.42	1	3.0
21.747	667.9	38.86	584.6	.838	99.1	284.7	933	245.7	0.10	0.2	18.23	16.25	19.77	1	3.5
21.543	661.9	38.88	579.0	.837	98.6	311.4	982	300.0	0.10	50.0	18.28	16.19	18.80	1	4.0
21.524	661.8	38.85	578.9	.837	98.5	306.2	973	300.0	0.10	50.0	18.26	16.20	18.92	1	5.0
21.522	661.7	38.85	578.9	.837	98.5	308.2	977	300.0	0.10	50.0	18.43	16.20	18.94	1	6.0
22.543	693.9	38.63	608.5	.841	99.6	194.8	745	181.3	0.10	0.2	18.77	16.46	17.85	2	0.
22.529	693.0	38.67	607.5	.840	99.6	201.8	761	186.3	0.10	0.2	18.76	16.44	18.29	2	1.0
22.447	687.7	38.85	602.6	.840	99.5	213.8	788	217.4	0.10	0.2	18.74	16.41	18.84	2	2.0
22.334	684.9	38.81	600.5	.840	99.4	204.1	766	217.4	0.10	0.2	18.78	16.43	19.19	2	2.5
22.110	676.4	38.95	592.6	.839	99.2	226.5	815	258.9	0.10	0.2	18.74	16.38	19.44	2	3.0
21.728	666.6	38.91	583.3	.838	99.1	286.7	937	258.9	0.10	0.2	18.80	16.24	19.76	2	3.5
21.520	661.2	38.89	578.4	.837	98.6	313.6	986	300.0	0.10	50.0	18.81	16.19	18.80	2	4.0
21.500	661.0	38.86	578.1	.837	98.5	312.4	984	300.0	0.10	50.0	18.80	16.19	18.92	2	5.0
21.499	661.0	38.86	578.1	.837	98.5	311.8	983	300.0	0.10	50.0	18.80	16.19	18.93	2	6.0
22.145	676.6	39.00	592.8	.839	99.5	218.2	798	246.9	0.10	0.2	19.33	16.40	18.35	3	0.
22.135	676.2	39.01	592.3	.839	99.5	233.5	830	246.9	0.10	0.2	19.33	16.36	18.98	3	1.0
22.096	674.3	39.08	590.3	.838	99.4	245.2	855	265.0	0.10	0.2	19.29	16.33	18.90	3	2.0
21.870	667.4	39.12	584.0	.838	99.2	264.1	893	300.0	0.10	0.2	19.34	16.29	19.52	3	3.0
21.375	656.7	38.93	574.0	.836	98.7	339.7	1033	300.0	0.10	50.0	19.35	16.14	18.80	3	4.0
21.357	656.5	38.91	573.9	.836	98.6	339.7	1033	300.0	0.10	50.0	19.34	16.14	18.91	3	5.0
21.355	656.5	38.90	573.9	.836	98.6	339.5	1032	300.0	0.10	50.0	19.34	16.14	18.92	3	6.0
21.156	646.5	39.22	564.4	.834	99.4	299.1	960	300.0	0.10	0.2	19.86	16.22	17.74	4	0.
21.153	646.5	39.22	564.3	.834	99.4	300.5	962	300.0	0.10	0.2	19.87	16.21	18.49	4	1.0
21.137	646.1	39.21	564.0	.834	99.4	304.7	970	300.0	0.10	0.2	19.86	16.20	18.97	4	2.0
21.041	644.1	39.18	561.9	.834	99.3	340.4	1034	300.0	0.10	0.2	19.86	16.13	19.53	4	3.0
20.751	638.7	39.01	556.8	.833	98.9	429.3	1179	300.0	0.10	50.0	19.87	15.97	18.77	4	4.0
20.736	638.6	38.99	556.7	.833	98.8	429.6	1180	300.0	0.10	50.0	19.87	15.97	18.89	4	5.0
20.734	638.6	38.99	556.7	.833	98.8	429.7	1180	300.0	0.10	50.0	19.87	15.97	18.90	4	6.0
19.650	608.9	39.04	528.2	.827	99.0	376.4	1095	300.0	0.10	0.4	20.39	16.07	17.72	5	0.
19.649	608.9	39.04	528.2	.827	99.0	378.2	1098	300.0	0.10	0.2	20.39	16.06	18.44	5	1.0
19.643	608.8	39.03	528.1	.827	99.0	386.0	1111	300.0	0.10	0.2	20.39	16.05	18.96	5	2.0
19.606	608.2	39.02	527.3	.826	98.9	423.9	1171	300.0	0.10	0.2	20.38	15.98	19.54	5	3.0
19.465	606.4	38.89	525.4	.825	98.6	524.1	1318	300.0	0.10	46.6	20.40	15.81	18.73	5	4.0
19.453	606.3	38.86	525.4	.825	98.5	528.3	1324	300.0	0.10	49.2	20.39	15.80	18.83	5	5.0
19.452	606.3	38.87	525.4	.825	98.5	523.1	1317	300.0	0.10	45.2	20.39	15.81	18.91	5	6.0
18.601	595.5	37.91	515.4	.824	96.1	385.7	1110	300.0	0.18	0.2	20.60	16.05	17.87	6	0.
18.601	595.4	37.92	515.4	.824	96.1	383.4	1106	300.0	0.18	0.2	20.60	16.05	18.38	6	1.0
18.596	595.5	37.91	515.4	.824	96.1	391.0	1119	300.0	0.18	0.2	20.60	16.04	18.97	6	2.0

eff	V_{oc}	J_{sc}	V_{mp}	ff	C_{eff}	τ_{bulk}	L_d	X_L	X_f	X_b	log D_0	log D_B	log D_L	log S_f	log S_b
18.566	595.2	37.88	514.9	.823	96.0	431.4	1183	300.0	0.18	0.2	20.60	15.97	19.49	6	3.0
18.449	593.0	37.83	512.5	.822	95.9	547.3	1350	300.0	0.18	43.6	20.60	15.77	18.71	6	4.0
18.438	593.2	37.80	512.7	.822	95.8	539.2	1339	300.0	0.18	40.0	20.60	15.78	18.93	6	5.0
18.436	593.0	37.81	512.5	.822	95.9	544.9	1347	300.0	0.18	45.1	20.60	15.77	18.87	6	6.0
18.421	597.1	37.43	517.0	.824	94.9	381.0	1102	300.0	0.23	0.2	20.60	16.06	17.64	7	0.
18.420	597.2	37.42	517.0	.824	94.9	380.7	1102	300.0	0.23	0.2	20.60	16.06	18.41	7	1.0
18.415	597.2	37.42	517.0	.824	94.9	389.8	1117	300.0	0.23	0.2	20.60	16.04	18.91	7	2.0
18.384	596.6	37.40	516.3	.824	94.8	430.9	1182	300.0	0.23	0.2	20.60	15.97	19.48	7	3.0
18.265	594.8	37.32	514.3	.823	94.6	537.4	1336	300.0	0.23	42.0	20.60	15.78	18.75	7	4.0
18.253	594.5	37.31	514.1	.823	94.6	535.3	1334	300.0	0.23	45.0	20.60	15.79	18.86	7	5.0
18.253	594.6	37.31	514.1	.823	94.6	537.6	1337	300.0	0.23	37.1	20.60	15.78	18.98	7	6.0
18.402	597.4	37.37	517.0	.824	94.7	380.1	1101	300.0	0.23	0.2	20.60	16.06	17.65	8	0.
18.401	597.4	37.37	517.2	.824	94.7	382.0	1104	300.0	0.23	0.2	20.60	16.06	18.38	8	1.0
18.396	597.4	37.36	517.2	.824	94.7	389.8	1117	300.0	0.24	0.2	20.60	16.04	18.96	8	2.0
18.365	596.8	37.36	516.4	.824	94.7	432.4	1184	300.0	0.24	0.2	20.60	15.97	19.51	8	3.0
18.246	594.9	37.27	514.4	.823	94.5	536.0	1335	300.0	0.24	35.9	20.60	15.79	18.81	8	4.0
18.234	594.6	37.27	514.1	.823	94.5	541.7	1342	300.0	0.23	44.2	20.60	15.78	18.87	8	5.0
18.233	594.8	37.26	514.3	.823	94.4	544.0	1346	300.0	0.23	38.4	20.60	15.77	18.96	8	6.0

Table 6.64 Effect of S_f and S_b at τ_{n0} = 1.0 ms, no BSF, $X_L \leq 300$ μm, $O_{pl} = 2$

eff	V_{oc}	J_{sc}	V_{mp}	ff	C_{eff}	τ_{bulk}	L_d	X_L	X_f	X_b	log D_0	log D_B	log D_L	log S_f	log S_b
22.645	702.5	38.26	617.0	.842	99.7	156.9	653	142.7	0.10	0.	17.87	16.57	0.	0	0.
22.559	698.2	38.33	613.6	.843	99.5	137.8	602	154.1	0.10	0.	17.89	16.63	0.	0	1.0
22.080	684.6	38.29	601.6	.842	98.5	98.5	487	192.4	0.10	0.	17.96	16.79	0.	0	2.0
20.967	667.7	37.44	585.2	.839	94.9	67.4	379	300.0	2.04	0.	17.77	16.96	0.	0	3.0
20.410	666.4	36.53	583.9	.838	92.6	44.7	286	300.0	2.11	0.	17.88	17.14	0.	0	4.0
20.331	666.4	36.40	583.9	.838	92.3	41.9	273	300.0	2.08	0.	17.90	17.17	0.	0	5.0
20.323	666.6	36.37	584.0	.838	92.2	41.1	269	300.0	2.02	0.	17.89	17.18	0.	0	6.0
22.630	701.4	38.30	615.9	.842	99.7	158.6	657	146.5	0.10	0.	18.25	16.56	0.	1	0.
22.545	697.4	38.35	612.9	.843	99.5	138.3	604	156.8	0.10	0.	18.27	16.63	0.	1	1.0
22.071	684.3	38.30	601.3	.842	98.5	98.6	487	193.4	0.10	0.	18.29	16.79	0.	1	2.0
20.960	667.6	37.43	585.2	.839	94.9	67.4	378	300.0	1.95	0.	17.82	16.97	0.	1	3.0
20.403	666.3	36.53	583.8	.838	92.6	44.9	287	300.0	2.06	0.	17.90	17.14	0.	1	4.0
20.324	666.3	36.39	583.8	.838	92.3	42.1	274	300.0	2.02	0.	17.92	17.17	0.	1	5.0
20.316	666.5	36.36	584.0	.838	92.2	41.1	269	300.0	1.97	0.	17.93	17.18	0.	1	6.0
22.536	695.5	38.49	610.6	.842	99.6	167.6	680	166.5	0.10	0.	18.79	16.54	0.	2	0.
22.461	692.5	38.50	608.3	.842	99.5	148.4	631	174.2	0.10	0.	18.79	16.60	0.	2	1.0
22.016	681.7	38.37	598.8	.842	98.5	104.3	505	204.1	0.10	0.	18.78	16.77	0.	2	2.0
20.908	668.1	37.27	586.0	.840	94.5	67.2	378	300.0	0.10	0.	18.78	16.97	0.	2	3.0
20.341	668.1	36.26	586.0	.840	91.9	42.5	276	300.0	0.10	0.	18.77	17.16	0.	2	4.0
20.262	668.3	36.11	586.1	.840	91.5	39.5	262	300.0	0.10	0.	18.79	17.19	0.	2	5.0
20.254	668.3	36.09	586.2	.840	91.5	39.1	260	300.0	0.10	0.	18.79	17.20	0.	2	6.0
22.142	677.3	38.93	593.7	.840	99.5	206.2	771	234.7	0.10	0.	19.33	16.43	0.	3	0.
22.088	676.0	38.90	592.7	.840	99.3	188.1	730	237.9	0.10	0.	19.33	16.48	0.	3	1.0
21.730	670.4	38.59	588.0	.840	98.4	126.7	571	249.2	0.10	0.	19.32	16.68	0.	3	2.0
20.717	661.8	37.33	579.9	.839	94.6	72.9	399	300.0	0.10	0.	19.30	16.93	0.	3	3.0
20.148	661.6	36.32	579.7	.838	92.1	47.0	296	300.0	0.10	0.	19.30	17.12	0.	3	4.0
20.068	661.8	36.16	579.9	.839	91.7	43.3	279	300.0	0.10	0.	19.30	17.15	0.	3	5.0
20.059	661.8	36.15	579.9	.839	91.6	42.9	278	300.0	0.10	0.	19.30	17.16	0.	3	6.0
21.153	646.5	39.21	564.4	.834	99.4	293.1	949	300.0	0.10	0.	19.86	16.23	0.	4	0.
21.119	646.0	39.17	564.0	.835	99.3	275.2	915	300.0	0.10	0.	19.87	16.27	0.	4	1.0
20.872	643.4	38.86	561.9	.835	98.5	198.1	753	300.0	0.10	0.	19.86	16.45	0.	4	2.0
20.010	639.1	37.53	558.1	.834	95.1	103.3	502	300.0	0.10	0.	19.83	16.77	0.	4	3.0
19.435	639.1	36.45	558.1	.834	92.4	64.1	366	300.0	0.10	0.	19.82	16.99	0.	4	4.0
19.349	639.4	36.26	558.5	.834	91.9	56.7	337	300.0	0.10	0.	19.82	17.04	0.	4	5.0
19.340	639.4	36.25	558.4	.834	91.9	57.1	338	300.0	0.10	0.	19.83	17.04	0.	4	6.0
19.648	608.9	39.04	528.2	.827	99.0	376.4	1095	300.0	0.10	0.	20.39	16.07	0.	5	0.
19.630	608.7	39.01	528.1	.827	98.9	364.2	1075	300.0	0.10	0.	20.39	16.09	0.	5	1.0
19.470	607.4	38.76	527.1	.827	98.3	300.6	963	300.0	0.10	0.	20.39	16.21	0.	5	2.0
18.766	604.3	37.54	524.7	.827	95.2	181.3	713	300.0	0.10	0.	20.36	16.50	0.	5	3.0
18.183	604.5	36.36	524.9	.827	92.2	101.6	496	300.0	0.10	0.	20.35	16.78	0.	5	4.0
18.088	604.6	36.16	525.1	.827	91.7	89.6	457	300.0	0.10	0.	20.35	16.84	0.	5	5.0
18.078	604.6	36.14	525.1	.827	91.6	88.2	453	300.0	0.10	0.	20.35	16.84	0.	5	6.0
18.600	595.2	37.94	515.1	.824	96.2	381.2	1103	300.0	0.18	0.	20.60	16.06	0.	6	0.
18.585	594.9	37.92	514.9	.824	96.1	372.4	1088	300.0	0.18	0.	20.60	16.07	0.	6	1.0
18.448	593.4	37.74	513.7	.824	95.7	326.3	1009	300.0	0.17	0.	20.60	16.16	0.	6	2.0
17.804	589.1	36.70	509.9	.824	93.0	218.5	798	300.0	0.15	0.	20.60	16.40	0.	6	3.0
17.232	588.8	35.52	509.9	.824	90.0	124.9	566	300.0	0.14	0.	20.60	16.68	0.	6	4.0
17.135	589.1	35.30	510.3	.824	89.5	105.0	507	300.0	0.14	0.	20.60	16.76	0.	6	5.0
17.125	589.2	35.28	510.3	.824	89.4	103.6	502	300.0	0.14	0.	20.60	16.77	0.	6	6.0
18.419	597.0	37.43	516.9	.824	94.9	381.0	1102	300.0	0.23	0.	20.60	16.06	0.	7	0.
18.403	596.8	37.41	517.0	.824	94.8	370.4	1085	300.0	0.23	0.	20.60	16.08	0.	7	1.0

eff	V_{oc}	J_{sc}	V_{mp}	ff	C_{eff}	τ_{bulk}	L_d	X_L	X_f	X_b	log D_0	log D_B	log D_L	log S_f	log S_b
18.264	595.2	37.23	515.5	.824	94.4	320.5	999	300.0	0.22	0.	20.60	16.17	0.	7	2.0
17.614	591.9	36.11	512.7	.824	91.5	213.5	787	300.0	0.20	0.	20.60	16.41	0.	7	3.0
17.043	591.0	34.99	512.0	.824	88.7	120.2	553	300.0	0.19	0.	20.60	16.70	0.	7	4.0
16.947	591.1	34.78	512.1	.824	88.2	103.5	502	300.0	0.19	0.	20.60	16.77	0.	7	5.0
16.937	591.2	34.75	512.3	.824	88.1	98.5	486	300.0	0.19	0.	20.60	16.79	0.	7	6.0
18.400	597.2	37.38	517.1	.824	94.8	380.1	1101	300.0	0.23	0.	20.60	16.06	0.	8	0.
18.385	597.0	37.36	517.1	.824	94.7	370.1	1085	300.0	0.23	0.	20.60	16.08	0.	8	1.0
18.245	595.4	37.17	515.6	.824	94.2	322.0	1002	300.0	0.22	0.	20.60	16.17	0.	8	2.0
17.595	591.2	36.11	512.1	.824	91.5	212.6	785	300.0	0.20	0.	20.60	16.41	0.	8	3.0
17.023	591.0	34.95	512.0	.824	88.6	120.8	554	300.0	0.19	0.	20.60	16.70	0.	8	4.0
16.927	591.4	34.72	512.4	.824	88.0	101.4	496	300.0	0.19	0.	20.60	16.78	0.	8	5.0
16.917	591.4	34.70	512.4	.824	88.0	99.4	489	300.0	0.19	0.	20.60	16.79	0.	8	6.0

Table 6.65 Effect of S_f and S_b at τ_{n0} = 0.7 ms, $X_L \leq 300$ μm, O_{pl} = 2

eff	V_{oc}	J_{sc}	V_{mp}	ff	C_{eff}	τ_{bulk}	L_d	X_L	X_f	X_b	log D_0	log D_B	log D_L	log S_f	log S_b
22.297	695.4	38.09	610.4	.842	99.6	114.6	560	131.2	0.10	0.2	17.86	16.55	17.34	0	0.
22.284	694.4	38.14	609.4	.841	99.6	118.2	571	134.7	0.10	0.2	17.86	16.54	18.23	0	1.0
22.209	689.8	38.28	605.2	.841	99.5	124.7	590	149.4	0.10	0.2	17.88	16.51	18.86	0	2.0
21.885	674.7	38.67	590.9	.839	99.2	161.5	690	207.9	0.10	0.2	17.91	16.37	19.47	0	3.0
21.326	657.1	38.81	574.4	.836	98.4	219.6	825	300.0	0.10	50.0	17.85	16.19	18.79	0	4.0
21.309	657.1	38.78	574.4	.836	98.3	215.2	816	300.0	0.10	50.0	17.86	16.20	18.90	0	5.0
21.308	656.9	38.79	574.2	.836	98.3	220.0	826	300.0	0.10	50.0	18.19	16.19	18.91	0	6.0
22.278	690.6	38.35	605.9	.841	99.5	121.6	581	156.3	0.10	0.2	18.27	16.52	17.50	1	0.
22.266	690.1	38.36	605.4	.841	99.5	121.8	582	157.9	0.10	0.2	18.25	16.52	18.23	1	1.0
22.196	686.9	38.44	602.4	.841	99.5	129.9	605	167.7	0.10	0.2	18.19	16.49	18.88	1	2.0
21.880	674.6	38.66	590.9	.839	99.2	158.9	683	207.5	0.10	0.2	18.23	16.38	19.46	1	3.0
21.323	657.2	38.80	574.5	.836	98.4	215.9	817	300.0	0.10	50.0	18.24	16.20	18.78	1	4.0
21.306	657.0	38.78	574.4	.836	98.3	214.9	815	300.0	0.11	50.0	18.23	16.20	18.90	1	5.0
21.305	657.0	38.78	574.3	.836	98.3	215.3	816	300.0	0.10	50.0	18.24	16.20	18.91	1	6.0
22.201	685.8	38.52	601.4	.840	99.4	126.9	597	176.3	0.10	0.2	18.79	16.50	17.65	2	0.
22.191	685.4	38.52	601.0	.840	99.4	128.1	600	177.5	0.10	0.2	18.80	16.49	18.25	2	1.0
22.130	682.9	38.58	598.7	.840	99.4	134.8	619	185.8	0.10	0.2	18.79	16.47	18.88	2	2.0
21.842	673.0	38.70	589.4	.839	99.2	163.7	695	212.1	0.10	0.2	18.77	16.36	19.46	2	3.0
21.303	656.5	38.81	573.8	.836	98.4	219.9	826	300.0	0.10	50.0	18.80	16.19	18.79	2	4.0
21.287	656.4	38.79	573.7	.836	98.3	217.7	821	300.0	0.10	50.0	18.79	16.19	18.90	2	5.0
21.285	656.4	38.79	573.7	.836	98.3	217.9	822	300.0	0.10	50.0	18.78	16.19	18.91	2	6.0
21.880	673.3	38.73	589.9	.839	99.4	147.4	653	206.4	0.10	0.2	19.32	16.42	17.69	3	0.
21.874	673.1	38.74	589.6	.839	99.4	151.0	662	206.4	0.10	0.2	19.32	16.41	18.27	3	1.0
21.836	671.8	38.76	588.4	.839	99.4	155.5	674	212.0	0.10	0.2	19.32	16.39	18.90	3	2.0
21.633	665.2	38.83	582.1	.837	99.2	180.1	735	235.0	0.10	0.2	19.33	16.31	19.48	3	3.0
21.180	652.5	38.86	569.9	.835	98.5	239.2	867	300.0	0.10	50.0	19.33	16.13	18.79	3	4.0
21.165	652.5	38.83	570.0	.835	98.4	233.3	855	300.0	0.10	50.0	19.33	16.15	18.90	3	5.0
21.163	652.5	38.83	570.0	.835	98.4	234.2	856	300.0	0.10	50.0	19.33	16.15	18.91	3	6.0
21.004	643.6	39.14	561.6	.834	99.2	211.3	807	300.0	0.10	0.2	19.85	16.21	17.70	4	0.
21.002	643.5	39.14	561.4	.834	99.2	215.6	817	300.0	0.10	0.2	19.86	16.20	18.32	4	1.0
20.987	643.3	39.14	561.2	.834	99.2	218.1	822	300.0	0.10	0.2	19.86	16.19	18.95	4	2.0
20.830	643.2	38.83	561.3	.834	99.4	234.1	856	222.6	0.10	0.2	19.84	16.15	19.49	4	3.0
20.626	636.3	38.95	554.4	.832	98.7	296.1	978	300.0	0.10	50.0	19.87	15.98	18.77	4	4.0
20.613	636.3	38.93	554.4	.832	98.7	293.9	974	300.0	0.10	50.0	19.87	15.99	18.88	4	5.0
20.611	636.2	38.93	554.4	.832	98.7	296.5	979	300.0	0.10	50.0	19.87	15.98	18.90	4	6.0
19.588	608.0	38.99	527.3	.826	98.8	276.6	941	300.0	0.10	0.2	20.39	16.03	17.59	5	0.
19.587	608.0	38.98	527.3	.826	98.8	276.1	940	300.0	0.10	0.2	20.40	16.04	18.35	5	1.0
19.581	607.9	38.99	527.1	.826	98.8	283.9	955	300.0	0.10	0.2	20.40	16.02	18.96	5	2.0
19.546	607.3	38.97	526.4	.826	98.8	302.8	991	300.0	0.10	0.2	20.39	15.97	19.53	5	3.0
19.409	605.5	38.84	524.6	.825	98.5	367.1	1103	300.0	0.10	50.0	20.38	15.81	18.69	5	4.0
19.397	605.4	38.82	524.5	.825	98.4	369.5	1107	300.0	0.10	50.0	20.40	15.80	18.82	5	5.0
19.396	605.4	38.81	524.6	.825	98.4	366.5	1102	300.0	0.10	50.0	20.40	15.81	18.82	5	6.0
18.552	593.3	37.99	513.2	.823	96.3	285.5	958	300.0	0.17	0.2	20.60	16.01	18.07	6	0.
18.551	593.1	38.00	513.0	.823	96.3	285.8	959	300.0	0.16	0.2	20.60	16.01	18.28	6	1.0
18.546	593.0	38.00	513.0	.823	96.3	288.5	964	300.0	0.16	0.2	20.60	16.00	18.96	6	2.0
18.519	592.4	38.00	512.2	.823	96.3	310.5	1005	300.0	0.16	0.2	20.60	15.95	19.54	6	3.0
18.406	590.3	37.94	510.0	.822	96.2	379.7	1124	300.0	0.16	45.6	20.60	15.78	18.69	6	4.0
18.394	590.3	37.92	509.9	.822	96.1	380.0	1124	300.0	0.16	47.2	20.60	15.78	18.81	6	5.0
18.392	590.4	37.91	510.0	.822	96.1	379.3	1123	300.0	0.16	49.6	20.60	15.78	18.80	6	6.0
18.369	595.1	37.47	515.0	.824	95.0	279.2	947	300.0	0.21	0.2	20.60	16.03	18.67	7	0.
18.368	595.3	37.46	515.1	.824	95.0	288.2	964	300.0	0.22	0.2	20.60	16.00	18.86	7	1.0

eff	V_{oc}	J_{sc}	V_{mp}	ff	C_{eff}	τ_{bulk}	L_d	X_L	X_f	X_b	log D_0	log D_B	log D_L	log S_f	log S_b
18.364	595.1	37.47	514.9	.823	95.0	287.5	962	300.0	0.21	0.2	20.60	16.01	18.97	7	2.0
18.336	594.6	37.46	514.4	.823	95.0	309.5	1003	300.0	0.22	0.2	20.60	15.95	19.54	7	3.0
18.219	592.2	37.41	511.8	.822	94.8	378.2	1121	300.0	0.21	48.5	20.60	15.78	18.66	7	4.0
18.208	592.7	37.35	512.4	.822	94.7	377.1	1120	300.0	0.21	50.0	20.60	15.78	18.78	7	5.0
18.205	592.1	37.39	511.7	.822	94.8	375.7	1117	300.0	0.20	50.0	20.60	15.79	18.80	7	6.0
18.350	595.2	37.43	515.1	.824	94.9	285.0	958	300.0	0.22	0.2	20.60	16.01	18.00	8	0.
18.348	594.8	37.46	514.7	.823	94.9	285.0	958	300.0	0.21	0.2	20.60	16.01	18.35	8	1.0
18.344	595.0	37.43	514.9	.823	94.9	286.6	961	300.0	0.22	0.2	20.60	16.01	18.97	8	2.0
18.316	594.5	37.43	514.3	.823	94.9	309.1	1002	300.0	0.22	0.2	20.60	15.95	19.53	8	3.0
18.197	591.9	37.39	511.6	.822	94.8	377.5	1120	300.0	0.21	50.0	20.60	15.78	18.66	8	4.0
18.187	592.4	37.34	512.0	.822	94.6	377.9	1121	300.0	0.21	50.0	20.60	15.78	18.79	8	5.0
18.186	592.4	37.33	512.1	.822	94.6	375.6	1117	300.0	0.21	50.0	20.60	15.79	18.80	8	6.0

Table 6.66 Effect of S_f and S_b at τ_{n0} = 0.4 ms, $X_L \leq 500$ μm, $O_{pl} = 2$

eff	V_{oc}	J_{sc}	V_{mp}	ff	C_{eff}	τ_{bulk}	L_d	X_L	X_f	X_b	log D_0	log D_B	log D_L	log S_f	log S_b
21.729	683.7	37.82	599.5	.840	99.5	69.7	440	115.2	0.10	0.2	17.99	16.52	17.31	0	0.
21.719	683.0	37.85	598.9	.840	99.5	70.9	444	117.3	0.10	0.2	17.87	16.51	18.02	0	1.0
21.666	679.7	37.96	595.8	.840	99.4	74.2	457	126.4	0.10	0.2	17.99	16.49	18.83	0	2.0
21.420	667.2	38.32	583.9	.838	99.1	93.4	524	168.3	0.10	0.2	18.14	16.36	19.42	0	3.0
20.911	649.7	38.55	567.4	.835	98.2	130.0	636	258.9	0.10	50.0	18.31	16.17	18.77	0	4.0
20.897	649.3	38.55	567.0	.835	98.1	129.8	636	266.1	0.10	50.0	17.89	16.17	18.87	0	5.0
20.896	649.3	38.55	566.9	.835	98.1	129.6	635	266.6	0.10	50.0	18.23	16.17	18.87	0	6.0
21.720	683.2	37.84	599.1	.840	99.5	69.9	440	116.3	0.10	0.2	18.21	16.52	17.84	1	0.
21.711	682.6	37.85	598.6	.840	99.5	70.0	441	117.9	0.10	0.2	18.12	16.52	18.23	1	1.0
21.659	679.3	37.97	595.4	.840	99.4	75.1	460	127.7	0.10	0.2	18.16	16.48	18.83	1	2.0
21.416	667.2	38.31	584.0	.838	99.1	91.2	517	167.5	0.10	0.2	18.20	16.38	19.43	1	3.0
20.909	649.3	38.58	567.0	.835	98.1	129.6	635	266.1	0.10	50.0	18.20	16.17	18.73	1	4.0
20.895	649.3	38.55	567.0	.835	98.1	128.8	633	266.3	0.10	50.0	18.21	16.17	18.85	1	5.0
20.894	649.2	38.55	566.9	.835	98.1	129.1	634	267.2	0.10	50.0	18.29	16.17	18.88	1	6.0
21.669	679.6	37.97	595.8	.840	99.4	72.9	452	126.3	0.10	0.2	18.76	16.50	17.80	2	0.
21.661	679.2	37.98	595.4	.840	99.4	73.6	454	127.5	0.10	0.2	18.76	16.49	18.13	2	1.0
21.614	676.5	38.07	592.8	.839	99.4	77.4	469	135.8	0.10	0.2	18.75	16.47	18.82	2	2.0
21.387	665.8	38.35	582.6	.838	99.1	93.9	526	172.1	0.10	0.2	18.76	16.36	19.43	2	3.0
20.893	649.0	38.56	566.8	.835	98.1	126.0	625	269.3	0.10	50.0	18.77	16.19	18.77	2	4.0
20.880	648.5	38.58	566.2	.835	98.1	131.7	641	269.5	0.10	50.0	18.76	16.16	18.86	2	5.0
20.879	648.4	38.58	566.1	.835	98.1	131.5	641	271.4	0.10	50.0	18.80	16.16	18.87	2	6.0
21.426	666.4	38.37	583.4	.838	99.3	87.3	504	166.4	0.10	0.2	19.32	16.40	18.03	3	0.
21.421	666.3	38.37	583.3	.838	99.3	87.3	504	166.4	0.10	0.2	19.32	16.40	18.03	3	1.0
21.390	665.0	38.40	582.0	.838	99.3	89.2	511	172.0	0.10	0.2	19.32	16.39	18.83	3	2.0
21.224	658.7	38.52	575.9	.836	99.1	103.3	557	195.0	0.10	0.2	19.33	16.31	19.44	3	3.0
20.800	645.4	38.63	563.3	.834	98.1	133.6	646	279.4	0.10	50.0	19.32	16.15	18.76	3	4.0
20.787	645.2	38.63	563.0	.834	98.1	137.0	656	279.6	0.10	50.0	19.32	16.13	18.85	3	5.0
20.786	645.2	38.63	563.0	.834	98.1	136.7	655	279.2	0.10	50.0	19.32	16.13	18.88	3	6.0
20.697	639.1	38.88	557.2	.833	99.0	125.0	622	259.3	0.10	0.2	19.85	16.19	18.08	4	0.
20.693	639.3	38.85	557.5	.833	99.0	123.5	618	252.4	0.10	0.2	19.86	16.20	18.98	4	1.0
20.683	638.8	38.87	556.9	.833	99.0	128.0	631	256.7	0.10	0.2	19.85	16.18	18.97	4	2.0
20.593	638.5	38.72	556.8	.833	99.1	131.4	640	222.6	0.10	0.2	19.84	16.16	19.47	4	3.0
20.362	630.6	38.85	549.0	.831	98.3	165.8	731	319.5	0.10	50.0	19.88	16.00	18.74	4	4.0
20.352	630.6	38.84	549.0	.831	98.3	164.0	726	322.7	0.10	50.0	19.87	16.01	18.86	4	5.0
20.351	630.8	38.82	549.2	.831	98.2	161.8	721	318.8	0.10	50.0	19.85	16.02	18.86	4	6.0
19.454	605.1	38.96	524.2	.825	98.4	173.6	750	351.4	0.10	0.2	20.39	15.97	18.06	5	0.
19.453	605.1	38.96	524.2	.825	98.3	173.0	749	351.5	0.10	0.2	20.40	15.97	18.96	5	1.0
19.448	605.0	38.96	524.0	.825	98.3	174.3	752	352.4	0.10	0.2	20.38	15.96	19.21	5	2.0
19.420	604.5	38.95	523.4	.825	98.3	180.7	767	357.8	0.10	0.2	20.39	15.93	19.57	5	3.0
19.309	602.3	38.92	521.1	.824	98.0	210.6	835	391.1	0.10	50.0	20.38	15.80	18.79	5	4.0
19.304	602.4	38.89	521.3	.824	97.9	205.0	823	391.8	0.10	50.0	20.40	15.83	18.82	5	5.0
19.303	602.4	38.89	521.3	.824	97.9	205.0	823	395.1	0.10	50.0	20.40	15.83	18.85	5	6.0
18.461	591.2	38.01	510.6	.822	95.8	182.7	772	370.8	0.17	0.2	20.60	15.93	18.78	6	0.
18.460	590.9	38.03	510.3	.821	95.9	184.9	777	375.5	0.16	0.2	20.60	15.92	19.13	6	1.0
18.457	590.9	38.02	510.4	.822	95.9	185.0	777	366.5	0.16	0.2	20.60	15.92	19.29	6	2.0
18.436	590.3	38.03	509.7	.821	95.9	193.6	797	368.2	0.16	0.2	20.60	15.88	19.52	6	3.0
18.353	588.3	38.04	507.4	.820	95.7	217.1	850	405.2	0.16	45.6	20.60	15.78	18.73	6	4.0
18.347	588.2	38.03	506.9	.820	95.7	217.3	850	410.0	0.16	47.2	20.60	15.78	18.85	6	5.0
18.347	588.3	38.01	507.5	.820	95.6	213.9	843	408.3	0.16	49.6	20.60	15.79	18.84	6	6.0
18.273	592.7	37.51	512.1	.822	94.6	185.8	779	368.2	0.21	0.2	20.60	15.91	19.18	7	0.
18.269	592.7	37.51	512.0	.822	94.4	183.5	774	399.9	0.22	0.2	20.60	15.92	19.31	7	1.0

eff	V_{oc}	J_{sc}	V_{mp}	ff	C_{eff}	τ_{bulk}	L_d	X_L	X_f	X_b	log D_0	log D_B	log D_L	log S_f	log S_b
18.270	592.8	37.49	512.1	.822	94.5	184.5	776	369.5	0.21	0.2	20.60	15.92	19.30	7	2.0
18.248	592.4	37.48	511.7	.822	94.5	192.0	794	369.3	0.22	0.2	20.60	15.89	19.50	7	3.0
18.163	589.8	37.53	508.9	.821	94.4	218.9	854	408.1	0.21	48.5	20.60	15.77	18.66	7	4.0
18.156	590.4	37.46	509.5	.821	94.2	215.6	846	408.6	0.21	50.0	20.60	15.78	18.82	7	5.0
18.156	589.8	37.51	509.0	.821	94.3	214.8	845	408.8	0.20	50.0	20.60	15.79	18.87	7	6.0
18.254	592.8	37.46	512.1	.822	94.4	185.0	777	376.1	0.22	0.2	20.60	15.92	18.97	8	0.
18.253	592.5	37.48	512.0	.822	94.5	184.1	775	365.9	0.21	0.2	20.60	15.92	19.06	8	1.0
18.250	592.7	37.46	512.1	.822	94.4	184.5	776	370.1	0.22	0.2	20.60	15.92	19.30	8	2.0
18.228	592.2	37.46	511.5	.822	94.4	191.6	793	374.0	0.22	0.2	20.60	15.89	19.59	8	3.0
18.143	589.6	37.50	508.7	.820	94.3	218.9	854	408.1	0.21	50.0	20.60	15.77	18.66	8	4.0
18.137	590.0	37.45	509.2	.821	94.2	216.0	847	409.8	0.21	50.0	20.60	15.78	18.86	8	5.0
18.136	590.1	37.44	509.3	.821	94.2	214.7	845	410.3	0.21	50.0	20.60	15.79	18.85	8	6.0

Table 6.67 Effect of S_f and S_b at τ_{n0} = 0.1 ms, $X_L \leq 300$ μm, O_{pl} = 2

eff	V_{oc}	J_{sc}	V_{mp}	ff	C_{eff}	τ_{bulk}	L_d	X_L	X_f	X_b	log D_0	log D_B	log D_L	log S_f	log S_b
20.318	655.8	37.05	573.4	.836	99.3	26.8	284	79.8	0.10	15.0	17.85	16.29	16.66	0	0.
20.277	657.0	36.91	574.5	.836	99.2	20.7	244	75.1	0.10	0.2	18.04	16.43	17.69	0	1.0
20.251	654.9	36.99	572.5	.836	99.2	21.6	250	79.1	0.10	0.2	18.03	16.41	18.60	0	2.0
20.127	647.4	37.24	565.4	.835	98.9	24.7	271	94.7	0.10	0.2	18.01	16.33	19.33	0	3.0
19.961	642.0	37.29	560.2	.834	98.8	27.4	288	100.0	0.10	0.2	17.89	16.27	19.63	0	3.5
19.696	629.1	37.67	547.9	.831	97.6	37.3	344	163.4	0.10	50.0	17.92	16.08	18.42	0	4.0
19.677	628.6	37.66	547.4	.831	97.4	37.2	344	168.9	0.10	50.0	17.81	16.08	18.58	0	5.0
19.675	628.6	37.66	547.4	.831	97.4	37.3	344	169.1	0.10	50.0	17.99	16.08	18.61	0	6.0
20.314	655.8	37.04	573.5	.836	99.3	26.8	284	79.6	0.10	14.6	18.03	16.29	16.65	1	0.
20.275	656.7	36.92	574.2	.836	99.2	20.7	244	75.6	0.10	0.2	18.16	16.43	17.70	1	1.0
20.248	654.9	36.98	572.5	.836	99.1	21.3	248	79.0	0.10	0.2	18.15	16.42	18.60	1	2.0
20.125	647.3	37.25	565.2	.835	98.9	24.9	272	95.1	0.10	0.2	18.14	16.33	19.33	1	3.0
19.958	641.9	37.29	560.2	.834	98.8	27.4	288	100.0	0.10	0.2	17.84	16.27	19.62	1	3.5
19.694	629.1	37.66	547.9	.831	97.6	37.4	345	162.3	0.10	50.0	18.43	16.07	18.41	1	4.0
19.676	628.6	37.66	547.4	.831	97.4	37.5	345	167.9	0.10	50.0	18.08	16.07	18.59	1	5.0
19.674	628.6	37.66	547.4	.831	97.4	37.5	345	168.3	0.10	50.0	18.32	16.07	18.61	1	6.0
20.311	653.4	37.19	571.1	.836	99.3	35.1	332	84.8	0.10	50.0	18.57	16.12	16.83	2	0.
20.253	654.9	36.99	572.5	.836	99.2	21.3	248	78.9	0.10	0.2	18.63	16.42	17.70	2	1.0
20.228	653.4	37.04	571.1	.836	99.1	21.7	250	81.8	0.10	0.2	18.63	16.41	18.59	2	2.0
20.110	646.4	37.28	564.5	.834	98.9	24.9	272	96.8	0.10	0.2	18.63	16.33	19.32	2	3.0
19.947	641.4	37.30	559.7	.834	98.8	27.9	291	100.0	0.10	0.2	18.63	16.26	19.63	2	3.5
19.687	628.5	37.69	547.3	.831	97.6	38.1	348	164.1	0.10	50.0	18.62	16.06	18.42	2	4.0
19.669	628.3	37.67	547.1	.831	97.4	37.5	345	168.5	0.10	50.0	18.62	16.07	18.58	2	5.0
19.667	628.3	37.66	547.1	.831	97.4	37.2	344	169.2	0.10	50.0	18.60	16.08	18.60	2	6.0
20.143	647.8	37.24	565.9	.835	99.0	23.3	262	92.4	0.10	0.2	19.27	16.37	17.28	3	0.
20.140	647.4	37.26	565.5	.835	99.0	23.5	263	93.6	0.10	0.2	19.26	16.36	17.71	3	1.0
20.120	646.3	37.30	564.4	.835	99.0	24.3	268	96.2	0.10	0.2	19.27	16.34	18.60	3	2.0
20.022	641.5	37.44	559.8	.834	98.8	26.9	285	107.1	0.10	0.2	19.25	16.29	19.33	3	3.0
19.871	639.0	37.32	557.5	.833	98.9	28.8	296	100.0	0.10	0.2	19.27	16.24	19.63	3	3.5
19.640	626.5	37.74	545.4	.831	97.6	39.1	353	168.4	0.10	50.0	19.27	16.04	18.41	3	4.0
19.622	626.3	37.72	545.1	.831	97.5	38.7	351	172.7	0.10	50.0	19.26	16.05	18.58	3	5.0
19.620	626.3	37.71	545.2	.831	97.4	38.3	349	173.2	0.10	50.0	19.27	16.06	18.60	3	6.0
19.790	627.4	37.94	546.5	.831	98.9	38.0	348	141.3	0.10	50.0	19.83	16.06	16.71	4	0.
19.714	627.3	37.81	546.8	.831	98.7	31.7	314	137.1	0.10	0.2	19.82	16.18	17.70	4	1.0
19.704	627.1	37.81	546.1	.831	98.6	31.4	312	138.3	0.10	0.2	19.82	16.19	18.70	4	2.0
19.651	625.2	37.84	544.2	.831	98.6	33.8	325	143.0	0.10	0.2	19.83	16.14	19.36	4	3.0
19.395	616.9	37.94	536.2	.829	97.6	43.2	374	192.1	0.10	50.0	19.84	15.97	18.40	4	4.0
19.379	617.0	37.90	536.3	.829	97.5	42.8	372	192.8	0.10	50.0	19.84	15.98	18.57	4	5.0
19.377	616.9	37.90	536.2	.829	97.5	43.2	374	192.3	0.10	50.0	19.84	15.97	18.58	4	6.0
18.866	598.8	38.20	518.8	.825	98.2	49.3	402	199.7	0.10	50.0	20.37	15.86	16.77	5	0.
18.796	598.6	38.07	518.6	.825	97.9	44.4	380	197.9	0.10	0.2	20.38	15.95	18.85	5	1.0
18.793	598.4	38.08	518.4	.825	97.8	44.9	382	199.9	0.10	0.2	20.37	15.94	18.73	5	2.0
18.770	598.0	38.07	517.9	.824	97.8	45.8	386	200.5	0.10	0.2	20.38	15.92	19.41	5	3.0
18.637	595.3	38.00	515.3	.824	97.6	51.8	414	204.9	0.10	21.8	20.38	15.82	18.90	5	4.0
18.628	594.6	38.04	514.6	.824	97.2	53.1	419	234.8	0.10	49.9	20.36	15.80	18.52	5	5.0
18.627	594.5	38.05	514.7	.823	97.2	53.5	421	235.4	0.10	50.0	20.36	15.79	18.55	5	6.0
17.913	583.7	37.37	504.2	.821	95.9	49.6	404	204.8	0.14	0.2	20.60	15.86	17.63	6	0.
17.910	583.0	37.43	503.4	.821	95.8	50.5	408	222.3	0.14	0.2	20.60	15.84	17.93	6	1.0
17.906	583.0	37.42	503.4	.821	95.8	50.6	408	222.9	0.14	0.2	20.60	15.84	18.04	6	2.0
17.893	582.5	37.42	503.0	.821	96.1	49.9	405	205.1	0.13	0.2	20.60	15.85	19.48	6	3.0
17.806	580.2	37.43	500.6	.820	95.7	57.1	437	230.4	0.13	31.0	20.60	15.73	18.67	6	4.0

eff	V_{oc}	J_{sc}	V_{mp}	ff	C_{eff}	τ_{bulk}	L_d	X_L	X_f	X_b	log D_0	log D_B	log D_L	log S_f	log S_b
17.802	579.6	37.47	500.0	.820	95.5	58.0	440	254.0	0.13	49.9	20.60	15.71	18.54	6	5.0
17.801	579.4	37.49	499.7	.819	95.4	58.6	443	260.8	0.13	49.6	20.60	15.70	18.55	6	6.0
17.714	585.2	36.84	505.7	.822	94.6	49.2	402	205.0	0.19	0.2	20.60	15.87	17.63	7	0.
17.709	584.3	36.91	504.6	.821	94.5	50.5	408	222.8	0.18	0.2	20.60	15.84	19.26	7	1.0
17.707	584.7	36.87	505.1	.821	94.4	49.5	403	219.4	0.18	0.2	20.60	15.86	19.29	7	2.0
17.694	584.7	36.84	505.1	.821	94.6	50.5	408	205.0	0.18	0.2	20.60	15.84	19.39	7	3.0
17.611	581.0	36.96	501.4	.820	94.2	58.1	441	251.6	0.17	49.9	20.60	15.71	18.33	7	4.0
17.601	580.6	36.98	501.0	.820	94.3	58.0	440	251.0	0.17	50.0	20.60	15.71	18.52	7	5.0
17.599	581.0	36.94	501.3	.820	94.1	57.8	440	257.1	0.17	50.0	20.60	15.71	18.54	7	6.0
17.691	584.9	36.82	505.3	.821	94.4	49.5	403	213.7	0.19	0.2	20.60	15.86	17.82	8	0.
17.688	584.9	36.82	505.3	.821	94.3	49.5	403	217.2	0.19	0.2	20.60	15.86	19.28	8	1.0
17.686	584.2	36.87	504.6	.821	94.4	50.3	407	222.2	0.18	0.2	20.60	15.85	19.26	8	2.0
17.673	584.9	36.78	505.4	.821	94.4	50.5	408	205.1	0.19	0.2	20.60	15.84	19.41	8	3.0
17.590	581.2	36.91	501.5	.820	94.0	58.1	441	252.8	0.18	50.0	20.60	15.71	18.33	8	4.0
17.607	580.9	36.96	501.3	.820	94.2	58.0	440	251.0	0.17	50.0	20.60	15.71	18.52	8	5.0
17.578	581.1	36.89	501.4	.820	93.9	57.9	440	257.0	0.18	50.0	20.60	15.71	18.54	8	6.0

Table 6.68 Effect of S_f and S_b at τ_{n0} = 0.1 ms, $X_L \leq 100$ μm, O_{pl} = 2

eff	V_{oc}	J_{sc}	V_{mp}	ff	C_{eff}	τ_{bulk}	L_d	X_L	X_f	X_b	log D_0	log D_B	log D_L	log S_f	log S_b
20.283	657.3	36.90	574.8	.836	99.2	20.6	243	74.6	0.10	0.2	18.13	16.44	17.24	0	0.
20.277	656.9	36.91	574.4	.836	99.2	20.7	244	75.2	0.10	0.2	18.04	16.43	17.69	0	1.0
20.251	655.0	36.99	572.5	.836	99.2	21.6	250	79.0	0.10	0.2	18.03	16.41	18.60	0	2.0
20.127	647.4	37.25	565.4	.835	98.9	24.7	271	94.8	0.10	0.2	18.05	16.33	19.33	0	3.0
19.555	636.3	36.91	554.7	.833	97.8	40.8	362	100.0	0.10	49.8	17.97	16.01	18.34	0	4.0
19.513	636.5	36.82	554.9	.833	97.5	40.5	361	100.0	0.10	49.8	18.30	16.02	18.51	0	5.0
19.510	636.5	36.81	554.9	.833	97.5	40.5	361	100.0	0.10	49.8	17.91	16.02	18.53	0	6.0
20.279	656.4	36.94	574.0	.836	99.2	20.7	244	76.8	0.10	0.2	18.31	16.43	17.28	1	0.
20.275	656.7	36.92	574.2	.836	99.2	20.7	244	75.6	0.10	0.2	18.16	16.43	17.70	1	1.0
20.248	654.9	36.98	572.6	.836	99.1	21.3	248	78.9	0.10	0.2	18.15	16.42	18.60	1	2.0
20.125	647.3	37.25	565.2	.835	98.9	24.9	272	95.1	0.10	0.2	18.14	16.33	19.33	1	3.0
19.553	636.2	36.92	554.6	.833	97.8	41.1	363	100.0	0.10	49.8	18.52	16.01	18.34	1	4.0
19.512	636.4	36.82	554.9	.833	97.5	40.9	363	100.0	0.10	49.8	17.99	16.01	18.53	1	5.0
19.508	636.5	36.81	555.0	.833	97.5	40.1	358	100.0	0.10	49.8	18.24	16.03	18.53	1	6.0
20.258	654.8	37.01	572.4	.836	99.2	21.3	248	79.8	0.10	0.2	18.66	16.42	17.14	2	0.
20.253	654.9	36.99	572.5	.836	99.2	21.3	248	78.9	0.10	0.2	18.63	16.42	17.69	2	1.0
20.228	653.4	37.04	571.1	.836	99.1	21.7	250	81.8	0.10	0.2	18.62	16.41	18.59	2	2.0
20.110	646.4	37.28	564.4	.834	98.9	24.9	272	97.1	0.10	0.2	18.65	16.33	19.30	2	3.0
19.544	635.9	36.91	554.4	.833	97.8	40.7	362	100.0	0.10	49.8	18.55	16.01	18.33	2	4.0
19.502	636.1	36.82	554.6	.833	97.5	40.7	361	100.0	0.10	49.8	18.56	16.01	18.51	2	5.0
19.498	636.2	36.81	554.6	.833	97.5	40.5	361	100.0	0.10	49.8	18.54	16.02	18.53	2	6.0
20.143	647.8	37.25	565.8	.835	99.0	23.3	262	92.6	0.10	0.2	19.25	16.37	17.44	3	0.
20.140	647.4	37.26	565.5	.835	99.0	23.5	263	93.6	0.10	0.2	19.26	16.36	17.71	3	1.0
20.120	646.3	37.30	564.4	.835	99.0	24.3	268	95.9	0.10	0.2	19.27	16.34	18.67	3	2.0
20.022	642.9	37.34	561.2	.834	98.9	26.1	280	100.0	0.10	0.2	19.27	16.30	19.33	3	3.0
19.483	633.9	36.93	552.5	.832	97.8	42.0	368	100.0	0.10	49.8	19.24	15.99	18.34	3	4.0
19.440	634.2	36.83	552.8	.832	97.6	41.4	365	100.0	0.10	49.8	19.23	16.00	18.51	3	5.0
19.436	634.2	36.82	552.8	.832	97.5	41.4	365	100.0	0.10	49.8	19.23	16.00	18.53	3	6.0
19.683	632.2	37.40	551.1	.832	99.1	28.9	297	100.0	0.10	0.5	19.84	16.24	16.58	4	0.
19.678	632.2	37.40	551.1	.832	99.1	28.7	296	100.0	0.10	0.2	19.84	16.25	17.70	4	1.0
19.666	631.9	37.40	550.8	.832	99.1	29.1	298	100.0	0.10	0.2	19.84	16.24	18.61	4	2.0
19.601	630.3	37.38	549.3	.832	99.0	30.8	308	100.0	0.10	0.2	19.84	16.20	19.34	4	3.0
19.169	623.9	37.00	543.0	.830	98.0	48.9	401	100.0	0.10	49.8	19.85	15.87	18.28	4	4.0
19.124	624.1	36.90	543.7	.830	97.7	48.5	399	100.0	0.10	49.8	19.85	15.88	18.47	4	5.0
19.120	624.2	36.89	543.3	.830	97.7	48.4	398	100.0	0.10	49.8	19.85	15.88	18.50	4	6.0
18.643	603.6	37.36	523.9	.827	98.9	51.0	410	100.0	0.10	50.0	20.40	15.83	16.78	5	0.
18.588	603.2	37.28	523.4	.827	98.8	40.2	359	100.0	0.10	0.2	20.38	16.02	18.77	5	1.0
18.585	603.1	37.28	523.3	.827	98.8	40.7	361	100.0	0.10	0.2	20.38	16.02	18.69	5	2.0
18.558	602.5	37.27	522.8	.826	98.7	41.7	367	100.0	0.10	0.2	20.38	16.00	19.34	5	3.0
18.355	599.0	37.12	519.3	.825	98.3	55.5	430	100.0	0.10	21.7	20.39	15.76	18.69	5	4.0
18.229	599.6	36.83	519.8	.825	97.6	62.1	457	100.0	0.10	49.8	20.39	15.64	18.36	5	5.0
18.224	599.5	36.82	519.7	.825	97.5	62.2	458	100.0	0.10	49.8	20.39	15.64	18.37	5	6.0
17.632	588.4	36.39	509.3	.823	96.4	43.7	376	100.0	0.15	0.2	20.60	15.96	17.58	6	0.
17.632	588.4	36.40	509.3	.823	96.4	44.5	380	100.0	0.15	0.2	20.60	15.95	17.89	6	1.0
17.628	588.3	36.39	509.2	.823	96.4	43.7	376	100.0	0.15	0.2	20.60	15.96	18.05	6	2.0
17.608	585.2	36.58	506.1	.822	96.9	49.5	403	100.0	0.13	0.2	20.60	15.86	19.44	6	3.0
17.433	584.8	36.25	505.7	.822	96.0	62.3	458	100.0	0.15	30.9	20.60	15.63	18.43	6	4.0
17.324	584.0	36.06	505.1	.822	95.5	63.4	462	100.0	0.14	49.8	20.60	15.61	18.38	6	5.0
17.320	583.9	36.07	505.0	.822	95.5	63.9	465	100.0	0.14	49.5	20.60	15.60	18.39	6	6.0
17.439	590.1	35.88	510.9	.824	95.0	43.6	376	100.0	0.20	0.2	20.60	15.96	17.58	7	0.
17.435	589.9	35.88	510.8	.824	95.0	44.0	378	100.0	0.20	0.2	20.60	15.96	19.17	7	1.0

eff	V_{oc}	J_{sc}	V_{mp}	ff	C_{eff}	τ_{bulk}	L_d	X_L	X_f	X_b	log D_0	log D_B	log D_L	log S_f	log S_b
17.433	589.8	35.88	510.7	.824	95.0	44.1	378	100.0	0.20	0.2	20.60	15.95	19.20	7	2.0
17.416	589.2	35.89	510.0	.823	95.1	47.1	392	100.0	0.20	0.2	20.60	15.90	19.33	7	3.0
17.178	585.5	35.65	506.5	.823	94.4	63.6	463	100.0	0.19	49.8	20.60	15.61	18.17	7	4.0
17.124	585.8	35.54	506.7	.822	94.1	67.4	478	100.0	0.19	49.8	20.60	15.54	18.30	7	5.0
17.119	585.7	35.54	506.5	.822	94.1	67.1	477	100.0	0.19	49.8	20.60	15.54	18.32	7	6.0

Table 6.69 Effect of S_f and S_b at τ_{n0} = 0.1 ms, no BSF, $X_L \leq 100$ μm, $O_{pl} = 2$

eff	V_{oc}	J_{sc}	V_{mp}	ff	C_{eff}	τ_{bulk}	L_d	X_L	X_f	X_b	log D_0	log D_B	log D_L	log S_f	log S_b
20.280	657.3	36.89	574.8	.836	99.2	20.6	243	74.3	0.10	0.	18.09	16.44	0.	0	0.
20.255	656.2	36.91	573.8	.836	99.1	20.1	239	76.3	0.10	0.	18.04	16.45	0.	0	1.0
20.055	650.4	36.90	568.6	.836	98.5	17.0	216	85.6	0.10	0.	18.03	16.54	0.	0	2.0
19.160	638.7	35.97	557.7	.834	95.3	11.2	166	100.0	0.10	0.	18.18	16.75	0.	0	3.0
18.015	628.6	34.55	547.2	.829	91.5	7.3	125	100.0	2.10	0.	17.85	16.95	0.	0	4.0
17.660	636.2	33.33	555.2	.833	88.3	5.0	96	100.0	0.11	0.	18.67	17.12	0.	0	5.0
17.627	636.1	33.28	555.1	.833	88.1	5.0	95	100.0	0.12	0.	18.63	17.13	0.	0	6.0
20.277	656.4	36.94	573.9	.836	99.2	20.7	244	76.8	0.10	0.	18.27	16.43	0.	1	0.
20.252	656.3	36.90	573.9	.836	99.1	20.0	239	75.6	0.10	0.	18.18	16.45	0.	1	1.0
20.051	652.1	36.78	570.3	.836	98.6	16.3	211	78.9	0.10	0.	18.15	16.56	0.	1	2.0
19.148	639.0	35.93	558.0	.834	95.4	11.0	164	95.1	0.10	0.	18.49	16.76	0.	1	3.0
17.955	635.3	33.93	554.4	.833	89.9	6.2	112	100.0	0.10	0.	18.64	17.03	0.	1	4.0
17.659	636.1	33.33	555.1	.833	88.3	5.1	97	100.0	0.10	0.	18.72	17.12	0.	1	5.0
17.626	636.2	33.26	555.2	.833	88.1	4.9	95	100.0	0.10	0.	18.71	17.13	0.	1	6.0
20.256	654.7	37.01	572.4	.836	99.2	21.3	248	79.8	0.10	0.	18.64	16.42	0.	2	0.
20.232	654.6	36.97	572.3	.836	99.1	20.4	242	78.9	0.10	0.	18.63	16.44	0.	2	1.0
20.035	650.7	36.83	569.0	.836	98.6	16.7	214	81.8	0.10	0.	18.62	16.55	0.	2	2.0
19.143	638.4	35.96	557.4	.834	95.4	11.2	166	97.1	0.10	0.	18.72	16.75	0.	2	3.0
17.946	635.5	33.90	554.6	.833	89.8	6.1	110	100.0	0.10	0.	18.68	17.04	0.	2	4.0
17.650	635.5	33.35	554.6	.833	88.3	5.2	98	100.0	0.10	0.	18.71	17.11	0.	2	5.0
17.617	635.6	33.28	554.6	.833	88.2	5.1	97	100.0	0.10	0.	18.71	17.12	0.	2	6.0
20.141	647.6	37.25	565.6	.835	99.0	23.3	262	93.3	0.10	0.	19.25	16.37	0.	3	0.
20.120	646.9	37.26	565.5	.835	99.0	23.0	260	94.6	0.10	0.	19.26	16.38	0.	3	1.0
19.940	643.3	37.14	561.9	.835	98.4	19.6	236	100.0	0.10	0.	19.27	16.46	0.	3	2.0
19.081	635.6	36.02	554.8	.833	95.4	11.8	171	100.0	0.10	0.	19.27	16.72	0.	3	3.0
17.887	632.7	33.95	552.0	.833	89.9	6.4	114	100.0	0.10	0.	19.27	17.01	0.	3	4.0
17.590	633.6	33.34	552.8	.833	88.3	5.1	98	100.0	0.10	0.	19.26	17.11	0.	3	5.0
17.557	633.7	33.28	552.9	.833	88.1	5.0	96	100.0	0.10	0.	19.25	17.12	0.	3	6.0
19.679	632.2	37.40	551.0	.832	99.1	28.9	297	100.0	0.10	0.	19.84	16.24	0.	4	0.
19.661	631.9	37.38	550.9	.832	99.0	28.2	293	100.0	0.10	0.	19.83	16.26	0.	4	1.0
19.512	630.1	37.21	549.4	.832	98.5	23.4	262	100.0	0.10	0.	19.84	16.37	0.	4	2.0
18.744	623.9	36.14	543.6	.831	95.7	14.1	192	100.0	0.10	0.	19.84	16.64	0.	4	3.0
17.578	621.4	34.06	541.2	.831	90.2	7.5	128	100.0	0.10	0.	19.80	16.94	0.	4	4.0
17.273	622.3	33.42	542.0	.831	88.5	5.9	108	100.0	0.10	0.	19.80	17.05	0.	4	5.0
17.238	622.4	33.34	542.1	.831	88.3	5.8	106	100.0	0.10	0.	19.80	17.06	0.	4	6.0
18.589	603.2	37.28	523.4	.827	98.8	39.9	357	100.0	0.10	0.	20.37	16.03	0.	5	0.
18.577	603.1	37.26	523.4	.827	98.7	39.0	353	100.0	0.10	0.	20.37	16.05	0.	5	1.0
18.473	602.1	37.12	522.5	.827	98.3	33.3	322	100.0	0.10	0.	20.37	16.15	0.	5	2.0
17.861	597.9	36.17	518.8	.826	95.8	21.0	246	100.0	0.10	0.	20.36	16.43	0.	5	3.0
16.751	595.8	34.06	516.8	.825	90.2	11.1	165	100.0	0.10	0.	20.35	16.75	0.	5	4.0
16.424	596.5	33.35	517.4	.825	88.3	8.5	138	100.0	0.10	0.	20.35	16.88	0.	5	5.0
16.387	596.6	33.27	517.5	.826	88.1	8.1	134	100.0	0.10	0.	20.34	16.90	0.	5	6.0
17.631	588.1	36.41	509.0	.823	96.4	43.7	376	100.0	0.15	0.	20.60	15.96	0.	6	0.
17.622	588.0	36.40	509.0	.823	96.4	42.6	371	100.0	0.15	0.	20.60	15.98	0.	6	1.0
17.537	586.7	36.31	507.9	.823	96.2	37.8	347	100.0	0.14	0.	20.60	16.07	0.	6	2.0
17.003	580.9	35.60	502.5	.822	94.3	26.0	279	100.0	0.12	0.	20.60	16.31	0.	6	3.0
15.944	577.0	33.64	498.9	.821	89.1	14.3	194	100.0	0.10	0.	20.60	16.63	0.	6	4.0
15.611	579.3	32.79	501.0	.822	86.9	10.2	156	100.0	0.11	0.	20.60	16.79	0.	6	5.0
15.570	578.2	32.78	499.9	.821	86.8	9.6	150	100.0	0.10	0.	20.60	16.82	0.	6	6.0
17.438	589.9	35.89	510.7	.824	95.1	42.9	372	100.0	0.20	0.	20.60	15.98	0.	7	0.
17.428	589.7	35.88	510.5	.824	95.0	42.3	369	100.0	0.20	0.	20.60	15.99	0.	7	1.0

eff	V_{oc}	J_{sc}	V_{mp}	ff	C_{eff}	τ_{bulk}	L_d	X_L	X_f	X_b	log D_0	log D_B	log D_L	log S_f	log S_b
17.342	588.5	35.78	509.6	.824	94.8	37.1	343	100.0	0.19	0.	20.60	16.08	0.	7	2.0
16.803	583.5	35.00	505.0	.823	92.7	24.8	272	100.0	0.17	0.	20.60	16.33	0.	7	3.0
15.741	579.0	33.08	500.8	.822	87.6	13.7	189	100.0	0.14	0.	20.60	16.65	0.	7	4.0
15.411	581.3	32.25	502.9	.822	85.4	9.8	152	100.0	0.15	0.	20.60	16.81	0.	7	5.0
15.373	581.5	32.16	503.1	.822	85.2	9.4	148	100.0	0.15	0.	20.60	16.84	0.	7	6.0

Table 6.70 Effect of S_f and S_b at τ_{n0} = 0.05 ms, $X_L \leq 100$ μm, O_{pl} = 2

eff	V_{oc}	J_{sc}	V_{mp}	ff	C_{eff}	τ_{bulk}	L_d	X_L	X_f	X_b	log D_0	log D_B	log D_L	log S_f	log S_b
19.546	644.8	36.35	562.9	.834	99.1	11.2	181	58.0	0.10	0.2	18.07	16.39	17.10	0	0.
19.542	644.5	36.36	562.6	.834	99.0	11.2	181	58.5	0.10	0.2	18.02	16.39	17.55	0	1.0
19.521	643.1	36.41	561.3	.834	99.0	11.5	184	60.5	0.10	0.2	18.00	16.37	18.43	0	2.0
19.429	637.1	36.62	555.6	.833	98.8	13.1	198	69.7	0.10	0.2	18.01	16.30	19.23	0	3.0
18.994	622.2	36.78	541.4	.830	97.4	21.7	265	100.0	0.10	50.0	17.95	15.97	18.10	0	4.0
18.951	622.8	36.66	541.9	.830	97.1	21.1	261	100.0	0.10	50.0	18.25	15.99	18.32	0	5.0
18.947	622.9	36.65	542.0	.830	97.1	21.1	261	100.0	0.10	50.0	17.85	15.99	18.36	0	6.0
19.536	640.4	36.61	558.8	.833	98.9	11.8	186	68.8	0.10	0.2	18.20	16.36	17.10	1	0.
19.534	640.8	36.58	559.1	.833	98.9	11.8	186	67.6	0.10	0.2	18.14	16.36	17.57	1	1.0
19.513	638.9	36.66	557.3	.833	98.9	12.5	193	70.9	0.10	0.2	18.13	16.33	18.45	1	2.0
19.412	631.9	36.93	550.7	.832	98.5	13.9	205	87.1	0.10	0.2	18.12	16.26	19.24	1	3.0
18.992	622.3	36.78	541.4	.830	97.4	21.6	264	100.0	0.10	50.0	18.47	15.97	18.13	1	4.0
18.951	622.8	36.66	541.9	.830	97.1	21.2	261	100.0	0.10	50.0	17.97	15.99	18.33	1	5.0
18.946	622.9	36.65	542.0	.830	97.1	21.1	261	100.0	0.10	50.0	18.21	15.99	18.37	1	6.0
19.520	638.8	36.68	557.2	.833	98.8	12.4	191	71.8	0.10	0.2	18.50	16.33	16.97	2	0.
19.518	639.1	36.66	557.5	.833	98.8	12.2	190	70.9	0.10	0.2	18.52	16.34	17.54	2	1.0
19.497	637.7	36.71	556.2	.833	98.8	12.4	191	73.8	0.10	0.2	18.54	16.33	18.42	2	2.0
19.400	631.1	36.96	549.9	.832	98.5	14.1	207	89.1	0.10	0.2	18.52	16.26	19.22	2	3.0
18.986	622.0	36.78	541.1	.830	97.4	21.7	265	100.0	0.10	50.0	18.49	15.97	18.11	2	4.0
18.944	622.6	36.66	541.7	.830	97.1	21.2	261	100.0	0.10	50.0	18.51	15.98	18.34	2	5.0
18.940	622.6	36.65	541.8	.830	97.1	21.1	261	100.0	0.10	50.0	18.48	15.99	18.36	2	6.0
19.433	632.7	36.92	551.4	.832	98.6	13.3	200	84.6	0.10	0.2	19.18	16.29	17.28	3	0.
19.429	632.2	36.94	550.9	.832	98.6	13.6	203	85.6	0.10	0.2	19.19	16.28	17.58	3	1.0
19.411	631.4	36.96	550.2	.832	98.5	13.6	203	87.9	0.10	0.2	19.17	16.28	18.48	3	2.0
19.330	627.0	37.10	546.0	.831	98.3	14.9	213	99.1	0.10	0.2	19.20	16.22	19.24	3	3.0
18.947	620.6	36.80	539.8	.830	97.5	22.2	268	100.0	0.10	50.0	19.20	15.95	18.10	3	4.0
18.904	621.2	36.68	540.4	.830	97.1	21.6	264	100.0	0.10	50.0	19.20	15.97	18.33	3	5.0
18.899	621.3	36.66	540.5	.830	97.1	21.5	264	100.0	0.10	50.0	19.20	15.97	18.35	3	6.0
19.127	620.0	37.18	539.4	.830	98.5	16.1	224	100.0	0.10	0.5	19.82	16.17	16.54	4	0.
19.124	620.1	37.17	539.5	.830	98.5	15.9	222	100.0	0.10	0.2	19.82	16.18	17.52	4	1.0
19.115	619.9	37.17	539.3	.830	98.4	16.0	222	100.0	0.10	0.2	19.82	16.18	18.60	4	2.0
19.069	618.7	37.16	538.2	.829	98.4	16.5	227	100.0	0.10	0.2	19.81	16.16	19.26	4	3.0
18.736	613.8	36.85	533.3	.828	97.6	24.3	282	100.0	0.10	50.0	19.82	15.88	18.05	4	4.0
18.689	614.3	36.73	533.9	.828	97.3	23.7	279	100.0	0.10	50.0	19.82	15.90	18.30	4	5.0
18.685	614.3	36.71	533.9	.828	97.3	23.7	278	100.0	0.10	50.0	19.81	15.90	18.32	4	6.0
18.387	598.3	37.23	518.8	.825	98.6	26.3	295	100.0	0.10	50.0	20.37	15.80	16.80	5	0.
18.297	597.8	37.09	518.3	.825	98.2	20.6	257	100.0	0.10	0.2	20.38	16.01	18.19	5	1.0
18.293	597.7	37.09	518.2	.825	98.2	20.7	258	100.0	0.10	0.2	20.37	16.00	18.43	5	2.0
18.269	597.2	37.08	517.6	.825	98.2	21.2	261	100.0	0.10	0.2	20.36	15.98	19.25	5	3.0
18.080	593.7	36.95	514.2	.824	97.9	26.2	294	100.0	0.10	21.8	20.38	15.81	18.49	5	4.0
17.980	594.6	36.68	515.1	.824	97.1	29.4	314	100.0	0.10	49.9	20.38	15.70	18.21	5	5.0
17.974	594.6	36.66	515.1	.824	97.1	29.4	314	100.0	0.10	50.0	20.38	15.70	18.24	5	6.0
17.427	583.3	36.35	504.4	.822	96.3	23.1	274	100.0	0.14	0.2	20.60	15.92	17.10	6	0.
17.427	583.1	36.36	504.2	.822	96.3	23.1	275	100.0	0.14	0.2	20.60	15.92	17.56	6	1.0
17.424	583.1	36.35	504.2	.822	96.3	23.1	274	100.0	0.14	0.2	20.60	15.92	18.40	6	2.0
17.408	581.8	36.41	502.9	.822	96.4	24.0	280	100.0	0.13	0.2	20.60	15.88	19.34	6	3.0
17.252	579.4	36.27	500.5	.821	96.1	30.1	318	100.0	0.13	31.0	20.60	15.67	18.18	6	4.0
17.155	579.4	36.06	500.6	.821	95.5	32.5	331	100.0	0.13	49.9	20.60	15.58	18.15	6	5.0
17.150	579.4	36.05	500.6	.821	95.5	32.4	331	100.0	0.13	49.6	20.60	15.58	18.19	6	6.0
17.226	584.8	35.81	505.9	.822	94.9	22.8	272	100.0	0.19	0.2	20.60	15.93	17.11	7	0.
17.225	584.5	35.83	505.6	.822	94.9	22.9	273	100.0	0.18	0.2	20.60	15.93	18.26	7	1.0

eff	V_{oc}	J_{sc}	V_{mp}	ff	C_{eff}	τ_{bulk}	L_d	X_L	X_f	X_b	log D_0	log D_B	log D_L	log S_f	log S_b
17.222	584.7	35.82	505.7	.822	94.9	23.0	274	100.0	0.18	0.2	20.60	15.92	18.43	7	2.0
17.205	584.2	35.81	505.3	.822	94.9	23.5	277	100.0	0.18	0.2	20.60	15.90	19.26	7	3.0
17.008	580.5	35.67	501.6	.821	94.5	32.8	333	100.0	0.17	49.9	20.60	15.57	17.84	7	4.0
16.948	580.3	35.56	501.4	.821	94.2	32.3	330	100.0	0.17	50.0	20.60	15.59	18.16	7	5.0
16.943	580.9	35.51	502.0	.821	94.0	32.2	330	100.0	0.17	50.0	20.60	15.59	18.19	7	6.0
17.205	584.8	35.77	505.9	.822	94.8	22.7	272	100.0	0.19	0.2	20.60	15.93	17.10	8	0.
17.204	584.9	35.76	506.0	.822	94.7	22.7	271	100.0	0.19	0.2	20.60	15.93	18.32	8	1.0
17.202	584.3	35.80	505.4	.822	94.8	23.0	274	100.0	0.18	0.2	20.60	15.92	18.38	8	2.0
17.184	584.5	35.75	505.6	.822	94.7	23.4	276	100.0	0.19	0.2	20.60	15.91	19.26	8	3.0
16.986	580.7	35.61	501.8	.821	94.3	32.7	333	100.0	0.18	50.0	20.60	15.57	17.84	8	4.0
16.927	580.6	35.49	501.7	.821	94.0	32.2	330	100.0	0.17	50.0	20.60	15.59	18.16	8	5.0
16.921	581.0	35.45	502.2	.821	93.9	32.2	330	100.0	0.18	50.0	20.60	15.60	18.19	8	6.0

Appendix C User's Manual

This appendix contains a user's manual for the code used in this work. The optimization code developed in this work is covered in detail, as is the information necessary to use the code with SCAP1D. Only those aspects of SCAP1D that were modified in this work are described in detail for the user. Those not familiar with the inputs to SCAP1D should check JPL publication #85-46[†]. The numbering of sections, figures, and tables in this appendix is independent of the previous sections.

[†]DOE/JPL-1012-107, A.R. Mokashi, T. Daud, and R.M. Kachare, "High-Efficiency Silicon Solar Cell Design Evaluation and Sensitivity Analysis"

C.1 Problem Definition

The code described in this manual is a nonlinear optimization code which was developed for the application of optimizing an output of a computer simulation with respect to the inputs. The computer simulation is a user supplied program which models a physical phenomenon or device. For example, the optimization code has been coupled with a one dimensional model of a silicon solar cell to optimize cell design. The code is not completely general in terms of constraints, as it is not anticipated that the inputs to a model will be heavily constrained.

The code is particularly effective for applications where the number of decision variables (dimension of **x**) is small and the objective function, f, is difficult to calculate (i.e., requires a nontrivial amount of CPU time). The code operates very reliably when using numerical approximations to the gradient (which must be used when optimizing a simulation). The code may also be used for optimizations in which a closed form expression for the objective and/or the gradient exist.

The code solves the following problem[†]:

$$\underset{\mathbf{x}}{\text{minimize}} \quad f(\mathbf{x})$$

$$\mathbf{lb} \le \mathbf{x} \le \mathbf{ub}$$

$$\mathbf{A}\,\mathbf{x} \le \mathbf{b} \quad .$$

x is an n dimensional vector of variables over which the function f will be minimized,

$$\mathbf{x} = [\, x_1, x_2, \ldots, x_n \,] \quad .$$

The vector **lb** represents the lower bounds for each of the components of **x**,

[†] Scalar quantities are represented by non-bold type (e.g., α), vectors by lower case bold type (e.g., **x**), a particular component of a vector by the vector symbol in normal type and a subscript denoting the component (e.g., x_1 = first component of vector **x**), a sequence of vectors by $\mathbf{x}^0$, $\mathbf{x}^1$, ..., and matrices by upper case bold type (e.g., **H**).

$$\mathbf{lb} = [\ lb_1,\ lb_2,\ ...,\ lb_n\ ] \quad .$$

The vector **ub** represents the upper bounds for each of the components of **x**,

$$\mathbf{ub} = [\ ub_1,\ ub_2,\ ...,\ ub_n\ ] \quad .$$

Any, or all, of the components of the vectors **lb** or **ub** may be undefined (i.e., there need not be upper and/or lower bounds on the components of **x**).

The matrix A and the right hand side vector **b** are used to enforce linear inequality constraints involving the decision vector, **x**. The code was not designed to handle large numbers of linear inequality constraints. Other methods may be coded that will solve optimization problems with large numbers of linear constraints more efficiently. Linear equality constraints should not be included in the problem. It is more efficient to eliminate linear equalities (see examples), which reduces the dimension of the problem. The code does not include logic to determine a feasible solution when starting from an infeasible starting point. Therefore, the user must be able to provide an initial estimate of the optimal solution which is feasible (satisfies all the constraints). The code is not designed to solve problems that include nonlinear constraints.

A maximization is simply a minimization of the negative of the objective function (e.g., maximize f(**x**) is equivalent to minimize -f(**x**)).

It is up to the user to provide subroutines to calculate the objective function (f), the gradient of the objective function with respect to the decision variables (optional), and a routine to initialize the problem (may not be necessary).

Another special adaptation of the code for use with computer simulations is the implementation of a two level optimization structure (see section C.5 for details).

The objective function is assumed to be reasonably smooth (e.g., continuous) and differentiable. The optimization code can only solve for a local minimum, which may or may not be the global minimum. Given certain conditions on the objective function (pseudo-convexity) a local minimum is a global minimum. However, such conditions are usually very difficult to establish for a general objective function. No techniques exist that can guarantee finding the global minimum of a general nonlinear objective function.

C.2 Method of Solution

Figure C.1 shows an overview of the algorithm used. The n-dimensional problem is solved by solving a series of one dimensional subproblems. The gradient is used to determine a favorable direction of search and then a one-dimensional optimization is carried out along that direction. The code iterates until one of the user specified convergence criteria is satisfied, at which point the n-dimensional problem is considered solved. The basic components of the algorithm are 1) initialization, 2) the calculation of the gradient, 3) definition of the search direction, 4) enforcing the constraints, 5) solution of the one dimensional subproblem, and 6) test for convergence. The paragraphs below describe each of these components in more detail and outline the steps of the algorithm.

(1) Set k=0, given $\mathbf{x}^k$ calculate $f^k = f(\mathbf{x}^k)$.

The user must supply the initial estimate of the optimal value of the decision vector ($\mathbf{x}^0$). The user also supplies the subroutine which, given the value $\mathbf{x}^k$, calculates the value of the objective function ($f^k = f(\mathbf{x}^k)$). The user may supply a subroutine to accomplish any activities that are unique to the problem being solved that should be done before the objective function can be evaluated (e.g., reading in data required for the objective function, echoing the input data file, etc.)

(2) Calculate $\mathbf{g}^k = \nabla f(\mathbf{x}^k)$.

The user may supply closed form expressions for any or all of the components of the gradient in a subroutine. If it is not possible to derive the expressions for any component of the gradient, that component will be approximated numerically by the code.

(3) If k=0, then $\mathbf{d}^0 = -\mathbf{g}^0$. Else, calculate the search direction using either:

(3a) Fletcher-Reeves conjugate gradient algorithm [†]

$$\mathbf{d}^k = -\mathbf{g}^k + \beta^k \mathbf{d}^{k-1} \qquad \beta^k = \frac{\mathbf{g}^{kt}\,\mathbf{g}^k}{\mathbf{g}^{k-1t}\,\mathbf{g}^{k-1}}$$

(3b) quasi-Newton algorithm

$\mathbf{d}^k = -\mathbf{H}^k\,\mathbf{g}^k$ Where $\mathbf{H}^k$ is calculated by one of the formulas below.

$$\mathbf{H}^k = \mathbf{H}^{k-1} + \left[1 + \frac{\boldsymbol{\gamma}^t\,\mathbf{H}^{k-1}\,\boldsymbol{\gamma}}{\boldsymbol{\delta}^t\,\boldsymbol{\gamma}}\right]\frac{\boldsymbol{\delta}\,\boldsymbol{\delta}^t}{\boldsymbol{\delta}^t\,\boldsymbol{\gamma}} - \left[\frac{\boldsymbol{\delta}\,\boldsymbol{\gamma}^t\,\mathbf{H}^{k-1} + \mathbf{H}^{k-1}\,\boldsymbol{\gamma}\,\boldsymbol{\gamma}^t}{\boldsymbol{\gamma}^t\,\boldsymbol{\gamma}}\right] \qquad \text{BFGS}$$

[†] $\mathbf{g}$ is a nx1 vector, whereas $\mathbf{g}^t$ denotes the transpose or a 1xn vector. Hence $\mathbf{g}^t\,\mathbf{g}$ is an inner product (the result of which is a scalar quantity).

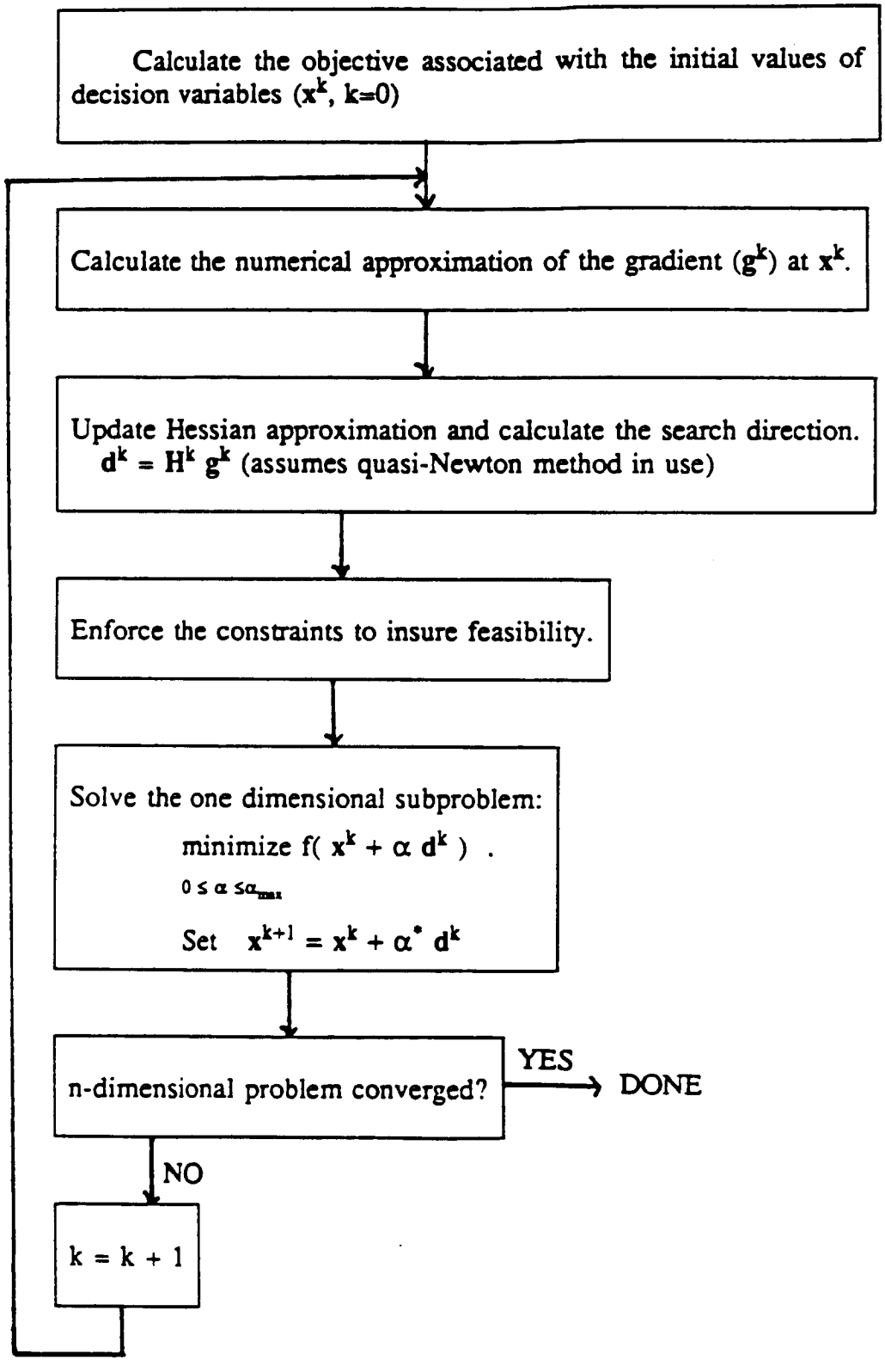

Figure C.1 Overview of Optimization Algorithm

$$H^k = H^{k-1} + \frac{\delta\,\delta^t}{\gamma\,\gamma^t} - \frac{H_{k-1}\,\gamma\,\gamma^t\,H_{k-1}}{\gamma^t\,H_{k-1}\,\gamma} \qquad \text{DFP}$$

$$H^k = (1-\alpha)\,H^k_{DFP} + \alpha\,H^k_{BFGS} \qquad \text{Broyden}$$

where $\delta = x^k - x^{k-1}$,and $\gamma = g^k - g^{k-1}$

The user may use any of the above formulas to calculate the search direction. The quasi-Newton methods use the quasi-Newton condition to develop an approximation of the inverse Hessian (the matrix of second partial derivatives) of the objective function. Several different formulas (DFP, BFGS, Broyden) for updating the inverse Hessian approximation are in the code. Quasi-Newton methods can be proven to converge to the optimal solution of a quadratic function in n (where n is the dimension of the problem) iterations if exact line searches are implemented. Since most functions can be approximated locally by a quadratic function, these methods exhibit good convergence properties on general functions (superior to always moving in the direction of steepest descent $d^k = -g^k$).

(4) Enforce the constraints to insure the direction d^k is a feasible direction, and calculate the maximum step size α_{max} (may be infinite) along the search direction for which the decision variables remain feasible (constraints are satisfied).

(5) Solve the one dimensional subproblem.

$$\text{minimize } f(x^k + \alpha\,d^k) \quad .$$
$$0 \le \alpha \le \alpha_{max}$$

The n-dimensional optimization is solved by iteratively solving the one dimensional subproblem. The one dimensional algorithm in the code uses successive polynomial approximations based on the information known about the function along the line (directional derivative and function values). As implemented in the code, the one dimensional minimization is an inexact algorithm. No attempt is made to solve the one dimensional problem to an ε tolerance (i.e., to within ε tolerance of the true optimal value of α), as this is not necessary to solve the n-dimensional problem. The one dimensional minimization is an iterative procedure, and the user defines the values of the convergence criterion.

(6) Test for convergence of the n-dimensional problem. Tests are based on the magnitude of the gradient, the magnitude of the change in the objective function, and the magnitude of the change in the vector x.

(6a) If $|g^k| <$ EPGRAD [†], done.

(6b) If $|f^k - f^{k-1}| <$ EPFUN for NSTOP consecutive iterations, done.

(6c) If $|x_i^k - x_i^{k-1}| <$ EPX i=1,n for NSTOP consecutive iterations, done.

(6d) If none of the above holds increment iteration counter, k=k+1.

(6e) If k > ITMAX, limit on iterations reached, halt execution.

(6f) Else, return to step 2 for another iteration.

The result of the program is a sequence of vectors x^0, x^1, ..., x^k which approaches a local minimum x^* and a sequence of function values f^0, f^1, ..., f^k which approaches the value of the objective function at the local minimum, $f^* = f(x^*)$.

[†] Capitalized variables refer to program inputs, which are described in the next section.

C.3 Description of Inputs

The inputs to the code are described below in the order that they appear in the input file. Where appropriate, a value is suggested for each input. Several input options are provided to tailor the code for the more specialized purpose of optimizing the output of a simulation program with respect to the inputs.

NDIM The dimension of the problem, which is the dimension of the decision vector $\mathbf{x} = [x_1, x_2, \ldots, x_{NDIM}]$.

ILOOP Always set equal to **one** (unless using two level optimization).

IPRINT Print flag for the main iteration loop of the code (suggested value is **1**).

- =0 No output from the main iteration loop of the code. Useful only for two level optimization when no output is desired from the inner loop.
- =1 Only the initial and final points of the optimization are output along with a summary of the run statistics (e.g., # of iterations, # of function calls, etc.)
- =2 Information is output at each iteration (e.g., $\mathbf{x}^k$, $\mathbf{g}^k$, f^k, etc.)
- =3 Highest level of output, details the optimization run.

IPR Output flag for the one dimensional subproblem. Note, the one dimensional problem is solved at each main loop iteration (k=0,1,2,...). (suggested value is **0**).

- =0 No output from the one dimensional subproblem.
- =1 Summary of the one dimensional subproblem including # of function evaluations, best step size, etc.
- =2 Output each step size and associated function value made along the line of search.

INTLIM # (≥ 0) of successful polynomial interpolations before the one dimensional subproblem is considered to have converged (suggested value = **2**).

KFAIL # (≥ 0) of unsuccessful polynomial interpolations before the one dimensional subproblem is considered to have converged (suggested value = **1**).

BIGSTP Specialized input useful when optimization code is used with numerical simulations. BIGSTP should represent a significant change in the magnitude of the decision vector ($|\mathbf{x}|$). Not a critical input for less specialized use, but should be interpreted in the same manner (suggested value is **1.0**).

NPROB Input used for user documentation purposes to label different problems.

IFORM Flag which denotes the method used to calculate the search direction (suggested value is **1**, unless value of NDIM is so large that array storage is a problem, in which case conjugate gradient algorithm should be used because it requires less storage).

- =1 Quasi-Newton method will be used.
- =2 Self-scaling quasi-Newton method will be used.
- =3 Conjugate gradient method will be used.

FORMLA If quasi-Newton calculation of the search direction is chosen (IFORM =1 or 2), this input determines which formula will be used to update the approximation of the inverse Hessian (suggested value is **1.0**).

- =0.0 Davidon-Fletcher-Powell (DFP)
- =1.0 Broyden-Fletcher-Goldfarb-Shanno (BFGS)
- $=\alpha$ Any other value results in the appropriate Broyden family member, which is a linear combination of the DFP and BFGS formulas.

IBOND Flag denotes whether any of the decision variables has upper or lower bounds (=1 there are bounds, =0 no bounds).

ICONST Flag which denotes whether or not the problem has linear constraints (=1 there are linear constraints, =0 no linear constraints).

NROWS # of linear constraints (rows in matrix A). Ignored if ICONST = 0.

NCOLS # of components of the decision vector involved in the linear constraints (columns in matrix A). Ignored if ICONST = 0.

ISCALE Flag to determine if the decision variables are to be prescaled (=0 no prescaling, =1 prescaled).

ITMAX Maximum # of iterations to be executed. If the code reaches this limit, it will halt and output the best point to date (suggested value is **100**).

IRSTRT Number of times the code should restart the direction finding algorithm if the convergence is sensed on the change in the magnitude of the objective function or the decision vector (suggested value is **0**). Note, a positive input should be supplied here only if the user wishes to solve the problem very accurately and is not particularly concerned with the number of iterations (computational effort) required.

NSTOP The number of consecutive iterations that a lack of progress in the objective function (as measured by EPFUN) or the decision vector (as measured by EPX) before the problem is considered to have converged (suggested value is **3**).

EPGRAD The magnitude of the gradient that will imply convergence. For analytical expressions of the gradient the suggested value is 10^{-4}. When

closed form expressions for the gradient are not supplied by the user, the criterion should be considerably tighter, due to the inaccuracies inherent when numerically approximating the gradient. The suggested value is 10^{-8} and possibly smaller if the objective function is calculated by a complex simulation (a very small value forces one of the other convergence criterion to be satisfied).

EPFUNC If the objective value changes by less than EPFUNC (in absolute magnitude or percent difference) for NSTOP consecutive iterations the problem is considered to have converged (if IRSTRT is non-zero this must occur IRSTRT times). This input depends on the accuracy desired by the user; 10^{-4} is a reasonable value for most problems.

EPX If each component of the decision vector changes by less than EPX (in absolute magnitude or percent difference) for NSTOP consecutive iterations, the problem is considered to have converged (if IRSTRT is non-zero this must occur IRSTRT times). 10^{-6} is a reasonable value for most problems. But, for use with simulations EPX should be set equal to OFFDIF, both of which should represent the accuracy desired in the decision variables.

INUM Flag denotes whether or not it will be necessary to numerically approximate any components of the gradient.

- =1 User has supplied expressions for all the components of the gradient in the subroutine *GRADNT*.
- =2 User has not supplied expressions for all the components of the gradient in the subroutine *GRADNT*, so that it will be necessary to numerically calculate some or all of the components of the gradient.

ISAVE Option that is best suited for use when the objective function is calculated by a simulation and/or requires considerable computational effort. For standard use suggested value is **0** .

- =0 Follows standard methods of calculating the gradient.
- =1 Attempts to save one objective evaluation when calculating the numerical gradient by making use of information along the line of search.

OFFDIF Percentage offset for the numerical approximation of the derivative. For standard use, the suggested value is **0.0001**. For more complex objective functions (outputs of simulation), the value must reflect the accuracy that can be attained in the decision variables, generally 0.001 (0.1%) or less.

IPARSH Used only if INUM $\neq$ 1. N vector of inputs that represents the manner in which each component of the gradient should be calculated. A value is entered for each of the NDIM components. Suggested values are **1** if

an analytic expression is available for the particular component, or 2 if no analytic expression is supplied. Forward differences (2) converts to modified central differences if the algorithm gets stuck (line search in the direction of steepest descent does not improve the objective function), so that the use of forward differences is very reliable.

=1 Use expression in subroutine *GRADNT*.

=2 Use the forward difference formula.

=3 Use the modified central difference formula.

=4 Use central difference, but take second function evaluation only if first offset does not improve the objective value.

=5 Use forward differences until a lack of progress is sensed in either the objective function or decision variables then switches to central differences.

X N vector used to read in the initial estimate of the solution.

IBOUND Ignored if IBOND = 0. Else, an NDIM vector used to denote if upper and/or lower bounds are in use for each component of the decision vector.

=1 Only lower bound is in use.

=2 Only upper bound is in use.

=3 Upper bound and lower bound are in use.

=4 Variable is free, no upper or lower bounds.

=5 Variable is fixed. The value of the variable will not be changed by the optimization (e.g., the variable will not take part in the optimization).

LB Ignored unless IBOND = 1 and IBOUND(i) = 1 or 3. N vector which contains the lower bound for each of the decision variables.

UB Ignored unless IBOND = 1 and IBOUND(i) = 2 or 3. N vector which contains the upper bound for each of the decision variables.

XSCALE Ignored if ISCALE = 0. N vector which represents prescaling to be done on each variable.

ICOL Ignored if ICONST = 0. Else, a NCOLS vector that denotes which components of the decision vector that are involved in the linear constraints.

AMAT Ignored if ICONST = 0. Else, the matrix representing the linear constraints entered by row (e.g., see section C.4.2).

BRHS Ignored if ICONST = 0. The NROWS vector representing the right hand side of the linear constraints.

ITYPE Ignored if ICONST = 0. Else, an NROWS vector specifying the relation to be enforced for each linear constraint.

=0 Equality (=) is to be enforced for the linear constraint. Linear equality constraints should be removed by elimination in order to reduce the dimensionality of the problem and, hence, the computational effort required to solve the problem (e.g., see sections C.4.3 and C.4.4). Also, inclusion of equality constraints may deteriorate the convergence rate of the algorithm.

=1 The linear expression of the variables must be greater than or equal to ($\geq$) the right hand side.

=2 The linear expression of the variables must be less than or equal to ($\leq$) the right hand side.

C.4 Example Inputs and Outputs

Several examples will be given to illustrate how the user starts from the problem definition given in the first section of this manual and prepares the files and subroutines needed to solve the problem using the code. The first three examples are standard functions, and the required input and resulting output are given. The last example illustrates how the code is used with a simulation program and presents some of the major concerns involved.

C.4.1 Example #1

$$\underset{x_1,x_2}{\text{minimize}} \sin(x_1 + x_2) + (x_1 - x_2)^2 - 1.5x_1 + 2.5x_2 + 1.0$$

$$-1.5 \le x_1 \le 4.0$$

$$-3.0 \le x_2 \le 3.0$$

The problem to be solved is mathematically described above. The problem is initiated from the point $\mathbf{x} = [0, 0]$. The input file for this problem is shown in figure C.2, which is supplied with the manual as the file inex1.d . The input file is read using list directed read statements (format=*). Associated with each read statement in the program is a comment line which describes the input that should be entered. The comment line and at least one input line must appear, even though some of the data is optional. As many lines as are required can be used if the data is to be read (i.e., more than one line may be required to enter the initial point), but exactly one line must be skipped after the comment line if the option is not in use (i.e., the data is to be ignored). Upper and lower bounds are used (IBOND = 1), so that the data required to read in the bound information (IBOUND, LB, and UB) appears following the comment lines. Since scaling is not used (ISCALE = 0) and there are no linear constraints (ICONST = 0), no input need appear after the associated comment lines, but one line must be skipped. The comment lines clearly display the organization of the data file so that the user can alter existing data files without having to refer back to a manual.

Figure C.3 shows the user supplied subroutines. Code that is written by the user for the particular problem to be solved is shown in bold type. The remainder of the subroutines are standardized and should always appear as shown in figure C.3 . In this example, the user supplied initialization routine, *INITLZ*, is used to write the input file to the output file (this helps document the problem). The code shown in figure C.3 is supplied with the manual in the module ex1.f . The module ex1.f includes two other short routines (described later in this manual) and additional comment lines to explain the variables that are passed into the routines.

The output of the program is shown in figure C.4. Figure C.4 may be used with the module ex1.f and the input file inex1.d to verify correct installation of the code. The convergence criterion on the magnitude of the gradient was reached after 5 iterations (e.g., k=4 in section C.2). If linear constraints are included, this is referred to as a K-T (Kuhn-Tucker) point. Only the magnitude of the gradient that corresponds to a feasible direction need be less than the input EPGRAD (e.g., see figure C.7). Sixteen objective evaluations and 6 evaluations of the gradient were required for convergence to the point [-0.5471978, -1.547197], which has an objective function equal to -1.913223. The inverse Hessian is by definition a symmetric matrix and is therefore stored as a lower triangular matrix to conserve storage.

The variables in the calling list of *INITLZ* are defined below.

NDIM = dimension of the problem
IIN = device number for the input file
IOUT = device number of the output file
IOUT2 and IPR2 are not used in this version of the program
IPRINT = flag for print level of n-dimensional optimization

The subroutine *FUNCTN* is called to calculate the objective function. The variables in the calling list of *FUNCTN* are defined below.

N = problem dimension
X = n vector containing current values of the decision variables
F = value of objective function (output)
ITER = iteration of the n-dimensional subroutine
IGRAD = component of gradient being solved for (if INUM=2), or 0 if in a line search.
SDIREC = n vector containing the current search direction (if IGRAD =0)
NPROB = problem number
IOUT = device number of output file
IPRINT = flag for print level of n-dimensional optimization

The subroutine *GRADNT* is called to calculate the gradient. The variables in the calling list of *GRADNT* are defined below.

N = problem dimension
X = n vector containing current values of the decision variables
G = value of gradient (output)
ITER = iteration of the n-dimensional subroutine
NPROB = problem number
IGRAD = component of gradient being solved for (if INUM=2).

All of the above definitions are included in their respective routines as comments (i.e., in ex1.f), but were not printed in the examples to save space.

```
NDIM    ILOOP   IPRINT   IPR
  2       1       1       0
INTLIM  KFAIL  BIGSTP  NPROB
  2       1      1.0      1
IFORM   FORMLA  IBOND   ICONST   NROWS   NCOLS  ISCALE
  1       1.0     1        0       1       1       0
ITMAX   IRSTRT  NSTOP   EPGRAD   EPFUN   EPX
 100      0       3      0.1E-03  0.1E-03  0.1E-05
INUM    ISAVE   OFFDIF
  1       1      0.0001
IPARSH(NDIM) 1=ANALYTIC 2=FORWARD 3=CENTRAL 4=CENTRAL1 5=AUTO F/C
(not in use)
X(NDIM)    INITIAL VALUE FOR THE DECISION VECTOR
 0.0  0.0
IBOUND(NDIM)  1=LB ACTIVE  2=UB ACTIVE  3=BOTH ACTIVE  4=FREE  5=FIXED
 3  3
XLB(NDIM)    LOWER BOUNDS
 -1.5  -3.0
XUB(NDIM)    UPPER BOUNDS
  4.0   3.0
XSCALE(NDIM) PRESCALING OF DECISION VARIABLES
(not in use)
ICOL(NCOL)   COMPONENTS OF DECISION VECTOR INVOLVED IN LINEAR CONSTRAINTS
(not in use)
AMAT(NROWS,NCOL) LINEAR CONSTRAINT MATRIX
(not in use)
BRHS(NROWS)  RIGHT HAND SIDE OF LINEAR CONSTRAINTS
(not in use)
ITYPE(NROWS)   0=(EQUALITY) 1=(≥)  2=(≤)
(not in use)
```

figure C.2 The file inex1.d

```
C*****
C     USER SUPPLIED SUBROUTINE TO INITIALIZE THE PROBLEM.
C
      SUBROUTINE INITLZ(NDIM,IIN,IOUT,IOUT2,IPR2,IPRINT)
      IMPLICIT DOUBLE PRECISION (A-H,O-Z)
C
      CHARACTER*80 IDUM
C     ECHO THE DATA FILE
      REWIND IIN
      DO 5 I=1,1000
        READ(IIN,10,END=20) IDUM
        WRITE(IOUT,10) IDUM
   10   FORMAT(A80)
    5 CONTINUE
C
C     DONE WRITING INPUT FILE TO OUTPUT, REALIGN INPUT FILE.
   20 CONTINUE
      REWIND IIN
      READ(IIN,*)
      READ(IIN,*)
      RETURN
      END
C*****
C     USER SUPPLIED SUBROUTINE TO EVALUATE THE FUNCTION.
C
      SUBROUTINE FUNCTN(N,X,F,ITER,IGRAD,SDIREC,NPROB,
     1                  IOUT,IPRINT)
      IMPLICIT DOUBLE PRECISION (A-H,O-Z)
      DIMENSION X(N),SDIREC(N)
C
      X1 = X(1)
      X2 = X(2)
      F = DSIN(X1+X2) + (X1-X2)**2 - 1.5D0*X1 + 2.5*X2 +1.D0
      RETURN
      END
C*****
C     USER SUPPLIED SUBROUTINE TO EVALUATE THE GRADIENT
C
      SUBROUTINE GRADNT(N,X,G,ITER,NPROB,IGRAD)
      IMPLICIT DOUBLE PRECISION (A-H,O-Z)
      DIMENSION X(N),G(N)
C
      X1 = X(1)
      X2 = X(2)
      G(1) = DCOS(X1+X2) + 2.D0*(X1-X2) - 1.5D0
      G(2) = DCOS(X1+X2) - 2.D0*(X1-X2) + 2.5D0
      RETURN
      END
```

figure C.3 Part of the module ex1.f

```
NDIM    ILOOP  IPRINT  IPR
  2       1       1      0
INTLIM  KFAIL  BIGSTP  NPROB
  2       1      1.0     1
IFORM   FORMLA  IBOND   ICONST  NROWS   NCOLS  ISCALE
  1       1.0     1       0       1       1      0
ITMAX   IRSTRT  NSTOP   EPGRAD  EPFUN   EPX
 100      0       3     0.1E-03 0.1E-03 0.1E-05
INUM    ISAVE  OFFDIF
  1       1     0.0001
IPARSH(NDIM) 1=ANALYTIC 2=FORWARD 3=CENTRAL 4=CENTRAL1 5=AUTO F/C
(not in use)
X(NDIM)    INITIAL VALUE FOR THE DECISION VECTOR
 0.0  0.0
IBOUND(NDIM)  1=LB ACTIVE  2=UB ACTIVE  3=BOTH ACTIVE  4=FREE  5=FIXED
 3  3
XLB(NDIM)    LOWER BOUNDS
 -1.5  -3.0
XUB(NDIM)    UPPER BOUNDS
  4.0  3.0
XSCALE(NDIM) PRESCALING OF DECISION VARIABLES
(not in use)
ICOL(NCOL)   COMPONENTS OF DECISION VECTOR INVOLVED IN LINEAR CONSTRAINTS
(not in use)
AMAT(NROWS,NCOL) LINEAR CONSTRAINT MATRIX
(not in use)
BRHS(NROWS)  RIGHT HAND SIDE OF LINEAR CONSTRAINTS
(not in use)
ITYPE(NROWS)  0=(EQUALITY) 1=(≥)  2=(≤)
(not in use)
  PROBLEM #  1
  EXECUTING THE BROYDEN FAMILY MEMBER
  0.00E+00 DFP +  1.0    BFGS

  BEGIN ITERATION #   0
  THE OBJ =    1.000000000
  THE POINT IS =
 0.00000000000E+00  0.00000000000E+00

  ISTOP=  1 CONVERGENCE ON MAGNITUDE OF DERIVATIVE SATISFIED. MAG<   0.1000000E-03

       PROBLEM SUMMARY
  # ITERATIONS =    5  # OBJ EVALS =   16  # GRAD EVALS =    6
  # OF RESETS =    0  # FAILED INTRPS=    0
  THE MINIMUM OBJECTIVE =   -1.913223
  THE OPTIMAL POINT IS =
-0.5471978      -1.547197
  THE MAGNITUDE OF THE GRADIENT AT THE MIN =   0.12602113E-05
  THE GRADIENT AT MIN =
  -0.92481E-06   0.85607E-06
  THE UPDATED (  4) HESSIAN INVERSE (LOW TRIANG)
   0.41309        0.16483        0.41345
   ALL PROBLEMS HAVE BEEN COMPLETED
```

figure C.4 Output using ex1.f and inex1.d

C.4.2 Example #2

$$\underset{x}{\text{minimize}}\ x_1 - x_2 - x_3 - x_1 x_3 + x_1 x_4 + x_2 x_3 - x_2 x_4$$

$$\begin{aligned}
-x_1 - 2x_2 &\geq -8.0 \\
-4x_1 - x_2 &\geq -12.0 \\
-3x_1 - 4x_2 &\geq -12.0 \\
-2x_3 - x_4 &\geq -8.0 \\
-x_3 - 2x_4 &\geq -8.0 \\
-x_3 - x_4 &\geq -5.0 \\
0 \leq x_i &\leq 20 \quad i=1,...,4
\end{aligned}$$

The problem to be solved is mathematically described above. The problem is initiated from the point $x = [0, 0, 0, 0]$. The input file for this problem is shown in figure C.5, which is supplied with the manual as the file inex2.d . This example shows how linear constraints are input to the problem. The flag ICONST = 1 and the appropriate inputs are given for NCOL, NROWS, ICOL, AMAT, BRHS, and ITYPE. Any variables that are involved in the linear inequality constraints **must** have upper and lower bounds. If such bounds do not appear naturally in the formulation of the problem, then extremely loose bounds which will not affect the optimization should be specified for the variables.

Figure C.6 shows the user supplied subroutines. Code that is written by the user for the particular problem to be solved is shown in bold type. The remainder of the subroutines are standardized and should always appear as shown in figure C.6 . The code shown in figure C.6 is supplied with the manual in the module ex2.f . The module ex1.f includes two other short routines (described later in this manual) and additional comment lines to explain the variables that are passed into the routines. In this example, the data file is not written out to the output. Although nothing is accomplished in the user supplied routine *INITLZ* it must still be included when linking the programs. The subroutine *FUNCTN* is called to calculate the objective function. The subroutine *GRADNT* is called to calculate the gradient. The output of the program is shown in figure C.7 . Figure C.7 may be used with the module ex2.f and the input file inex2.d to verify correct installation of the code.

```
NDIM    ILOOP   IPRINT   IPR
  4       1       1       0
INTLIM  KFAIL   BIGSTP   NPROB
  2       1      1.0      2
IFORM   FORMLA  IBOND   ICONST   NROWS   NCOLS   ISCALE
  1       1.0     1       1       6       4       0
ITMAX   IRSTRT  NSTOP   EPGRAD   EPFUN   EPX
 100      0       3     0.1E-03  0.1E-03  0.1E-05
INUM    ISAVE   OFFDIF
  1       1      0.0001
IPARSH(NDIM) 1=ANALYTIC 2=FORWARD 3=CENTRAL 4=CENTRAL1 5=AUTO F/C
(not in use)
X(NDIM)    INITIAL VALUE FOR THE DECISION VECTOR
 0.0  0.0  0.0  0.0
IBOUND(NDIM)  1=LB ACTIVE  2=UB ACTIVE  3=BOTH ACTIVE  4=FREE  5=FIXED
 3  3  3  3
XLB(NDIM)    LOWER BOUNDS
  0.0   0.0   0.0   0.0
XUB(NDIM)    UPPER BOUNDS
 20.0   20.0   20.0   20.0
XSCALE(NDIM) PRESCALING OF DECISION VARIABLES
(not in use)
ICOL(NCOL)  COMPONENTS OF DECISION VECTOR INVOLVED IN LINEAR CONSTRAINTS
1  2  3  4
AMAT(NROWS,NCOL) LINEAR CONSTRAINT MATRIX
-1  -2  0  0
-4  -1  0  0
-3  -4  0  0
 0   0 -2 -1
 0   0 -1 -2
 0   0 -1 -1
BRHS(NROWS)  RIGHT HAND SIDE OF LINEAR CONSTRAINTS
-8.0  -12.0  -12.0  -8.0  -8.0  -5.0
ITYPE(NROWS)  0=(EQUALITY) 1=(≥)  2=(≤)
1  1  1  1  1  1
```

figure C.5 The file inex2.d

```
C*****
C     USER SUPPLIED SUBROUTINE TO INITIALIZE THE PROBLEM.
C
      SUBROUTINE INITLZ(NDIM,IIN,IOUT,IOUT2,IPR2,IPRINT)
      IMPLICIT DOUBLE PRECISION (A-H,O-Z)
C
      RETURN
      END
C*****
C     USER SUPPLIED SUBROUTINE TO EVALUATE THE FUNCTION.
C
      SUBROUTINE FUNCTN(N,X,F,ITER,IGRAD,SDIREC,NPROB,
     1                  IOUT,IPRINT)
      IMPLICIT DOUBLE PRECISION (A-H,O-Z)
      DIMENSION X(N),SDIREC(N)
C
      F = X(1) - X(2) - X(3) -X(1)*X(3) + X(1)*X(4) + X(2)*X(3) - X(2)*X(4)
      RETURN
      END
C*****
C     USER SUPPLIED SUBROUTINE TO EVALUATE THE GRADIENT
C
      SUBROUTINE GRADNT(N,X,G,ITER,NPROB,IGRAD)
      IMPLICIT DOUBLE PRECISION (A-H,O-Z)
      DIMENSION X(N),G(N)
C
      G(1) =  1 - X(3) + X(4)
      G(2) = -1 + X(3) - X(4)
      G(3) = -1 - X(1) + X(2)
      G(4) =      X(1) - X(2)
      RETURN
      END
```

figure C.6 Part of the module ex2.f

```
PROBLEM #   2


EXECUTING THE BROYDEN FAMILY MEMBER
0.00E+00 DFP +  1.0     BFGS



BEGIN ITERATION #    0
THE OBJ =   0.0000000000E+00
THE POINT IS =
0.00000000000E+00 0.00000000000E+00 0.00000000000E+00 0.00000000000E+00

ISTOP=  1  K-T POINT, IKT= 2



     PROBLEM SUMMARY

 # ITERATIONS =    5   # OBJ EVALS =   13   # GRAD EVALS =    6
 # OF RESETS =    4   # FAILED INTRPS=    0
 THE MINIMUM OBJECTIVE =   -15.00000
 THE OPTIMAL POINT IS =
0.0000000E+00   3.000000      0.0000000E+00   4.000000
 THE MAGNITUDE OF THE GRADIENT AT THE MIN =    7.9372539
 THE GRADIENT AT MIN =
  5.0000        -5.0000         2.0000        -3.0000
 THE UPDATED (  0) HESSIAN INVERSE (LOW TRIANG)
  1.0000        0.00000E+00    0.00000E+00    0.00000E+00     1.0000        0.00000E+00
 0.00000E+00     1.0000        0.00000E+00     1.0000
 ALL PROBLEMS HAVE BEEN COMPLETED
```

figure C.7 Output using ex2.f and inex2.d

C.4.3 Example #3

$$\underset{x}{\text{minimize}} \; (x_1 - 1)^2 + (x_2 - x_3)^2 + (x_4 - x_5)^2$$

$$x_1 + x_2 + x_3 + x_4 + x_5 - 5 = 0$$

$$x_3 - 2 (x_4 + x5) + 3 = 0$$

The problem to be solved is mathematically described above. The problem is initiated from the point x = [3, 5, -3, 2, -2] The linear equality constraints can be used to eliminate two of the variables from the problem. In this example, x_1 and x_3 may be eliminated by the equations:

$$x_1 = -x_2 - x_3 - x_4 - x_5 + 5$$

$$x_3 = 2 (x_4 + x5) - 3$$

Eliminating x_3 from the equation for x_1 gives:

$$x_1 = -x_2 - 3 x_4 - 3 x_5 + 8$$

The expressions for x_1 and x_3 are then substituted into the objective function. The resulting problem is:

$$\underset{x_2,x_4,x_5}{\text{minimize}} \; (-x2 - 3 x_4 - 3 x_5 + 7)^2 + (x2 - 2 x_4 - 2 x_5 + 3)^2 + (x4 - x5)^2$$

This results in an unconstrained problem in three dimensions, which is much easier to solve. The input file for this formulation is shown in figure C.8, which is supplied with the manual as the file inex3.d . It is important to note that in the input data file x_1 corresponds to x_2, x_2 corresponds to x_4, and x_3 corresponds to x_5 in the problem statement given above. It is up to the user to go back and determine the values of the original variables x_1 and x_3, which were eliminated from the problem. The user supplied subroutines are shown in figure C.9 . The code shown in figure C.9 is supplied with the manual in the module ex3.f . The module ex1.f includes two other short routines (described later in this manual) and additional comment lines to explain the variables that are passed into the routines. Because there are no constraints in the new formulation, IBOND = 0 and ICONST = 0. It should be noted that IBOND = 0 is the same as IBOND = 1 and IBOUND = 4 for each component, but the latter requires more storage and a slight increase in execution time (both of which may be important if the dimension of the problem is very large). Since the linear constraints and bounds are not in use anything can be on the lines associated with IBOUND, XLB, XUB, ICOL, AMAT, BRHS, and ITYPE, as those lines are skipped. The values associated with the previous example were left in to illustrate this. But, there can be only one line after the comment

lines. For example, had all the data lines associated with AMAT from the previous problem been left in, the code would have flagged an I/O error. The output for this problem is shown in figure C.10. Figure C.10 may be used with the module ex3.f and the input file inex3.d to verify correct installation of the code.

```
NDIM    ILOOP  IPRINT   IPR
  3       1       1       0
INTLIM  KFAIL  BIGSTP  NPROB
  2       1      1.0      3
IFORM   FORMLA IBOND   ICONST  NROWS   NCOLS  ISCALE
  1       1.0      0       0       1       1       0
ITMAX   IRSTRT NSTOP   EPGRAD  EPFUN   EPX
 100      0      3      0.1E-03  0.1E-03  0.1E-05
INUM    ISAVE  OFFDIF
  1       0      0.001
IPARSH(NDIM) 1=ANALYTIC 2=FORWARD 3=CENTRAL 4=CENTRAL1 5=AUTO F/C
(not in use)
X(NDIM)    INITIAL VALUE FOR THE DECISION VECTOR
 5.0  2.0  -2.0
IBOUND(NDIM)  1=LB ACTIVE  2=UB ACTIVE  3=BOTH ACTIVE  4=FREE  5=FIXED
  1  1  1  1
XLB(NDIM)    LOWER BOUNDS
  0.0  0.0  0.0   0.0
XUB(NDIM)    UPPER BOUNDS
    0.0  0.0  0.0   0.00
XSCALE(NDIM) PRESCALING OF DECISION VARIABLES
(not in use)
ICOL(NCOL)  COMPONENTS OF DECISION VECTOR INVOLVED IN LINEAR CONSTRAINTS
1  2  3  4
AMAT(NROWS,NCOL) LINEAR CONSTRAINT MATRIX
-1  -2  0  0
BRHS(NROWS)  RIGHT HAND SIDE OF LINEAR CONSTRAINTS
-8.0  -12.0  -12.0  -8.0  -8.0  -5.0
ITYPE(NROWS)  0=(EQUALITY) 1=(≥)  2=(≤)
1  1  1  1  1  1
```

figure C.8 The file inex3.d

```
C*****
C     USER SUPPLIED SUBROUTINE TO INITIALIZE THE PROBLEM.
C
      SUBROUTINE INITLZ(NDIM,IIN,IOUT,IOUT2,IPR2,IPRINT)
      IMPLICIT DOUBLE PRECISION (A-H,O-Z)
C
      RETURN
      END
C*****
C     USER SUPPLIED SUBROUTINE TO EVALUATE THE FUNCTION.
C
      SUBROUTINE FUNCTN(N,X,F,ITER,IGRAD,SDIREC,NPROB,
     1                  IOUT,IPRINT)
      IMPLICIT DOUBLE PRECISION (A-H,O-Z)
      DIMENSION X(N),SDIREC(N)
C
      P1 =  -X(1) - 3*X(2) -3*X(3) + 7
      P2 =  X(1) - 2*X(2) -2*X(3) + 3
      F =  P1**2 + P2**2 + ( X(2) - X(3) )**2
      RETURN
      END
C*****
C     USER SUPPLIED SUBROUTINE TO EVALUATE THE GRADIENT
C
      SUBROUTINE GRADNT(N,X,G,ITER,NPROB,IGRAD)
      IMPLICIT DOUBLE PRECISION (A-H,O-Z)
      DIMENSION X(N),G(N)
C
      P1 =  -X(1) - 3*X(2) -3*X(3) + 7
      P2 =  X(1) - 2*X(2) -2*X(3) + 3
      G(1) =  -2*P1 + 2*P2
      G(2) =  -6*P1 - 4*P2 + 2*( X(2) - X(3) )
      G(3) =  -6*P1 - 4*P2 - 2*( X(2) - X(3) )
      RETURN
      END
```

figure C.9 Part of the module ex3.f

```
PROBLEM #  3


EXECUTING THE BROYDEN FAMILY MEMBER
0.00E+00 DFP +  1.0    BFGS



BEGIN ITERATION #    0
THE OBJ =    84.00000000
THE POINT IS =
5.0000000000      2.0000000000      -2.0000000000

ISTOP=  1 CONVERGENCE ON MAGNITUDE OF DERIVATIVE SATISFIED. MAG<   0.1000000E-03



     PROBLEM SUMMARY

# ITERATIONS =     6   # OBJ EVALS =   19   # GRAD EVALS =    7
# OF RESETS =    0   # FAILED INTRPS=   3
THE MINIMUM OBJECTIVE =   0.2898624E-21
THE OPTIMAL POINT IS =
1.0000000       1.000000       1.0000000
THE MAGNITUDE OF THE GRADIENT AT THE MIN =   0.48439666E-10
THE GRADIENT AT MIN =
-0.10283E-10   0.37774E-10   -0.28527E-10
THE UPDATED (   5) HESSIAN INVERSE (LOW TRIANG)
 0.26000       -0.10000E-01   -0.99997E-02   0.13500       -0.11500       0.13500

 ALL PROBLEMS HAVE BEEN COMPLETED
```

figure C.10 Output using ex3.f and inex3.d

C.4.4 Example #4

This example illustrates the use of the algorithm to optimize an output of a simulation with respect to the inputs. An example formulation is as follows. Assume a simulation, *SIMLAT*, has been written by the user to predict the efficiency of a solar cell (note this is for illustrative purposes only, no such code is supplied with this manual). The objective is to maximize the efficiency of the solar with respect to six inputs to the simulation.

$$\underset{x}{\text{maximize}} \quad \text{efficiency } (x_1, x_2, x_3, x_4, x_5, x_6)$$

$$x_5 + x_6 = 5$$

$$x_3 + x_4 \leq 100.5$$

$$0 \leq x_1$$

$$1 \leq x_3 \leq 2$$

$$30 \leq x_4 \leq 100$$

$$1 \leq x_5$$

$$2 \leq x_6 \leq 4$$

The initial value for the decision vector, which should be the best available estimate of the optimal solution, is assumed for illustrative purposes to be [0, 4, 1.5, 50, 2, 3].

The linear equality constraint can be used to eliminate the variable x_6 from the problem (e.g., $x_6 = 5-x_5$). Because of the bounds on the eliminated variable, it is necessary to redefine the bounds on the variable x_5. Resulting in the constraint,

$$1 \leq x_5 \leq 3 \quad .$$

However, unlike the previous example, there is no way to substitute the expression x_6 directly into the objective function. Instead, the variable x_6 is entered as a fixed variable in the optimization (effectively reducing the dimension of the optimization by one), and the equality for its value is coded into the routine *FUNCTN*. Since the objective is a result of a complex simulation, there are no analytical expressions for the gradient, as in the previous examples. Therefore, the gradient is approximated numerically (INUM = 2) using forward differences (IPARSH = 2 for each component). Figure C.11 shows the input data file for this problem formulation. The value of EPGRAD should be decreased when numerical gradients are used. The flag ISAVE is set to one, which may result in saving an objective function evaluation each time the gradient is calculated.

Convergence can be slowed if the objective function is particularly insensitive to one of the decision variables. The prescaling vector XSCALE is provided if prior to the optimization such knowledge is known (perhaps from previous optimization runs or the physics of the phenomenon being modeled). For example, if it is known that the simulation is particularly insensitive to the variable x_4 that variable may be prescaled by 10. Interior to the optimization code, the variable x_4 is then treated as the variable $\frac{x_4}{10}$, which has as its bounds $3 \leq \frac{x_4}{10} \leq 10$. The data file in figure C.11 shows how prescaling is input to the program. The user only supplies the prescaling vector, but does not transform any of the constraints or bounds as this is done automatically inside the code. Also, the decision vector is passed to the user supplied routines as though no scaling had been done (i.e., the scaling is totally transparent to the user).

The input BIGSTP is used to signify a significant change in the decision vector. This input is particularly useful if the previous execution of the simulation is being used to initiate the next solution of the simulation (the objective function). For example, such a scheme may result in significant savings if the simulation requires the numerical solution of differential equations using indirect solution procedures (e.g., Newton's method, etc.).

The inputs OFFDIF and EPX are set equal to the accuracy desired in the decision variables. The output of the simulation must be able to dependably reflect the accuracy desired (e.g., there may be significant roundoff error or nonzero convergence tolerance(s) for iterative algorithms within the simulation). Generally this will require some experimentation on the part of the user to determine the accuracy that should be pursued in the optimization.

Figure C.12 shows the user supplied subroutines. It is up to the user to adapt the simulation (in this case SIMLAT) so that the inputs and output are passed appropriately. The inputs and output could have been passed to the simulation using COMMON statements in the routine *FUNCTN* and the simulation. Considerable coding may be required to provide an interface between the simulation and the optimization code. Almost always, some modifications will have to be made to the simulation. The routine *INITLZ* may be coded by the user to execute any activities that may be required to initialize the simulation prior to the optimization (e.g., reading input data not involved in the optimization, designing a flexible interface so that the user can choose different outputs as the objective function and/or different inputs as decision variables in the optimization, etc.)

The device numbers of the optimization input and output files can be easily changed so that they do not coincide with those used in the simulation program (see section C.6.2).

```
NDIM    ILOOP   IPRINT   IPR
  6       1       1       0
INTLIM  KFAIL  BIGSTP  NPROB
  2       1      0.2      3
IFORM   FORMLA IBOND   ICONST  NROWS   NCOLS  ISCALE
  1       1.0      1       1       1       2       1
ITMAX   IRSTRT NSTOP   EPGRAD  EPFUN   EPX
 100      0       3      0.1E-07   0.1E-03    0.001
INUM    ISAVE  OFFDIF
  2       1      0.001
IPARSH(NDIM) 1=ANALYTIC 2=FORWARD 3=CENTRAL 4=CENTRAL1 5=AUTO F/C
2 2 2 2 2 2
X(NDIM)    INITIAL VALUE FOR THE DECISION VECTOR
 0  4  1.5  50  2  3
IBOUND(NDIM)  1=LB ACTIVE  2=UB ACTIVE  3=BOTH ACTIVE  4=FREE  5=FIXED
 1 4 3 3 3 5
XLB(NDIM)    LOWER BOUNDS
  0.0  0.0  1.0  30.0 1.0  0.0
XUB(NDIM)    UPPER BOUNDS
  0.0  0.0  2.0  100.0 3.0  0.0
XSCALE(NDIM) PRESCALING OF DECISION VARIABLES
1.0  1.0  1.0  10.0 1.0  1.0
ICOL(NCOL)  COMPONENTS OF DECISION VECTOR INVOLVED IN LINEAR CONSTRAINTS
 3  4
AMAT(NROWS,NCOL) LINEAR CONSTRAINT MATRIX
1  1
BRHS(NROWS)  RIGHT HAND SIDE OF LINEAR CONSTRAINTS
5.0
ITYPE(NROWS)  0=(EQUALITY) 1=(≥)  2=(≤)
2
```

figure C.11

```
C*****
C     USER SUPPLIED SUBROUTINE TO INITIALIZE THE PROBLEM.
C
      SUBROUTINE INITLZ(NDIM,IIN,IOUT,IOUT2,IPR2,IPRINT)
      IMPLICIT DOUBLE PRECISION (A-H,O-Z)
C
C     CODING TO INITIALIZE THE OPTIMIZATION
C
      RETURN
      END
C*****
C     USER SUPPLIED SUBROUTINE TO EVALUATE THE FUNCTION.
C
      SUBROUTINE FUNCTN(N,X,F,ITER,IGRAD,SDIREC,NPROB,
     1                  IOUT,IPRINT)
      IMPLICIT DOUBLE PRECISION (A-H,O-Z)
      DIMENSION X(N),SDIREC(N)
C
      X(6) = 5.0 -x(5)
      CALL SIMLAT( X(1), X(2), X(3), X(4), X(5), X(6), OUTPUT)
      F = OUTPUT
      RETURN
      END
C*****
C     USER SUPPLIED SUBROUTINE TO EVALUATE THE GRADIENT
C
      SUBROUTINE GRADNT(N,X,G,ITER,NPROB,IGRAD)
      IMPLICIT DOUBLE PRECISION (A-H,O-Z)
      DIMENSION X(N),G(N)
C
C     NUMERICAL GRADIENTS USED
C
      RETURN
      END
```

figure C.12

C.5 Two Loop Optimizations

When optimizing a simulation, it may take considerably less effort to calculate the objective function for changes in some variables than others. An example would be a time simulation in which the objective function is integrated over the time interval being simulated (say t=0 to t=100). Two of the variables may affect the objective throughout the time interval. There may be three other variables which affect the results of the simulation only over very limited time increments (t=5 to t=6 and t=80 to t=82). For changes in the latter three variables, the objective can be evaluated by retaining the integral over the other times and simply reintegrating over the time intervals that are affected by those variables (t=5 to t=6 and t=80 to t=82). To take advantage of this fact, a two level optimization scheme may be used.

$$\underset{x_1,x_2}{\text{minimize}} \quad f(x_1, x_2, x_3, x_4, x_5)$$

$$\underset{x_3,x_4,x_5}{\text{minimize}} \quad f(x_1, x_2, x_3, x_4, x_5)$$

$$\mathbf{lb} \leq \mathbf{x} \leq \mathbf{ub}$$

$$\mathbf{A}\,\mathbf{x} \leq \mathbf{b} \quad .$$

The linear constraints must not link variables to be optimized in different levels.

If the variables can be treated separably (e.g., if x_1 and x_2 had no impact in the time intervals t=5 to t=6 and t=80 to t=82), then the two optimizations should be solved separately. Hence, for this formulation to make sense, it must not be possible to separate the effects of the variables. The inability to separate the effects of the variables in the example shown above is denoted by showing that f, the objective function, is a function of all five variables (for all time t=0 to t=100).

The inner loop optimization over the variables x_3, x_4, and x_5 is executed for each combination of the variables x_1 and x_2 arrived at during the outer loop optimization. The inner loop optimization will require iterative objective evaluations to converge. In the inner loop optimization, however, only the variables x_3, x_4, and x_5 are varied so less effort is required to determine the objective function. If all five variables were optimized simultaneously, then most of the function calls would involve changes in all five variables, nullifying the savings in computational effort described above. The savings in computational effort afforded by holding x_1 and x_2 fixed in the inner loop optimization must be substantial to justify the above formulation.

For illustrative purposes, no constraints will be assumed for the variables x_1, x_2, x_3, x_4, and x_5. Two input data files are prepared to reflect the inner and outer loop optimizations in essentially the same manner already illustrated in section C.4. For the data file associated with the outer loop optimization, the input ILOOP = 2 (figure C.13); while for the inner loop, ILOOP=1 (figure C.14). The components of the decision vector to be involved in the outer loop optimization are fixed in the inner loop optimization input file (IBOUND = 5). Similarly, the components of the decision vector involved in the inner loop optimization are fixed in the outer loop optimization input file (IBOUND = 5). Although no upper or lower bounds are in use, the input IBOND must be entered as a one so that the fixed variables may be identified. Also, the print level for the inner loop optimization (IPRINT = 0) will result in no output from the inner level.

```
NDIM    ILOOP  IPRINT   IPR
  5       2       1       0
INTLIM  KFAIL  BIGSTP  NPROB
  2       1      0.2      1
IFORM   FORMLA IBOND   ICONST  NROWS   NCOLS  ISCALE
  1       1.0     1       0       1       1       0
ITMAX   IRSTRT NSTOP   EPGRAD  EPFUN   EPX
 100      0      3      0.1E-07  0.1E-03  0.001
INUM    ISAVE  OFFDIF
  2       1      0.001
IPARSH(NDIM) 1=ANALYTIC 2=FORWARD 3=CENTRAL 4=CENTRAL1 5=AUTO F/C
2 2 2 2 2 2
X(NDIM)    INITIAL VALUE FOR THE DECISION VECTOR
 1  1  1  1  1
IBOUND(NDIM)  1=LB ACTIVE  2=UB ACTIVE  3=BOTH ACTIVE  4=FREE  5=FIXED
 4 4 5 5 5
XLB(NDIM)    LOWER BOUNDS
  0.0  0.0  0.0  0.0 0.0
XUB(NDIM)    UPPER BOUNDS
  0.0  0.0  0.0 0.0  0.0
XSCALE(NDIM) PRESCALING OF DECISION VARIABLES
(not in use)
ICOL(NCOL)  COMPONENTS OF DECISION VECTOR INVOLVED IN LINEAR CONSTRAINTS
(not in use)
AMAT(NROWS,NCOL) LINEAR CONSTRAINT MATRIX
(not in use)
BRHS(NROWS)  RIGHT HAND SIDE OF LINEAR CONSTRAINTS
(not in use)
ITYPE(NROWS)  0=(EQUALITY) 1=(≥)  2=(≤)
(not in use)
```

figure C.13

```
NDIM    ILOOP   IPRINT   IPR
5         1        0        0
INTLIM   KFAIL   BIGSTP   NPROB
2         1       0.2        1
IFORM    FORMLA  IBOND    ICONST   NROWS    NCOLS   ISCALE
  1        1.0       1         0         1         1         0
ITMAX    IRSTRT  NSTOP    EPGRAD   EPFUN    EPX
 100         0        3       0.1E-07    0.1E-03     0.001
INUM     ISAVE   OFFDIF
  2         1        0.001
IPARSH(NDIM) 1=ANALYTIC 2=FORWARD 3=CENTRAL 4=CENTRAL1 5=AUTO F/C
2 2 2 2 2 2
X(NDIM)     INITIAL VALUE FOR THE DECISION VECTOR
 1  1  1  1  1
IBOUND(NDIM)  1=LB ACTIVE  2=UB ACTIVE  3=BOTH ACTIVE  4=FREE  5=FIXED
 5 5 4 4 4
XLB(NDIM)     LOWER BOUNDS
  0.0  0.0  0.0  0.0 0.0
XUB(NDIM)     UPPER BOUNDS
  0.0  0.0  0.0 0.0  0.0
XSCALE(NDIM) PRESCALING OF DECISION VARIABLES
(not in use)
ICOL(NCOL)   COMPONENTS OF DECISION VECTOR INVOLVED IN LINEAR CONSTRAINTS
(not in use)
AMAT(NROWS,NCOL) LINEAR CONSTRAINT MATRIX
(not in use)
BRHS(NROWS)  RIGHT HAND SIDE OF LINEAR CONSTRAINTS
(not in use)
ITYPE(NROWS)   0=(EQUALITY) 1=(≥)  2=(≤)
(not in use)
```

figure C.14

As another example, suppose there are five variables related to the performance of a solar cell. Two of the variables x_1 and x_2 are related to changes in design that are relatively costly (e.g., extra processing or material costs), and the performance level of the solar cell design can be considered essentially monotonicly increasing with respect to x_1 and x_2. Where as, the variables x_3, x_4, and x_5 may be changed with little effect on the cost of the design.

It is desired to reach a certain level of performance (denoted as Target). The least squares objective is:

$$\underset{x_1,x_2,x_3,x_4,x_5}{\text{minimize}} \; (\text{Target} - f(x_1, x_2, x_3, x_4, x_5))^2$$

The function "f", which is obtained from a simulation, is the measure of solar cell

performance. Furthermore, it is desirable to reach the target without using values for x_1 and x_2 that lead to an expensive design.

If all the variables are optimized simultaneously, the optimization may move primarily in the subspace associated with x_1 and x_2, resulting in an expensive design. The true objective is to find the best design with respect to x_3, x_4, and x_5 for a combination of the variables x_1 and x_2 that just achieves the target. This is formulated as follows:

$$\underset{x_1,x_2}{\text{minimize}} \ (\text{Target} - mf (x_1, x_2))$$

$$mf = \underset{x_3,x_4,x_5}{\text{maximize}} \ f (x_1, x_2, x_3, x_4, x_5)$$

The value of f is passed in directly from the simulation that the optimization code is coupled with. Unlike the previous example, the outer loop optimization no longer has the same objective function. The routine fouter.f (given below) is used if the outer and inner loop optimizations involve different objective functions.

```
      DOUBLE PRECISION FUNCTION FOUTER(F,X,N)
      IMPLICIT DOUBLE PRECISION (A-H,O-Z)
      DIMENSION X(N)
C
C     F = FUNCTION VALUE FROM INNER LOOP OPTIMIZATION
C     X = DECISION VECTOR (OUTER AND INNER LOOP)
C     N = DIMENSION OF DECISION VECTOR
C     FOUTER = FUNCTION VALUE OF OUTER LOOP
C
      FOUTER = (TARGET-F)**2
      RETURN
      END
```

The user must supply the routine fouter.f (a dummy routine that simply uses the statement FOUTER = F is supplied with the code). The outer loop optimization must be related in some way to the objective function or the values of the variables involved in the inner loop.

C-4

C.6 Implementation Instructions and Environment

This section will detail what is required of the user to prepare the program for execution. It will also detail how the user calculates the amount of array storage needed to solve a problem and how to change the device numbers associated with the input and output files.

6.1 The Code

The code is broken into 8 modules (opt.f, update.f, redgrd.f, onedim.f interloop.f, opt2.f, one2.f, and user.f). User.f contains the routines *MAIN, FOUTER, INITLZ, FUNCTN*, and *GRADNT*, which must be partially coded by the user. The latter three routines are described in section C.4, while the user supplied *MAIN* for the program is described in the next two sections. *FOUTER* is described in section C.5 . Three examples of the user.f module, ex1.f, ex2.f, and ex3.f, which correspond to the first three examples described in the manual, have been supplied with the code. When coding a new problem, it is strongly suggested that the user modify one of the example modules. This will minimize the possibility of any errors in that portion of the code which must remain constant (e.g., calling sequences for subroutines, etc.).

The source code requires approximately 190K bytes of storage (not including the user.f module, which may be short or include a user supplied simulation program). The user must generate object code for each module with a Fortran 77 compiler. The object codes are then linked to form one executable module. An example of how the program would be compiled on a UNIX operating system is given below (the modules can be compiled one at a time, a single command is used below simply to save space in this report).

```
f77 -c opt.f update.f redgrd.f onedim.f interloop.f opt2.f one2.f
```

Depending on the compiler used some warning messages may be generated due to the use of dummy routines (subroutines which must be supplied but the user does not make use of). Any warnings with respect to nonreference of dummy variables passed to subroutines should be ignored during the above compilation and all others to be described. This generates the object files (opt.o, update.o, redgrd.o, onedim.o, interloop.o, opt2.o, and one2.o) for each of the above modules which should never change. The user may then prepare user.f to his/her exact needs and compile it.

```
f77 -c user.f
```

All the object codes are then combined to form the executable module (in this example named opt.out). For this step, all the object modules must be included in the single command below (or a similar one on a different operating system).

```
f77 -o opt.out   opt.o update.o redgrd.o onedim.o interloop.o
                 opt2.o one2.o main.o user.o
```

To solve future problems, the user will only have to change the module user.f, so only the latter two steps need to be executed again. The executable module would be run in foreground by entering:

```
opt.out <inputfile >outputfile
```

"inputfile" is the name of the input file, and "outputfile" is the name of the output file. **Note**, for use at JPL on the Univac and VAX computers the inputfile has been associated with the device number 8. Therefore, the user simply uses the usual JCL to connect the input file to the number 8. For example, to run the first example, ex1.f is compiled and linked with the optimization object modules and then JCL is written to associate device number 8 with the input file inex1.d. When solving example problem two, ex2.f must be compiled and linked with the optimization object modules, and the JCL changed so that inex2.d is associated with device number 8.

The amount of storage required for the object code modules is machine dependent (274K on a Pyramid 90X minicomputer), but will generally be 1.3 to 2 times greater than the storage required for the source. The size of the executable module is also machine dependent (275K on a Pyramid 90X minicomputer). The size of the executable module quoted above does not include data storage (primarily array storage). The program was developed on a minicomputer, but it should fit on most personal computers, depending on problem size and the size of the *FUNCTN* routine (which may call a simulation program).

If the two level optimization scheme is not going to be used (section C.5), storage may be saved by substituting dopt2.f and done2.f for opt2.f and one2.f. The former routines are dummy routines which do not contain the coding required for the two level optimization. Hence, they require very little storage. Using the dummy routines, the source coding is only 112K, the object codes are only 170K, and the executable module is only 193K (the latter two figures are for a Pyramid 90X minicomputer).

6.2 Array Storage and I/O

The amount of array storage needed to solve a problem is dependent on the dimension of the problem and whether or not bounds, prescaling, and linear constraints are used. Rather than fix the dimension of the code to a maximum problem size, the array storage is passed using variable dimensions through the fixed modules of the code. Using the module main.f, which is a very simple routine, the user may fix the amount of array storage needed to solve any given problem.

Figure C.15 shows an example of the *MAIN* that is in ex1.f, ex2.f and ex3.f. The user may fix the values of the dimension statements and the values of the variables ZCORE and ICORE (shown in bold) in main.f according to the equations given in figure C.15 to assure that there is sufficient storage to solve the problem. The values of ZCORE and ICORE can be larger than required for the problem, so that it is best to use values that will suffice for most problems. Then, the user only has to change the dimensions if the problem is very large or machine storage is limited. From figure C.15 it is seen that using the conjugate gradient algorithm to calculate the search direction requires less array storage than a quasi-Newton algorithm. Also, the use of upper and lower bounds, prescaling, and/or linear constraints increases the storage requirements.

The Fortran device numbers associated with the input and output files for the optimization (only one of each is used) are given in the variables IIN and IOUT, respectively. They may be easily changed if the values given in figure C.15 lead to a conflict with another program to be coupled with the optimization code through the *FUNCTN* routine. However, on the UNIX system that the code was developed on it is not necessary to use the Fortran 77 statement OPEN for the device numbers 5 (standard input) and 6 (standard output). If the device numbers are changed, OPEN statements should be included in the *MAIN* to connect the files to be used to the device numbers. Other operating systems may require an open statement for the device numbers 5 and 6 (and others) as well as job control language to insure the files are connected. Where as, some operating systems will not require an OPEN statement for any device number as long as the appropriate JCL is used.

```
C
C    USER MAY USE THIS ROUTINE TO CHANGE THE AMOUNT OF ARRAY STORAGE
C    as follows:
C    IFORM = 1 or 2    ZCORE = 6*n + n*(n+1)/2 + 15   ICORE = 2*n + 7
C    IFORM = 3         ZCORE = 4*n + 15               ICORE = 2*n + 7
C    for both case above
C    if IBOND = 1   ZCORE = ZCORE + 2*n    ICORE = ICORE + 2*n
C    if ISCAL  = 1  ZCORE = ZCORE + n
C    if ICONST = 1  ZCORE = ZCORE + 2*(nr*nc) + nr*nr + 3*nr + 2*nc
C                   ICORE = ICORE + 3*nc + 3*nr
C    where: n= NDIM, nr = NROWS, nc = NCOLS
C
C    IIN = input file device number
C    IOUT = output file device number
C
C    ************do not forget OPEN statements if needed*****************
C
     INTEGER ZCORE,ICORE
     DOUBLE PRECISION Z(5000)
     INTEGER I(1000)
C
C    NOTE THE VALUES ABOVE AND THE VALUES OF ZCORE AND ICORE MUST AGREE
C
     ZCORE = 5000
     ICORE = 1000
     IIN = 5
     IOUT = 6
     CALL START(Z,I,ZCORE,ICORE,IIN,IOUT)
     STOP
     END
```

figure C.15

C.7 Use With SCAP1D

The optimization routine described in the previous six sections has been coupled with a numerical model of a silicon solar cell, Solar Cell Analysis Program in 1 Dimension (SCAP1D), which was obtained from JPL. SCAP1D was extensively modified and a very flexible interface was written to couple SCAP1D to the optimization code. The optimization variables are inputs to SCAP1D and the objective function is an output from SCAP1D. All the coding required to interface the two programs has been provided (e.g., the user.f module) as well as additional routines written to decrease the computational effort required to solve an optimization. In addition, several changes have been made to the SCAP1D model to include additional variables related to solar cell performance and to generalize the model. This section will detail the modifications made to SCAP1D and the input files required to run the program.

7.1 Modifications to SCAP1D

Only those modifications that affect the SCAP1D input file are described in this section. The format of the SCAP1D input file has been changed from name list input format to list directed input format because the former is not standard Fortran 77. The new format for the SCAP1D data file is similar to the optimization data file described in section C.4 (i.e., the organization of the file is clearly illustrated by comment lines with the data entered on the line(s) below the comment line).

Figure C.16 is an example of a SCAP1D file. Two lines are provided at the top of the file for comments to document the input file. The two comment lines must be included, but they are skipped when the data is read in. In list directed format, the occurrence of a slash, "/", implies that the rest of the data in that read statement (the inputs associated with a single comment line) will not be read. If a read statement is used (no slash), the data need not necessarily appear on a single line. But if a slash is used, exactly one line must be skipped after the comment line. Inputs that are not read in will take on the default values assigned in SCAP1D. If data is read in for a variable, it supersedes the default values assigned in SCAP1D.

All the input variables in figure C.16 that are in normal type are unchanged from their interpretation in the original version of SCAP1D, which is described in JPL publication #85-46[†]. All the entries shown in bold in figure C.16 are either new variables or new interpretations of variables that were in the original version.

[†]DOE/JPL-1012-107, A.R. Mokashi, T. Daud, and R.M. Kachare, "High-Efficiency Silicon Solar Cell Design Evaluation and Sensitivity Analysis"

The paragraphs below describe the bold entries in the order they occur in the data file.

The input SHADOW has been changed from a shadowing and reflection factor to a shadowing factor only. The input SHADOW determines the active area of the cell (e.g., the area of the cell exposed to the incoming illumination). The definition of the active area of the cell is A_{act} = (1-SHADOW) AREA. This input accounts for the shadowing of the illuminated surface of the cell by the current collection grid that occurs in a conventional cell design. Hence, the incoming illumination is no longer affected by the input SHADOW. The new input REFLCT reduces the incoming irradiation by the factor (1 -REFLCT), which is constant over all wavelengths (this is what SHADOW used to do).

The inputs RADCOF and RADREC relate to radiative recombination. If the flag RADREC is true, then radiative recombination will be included in the analysis. The input RADCOF is the coefficient for radiative recombination (see equation A.3).

The inputs RFRONT and INTREF are used to implement light trapping in the cell. Light trapping occurs when the light is reflected back to the front surface at an angle greater than the critical angle, resulting in total internal reflection. The input RFRONT is analogous to RBACK for a back surface reflector. It represents the percent of the light that is reflected from the front surface back into the cell (e.g., RFRONT = 1.0 is a perfect reflector, all light arrives at the front surface at an angle greater than the critical angle). The input INTREF is an integer that represents the number of times the light will be internally reflected from the front surface. At each reflection, 1-RFRONT of the irradiation will be lost at the front surface. The value of INTREF in the original version of SCAP1D was effectively zero, since light trapping was not included in the code.

A print level of -1 has been added to SCAP1D, which results in absolutely no output from SCAP1D (unless an error occurs). This print level should be used when running an optimization.

The last input line in figure C.16 relates to the use of anti-reflection coatings. The logical input MODULE is related to passing the incident radiation through the materials that make up the module. This logic has not been implemented, so MODULE should always be false. If the logical input variable ARFILM is true, then the incident illumination will be passed through an anti-reflection coating(s). XRMED = the index of refraction of the surrounding medium. NLAY = the number of layers (1 or 2). XRFILM = the index of refraction of each layer, which is assumed constant over all wavelengths. XTHICK = the thickness of each layer in μm. The number of entries for XRFILM and XTHICK must agree with NLAY or erroneous results will occur. If the logical input ARPRNT is true, the reflectivity will be output as a function of wavelength.

The formulas used to calculate the reflection of the incident illumination with the inclusion of anti-reflection coating(s) are based on thin film optics. To use these formulas the real and imaginary components of the index of refraction of silicon as a function of wavelength must be known. The files used to read in the incident irradiation (AM0, AM1, or AM15) have been expanded to include the refraction index of silicon. These files are only valid for use with silicon solar cells, if the antireflection logic is in use. Figure C.17 is the top portion of the new AM15 data file. The data file now contains the wavelength, the irradiance per μm at the wavelength, and the real and the imaginary (extinction coefficient) parts of the index of refraction for silicon at the wavelength.

```
THIS IS A TITLE LINE FOR DOCUMENTATION PURPOSES.
THIS IS A TITLE LINE FOR DOCUMENTATION PURPOSES.
IRUNUM   TEMP  SOLAR    RS      AREA      SI       GE
 1001      28.  .TRUE.    0.000    4.00  .TRUE.  .FALSE.
 ZKN    ZKP   RADCOF    AN     AP     BGNON BGNOP  NCRITP  NCRITN
7.1D15  7.1D15  2.0E-15  2.8E-31 9.9E-32 /
 EG0   NV0    NC0      EP(2)   EGD0 EG20 EG10    AD       A(2)     C(2)
/
 GMMAA  BETA  GMMAM  ETAN  ETAP  NREFP  NREFN  ALPHAP
/
 ALPHAN  UPMIN  UNMIN  UPMAX  UNMAX DOSNI  EGNI   CS
/
    PI        HP       M0  MH  ME     KB     E0     K0     Q
/
    FRONT   BACK   BOTH     SF     SB
  .FALSE.  .FALSE.  .FALSE.   1.0D2  1.0D2
  NODES    ITMAXQ   ITMAX  RESQAXQ   RESIDMX   DELMAXQ
   250         30         25  /
  DELMAX   REDUCE   APPROX   VINCR   DROP   DELSUN
 /
  ND  NXD(20)     XD(20)       FAC    ATOMSH   XDMAX
  1    25 19*0  100.D0 19*0.D0 10.0D0   .TRUE.    280
 BORON  PHOS  STEP   ERFC   FAIRT   DDOP    DDOPS   UDOP
.TRUE.  .TRUE. .FALSE. .TRUE.  .FALSE.  .FALSE.  .FALSE.  .FALSE.
  XJF   XJB   DOP0  DOPBLK   DOPL   DIFTIM   DIFTMP
  0.2     0.0   2.D20   -1.D19   -1.D19      0.D0      0.D0
  PHOSFR    PHOSBK    DFILES   ASCII   BINARY
  .FALSE.    .FALSE.         0      .FALSE.  .FALSE.
  SBBGN     LTBGN    UBGN    IGAM   UGAM
  .TRUE.    .FALSE.  .FALSE.     0     .FALSE.
  AUGER    RADREC      ET    MIDG      TAUP    TAUN
  .TRUE.   .FALSE. -1.D5   .FALSE.     1.0D-3    2.0D-3
   AM1    AM15   UNIFRM   MONO    DARK    UGEN   CONCEN
  .FALSE.  .TRUE.  .FALSE.  .FALSE.  .FALSE.  .FALSE.  1.2022
   SHADOW  REFLCT WAVEL   FLUXQ   FILTER   WFILTR   BBODY   TBB
    0.00        0.07      0.5D0 /
  IBC    PWRINC   AM0    ER203   RBACK RFRONT  INTREF   ANGLE   GDATA
 .FALSE.  0.0D0    .FALSE. .FALSE.  1.0    0.0       0       0.0      .FALSE.
   SPECRS     ISR   VSR   JSR      WL(20)
   .FALSE.      11   0.D0  1.D-6 /
  IVNUM   VSTART    VSTOP   VDEL   VA
    0        0.0          1.0       0.1 /
  SOLCEL
  .TRUE.
   IPRINT    PSTEP    TABL   TABLQ
   -1           5      .FALSE.  .FALSE.
  SAVE
 .FALSE.
  DOCAP   DELVC  CAPERR    CAP(25)
 .FALSE.   .001D0 /
 MODULE  ARFILM XRMED  NLAY XRFILM(NLAY) XTHICK(NLAY)   IRPRNT
.FALSE.   .FALSE.      1.0      1       1.0        1       0.0       .FALSE.
```

figure C.16

AM1.5
0.0831812
3.61800E17
125
0.295000 0. 4.28282 4.64986
0.305000 1.32000 4.83000 3.95734
0.315000 20.9600 4.98630 3.50163
0.325000 113.480 5.06128 3.29837
0.335000 182.230 5.14183 3.09512
0.345000 234.430 5.53088 2.90808
0.355000 286.010 6.04100 3.07517
0.365000 355.880 6.45103 2.57856
0.375000 386.800 6.86105 2.08195
0.385000 381.780 6.38547 1.58534
0.395000 492.180 5.85202 1.08873
0.405000 751.720 5.39246 0.592119
0.415000 822.450 4.98823 0.169314
0.425000 842.260 4.90758 0.164743
0.435000 890.550 4.82694 0.160171
0.445000 1077.07 4.74630 0.155600
0.455000 1162.43 4.66566 0.151029
0.465000 1180.61 4.58502 0.146457
0.475000 1212.72 4.51213 0.141886
0.485000 1180.43 4.43944 0.137314
0.495000 1253.83 4.36676 0.132743
0.505000 1242.28 4.29407 0.128171
0.515000 1211.01 4.22139 0.123600
0.525000 1244.87 4.14870 0.119029
0.535000 1299.51 4.08572 0.114457
0.545000 1273.47 4.04246 0.109886
0.555000 1276.14 3.99920 0.105314
0.565000 1277.74 3.95593 0.100743
0.575000 1292.51 3.91267 9.61714e-02
0.585000 1284.55 3.86941 9.16000e-02
0.595000 1262.61 3.82614 8.70286e-02
0.605000 1261.79 3.78288 8.24571e-02
0.615000 1255.43 3.73962 7.78857e-02
0.625000 1240.19 3.71229 7.33143e-02
0.635000 1243.79 3.70309 6.87428e-02
0.645000 1233.96 3.69388 6.41714e-02
0.655000 1188.32 3.68467 5.96000e-02

figure C.17

7.2 The Optimization Data File

The optimization data file for use with SCAP1D is similar in format to the file format detailed in sections C.4.1, C.4.2, C.4.3 and C.4.4. The interface between the optimization and SCAP1D has been generalized so that a number of variables may be included or left out of the optimization. Also, the user may choose between a number of different objective functions. This generalization is provided by the *INITLZ* routine and requires several additional lines in the optimization data file. The additional lines occur after the initial comment and data file line in a standard file (see figure C.18). The additional lines identify the objective, read in any constants to be used in the objective, and identify the variables to be used in the optimization.

A complete list of the possible optimization variables is given below. The variable name must be entered in the input file starting in column *one* so that the optimization correctly passes the decision vector (x) to SCAP1D.

XJF Front junction depth measured from the front surface of the cell (μm).

XJB Back junction depth measured from the back surface of the cell (μm).

XDMAX Cell thickness (μm).

DOP0 † $\pm$Log$_{10}$ of front surface doping concentration, which is in atoms/cm^3

DOPBLK † $\pm$Log$_{10}$ of bulk doping concentration, which is in atoms/cm^3

DOPL † $\pm$Log$_{10}$ of back surface doping concentration, which is in atoms/cm^3

SF Log$_{10}$ of effective front surface recombination velocity, which is in cm/second.

SB Log$_{10}$ of effective back surface recombination velocity, which is in cm/second.

TAUN Electron minority carrier lifetime for a lightly doped or intrinsic substrate (saturation lifetime) in milliseconds. The hole saturation minority carrier lifetime (TAUP) is taken as one half the value of TAUN.

SHADOW Shadowing factor, percent of cell covered by front contact grid (entered as a decimal %/100).

REFLCT Reflection factor, percent of incoming radiation lost to reflection, constant over all wavelengths (entered as a decimal %/100).

RS Contact resistance and grid resistance (Ω).

CONCEN Concentration factor for illumination (e.g., 1.2022 with AM15 illumination for global power incidence).

† A positive value implies a net n-type or donor impurity, while a negative value implies a net p-type or acceptor impurity (e.g., 19 is 10^{19} P atoms/cm^3 and -19 is 10^{19} B atoms/cm^3).

XRFILM Index of refraction for anti-reflection layer(s). If there are n layers, XRFILM should appear n times (n=1 or 2). The first incidence of XRFILM is for the layer nearest the medium, last is for the layer nearest the cell.

XTHICK Thickness of anti-reflection layer(s) in μm. If there are n layers, XTHICK should appear n times (n=1 or 2). The first incidence of XTHICK is for the layer nearest the medium, last is for the layer nearest the cell.

UDOP1 Variable which will not affect the finite difference mesh (e.g., doping concentration) to be used in user written *UDOP* routine. UDOP1 may appear as many times as desired. The entire decision vector is passed to the *UDOP* routine so the user determines how the variable is used.

UDOP2 Variable which will affect the finite difference mesh (e.g., junction depth) to be used in user written *UDOP* routine. UDOP2 may appear as many times as desired. The entire decision vector is passed to the *UDOP* routine so the user determines how the variable is used.

All of the variables above also appear in the SCAP1D input file (except UDOP1 and UDOP2). The value of any variable read in the optimization file *supersedes* the value that appears in the SCAP1D input file. In general, the user will include only a subset of the variables listed above in the optimization data file. Any variables not included then get their values from the SCAP1D input file (or by default). The situation is complicated by the logical entries in the SCAP1D data file. If any of the inputs FRONT, BACK, or BOTH are entered as true in the SCAP1D input file, ohmic surfaces are used in the simulation and the inputs for SF and/or SB are ignored in both data files. If the input ARFILM is false, the logic associated with anti-reflection coatings will not be executed regardless of the values of the variables XTHICK and XRFILM. Also, a nonzero number of occurrences of the variables XTHICK and XRFILM in the optimization file (must be the same and both must occur, but any of the values may be held fixed during the optimization) will supersede the value of the variable NLAY in the SCAP1D data file.

A complete list of the objective functions that may be optimized is given below. The first column is the identifier, which must be entered in the data file starting in column *one* so the code may determine which objective function is to be used. A brief explanation is given for each objective function. A more complete description is given for each objective function in the main body of the report. The decision vector for which the objective will be optimized is determined by the user using the variable inputs described above. Along with the identifier, the user may have to enter some constants that are used in the objective function. The constants required are described for each objective.

MAXEFF Maximize the efficiency as calculated in the original version of SCAP1D (no user supplied constants).

MAXEFFLR Maximize the efficiency with a correction for lateral resistance through the emitter, which was not included in the original version of SCAP1D. The user must also supply one constant, which represents the distance between the grid lines in *centimeters*. This input is used in the formula for determining the correction for lateral resistance.

MAXVOC Maximize the open circuit voltage (no user supplied constants).

MAXJSC Maximize the short circuit current density (no user supplied constants).

MAXGEN Maximize the electron-hole pair generation rate in the cell (no user supplied constants).

Figure C.18 shows an example data file used to optimize the efficiency with the lateral resistance correction term. The problem is stated mathematically below.

$$\text{maximize effir(XJF, XJB, XDMAX, DOP0, DOPBLK, DOPL)}$$

$$0.1 \le \text{XJF} \le 10.0$$

$$0.2 \le \text{XJB} \le 50.0$$

$$10.0 \le \text{XDMAX} \le 300.0$$

$$14 \le \text{DOP0} \le 20.6$$

$$-20.6 \le \text{DOPBLK} \le -14.0$$

$$-20.6 \le \text{DOPL} \le -14.0$$

$$-0.4 \le \text{DOPL} - \text{DOPBLK}$$

The data file is identical to a normal optimization data file already discussed except for the additional entries that occur between the data line associated with the dimension etc. and the comment line for INTLIM etc. The additional lines also use comment lines to show the organization. The first data line is the name of the SCAP1D data file that will be used (figure C.16). The second data line is the name which identifies the objective function, in this case a maximization of efficiency including a correction for lateral resistance. The objective name must start in the first column. The third data line is for the user supplied constants in the objective function, in this case the distance between grid lines in centimeters. Even if the objective function to be used does not require user supplied constants, a comment and data line must occur in the input file. One comment line identifies that the next NDIM lines will be used to identify the decision vector. There must be NDIM entries following the comment line. The order of the variables must correspond to the order that they appear in the decision vector (e.g., x(1) is first, x(NDIM) is last). Each variable name must be on a separate line and start in the

first column. In this example, twelve of the variables from the list are to be read in from the optimization file. The variables involved in the optimization are XJF, XJB, XDMAX, DOP0, DOPBLK, and DOPL. Although the variables SF, SB, TAUN, SHADOW, RS, and CONCEN are read in from the optimization file, they are held fixed (IBOUND = 5) and are not varied during the optimization. The output associated with the input file shown in figure C.18 is given in figure C.19 .

In figure C.20, the objective is to maximize the generation rate. The variables to be involved in the optimization (IBOUND ≠ 5) represent the design of a double layer anti-reflection coating. The problem is stated mathematically below.

maximize genrationrate(XRFILM(1), XTHICK(1), XRFILM(2), XTHICK(2))

$1.45 \leq$ XRFILM(1) ≤ 2.3

$0.01 \leq$ XTHICK(1) ≤ 1.5

$1.45 \leq$ XRFILM(2) ≤ 2.3

$0.01 \leq$ XTHICK(2) ≤ 1.5

The output associated with the above problem statement and the input file given in figure C.20 is given in figure C.21 .

Figure C.22 shows an example data file used to optimize the efficiency without the lateral resistance correction term (the original definition of efficiency from SCAP1D). The problem is stated mathematically below.

maximize eff(XJF, XJB, XDMAX, DOP0, DOPBLK, DOPL)

$0.1 \leq$ XJF ≤ 10.0

$0.2 \leq$ XJB ≤ 50.0

$10.0 \leq$ XDMAX ≤ 300.0

$14 \leq$ DOP0 ≤ 20.6

$-20.6 \leq$ DOPBLK ≤ -14.0

$-20.6 \leq$ DOPL ≤ -14.0

$-0.4 \leq$ DOPL − DOPBLK

The output associated with the above problem statement and the input file given in figure C.22 is given in figure C.23 .

Figure C.24 shows an example data file used to optimize the open circuit voltage. The problem is stated mathematically below.

maximize voc(XJF, XJB, XDMAX, DOP0, DOPBLK, DOPL)

$0.1 \leq$ XJF ≤ 10.0

$$0.2 \leq XJB \leq 50.0$$

$$10.0 \leq XDMAX \leq 300.0$$

$$14 \leq DOP0 \leq 20.6$$

$$-20.6 \leq DOPBLK \leq -14.0$$

$$-20.6 \leq DOPL \leq -14.0$$

$$-0.4 \leq DOPL - DOPBLK$$

The output associated with the above problem statement and the input file given in figure C.24 is given in figure C.25 .

Figure C.26 shows an example data file used to optimize the short circuit current density. The problem is stated mathematically below.

maximize jsc(XJF, XJB, XDMAX, DOP0, DOPBLK, DOPL)

$$0.1 \leq XJF \leq 10.0$$

$$0.2 \leq XJB \leq 50.0$$

$$10.0 \leq XDMAX \leq 300.0$$

$$14 \leq DOP0 \leq 20.6$$

$$-20.6 \leq DOPBLK \leq -14.0$$

$$-20.6 \leq DOPL \leq -14.0$$

$$-0.4 \leq DOPL - DOPBLK$$

The output associated with the above problem statement and the input file given in figure C.26 is given in figure C.27 .

```
NDIM    ILOOP  IPRINT   IPR
 12      1       1       0
THE NAME OF THE INPUT FILE FOR SCAP1D
INSCAP.D
NAME OF THE OBJECTIVE FUNCTION
MAXEFFLR
INPUT FOR OBJECTIVE (FOR THIS CASE DISTANCE BETWEEN GRID LINES IN CM)
0.1
VARIABLE NAMES, IN ORDER THEY APPEAR IN THE OPTIMIZATION VECTOR X
XJF
XJB
XDMAX
DOP0
DOPBLK
DOPL
SF
SB
TAUN
SHADOW
RS
CONCEN
INTLIM  KFAIL  BIGSTP  NPROB
  2      1      0.1      1
IFORM   FORMLA  IBOND   ICONST  NROWS   NCOLS  ISCALE
  1      1.0     1       1       1       2      1
ITMAX   IRSTRT  NSTOP   EPGRAD  EPFUN   EPX
 100      0      3     0.1E-09 0.1E-03 0.1E-03
INUM    ISAVE  OFFDIF
  2       1     0.001
IPARSH(NDIM) 1=ANALYTIC 2=FORWARD 3=CENTRAL 4=CENTRAL1 5=AUTO F/C
2 2 2 2 2 2 2 2 2 2 2 2
X(NDIM)    INITIAL VALUE FOR THE DECISION VECTOR
 0.1  0.2 280.1  19.4031 -16.2986  -19.507  3.0
 3.0  1.0   0.00   0.0    1.2022
IBOUND(NDIM)  1=LB ACTIVE  2=UB ACTIVE  3=BOTH ACTIVE  4=FREE  5=FIXED
3 3 3 3 3 3 5  5 5 5 5 5
XLB(NDIM)     LOWER BOUNDS
0.1   0.2   10.0   14.0  -20.6  -20.6  -5.0  -5.0
XUB(NDIM)     UPPER BOUNDS
15.0  50.0  300.0  20.6  -14.0   -14.0   16.0  16.0  10000.0
 10.0  30.0  300.0
XSCALE(NDIM) PRESCALING OF DECISION VARIABLES
0.4  1.0  100.0  1.0  1.0  1.0  1.0  1.0  1.0  1.0  1.0  1.0  1.0 1.0
ICOL(NCOL)   COMPONENTS OF DESICION VECTOR INVLOVED IN LINEAR CONSTRAINTS
  5   6
AMAT(NROWS,NCOL) LINEAR CONSTRAINT MATRIX
 -1  1
BRHS(NROWS)  RIGHT HAND SIDE OF LINEAR CONSTRAINTS
 -0.4
ITYPE(NROWS)   0=(EQUALITY) 1=(>)  2=(<)
 2
```

figure C.18 The file inefflr.d

```
   INPUT DATA FILE

(DATA FILE WRITTEN OUT HERE, SEE FIGURE C.18)


  PROBLEM #  1


  EXECUTING THE BROYDEN FAMILY MEMBER
  0.00E+00 DFP +  1.0    BFGS



  BEGIN ITERATION #   0
  THE OBJ =  -20.84767454
  THE POINT IS =
 0.10000000000     0.20000000000     280.10000000     19.403100000     -16.298600000     -19.507000000
 3.0000000000      3.0000000000      1.0000000000     0.00000000000E+00 0.00000000000E+00 1.2022000000


  ISTOP=  1 CONVERGENCE ON MAGNITUDE OF DERIVATIVE SATISFIED. MAG<  0.1000000E-09



      PROBLEM SUMMARY

  # ITERATIONS =    9  # OBJ EVALS =  104  # GRAD EVALS =  10
  # OF RESETS =   2  # FAILED INTRPS=   4
   64 OF THE OBJECTIVE EVALUATIONS WERE FOR NUMERICAL DERIVATIVES
  THE MINIMUM OBJECTIVE =  -21.76188
  THE OPTIMAL POINT IS =
 0.5975804      0.2000000      290.4114      19.21597      -16.23632      -19.54320
 3.000000       3.000000       1.000000      0.0000000E+00 0.0000000E+00  1.202200

  THE MAGNITUDE OF THE GRADIENT AT THE MIN =   223.93014
  THE GRADIENT AT MIN =
   197.54       -0.00000E+00    101.61        15.471        18.242        15.093
 -0.00000E+00   -0.00000E+00   -0.00000E+00  -0.00000E+00  -0.00000E+00   -246.08

  ALL PROBLEMS HAVE BEEN COMPLETED
```

figure C.19 Output for input file inefflr.d

```
NDIM    ILOOP   IPRINT   IPR
 7       1        1       0
THE NAME OF THE INPUT FILE FOR SCAP1D
INSCAPG.D
NAME OF THE OBJECTIVE FUNCTION
MAXGEN
INPUT FOR OBJECTIVE (FOR THIS CASE DISTANCE BETWEEN GRID LINES IN CM)
(not in use)
VARIABLE NAMES, IN ORDER THEY APPEAR IN THE OPTIMIZATION VECTOR X
XRFILM
XTHICK
XRFILM
XTHICK
XDMAX
SHADOW
REFLCT
INTLIM  KFAIL  BIGSTP  NPROB
 2      1      1.0      2
IFORM   FORMLA IBOND   ICONST  NROWS   NCOLS   ISCALE
 1      1.0    1       0       1       1       1
ITMAX   IRSTRT NSTOP   EPGRAD  EPFUN   EPX
 100    0      3       0.1E-09 0.1E-03 0.1E-03
INUM    ISAVE  OFFDIF
 2      1      0.001
IPARSH(NDIM) 1=ANALYTIC 2=FORWARD 3=CENTRAL 4=CENTRAL1 5=AUTO F/C
2 2 2 2 2 2 2 2 2 2 2 2
X(NDIM)    INITIAL VALUE FOR THE DECISION VECTOR
 1.45  0.2  2.3  0.2 100.0 0.02  0.0
IBOUND(NDIM)  1=LB ACTIVE  2=UB ACTIVE  3=BOTH ACTIVE  4=FREE  5=FIXED
3 3 3 3  5  5 5
XLB(NDIM)     LOWER BOUNDS
 1.45  .01  1.45 .01 10 0.0  0.0
XUB(NDIM)     UPPER BOUNDS
 2.3  1.5  2.3  1.5  300.0 1.0  1.0
XSCALE(NDIM) PRESCALING OF DECISION VARIABLES
1.0   1.0   1.0   1.0  1.0  1.0 1.0
ICOL(NCOL)   COMPONENTS OF DESICION VECTOR INVLOVED IN LINEAR CONSTRAINTS
(not in use)
AMAT(NROWS,NCOL) LINEAR CONSTRAINT MATRIX
(not in use)
BRHS(NROWS)  RIGHT HAND SIDE OF LINEAR CONSTRAINTS
(not in use)
ITYPE(NROWS)  0=(EQUALITY) 1=(>)  2=(<)
(not in use)
```

figure C.20 The file inmaxgen.d

```
   INPUT DATA FILE

(INPUT DATA FILE WRITTEN OUT HERE, SEE FIGURE C.20)


  PROBLEM #   2


  EXECUTING THE BROYDEN FAMILY MEMBER
  0.00E+00 DFP +  1.0     BFGS



  BEGIN ITERATION #    0
  THE OBJ =  -34.20296827
  THE POINT IS =
  1.4500000000     0.20000000000     2.3000000000     0.20000000000     100.00000000     0.20000000000E-01
0.00000000000E+00

  ISTOP= 2 CONVERGENCE ON OBJECTIVE VALUE SATISFIED.
  CHANGE IN OBJECTIVE <  0.1000000E-03 FOR LAST   3 ITERATIONS



       PROBLEM SUMMARY

  # ITERATIONS =    8   # OBJ EVALS =  54   # GRAD EVALS =   8
  # OF RESETS =   2   # FAILED INTRPS=   3
   26 OF THE OBJECTIVE EVALUATIONS WERE FOR NUMERICAL DERIVATIVES
  THE MINIMUM OBJECTIVE =  -37.60268
  THE OPTIMAL POINT IS =
  1.478805     0.1077049     2.300000     0.2547077     100.0000     0.2000000E-01
0.0000000E+00
  THE MAGNITUDE OF THE GRADIENT AT THE MIN =   1.0453586
  THE GRADIENT AT MIN =
  -0.45086     -0.25284E-01  -0.00000E+00  -0.94279     -0.00000E+00  -0.00000E+00
  -0.00000E+00
   ALL PROBLEMS HAVE BEEN COMPLETED
```

figure C.21 Output for input file inmaxgen.d

```
NDIM    ILOOP  IPRINT   IPR
 12      1      1       0
THE NAME OF THE INPUT FILE FOR SCAP1D
INSCAP.D
NAME OF THE OBJECTIVE FUNCTION
MAXEFF
INPUT FOR OBJECTIVE (FOR THIS CASE DISTANCE BETWEEN GRID LINES IN CM)
0.1
VARIABLE NAMES, IN ORDER THEY APPEAR IN THE OPTIMIZATION VECTOR X
XJF
XJB
XDMAX
DOP0
DOPBLK
DOPL
SF
SB
TAUN
SHADOW
RS
CONCEN
INTLIM  KFAIL  BIGSTP  NPROB
 2      1      0.1      1
IFORM   FORMLA IBOND   ICONST  NROWS   NCOLS  ISCALE
 1      1.0    1       1       1       2      1
ITMAX   IRSTRT NSTOP   EPGRAD  EPFUN   EPX
 100    0      3       0.1E-09 0.1E-03 0.1E-03
INUM    ISAVE  OFFDIF
 2      1      0.001
IPARSH(NDIM) 1=ANALYTIC 2=FORWARD 3=CENTRAL 4=CENTRAL1 5=AUTO F/C
2 2 2 2 2 2 2 2 2 2 2 2
X(NDIM)    INITIAL VALUE FOR THE DECISION VECTOR
 0.2  0.2 250.0  20.4031 -17.2986  -19.507  3.0
 3.0  1.0   0.00   0.0    1.2022
IBOUND(NDIM)  1=LB ACTIVE  2=UB ACTIVE  3=BOTH ACTIVE  4=FREE  5=FIXED
3 3 3 3 3 3 5  5 5 5 5 5
XLB(NDIM)    LOWER BOUNDS
0.1   0.2   10.0   14.0  -20.6  -20.6  -5.0  -5.0
XUB(NDIM)    UPPER BOUNDS
15.0  50.0  300.0  20.6  -14.0   -14.0   16.0  16.0  10000.0
 10.0  30.0  300.0
XSCALE(NDIM) PRESCALING OF DECISION VARIABLES
0.4  1.0  100.0  1.0  1.0  1.0  1.0  1.0  1.0  1.0  1.0  1.0  1.0 1.0
ICOL(NCOL)   COMPONENTS OF DESICION VECTOR INVLOVED IN LINEAR CONSTRAINTS
 5   6
AMAT(NROWS,NCOL) LINEAR CONSTRAINT MATRIX
-1  1
BRHS(NROWS)  RIGHT HAND SIDE OF LINEAR CONSTRAINTS
-0.4
ITYPE(NROWS)   0=(EQUALITY) 1=(>)  2=(<)
 2
```

figure C.22 The file ineff.d

```
   INPUT DATA FILE

(INPUT DATA FILE WRITTEN OUT HERE, SEE FIGURE C.22)


  PROBLEM #  3


  EXECUTING THE BROYDEN FAMILY MEMBER
  0.00E+00 DFP +  1.0    BFGS



  BEGIN ITERATION #   0
  THE OBJ =  -18.87970504
  THE POINT IS =
 0.20000000000    0.20000000000     250.00000000     20.403100000    -17.298600000    -19.507000000
  3.0000000000     3.0000000000     1.0000000000    0.00000000000E+00 0.00000000000E+00  1.2022000000


  ISTOP= 2 CONVERGENCE ON OBJECTIVE VALUE SATISFIED.
  CHANGE IN OBJECTIVE <  0.1000000E-03 FOR LAST  3 ITERATIONS



      PROBLEM SUMMARY

  # ITERATIONS =   10  # OBJ EVALS =  90  # GRAD EVALS =  10
  # OF RESETS =   4  # FAILED INTRPS=   6
   54 OF THE OBJECTIVE EVALUATIONS WERE FOR NUMERICAL DERIVATIVES
  THE MINIMUM OBJECTIVE =  -21.87110
  THE OPTIMAL POINT IS =
 0.1000000     0.2000000     282.2181     19.32295     -16.28486     -19.53169
  3.000000     3.000000     1.000000    0.0000000E+00 0.0000000E+00  1.202200

  THE MAGNITUDE OF THE GRADIENT AT THE MIN =  0.34966550E-01
  THE GRADIENT AT MIN =
 -0.00000E+00  -0.00000E+00  -0.11244E-01  0.65867E-02  0.32438E-01  -0.79882E-03
 -0.00000E+00  -0.00000E+00  -0.00000E+00  -0.00000E+00  -0.00000E+00  -0.00000E+00

   ALL PROBLEMS HAVE BEEN COMPLETED
```

figure C.23 Output for input file ineff.d

```
NDIM    ILOOP  IPRINT   IPR
 12      1       1       0
THE NAME OF THE INPUT FILE FOR SCAP1D
INSCAP.D
NAME OF THE OBJECTIVE FUNCTION
MAXVOC
INPUT FOR OBJECTIVE (FOR THIS CASE DISTANCE BETWEEN GRID LINES IN CM)
0.1
VARIABLE NAMES, IN ORDER THEY APPEAR IN THE OPTIMIZATION VECTOR X
XJF
XJB
XDMAX
DOP0
DOPBLK
DOPL
SF
SB
TAUN
SHADOW
RS
CONCEN
INTLIM   KFAIL   BIGSTP   NPROB
  2       1       0.1       1
IFORM    FORMLA  IBOND   ICONST   NROWS   NCOLS   ISCALE
  1       1.0     1       1       1       2       1
ITMAX    IRSTRT  NSTOP   EPGRAD   EPFUN    EPX
 100       0       3     0.1E-09  0.1E-03  0.1E-03
INUM     ISAVE   OFFDIF
  2       1       0.001
IPARSH(NDIM) 1=ANALYTIC 2=FORWARD 3=CENTRAL 4=CENTRAL1 5=AUTO F/C
2 2 2 2 2 2 2 2 2 2 2 2
X(NDIM)     INITIAL VALUE FOR THE DECISION VECTOR
 0.1  0.2 45.0  19.8 -14.5  -19.8  3.0
 3.0  1.0   0.00   0.0    1.2022
IBOUND(NDIM)  1=LB ACTIVE  2=UB ACTIVE  3=BOTH ACTIVE  4=FREE  5=FIXED
3 3 3 3 3 3 5  5 5 5 5 5
XLB(NDIM)     LOWER BOUNDS
0.1   0.2   10.0   14.0  -20.6  -20.6  -5.0  -5.0
XUB(NDIM)     UPPER BOUNDS
15.0  50.0  300.0  20.6  -14.0   -14.0   16.0  16.0  10000.0
 10.0  30.0  300.0
XSCALE(NDIM) PRESCALING OF DECISION VARIABLES
0.4  1.0  100.0  1.0  1.0  1.0  1.0  1.0  1.0  1.0  1.0  1.0  1.0 1.0
ICOL(NCOL)   COMPONENTS OF DESICION VECTOR INVLOVED IN LINEAR CONSTRAINTS
  5   6
AMAT(NROWS,NCOL) LINEAR CONSTRAINT MATRIX
 -1  1
BRHS(NROWS)  RIGHT HAND SIDE OF LINEAR CONSTRAINTS
 -0.4
ITYPE(NROWS)   0=(EQUALITY) 1=(>)  2=(<)
 2
```

figure C.24 The file invoc.d

```
   INPUT DATA FILE

(INPUT DATA FILE WRITTEN OUT HERE, SEE FIGURE C.24)


  PROBLEM #  4


  EXECUTING THE BROYDEN FAMILY MEMBER
  0.00E+00 DFP +  1.0    BFGS



  BEGIN ITERATION #   0
  THE OBJ =  -676.8508655
  THE POINT IS =
 0.10000000000    0.20000000000    45.000000000    19.800000000    -14.500000000    -19.800000000
 3.0000000000     3.0000000000     1.0000000000    0.00000000000E+00 0.00000000000E+00 1.2022000000


  ISTOP= 2 CONVERGENCE ON OBJECTIVE VALUE SATISFIED.
  CHANGE IN OBJECTIVE <  0.1000000E-03 FOR LAST  3 ITERATIONS



      PROBLEM SUMMARY

  # ITERATIONS =    9  # OBJ EVALS =  80  # GRAD EVALS =  9
  # OF RESETS =   5  # FAILED INTRPS=  3
   49 OF THE OBJECTIVE EVALUATIONS WERE FOR NUMERICAL DERIVATIVES
  THE MINIMUM OBJECTIVE =  -683.1086
  THE OPTIMAL POINT IS =
 0.1000000     0.2000000     36.71090     19.38476     -14.44830     -19.44760
 3.000000      3.000000      1.000000     0.0000000E+00 0.0000000E+00 1.202200

  THE MAGNITUDE OF THE GRADIENT AT THE MIN =  0.81529998
  THE GRADIENT AT MIN =
 -0.00000E+00  -0.00000E+00  0.00000E+00  0.26264     -0.63041     0.44533
 -0.00000E+00  -0.00000E+00  -0.00000E+00  -0.00000E+00  -0.00000E+00  -0.00000E+00

  ALL PROBLEMS HAVE BEEN COMPLETED
```

figure C.25 Output for input file invoc.d

```
NDIM    ILOOP  IPRINT   IPR
 12      1       1       0
THE NAME OF THE INPUT FILE FOR SCAP1D
INSCAP.D
NAME OF THE OBJECTIVE FUNCTION
MAXJSC
INPUT FOR OBJECTIVE (FOR THIS CASE DISTANCE BETWEEN GRID LINES IN CM)
0.1
VARIABLE NAMES, IN ORDER THEY APPEAR IN THE OPTIMIZATION VECTOR X
XJF
XJB
XDMAX
DOP0
DOPBLK
DOPL
SF
SB
TAUN
SHADOW
RS
CONCEN
INTLIM  KFAIL  BIGSTP  NPROB
  2      1      0.1      1
IFORM   FORMLA  IBOND   ICONST  NROWS   NCOLS  ISCALE
  1      1.0     1       1       1       2      1
ITMAX   IRSTRT  NSTOP   EPGRAD  EPFUN   EPX
 100      0      3     0.1E-09 0.1E-03 0.1E-03
INUM    ISAVE   OFFDIF
  2       1     0.001
IPARSH(NDIM) 1=ANALYTIC 2=FORWARD 3=CENTRAL 4=CENTRAL1 5=AUTO F/C
2 2 2 2 2 2 2 2 2 2 2 2
X(NDIM)    INITIAL VALUE FOR THE DECISION VECTOR
 0.1  0.2 250.0  19.8 -14.5  -19.8  3.0
 3.0  1.0   0.00   0.0    1.2022
IBOUND(NDIM)  1=LB ACTIVE  2=UB ACTIVE  3=BOTH ACTIVE  4=FREE  5=FIXED
3 3 3 3 3 3 5  5 5 5 5 5
XLB(NDIM)     LOWER BOUNDS
0.1   0.2   10.0   14.0  -20.6  -20.6  -5.0  -5.0
XUB(NDIM)     UPPER BOUNDS
15.0  50.0  300.0  20.6  -14.0   -14.0   16.0  16.0  10000.0
 10.0  30.0  300.0
XSCALE(NDIM) PRESCALING OF DECISION VARIABLES
0.4  1.0  100.0  1.0  1.0  1.0  1.0  1.0  1.0  1.0  1.0  1.0  1.0 1.0
ICOL(NCOL)   COMPONENTS OF DESICION VECTOR INVLOVED IN LINEAR CONSTRAINTS
  5   6
AMAT(NROWS,NCOL) LINEAR CONSTRAINT MATRIX
 -1  1
BRHS(NROWS)  RIGHT HAND SIDE OF LINEAR CONSTRAINTS
 -0.4
ITYPE(NROWS)   0=(EQUALITY) 1=(>)  2=(<)
 2
```

figure C.26 The file injsc.d

```
   INPUT DATA FILE

(INPUT DATA FILE WRITTEN OUT HERE, SEE FIGURE C.26)


  PROBLEM #  5


  EXECUTING THE BROYDEN FAMILY MEMBER
  0.00E+00 DFP +  1.0    BFGS



  BEGIN ITERATION #   0
  THE OBJ =  -39.19861078
  THE POINT IS =
 0.10000000000    0.20000000000     250.00000000     19.800000000    -14.500000000    -19.800000000
 3.0000000000     3.0000000000      1.0000000000    0.00000000000E+00 0.00000000000E+00 1.2022000000


  ISTOP= 2 CONVERGENCE ON OBJECTIVE VALUE SATISFIED.
  CHANGE IN OBJECTIVE <  0.1000000E-03 FOR LAST  3 ITERATIONS



      PROBLEM SUMMARY

  # ITERATIONS =    5  # OBJ EVALS =  49  # GRAD EVALS =  5
  # OF RESETS =   0  # FAILED INTRPS=  1
   28 OF THE OBJECTIVE EVALUATIONS WERE FOR NUMERICAL DERIVATIVES
  THE MINIMUM OBJECTIVE =  -39.43213
  THE OPTIMAL POINT IS =
 0.1231489     0.2713563      300.0000      19.03269     -14.00000     -17.06288
 3.000000      3.000000       1.000000     0.0000000E+00 0.0000000E+00 1.202200

  THE MAGNITUDE OF THE GRADIENT AT THE MIN =  0.29160733E-01
  THE GRADIENT AT MIN =
   0.10014E-01  -0.44007E-05  -0.00000E+00   0.13807E-02  -0.27352E-01   0.14331E-03
  -0.00000E+00  -0.00000E+00  -0.00000E+00  -0.00000E+00  -0.00000E+00  -0.00000E+00

   ALL PROBLEMS HAVE BEEN COMPLETED
```

figure C.27 Output for input file injsc.d

7.3 Implementation

As well as the program modules required for the optimization program, which were discussed in section C.6, to run the optimization coupled with SCPAP1D additional modules are required. The module interscap.f is used in place of interopto.f. The additional modules are main.f, fouter.f, optoscap.f, mainscap.f, scap1.f, scap2.f, scap3.f, scap4.f, scap5.f, scap6.f, scap7.f, scap8.f, setgen.f, linpack.f, addscap.f, and udop.f. The main.f and the fouter.f module have been separated from optoscap.f so that they may be altered without having to recompile the module optoscap.f, which is a rather lengthy interface module (includes the routines *FUNCTN, GRADNT,* and *INITLZ*). The method of compiling the source codes to get object codes and linking the object codes to get the executable module is the same as discussed in section C.6.

The optimization and SCAP1D source codes together require approximately 472K bytes of storage (this assumes the dummy outer loop routines dopt2.f and done2.f are used). The user must generate object code for each module with a Fortran 77 compiler. The object codes are then linked to form one executable module. An example of how the program would be compiled on a UNIX operating system is given below (the modules can be compiled one at a time, a single command is used below simply to save space in this report).

```
f77 -c -w opt.f update.f redgrd.f onedim.f interscap.f done2.f done2.f
        main.f fouter.f optoscap.f mainscap.f scap1.f scap2.f scap3.f
        scap4.f scap5.f scap6.f scap7.f scap8.f setgen.f linpack.f
        addscap.f udop.f
```

If the steps in section C.6 were already completed it is not necessary to recompile the modules opt.f, update.f, redgrd.f, onedim.f, dopt2.f, and done2.f. The -w flag invokes the compiler option that warnings not be printed out. There are numerous (thousands) of warnings in the modules that make up SCAP1D and the warning flag should be shut off to avoid voluminous output from the compile step. The warnings will not halt the compilation and do not lead to any errors in the execution of the program. This generates the object files. Then all the object codes are combined to form the executable module (in this example named opt.x). For this step all the object modules must be included in the single command below (or similar one on a different operating system).

```
f77 -o opt.x    opt.o update.o redgrd.o onedim.o interscap.o
                dopt2.o done2.o main.o fouter.o optoscap.o
                mainscap.o scap1.o scap2.o scap3.o
                scap4.o scap5.o scap6.o scap7.o scap8.o setgen.o
                linpack.o scapblk.o setgen.o linpack.o addscap.o
```

udop.o

To solve different problems (e.g., different objective functions or decision vectors supplied by the interface) the user need only change the input data files. The executable module would be run in foreground by entering:

opt.out <inputfile >outputfile

where inputfile is the name of the optimization input file (e.g., figure C.18 or figure C.19) and outputfile is the name of the output file (e.g., figure C.20 or figure C.21). Since the program takes considerable time to execute it should be run in batch (background) mode. **Note**, for use at JPL on the Univac and the VAX computers the optimization input file has been associated with the device number 8. To run different data files (e.g., the different examples provided with this code) it is only necessary to change the JCL to associate the desired optimization input data file with the device number 8 (e.g., to reproduce the output in figure C.19, the file inefflr.d must be associated with unit 8). It is not necessary to recompile or relink the program modules to run a different optimization (defined by a different data file).

The amount of storage required for the object code modules is machine dependent (535K on a Pyramid 90X minicomputer), but will generally be 1.3 to 2 times greater than the storage required for the source. The size of the executable module is also machine dependent (484K on a Pyramid 90X minicomputer). The size of the executable module quoted above does not include data storage (primarily array storage). A significant amount of array storage is required by the SCAP1D program.

The executable module is run with the three input data files already discussed in this section. The device numbers are 5 (optimization input file), 9 (SCAP1D input file), and 36 (incident radiation input file). The device number for the optimization output (and SCAP1D output) is 6. In addition, if the flag IRPRNT is true the program uses the output files SPECTRUM (device number 10) and REFLECTED (device number 11). As already mentioned in section C.6 the device numbers 5 and 6 can be altered by changing the module main.f . However, the data files associated with SCAP1D are set in the code and cannot be changed without considerable effort.

To use the optimization code to run SCAP1D a single time set the input ITMAX = 0 and/or IBOUND = 5 for each component of the decision vector.

Program installation can be checked by running the executable module with the input file inxr.d (optimization input file associated with device #5 and shown in figure C.19), which is supplied with this manual. The output that should result is shown in figure C.21 . Figure C.18, the input file inlr.d, can also be run but

requires considerably more computational effort to complete. The resulting output is shown in figure C.20 . Note that the appropriate SCAP1D data files (INSCAP.D and INSCAP1.D) are also supplied for the runs.